

SOME STUDIES ON TWO-BODY RANDOM MATRIX ENSEMBLES

Thesis submitted to



The Maharaja Sayajirao University of Baroda
Vadodara - 390 002, India

for the degree of

Doctor of Philosophy in Physics

by

MANAN VYAS



Theoretical Physics Division
Physical Research Laboratory
Ahmedabad - 380 009, India

May, 2011

To my family

Declaration

I hereby declare that the work presented in this thesis is original and has not formed the basis for the award of any degree or diploma by any university or institution.

.....

Ms. Manan Vyas

(Candidate)

Place: Ahmedabad

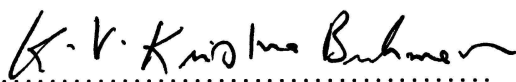
Date: May 04, 2011

Theoretical Physics division

Physical Research Laboratory

Ahmedabad - 380 009, India.

Certified by:

.....


Prof. Venkata Krishna Brahmam Kota

(Guide)

Theoretical Physics division

Physical Research Laboratory

Ahmedabad - 380 009, India.

.....

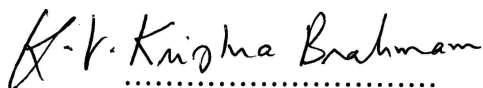
Head, Department of Physics

The Maharaja Sayajirao University of Baroda

Vadodara - 390 002, India.

Certificate

This is to certify that Ms. Manan Vyas has regularly attended Physical Research Laboratory, Ahmedabad and has put more than 200 days of attendance with me at Physical Research Laboratory for her thesis work.



Prof. Venkata Krishna Brahman Kota

(Guide)

Place: Ahmedabad

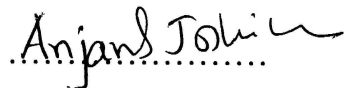
Date: 3/5/2011

Theoretical Physics division

Physical Research Laboratory

Ahmedabad - 380 009, India.

Endorsed by:



Prof. Anjan S. Joshipura

(Dean)

Physical Research Laboratory

Ahmedabad - 380 009, India.



प्रो. ए. एस. जोशीपुरा
Prof. A.S. JOSHIPURA

विशिष्ट वैज्ञानिक एवं डीन Outstanding Scientist & Dean

भौतिक अनुसंधान प्रयोगशाला

Physical Research Laboratory

(भारत सरकार, अंतरिक्ष विभाग की यूनिट)

(A Unit of Department of Space, Govt. of India)

नवरंगपुरा, अहमदाबाद-380 009, भारत

Navrangpura, Ahmedabad-380 009, INDIA

Acknowledgments

This dissertation would not have been possible without the meticulous guidance of Prof. V. K. B. Kota. First of all, I am grateful to him for giving me an opportunity to work with him. His motivation, enthusiasm, immense knowledge, and attention to details has helped me a lot in all the time of research and writing of this thesis. I sincerely thank him for his patience and efforts to educate me with the basics necessary for the work in this thesis.

During this work I have collaborated with Dr. K. B. K. Mayya, Dr. N. D. Chavda, and Dr. P. C. Srivastava and I extend my warmest thanks to them. I am thankful to Dr. N. D. Chavda for his help in the initial stages of my thesis work. I am grateful to Prof. V. N. Potbhare and Dr. N. D. Chavda for their help during my visits to M. S. University of Baroda. I thank Prof. A. C. Sharma for his interest in the thesis work. I am grateful to him for his guidance, encouragement and help. I wish to express my warm and sincere thanks to Prof. Steven Tomsovic for some useful discussions. I sincerely thank Dr. Dilip Angom for encouragement and discussions. I also offer my sincere thanks to Prof. Panigrahi for guiding me in my initial stages of research. I thank Prof. A. K. Dutta and Prof. K. P. Maheshwari for their excellent teaching of basic physics in my master degree course.

This acknowledgment will be incomplete if I do not express my gratitude to the various facilities availed in PRL and the people associated with them. To mention a few, this includes Dr. P. Sharma, Mr. G. Dholakia, Mrs. Nishtha AnilKumar, Mrs. Pauline Joseph, Mrs. Parul Parikh, Miss Jayshree, Mr. Shashi, Mr. Gangadhar, Mr. B. M. Joshi, Mr. Ghanshyam Patel, Mr. Ranganathan, Dr. Sheetal Patel, Miss Pragya, Mr. N. P. M. Nair, Miss Miral Patel, and Mrs. Sujata. I have extensively used POWER5 machine and HPC facility for my thesis work with the help of computer center staff.

I also extend my thanks to the staff of M. S. University of Baroda for their kind co-operation and prompt services.

I express my special gratitude to Prof. V. K. B. Kota and Mrs. Vijayalakshmi Kota for hospitality during my academics related visits to their place. I am deeply touched by Mrs. Kota's motherly care during these visits. Thanks are also due to all my friends in PRL for their affectionate company and best wishes. Dr. Rajneesh Atre has been a great senior and has stood with me in thick and thin. Eventually, he has become a part of my family. I thank him for everything he has done for me. I express my gratitude to my parents and my brother Manthan for their loving support and encouragement. My sincere thanks are due to my parents-in-law for their untiring efforts and boundless love. Words fail me to express my appreciation for my husband Harinder whose patience and encouragement have never let my spirits down. I thank him for his unconditional support. I wish to thank my entire extended family for their patience and moral support.

Finally, I feel great pleasure to express my gratitude to all others who have directly or indirectly contributed to this thesis.

Abstract

Random matrix theory (RMT) has been established to be one of the central themes in quantum physics during the end of 20th century. This theory has emerged as a powerful statistical approach leading to paradigmatic models describing generic properties of complex systems. On the other hand, with scientific developments it was clear by mid 20th century that deterministic ideas are not valid for microscopic systems and this led to the development of a new field of research called ‘quantum chaos’. One-body chaos is well understood by 90’s with RMT playing a key role. More specifically, the spectral statistics predicted by RMT is a characteristic of quantum systems whose classical analogue is chaotic. However, most of the real systems are many-body in character. The classical Gaussian orthogonal (GOE), unitary (GUE) and symplectic (GSE) ensembles, introduced by Wigner and Dyson, are ensembles of multi-body interactions. In various quantum many-body systems such as nuclei, atoms, mesoscopic systems like quantum dots and small metallic grains, interacting spin systems modeling quantum computing core and BEC, the interparticle interactions are essentially two-body in nature. This together with nuclear shell-model examples led to the introduction of random matrix ensembles generated by two-body interactions in 1970-1971. These two-body ensembles are defined by representing the two-particle Hamiltonian by one of the classical ensembles and then the m ($m > 2$) particle H -matrix is generated by the Hilbert space geometry. Thus the random matrix ensemble in the two-particle spaces is embedded in the m -particle H -matrix and therefore these ensembles are generically called embedded ensembles (EEs). Simplest of these ensembles is the embedded Gaussian orthogonal ensemble of random matrices generated by two-body interactions for spinless fermion [boson] systems, denoted by EGOE(2) [BEGOE(2); here ‘B’ stands for bosons]. In addition to the complexity gener-

ating two-body interaction, Hamiltonians for realistic systems consist of a mean-field one-body part. Then the appropriate random matrix ensembles are $EE(1+2)$. The spinless fermion/boson EGEs (orthogonal and unitary versions) have been explored in detail from 70's with a major revival from 1994. It is now well understood that EGEs generate paradigmatic models for many-body chaos or stochasticity exhibited by isolated finite interacting quantum systems. Besides the mean-field and the two-body character, realistic Hamiltonians also carry a variety of symmetries. In many applications of EGEs, generic properties of EGE for spinless fermions are 'assumed' to extend to symmetry subspaces. More importantly, there are several properties of real systems that require explicit inclusion of symmetries and they are defined by a variety of Lie algebras. The aim of the present thesis is to identify and systematically analyze many different physically relevant EGEs with symmetries by considering a variety of quantities and measures that are important for finite interacting quantum systems mentioned above. The embedded ensembles investigated to this end and the corresponding results are as follows.

The thesis contains nine chapters. Chapter 1 gives an introduction to the subject of two-body random matrix ensembles. Also, the known results for spinless fermion/boson EGEs are described briefly for completeness and for easy reference in the following chapters.

Finite interacting Fermi systems with a mean-field and a chaos generating two-body interaction are modeled, more realistically, by one plus two-body embedded Gaussian orthogonal ensemble of random matrices with spin degree of freedom [called $EGOE(1+2)-s$]. Numerical calculations are used to demonstrate that, as λ , the strength of the interaction (measured in the units of the average spacing of the single particle levels defining the mean-field), increases, generically there is Poisson to GOE transition in level fluctuations, Breit-Wigner to Gaussian transition in strength functions (also called local density of states) and also a duality region where information entropy will be the same in both the mean-field and interaction defined basis. Spin dependence of the transition points λ_c , λ_F and λ_d , respectively, is described using the propagator for the spectral variances and the analytical formula for the propagator is derived. We further establish that the duality region corresponds to a region of thermalization. For this purpose we have compared the single particle entropy de-

finied by the occupancies of the single particle orbitals with thermodynamic entropy and information entropy for various λ values and they are very close to each other at $\lambda = \lambda_d$. All these results are presented in Chapter 2.

EGOE(1+2)-s also provides a model for understanding general structures generated by pairing correlations. In the space defined by EGOE(1+2)-s ensemble for fermions, pairing defined by the algebra $U(2\Omega) \supset Sp(2\Omega) \supset SO(\Omega) \otimes SU_S(2)$ is identified and some of its properties are derived. Using numerical calculations it is shown that in the strong coupling limit, partial densities defined over pairing subspaces are close to Gaussian form and propagation formulas for their centroids and variances are derived. As a part of understanding pairing correlations in finite Fermi systems, we have shown that pair transfer strength sums (used in nuclear structure) as a function of excitation energy (for fixed S), a statistic for onset of chaos, follows, for low spins, the form derived for spinless fermion systems, i.e., it is close to a ratio of Gaussians. Going further, we have considered a quantity in terms of ground state energies, giving conductance peak spacings in mesoscopic systems at low temperatures, and studied its distribution over EGOE(1+2)-s by including both pairing and exchange interactions. This model is shown to generate bimodal to unimodal transition in the distribution of conductance peak spacings. All these results are presented in Chapter 3.

For m fermions in Ω number of single particle orbitals, each four-fold degenerate, we have introduced and analyzed in detail embedded Gaussian unitary ensemble of random matrices generated by random two-body interactions that are $SU(4)$ scalar [EGUE(2)- $SU(4)$]. Here, the $SU(4)$ algebra corresponds to the Wigner's supermultiplet $SU(4)$ symmetry in nuclei. Embedding algebra for the EGUE(2)- $SU(4)$ ensemble is $U(4\Omega) \supset U(\Omega) \otimes SU(4)$. Exploiting the Wigner-Racah algebra of the embedding algebra, analytical expression for the ensemble average of the product of any two m -particle Hamiltonian matrix elements is derived. Using this, formulas for a special class of $U(\Omega)$ irreducible representations (irreps) $\{4^r, p\}$, $p = 0, 1, 2, 3$ are derived for the ensemble averaged spectral variances and also for the covariances in energy centroids and spectral variances. On the other hand, simplifying the tabulations available for $SU(\Omega)$ Racah coefficients, numerical calculations are carried out for general $U(\Omega)$ irreps. Spectral variances clearly show, by applying the so-called Jacquod and

Stone prescription, that the EGUE(2)- $SU(4)$ ensemble generates ground state structure just as the quadratic Casimir invariant (C_2) of $SU(4)$. This is further corroborated by the calculation of the expectation values of $C_2[SU(4)]$ and the four periodicity in the ground state energies. Secondly, it is found that the covariances in energy centroids and spectral variances increase in magnitude considerably as we go from EGUE(2) for spinless fermions to EGUE(2) for fermions with spin to EGUE(2)- $SU(4)$ implying that the differences in ensemble and spectral averages grow with increasing symmetry. Also for EGUE(2)- $SU(4)$ there are, unlike for GUE, non-zero cross-correlations in energy centroids and spectral variances defined over spaces with different particle numbers and/or $U(\Omega)$ [equivalently $SU(4)$] irreps. In the dilute limit defined by $\Omega \rightarrow \infty$, $r \gg 1$ and $r/\Omega \rightarrow 0$, for the $\{4^r, p\}$ irreps, we have derived analytical results for these correlations. All correlations are non-zero for finite Ω and they tend to zero as $\Omega \rightarrow \infty$. All these results are presented in Chapter 4.

One plus two-body embedded Gaussian orthogonal ensemble of random matrices with parity [EGOE(1+2)- π] generated by a random two-body interaction (modeled by GOE in two particle spaces) in the presence of a mean-field, for spinless identical fermion systems, is defined in terms of two mixing parameters and a gap between the positive ($\pi = +$) and negative ($\pi = -$) parity single particle states. Numerical calculations are used to demonstrate, using realistic values of the mixing parameters, that this ensemble generates Gaussian form (with corrections) for fixed parity state densities. The random matrix model also generates many features in parity ratios of state densities that are similar to those predicted by a method based on the Fermi-gas model for nuclei. We have also obtained a simple formula for the spectral variances defined over fixed- (m_1, m_2) spaces where m_1 is the number of fermions in the +ve parity single particle states and m_2 is the number of fermions in the -ve parity single particle states. The smoothed densities generated by the sum of fixed- (m_1, m_2) Gaussians with lowest two shape corrections describe the numerical results in many situations. The model also generates preponderance of +ve parity ground states for small values of the mixing parameters and this is a feature seen in nuclear shell-model results. All these results are presented in Chapter 5.

For m number of bosons, carrying spin ($\mathbf{s} = \frac{1}{2}$) degree of freedom, in Ω number of single particle orbitals, each doubly degenerate, we have introduced and an-

alyzed embedded Gaussian orthogonal ensemble of random matrices generated by random two-body interactions that are spin (S) scalar [BEGOE(2)- \mathbf{s}]. The ensemble BEGOE(2)- \mathbf{s} is intermediate to the BEGOE(2) for spinless bosons and for bosons with spin $\mathbf{s} = 1$ which is relevant for spinor BEC. Embedding algebra for the BEGOE(2)- \mathbf{s} ensemble and also for BEGOE(1+2)- \mathbf{s} that includes the mean-field one-body part is $U(2\Omega) \supset U(\Omega) \otimes SU(2)$ with $SU(2)$ generating spin. A method for constructing the ensembles in fixed- (m, S) spaces has been developed. Numerical calculations show that the fixed- (m, S) density of states is close to Gaussian and generically there is Poisson to GOE transition in level fluctuations as the interaction strength (measured in the units of the average spacing of the single particle levels defining the mean-field) is increased. The interaction strength needed for the onset of the transition is found to decrease with increasing S . Propagation formulas for the fixed- (m, S) space energy centroids and ensemble averaged spectral variances are derived. Using these, covariances in energy centroids and spectral variances are analyzed. Variance propagator clearly shows that the BEGOE(2)- \mathbf{s} ensemble generates ground states with spin $S = S_{max}$. This is further corroborated by analyzing the structure of the ground states in the presence of the exchange interaction \hat{S}^2 in BEGOE(1+2)- \mathbf{s} . Natural spin ordering ($S_{max}, S_{max} - 1, S_{max} - 2, \dots, 0$ or $\frac{1}{2}$) is also observed with random interactions. Going beyond these, we have also introduced pairing symmetry in the space defined by BEGOE(2)- \mathbf{s} . Expectation values of the pairing Hamiltonian show that random interactions exhibit pairing correlations in the ground state region. All these results are presented in Chapter 6.

Parameters defining many of the important spectral distributions (valid in the chaotic region), generated by EGEs, involve traces of product of four two-body operators. For example, these higher order traces are required for calculating nuclear structure matrix elements for $\beta\beta$ decay and also for establishing Gaussian density of states generated by various embedded ensembles. Extending the binary correlation approximation method for two different operators and for traces over two-orbit configurations, we have derived formulas, valid in the dilute limit, for the skewness and excess parameters for EGOE(1+2)- π ensemble. In addition, we have derived a formula for the traces defining the correlation coefficient of the bivariate transition strength distribution generated by the two-body transition operator appropriate for

calculating $0\nu\text{-}\beta\beta$ decay nuclear transition matrix elements and also for other higher order traces required for justifying the bivariate Gaussian form for the strength distribution. With applications in the subject of regular structures generated by random interactions, we have also derived expressions for the coefficients in the expansions to order $[J(J+1)]^2$ for the energy centroids $E_c(m, J)$ and spectral variances $\sigma^2(m, J)$ generated by EGOE(2)- J ensemble members for the single- j situation. These expansion coefficients also involve traces of four two-body operators. All these results are presented in Chapter 7.

In Chapter 8, to establish random matrix structure of nuclear shell model Hamiltonian matrices, we have presented a comprehensive analysis of the structure of Hamiltonian matrices based on visualization of the matrices in three dimensions as well as in terms of measures for GOE, banded and embedded random matrix ensembles. We have considered two nuclear shell-model examples, ^{22}Na with $J^\pi T = 2^+0$ and ^{24}Mg with $J^\pi T = 0^+0$ and, for comparison we have also considered SmI atomic example with $J^\pi = 4^+$. It is clearly established that the matrices are neither GOE nor banded. For the EGOE [strictly speaking, EGOE(2)- JT or EGOE(2)- J] structure we have examined the correlations between diagonal elements and eigenvalues, fluctuations in the basis states variances and structure of the two-body part of the Hamiltonian in the eigenvalue basis. Unlike the atomic example, nuclear examples show that the nuclear shell-model Hamiltonians can be well represented by EGOE.

Finally, Chapter 9 of the thesis gives conclusions and future outlook. To summarize, we have obtained large number of new results for embedded ensembles and in particular for EGOE(1+2)-**s**, EGUE(2)- $SU(4)$, EGOE(1+2)- π and BEGOE(1+2)-**s**, with EGUE(2)- $SU(4)$ introduced for the first time in this thesis. Moreover, some results are presented for EGOE(2)- J and for the first time BEGOE(1+2)-**s** has been explored in detail in this thesis. In addition, formulas are derived, by extending the binary correlation approximation method, for higher order traces for embedded ensembles with $U(N) \supset U(N_1) \oplus U(N_2)$ embedding and some of these are needed for new applications of statistical nuclear spectroscopy. Results of the present thesis establish that embedded Gaussian ensembles can be used gainfully to study a variety of problems in many-body quantum physics and this includes quantum information science and the thermodynamics of isolated finite interacting quantum systems.

Contents

Declaration	v
Certificate	vii
Abstract	xi
1 Introduction	1
1.1 Random Matrix Theory, Quantum Chaos and Finite Quantum Systems . . .	1
1.2 Embedded Ensembles for Spinless Fermion Systems	6
1.2.1 EGOE(2) and EGOE(k) ensembles	7
1.2.2 EGOE(1+2) ensemble	9
1.2.3 EGUE(2) and EGUE(k) ensembles	11
1.3 Embedded Ensembles for Spinless Boson Systems	12
1.4 Preview	15
2 EGOE(1+2)-s: Transition Markers	19
2.1 Introduction	19
2.2 EGOE(1+2)-s Ensemble: Preliminaries	20
2.3 Gaussian Level Densities and Ensemble Averaged Spectral Variances . .	23
2.3.1 Gaussian form for fixed- (m, S) eigenvalue densities	23
2.3.2 Propagation formulas for ensemble averaged spectral variances .	25
2.4 Poisson (or close to Poisson) to GOE Transition in Level Fluctuations . .	29
2.5 Breit-Wigner to Gaussian Transition in Strength Functions	34
2.6 Information Entropy and Duality Marker	37
2.7 Occupancies, Single-particle Entropy and Thermodynamic Region . . .	41
2.8 Some Results for $\lambda_0 \neq \lambda_1$	44

2.9	Results for $\gamma_2(m, S)$ for EGOE(1+2)-s	47
2.10	Summary	49
3	EGOE(1+2)-s: Pairing Correlations	53
3.1	Introduction	53
3.2	$U(2\Omega) \supset Sp(2\Omega) \supset SO(\Omega) \otimes SU_S(2)$ Pairing Symmetry	54
3.3	Fixed- (m, ν, S) Partial Densities and their Centroids and Variances	58
3.4	Expectation Values $\langle PP^\dagger \rangle^E$ of the Pairing Operator as Signature of Chaos	66
3.5	Distribution of $\Delta_2 = E_{gs}^{(m+1)} + E_{gs}^{(m-1)} - 2 E_{gs}^{(m)}$ With Pairing and Exchange Interactions	71
3.5.1	Brief introduction to mesoscopic systems	71
3.5.2	Conductance peak spacing (Δ_2) distribution	74
3.6	Summary	80
4	EGUE(2)-$SU(4)$: Group Theoretical Results	81
4.1	Introduction	81
4.2	Preliminaries of $U(4\Omega) \supset U(\Omega) \otimes SU(4)$ Algebra	82
4.2.1	Generators of $U(\Omega)$ and $SU(4)$ algebras	82
4.2.2	Quadratic Casimir operators of $U(\Omega)$ and $SU(4)$ and the Majorana operator	85
4.2.3	$SU(4)$ and $U(\Omega)$ irreps and identification of the ground state $U(\Omega)$ or $SU(4)$ irreps	86
4.3	Definition and Basic Properties of EGUE(2)- $SU(4)$	90
4.3.1	Definition of EGUE(2)- $SU(4)$	90
4.3.2	Matrix structure	93
4.3.3	Matrix construction	95
4.4	$U(4\Omega) \supset U(\Omega) \otimes SU(4)$ Wigner-Racah Algebra for Solving EGUE(2)- $SU(4)$	97
4.5	Exact Expressions for Spectral Variances, Lower Order Cross-correlations and Analytical Results for Lowest $U(\Omega)$ Irreps	101
4.5.1	Covariances in energy centroids $\overline{\langle H \rangle^{m, f_m} \langle H \rangle^{m', f_{m'}}$	101
4.5.2	Spectral variances $\overline{\langle H^2 \rangle^{m, f_m}}$	102
4.5.3	Cross-correlations in energy centroids $\Sigma_{11}(m, f_m; m', f_{m'})$	107
4.5.4	Cross-correlations in spectral variances $\Sigma_{22}(m, f_m; m', f_{m'})$	111

4.6	Numerical Results for Spectral Variances, Expectation Values of $C_2[SU(4)]$ and Four Periodicity in GS	116
4.6.1	Spectral variances	117
4.6.2	Expectation values $\langle C_2[SU(4)] \rangle^E$	118
4.6.3	Four-periodicity in the ground state energies	120
4.6.4	Conclusions	122
4.7	Numerical Results for Correlations in Energy Centroids and Spectral Variances	122
4.7.1	Self-correlations	122
4.7.2	Cross-correlations	123
4.7.3	Results for $\lambda_{\{2\}}^2 \neq \lambda_{\{1^2\}}^2$	127
4.7.4	Conclusions	128
4.8	Summary	128
5	EGOE(1+2)-π: Density of States and Parity Ratios	131
5.1	Introduction	131
5.2	EGOE(1+2)- π Ensemble	133
5.3	Energy Centroids, Variances, Skewness and Excess Parameters for Fixed- (m_1, m_2) Partial Densities	136
5.4	Numerical Results and Discussion	142
5.4.1	Gaussian form for fixed- π state densities	143
5.4.2	Parity ratios for state densities	151
5.4.3	Probability for +ve parity ground states	155
5.5	Summary	156
6	BEGOE(1+2)-s: Spectral Properties	159
6.1	Introduction	159
6.2	Definition and Construction of BEGOE(1+2)-s	160
6.3	Numerical Results for Eigenvalue Density and Level Fluctuations in the Dense Limit	163
6.4	Energy Centroids, Spectral Variances and Ensemble Averaged Spectral Variances and Covariances	169
6.4.1	Propagation formulas for energy centroids and spectral variances	169

6.4.2	Ensemble averaged spectral variances for BEGOE(2)- s	172
6.4.3	Ensemble averaged covariances in energy centroids and spectral variances for BEGOE(2)- s	174
6.5	Preponderance of $S_{max} = m/2$ Ground States and Natural Spin Order : Role of Exchange Interaction	179
6.5.1	Introduction to regular structures with random interactions . . .	179
6.5.2	$U(\Omega)$ algebra and space exchange operator	180
6.5.3	Numerical results for $S_{max} = m/2$ ground states and natural spin order	181
6.6	Pairing in BEGOE(2)- s	184
6.6.1	$U(2\Omega) \supset [U(\Omega) \supset SO(\Omega)] \otimes SU_S(2)$ Pairing symmetry	185
6.6.2	Pairing expectation values	188
6.7	Summary	191
7	Higher Order Traces and their Applications	195
7.1	Introduction	195
7.2	Application to EGOE(1+2)- π : Formulas for Skewness and Excess Param- eters	197
7.3	Application to $\beta\beta$ Decay: Formulas for the Bivariate Correlation Coeffi- cient and Fourth Order Cumulants for the Transition Strength Density .	208
7.3.1	Transition matrix elements and bivariate strength densities	208
7.3.2	Formulas for the bivariate moments	210
7.3.3	Numerical results for bivariate correlation coefficient and fourth order cumulants	214
7.4	EGOE(2)- J Ensemble: Structure of Centroids and Variances for Fermions in a Single- j Shell	217
7.4.1	Definition and construction of EGOE(2)- J	217
7.4.2	Expansions for centroids $E_c(m, J)$ and variances $\sigma^2(m, J)$	221
7.4.3	Propagation equations for bivariate cumulants $k_{rs}(m)$ for $(j)^m$ systems	224
7.4.4	Structure of centroids and variances	230
7.5	Summary	232

8	Hamiltonian Matrix Structure	233
8.1	Introduction	233
8.2	Matrix Structure by Visualization	234
8.3	Analysis in Terms of GOE and BRME	238
8.3.1	GOE structure: distribution of the off-diagonal matrix elements .	239
8.3.2	BRME structure: bandwidths and sparsity	240
8.4	Analysis Using Measures for EGOE Structure	243
8.4.1	Correlations between diagonal matrix elements and eigenvalues .	243
8.4.2	Fluctuations in the basis states spreading widths	245
8.4.3	Structure of the two-body part of the Hamiltonian in the eigen- value basis	247
8.4.4	Comments on deviations from EGOE in the atomic example . . .	249
8.5	Summary	251
9	Conclusions and Future Outlook	253
A	Unitary decomposition for a one plus two-body Hamiltonian for spinless fermions	261
B	Exact variance formula for a given member of EGOE(1+2)-s	263
C	EGUE(2)-s ensemble	267
D	$U(2\Omega) \supset [U(\Omega) \supset SO(\Omega)] \otimes SU(2)$ pairing symmetry	271
E	Some properties of $SU(\Omega)$ Wigner coefficients	275
F	Excess parameter $\gamma_2(m, f_m)$ in terms of $SU(\Omega)$ Racah coefficients	277
G	Further extensions of BEGOE(1+2)	281
H	Basic binary correlation results	285
I	Fixed-(m, M) occupation numbers	297
J	Bivariate edgeworth expansion	299
	Bibliography	301

Chapter 1

Introduction

1.1 Random Matrix Theory, Quantum Chaos and Finite Quantum Systems

Random matrix theory (RMT), starting with Wigner and Dyson's Gaussian random ensembles introduced to describe neutron resonance data, has emerged as a powerful statistical approach leading to paradigmatic models describing generic properties of complex systems. Importance of RMT has been recognized almost since its inception in physics by Wigner in 1955 [Wi-55] to explain the compound nucleus resonance data. Though random matrices were encountered much earlier in 1928 by Wishart [Wi-28] in the context of multivariate statistics and later in 1967 by Pastur [Ma-67], their extensive study began with the pioneering work of Wigner [Wi-67, Po-65]. Though not referred explicitly, Bohr's idea of compound nucleus [Bo-36] almost certainly motivated Wigner to introduce random matrices. Porter's book [Po-65] gives a good introduction to classical random matrix ensembles with a detailed derivation of the joint probability distribution for these ensembles along with an impressive and instructive collection of papers on the subject till 1965. Mathematical foundations of RMT are well described by Mehta [Me-04] (the first edition of Mehta's book was published in 1967). The classical random matrix ensembles are developed and applied during 1955-1972 by Dyson, Mehta, Porter and others [Po-65, Br-81]. In the last three decades, RMT has been successfully used in diverse areas, as shown in Fig. 1.1, with wide ranging applicability to various mathematical, physical and en-

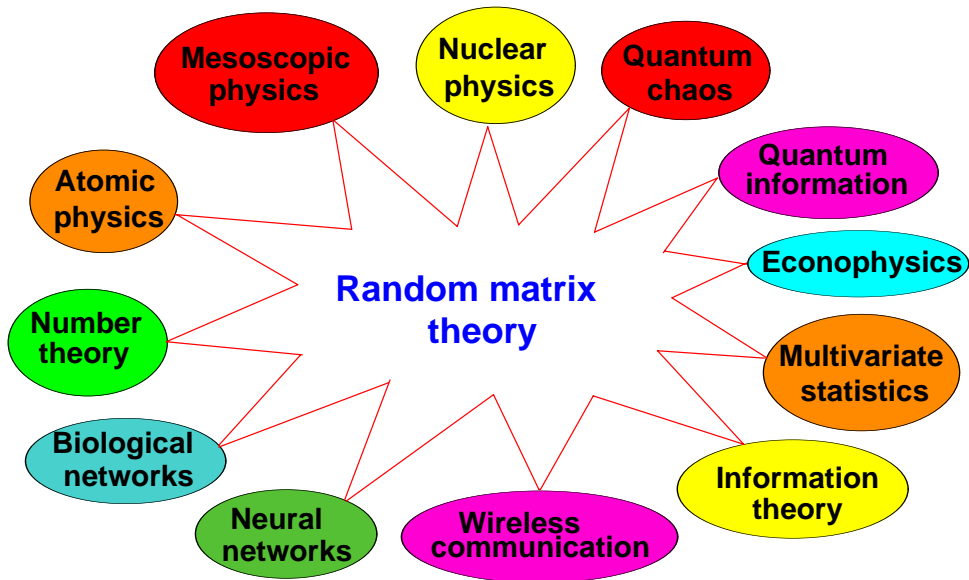


Figure 1.1: Figure showing wide ranging applications of random matrix theory.

gineering branches [Po-65, Me-04, Br-81, Gu-98, Tu-04, St-06, Br-06, Ul-08, We-09, Fo-10, Wr-10, An-10, Ba-10, Ha-10, Mi-10].

RMT helps to analyze statistical properties of physical systems whose exact Hamiltonian is too complex to be studied directly. The exact Hamiltonian of the system under consideration is represented by an ensemble of random matrices that incorporate generic symmetry properties of the system. As stated by Wigner [Wi-61]: *The assumption is that the Hamiltonian which governs the behavior of a complicated system is a random symmetric matrix, with no special properties except for its symmetric nature.* More importantly, as emphasized by French [Fr-95]: *with one short step beyond this, specifically replacing “complicated” by “non-integrable”, this paper would have led to the foundations of quantum chaos. Perhaps it should be so regarded even as it stands.* Depending on the global symmetry properties, namely rotational and time-reversal, Dyson classified the classical random matrix ensembles into three classes—Gaussian orthogonal (GOE), unitary (GUE) and symplectic (GSE) ensembles [Dy-62]. As the names suggest, these ensembles will be invariant under orthogonal, unitary, and symplectic transformations, respectively. The corresponding matrices will be real symmetric, complex hermitian and real quaternion matrices. In order to study symmetry breaking effects on level and strength fluctuations and order-chaos transitions, it is necessary to consider interpolating or deformed random matrix ensem-

bles [Pa-81, Fr-88]. Earliest examples include banded random matrix ensembles, the Porter-Rosenzweig model and 2×2 GOE due to Dyson [Po-65].

RMT has been established to be one of the central themes in quantum physics with the recognition that quantum systems whose classical analogues are chaotic, follow RMT. The BGS conjecture [Bo-84a] is the corner stone for this and the earlier work on this is due to McDonald and Kaufman [Mc-79], Casati et al [Ca-80] and Berry [Be-81]. The BGS conjecture is: *Spectra of time-reversal-invariant systems whose classical analogues are K systems show the same fluctuation properties as predicted by GOE.* Also as stated by BGS: *if this conjecture happens to be true, it will then have established the ‘universality of the laws of level fluctuations’ in quantal spectra already found in nuclei and to a lesser extent in atoms. Then, they should also be found in other quantal systems, such as molecules, hadrons etc.* The details of the developments establishing the connection between RMT and the spectral fluctuation properties of quantum systems whose classical analogues are chaotic are summarized in [Ha-10, St-06]. Recently, Haake et al gave a proof for the BGS conjecture using semi-classical methods [He-07]. Combining BGS work with that of Berry on integrable systems [Be-77], as summarized by Altshuler in the abstract of the colloquium he gave in memory of J.B. French at the university of Rochester in 2004: *Classical dynamical systems can be separated into two classes - integrable and chaotic. For quantum systems this distinction manifests itself, e.g. in spectral statistics. Roughly speaking integrability leads to Poisson distribution for the energies while chaos implies Wigner-Dyson statistics of levels, which are characteristic for the ensemble of random matrices. The onset of chaotic behavior for a rather broad class of systems can be understood as a delocalization in the space of quantum numbers that characterize the original integrable system ...* Following this, as stated by Papenbrock and Weidenmüller [Pa-07]: *We speak of chaos in quantum systems if the statistical properties of the eigenvalue spectrum coincide with predictions of random-matrix theory.* For example, the nearest neighbor spacing distribution (NNSD) showing von-Neumann Wigner [Ne-29] ‘level repulsion’ and the Dyson-Mehta [Dy-63] Δ_3 statistic showing ‘spectral rigidity’ are exhibited by quantum systems whose classical analogues are chaotic; see Fig. 1.2. It is now well recognized that chaos is a typical feature of atomic nuclei and other self bound Fermi systems.

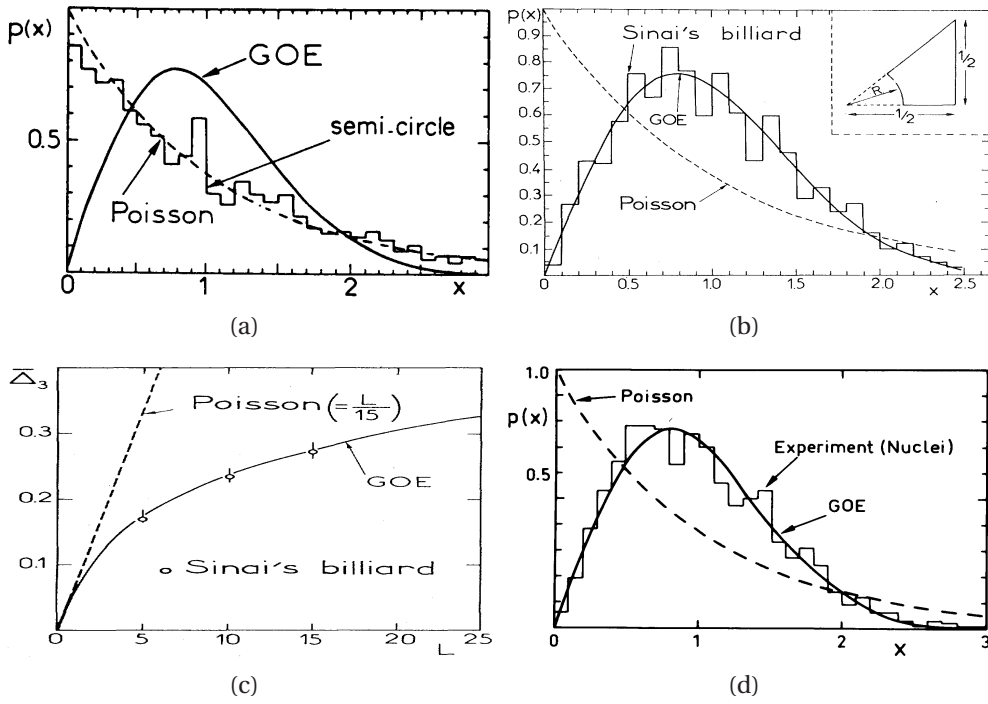


Figure 1.2: Figure illustrating the connection between RMT and quantum chaos. (a) NNSD for the regular (integrable) semi-circular billiard follows Poisson distribution $P(X)dX = e^{-X}dX$ (taken from [Bo-84]); (b) NNSD for the chaotic Sinai billiard follows GOE (taken from [Bo-84a]) and the GOE Wigner form is $P(X)dX = \frac{\pi}{2}X \exp -\frac{\pi X^2}{4}dX$; (c) Dyson-Mehta statistic $\Delta_3(L)$ for Sinai billiard also follows GOE (taken from [Bo-84a]) and for GOE, $\Delta_3(L) \sim \ln L$; and (d) NNSD for the nuclear data ensemble (NDE) follows GOE [Bo-83]. Though we haven't shown, the $\Delta_3(L)$ for $L \leq 20$ also follows GOE for the NDE [Ha-82a]. Note that X is the level spacing normalized to the average level spacing and L is the length of the energy interval over which Δ_3 is calculated. It is clearly seen that, unlike regular billiard, chaotic billiard follows RMT and more importantly, the NDE follows RMT establishing that the neutron resonance region is a region of chaos.

Finite quantum systems such as nuclei, atoms, quantum dots, small metallic grains, interacting spin systems modeling quantum computing core and BEC, share one common property - their constituents (predominantly) interact via two-particle interactions. As pointed out by French [Fr-80]: *The GOE, now almost universally regarded as a model for a corresponding chaotic system is an ensemble of multi-body, not two-body interactions. This difference shows up both in one-point (density of states) and two-point (fluctuations) functions generated by nuclear shell model.* Therefore, it is more appropriate to represent an isolated finite interacting quantum system by random matrix models generated by random *two-body* interactions (in general, by k -body interactions with $k < \text{particle number } m$). Matrix ensembles generated by random two-body interactions, called two-body random ensembles (TBRE), model

what one may call many-body chaos or stochasticity or complexity exhibited by these systems. These ensembles are defined by representing the two-particle Hamiltonian by one of the classical ensembles (GOE or GUE or GSE) and then the $m > 2$ particle H matrix is generated by the m -particle Hilbert space geometry [Fr-70, Bo-71, Mo-75] and with GOE(GUE) embedding, they will be EGOE(EGUE). The key element here is the recognition that there is a Lie algebra that transports the information in the two-particle spaces to many-particle spaces [Mo-75, Ko-05, Be-01a]. Thus the random matrix ensemble in the two-particle spaces is embedded in the m -particle H matrix and therefore these ensembles are more generically called embedded ensembles (EE) [Mo-75, Br-81]. Due to the two-body selection rules, many of the m -particle matrix elements will be zero. Figure 1.3 gives an example of a H -matrix displaying the structure due to two-body selection rules which form the basis for the EE description. At this stage, it is appropriate to recall the purpose, as stated by the organizers Altshuler, Bohigas and Weidenmüller, of a workshop (held at ECT*, Trento in February 1997) on chaotic dynamics of many-body systems: *The study of quantum manifestations of classical chaos has known important developments, particularly for systems with few degrees of freedom. Now, we understand much better how the universal and system-specific properties of ‘simple chaotic systems’ are connected with the underlying classical dynamics. The time has come to extend, from this perspective, our understanding to objects with many degrees of freedom, such as interacting many-body systems. Problems of nuclear, atomic, and molecular theory as well as the theory of mesoscopic systems will be discussed at the workshop.* Note that, chaos implies RMT and the new emphasis is on many-body chaos. Recent thinking is that EE generate paradigmatic models for many-body chaos [Ko-01, Go-11] (one-body chaos is well understood using classical ensembles). The present thesis is devoted to developing and analyzing a variety of EE so that one can quantify and apply the results of many-body chaos.

Simplest of EE is the embedded Gaussian orthogonal ensemble of random matrices for spinless fermion/boson systems generated by random two-body interactions. However, unlike for fermion systems, there are only a few EE investigations for finite interacting boson systems [Pa-00, Ag-01, Ag-02, Ch-03, Ch-04]; the corresponding EE are called BEE (B stands for bosons). The spinless fermion/boson EGEs (orthogonal

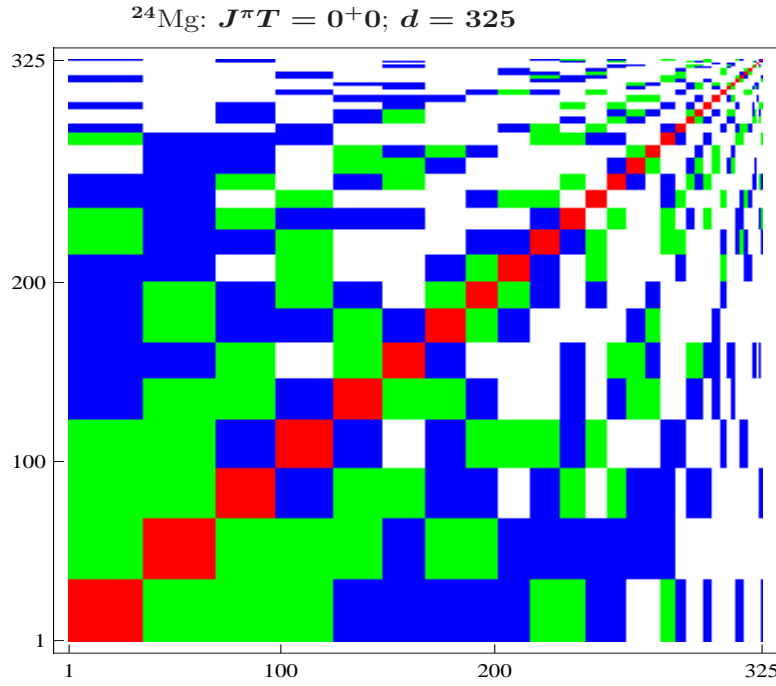


Figure 1.3: Block matrix structure of the H matrix of ^{24}Mg displaying two-body selection rules. Total number of blocks are 33, each labeled by the spherical configurations (m_1, m_2, m_3) . The diagonal blocks are shown in red and within these blocks there will be no change in the occupancy of the nucleons in the three sd orbits. Green corresponds to the region (in the matrix) connected by the two-body interaction that involve change of occupancy of one nucleon. Similarly, blue corresponds to change of occupancy of two nucleons. Finally, white correspond to the region forbidden by the two-body selection rules. This figure was first reported by us in [Ma-10c] and a similar figure was given earlier in [Pa-05] for ^{28}Si with $(J^\pi T) = (0^+ 0)$. Section 8.2 gives further discussion.

and unitary versions) have been explored in detail from 70's [Br-81, Ko-01, Go-11] with a major revival from mid 90's [Fl-94, Fl-96, Fl-97, Ho-95, Fr-96, Ja-97, Ko-98]. Before proceeding further, we briefly describe the known results for spinless fermion/boson EGEs for completeness and for easy reference in the following chapters.

1.2 Embedded Ensembles for Spinless Fermion Systems

The embedding algebra for $\text{EGOE}(k)$ and $\text{EGUE}(k)$ [also $\text{BEGOE}(k)$ and $\text{BEGUE}(k)$] for a system of m spinless particles (fermions or bosons) in N single particle (sp) states with k -body interactions ($k < m$) is $SU(N)$. These ensembles are defined by the three parameters (N, m, k) . A large number of asymptotic results are derived for $\text{EGOE}(k)$ and $\text{EGUE}(k)$ using Wigner's binary correlation approximation [Mo-75, Br-81, Fr-88] and, more importantly, also some exact analytical results are derived using

$SU(N)$ Wigner-Racah algebra [Ko-05, Be-01a, Pl-02]. For bosons, the dense limit studies are interesting as this limit does not exist for fermion systems [Ko-80, Pa-00, Ag-01, Ag-02, Ch-03, Ch-04]. Now we will briefly discuss the definition, construction and the known results for these ensembles.

1.2.1 EGOE(2) and EGOE(k) ensembles

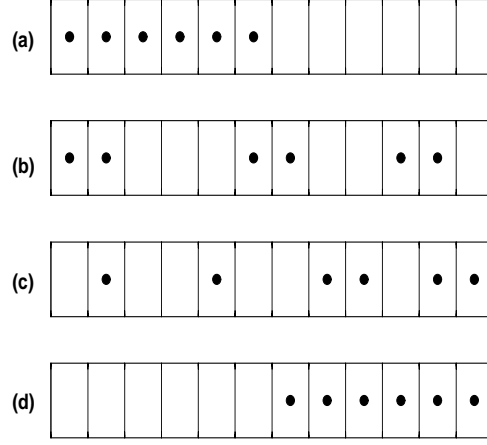


Figure 1.4: Figure showing some configurations for the distribution of $m = 6$ spinless fermions in $N = 12$ single particle states. Distributing the m fermions in all possible ways in N single particle states generates the m -particle configurations or basis states. This is similar to distributing m particles in N boxes with the conditions that the occupancy of each box can be either zero or one and the total number of occupied boxes equals m . In the figure, (a) corresponds to the basis state $|\nu_1 \nu_2 \nu_3 \nu_4 \nu_5 \nu_6\rangle$, (b) corresponds to the basis state $|\nu_1 \nu_2 \nu_6 \nu_7 \nu_{10} \nu_{11}\rangle$, (c) corresponds to the basis state $|\nu_2 \nu_5 \nu_8 \nu_9 \nu_{11} \nu_{12}\rangle$ and (d) corresponds to the basis state $|\nu_7 \nu_8 \nu_9 \nu_{10} \nu_{11} \nu_{12}\rangle$.

The EGOE(2) ensemble for spinless fermion systems is generated by defining the two-body Hamiltonian H to be GOE in two-particle spaces and then propagating it to many-particle spaces by using the geometry of the many-particle spaces [this is in general valid for k -body Hamiltonians, with $k < m$, generating EGOE(k)]. Let us consider a system of m spinless fermions occupying N sp states. Each possible distribution of fermions in the sp states generates a configuration or a basis state; see Fig. 1.4. Given the sp states $|\nu_i\rangle$, $i = 1, 2, \dots, N$, the EGOE(2) is defined by the Hamiltonian operator,

$$\hat{H} = \sum_{\nu_i < \nu_j, \nu_k < \nu_\ell} \langle \nu_k \nu_\ell | \hat{H} | \nu_i \nu_j \rangle a_{\nu_\ell}^\dagger a_{\nu_k}^\dagger a_{\nu_i} a_{\nu_j}. \quad (1.2.1)$$

The action of the Hamiltonian operator defined by Eq. (1.2.1) on the basis states

$|v_1 v_2 \cdots v_m\rangle$ (see Fig. 1.4 for examples) generates the EGOE(2) ensemble in m -particle spaces. The symmetries for the antisymmetrized two-body matrix elements $\langle v_k v_\ell | \hat{H} | v_i v_j \rangle$ are

$$\begin{aligned}\langle v_k v_\ell | \hat{H} | v_j v_i \rangle &= -\langle v_k v_\ell | \hat{H} | v_i v_j \rangle, \\ \langle v_k v_\ell | \hat{H} | v_i v_j \rangle &= \langle v_i v_j | \hat{H} | v_k v_\ell \rangle.\end{aligned}\tag{1.2.2}$$

Note that a_{v_i} and $a_{v_i}^\dagger$ in Eq. (1.2.1) annihilate and create a fermion in the sp state $|v_i\rangle$, respectively. The Hamiltonian matrix $H(m)$ in m -particle spaces contains three different types of non-zero matrix elements (all other matrix elements are zero due to two-body selection rules) and explicit formulas for these are [Ko-01],

$$\begin{aligned}\langle v_1 v_2 \cdots v_m | \hat{H} | v_1 v_2 \cdots v_m \rangle &= \sum_{v_i < v_j \leq v_m} \langle v_i v_j | \hat{H} | v_i v_j \rangle, \\ \langle v_p v_2 v_3 \cdots v_m | \hat{H} | v_1 v_2 \cdots v_m \rangle &= \sum_{v_i=v_2}^{v_m} \langle v_p v_i | \hat{H} | v_1 v_i \rangle, \\ \langle v_p v_q v_3 \cdots v_m | \hat{H} | v_1 v_2 v_3 \cdots v_m \rangle &= \langle v_p v_q | \hat{H} | v_1 v_2 \rangle.\end{aligned}\tag{1.2.3}$$

Note that, in Eq. (1.2.3), the notation $|v_1 v_2 \cdots v_m\rangle$ denotes the orbits occupied by the m spinless fermions. The EGOE(2) is defined by Eqs. (1.2.2) and (1.2.3) with GOE representation for \hat{H} in the two-particle spaces, i.e.,

$\langle v_k v_\ell | \hat{H} | v_i v_j \rangle$ are independent Gaussian random variables

$$\overline{\langle v_k v_\ell | \hat{H} | v_i v_j \rangle} = 0,\tag{1.2.4}$$

$$\overline{|\langle v_k v_\ell | \hat{H} | v_i v_j \rangle|^2} = v^2 (1 + \delta_{(ij),(k\ell)}).$$

In Eq. (1.2.4), ‘overline’ indicates ensemble average and v is a constant. Now the m -fermion EGOE(2) Hamiltonian matrix ensemble is denoted by $\{H(m)\}$ where $\{\dots\}$ denotes ensemble, with $\{H(2)\}$ being GOE. Note that, the m -particle H -matrix dimension is $d_f(N, m) = \binom{N}{m}$ and the number of independent matrix elements is $d_f(N, 2)[d_f(N, 2) + 1]/2$; the subscript ‘ f ’ in $d_f(N, m)$ stands for ‘fermions’. A com-

puter code for constructing EGOE(2) ensemble is available in our group [Ko-01]; many other groups in the world have also developed codes for EGOE(2).

Just as the EGOE(2) ensemble, it is possible to define k -body ($k < m$) ensembles EGOE(k) (these are also called 2-BRE, 3-BRE, \dots in [Vo-08]). Some of the generic results, derived numerically and analytically, for EGOE(k) are as follows: (i) state densities approach Gaussian form for large m and they exhibit, as m increases from k , semi-circle to Gaussian transition with $m = 2k$ being the transition point [Br-81, Be-01a]; (ii) level and strength fluctuations follow GOE (as far as one can infer from numerical examples) [Br-81]; (iii) there is average fluctuation separation with increasing m and the averages are determined by a few long wavelength modes in the normal mode decomposition of the density of states [Mo-75, Br-81, Le-08]; (iv) smoothed (ensemble averaged) transition strength densities take bivariate Gaussian form and as a consequence transition strength sums originating from a given eigenstate will be close to a ratio of two Gaussians [Fr-88]; (v) cross-correlations between spectra with different particle numbers will be non-zero [Pa-06, Ko-06a]. For reviews on EGOE, see [Br-81, Be-03, Ko-01].

1.2.2 EGOE(1+2) ensemble

Besides the two-body interaction, Hamiltonians for realistic systems also contain a mean field one-body part (generating shell structure) and therefore a more appropriate random matrix ensemble for finite quantum systems is EGOE(1+2)^a, the embedded GOE of one plus two-body interactions [Fl-96, Fl-96a, Fl-97, Ko-01]. Given the mean-field Hamiltonian $\hat{h}(1) = \sum_i \epsilon_i \hat{n}_i$, where \hat{n}_i are number operators and ϵ_i , $i = 1, 2, \dots, N$ are the sp energies, and the two-body interaction $\hat{V}(2)$ (this is same as $\hat{H}(2)$ defined in Sec. 1.2.1), EGOE(1+2) is defined by the operator

$$\{\hat{H}\} = \hat{h}(1) + \lambda \{\hat{V}(2)\}. \quad (1.2.5)$$

^aAt this point it is also useful to mention that EGOE(1+2)'s [and EGOE(2)'s] are also called TBRE in literature; Sec. 5.7 in [Go-11] gives clarifications on this nomenclature. As Brody et al state [Br-81]: *The most severe mathematical difficulties with TBRE are due to angular momentum constraints ... Another type of ensemble, ... much closer to being mathematical tractable abandons the J restrictions entirely ... an embedded GOE, or EGOE for short.*

The $\{\hat{V}(2)\}$ ensemble in two-particle spaces is represented by GOE(1) and λ is the strength of $\hat{V}(2)$. Note that $\text{GOE}(\nu^2)$ means GOE with variance ν^2 for the off-diagonal matrix elements and $2\nu^2$ for the diagonal matrix elements; see Eq. (1.2.4). The mean-field one-body Hamiltonian $\hat{h}(1)$ in Eq. (1.2.5), in our studies, is a fixed one-body operator defined by the sp energies ϵ_i with average spacing Δ . It is important to note that the operators $h(1)$ and $V(2)$ are independent. Without loss of generality, we put $\Delta = 1$ so that λ , the strength of the interaction, is in the units of Δ . Thus, EGOE(1+2) is defined by the three parameters (N, m, λ) . It is possible to draw the ϵ_i 's from the eigenvalues of a random ensemble and then the corresponding EGOE(1+2) is called two-body random interaction model (TBRIM) [Fl-97] or from the center of a GOE and then the corresponding EGOE(1+2) is called random interaction matrix model (RIMM) [Al-00, Al-01]. Construction of the EGOE(1+2) ensemble in m -fermion spaces follows easily from the results in Sec. 1.2.1. The notation used in Eq. (1.2.5) implies that the action of the operator $\{\hat{H}\}$ on the m -particle basis space generates EGOE(1+2) Hamiltonian matrix ensemble in m -particle spaces. It should be noted that the embedding for EGOE(1+2) is also generated by the $SU(N)$ group and the propagation formulas for the energy centroids and variances of the eigenvalue densities follow from the unitary decomposition of H with respect to the $U(N)$ algebra; see Appendix A.

The most significant aspect of EGOE(1+2) is that the ensemble admits three chaos markers as λ is increased from zero. Firstly, eigenvalue (state) densities approach Gaussian form for large m for all values of λ . As the value of λ increases from zero, level fluctuations exhibit transition from Poisson to GOE at $\lambda = \lambda_c$ [Ja-97]. With further increase in the λ value, strength functions (also called local density of states) make a transition from Breit-Wigner (BW) to Gaussian form at $\lambda = \lambda_F \gg \lambda_c$ [Ge-97, Ko-01a, Ja-02]. Beyond this point, there is a region around $\lambda = \lambda_d$ where entropies and other statistics become same in the eigenbasis of the mean-field Hamiltonian and the pure two-body Hamiltonian [Ho-95, Ko-02] (though not yet proved, this result perhaps extends to any basis [Ko-03]). Equivalently, all different definitions for thermodynamic properties like entropy, temperature etc. coincide at $\lambda = \lambda_d$. It should be stressed that the chaos markers form the basis [Ko-03] for statistical spectroscopy [Ko-01, Fr-82, Ka-94, Fl-99, Fr-06, Ko-10]. The parametric dependence of λ_c , λ_F and

λ_d is also known and this will be discussed in detail in Chapter 2. Besides these, generic properties of EGOE(2) are valid for EGOE(1+2) in the strong coupling limit; i.e., for $\lambda \gg \lambda_F$. Detailed discussion of the three chaos markers $(\lambda_c, \lambda_F, \lambda_d)$ generated by EGOE(1+2) and also applications of the ensemble are given in [Ko-01, Ko-03, An-04, Br-08, Go-11] and references therein. Now, we will turn to embedded Gaussian unitary ensembles for spinless fermions.

1.2.3 EGUE(2) and EGUE(k) ensembles

For a system of m fermions occupying N sp states, all the $N_m = d_f(N, m) = \binom{N}{m}$ antisymmetric states transform as the irreducible representation (irrep) $f_m = \{1^m\}$, in Young tableaux notation, with respect to the $U(N)$ algebra. With only two-body interactions among the fermions, the Hamiltonian operator is

$$\hat{H} = \sum_{v_a, v_b} V_{v_a v_b}(2) A^\dagger(f_2 v_b) A(f_2 v_a). \quad (1.2.6)$$

Here, $f_2 = \{1^2\}$ and v_r 's denote irreps of the groups in the subgroup chain of $U(N)$ that supply the labels for a complete specification of any two-particle state; similarly, for any m , the states are $|f_m v_m\rangle$. Note that A^\dagger and A in Eq. (1.2.6) are normalized two-particle creation and destruction operators, respectively and $V_{v_a v_b}(2)$ are two-particle matrix elements. The EGUE(2) ensemble in m -particle spaces, with matrix dimension $N_m = d_f(N, m)$, is generated by the \hat{H} operator in Eq. (1.2.6) with GUE representation in two-particle spaces and then propagating it to the m -particle spaces using the direct product structure of the m -particle states [Ko-05]. With the two-particle matrix elements $V_{v_a v_b}(2)$ [the $V(2)$ matrix being complex hermitian] drawn from a GUE, $V_{v_a v_b}(2)$ are independent Gaussian variables with zero center and variance given by,

$$\overline{V_{v_a v_b}(2) V_{v_c v_d}(2)} = \lambda^2 \delta_{v_a v_d} \delta_{v_b v_c}. \quad (1.2.7)$$

Here, $\lambda^2 N_2$ is the ensemble averaged two-particle variance. As in [Ko-05], the $U(\Omega) \leftrightarrow SU(\Omega)$ correspondence is used and therefore we use $U(\Omega)$ and $SU(\Omega)$ interchangeably when there is no confusion. Important step in the analytical study of EGUE(2) is the unitary decomposition of \hat{H} in terms of the $SU(N)$ tensors $B(g_v \omega_v)$

with $g_v = \{0\}, \{21^{N-2}\}$ and $\{2^2 1^{N-4}\}$,

$$B(g_v \omega_v) = \sum_{v_a, v_b} \left\langle f_2 v_a \overline{f_2 v_b} \mid g_v \omega_v \right\rangle A^\dagger(f_2 v_a) A(f_2 v_b), \quad (1.2.8)$$

where \overline{f} is the irrep conjugate to f and $\left\langle f_2 v_a \overline{f_2 v_b} \mid g_v \omega_v \right\rangle$ is a $SU(N)$ Wigner coefficient. For $f_2 = \{1^2\}$ we have, $\overline{f_2} = \{1^{N-2}\}$ and it also contains a phase factor as discussed in [Ko-05]. Then we have $\hat{H} = \sum_{g_v, \omega_v} W(g_v \omega_v) B(g_v \omega_v)$. A significant property of the expansion coefficients W 's is that they are also independent Gaussian random variables, just as V 's, with zero center and variance given by $\overline{W(g_v \omega_v) W(g_\mu \omega_\mu)} = \lambda^2 \delta_{g_v g_\mu} \delta_{\omega_v \omega_\mu}$. Using Wigner-Eckart theorem, the matrix elements of B 's in f_m space can be decomposed into a reduced matrix element and a $SU(\Omega)$ Wigner coefficient. Using this and the expansion of \hat{H} in terms of B 's, exact analytical formulas are derived for the ensemble averaged spectral variances, cross-correlations in energy centroids and also for the cross-correlations in spectral variances for EGUE(2) [Ko-05]. In addition, exact result for the ensemble averaged excess parameter (this involves fourth moment) for the density of eigenvalues is also derived [Ko-05]. An alternative derivation was given by Benet et al [Be-01a, Be-01b]. More significantly, all these results extend to EGUE(k); i.e., EGUE generated by k -body interactions. Two significant results for EGUE(k) are: (i) for $k \leq m < 2k$, the density of eigenvalues is semi-circular whereas the density is Gaussian for $m >> 2k$ with $m = 2k$ being the transition point; (ii) EGUE(k) generates non-zero cross-correlations between states with different particle numbers while they will be zero for GUE representation for the m -particle H matrices. See [Ko-05, Be-01a, Be-01b, Pl-02, Ko-06a] for further details; cross-correlations are defined and further explored in Chapters 4 and 6 ahead.

1.3 Embedded Ensembles for Spinless Boson Systems

The BEGOE(2)/BEGUE(2) ensemble for spinless boson systems is generated by defining the two-body Hamiltonian H to be GOE/GUE in two-particle spaces and then propagating it to many-particle spaces by using the geometry of the many-particle spaces [this is in general valid for k -body Hamiltonians, with $k < m$, generating BEGOE(k)/BEGUE(k)]. Consider a system of m spinless bosons occupying N sp states $|v_i\rangle$, $i = 1, 2, \dots, N$; see Fig. 1.5. Then, BEGOE(2) is defined by the Hamilto-

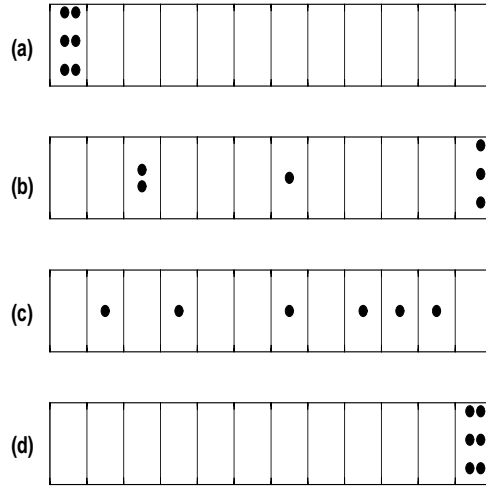


Figure 1.5: Figure showing some configurations for the distribution of $m = 6$ spinless bosons in $N = 12$ single particle states. Distributing the m bosons in all possible ways in N single particle states generates the m -particle configurations or basis states. This is similar to distributing m particles in N boxes with the conditions that occupancy of each box lies between zero and m and the maximum number of occupied boxes equals m . In the figure, (a) corresponds to the basis state $|(v_1)^6\rangle$, (b) corresponds to the basis state $|(v_3)^2 v_7 (v_{12})^3\rangle$, (c) corresponds to the basis state $|v_2 v_4 v_7 v_9 v_{10} v_{11}\rangle$ and (d) corresponds to the basis state $|(v_{12})^6\rangle$.

nian operator,

$$\hat{H} = \sum_{v_i \leq v_j, v_k \leq v_l} \frac{\langle v_k v_l | \hat{H} | v_i v_j \rangle}{\sqrt{(1 + \delta_{ij})(1 + \delta_{kl})}} b_{v_k}^\dagger b_{v_l}^\dagger b_{v_i} b_{v_j}, \quad (1.3.1)$$

with the symmetries for the symmetrized two-body matrix elements $\langle v_k v_l | \hat{H} | v_i v_j \rangle$ being,

$$\begin{aligned} \langle v_k v_l | \hat{H} | v_j v_i \rangle &= \langle v_k v_l | \hat{H} | v_i v_j \rangle, \\ \langle v_k v_l | \hat{H} | v_i v_j \rangle &= \langle v_i v_j | \hat{H} | v_k v_l \rangle. \end{aligned} \quad (1.3.2)$$

The action of the Hamiltonian operator defined by Eq. (1.3.1) on an appropriately chosen basis states (see Fig. 1.5 for examples) generates the BEGOE(2) ensemble. Note that b_{v_i} and $b_{v_i}^\dagger$ in Eq. (1.3.1) annihilate and create a boson in the sp state $|v_i\rangle$, respectively. The Hamiltonian matrix $H(m)$ in m -particle spaces contains three different types of non-zero matrix elements and explicit formulas for these are [Pa-00],

$$\left\langle \prod_{r=i,j,\dots} (v_r)^{n_r} | \hat{H} | \prod_{r=i,j,\dots} (v_r)^{n_r} \right\rangle = \sum_{i \geq j} \frac{n_i (n_j - \delta_{ij})}{(1 + \delta_{ij})} \langle v_i v_j | \hat{H} | v_i v_j \rangle,$$

$$\left\langle (v_i)^{n_i-1} (v_j)^{n_j+1} \prod_{r'=k,l,\dots} (v_{r'})^{n_{r'}} | \hat{H} | \prod_{r=i,j,\dots} (v_r)^{n_r} \right\rangle = \quad (1.3.3)$$

$$\sum_{k'} \left[\frac{n_i (n_j + 1) (n_{k'} - \delta_{k'i})^2}{(1 + \delta_{k'i}) (1 + \delta_{k'j})} \right]^{1/2} \langle v_{k'} v_j | \hat{H} | v_{k'} v_i \rangle ,$$

$$\left\langle (v_i)^{n_i+1} (v_j)^{n_j+1} (v_k)^{n_k-1} (v_l)^{n_l-1} \prod_{r'=m,n,\dots} (v_{r'})^{n_{r'}} | \hat{H} | \prod_{r=i,j,\dots} (v_r)^{n_r} \right\rangle =$$

$$\left[\frac{n_k (n_l - \delta_{kl}) (n_i + 1) (n_j + 1 + \delta_{ij})}{(1 + \delta_{ij}) (1 + \delta_{kl})} \right]^{1/2} \langle v_i v_j | \hat{H} | v_k v_l \rangle .$$

Note that all other m -particle matrix elements are zero due to two-body selection rules. In the second equation in Eq. (1.3.3), $i \neq j$ and in the third equation, four combinations are possible: (i) $k = l$, $i = j$, $k \neq i$; (ii) $k = l$, $i \neq j$, $k \neq i$, $k \neq j$; (iii) $k \neq l$, $i = j$, $i \neq k$, $i \neq l$; and (iv) $i \neq j \neq k \neq l$. BEGOE(2) for spinless boson systems is defined by Eqs. (1.3.2) and (1.3.3) with the H matrix in two-particle spaces represented by $\text{GOE}(v^2)$ [see Eq. (1.2.4) and discussion below Eq. (1.2.5) for $\text{GOE}(v^2)$]. Now the m -boson BEGOE(2) Hamiltonian matrix ensemble is denoted by $\{H(m)\}$, with $\{H(2)\}$ being a GOE. Note that the $H(m)$ matrix dimension is $d_b(N, m) = \binom{N+m-1}{m}$ and the number of independent matrix elements is $d_b(N, 2)[d_b(N, 2) + 1]/2$. The subscript ' b ' in $d_b(N, m)$ stands for 'bosons'. Using Eqs. (1.3.2) and (1.3.3) with GOE representation for H in two-particle spaces, we have developed a computer code for constructing BEGOE(2) ensemble. The extension of BEGOE(2) code to construct BEGOE(1+2) incorporating mean-field one-body part is straightforward. It is important to stress that, unlike for fermionic EE, there are only a few BEE investigations [Pa-00, Ag-01, Ag-02, Ch-03, Ch-04].

Firstly, it is important to mention that, unlike fermion systems, for interacting spinless boson systems with m bosons in N sp orbitals, dense limit defined by $m \rightarrow \infty$, $N \rightarrow \infty$ and $m/N \rightarrow \infty$ is also possible as m can be greater than N for bosons. Also the results for bosons can be obtained from those for fermions by using $N \rightarrow -N$ symmetry [Ko-80]. It is now well understood that BEGOE(2) [also BEGUE(2)] generates in the dense limit, eigenvalue density close to a Gaussian [Ko-80, Pa-00, Ag-02]. Also the ergodic property is found to be valid in the dense limit with sufficiently large

N [Ch-03]; there are deviations for small N [Ag-01]. Similarly, for BEGOE(1+2), as the strength λ of the two-body interaction increases, there is Poisson to GOE transition in level fluctuations [Ch-03] and with further increase in λ , there is Breit-Wigner to Gaussian transition in strength functions [Ch-04]. For BEGUE(k), exact analytical results for the lowest two moments of the two-point function have been derived by Agasa et al [Ag-02]. Level fluctuations and wavefunction structure in interacting boson systems are also studied using interacting boson models of atomic nuclei [Al-91, Wh-93, Ca-00] and a symmetrized two coupled rotors model [Bo-98a, Bo-98b] and the results are understood in terms of random matrix theory. In addition, using random interactions in interacting boson models, there are several studies on the generation of regular structures in boson systems with random interactions [Ku-97, Bi-00, Ko-04, Yo-09]. Finally, there are also studies on thermalization in finite quantum systems using boson systems and here also random matrix theory plays an important role; see [Ri-09, Sa-10, Sa-10a, Ol-09, Ko-11] and references therein.

1.4 Preview

Besides the mean-field and the two-body character, realistic Hamiltonians also carry a variety of symmetries. In many applications of EGEs, generic properties of EGE for spinless fermions are ‘assumed’ to extend to symmetry subspaces. More importantly, there are several properties of real systems that require explicit inclusion of symmetries and they are defined by a variety of Lie algebras. For example, spin S is a good quantum number for atoms and quantum dots, angular-momentum J and parity π are good quantum numbers for nuclei and so on. Therefore, it is more appropriate to study EE with good symmetries and symmetries in principle provide a systematic classification of EE. Figure 1.6 shows some EE/BEE with symmetries. It is well acknowledged that these extended ensembles are notoriously difficult and to derive their generic properties is thus, quite complicated. As stated by French [Fr-80]: *... For most purposes, the resulting embedded GOE (or EGOE) is very difficult to deal with, but by good luck, we can use it to study the questions we have posed and the answers are different from, and much more enlightening than, those which would come from GOE.* EGEs operating in many-particle spaces generate forms for distributions of various physical quantities with respect to energy and other quantum numbers. The separa-

tion of the energy evolution of various observables into a smoothed and a fluctuating part (with fluctuations following GOE/GUE/GSE) provides the basis for statistical spectroscopy [Ko-10, Ko-89, Fr-82]. In statistical spectroscopy, methods are developed to determine various moments defining the distributions (predicted by EGEs) for the smoothed parts (valid in the chaotic region) without recourse to many-body Hamiltonian construction [this part of statistical spectroscopy is also often referred to as spectral distribution theory or spectral distribution methods].

The aim of the present thesis is to identify and systematically analyze many different physically relevant EGEs with symmetries by considering a variety of quantities and measures that are important for finite interacting quantum systems. Numerical as well as analytical study of these more general ensembles is challenging due to the complexities of group theory and also due to large matrix dimensions for $m \geq 10$. It is useful to mention that many diversified methods like numerical Monte-Carlo methods, binary correlation approximation, trace propagation, group theory and perturbation theory are used to derive generic properties of EE [Mo-75, Be-01a, Ko-05, Ko-07, Pa-11]. Towards this end, we have obtained large number of new results for embedded ensembles and in particular for EGOE(1+2)-**s**, EGUE(2)- $SU(4)$, EGOE(1+2)- π , BEGOE(1+2)-**s** and EGOE(2)- J ensembles. In addition, derived are formulas for several fourth order traces that are needed in the analysis of EGOE's and also in the applications of spectral distribution theory generated by EGEs. We have also obtained further evidence for EGOE representation of nuclear Hamiltonian matrices. Results of the present thesis together with earlier investigations establish that embedded Gaussian ensembles can be used gainfully to study a variety of problems in many-body quantum physics and this includes some of the new areas of research in physics such as quantum information science (QIS) and the thermodynamics of isolated finite interacting quantum systems. It should be noted that some of the work in the present thesis is also reviewed in [Go-11].

Before going further, for completeness, we mention that, besides the EE(BEE)'s that will be described in detail in Chapters 2-8, there are a few other EE(BEE)'s that have received limited attention in the literature. They are: (i) EGOE invariant under particle-hole symmetry, called random quasi-particle ensembles [Jo-98, Ki-07], (ii) a fixed Hamiltonian plus EGOE called K +EGOE [Ko-01] and similarly displaced

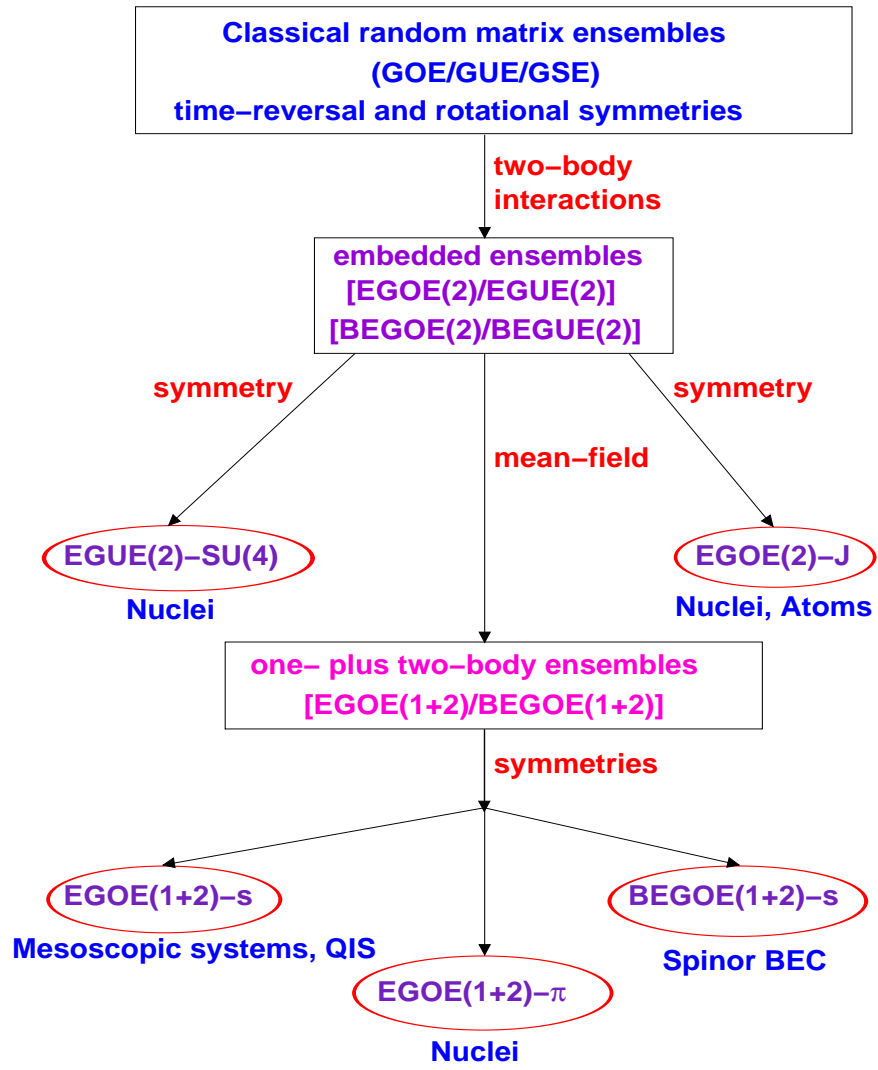


Figure 1.6: Figure showing the information content of various random matrix ensembles. Also shown are the areas in which embedded ensembles with various symmetries are relevant. Here, s denotes two-particle spin, $SU(4)$ denotes spin-isospin supermultiplet symmetry, π denotes parity and J denotes total angular-momentum. Note that the symplectic ensembles EGSE/BEGSE and the one plus two-body unitary ensembles EGUE(1+2)/BEGUE(1+2) are not shown as there are no studies of these ensembles till today.

TBRE [Ve-02, Co-82] where a constant is added to all the two-body interaction matrix elements, (iii) EGOE with a partitioned GOE in the two-particle spaces, called p -EGOE [Ko-99, Fr-83], (iv) in mesoscopic systems such as quantum dots, randomness of the sp states induces randomness in the two-body part of the Hamiltonian and these then give rise to induced-TBRE depending on the underlying space-time symmetries as well as on the features of the two-body interaction [Al-05], and (v) BEGOE(1+2) with orbital angular-momentum L , denoted as BEGOE(1+2)- L or BTRBE- L , for bosons in sp orbits [Ku-00] and sd orbits [Bi-01] and also BEGOE(2) with

$SO(N_1) \oplus SO(N_2)$ symmetry in IBM [Ko-04]. Now we will give a preview of the thesis.

Results for transitions in eigenvalue and wavefunction structure in one plus two-body random matrix ensembles with spin [EGOE(1+2)-**s**] are given in Chapter 2. Chapter 3 gives the results for pairing correlations generated by EGOE(1+2)-**s**. Spectral properties of embedded Gaussian unitary ensemble of random matrices generated by two-body interactions with Wigner's $SU(4)$ symmetry [EGUE(2)- $SU(4)$] are derived and discussed in Chapter 4. It is important to mention that EGUE(2)- $SU(4)$ is introduced for the first time in the present thesis. Chapter 5 gives the results for density of states and parity ratios for one plus two-body random matrix ensembles with parity [EGOE(1+2)- π]. Spectral properties of one plus two-body random matrix ensembles for boson systems with spin [BEGOE(1+2)-**s**] are presented in Chapter 6. Although BEGOE(1+2)-**s** was known in literature before, it is explored in detail for the first time in this thesis. Chapter 7 gives the results for higher order averages, derived by extending Mon and French's binary correlation method to two-orbits, required in many applications. In addition, given also are some results for the traces needed for the embedded Gaussian orthogonal ensemble of two-body interactions with angular-momentum J symmetry [EGOE(2)- J] for fermions in a single j -shell. Chapter 8 gives a comprehensive analysis of the structure of H matrices to establish EGOE structure of nuclear shell model H -matrices. Finally, Chapter 9 gives conclusions and future outlook. Before turning to Chapter 2, we would like to add that there will be some unavoidable repetition in Chapters 2-8 as they deal with different embedded ensembles with applications in different physical systems.

Chapter 2

EGOE(1+2)-s: Transition Markers

2.1 Introduction

First non-trivial but at the same time important (from the point of view of its applications) embedded ensembles are $EE(2)\text{-s}$ and $EE(1+2)\text{-s}$ with spin degree of freedom, for a system of interacting fermions. In the last decade, the GOE version, the embedded Gaussian orthogonal ensemble of one plus two-body interactions with spin degree of freedom [$EGOE(1+2)\text{-s}$], has received considerable attention. Both numerical [Ko-06, Tu-06] and analytical [Ka-00, Ko-02a] methods for analyzing and applying this ensemble have been developed. Using these, several results are obtained and briefly they are as follows: (i) fixed- (m, S) density of levels is established, using numerical results, to be Gaussian [Ko-06, Ja-01, Ka-00]; (ii) lower order cross-correlations in spectra with different (m, S) are studied both numerically and analytically and they are found to be larger compared to those for the spinless fermion systems [Ko-06, Ko-06a]; (iii) ground-state (gs) spin structure investigated using second and fourth moments established that with random interactions there is preponderance of $S = 0$ ground states [Ka-00, Ko-02a]; (iv) delay in Stoner instability in itinerant magnetic systems due to random interactions has been established and thus with random interactions much stronger exchange interaction is needed for gs magnetization in irregular quantum dots [Ja-00, Ja-01]; and (v) it is shown that the odd-even staggering in the gs energies of nm-scale metallic grains, attributed normally due to mean-field orbital energy effects or coherent pairing effects, can also come from purely random two-body Hamiltonians [Pa-02, Ko-02a]. Thus, although the gs structures generated

by EGOE(1+2)-**s** and also some results in the strong-coupling region have been investigated in some detail, the important question of chaos or transition markers generated by the ensemble hasn't yet been investigated in any detail. It should be stressed that the chaos markers form the basis [Ko-03] for statistical spectroscopy [Ko-01, Fr-82, Ka-94, Fl-99, Fr-06] and also the BW to Gaussian transition plays an important role in characterizing multi-partite entanglement and fidelity decay relevant for QIS [Mo-06, Br-08, Pi-07]. Our purpose in this chapter is to establish that the EGOE(1+2)-**s** ensemble exhibits three chaos markers just as the EGOE(1+2) for spinless fermion systems and more importantly, by deriving the exact formula for the propagator of the spectral variances, the spin dependence of the markers is explained. These results, derived for the first time using an ensemble with additional symmetry (besides particle number), provide much stronger basis for statistical (nuclear and atomic) spectroscopy. In addition, as recognized only recently, entanglement and strength functions essentially capture the same information about eigenvector structure and therefore the change in the form (δ -function to BW to Gaussian) of the strength functions in different regimes defined by the chaos markers determines entanglement properties in multi-qubit systems [Mo-06, Br-08, Pi-07, Me-05]. Similarly, the chaos marker λ_d discussed in the present chapter allows us to define a region of thermalization in finite interacting quantum systems modeled by EGOE and thermalization in generic isolated quantum systems has applications in QIS as emphasized in some recent papers [Ri-08, Ca-09, De-91, Sr-94]. All the results presented in this chapter are published in [Ma-10a].

2.2 EGOE(1+2)-**s** Ensemble: Preliminaries

Let us begin with a system of m ($m > 2$) fermions distributed say in Ω number of sp orbitals each with spin $\mathbf{s} = \frac{1}{2}$ so that the number of sp states $N = 2\Omega$. The sp states are denoted by $|i, m_s = \pm \frac{1}{2}\rangle$ with $i = 1, 2, \dots, \Omega$ and similarly the two-particle antisymmetric states are denoted by $|(ij)s, m_s\rangle$ with $s = 0$ or 1 . For one plus two-body Hamiltonians preserving m -particle spin S , the one-body Hamiltonian is $\hat{h}(1) = \sum_{i=1,2,\dots,\Omega} \epsilon_i \hat{n}_i$. Here the orbitals i are doubly degenerate, \hat{n}_i are number operators and ϵ_i are sp energies [it is in principle possible to consider $\hat{h}(1)$ with off-diagonal energies ϵ_{ij}]. Similarly the two-body Hamiltonian $\hat{V}(2)$ is defined by the two-body ma-

trix elements $\lambda_s V_{ijkl}^s = \langle (kl)s, m_s | \hat{V}(2) | (ij)s, m_s \rangle$ with the two-particle spins $s = 0$ and 1 . These matrix elements are independent of the m_s quantum number. Note that the λ_s are constants and for $s = 1$, only $i \neq j$ and $k \neq l$ matrix elements exist. Thus $\hat{V}(2) = \lambda_0 \hat{V}^{s=0}(2) + \lambda_1 \hat{V}^{s=1}(2)$ and the V matrix in two-particle spaces is a direct sum matrix with the $s = 0$ and $s = 1$ space matrices having dimensions $\Omega(\Omega + 1)/2$ and $\Omega(\Omega - 1)/2$, respectively. Now, EGOE(2)-**s** for a given (m, S) system is generated by defining the two parts of the two-body Hamiltonian to be independent GOE's [one for $\hat{V}^{s=0}(2)$ and other for $\hat{V}^{s=1}(2)$] in two-particle spaces and then propagating the $V(2)$ ensemble $\{\hat{V}(2)\} = \lambda_0 \{\hat{V}^{s=0}(2)\} + \lambda_1 \{\hat{V}^{s=1}(2)\}$ to the m -particle spaces with a given spin S by using the geometry (direct product structure), defined by $U(2\Omega) \supset U(\Omega) \otimes SU(2)$ algebra (see Appendix D and Chapter 3), of the m -particle spaces. Then EGOE(1+2)-**s** is defined by the operator

$$\{\hat{H}\}_{\text{EGOE}(1+2)\text{-}\mathbf{s}} = \hat{h}(1) + \lambda_0 \{\hat{V}^{s=0}(2)\} + \lambda_1 \{\hat{V}^{s=1}(2)\}, \quad (2.2.1)$$

where $\{\hat{V}^{s=0}(2)\}$ and $\{\hat{V}^{s=1}(2)\}$ in two-particle spaces are GOE(1) and λ_0 and λ_1 are the strengths of the $s = 0$ and $s = 1$ parts of $\hat{V}(2)$, respectively. From now onwards we drop the “hat” symbol over H , h and V operators when there is no confusion.

The mean-field one-body Hamiltonian $h(1)$ in Eq. (2.2.1) is a fixed one-body operator defined by the sp energies ϵ_i with average spacing Δ (it is possible to draw the ϵ_i 's from the eigenvalues of a random ensemble [Ja-01] or from the center of a GOE [Al-00a]). Without loss of generality we put $\Delta = 1$ so that λ_0 and λ_1 are in the units of Δ . Thus, EGOE(1+2)-**s** in Eq. (2.2.1) is defined by the five parameters $(\Omega, m, S, \lambda_0, \lambda_1)$. The action of the Hamiltonian operator defined by Eq. (2.2.1) on an appropriately chosen fixed- (m, S) basis states generates the EGOE(1+2)-**s** ensemble in (m, S) spaces. The H matrix dimension $d_f(\Omega, m, S)$ for a given (Ω, m, S) , i.e., number of levels in the (m, S) space [with each of them being $(2S + 1)$ -fold degenerate], is

$$d_f(\Omega, m, S) = \frac{(2S + 1)}{(\Omega + 1)} \binom{\Omega + 1}{m/2 + S + 1} \binom{\Omega + 1}{m/2 - S}, \quad (2.2.2)$$

satisfying the sum rule $\sum_S (2S + 1) d_f(\Omega, m, S) = \binom{N}{m}$. Note that the subscript ‘ f ’ in Eq. (2.2.2) stands for ‘fermions’. For example for $\Omega = m = 8$, the dimensions are 1764,

2352, 720, 63, and 1 for $S = 0, 1, 2, 3$, and 4, respectively. Similarly for $\Omega = m = 10$, the dimensions are 19404, 29700, 12375, 1925, 99, and 1 for $S = 0 - 5$ and for $\Omega = m = 12$, they are 226512, 382239, 196625, 44044, 4214, 143, and 1 for $S = 0 - 6$. It is useful to note that for the EGOE(1+2)-**s** ensemble three group structures are relevant and they are $U(\Omega) \otimes SU(2)$, $\sum_{S=0,1} O(N_{2,S}) \oplus$ and $\sum_S O(N_{m,S}) \oplus$, $m > 2$. Here $N_{m,S} = d_f(\Omega, m, S)$, the symbol \oplus stands for direct sum and $O(r)$ is the orthogonal group in r dimensions. The $U(\Omega) \otimes SU(2)$ algebra defines the embedding. The EGOE(2) ensemble has orthogonal invariance with respect to the $\sum_{S=0,1} O(N_{2,S}) \oplus$ group acting in two-particle spaces. However it is not invariant under the $\sum_S O(N_{m,S}) \oplus$ group for $m > 2$. This group is appropriate if GOE representation for fixed- (m, S) H matrices is employed; i.e., there is an independent GOE for each (m, S) subspace.

Given the sp energies ϵ_i and the two-body matrix elements V_{ijkl}^s , the many-particle Hamiltonian matrix for a given (m, S) can be constructed either using the M_S representation and a spin (S) projection operator [Ko-06] or directly in a good S basis using angular-momentum algebra [Tu-06]. The former is equivalent to employing the algebra $U(2\Omega) \supset U(\Omega) \oplus U(\Omega)$ and the latter corresponds to $U(2\Omega) \supset U(\Omega) \otimes SU(2)$. Just as in the earlier papers by our group [Ko-06], we have employed the M_S representation for constructing the H matrices and the \hat{S}^2 operator for projecting states with good S . Then the dimension of the basis space is $\mathcal{D}(M_S^{min}) = \sum_S d_f(\Omega, m, S)$; $M_S^{min} = 0$ for m even and $1/2$ for m odd. For example, for $\Omega = m = 8$ we have $\mathcal{D}(M_S^{min}) = 4900$, for $\Omega = 8, m = 6$, $\mathcal{D}(M_S^{min}) = 3136$ and for $\Omega = m = 10$ we have $\mathcal{D}(M_S^{min}) = 63404$. It is important to note that here the construction of the m -particle H matrix reduces to the problem of EGOE(1+2) for spinless fermion systems and hence Eqs. (1.2.1)- (1.2.4) of Chapter 1 will apply. From the dimensions given above, it is clear that numerical calculations will be prohibitive for $m \geq 10$ even on best available computers. Therefore, most of the numerical investigations are restricted to $m \leq 8$. For properties related to a few lowest eigenvalues it is possible to go beyond $m = 8$ [Pa-02]. Now, before presenting the results for the three chaos markers generated by EGOE(1+2)-**s**, we will consider the ensemble averaged fixed- (m, S) density of levels and present the exact formula for its variance.

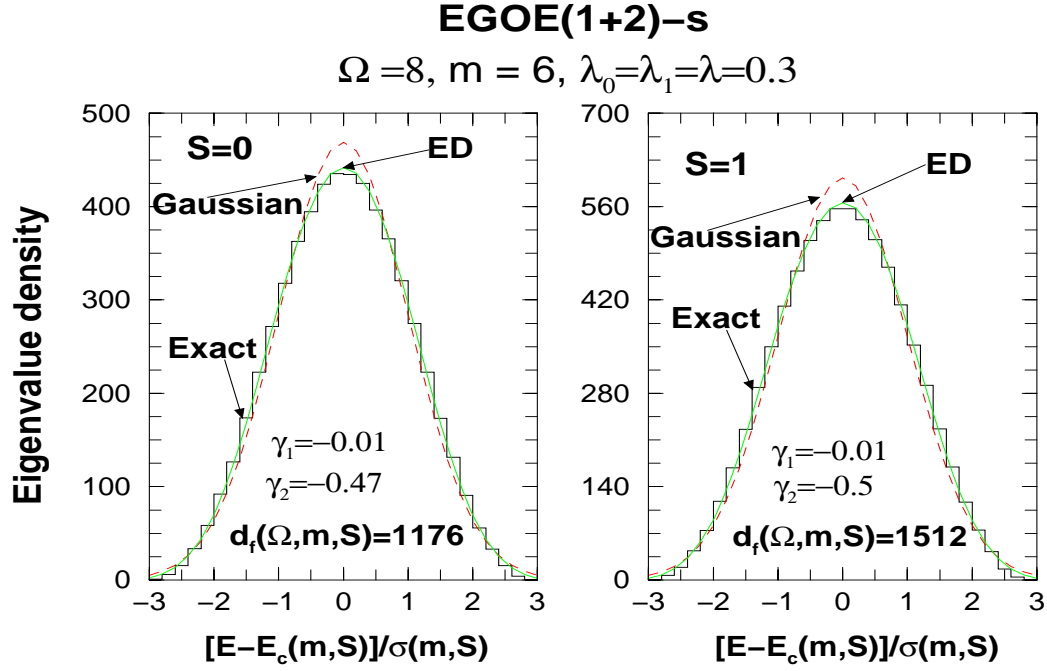


Figure 2.1: Ensemble averaged eigenvalue density for a 20 member EGOE(1+2)-s ensemble with $\Omega = 8$, $m = 6$ and spins $S = 0$ and 1 . The dashed curves give Gaussian representation and the continuous curves give Edgeworth corrected Gaussians [ρ_{ED} in Eq. (2.3.2)]. Values of the skewness and excess parameters are also given in the figure. In the plots, the densities for a given spin are normalized to the dimension $d_f(\Omega, m, S)$. Note that the $E_c(m, S)$ and $\sigma(m, S)$ are fixed- (m, S) energy centroids and spectral widths, respectively of the eigenvalue densities. See text for further details.

2.3 Gaussian Level Densities and Ensemble Averaged Spectral Variances

2.3.1 Gaussian form for fixed- (m, S) eigenvalue densities

Using the M_S representation, we have numerically constructed the H matrix in large number of examples and by diagonalizing them obtained the ensemble averaged eigenvalue (level) densities $\overline{\rho^{m,S}(E)} = \langle \delta(\hat{H} - E) \rangle^{m,S}$. In general, given m -particle space it is possible to decompose it into subspaces Γ such that the H preserving Γ symmetry will be a direct sum matrix of H matrices for each Γ subspace (as H will not connect states with different Γ). Then, the one-point function $\overline{\rho^{m,\Gamma}(E)}$, the ensemble averaged density of eigenvalues over each Γ subspace, is given by

$$\overline{\rho^{m,\Gamma}(E)} = \langle \delta(\hat{H} - E) \rangle^{m,\Gamma}. \quad (2.3.1)$$

For EGOE(1+2)-**s**, Γ denotes the m -particle spin S . For EGUE(2)- $SU(4)$ ensemble discussed in Chapter 4, Γ represents a m -particle $SU(4)$ irrep F_m . Similarly, for EGOE(1+2)- π , ensemble discussed in Chapter 5, $\Gamma = \pi$ and for BEGOE(1+2)-**s** ensemble discussed in Chapter 6, $\Gamma = S$. Note that the trace of an operator \mathcal{O} over a fixed- (m, S) space is defined by $\langle\langle\mathcal{O}\rangle\rangle^{m,S} = (2S+1)^{-1} \sum_{\alpha} \langle m, S, \alpha | \mathcal{O} | m, S, \alpha \rangle$ and similarly (m, S) space average is $\langle\mathcal{O}\rangle^{m,S} = [d_f(\Omega, m, S)]^{-1} \langle\langle\mathcal{O}\rangle\rangle^{m,S}$. From now onwards, we drop the “overline” over ρ when there is no confusion. Results are shown for $\Omega = 8$ and $m = 6$ with $S = 0$ and 1 and $\lambda_0 = \lambda_1 = \lambda = 0.3$ in Fig. 2.1. In these calculations and also for all other calculations reported in this chapter, we have chosen the sp energies to be $\epsilon_i = i + 1/i$ with $i = 1, 2, \dots, \Omega$ just as in many of the earlier papers [Fl-96, Fl-96a, Ko-02, Ko-06]. Note that the second term $(1/i)$ in ϵ_i has been added, as discussed first in [Fl-96, Fl-96a], to avoid the degeneracy of many-particle states for small λ . To construct the eigenvalue density, we first make the centroids $E_c(m, S)$ of all the members of the ensemble to be zero and variance $\sigma^2(m, S)$ to be unity, i.e., for each member we change the eigenvalues E to the standardized variables $\hat{E} = [E - E_c(m, S)]/\sigma(m, S)$. Note that the parameters $E_c(m, S)$ and $\sigma^2(m, S)$ depend also on Ω . But for convenience, we shall drop Ω in $E_c(m, S)$ and $\sigma^2(m, S)$ throughout this chapter. Then, using a bin-size $\Delta\hat{E} = 0.2$, histograms for $\rho^{m,S}(E)$ are generated. The calculated results are compared with both the Gaussian ($\rho_{\mathcal{G}}$) and Edgeworth (ED) corrected Gaussian (ρ_{ED}) forms [St-87],

$$\rho_{\mathcal{G}}(\hat{E}) = \frac{1}{\sqrt{2\pi}} \exp\left(-\frac{\hat{E}^2}{2}\right), \quad (2.3.2)$$

$$\rho_{ED}(\hat{E}) = \rho_{\mathcal{G}}(\hat{E}) \left\{ 1 + \left[\frac{\gamma_1}{6} He_3(\hat{E}) \right] + \left[\frac{\gamma_2}{24} He_4(\hat{E}) + \frac{\gamma_1^2}{72} He_6(\hat{E}) \right] \right\}.$$

Here γ_1 is the skewness and γ_2 is the excess parameter. Similarly, He are the Hermite polynomials: $He_3(x) = x^3 - 3x$, $He_4(x) = x^4 - 6x^2 + 3$, and $He_6(x) = x^6 - 15x^4 + 45x^2 - 15$. From the results in Fig. 2.1, it is seen that the agreement between the exact and ED corrected Gaussians is excellent. Further numerical examples are given in [Ko-06, Ja-01] up to $m = 8$. It has been well established that the ensemble averaged eigenvalue density takes Gaussian form in the case of spinless fermion as well as boson sys-

tems [Mo-75, Ko-01, Be-01a, Ch-03]. Combining these with the numerical results for the fixed- (m, S) level densities, it can be concluded that the Gaussian form is generic for the embedded ensembles extending to those with good quantum numbers. This is further substantiated by the analytical results for the ensemble averaged $\gamma_2(m, S)$ as discussed in Section 2.9 ahead. We will present the analytical formula for the ensemble averaged spectral variances $\overline{\sigma^2(m, S)}$; i.e., for the variance of $\overline{\rho^{m, S}(E)}$ in Sec. 2.3.2.

It is important to point out that the variances $\overline{\sigma^2(m, S)}$ propagate in a simple manner [Pa-78, Qu-75] from the corresponding three defining space variances, the variance in one-particle space $\sigma^2(1, \frac{1}{2})$ and the two two-particle variances $\overline{\sigma^2(2, s)} = \lambda_s^2 [d_f(\Omega, m, S) + 1]$, $s = 0, 1$. Thus the (m, S) space variances are a linear combination of these three basic variances with the multiplying factors being simple functions of (Ω, m, S) . These functions are called variance propagators as they carry the variance information from the defining space to the final (m, S) spaces and it is easy to derive formulas for them as given in Sec. 2.3.2. For example, the variances generated by the two-body part of the Hamiltonian for $\lambda_0^2 = \lambda_1^2 = \lambda^2$ are of the form $\overline{\sigma_{V(2)}^2(m, S)} = \lambda^2 P(\Omega, m, S)$. The variance propagator $P(\Omega, m, S)$, given by Eq. (2.3.12) ahead, determines much of the behavior of the transitions in eigenvalue and wavefunction structure as discussed ahead.

2.3.2 Propagation formulas for ensemble averaged spectral variances

Let us start with the fixed- (m, S) energy centroids $E_c(m, S) = \langle H \rangle^{m, S}$ for a one plus two-body Hamiltonian $H = h(1) + V(2) = h(1) + [\lambda_0 V^{s=0}(2) + \lambda_1 V^{s=1}(2)]$. The operator generating $\langle H \rangle^{m, S}$ will be a polynomial, in the scalar operators \hat{n} and \hat{S}^2 , of maximum body rank 2. A two-body operator is said to be of body rank 2, a three-body operator of body rank 3 and so on [Mo-75]. Note that \hat{n} is a one-body operator and \hat{S}^2 is a one plus two-body operator. Hence only \hat{n} , \hat{n}^2 and \hat{S}^2 are operators of maximum body rank 2 (for example, the operator $\hat{n}\hat{S}^2$ is of maximum body rank 3). Then, $E_c(m, S) = a_0 + a_1 m + a_2 m^2 + a_3 S(S+1)$. Solving for the a_i 's in terms of E_c for $m \leq 2$, we obtain

the well-known propagation formula for the energy centroids [Pa-78],

$$\begin{aligned}
E_c(m, S) &= \left[\langle h(1) \rangle^{1, \frac{1}{2}} \right] m + \lambda_0 \langle \langle V^{s=0}(2) \rangle \rangle^{2,0} \frac{P^0(m, S)}{4\Omega(\Omega+1)} \\
&+ \lambda_1 \langle \langle V^{s=1}(2) \rangle \rangle^{2,1} \frac{P^1(m, S)}{4\Omega(\Omega-1)}; \\
P^0(m, S) &= [m(m+2) - 4S(S+1)], \\
P^1(m, S) &= [3m(m-2) + 4S(S+1)],
\end{aligned} \tag{2.3.3}$$

$$\langle h(1) \rangle^{1, \frac{1}{2}} = \Omega^{-1} \sum_{i=1}^{\Omega} \epsilon_i, \quad \langle \langle V^{s=0}(2) \rangle \rangle^{2,0} = \sum_{i \leq j} V_{ijij}^{s=0}, \quad \langle \langle V^{s=1}(2) \rangle \rangle^{2,1} = \sum_{i < j} V_{ijij}^{s=1}.$$

Trivially the ensemble average of E_c from the $V(2)$ part will be zero. However, the covariances in the energy centroids generated by the two-body part $H(2) = V(2)$ of H are non-zero,

$$\begin{aligned}
&\overline{\langle H(2) \rangle^{m,S} \langle H(2) \rangle^{m',S'}} = \\
&\frac{\lambda_0^2}{16\Omega(\Omega+1)} P^0(m, S) P^0(m', S') + \frac{\lambda_1^2}{16\Omega(\Omega-1)} P^1(m, S) P^1(m', S').
\end{aligned} \tag{2.3.4}$$

The spectral variances $\sigma^2(m, S) = \langle H^2 \rangle^{m,S} - [\langle H \rangle^{m,S}]^2$ are generated by an operator that is a polynomial, in the scalar operators \hat{n} and \hat{S}^2 , of maximum body rank 4. This gives $\sigma^2(m, S) = \sum_{p=0}^4 a_p m^p + \sum_{q=0}^2 b_q m^q S(S+1) + c_0 [S(S+1)]^2$. The nine parameters (a_i, b_i, c_i) can be written in terms of ϵ_i and the two-body matrix elements $V_{ijkl}^{s=0,1}$ using the embedding algebra $U(N) \supset U(\Omega) \otimes SU(2)$. The final result is given by Eq. (B2) of Appendix B (this is derived using the results in [He-74]). We have carried out the ensemble average of $\sigma_H^2(m, S)$ over EGOE(1+2)-s ensemble assuming that $h(1)$ is fixed and the final result is as follows. Firstly, the ensemble averaged variance is,

$$\overline{\sigma_H^2(m, S)} = \overline{\sigma_{h(1)}^2(m, S)} + \overline{\sigma_{V(2)}^2(m, S)}. \tag{2.3.5}$$

The propagation formula for $\sigma_{h(1)}^2$ is simple,

$$\sigma_{h(1)}^2(m, S) = \frac{(\Omega+2)m(\Omega-m/2) - 2\Omega S(S+1)}{(\Omega-1)(\Omega+1)} \sigma_{h(1)}^2\left(1, \frac{1}{2}\right). \tag{2.3.6}$$

The two parts $V^{s=0}(2)$ and $V^{s=1}(2)$ of $V(2)$ will have a scalar part, an effective one-

body part and an irreducible two-body part denoted by $V^{s,\nu}(2)$, with $\nu = 0, 1$, and 2 , respectively with respect to $U(N) \supset U(\Omega) \otimes SU(2)$ algebra. The two $\nu = 0$ parts generate the centroids and they can be identified from Eq. (2.3.3). As the ν decomposition is an orthogonal decomposition, we have

$$\overline{\sigma_{V(2)}^2(m, S)} = \sum_{s=0,1} \lambda_s^2 \sum_{\nu=1,2} \overline{\langle [V^{s,\nu}(2)]^2 \rangle^{m,S}}. \quad (2.3.7)$$

As seen from Eq. (B2), for evaluating $\overline{\langle [V^{s,\nu=1}(2)]^2 \rangle^{m,S}}$ we need $\sum_{i,j} \overline{\lambda_{i,j}^2(s)}$ where the $\lambda(s)$'s are the so called induced one-particle matrix elements generated by V^s ,

$$\begin{aligned} \lambda_{i,i}(s) &= \sum_j V_{ijij}^s (1 + \delta_{ij}) - (\Omega)^{-1} \sum_{k,l} V_{klkl}^s (1 + \delta_{kl}), \\ \lambda_{i,j}(s) &= \sum_k \sqrt{(1 + \delta_{ki})(1 + \delta_{kj})} V_{kikj}^s \text{ for } i \neq j. \end{aligned} \quad (2.3.8)$$

Similarly for evaluating $\overline{\langle [V^{s,\nu=2}(2)]^2 \rangle^{m,S}}$, we need $\overline{\langle [V^{s,\nu=2}(2)]^2 \rangle^{2,s}}$. Firstly, applying the fact that the V^s matrix elements are independent Gaussian random variables with zero center and variance unity (except for the diagonal matrix elements it is 2) and simplifying using Eq. (2.3.8), we obtain

$$\begin{aligned} \sum_{i,j} \overline{\lambda_{i,j}^2(0)} &= (\Omega - 1)(\Omega + 2)^2, \\ \sum_{i,j} \overline{\lambda_{i,j}^2(1)} &= (\Omega - 1)(\Omega - 2)(\Omega + 2). \end{aligned} \quad (2.3.9)$$

Also, $\overline{\langle [V^s(2)]^2 \rangle^{2,s}} = [d_f(\Omega, 2, s) + 1]$. This along with Eqs. (B2), (2.3.3) and (2.3.9) will give $\overline{\langle [V^{s,\nu=2}(2)]^2 \rangle^{2,s}}$,

$$\begin{aligned} \overline{\langle [V^{s=0,\nu=2}(2)]^2 \rangle^{2,0}} &= \frac{1}{2}(\Omega - 1)(\Omega + 2), \\ \overline{\langle [V^{s=1,\nu=2}(2)]^2 \rangle^{2,1}} &= \frac{(\Omega - 3)(\Omega^2 + \Omega + 2)}{2(\Omega - 1)}. \end{aligned} \quad (2.3.10)$$

Substituting the results in Eqs. (2.3.3), (2.3.7), (2.3.9), and (2.3.10) in Eq. (B2) gives the

final result,

$$\begin{aligned}
\overline{\sigma_{V(2)}^2(m, S)} &= \frac{\lambda_0^2}{\Omega(\Omega+1)/2} \left[\frac{\Omega+2}{\Omega+1} Q^1(\{2\} : m, S) + \frac{\Omega^2+3\Omega+2}{\Omega^2+3\Omega} Q^2(\{2\} : m, S) \right] \\
&+ \frac{\lambda_1^2}{\Omega(\Omega-1)/2} \left[\frac{\Omega+2}{\Omega+1} Q^1(\{1^2\} : m, S) + \frac{\Omega^2+\Omega+2}{\Omega^2+\Omega} Q^2(\{1^2\} : m, S) \right]; \\
Q^1(\{2\} : m, S) &= [(\Omega+1)P^0(m, S)/16] [m^x(m+2)/2 + \langle S^2 \rangle], \\
Q^2(\{2\} : m, S) &= [\Omega(\Omega+3)P^0(m, S)/32] [m^x(m^x+1) - \langle S^2 \rangle], \\
Q^1(\{1^2\} : m, S) &= \frac{(\Omega-1)}{16(\Omega-2)} [(\Omega+2)P^1(m, S)P^2(m, S) \\
&+ 8\Omega(m-1)(\Omega-2m+4)\langle S^2 \rangle], \\
Q^2(\{1^2\} : m, S) &= \frac{\Omega}{8(\Omega-2)} [(3\Omega^2-7\Omega+6)(\langle S^2 \rangle)^2 \\
&+ 3m(m-2)m^x(m^x-1)(\Omega+1)(\Omega+2)/4 \\
&+ \langle S^2 \rangle \{-mm^x(5\Omega-3)(\Omega+2) + \Omega(\Omega-1)(\Omega+1)(\Omega+6)\}], \\
P^2(m, S) &= 3m^x(m-2)/2 - \langle S^2 \rangle, \quad m^x = \left(\Omega - \frac{m}{2}\right).
\end{aligned} \tag{2.3.11}$$

Note that the $\nu = 1$ terms (they correspond to the Q^1 's) are $1/\Omega^2$ times smaller as compared to the $\nu = 2$ terms (they correspond to the Q^2 's). Therefore in the dilute limit defined by $\Omega \rightarrow \infty$, $m \rightarrow \infty$, $m/\Omega \rightarrow 0$ and $m \gg S$, the $V^{s=0,1;\nu=2}$ parts determine the variances $\sigma_H^2(m, S)$. As a result, formula for the ensemble averaged variances given in [Ko-02a] is same as the sum of the two $\nu = 2$ terms in Eq. (2.3.11).

In most of the numerical examples discussed in the remaining part of the present chapter (except in Sec. 2.8) we employ $\lambda_0 = \lambda_1 = \lambda$ and for this $\overline{\sigma_{V(2)}^2(m, S)}$ takes the form

$$\begin{aligned}
\overline{\sigma_{V(2)}^2(m, S)} &\xrightarrow{\lambda_0=\lambda_1=\lambda} \lambda^2 P(\Omega, m, S); \\
P(\Omega, m, S) &= \frac{1}{\Omega(\Omega+1)/2} \left[\frac{\Omega+2}{\Omega+1} Q^1(\{2\} : m, S) + \frac{\Omega^2+3\Omega+2}{\Omega^2+3\Omega} Q^2(\{2\} : m, S) \right] \\
&+ \frac{1}{\Omega(\Omega-1)/2} \left[\frac{\Omega+2}{\Omega+1} Q^1(\{1^2\} : m, S) + \frac{\Omega^2+\Omega+2}{\Omega^2+\Omega} Q^2(\{1^2\} : m, S) \right].
\end{aligned} \tag{2.3.12}$$

Note that we are showing Ω explicitly in the formula for the variance propagator $P(\Omega, m, S)$ as Ω plays an important role in determining the transition markers. Figure 2.2 shows a plot of $P(\Omega, m, S)/P(\Omega, m, 0)$ vs S for various values of m and Ω . As

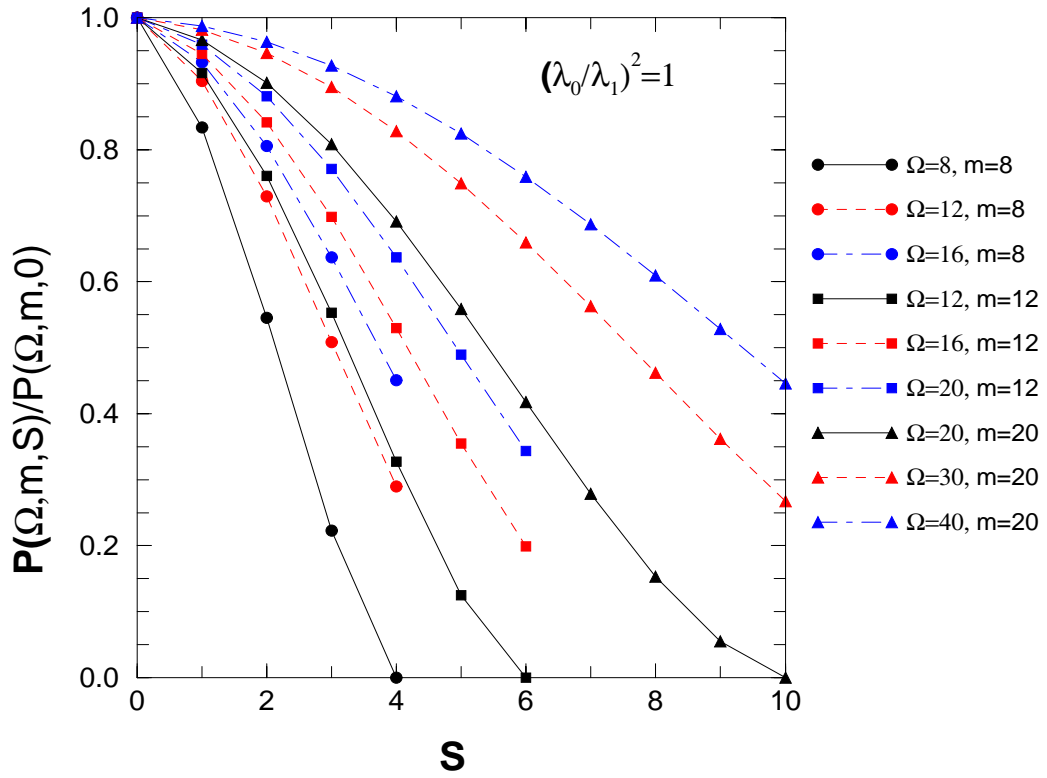


Figure 2.2: Variance propagator $P(\Omega, m, S)$ vs S for different values of Ω and m . Eq. (2.3.12) gives the formula for $P(\Omega, m, S)$.

seen from Fig. 2.2, $P(\Omega, m, S)$ decreases with spin and this plays an important role in understanding the properties of EGOE(1+2)-s as will be seen in the following sections. Now, we will discuss the results for transition markers generated by EGOE(1+2)-s.

2.4 Poisson (or close to Poisson) to GOE Transition in Level Fluctuations

Fluctuations in the eigenvalues of a fixed- (m, S) spectrum derive from the two and higher point correlation functions. For example, the two-point function is given by Eq. (4.4.6) with $\Gamma = S$ and $\Gamma' = S'$. The commonly used Dyson-Mehta Δ_3 statistic is an exact two-point measure while variance $\sigma^2(0)$ of the nearest neighbor spacing distribution (NNSD) is essentially a two-point measure [Br-81]. Note that, due to a convention as stated in the footnote 14 of [Br-81], the variance of the NNSD is $\sigma^2(0)$, the second nearest $\sigma^2(1)$ etc. In all the discussion in this Sec. and all other remaining Secs. 2.5-2.7 (except Sec. 2.8), we use $\lambda_0 = \lambda_1 = \lambda$, i.e., we employ EGOE(1+2)-s

Hamiltonian,

$$H_\lambda = h(1) + \lambda[V^{s=0}(2) + V^{s=1}(2)] . \quad (2.4.1)$$

The NNSD and Δ_3 statistics show Poisson character in general [Mu-06] for very small values of λ due to the presence of many good quantum numbers defined by $h(1)$. As the value of λ increases, there is delocalization in the Fock space, i.e., the eigenstates spread over all the basis states leading to complete mixing of the basis states. Hence, one expects GOE behavior for large λ values.

For a 20 member EGOE(1+2)-s ensemble with $\Omega = m = 8$ and spins $S = 0, 1$, and 2, we have constructed NNSD and Δ_3 for various λ values changing from 0.01 to 0.3. In the calculations: (i) the spectrum for each member of the ensemble is unfolded using ED corrected Gaussian for the eigenvalue density so that the average spacing is unity; (ii) we drop 5% of the levels from the two spectrum ends; (iii) with this we have constructed the ensemble averaged NNSD histograms and calculated their variances $\sigma^2(0)$; (iv) for the Δ_3 statistic, overlap interval of 0.5 (for the unfolded spectrum) is used and $\overline{\Delta_3}(L)$ for $L \leq 60$ are calculated following Ref. [Bo-83]; L is the energy interval, measured in units of average level spacing, over which Δ_3 is calculated. Results for NNSD and Δ_3 statistic are shown in Figs. 2.3 and 2.4, respectively. As mentioned in Sec. 2.3.1, in our calculation the mean-field Hamiltonian is of a special form defined by the sp energies $\epsilon_i = i + 1/i$. For this Hamiltonian, it is easy to see that in the dilute regime, the majority of many-body eigenvalues approach a perturbed picket-fence spectrum. Away from the dilute limit, the spectrum is not picket-fence and deviates from Poisson as can be seen from Figs. 2.3 and 2.4. However, if we had used sp energies drawn from the center of a GOE or from the eigenvalues of an irregular system, the fluctuations will be generically Poisson [Mu-06]. Therefore we call the transition seen in Figs. 2.3 and 2.4, Poisson to GOE transition and it should be kept in mind that, the sp spectrum we have chosen gives level fluctuations that are close to Poisson but not strictly Poisson for $\lambda = 0$. For further discussion we focus on the NNSD and its variance $\sigma^2(0)$.

As we increase λ , NNSD changes rapidly from a form close to Poisson to a form close to that of GOE (Wigner distribution) as seen from Fig. 2.3. However, the complete convergence to GOE form is very slow. Therefore, although the transition to

EGOE(1+2)-s

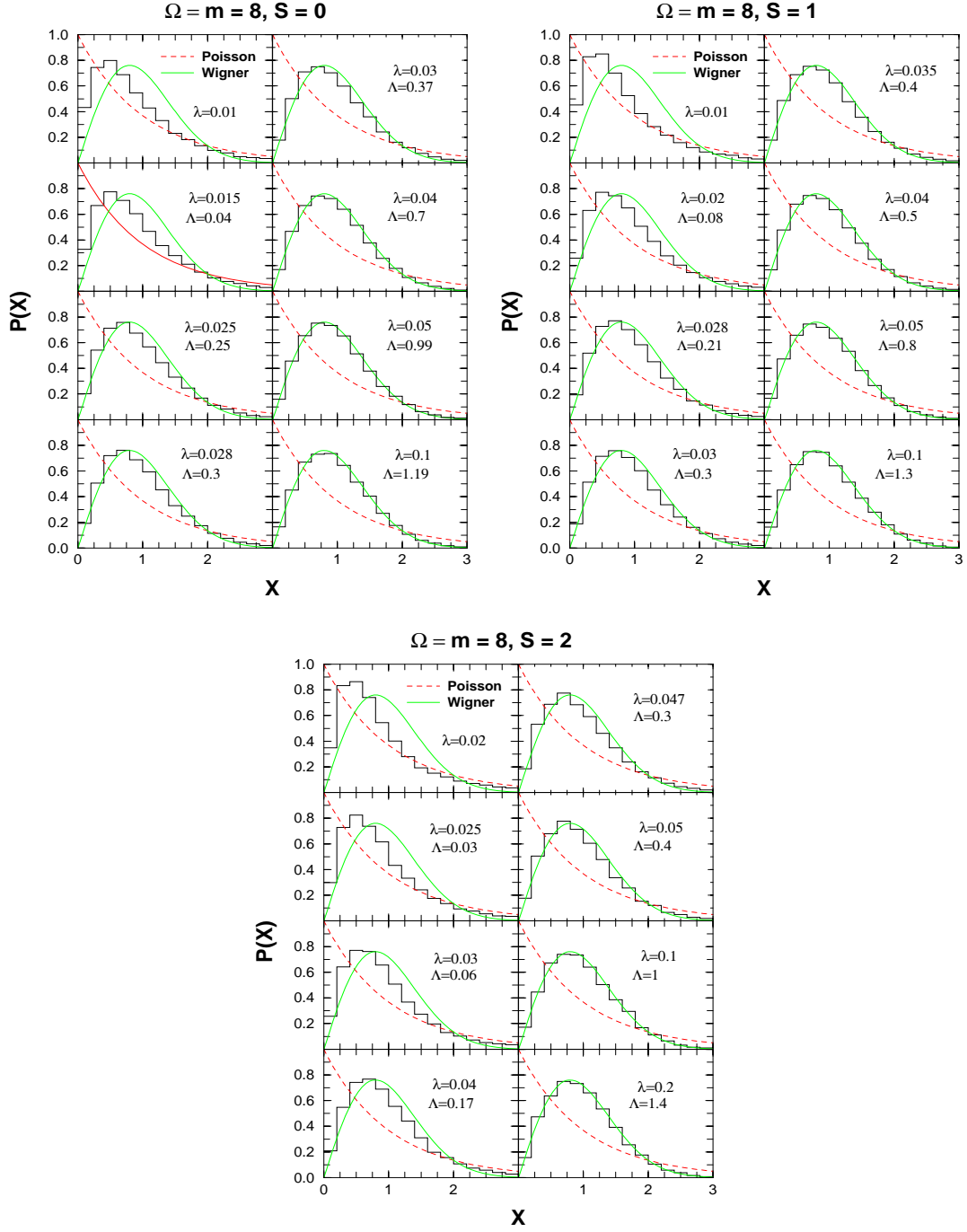


Figure 2.3: NNSD for a 20 member EGOE(1+2)-s ensemble with $\Omega = m = 8$ and spins $S = 0, 1$, and 2 , respectively. Calculated NNSD are compared to the Poisson and Wigner (GOE) forms. Values of the interaction strength λ and the transition parameter Λ are given in the figure. The chaos marker λ_c corresponds to $\Lambda = 0.3$. Bin-size for the histograms is 0.2 . As discussed in the text, for very small values of λ , the NNSD, for the sp spectrum employed in the calculations, is not strictly a Poisson. Therefore, the Λ values are not given for $\lambda = 0.01$ for spins $S = 0$ and 1 and for $\lambda = 0.02$ for spin $S = 2$.

GOE in level fluctuations is not a phase transition, we can still define a transition point $\lambda = \lambda_c$ where Poisson-like fluctuations start changing to GOE character and we need a criterion to determine λ_c . For this purpose we employ $\sigma^2(0)$ given by a simple 2×2 random matrix model for Poisson to GOE transition [Ko-99b] as used in some of the earlier studies [Ch-03]. In this model, in terms of a transition parameter Λ (Λ is mean squared admixing GOE matrix element divided by the square of the mean spacing D_0 of the Poisson spectrum), $\sigma_{P \rightarrow GOE}^2(0 : \Lambda) = (8\Lambda + 2)/[\pi(\Psi(-0.5, 0, 2\Lambda))]^2 - 1$. Here Ψ is the Kummer function. It can be argued that the transition to GOE is nearly complete for $\Lambda \sim 0.3$ which corresponds to NNSD variance $\sigma^2(0) = 0.37$. A plot of $\sigma_{P \rightarrow GOE}^2(0 : \Lambda)$ vs Λ [Ko-99b] shows that the variance decreases fast from Poisson value $\sigma^2(0) = 1$ up to $\Lambda \sim 0.37$ and then converges slowly to the GOE value $\sigma^2(0) = 0.27$. For the NNSD that are constructed for various EGOE(1+2)-s examples, the calculated $\sigma^2(0)$ are used to deduce, from the 2×2 matrix formula, the values of Λ . In Fig. 2.3, the values of the Λ parameter are given for different λ values and it is seen that the transition point λ_c is 0.028, 0.030, and 0.047 for $S = 0, 1$, and 2, respectively. In Fig. 2.4, we show $\overline{\Delta_3}(L)$ vs L for some values of λ and clearly there is a transition to GOE statistics. It should be stressed that one expects the λ_c needed to approach GOE statistics for $\overline{\Delta_3}(L)$ to scale as $L^{1/2}$ [Gu-89] although the scaling of λ_c with other parameters (m, S, Ω) will be same for any given L . In the present example, up to $L = 20$, the λ_c deduced from NNSD could be considered as the transition point for $\overline{\Delta_3}(L)$. However the L dependence of λ_c is not probed further in the present chapter.

For a qualitative understanding of the variation of λ_c with spin S , it is plausible to use the same arguments used for spinless fermion systems and they are based on perturbation theory [Ja-97]. As λ is increased from zero, the m -particle states generated by $h(1)$ will be mixed by $V(2)$ and in lowest-order perturbation the first stage of mixing will be between states that are directly coupled by the two-body interaction. Poisson to GOE transition occurs when λ is of the order of the spacing Δ_c between the m -particle states that are directly coupled by the two-body interaction. Given the two-particle spectrum span to be B_2 and the number of fixed- (m, S) states directly coupled by the two-body interaction to be $K(\Omega, m, S)$, we have $\Delta_c(\Omega, m, S) \propto B_2/K(\Omega, m, S)$ and therefore, $\lambda_c \propto B_2/K(\Omega, m, S)$. Using the $h(1)$ spectrum, it is easy to see that

EGOE(1+2)-s

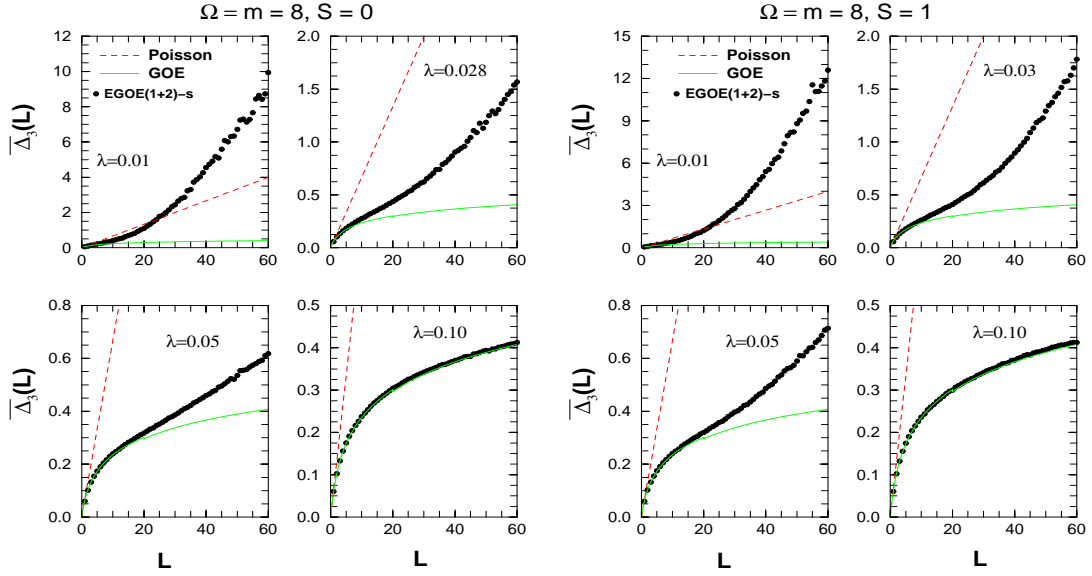


Figure 2.4: $\overline{\Delta}_3(L)$ vs L for a 20 member EGOE(1+2)-s ensemble with $\Omega = m = 8$ and spins $S = 0$ and 1. Calculated results are compared with the Poisson and GOE forms.

$B_2 \propto \Omega$. Following the arguments in [Ja-01] (see also [Ko-02a]), the spectral variances generated by $V(2)$ can be written as $\overline{\sigma_{V(2)}^2(m, S)} \approx \lambda^2 K(\Omega, m, S)$ and applying Eq. (2.3.12) gives $K(\Omega, m, S) \approx P(\Omega, m, S)$. With this, we have

$$\lambda_c(S) \propto \frac{\Omega}{P(\Omega, m, S)}. \quad (2.4.2)$$

From the results in Fig. 2.2 for $P(\Omega, m, S)$, it is clear that λ_c should increase with spin S . For $\Omega = m = 8$, Eq. (2.4.2) and the formula for $P(\Omega, m, S)$ gives $P(8, 8, S = 1)/P(8, 8, S = 0) = 0.834$ and $P(8, 8, S = 2)/P(8, 8, S = 0) = 0.55$. These and the result $\lambda_c(S = 0) = 0.028$ from Fig. 2.3 will give $\lambda_c(S = 1) = 0.034$ and $\lambda_c(S = 2) = 0.05$. These predictions are close to the numerical results shown in Fig. 2.3. Therefore Eq. (2.4.2) gives a good qualitative understanding of the $\lambda_c(S)$ variation with S . In the dilute limit (sometimes also called asymptotic limit), as defined just after Eq. (2.3.11), it is easily seen that $P(\Omega, m, S) \rightarrow m^2 \Omega^2$ and hence $\lambda_c \rightarrow 1/m^2 \Omega$. Thus we recover the result known [Ja-97] for spinless fermion systems as a limiting case.

2.5 Breit-Wigner to Gaussian Transition in Strength Functions

Wavefunction structure is understood usually in terms of strength functions $[F_k(E)]$ and information entropy $[S^{info}(E)]$. Both of these are basis dependent. In our (also by all others [Ja-01, Ka-00, Tu-06, Pa-02, Ko-06]) construction of the H matrices, the basis states chosen are eigenstates of both $\hat{h}(1)$ and \hat{S}^2 operators (we drop M_S^{min} everywhere although all the states have $M_S = M_S^{min}$). Given the mean field $h(1)$ basis states (denoted by $|k\rangle$) expanded in the H eigenvalue (E) basis,

$$|k, S, M_S\rangle = \sum_E C_{k,S}^{E,S} |E, S, M_S\rangle, \quad (2.5.1)$$

the strength functions $F_{k,S}(E, S)$ and information entropy $S^{info}(E, S)$ are defined by,

$$\begin{aligned} F_{k,S}(E, S) &= \sum_{E'} \left| C_{k,S}^{E',S} \right|^2 \delta(E - E') = \left| \mathcal{C}_{k,S}^{E,S} \right|^2 d_f(\Omega, m, S) \rho^{m,S}(E), \\ S^{info}(E, S) &= -\frac{1}{d_f(\Omega, m, S) \rho^{m,S}(E)} \sum_{E'} \sum_k \left| C_{k,S}^{E',S} \right|^2 \ln \left| C_{k,S}^{E',S} \right|^2 \delta(E - E'), \end{aligned} \quad (2.5.2)$$

where $\left| \mathcal{C}_{k,S}^{E,S} \right|^2$ denotes the average of $\left| C_{k,S}^{E,S} \right|^2$ over the eigenstates with the same energy E . The strength functions give the spreading of the basis states over the eigenstates. For $\lambda = 0$, the strength functions will be δ -functions at the $h(1)$ eigenvalues. As λ increases from zero, the strength functions first change from δ -function form to BW form at $\lambda = \lambda_\delta$ where λ_δ is very small; see Eq. (2.5.5) ahead. The BW form, with Γ_{BW} denoting the spreading width, is defined by,

$$F_{k,BW}(E) = \frac{1}{2\pi} \frac{\Gamma_{BW}}{(E - \xi_k)^2 + \Gamma_{BW}^2/4}. \quad (2.5.3)$$

The energies $\xi_k = \langle \phi_k | H | \phi_k \rangle$ are the diagonal matrix elements of H and they are the basis state energies. Information entropy S^{info} is a measure of complexity or chaos in wavefunctions and the GOE value for $\exp[S^{info}(E, S)]$ is $0.48 d_f(\Omega, m, S)$ independent of E . Our purpose is to investigate the change in $F_{k,S}(E, S)$ and $S^{info}(E, S)$ as we change λ . In the present Sec. we consider strength functions and in the next Sec. information entropy.

EGOE(1+2)-s

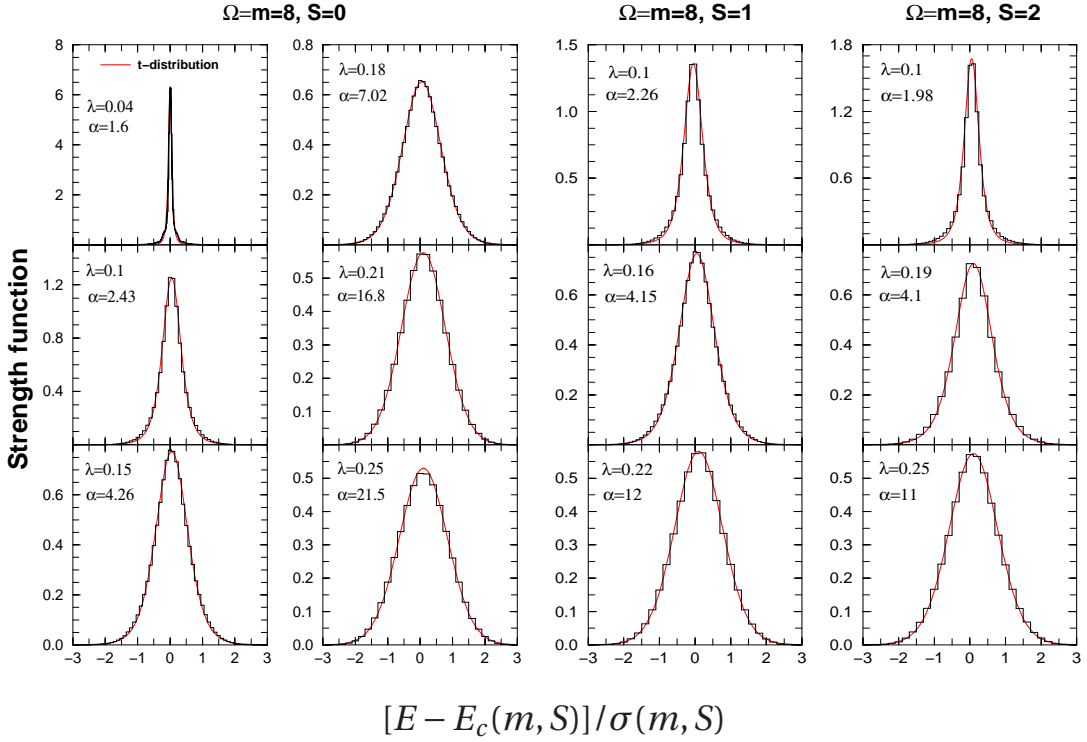


Figure 2.5: Strength functions as a function of λ for a 20 member EGOE(1+2)-s ensemble. Calculations (histograms) are for a $\Omega = m = 8$ system with spins $S = 0, 1$ and 2 . Note that the widths $\sigma_{F_k}(m, S)$ of the strength functions are different from the spectral widths $\sigma(m, S)$. Continuous curves in the figures correspond to the t -distribution given by Eq. (2.5.4). See text for details.

Figure 2.5 shows strength functions as a function of λ for 8 particles in 8 sp levels ($\Omega = m = 8$) with spins $S = 0, 1$, and 2 . The centroids (ϵ) of the ξ_k spectra are same as that of the eigenvalue (E) spectra but their widths are different. In the calculations, E and ξ_k are zero centered for each member and scaled by the width of the eigenvalue spectrum. The new energies are called \hat{E} and \hat{E}_k , respectively. For each member $|C_{k,S}^{E,S}|^2$ are summed over the basis states in the energy window $\hat{E}_k \pm \Delta_k$ and then the ensemble averaged $F_k(\hat{E}, S)$ vs \hat{E} are constructed as histograms. We have chosen $\Delta_k = 0.025$ for $\lambda < 0.1$ and beyond this $\Delta_k = 0.1$. In the plots $\int F_k(\hat{E}, S) d\hat{E} = 1$. Clearly, strength functions exhibit transition from BW to Gaussian form. To describe this transition, a simple linear interpolation of BW and Gaussian forms, with three parameters, as employed in [Ch-04] could be used. However, an alternative form is given by the one-parameter t -distribution well known in statistics and it is used

in [An-04]. In the following we employ the t -distribution.

Student's t -distribution, with a shape parameter α , such that $\alpha = 1$ gives BW and $\alpha \rightarrow \infty$ gives Gaussian, is a good interpolating function for BW to Gaussian transition and it is given by,

$$F_k^{stud}(E, S; \alpha, \beta) dE = \frac{(\alpha\beta)^{\alpha-1/2}\Gamma(\alpha)}{\sqrt{\pi}\Gamma(\alpha-1/2)} \frac{dE}{[(E-E_k)^2 + \alpha\beta]^\alpha}. \quad (2.5.4)$$

Note that the Γ function in Eq. (2.5.4) shall not be confused with the Γ notation used to denote subspaces; see Eq. (2.3.1). The parameter β defines the energy spread and hence, it is determined by the variance of the strength function $\sigma_{F_k}^2$, i.e., $\beta = \sigma_{F_k}^2 (2\alpha - 3)/\alpha$ for $\alpha > 1.5$. For $\alpha \leq 1.5$, the spreading width determines the parameter β . Numerical results for the strength functions are compared with the best-fit $F_k^{stud}(E, S)$ and they are shown as continuous curves in Fig. 2.5 along with the values of the parameter α . Although only the results for $S = 0, 1, 2$ and $\hat{E}_k = 0$ are shown in the figures, we have also performed calculations for $S = 0$ with $\hat{E}_k = \pm 0.5$. As seen from the figures, the fits are excellent over a wide range of λ values. The parameter α rises slowly up to λ_F , then it increases sharply (for $\alpha > 16$ the curves are indistinguishable from Gaussian). Following [An-04], the criterion $\alpha \sim 4$ defines the transition point λ_F . From the results in Fig. 2.5 it is seen that the transition point λ_F is 0.15 and 0.16 for $S = 0$ and 1, respectively. In addition, $\lambda_F = 0.19$ for $S = 2$ (for $\lambda = 0.075$ and 0.15, $\alpha = 1.69$ and 2.73, respectively). Similarly for $S = 0$ and $\hat{E}_k = \pm 0.5$, the λ_F value is 0.16. Thus λ_F increases slowly with \hat{E}_k .

For a qualitative understanding of the variation of λ_F with spin S , we consider the spreading width $\Gamma(S)$ and the inverse participation ratio (IPR) $\zeta(S)$. First, Fermi golden rule gives $\Gamma_{BW}(S) = 2\pi\lambda^2/\overline{D(S)}$ with $\overline{D(S)} = \Delta_c(\Omega, m, S)$ as established in [Ge-97]. Therefore, using Eq. (2.4.2) gives $\Gamma_{BW}(S) \propto 2\pi\lambda^2 P(\Omega, m, S)/\Omega$. Similarly, $\zeta(S) \sim \Gamma_{BW}(S)/\Delta_m(S)$ with $\Delta_m(S)$ being the average spacing of the m -particle fixed- S spectrum. The total spectrum span considering only $h(1)$ is $B_m \propto m\Omega$ and therefore $\Delta_m(S) \propto m\Omega/d_f(\Omega, m, S)$. In the BW domain, $\Gamma_{BW}(S)$ and $\zeta(S)$ should be such that (i) $\Gamma_{BW}(S) < f_0 B_m$ and (ii) $\zeta(S) \gg 1$ where $f_0 < 1$. Condition (i) gives, $\lambda^2 < C_0 m\Omega^2/P(\Omega, m, S)$ and condition (ii) gives, $\lambda^2 \gg B_0 m\Omega^2/P(\Omega, m, S) d_f(\Omega, m, S)$.

Note that the constants C_0 and B_0 are positive. Therefore,

$$\sqrt{\frac{B_0 m \Omega^2}{P(\Omega, m, S) d_f(\Omega, m, S)}} \ll \lambda < \sqrt{\frac{C_0 m \Omega^2}{P(\Omega, m, S)}} \Rightarrow \lambda_F(S) \propto \sqrt{\frac{m \Omega^2}{P(\Omega, m, S)}}. \quad (2.5.5)$$

This equation shows that just as λ_c , the marker λ_F is essentially determined by the variance propagator $P(\Omega, m, S)$. Also as λ increases from zero, the BW form sets in fast as $d_f(\Omega, m, S)$ is usually very large. From the results in Fig. 2.2, it is clear that λ_F should increase with S . This prediction is close to the numerical results shown in Fig. 2.5. Equation (2.5.5) with the result $\lambda_F(S = 0) = 0.15$ gives $\lambda_F(S = 1) = 0.16$ and $\lambda_F(S = 2) = 0.2$. Therefore Eq. (2.5.5) gives a good qualitative understanding of $\lambda_F(S)$ variation with S just as for $\lambda_c(S)$. In the dilute limit with $P(\Omega, m, S) \rightarrow m^2 \Omega^2$, we have $\lambda_F \rightarrow 1/\sqrt{m}$ and thus reducing to the result known [Ja-02] for spinless fermion systems.

2.6 Information Entropy and Duality Marker

Figure 2.6 shows information entropy $S^{info}(E, S)$ as a function of E for a 20 member EGOE(1+2)-**s** ensemble with spins $S = 0$ and 1 and for different λ values. These results are compared with the EGOE(1+2) formula for S^{info} given in [Ko-01a] (strictly valid only for $\lambda > \lambda_F$) by replacing the fixed- m variances by fixed- (m, S) variances,

$$\exp(S^{info}(E, S) - S_{GOE}^{info})^{EGOE(1+2)-s} \sqrt{1 - \xi^2} \exp\left(\frac{\xi^2}{2}\right) \exp\left(-\frac{\xi^2 \hat{E}^2}{2}\right); \quad (2.6.1a)$$

$$\xi^2 = 1 - \frac{\sigma_{\text{off-diagonal}}^2(m, S)}{\sigma^2(m, S)} \sim \frac{\sigma_{h(1)}^2(m, S)}{\sigma_{h(1)}^2(m, S) + \sigma_{V(2)}^2(m, S)}. \quad (2.6.1b)$$

Note that \hat{E} is defined just before Eq. (2.3.2) and ξ is a correlation coefficient. The results given by Eq. (2.6.1a) are compared with the numerical results in Fig. 2.6. It is seen that the numerical results for $\lambda \geq \lambda_F$ are described well by the EGOE formula. There are deviations at the tails because the result given by Eq. (2.6.1a) assumes Gaussian form for the strength functions while in practice there will be corrections to the Gaussian form. Thus results of EGOE(1+2) extend to EGOE(1+2)-**s** with parameters calculated in (m, S) spaces. Similar analysis was done for number of principal components or IPR in [Ko-06].

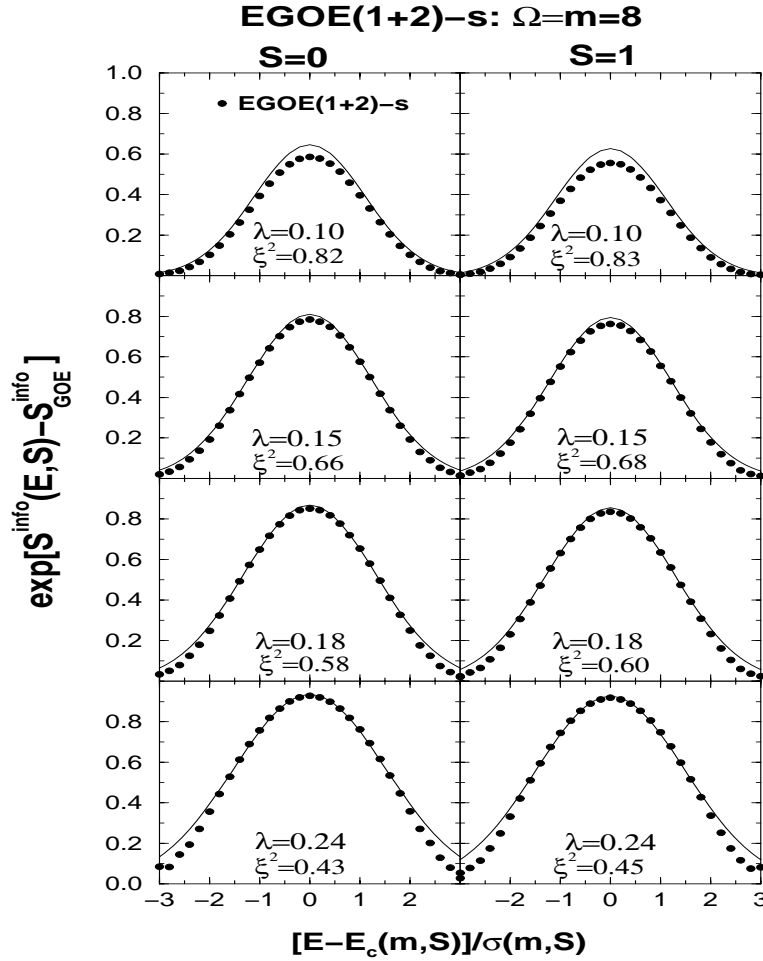


Figure 2.6: $\exp[S^{\text{info}}(E, S) - S_{\text{GOE}}^{\text{info}}]$ for a 20 member EGOE(1+2)-s ensemble with $\Omega = m = 8$ and spins $S = 0$ and 1 for different λ values. Values averaged over bin-size 0.2 are shown as filled circles. The continuous curves correspond to Eq. (2.6.1a). See text for details.

For the EGOE(1+2)-s Hamiltonian, two asymptotic natural basis emerge and they are (i) the non-interacting basis defined by $\lambda_0 = \lambda_1 = 0$ and (ii) the infinite interaction strength basis defined by $\lambda_0 = \lambda_1 = \infty$. In principle two more basis defined by $\lambda_0 = 0, \lambda_1 = \infty$ and $\lambda_0 = \infty, \lambda_1 = 0$ are possible but they are not considered in the present section. Therefore just as in the previous discussion we put $\lambda_0 = \lambda_1 = \lambda$. An important question is [Ja-02, An-04]: is there a point $\lambda = \lambda_d \geq \lambda_F$ where quantities defining wavefunction properties like entropy, strength functions, temperature etc. are basis independent? To examine this question, we compare $S^{\text{info}}(E, S)$ in $\lambda = 0$ and $\lambda = \infty$ basis by varying λ . In the $\lambda = 0$ basis, $S^{\text{info}}(E, S)$ is determined by Eq. (2.6.1a) with the correlation coefficient $\xi^2 = \xi_0^2$ defined in Eq. (2.6.1b). Similarly, in the $\lambda = \infty$ basis, Eq. (2.6.1a) applies with $\xi^2 = \xi_\infty^2 = \sigma_{V(2)}^2(m, S) / [\sigma_{h(1)}^2(m, S) + \sigma_{V(2)}^2(m, S)]$; note

that $\sigma_{V(2)}^2(m, S)$ depends on λ^2 . Therefore we can determine λ_d by using the condition that $\xi_0^2 = \xi_\infty^2$ (this is equivalent to the condition that the spreadings produced by $h(1)$ and $V(2)$ are equal). Then we have $\xi^2 = \xi_0^2 = \xi_\infty^2 = 0.5$ at $\lambda = \lambda_d$; see [An-04] for more details. Further, it can be argued that the duality region (defined by $\lambda \sim \lambda_d$) corresponds to the thermodynamic region for finite quantum systems and this will be discussed in Sec. 2.7.

Figure 2.7 shows numerical results for the information entropy in the $h(1)$ and $V(2)$ basis for a 20 member EGOE(1+2)-s ensemble with $\Omega = m = 8$ and spins $S = 0$ and 1 for different λ values ranging from $\lambda = 0.18$ to 0.3. It is seen from Fig. 2.7 that the duality marker $\lambda_d = 0.21$ for spin $S = 0$ and 0.22 for $S = 1$. For λ values below and above λ_d clearly there are differences in $S^{info}(E, S)$ in the two basis. The $S^{info}(E, S)$ values in the $h(1)$ basis are smaller compared to those in the $V(2)$ basis for $\lambda < \lambda_d$. The two entropies coincide at $\lambda = \lambda_d$ and beyond that, S^{info} in the $h(1)$ basis is comparatively larger. For a qualitative understanding of the variation of λ_d with S , we use the criterion that around the duality region, spreadings produced by $h(1)$ and $V(2)$ are equal. This leads to the condition,

$$\sigma_{h(1)}^2(m, S) = \lambda_d^2 P(\Omega, m, S). \quad (2.6.2)$$

To determine $\sigma_{h(1)}^2(m, S)$, we consider a uniform spectrum with $\Delta = 1$. This gives, $\sigma_{h(1)}^2(1, \frac{1}{2}) = (\Omega^2 - 1)/12$. Then, using Eq. (2.3.6),

$$\sigma_{h(1)}^2(m, S) = \mathcal{H}(\Omega, m, S) = \frac{1}{12} [m(\Omega + 2)(\Omega - m/2) - 2\Omega S(S + 1)]. \quad (2.6.3)$$

Combining this with Eqs. (2.3.12) and (2.6.2) will give finally

$$\lambda_d(S) \propto \sqrt{\frac{\mathcal{H}(\Omega, m, S)}{P(\Omega, m, S)}}. \quad (2.6.4)$$

Eq. (2.6.4) with the result $\lambda_d(S = 0) = 0.21$ gives $\lambda_d(S = 1) = 0.22$ and $\lambda_d(S = 2) = 0.24$. These predictions are close to the numerical results shown in Fig. 2.7. Therefore Eq. (2.6.4) gives a good qualitative understanding of $\lambda_d(S)$ variation with S . In the dilute limit, simplifying the \mathcal{H} and P factors, we have $\lambda_d \rightarrow 1/\sqrt{m}$ and this is the result

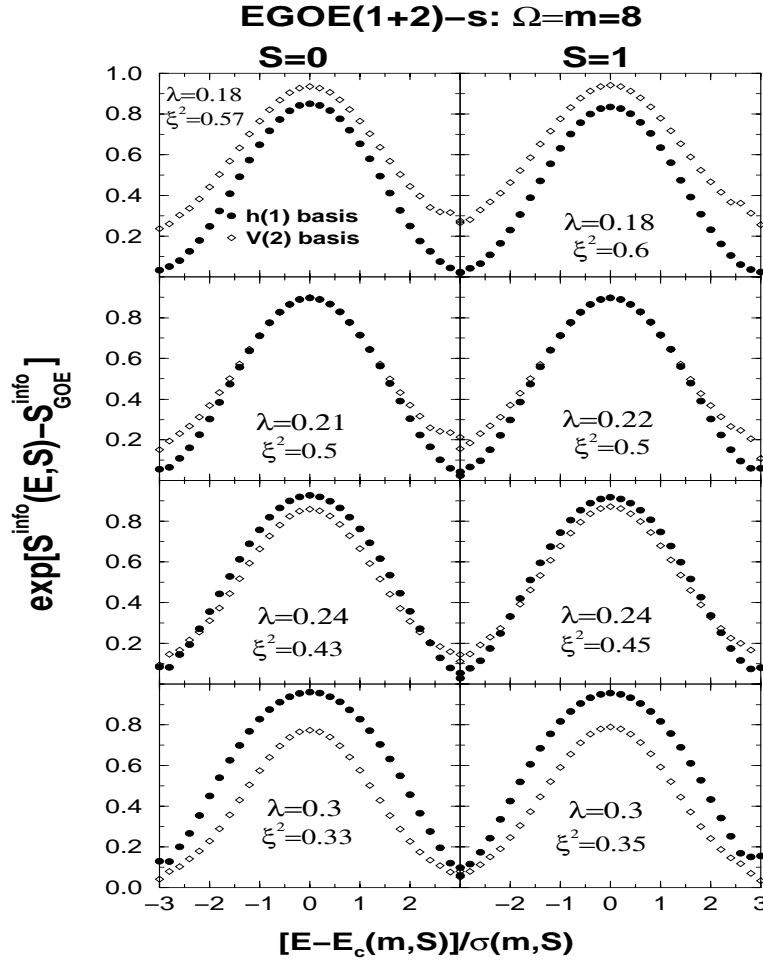


Figure 2.7: $\exp[S^{\text{info}}(E, S) - S^{\text{info}}_{\text{GOE}}]$ in $h(1)$ and $V(2)$ basis for a 20 member EGOE(1+2)-s ensemble with $\Omega = m = 8$ and spins $S = 0$ and 1 for different λ values. Results averaged over bin-size 0.2 are shown as circles; filled circles correspond to $h(1)$ basis and open circles correspond to $V(2)$ basis. The ξ^2 values defined by Eq. (2.6.1b) are also given in the figure. The duality point λ_d corresponds to $\xi^2 = 0.5$. See text for details.

for spinless fermion systems [An-04]. This also shows that in the dilute limit λ_d and λ_F have same scale. However these scales differ parametrically as m approaches Ω (for $m > \Omega$ one has to consider holes) and $S \gtrsim m/4$. In this situation there is strong spin dependence for the ratio λ_d / λ_F as seen from Eqs. (2.5.5), (2.6.3), and (2.6.4) that give $\lambda_d / \lambda_F \propto \sqrt{\frac{[m(\Omega+2)(\Omega-m/2)-2\Omega S(S+1)]}{m\Omega^2}}$. Thus the variance propagator determines the behavior of the three transition markers λ_c , λ_F , and λ_d .

2.7 Occupancies, Single-particle Entropy and Thermodynamic Region

A very important question for isolated finite interacting particle systems is the following [Ho-95, Fl-97, Be-01, Ko-01, Ri-08]: in the chaotic domain will there be a point or a region where thermalization occurs; i.e., will there be a region where different definitions of entropy, temperature, specific heat, and other thermodynamic variables give the same results (as valid for infinite particle systems)? Toward answering this question within EGOE(1+2)-s, we consider three different entropies, i.e., thermodynamic entropy defined by the eigenvalue density, information entropy and sp entropy defined by the occupancies of the sp orbitals. Before comparing these three different entropies for various values of λ , now let us first consider occupancies in some detail.

Occupation probability for a sp orbital i is given by the expectation value of n_i , i.e., $\langle n_i \rangle^{m,S,E}$. It is possible to write this as a ratio of two densities,

$$\begin{aligned} \langle n_i \rangle^{m,S,E} &= \frac{\langle n_i \delta(H-E) \rangle^{m,S}}{\langle \delta(H-E) \rangle^{m,S}} \\ &= \langle n_i \rangle^{m,S} \frac{\rho_{n_i}^{m,S}(E)}{\rho^{m,S}(E)}. \end{aligned} \quad (2.7.1)$$

As n_i is a positive-definite operator, the occupancy density $\rho_{n_i}^{m,S}(E)$ can be represented by a probability density with moments $M_p(n_i) = \langle n_i H^p \rangle^{m,S} / \langle n_i \rangle^{m,S}$. The corresponding lower order central moments define Edgeworth corrected Gaussian form for $\rho_{n_i}^{m,S}(E)$. For $\lambda > \lambda_c$, fluctuations follow GOE and hence $\langle n_i \rangle^{m,S,E}$ take a smoothed form and they can be written as the ratio of the smoothed forms for the densities in Eq. (2.7.1). As the fixed- (m, S) eigenvalue density is Gaussian, the fixed- (m, S) occupancy densities also follow Gaussian form (as discussed ahead, this is verified by calculating the excess parameter). Therefore,

$$\langle n_i \rangle^{m,S,E} \xrightarrow{\lambda \geq \lambda_c} \langle n_i \rangle^{m,S} \frac{\rho_{n_i:\mathcal{G}}^{m,S}(E)}{\rho_{\mathcal{G}}^{m,S}(E)}. \quad (2.7.2)$$

Section 3.4 gives extensions of Eq. (2.7.2) to pairing Hamiltonian with further dis-

cussion on expectation value densities. Figure 2.8(a) shows occupation numbers for a 200 member EGOE(1+2)-s ensemble with $\Omega = m = 6$ and spin $S = 0$ as a function of E for various λ values. Results are shown for the lowest three sp orbitals. As discussed in Sec. 2.8 (see also Fig. 2.10 ahead), $\lambda_c = 0.05$ and $\lambda_F = 0.18$ for the present example. It is clearly seen from Fig. 2.8(a) that the fluctuations are large for $\lambda < \lambda_c$ as expected. Beyond this, the occupancies start taking a smoothed form. The numerical results for $\lambda \gg \lambda_c$ are compared with the smoothed form given by Eq. (2.7.2). Here Edgeworth corrections are added to the Gaussian densities. For example, for $\lambda = 0.1$, the difference between the occupancy density centroids and the energy centroids (in units of the spectral widths) are -0.4 , -0.29 , and -0.12 for the sp orbitals 1, 2, and 3, respectively. Similarly the occupancy density widths (in units of the spectral widths) are 0.91 , 0.96 , and 0.99 and γ_2 values are -0.39 , -0.43 , and -0.4 for the sp orbitals 1, 2, and 3, respectively. Note that $|\gamma_1| \sim 0$ in all the cases. For the eigenvalue density, the excess parameter $\gamma_2(m, S) = -0.38$. Agreement between Eq. (2.7.2) and the numerical results is excellent except at the spectrum ends as here the states are not sufficiently complex. We have also verified this for $S = 1$ and $S = 2$ examples. Therefore in the $\lambda < \lambda_c$ region, fluctuations being large (they follow Poisson), smoothed forms are not meaningful. On the other hand, in the chaotic domain defined by $\lambda > \lambda_c$, occupation probabilities take a smoothed form as the fluctuations here follow GOE (hence they are small). The smoothed form is well described by Eq. (2.7.2). It is interesting to note that the fluctuations even in the gs region are small for $\lambda \gg \lambda_F$. All these conclusions are also verified for a 20 member EGOE(1+2)-s ensemble with $\Omega = m = 8$ and $S = 0$ and some of these results are shown in Fig. 2.8(b).

Given the fractional occupation probabilities $f_i(E, S) = \frac{1}{2} \langle n_i \rangle^{m, S, E}$, the sp entropy $S^{sp}(E, S)$ is defined by,

$$S^{sp}(E, S) = - \sum_i 2 \{ f_i(E, S) \ln f_i(E, S) + [1 - f_i(E, S)] \ln [1 - f_i(E, S)] \} . \quad (2.7.3)$$

To establish that the $\lambda = \lambda_d$ region corresponds to the thermodynamic region, we will compare the thermodynamic entropy $S^{ther}(E) = \ln \rho^{m, S}(E)$ and the information entropy defined by Eqs. (2.5.2) and (2.6.1a) with the sp entropy for different λ values just as it was done before for EGOE(1+2) and the nuclear shell-model examples [Ho-

EGOE(1+2)-s

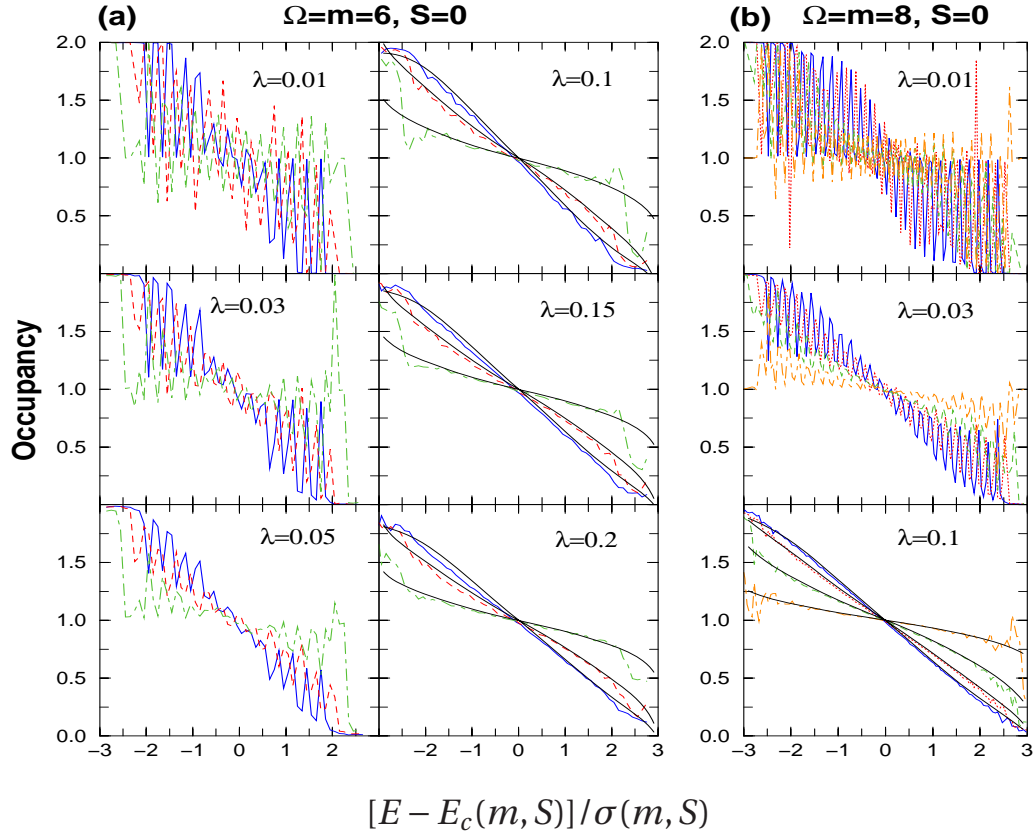


Figure 2.8: Occupation numbers as a function of $\hat{E} = [E - E_c(m, S)] / \sigma(m, S)$. (a) For a 200 member EGOE(1+2)-s ensemble with $\Omega = m = 6$ and spin $S = 0$, shown are the results for the three lowest sp levels (solid blue, dashed red and dot-dashed green, respectively). They are compared with the EGOE smoothed form (black) given by Eq. (2.7.2) for $\lambda > \lambda_c = 0.05$. (b) For a 20 member EGOE(1+2)-s ensemble with $\Omega = m = 8$ and spin $S = 0$, shown are the results for the four lowest sp levels (solid blue, dotted red, dashed green and dot-dashed orange, respectively). They are compared with the EGOE smoothed form (black) given by Eq. (2.7.2) for $\lambda = 0.1$. For this system, $\lambda_c = 0.028$. Note that for the results in the figures, occupancies are averaged over bin-size 0.1 for $\Omega = m = 6$ and 0.05 for $\Omega = m = 8$, respectively. See text for further details.

95, Ko-02]. For $\Omega = m = 8$ and $S = 0$ system with 20 members, we show in Fig. 2.9 results for $\lambda = \lambda_d = 0.21$, $\lambda = 0.01 \ll \lambda_d$ and $\lambda = 2 \gg \lambda_d$. Note that $\exp[S^{ther}(E, S) - S_{max}^{ther}] \rightarrow \exp[-\frac{1}{2}\hat{E}^2]$ for all λ values as the eigenvalue density is a Gaussian essentially independent of λ . Similarly, Eq. (2.6.1a) gives the formula for $\exp[S^{info}(E, S) - S_{GOE}^{info}]$. We have also verified that the extension of the EGOE(1+2) formula for the sp entropy [Ko-02] with centroids and variances replaced by fixed- (m, S) centroids and variances

is a good approximation for fixed- (E, S) sp entropy and then the formula is,

$$\exp[S^{sp}(E, S) - S_{max}^{sp}] = \exp -\frac{1}{2}\xi^2 \widehat{E}^2. \quad (2.7.4)$$

For the three examples shown in Fig. 2.9, $\xi^2 = 0.998, 0.5$, and 0.039 for $\lambda = 0.01, 0.21$, and 2 , respectively. It is clearly seen from Fig. 2.9 that the three entropies differ as we go away from $\lambda = \lambda_d$ and at $\lambda = \lambda_d$ they all look similar, i.e., as stated in [Ho-95] “the thermodynamic entropy defined via the global level density or in terms of occupation numbers behaves similar to the information entropy.” Therefore, $\lambda = \lambda_d$ region can be interpreted as the thermodynamic region in the sense that all different definitions of entropy coincide in this region.

2.8 Some Results for $\lambda_0 \neq \lambda_1$

All the discussion in Secs. 2.4-2.7 is restricted to $\lambda_0 = \lambda_1 = \lambda$ in Eq. (2.2.1) i.e., for equal strengths of the $s = 0$ and $s = 1$ parts of the interaction. However, for completeness, here we present some results for the change in the eigenvalue and wavefunction structure for $\lambda_0^2 \neq \lambda_1^2$. To investigate this, we have examined NNSD and strength functions by fixing the value for the ensemble averaged two-particle spectral variance $\sigma_{V(2)}^2(2)$ generated by the two-body part of H and then varying λ_0 (λ_1). The two-particle spectral variance for $\Omega \gg 1$ is $\sigma_{V(2)}^2(2) = (\lambda_0^2 + 3\lambda_1^2)/16$. Therefore we have considered the following Hamiltonian,

$$H_{(\lambda_0, \lambda_1; \lambda)} = h(1) + \lambda_0 V^{s=0}(2) + \lambda_1 V^{s=1}(2); \quad (\lambda_0^2 + 3\lambda_1^2)/4 = \lambda^2, \quad (2.8.1)$$

and carried out calculations for various fixed values of λ and varying λ_0 (λ_1) with the constraint $(\lambda_0^2 + 3\lambda_1^2)/4 = \lambda^2$. For a 200 member EGOE(1+2)-s ensemble defined by $H_{(\lambda_0, \lambda_1; \lambda)}$ with $\Omega = m = 6$ and $S = 0$, results are presented in Fig. 2.10 for NNSD and strength functions. In the calculations, we have chosen $\lambda = 0.05$ for NNSD and $\lambda = 0.18$ for the strength functions. For the choice $\lambda_0 = \lambda_1 = \lambda$, they correspond to λ_c and λ_F , respectively for the $\Omega = m = 6$ and $S = 0$ system. This is clearly seen in Fig. 2.10. Results are also shown for the two extreme choices $\lambda_0 = 0$, $\lambda_1 = \sqrt{4/3}\lambda$ and $\lambda_0 = 2\lambda$, $\lambda_1 = 0$. For $\lambda_0 = 0$, the NNSD is closer to Poisson

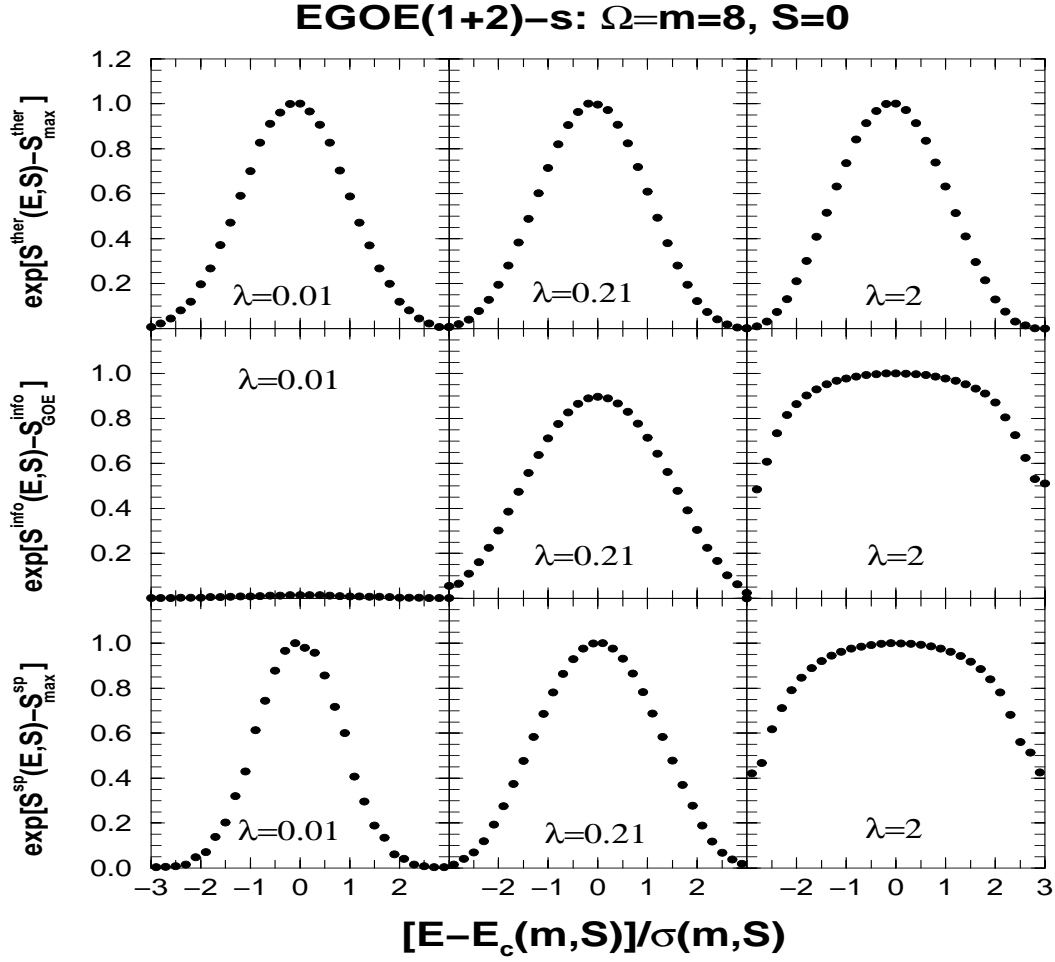


Figure 2.9: Thermodynamic entropy $\exp[S^{ther}(E, S) - S_{max}^{ther}]$, information entropy $\exp[S^{info}(E, S) - S_{GOE}^{info}]$ and single-particle entropy $\exp[S^{sp}(E, S) - S_{max}^{sp}]$ vs $\hat{E} = [E - E_c(m, S)]/\sigma(m, S)$ for a 20 member EGOE(1+2)-s ensemble with $\Omega = m = 8$ and $S = 0$ for different λ values. Entropies averaged over bin-size 0.2 are shown as filled circles. Note that for $\lambda = 0.01$, $\exp[S^{info}(E, S) - S_{GOE}^{info}]$ is close to zero for all \hat{E} values. See text for details.

while for $\lambda_1 = 0$, NNSD is much closer to the Wigner form. Similarly, for $\lambda_0 = 0$, the strength function is more closer to BW while for $\lambda_1 = 0$, it is closer to Gaussian. We can easily infer these changes in the structures from the propagator ratio $R_{(\lambda_0, \lambda_1; \lambda)}(\Omega, m, S) = \sigma_{(\lambda_0, \lambda_1; \lambda)}^2(m, S) / [\lambda^2 P(\Omega, m, S)]$. Note that $\sigma_{(\lambda_0, \lambda_1; \lambda)}^2(m, S)$ is same as $\sigma_{V(2)}^2(m, S)$ given by Eq. (2.3.11). For our example with $\Omega = m = 6$ and $S = 0$, we have $R_{(\lambda_0, \lambda_1; \lambda)}(\Omega, m, S) = 0.93, 0.94, 1, 1.1, 1.22$ for $\lambda = 0.05$ and $\lambda_0 = 0, 0.02, 0.05, 0.075$, and 0.1 , respectively. Therefore for $\lambda_0 < 0.05$, we have $R_{(\lambda_0, \lambda_1; \lambda)}(\Omega, m, S) < 1$ and this implies [as seen from Eq. (2.4.2)] that the level fluctuations change from Poisson-like to GOE as the value of λ_0 is increased from $\lambda_0 = 0$ as seen in Fig. 2.10(a).

$$\Omega=m=6, S=0$$

$$(\lambda_0^2 + 3\lambda_1^2)/4 = \lambda^2$$

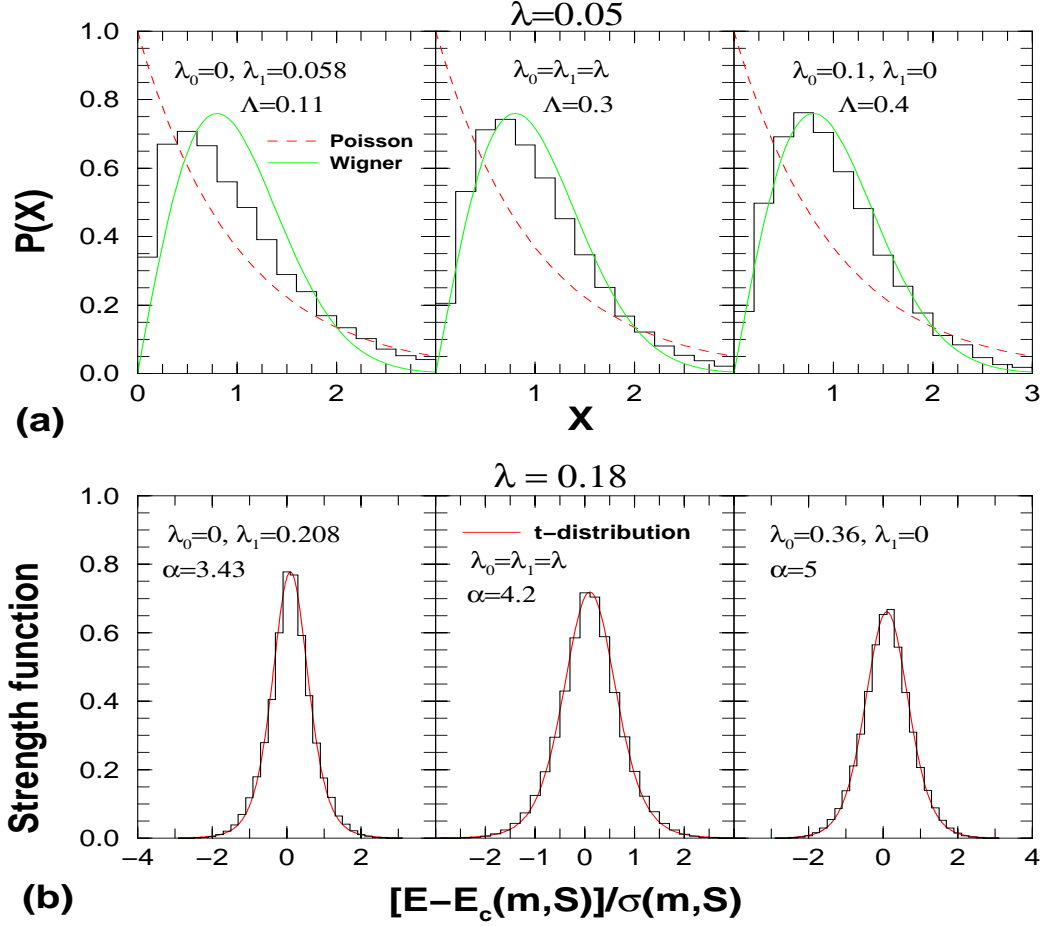


Figure 2.10: Variation in the nearest neighbor spacing distributions $P(X)$ and the strength functions $F_k(E, S)$ with λ_0 and λ_1 , for a 200 member EGOE(1+2)-s ensemble with $\Omega = m = 6$ and spin $S = 0$. Calculations are carried out with the constraint $(\lambda_0^2 + 3\lambda_1^2)/4 = \lambda^2$ and the results are shown for (a) $\lambda = 0.05$ and (b) $\lambda = 0.18$ with three different values for λ_0 . Strength functions are shown for $\hat{E}_k = 0$. Histograms, with bin-size 0.2, are the calculated results. See text for details.

Similarly, $R_{(\lambda_0, \lambda_1; \lambda)}(\Omega, m, S) = 0.93, 0.95, 1, 1.07, 1.22$ for $\lambda = 0.18$ and $\lambda_0 = 0, 0.1, 0.18, 0.25$, and 0.36 , respectively. Therefore for $\lambda_0 < 0.18$, we have $R_{(\lambda_0, \lambda_1; \lambda)}(\Omega, m, S) < 1$ and this implies [as seen from Eq. (2.5.5)] that the strength functions change from BW to Gaussian form as the value of λ_0 is increased from $\lambda_0 = 0$ as seen in Fig. 2.10(b). Thus we can conclude that the general structure of the transitions, as discussed in Fig. 2.11, remains same even for $\lambda_0^2 \neq \lambda_1^2$. We have also made calculations by varying λ_0 and λ_1 without any constraint. Here also the variance propagator gives predictions for the changes in NNSD and strength functions and we have verified these predic-

tions in some examples. Before summarizing the results on transition markers, we now present the results for the excess parameter $\gamma_2(m, S)$ for EGOE(1+2)-s.

2.9 Results for $\gamma_2(m, S)$ for EGOE(1+2)-s

Towards providing a basis for the Gaussian form for the eigenvalue density generated by EGOE(1+2)-s, we derive first the exact formula for $\gamma_2(m, S)$ for a general $h(1)$ operator and then discuss $\gamma_2(m, S)$ for EGOE(2)-s. Given $h(1) = \sum_i \epsilon_i n_i$, the $\gamma_2(m, S)$ is defined by the fourth central moment $\langle \tilde{h}^4(1) \rangle^{m, S}$ and the variance or the second central moment $\langle \tilde{h}^2(1) \rangle^{m, S}$. Note that,

$$\tilde{h}(1) = \sum_{i=1}^{\Omega} \tilde{\epsilon}_i n_i; \quad \tilde{\epsilon}_i = \epsilon_i - \frac{1}{\Omega} \sum_{i=1}^{\Omega} \epsilon_i. \quad (2.9.1)$$

To derive the formula for the fourth moment, we will decompose first $\tilde{h}^2(1)$ into one and two body parts and apply Eq. (B2). The one-body part of $\tilde{h}^2(1)$ is defined by the sp energies $\tilde{\epsilon}_i^2$ and the two-body matrix elements $V_{ijij}^s = 2\tilde{\epsilon}_i \tilde{\epsilon}_j$ with all other matrix elements being zero; note that $i \neq j$ for $s = 1$. Then the λ 's and other averages in Eqs. (2.3.8)-(2.3.10) are,

$$\begin{aligned} \lambda_{i,i}^{s=0} &= -\lambda_{i,i}^{s=1} = 2\tilde{\epsilon}_i^2 - \frac{2}{\Omega} \sqrt{X}, \quad \langle V(2) \rangle^{2,s} = \frac{2(-1)^s}{\Omega[\Omega + (-1)^s]} \sqrt{X}, \\ \langle [V(2)]^2 \rangle^{2,s} &= \frac{4}{\Omega[\Omega + (-1)^s]} [X + (-1)^s Y], \\ \langle [V^{s:v=2}(2)]^2 \rangle^{2,s} &= \frac{4(-1)^s}{[\Omega + (-1)^s][\Omega + 2(-1)^s]} Y + \frac{4(\Omega^2 + 3(-1)^s \Omega + 3)}{\Omega[\Omega + (-1)^s]^2 [\Omega + 2(-1)^s]} X; \\ X &= \left(\sum_k \tilde{\epsilon}_k^2 \right)^2, \quad Y = \sum_k \tilde{\epsilon}_k^4. \end{aligned} \quad (2.9.2)$$

Using Eq. (B2) with Eq. (2.9.2), the final propagation formulas are,

$$\begin{aligned} \left[\langle \tilde{h}^2(1) \rangle^{m, S} \right]^2 &= \frac{[m(m - 2\Omega)(\Omega + 2) + 4\Omega S(S + 1)]^2}{4\Omega^2(\Omega^2 - 1)^2} X, \\ \langle \tilde{h}^4(1) \rangle^{m, S} &= \left[\langle \tilde{h}^2(1) \rangle^{m, S} \right]^2 - \frac{12\mathcal{H}(\Omega, m, S)}{\Omega^2(\Omega^2 - 1)} (X - \Omega Y) \end{aligned}$$

$$\begin{aligned}
& + \frac{[-m(m-2\Omega)\{-4(\Omega+1)+m(\Omega+4)\}+4\Omega(2\Omega-3m+2)S(S+1)]}{\Omega^2(\Omega+1)(\Omega-1)(\Omega-2)}(X-\Omega Y) \\
& + \frac{1}{2\Omega^2(\Omega^2-1)(\Omega-2)^2(\Omega+2)} \left[m(m-2\Omega)\{-4(\Omega+1)+m(\Omega+4)\}^2 \right. \\
& \quad \left. + 8\Omega S(S+1)\{2(\Omega+1)(3\Omega+2)+m^2(3\Omega+8)-m(3\Omega^2+16\Omega+12)\} \right. \\
& \quad \left. + 16\Omega^2\{S(S+1)\}^2 \right] (X-\Omega Y) \\
& + \frac{4}{\Omega^2(\Omega-1)(\Omega+3)} Q^2(\{2\}:m,S) \langle [V^{s=0:v=2}(2)]^2 \rangle^{2,0} \\
& + \frac{4}{\Omega^2(\Omega+1)(\Omega-3)} Q^2(\{1^2\}:m,S) \langle [V^{s=1:v=2}(2)]^2 \rangle^{2,1}.
\end{aligned} \tag{2.9.3}$$

Note that \mathcal{H} is defined in Eq. (2.6.3) and Q 's are defined in Eq. (2.3.11) respectively.

Using Eq. (2.9.3), we can calculate $\gamma_2(m, S)$ for any set of ϵ_i 's and (Ω, m, S) where,

$$\gamma_2(m, S) = \frac{\langle \tilde{h}^4(1) \rangle^{m,S}}{\left[\langle \tilde{h}^2(1) \rangle^{m,S} \right]^2} - 3. \tag{2.9.4}$$

Expanding the expression, by combining Eqs. (2.9.3) and (2.9.4), for $\gamma_2(m, S)$ in powers of $1/\Omega$ and retaining terms up to $1/\Omega$, we have

$$\gamma_2(m, S) = \frac{\gamma_2(1, \frac{1}{2})}{m} - \frac{\{m(m-4)+4S(S+1)\}\{5\gamma_2(1, \frac{1}{2})+6\}}{2m^2\Omega} + O\left(\frac{1}{\Omega^2}\right). \tag{2.9.5}$$

Therefore, for the $h(1)$ operators with $|\gamma_2(1)| \sim 1$, the excess parameter $\gamma_2(m, S) \rightarrow 0$ for sufficiently large m and also the spin dependence is weak. Therefore $h(1)$ operators in general generate Gaussian eigenvalue densities for large m values. With $S = m/2$ and $N = 2\Omega$, Eq. (2.9.5) reduces to,

$$\gamma_2(m, S) = \frac{\gamma_2(1, \frac{1}{2})}{m} + \frac{1}{N} \left[\frac{\{5\gamma_2(1, \frac{1}{2})+6\}}{m} - \left\{ 5\gamma_2\left(1, \frac{1}{2}\right) + 6 \right\} \right]. \tag{2.9.6}$$

This is same as the result that follows from the exact formula for $\gamma_2(N, m)$ for spinless fermion systems [Fr-06].

Turning to two-body interactions, first it should be mentioned that a formalism for obtaining exact results for $\gamma_2(m, S)$ for a given $V(2)$ is given in [Ka-95, Pl-

96] and also they can be obtained via a subtraction procedure using the formula discussed in [Wo-86]. As seen from [Ka-95], the analytical result for $\gamma_2(m, S)$ is complicated and contains too many terms. Therefore it is not easy to derive an easy to understand analytical formula for $\overline{\gamma_2(m, S)}$ for EGOE(2)-**s**. However, an analytical understanding is possible in the dilute limit. Then, as argued in [Pl-97], the spin dependence of $\gamma_2(m, S)$ will be weak and the first correction is of the form $C_0[1 + 4S(S+1)/m^2]$ where C_0 is a constant. Strikingly, Eq. (2.9.5), for the $h(1)$ operator, also gives the same result. Then one can conclude that EGOE(2)-**s** gives Gaussian eigenvalue densities. Combining the analytical results given by Eqs. (2.9.3) and (2.9.5) for $\gamma_2(m, S)$ for the $h(1)$ operator and the asymptotic result for a general two-body Hamiltonian preserving spin given in [Pl-97], it is plausible to argue that the eigenvalue density for EGOE(1+2)-**s** will be in general of Gaussian form.

2.10 Summary

In summary, we have presented in Secs. 2.4-2.7, a comprehensive set of calculations for the changes in level fluctuations, strength functions, information entropy and occupancies as a function of the λ parameter in EGOE(1+2)-**s** Hamiltonian given by Eq. (2.2.1) with $\lambda_0 = \lambda_1 = \lambda$. The final results are summarized in Fig. 2.11 (the basic structure of the transitions remains same even for $\lambda_0^2 \neq \lambda_1^2$ as discussed briefly in Sec. 2.8). In addition, we have derived the exact formula for the ensemble averaged fixed- (m, S) spectral variances and for the $V(2)$ part it is of the form $\lambda^2 P(\Omega, m, S)$. We have demonstrated that the variance propagator $P(\Omega, m, S)$ in Eq. (2.3.12) gives a good explanation for the spin dependence of the Poisson to GOE and BW to Gaussian crossover points λ_c and λ_F for level fluctuations and strength functions, respectively, and similarly for the duality or thermodynamic region marked by λ_d (obtained from information entropy and occupancies). The three chaos markers λ_c , λ_F and λ_d in terms of $P(\Omega, m, S)$ are given by Eqs. (2.4.2), (2.5.5), and (2.6.4), respectively. As seen from Fig. 2.2, P decreases with S and using this in Eqs. (2.4.2), (2.5.5), and (2.6.4), establishes that the λ_c , λ_F and λ_d values will increase with S (as $S = m/2$ corresponds to spinless fermions, it may be possible to investigate further, using EGOE(1+2)-**s**, the recent claim by Papenbrock and Weidenmüller [Pa-05] that symmetries are responsible for chaos in nuclear shell-model). Thus, introduction of the spin quantum

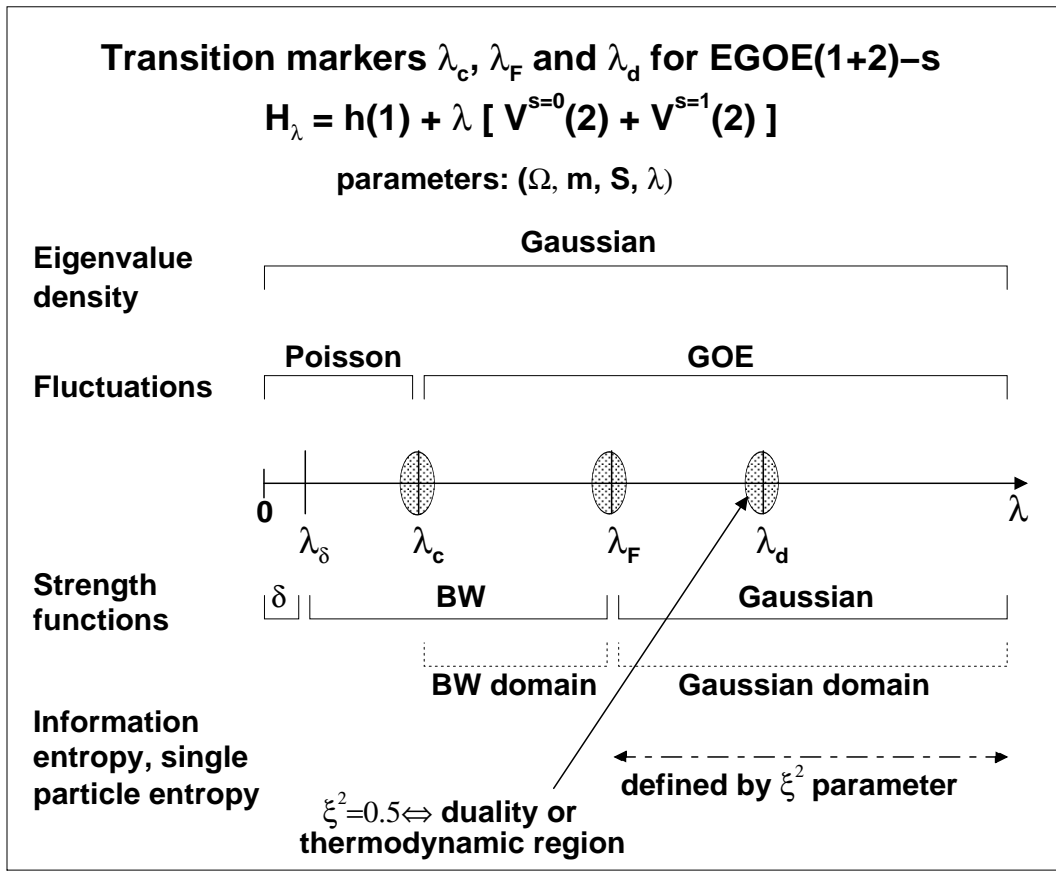


Figure 2.11: Transition (chaos) markers for EGOE(1+2)-s. Results in the figure are obtained using the Hamiltonian H_λ given in Eq. (2.4.1), i.e., $\lambda_0 = \lambda_1 = \lambda$ in Eq. (2.2.1). Note that λ is in the units of the average spacing Δ of the sp levels defining $h(1)$. As discussed in the text, strength functions take δ -function form (denoted by δ in the figure) for $\lambda < \lambda_\delta$ with $\lambda_\delta \ll \lambda_c$ and they start taking BW form as λ crosses λ_δ . The BW domain is defined by $\lambda_c < \lambda < \lambda_F$ and here the strength functions take BW form and the fluctuations are GOE. Similarly, in the Gaussian domain, defined by $\lambda > \lambda_F$, the strength functions take Gaussian form and the fluctuations are GOE. Also in this region, the information entropy and single-particle entropy are defined by the ξ^2 parameter given in Eq. (2.6.1b). The basic structure of the transitions remains same even for $\lambda_0^2 \neq \lambda_1^2$ as discussed in Sec. 2.8. See text for further details.

number preserves the general structures, generated by spinless fermion EGOE(1+2) ensemble, although the actual values of the markers vary with the m -particle spin S . It should be emphasized that the first example for the transition markers exhibited by EGOE(1+2) with additional good quantum number besides the particle number m are derived and presented using EGOE(1+2)-s in this chapter.

The transition markers as described in Fig. 2.11 provide a basis for statistical spectroscopy. For example, for $\lambda \geq \lambda_c$ as GOE fluctuations are small they can be ignored. Then the smoothed eigenvalue densities will be Gaussian. Similarly the strength

functions and other related distributions will take BW or Gaussian form. Using these it is possible to derive distributions (with respect to the energy eigenvalues) for various spectroscopic observables [Ko-01, Ko-03, Br-81, Fl-99, Ka-94] and employ them in applications in nuclear and atomic physics. Moreover if the system is in the thermodynamic region, then Gaussian form can be used for the strength functions (or partial densities) defined over sub-spaces generated by any symmetry algebra [Ko-03] and this will allow one to study goodness of group symmetries [Pa-78, Wo-86].

Chapter 3

EGOE(1+2)-s: Pairing Correlations

3.1 Introduction

Pairing correlations play very important role in finite interacting Fermi systems such as nuclei [Ho-07, Ka-00], small metallic grains [Pa-02, Sc-08], quantum dots [Lu-01, Al-05] and so on. The EGOE(1+2)-s discussed in Chapter 2 provides a model for understanding general structures generated by pairing correlations [Pa-02, Al-05]. We adopt an algebraic approach to pairing rather than the BCS approach. Our purpose in this chapter is to study first the pairing symmetry in the space defined by EGOE(1+2)-s and then the measures for pairing, using EGOE(1+2)-s ensemble, that are of interest for nuclei (see [Ho-07]), quantum dots and small metallic grains (see [Sc-08]). In the space defined by EGOE(1+2)-s ensemble, pairing symmetry is defined by the algebra $U(2\Omega) \supset Sp(2\Omega) \supset SO(\Omega) \otimes SU_S(2)$. Starting with the details of this algebra we show that the state density generated by the pairing Hamiltonian will be a highly skewed distribution. In contrast, the partial densities over pairing subspaces follow Gaussian form and the propagation formulas for their centroids and variances, defined over subspaces given by the algebra $U(2\Omega) \supset Sp(2\Omega) \supset SO(\Omega) \otimes SU_S(2)$, are derived. Pair transfer strength sum as a function of excitation energy (for fixed S), a statistic for onset of chaos, is shown to follow, for low spins, the form derived for spinless fermion systems. The parameters defining this form are easy to calculate using propagation equations. In addition, we consider a quantity in terms of gs energies, giving conductance peak spacings in mesoscopic systems at low temperatures, and study its distribution over EGOE(1+2)-s by including both pairing and exchange interactions.

All the results presented in this chapter are published in [Ma-09, Ma-10].

3.2 $U(2\Omega) \supset Sp(2\Omega) \supset SO(\Omega) \otimes SU_S(2)$ Pairing Symmetry

Pairing algebra to be discussed here is presumably familiar to others. However to our knowledge the details presented here are not reported elsewhere (for a short related discussion see [Fl-64]). Note that, we drop the “hat” symbol over \hat{H} , \hat{h} and \hat{V} when there is no confusion as in Chapter 2.

Consider m fermions distributed in Ω number of sp levels each with spin $\mathbf{s} = 1/2$. Therefore total number of sp states is $N = 2\Omega$ and they are denoted by $a_{i,\mathbf{s}=\frac{1}{2},m_s}^\dagger |0\rangle = |i, \mathbf{s} = \frac{1}{2}, m_s = \pm \frac{1}{2}\rangle$ with $i = 1, 2, \dots, \Omega$. Similarly,

$$\frac{1}{\sqrt{1 + \delta_{i,j}}} \left(a_{i,\mathbf{s}=\frac{1}{2}}^\dagger a_{j,\mathbf{s}=\frac{1}{2}}^\dagger \right)_{m_s}^s |0\rangle = \left| \left(i, \mathbf{s} = \frac{1}{2}; j, \mathbf{s} = \frac{1}{2} \right) s, m_s \right\rangle$$

denotes two-particle antisymmetric states with the two-particle in the levels i and j and the two-particle spin $s = 0$ or 1 . From now on we will drop the index $\mathbf{s} = \frac{1}{2}$ for simplicity and then the two-particle antisymmetric states, in spin coupled representation, are

$$|(i, j) s, m_s\rangle = \frac{1}{\sqrt{1 + \delta_{i,j}}} \left(a_i^\dagger a_j^\dagger \right)_{m_s}^s |0\rangle.$$

In constructing EGOE(1+2)- \mathbf{s} , only spin invariant Hamiltonians are considered. Thus the m -particle states carry good spin(S) quantum number [Ko-06, Tu-06]. Now the pair creation operator P_i for the level i and the generalized pair creation operator (over the Ω levels) P are

$$P = \frac{1}{\sqrt{2}} \sum_i \left(a_i^\dagger a_i^\dagger \right)^0 = \sum_i P_i, \quad P^\dagger = -\frac{1}{\sqrt{2}} \sum_i (\tilde{a}_i \tilde{a}_i)^0. \quad (3.2.1)$$

In Eq. (3.2.1), $\tilde{a}_{i,\mathbf{s}=\frac{1}{2},m_s} = (-1)^{\frac{1}{2}+m_s} a_{i,\mathbf{s}=\frac{1}{2},-m_s}$. Therefore in the space defining EGOE(1+2)- \mathbf{s} , the pairing Hamiltonian H_p and its two-particle matrix elements are,

$$H_p = P^2 = PP^\dagger, \quad (3.2.2)$$

$$\langle (k, \ell) s, m_s | H_p | (i, j) s', m_{s'} \rangle = \delta_{s,0} \delta_{i,j} \delta_{k,\ell} \delta_{s,s'} \delta_{m_s, m_{s'}}.$$

Note that the two-particle matrix elements of H_p (also true for H) are independent

of the m_s quantum number. With this, we will proceed to identify and analyze the pairing algebra. Firstly, it is easily seen that the $4\Omega^2$ number of one-body operators $u_\mu^r(i, j) = (a_i^\dagger \tilde{a}_j)_\mu^r$, $r = 0, 1$ generate $U(2\Omega)$ algebra; see Appendix D. They satisfy the following commutation relations,

$$\begin{aligned} \left[u_\mu^r(i, j), u_{\mu'}^{r'}(k, l) \right]_- &= \sum_{r''} (-1)^{r+r'} \langle r \mu r' \mu' | r'' \mu'' \rangle \sqrt{(2r+1)(2r'+1)} \\ &\times \left\{ \begin{array}{ccc} r & r' & r'' \\ 1/2 & 1/2 & 1/2 \end{array} \right\} \left[u_{\mu''}^{r''}(k, j) \delta_{il} - (-1)^{r+r'+r''} u_{\mu''}^{r''}(i, l) \delta_{jk} \right]. \end{aligned} \quad (3.2.3)$$

Here, $\langle \dots | \dots \rangle$ are CG coefficients and $\{ \dots \}$ are $6j$ -symbols. The $U(2\Omega)$ irreducible representations (irreps) are denoted trivially by the particle number m as they must be antisymmetric irreps $\{1^m\}$. The $2\Omega(\Omega-1)$ number of operators $V_\mu^r(i, j)$,

$$V_\mu^r(i, j) = \sqrt{(-1)^{r+1}} \left[u_\mu^r(i, j) - (-1)^r u_\mu^r(j, i) \right]; \quad i > j, \quad r = 0, 1 \quad (3.2.4)$$

along with the 3Ω number of operators $u_\mu^1(i, i)$ form $Sp(2\Omega)$ subalgebra of $U(2\Omega)$ and this follows from the results in [Ko-06b]. Using anti-commutation relations for fermion creation and destruction operators and carrying out angular-momentum algebra [Ed-74], we have

$$\begin{aligned} &\left[(a_i^\dagger \tilde{a}_j)^k (a_j^\dagger \tilde{a}_i)^k \right]^0 \\ &= (-1)^k \sqrt{\frac{2k+1}{2j+1}} (a_i^\dagger \tilde{a}_i)^0 - \sum_{k'} \chi \left\{ \begin{array}{ccc} 1/2 & 1/2 & k \\ 1/2 & 1/2 & k \\ k' & k' & 0 \end{array} \right\} [(a_i^\dagger a_j^\dagger)^{k'} (\tilde{a}_j \tilde{a}_i)^{k'}]^0, \\ &\left[(a_i^\dagger \tilde{a}_j)^k (a_i^\dagger \tilde{a}_j)^k \right]^0 = -\chi \left\{ \begin{array}{ccc} 1/2 & 1/2 & k \\ 1/2 & 1/2 & k \\ 0 & 0 & 0 \end{array} \right\} (a_i^\dagger a_i^\dagger)^0 (\tilde{a}_j \tilde{a}_j)^0. \end{aligned} \quad (3.2.5)$$

Here, $\chi\{\dots\dots\dots\}$ are $9j$ coefficients (they are not $9j$ -symbols). Note that

$$\chi \left\{ \begin{array}{ccc} 1/2 & 1/2 & k \\ 1/2 & 1/2 & k \\ s & s & 0 \end{array} \right\} = \sqrt{\frac{2s+1}{4}} \text{ for } k=0, \quad (3.2.6)$$

$$= \sqrt{\frac{2s+1}{3}} \left[\frac{3}{2} - s(s+1) \right] \text{ for } k=1.$$

We will show that the irreps of $Sp(2\Omega)$ algebra are uniquely labeled by the seniority quantum number ‘v’ discussed in the context of identical particle pairing in nuclear structure [Ta-93] and they in turn define the eigenvalues of H_p . The quadratic Casimir operators of the $U(2\Omega)$ and $Sp(2\Omega)$ algebras are [Ko-06b],

$$C_2[U(2\Omega)] = \sum_{i,j,r} u^r(i,j) \cdot u^r(j,i), \quad (3.2.7)$$

$$C_2[Sp(2\Omega)] = 2 \sum_i u^1(i,i) \cdot u^1(i,i) + \sum_{i>j,r} V^r(i,j) \cdot V^r(i,j).$$

Simplifying these expressions using relations in Eqs. (3.2.5) and (3.2.6) [with \hat{n} being the number operator], we have

$$C_2[U(2\Omega)] = 2\hat{n}\Omega - 2 \sum_i P_i P_i^\dagger - \sum_{i \neq j, s} \sqrt{2s+1} [s(s+1) - 1] \left[\left(a_i^\dagger a_j^\dagger \right)^s \left(\tilde{a}_j \tilde{a}_i \right)^s \right]^0,$$

$$C_2[Sp(2\Omega)] = (2\Omega + 1)\hat{n} - 6 \sum_i P_i P_i^\dagger - 4 \sum_{i>j} (P_i P_j^\dagger + P_j P_i^\dagger)$$

$$- \sum_{i \neq j, s} \sqrt{2s+1} [s(s+1) - 1] \left[\left(a_i^\dagger a_j^\dagger \right)^s \left(\tilde{a}_j \tilde{a}_i \right)^s \right]^0,$$

$$\Rightarrow C_2[U(2\Omega)] - C_2[Sp(2\Omega)] = 4 P P^\dagger - \hat{n}. \quad (3.2.8)$$

It is also seen that the operators P , P^\dagger and P_0 form $SU(2)$ algebra,

$$[P, P^\dagger] = \hat{n} - \Omega = 2 P_0, \quad [P_0, P] = P, \quad [P_0, P^\dagger] = -P^\dagger. \quad (3.2.9)$$

The corresponding spin is called quasi-spin Q . As M_Q , the P_0 eigenvalue, is $(m -$

$\Omega)/2$, we obtain $Q = (\Omega - v)/2$. Then, for $m \leq \Omega$, v take values $v = m, m-2, \dots, 0$ or 1 .

Therefore eigenvalues of the pairing Hamiltonian H_p are given by,

$$E_p(m, v, S) = \langle H_p \rangle^{m, v, S} = \langle PP^\dagger \rangle^{m, v, S} = \frac{1}{4}(m - v)(2\Omega + 2 - m - v). \quad (3.2.10)$$

As $\langle C_2[U(2\Omega)] \rangle^{\{1^m\}} = m(2\Omega + 1 - m)$, Eqs. (3.2.8) and (3.2.10) will give

$$C_2[Sp(2\Omega)] = 2v \left(\Omega + 1 - \frac{v}{2} \right). \quad (3.2.11)$$

Comparing Eq. (3.2.11) with the general formula for the eigenvalues of the quadratic Casimir invariant of $Sp(2\Omega)$ [Wy-74], it follows that the seniority quantum number ' v ' corresponds to totally antisymmetric irrep $\langle 1^v \rangle$ of $Sp(2\Omega)$. Thus $Sp(2\Omega)$ corresponds to $SU(2)$ quasi-spin algebra generated by (P, P^\dagger, P_0) . More explicitly,

$$|m, v, S, \alpha\rangle = \sqrt{\frac{(\Omega - v - p)!}{(\Omega - v)! p!}} P^p |m = v, v, S, \alpha\rangle; \quad p = \frac{m - v}{2}. \quad (3.2.12)$$

Thus the spin S is generated by ' v ' free particles and therefore $v \geq 2S$. Then, for a given (m, S) we have

$$v = m, m-2, \dots, 2S, \quad (m \leq \Omega). \quad (3.2.13)$$

Number of states or dimension $D(m, v, S)$, without the $(2S + 1)$ degeneracy factor, for a fixed- (m, v, S) is,

$$D(m, v, S) = d_f(\Omega, m = v, S) - d_f(\Omega, m = v - 2, S). \quad (3.2.14)$$

Note that the fixed- (m, S) dimensions $d_f(\Omega, m, S)$ are given by Eq. (2.2.2). Table 3.1 gives the reductions $m \rightarrow S \rightarrow v$, $D(m, v, S)$ and also $E_p(m, v, S)$ for some examples. Let us point out $Sp(2\Omega) \supset SO(\Omega) \otimes SU(2)$ but $SO(\Omega)$ carries no extra information. In fact there is one-to-one correspondence between the $Sp(2\Omega)$ chain and the alternative group-subgroup chain $U(2\Omega) \supset U(\Omega) \otimes SU(2) \supset SO(\Omega) \otimes SU(2)$. This is verified by comparing the results in Table 3.1 with the irrep reductions for $U(\Omega) \supset SO(\Omega)$ that are given in Appendix D. It is useful to note that Eqs. (3.2.10), (3.2.13) and (3.2.14) will allow one to construct the state density generated by the pairing Hamiltonian

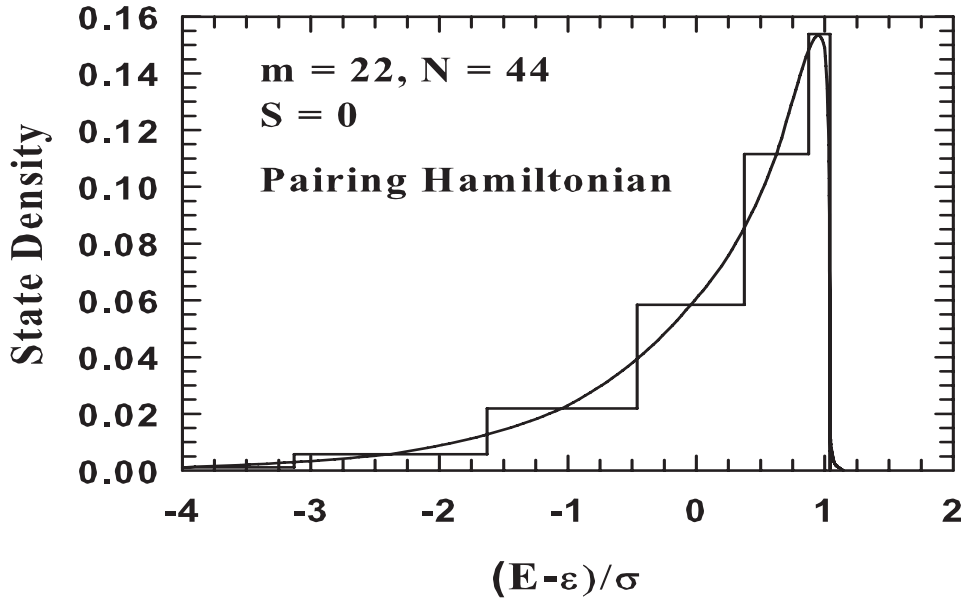


Figure 3.1: State density for the pairing Hamiltonian $H = -H_p$ for a system of 22 fermions in $\Omega = 22$ orbits ($N = 44$) and total spin $S = 0$. In the histogram, $\rho(E)$ for a given $\hat{E} = (E - \epsilon)/\sigma$ is plotted with \hat{E} as center with width given by $\Delta\hat{E} = \Delta E/\sigma$ (see Eq. (3.2.15) and the following discussion). The smooth curve is obtained by joining the center points to guide the eye. A similar plot was shown before by Ginocchio [Gi-80] but for a system of identical fermions in a large single- j shell.

$H = -H_p$. The dimensions $d_f(\Omega, m, S)$ and $D(m, \nu, S)$ along with the energy E_p of H_p will give the normalized density $\rho(E)$ to be

$$\rho_{(-H_p)}(E) = \frac{D(m, \nu, S)}{d_f(\Omega, m, S) \Delta E}; \quad \Delta E = E_p(m, \nu+1, S) - E_p(m, \nu-1, S) = \Omega - \nu + 1. \quad (3.2.15)$$

Figure 3.1 gives $\rho(\hat{E})$ vs \hat{E} plot for $\Omega = 22$ (i.e., $N = 44$), $m = 22$ and $S = 0$. For this system, the spectrum spread is 132 (note that $\nu_{max} = 22$), centroid $\epsilon \sim 5.7$ and width $\sigma \sim 6$; note that $\hat{E} = (E - \epsilon)/\sigma$. Clearly, it is a highly skewed distribution (see also the $\alpha = 0$ plot in Fig. 3.4 ahead).

3.3 Fixed- (m, ν, S) Partial Densities and their Centroids and Variances

Expansion of a given $|m, \nu, S, \alpha\rangle$ basis state in terms of the H eigenstates $|E; (m, S)\rangle$, with the expansion coefficients being $C_E^{m, \nu, S, \alpha}$ will allow us to define the fixed- (m, ν, S)

Table 3.1: Classification of states in the $U(2\Omega) \supset Sp(2\Omega) \supset SO(\Omega) \otimes SU_5(2)$ limit for $\Omega = 6$ with $m = 0 - 6$ and $\Omega = 8$ with $m = 6 - 8$. Given are (m, S, v) labels, the corresponding dimensions $D(m, v, S)$ and eigenvalues $E_p(m, v, S)$. Note that $\sum_{v, S} (2S + 1) D(m, v, S) = \binom{2\Omega}{m}$ and $\sum_v D(m, v, S) = d_f(\Omega, m, S)$.

Ω	m	S	v	$D(m,v,S)$	$E_p(m,v,S)$	Ω	m	S	v	$D(m,v,S)$	$E_p(m,v,S)$		
6	0	0	0	1	0	8	6	0	6	840	0		
			$\frac{1}{2}$	1	6				0	4	300	4	
			2	0	2				20	0	2	35	12
	2	0	0	1	6				0	1	18		
			1	2	15				0	1	6	1134	0
			$\frac{1}{2}$	3	64				0	4	350	4	
	3	$\frac{1}{2}$	1	6	5				2	28	10		
			$\frac{3}{2}$	3	20				0	2	6	350	0
			4	0	4				84	0	4	70	4
	4	0	2	20	4				3	6	28	0	
			0	1	10				7	$\frac{1}{2}$	7	1344	0
			1	4	90				0	5	840	3	
	5	$\frac{1}{2}$	2	15	4				3	160	8		
			4	15	0				1	8	15		
			5	5	140				0	$\frac{3}{2}$	7	840	0
	6	$\frac{1}{2}$	3	64	3				5	448	3		
			1	6	8				3	56	8		
			$\frac{3}{2}$	5	64				0	$\frac{5}{2}$	7	160	0
	7	$\frac{1}{2}$	3	20	3				5	56	3		
			5	6	0				$\frac{7}{2}$	7	8	0	
			6	0	6				70	0	8	588	0
	8	0	4	84	2				0	8	840	2	
			2	20	6				6	300	6		
			0	1	12				2	35	12		
	9	0	1	6	84				0	0	1	20	
			4	90	2				1	8	840	0	
			2	15	6				6	1134	2		
	10	0	6	20	0				4	350	6		
			4	15	2				2	28	12		
			3	6	1				0	2	8	300	0
	11	0							6	350	2		
									4	70	6		
									3	8	35	0	
	12	0							6	28	2		
									4	8	1	0	

partial densities $\rho^{m,v,S}(E)$,

$$\begin{aligned}\rho^{m,v,S}(E) &= \langle \delta(H - E) \rangle^{m,v,S} = \frac{1}{D(m,v,S)} \sum_{\alpha} \left| C_E^{m,v,S,\alpha} \right|^2 \\ \Rightarrow I^{m,v,S}(E) &= D(m,v,S) \rho^{m,v,S}(E) = \sum_{\alpha} \left| C_E^{m,v,S,\alpha} \right|^2.\end{aligned}\tag{3.3.1}$$

Often it is convenient to use total densities $I(E)$ rather than the normalized densities $\rho(E)$. It is important to note that fixed- (m, S) density of states $\rho^{m,S}(E)$ decompose into a sum of fixed- (m, v, S) partial densities,

$$\begin{aligned}\rho^{m,S}(E) &= \sum_v \frac{D(m,v,S)}{d_f(\Omega, m, S)} \rho^{m,v,S}(E) \\ \Rightarrow I^{m,S}(E) &= \sum_v I^{m,v,S}(E).\end{aligned}\tag{3.3.2}$$

The partial densities are defined over broken symmetry subspaces and they are also called ‘strength functions’ or ‘local density of states’ [Ko-01, Ko-03]. Partial densities $\rho^{m,v,S}(E)$ give intensity distribution of a given basis state $|m, v, S\rangle$ over the eigenstates $|E\rangle$, i.e., distribution of the expansion coefficients $|C_E^{m,v,S}|^2$ vs E . The partial densities have same structure as that for the strength functions defined in Eq. (2.5.2) as partial sums over the strength functions give partial densities. We will also encounter partial densities in Chapter 5.

In the $\lambda > \lambda_F$ region, as discussed in Chapter 2, strength functions take Gaussian form and therefore partial densities are expected to be Gaussian in this region. Extension of this result to EGOE(1+2)- J [Pa-07] with subspaces defined by the pairing Hamiltonian, i.e., fixed- (m, v, J) partial densities are Gaussian is often used in nuclear physics [Qu-74, Qu-77]. In Fig. 3.2 we present tests of this assumption for EGOE(1+2)- s with J replaced by S . In order to discuss these results, we will start with the EGOE(1+2)- s Hamiltonian defined by Eq. (2.2.1). We choose, in all the calculations reported in this chapter, $\epsilon_i = i + (1/i)$, $i = 1, 2, \dots, \Omega$ and $\lambda_0 = \lambda_1 = \lambda = 0.3$. Results in Chapter 2 confirm that $\lambda = 0.3$ corresponds to strong coupling region. Before going further, let us add that we will later consider extensions of H with the inclusion of pairing and exchange interactions (they are not random). For a $\Omega = m = 8$ system

with 50 members, we have extracted the partial densities $\rho^{m,v,S}(E)$ in Eq. (3.3.1) by numerically constructing the H matrix in good S basis and then changing it into good (m,v,S) basis with an auxiliary diagonalization of H_p in the good S basis. Results for the ensemble averaged partial densities are shown for $S = 0$ and 1 in Fig. 3.2 and the results are compared with the Gaussian (\mathcal{G}) and ED corrected Gaussian forms given by Eq. (2.3.2). From the results in Fig. 3.2, it is seen that the agreement between the exact and ED corrected Gaussians is excellent. For $v = 0$ (this is one dimensional) the deviations are some what larger. Similar results are also obtained for a smaller example (these are not shown in the figure) with $\Omega = m = 6$ and $S = 0, 1$ and for this system we have carried out calculations with 500 members. This shows fixed- (m,v,S) partial densities take close to Gaussian form, just as fixed- (m,S) densities, in the strong coupling region. Thus the EGOE(1+2)-s densities follow EGOE(1+2) even in pairing subspaces. This is a result assumed in statistical nuclear spectroscopy (see for example [Da-80, Fr-82]).

For constructing Gaussian partial (m,v,S) densities, we need fixed- (m,v,S) centroids $E_c(m,v,S) = \langle H \rangle^{m,v,S}$ and variances $\sigma^2(m,v,S) = \langle H^2 \rangle^{m,v,S} - [E_c(m,v,S)]^2$. An important result here is, these parameters can be calculated for any (Ω, m, v, S) with $m > 4$ without recourse to H matrix construction in (m,S) spaces. This derives from the fact that simple (Casimir) propagation is possible for $E_c(m,v,S)$ in terms of the corresponding E_c for $m \leq 2$ and for $\sigma^2(m,v,S)$ in terms of the corresponding σ^2 for $m \leq 4$. From Table 3.1 one can see that the number of (m,v,S) irreps Λ_i is 5 for m up to 2 and there are 5 simple scalar operators \hat{C}_i of maximum body rank 2, $\hat{C}_i = 1, \hat{n}, \binom{\hat{n}}{2}, H_p$, and \hat{S}^2 for $i = 1 - 5$, respectively. Note that $\langle H_p \rangle^{m,v,S}$ and $\langle \hat{S}^2 \rangle^{m,v,S}$ are $E_p(m,v,S)$ [see Eq. (3.2.10)] and $S(S+1)$, respectively. More remarkable is that, for $m \leq 4$, the number of (m,v,S) irreps Υ_i is 14 as seen from Table 3.1 and also the available simple scalars $\hat{\mathcal{C}}_i$ of maximum body rank 4 are exactly 14. These are $\hat{\mathcal{C}}_i = 1, \hat{n}, \binom{\hat{n}}{2}, \binom{\hat{n}}{3}, \binom{\hat{n}}{4}, H_p, \hat{n}H_p, \binom{\hat{n}}{2}H_p, (H_p)^2, H_p\hat{S}^2, \hat{S}^2, \hat{n}\hat{S}^2, \binom{\hat{n}}{2}\hat{S}^2$ and $(\hat{S}^2)^2$ for $i = 1 - 14$, respectively. Therefore, the spectral variances over (m,v,S) spaces propagate simply and they will be linear combinations of the eigenvalues of the 14 operators above. The constants in the expansion will follow from the variances for $m \leq 4$. Then, fixed- (m,v,S) energy centroids with $\mathcal{S}^2 = S(S+1)$, $X(m,S) = m(m+2) - 4S(S+1)$ and

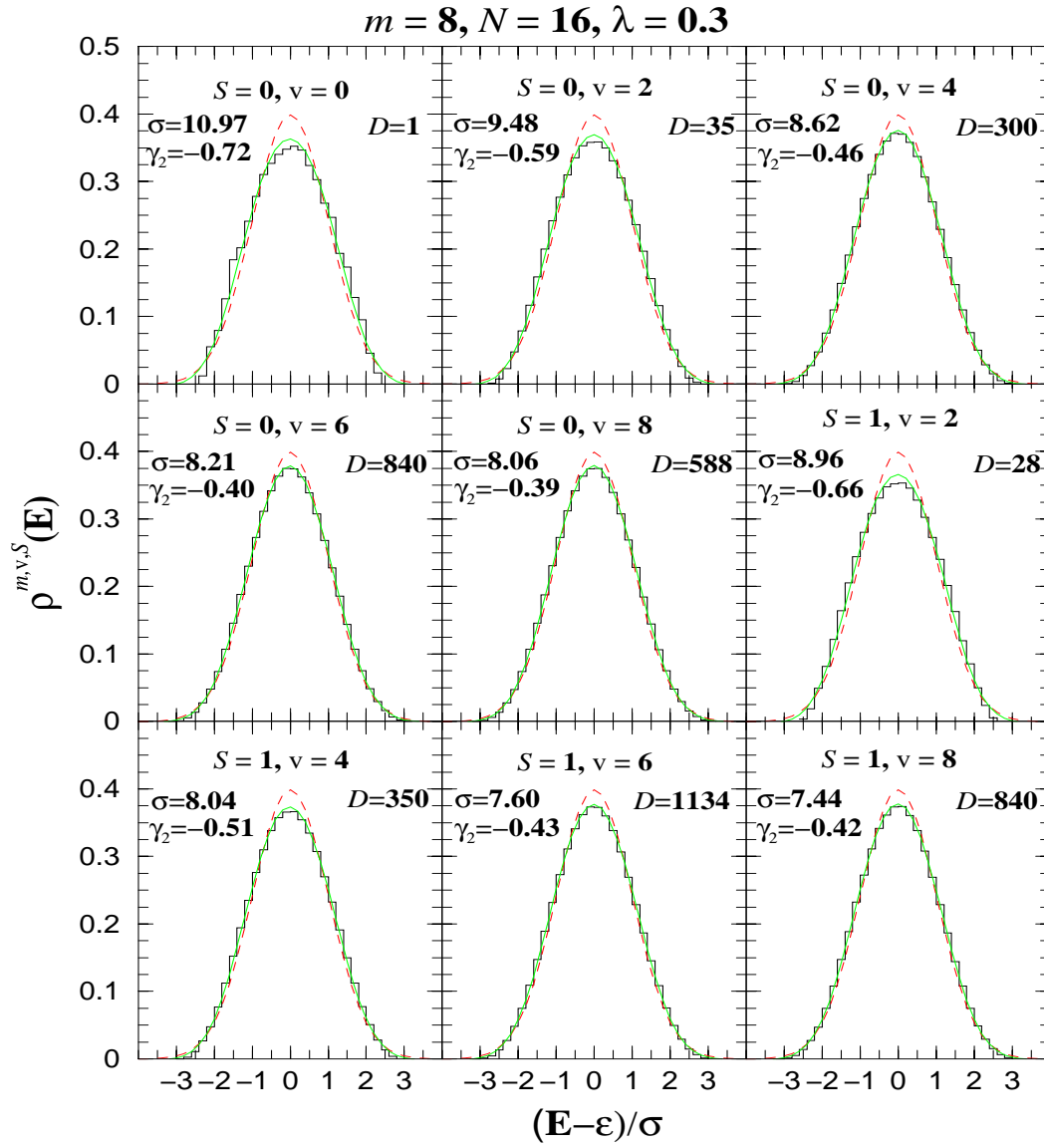


Figure 3.2: Partial densities $\rho^{m,v,S}(E)$ vs E for a EGOE(1+2)-s ensemble H defined in the text. The values of (v, S) , dimension D , width σ and γ_2 for the densities are given in the figure. Note that $\gamma_1 \sim 0$ in all cases. The energies E are zero centered with respect to the centroid ϵ and scaled with the width σ of $\rho^{m,v,S}(E)$. The histograms (with 0.2 bin size) are exact results, dashed curves are Gaussians and the continuous curves are Edgeworth corrected Gaussians. See text for further details.

$Y(m, S) = m(m - 2) - 4S(S + 1)$, are given by

$$\langle H \rangle^{m,v,S} = E_c(m, v, S) = a_0 + a_1 m + a_2 \binom{m}{2} + a_3 \mathcal{S}^2 + a_4 E_p(m, v, S) \quad (3.3.3)$$

$$\Rightarrow E_c(m, v, S) = \frac{1}{2}(m - 1)(m - 2) E_c(0, 0, 0) - m(m - 2) E_c(1, 1, \frac{1}{2})$$

$$\begin{aligned}
& + \frac{1}{8\Omega} \left[-8E_p(m, v, S) + \Omega X(m, S) \right] E_c(2, 2, 0) + \frac{1}{\Omega} E_p(m, v, S) E_c(2, 0, 0) \\
& + \frac{1}{8} [4m(m-2) - Y(m, S)] E_c(2, 2, 1).
\end{aligned}$$

Similarly, fixed- (m, v, S) spectral variances are

$$\begin{aligned}
\langle H^2 \rangle^{m, v, S} &= \frac{1}{24} (m-1)(m-2)(m-3)(m-4) \langle H^2 \rangle^{0,0,0} \\
& - \frac{1}{6} m(m-2)(m-3)(m-4) \langle H^2 \rangle^{1,1,\frac{1}{2}} \\
& + \frac{1}{16\Omega} (m-3)(m-4) [\Omega X(m, S) - 8E_p(m, v, S)] \langle H^2 \rangle^{2,2,0} \\
& + \frac{1}{2\Omega} (m-3)(m-4) E_p(m, v, S) \langle H^2 \rangle^{2,0,0} \\
& + \frac{1}{16} (m-3)(m-4) [3m(m-2) + 4\mathcal{S}^2] \langle H^2 \rangle^{2,2,1} \\
& - \frac{(m-2)(m-4)}{12(\Omega-1)} [(\Omega-1)X(m, S) - 12E_p(m, v, S)] \langle H^2 \rangle^{3,3,\frac{1}{2}} \\
& - \frac{1}{\Omega-1} (m-2)(m-4) E_p(m, v, S) \langle H^2 \rangle^{3,1,\frac{1}{2}} \tag{3.3.4} \\
& - \frac{1}{12} (m-2)(m-4) [m(m-4) + 4\mathcal{S}^2] \langle H^2 \rangle^{3,3,\frac{3}{2}} \\
& + \frac{1}{192(\Omega-2)(\Omega-1)} \left[96 \{E_p(m, v, S)\}^2 + 24 \{-(\Omega-1)m^2 + 2(\Omega+1)m \right. \\
& + 4(\Omega-1)\mathcal{S}^2 - 4(\Omega+2)\} E_p(m, v, S) \\
& + (\Omega-1)(\Omega-2)X(m, S)Y(m, S) \left. \right] \langle H^2 \rangle^{4,4,0} \\
& + \frac{1}{8\Omega(\Omega-2)} E_p(m, v, S) \\
& \times [\Omega \{m(m-2) - 4\mathcal{S}^2 + 8\} - 8 \{E_p(m, v, S) + m - 2\}] \langle H^2 \rangle^{4,2,0}
\end{aligned}$$

$$\begin{aligned}
& + \frac{1}{2\Omega(\Omega-1)} E_p(m, v, S) \{E_p(m, v, S) + m - \Omega - 2\} \langle H^2 \rangle^{4,0,0} \\
& + \frac{[3m(m-6) + 4\mathcal{S}^2 + 24]}{128(\Omega-2)} \\
& \times [(\Omega-2)X(m, S) - 16E_p(m, v, S)] \langle H^2 \rangle^{4,4,1} \\
& + \frac{1}{8(\Omega-2)} E_p(m, v, S) [3m(m-6) + 4\mathcal{S}^2 + 24] \langle H^2 \rangle^{4,2,1} \\
& + \frac{1}{384} [16(\mathcal{S}^2)^2 + 40m^2 \mathcal{S}^2 - 240m \mathcal{S}^2 + 288\mathcal{S}^2 \\
& + 5m(m-2)(m-4)(m-6)] \langle H^2 \rangle^{4,4,2}.
\end{aligned}$$

Using EGOE(1+2)-s computer codes, it is easy to construct, even for large Ω values, the input averages $\langle H \rangle^{m,v,S}$, $m \leq 2$ for centroids and $\langle H^2 \rangle^{m,v,S}$, $m \leq 4$ for variances propagation. For a 100 member ensemble with $\Omega = 12$ and m changing from 8 to 12, we have calculated, for three lowest spins (i.e., for even m , with $S = 0, 1$ and 2 and odd m with $S = \frac{1}{2}, \frac{3}{2}$ and $\frac{5}{2}$), the ensemble averaged variances using Eq. (3.3.4). We use the EGOE(1+2)-s Hamiltonian defined by Eq. (2.2.1) with $\lambda = 0.3$. The ensemble averaged centroids do not change with ‘v’ as expected and therefore we will discuss the structure of variances. The results are shown in Fig. 3.3. It is observed that as the ‘v’ value increases from $2S$ to m , there is decrease in the variances. However the dimensions increase as ‘v’ increases. For example, for $S = 0$ and $m = 10$ the widths and dimensions are $(\sigma, D) = (20.93, 1), (18.6, 77), (17, 1638), (16, 14014), (15.44, 55055)$, and $(15.17, 99099)$ for $v = 0, 2, \dots, 10$. The decrease in variances with increasing ‘v’ is necessary for the gs to be dominated by $v = 0$, i.e., by pairing structure. As we shall discuss later, this indeed happens. Going beyond the averages, we have also calculated the variation over the ensemble for both centroids and variances as they will give information about fluctuations and ergodicity [Br-81, Be-01a, Ko-07]. We have calculated the ensemble variances for these, say $\mathcal{V}^2[E_c(m, v, S)]$ and $\mathcal{V}^2[\sigma^2(m, v, S)]$, respectively and then the corresponding scaled widths $\Delta_c(m, v, S) = \mathcal{V}[E_c(m, v, S)] / \{\overline{\sigma^2(m, v, S)}\}^{1/2}$ and $\Delta_s(m, v, S) = \mathcal{V}[\sigma^2(m, v, S)] / \overline{\sigma^2(m, v, S)}$. It is observed that Δ_c varies from 5 – 7% for $m = 8$, 7 – 9% for $m = 9$, 8 – 10% for $m = 10$, 9 – 13% for $m = 11$ and 10 – 14% for

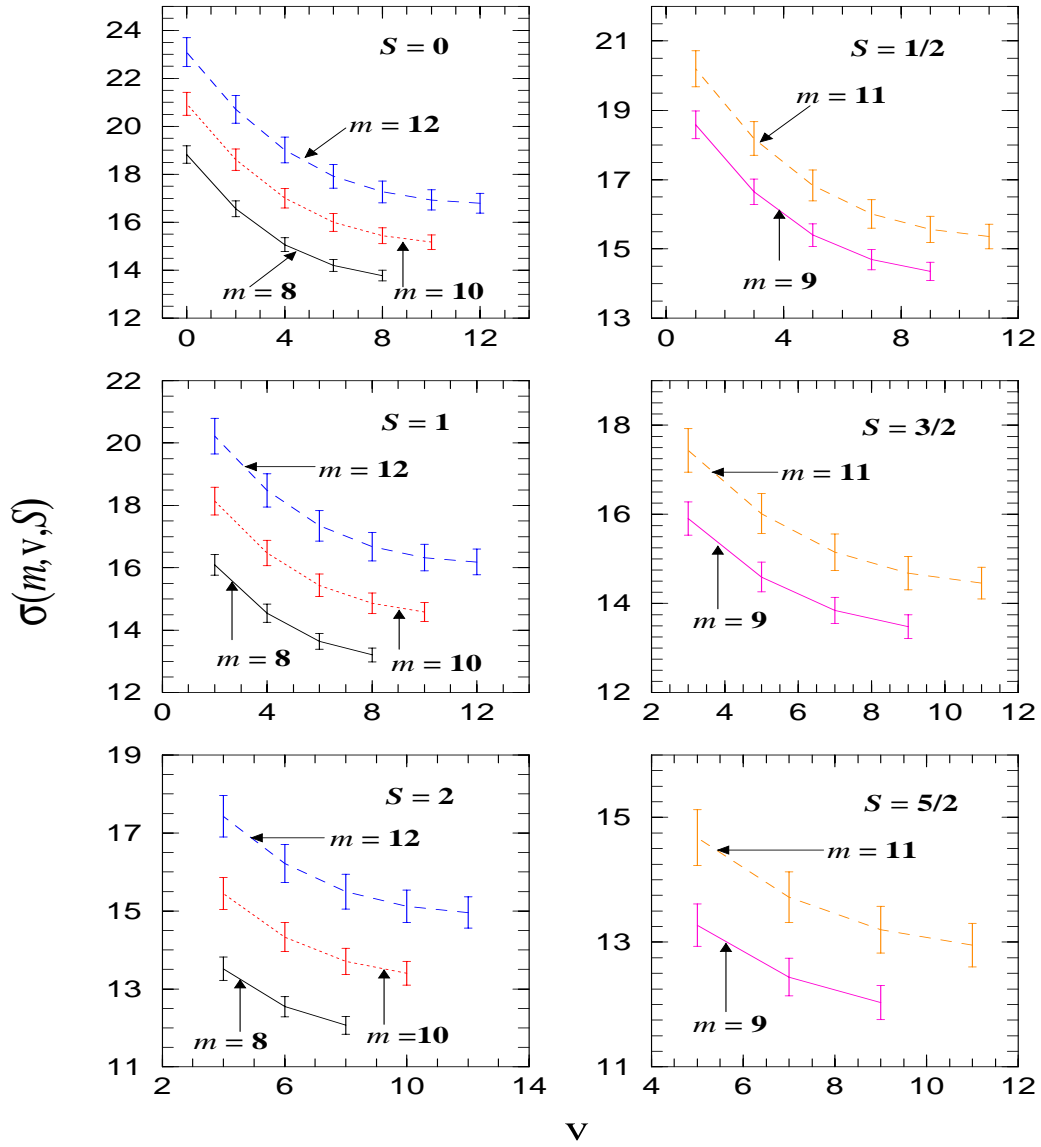


Figure 3.3: Ensemble averaged widths $\sigma(m, v, S)$ vs ' v ' for EGOE(1+2)-s ensembles with $\Omega = 12$ and (m, S) values as given in the figures. Shown also in the figures are the r.m.s. deviations (over the ensemble) in the widths as error bars. For $m = 12$, the results are shifted by one unit to avoid overlapping of the error bars. See text for details.

$m = 12$. Thus centroid fluctuations are large just as the situation with EGOE for spinless fermion systems [Br-81, Be-01a]. However the variance fluctuations, as given by Δ_s are small, $\lesssim 5\%$. Therefore the widths are $\sigma(m, v, S) \sim \left[\overline{\sigma^2(m, v, S)} \right]^{1/2} \{1 \pm \frac{\Delta_s}{2}\}$. In Fig. 3.3 shown also are the fluctuations in widths.

3.4 Expectation Values $\langle PP^\dagger \rangle^E$ of the Pairing Operator as Signature of Chaos

A series of studies in the past, using Gamow-Teller, electric quadrupole and magnetic dipole transition operators, have established that transition strength sums can be considered as a statistic able to distinguish between regular and chaotic motion [Ko-99a, Go-01, Go-03]. Moreover, for EGOE(1+2) for spinless fermions in the strong coupling region, it is well understood that the strength sums vary with the excitation energy as ratio of two Gaussians [Fr-88, Ko-00, Ko-01, Ko-03]. This result was derived using the fact that (proved using the so-called binary correlation approximation) the transition strength densities, transition strengths multiplied by the state densities at the two energies involved, for EGOE(1+2) with $\lambda > \lambda_F$, take bivariate Gaussian form and hence, being the marginal densities, the strength sum densities (see ahead for the definition) will be Gaussian; see Chapter 7 for transition strength densities. It is now well established that the EGOE(1+2) (but not the GOE) provides a good description of strength sums in nuclear shell-model in the chaotic domain [Ko-99a, Go-01, Go-03]. Our interest is in calculating the expectation value of PP^\dagger over fixed- (m, S) spaces, which is a measure of the pairing correlations, and this is nothing but the strength sum for pair removal,

$$\langle PP^\dagger \rangle^{m,S,E} = \langle m, S, E | PP^\dagger | m, S, E \rangle = \sum_{E_f} \left| \langle m-2, S, E_f | P^\dagger | m, S, E \rangle \right|^2. \quad (3.4.1)$$

Recently Horoi and Zelevinsky [Ho-07] re-emphasized, in the context of pairing correlations in nuclei, the importance of $\langle PP^\dagger \rangle^E$ measure. Given a transition operator \mathcal{O} , in terms of the transition strength sum density $\rho_{\mathcal{O}^\dagger \mathcal{O}}(E)$, the expectation value $\langle \mathcal{O}^\dagger \mathcal{O} \rangle^E$ is

$$\langle \mathcal{O}^\dagger \mathcal{O} \rangle^E = \frac{\langle \mathcal{O}^\dagger \mathcal{O} \delta(H-E) \rangle}{\rho(E)} = \langle \mathcal{O}^\dagger \mathcal{O} \rangle \rho_{\mathcal{O}^\dagger \mathcal{O}}(E) / \rho(E). \quad (3.4.2)$$

As stated before, the normalized $\mathcal{O}^\dagger \mathcal{O}$ -density $\rho_{\mathcal{O}^\dagger \mathcal{O}}$ also takes Gaussian form for EGOE(1+2) with $\lambda > \lambda_F$ and it is defined by the centroid $\epsilon_{\mathcal{O}^\dagger \mathcal{O}} = \langle \mathcal{O}^\dagger \mathcal{O} H \rangle / \langle \mathcal{O}^\dagger \mathcal{O} \rangle$ and variance $\sigma_{\mathcal{O}^\dagger \mathcal{O}}^2 = \langle \mathcal{O}^\dagger \mathcal{O} H^2 \rangle / \langle \mathcal{O}^\dagger \mathcal{O} \rangle - \epsilon_{\mathcal{O}^\dagger \mathcal{O}}^2$. Similarly, skewness $\gamma_1(\mathcal{O}^\dagger \mathcal{O})$ and excess $\gamma_2(\mathcal{O}^\dagger \mathcal{O})$ for the $\mathcal{O}^\dagger \mathcal{O}$ -density are defined. The normalization factor $\langle \mathcal{O}^\dagger \mathcal{O} \rangle$ is the aver-

age value of $\mathcal{O}^\dagger \mathcal{O}$ over the complete space [in our examples this is fixed- (m, S) space]. Therefore the ensemble averaged strength sum density reduces to the ratio of two Gaussians or two ED corrected Gaussians [Fr-88, Ko-00, Ko-01, Ko-03],

$$\frac{\langle \mathcal{O}^\dagger \mathcal{O} \rangle^E}{\langle \mathcal{O}^\dagger \mathcal{O} \rangle} \xrightarrow{\text{EGOE}(1+2)} \rho_{\mathcal{O}^\dagger \mathcal{O}; \mathcal{G}}(E) / \rho_{\mathcal{G}}(E) \longrightarrow \rho_{\mathcal{O}^\dagger \mathcal{O}; \text{ED}}(E) / \rho_{\text{ED}}(E). \quad (3.4.3)$$

We will now test how well the EGOE(1+2) theory given by Eq. (3.4.3) extends to systems with spin, i.e., for EGOE(1+2)-s in the strong coupling regime and for the operator $\mathcal{O} = P^\dagger$. Note that in applying Eq. (3.4.3), all the averages and the densities will be over fixed- (m, S) spaces. As $H_p = PP^\dagger$ generates a highly skewed distribution for density of states, a priori it is expected that Eq. (3.4.3) may not be a good statistical formula for $\langle PP^\dagger \rangle^{m, S, E}$. Now we will investigate this using three numerical examples.

Just as in Section 3.3, first we have used the random EGOE(1+2)-s Hamiltonian defined in Eq. (2.2.1) and calculated $\langle PP^\dagger \rangle^{m, S, E}$ for various values of the λ parameter using a 500 member ensemble for 6 fermions ($m = 6$) in 6 orbits ($\Omega = 6$) and total spins $S = 0$ and 1. Results are shown in Fig. 3.4(a). Numerical results are compared with the EGOE(1+2) formula given by Eq. (3.4.3) both with and without ED corrections. For $\lambda = 0.1$, we have $\epsilon_{PP^\dagger} \sim 0$, $|\gamma_1(PP^\dagger)| \sim 0$, $\hat{\sigma}_{PP^\dagger} = \sigma_{PP^\dagger} / \sigma_H \sim 1.07$, $\gamma_2(PP^\dagger) \sim -0.47$ and $\langle PP^\dagger \rangle^{m, S} \sim 1.71$ for $S = 0$. Similarly, for $\lambda = 0.3$, $\gamma_2(PP^\dagger) \sim -0.55$ for $S = 0$ and ~ -0.63 for $S = 1$. Large values of $\gamma_2(PP^\dagger)$ imply that ED corrections are important in the examples considered and this is clearly seen in Fig. 3.4(a). The average value of PP^\dagger follows easily from the centroid formula given by Eq. (3.3.3),

$$\langle PP^\dagger \rangle^{m, S} = \frac{2}{\Omega + 1} \left\{ \frac{m(m+2)}{8} - \frac{S(S+1)}{2} \right\} \quad (3.4.4)$$

and this has been used to verify numerical calculations. As expected, the EGOE(1+2) smoothed form is not a good approximation to the exact results in the case of regular motion. Here there are large fluctuations due to approximate good quantum numbers and the level fluctuations will be close to that of Poisson. However, as λ increases and after the onset of chaos, in our example for $\lambda \gtrsim 0.1$, the interacting particle system is chaotic, giving a smoothed form for pair transfer strength sums (with fluctuations following GOE). This behavior is clearly seen in Fig. 3.4(a). To strengthen

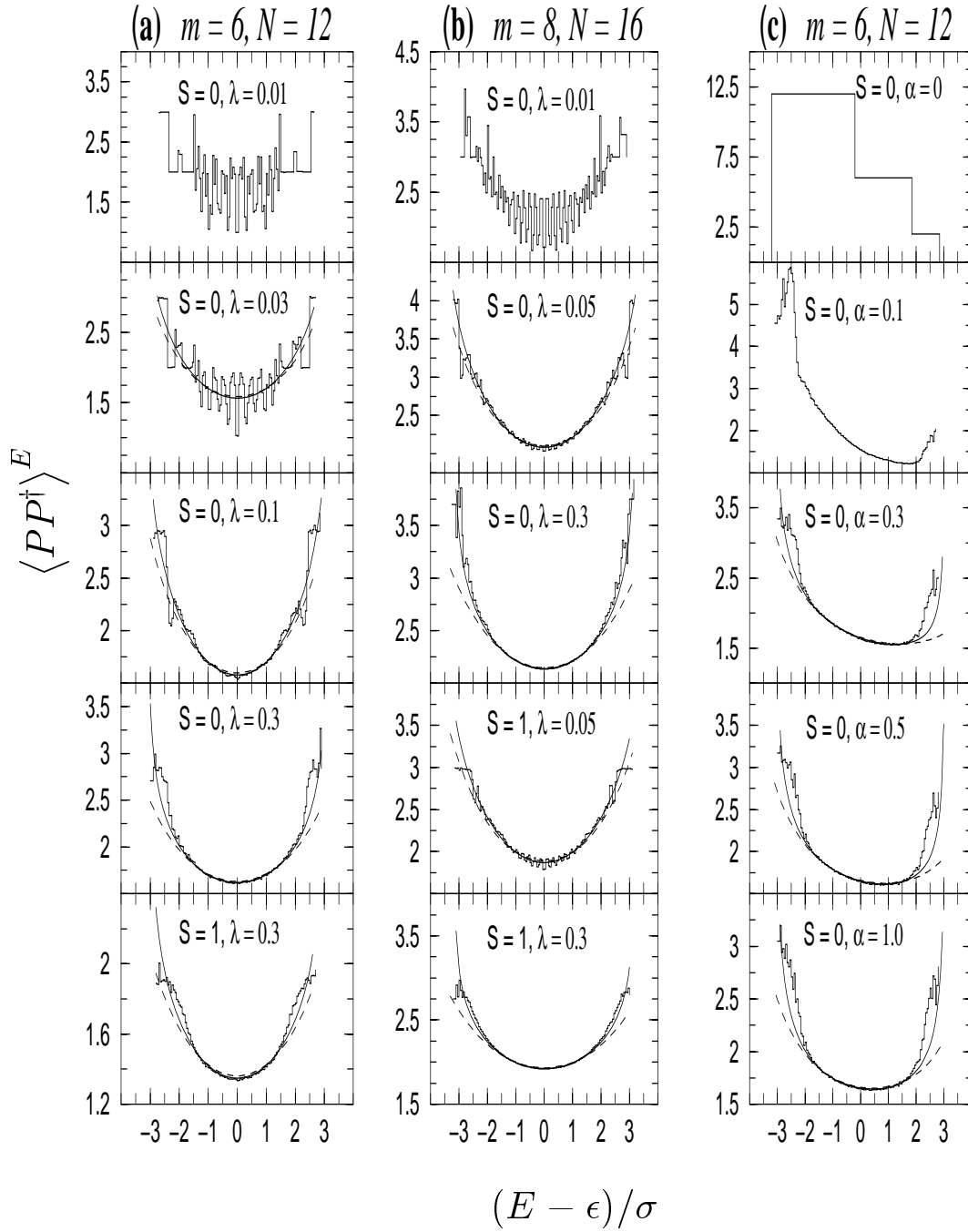


Figure 3.4: Ensemble averaged pairing expectation value $\langle PP^\dagger \rangle^{m,S,E}$ vs E for 3 different EGOE(1+2)-s examples. (a) For various values of λ in Eq. (2.2.1) with $\Omega = m = 6$ and $S = 0, 1$. (b) For various values of λ in Eq. (2.2.1) with $\Omega = m = 8$ and $S = 0, 1$. (c) For various values of α in Eq. (3.4.5) with $\Omega = m = 6$ and $S = 0$. Results are compared with the EGOE(1+2) formula given by Eq. (3.4.3), using Gaussian (dashed curves) and Edgeworth corrected Gaussian (solid curves) forms. The energies E are zero centered with respect to the centroid ϵ and scaled with the width σ of $\rho^{m,S}(E)$. See text for details.

these observations, calculations are repeated for a 50 member EGOE(1+2)-**s** ensemble with $\Omega = m = 8$ and total spins $S = 0$ and 1 . The results are shown in Fig. 3.4(b). In this example, for $\lambda \gtrsim 0.05$ [note that for EGOE(1+2) there is scaling by $\sim 1/(m^2\Omega)$], the EGOE(1+2) form is in good agreement with numerical results. For $\lambda = 0.05$, we have $\epsilon_{PP^\dagger} \sim 0$, $|\gamma_1(PP^\dagger)| \sim 0$, $\hat{\sigma}_{PP^\dagger} \sim 1.06$, $\gamma_2(PP^\dagger) \sim -0.33$ and $\langle PP^\dagger \rangle^{m,S} \sim 2.22$ for $S = 0$. Similarly, $\gamma_2(PP^\dagger) \sim -0.37$ and $\langle PP^\dagger \rangle^{m,S} \sim 2$ for $S = 1$. For $\lambda = 0.3$, we have $\gamma_2(PP^\dagger) \sim -0.44$ for $S = 0$ and ~ -0.47 for $S = 1$. Thus, as seen from Figs. 3.4(a) and 3.4(b), pair expectation values follow, in the chaotic domain the simple EGOE(1+2) law given by Eq. (3.4.3). Also it is seen from the figures that at low energies the pair expectation value is large (but still much smaller than that for the pure pairing Hamiltonian) and then decreases as we go to the center (after that it will again increase as the space is finite). This trend is easily understood from the fact that $\hat{\sigma}_{PP^\dagger} > 1$. Also expectation values in the gs domain for $S = 0$ are always larger than for $S = 1$ and this is consistent with previously known results [Ho-07]. Thus random interactions, even in the chaotic domain, exhibit strong pairing correlations in the gs region and they decrease as we go up in the energy. Perhaps this explains the preponderance of 0^+ ground states seen in nuclear shell-model examples [Ze-04].

Going further, to understand the interplay between random interactions and pairing, calculations are carried out for $\langle PP^\dagger \rangle^{m,S,E}$ using the Hamiltonian,

$$H = \alpha [\{V^{s=0}\} + \{V^{s=1}\}] + [-H_p/\Omega] , \quad (3.4.5)$$

which explicitly contains the pairing part. Here we divide H_p by Ω so that the pairing gap (the gap between $v = 0$ and $v = 2$ states generated by H_p) is unity. Therefore the parameter α in Eq. (3.4.5) is the strength of the random part of the Hamiltonian in units of the pairing gap. Using a 500 member EGOE(1+2)-**s** ensemble, with H given by Eq. (3.4.5), for $\Omega = m = 6$ and $S = 0$, pair transfer strength sums are calculated as a function of energy for various α values. Results are shown in Fig. 3.4(c). For $\alpha = 0$, we have pure pairing Hamiltonian and this generates a staircase function. As the value of the strength of the random part increases to $\alpha > 0.3$, there is a transition to chaotic domain with $\langle PP^\dagger \rangle^{m,S,E}$ vs E taking a smoothed form (fluctuations being small and tending to that of GOE). The smooth behavior observed for $\alpha \geq 0.5$ is explained to

some extent by Eq. (3.4.3). For better description we use an expression (its derivation being straightforward) based on partial (m, v, S)-densities,

$$\langle PP^\dagger \rangle^{m,S,E} = \sum_v \frac{I_{ED}^{m,v,S}(E)}{I_{ED}^{m,S}(E)} \langle PP^\dagger \rangle^{m,v,S}. \quad (3.4.6)$$

Note that the formula for $\langle PP^\dagger \rangle^{m,v,S}$ is given by Eq. (3.2.10) and $I_{ED}^{m,S}(E)$ is sum of $I_{ED}^{m,v,S}(E)$. Following Section 3.3, we have constructed the partial densities appearing in Eq. (3.4.6) as ED corrected Gaussians. The results obtained with these are shown in Fig. 3.4(c). It is seen that the agreements even at the spectrum ends are good (without partitioning the expectation values are found to be much larger than the exact results). It can be concluded from Fig. 3.4(c) that for α of the order 0.5 times the pairing gap, pairing effects get washed out and the structure of the expectation values is well explained by the EGOE(1+2) smoothed formula (3.4.6). It is plausible that unlike Eq. (3.4.3) that has worked well for the Hamiltonian defined by Eq. (2.2.1), the partitioned version given by Eq. (3.4.6) should be used for the Hamiltonian defined by Eq. (3.4.5) as this explicitly involves H_p , i.e., a regular part (as already discussed, H_p produces highly skewed density of states).

Partial densities give information about the composition, in terms of the ‘ v ’ quantum number, of the wavefunctions for a given E . Note that $f(v) = I_{ED}^{m,v,S}(E)/I_{ED}^{m,S}(E)$ gives the fractional intensity of states with a given ‘ v ’ in the eigenstate with energy E ; see Eqs. (3.3.1) and (3.3.2). For the Hamiltonian in Eq. (3.4.5) with $\alpha = 0.3$, for $\hat{E} = -3$, the $f(v)$ for $v = 0, 2, 4$ and 6 are 16%, 34%, 33%, and 17%, respectively. However for the random Hamiltonian given by Eq. (2.2.1) with $\lambda = 0.3$, the $f(v)$ values are 7%, 33%, 42%, and 18%. Thus in the gs domain, although the pair expectation values are enhanced (see Fig. 3.4), the wavefunctions have relatively small strength for $v = 0$ states, i.e., they are not close to pure H_p eigenstates. This result is consistent with the nuclear shell-model results with random interactions, possessing J -symmetry, presented in [Zh-04]. Thus, some essential features of EGOE(1+2)- J are reproduced by EGOE(1+2)-s.

3.5 Distribution of $\Delta_2 = E_{gs}^{(m+1)} + E_{gs}^{(m-1)} - 2 E_{gs}^{(m)}$ With Pairing and Exchange Interactions

3.5.1 Brief introduction to mesoscopic systems

Mesoscopic systems are intermediate between microscopic systems (like nuclei and atoms) and macroscopic bulk matter. Quantum dots and ultrasmall metallic grains are good examples of mesoscopic systems whose transport properties can be measured [Im-97, Ja-01a]. When the electron's phase coherence length is comparable to or larger than the system size, the system is called mesoscopic. As the electron phase is preserved in mesoscopic systems, these are ideal to observe new phenomenon governed by the laws of quantum mechanics not observed in macroscopic conductors. Also, the transport properties of mesoscopic systems are readily measured with almost all system parameters (like the shape and size of the system, number of electrons in the system and the strength of coupling with the leads) under experimental control. The phase coherence length increases rapidly with decreasing temperature. For system size $\sim 100 \mu\text{m}$, the system becomes mesoscopic below $\sim 100 \text{ mK}$.

Quantum dots are artificial devices obtained by confining a finite number of electrons to regions with diameter $\sim 100 \text{ nm}$ by electrostatic potentials. Typically it consists of 10^9 real atoms but the number of mobile electrons is much lower, ~ 100 . Their level separation is $\sim 10^{-4} \text{ eV}$. If the transport in the quantum dot is dominated by electron scattering from impurities, the dot is said to be diffusive and if the transport is dominated by electron scattering from the structure boundaries, then dot is called ballistic. The coupling between a dot and its leads is experimentally controllable. When the dot is strongly coupled to the leads, the electron motion is classical and the dot is said to be open. In isolated or closed quantum dots, the coupling is weak and conductance occurs only by tunneling. Also the charge on the closed dot is quantized and they have discrete excitation spectrum. The tunneling of an electron into the dot is usually blocked by the classical Coulomb repulsion of the electrons already in the dot. This phenomenon is called Coulomb blockade. This repulsion can be overcome by changing the gate voltage. At appropriate gate voltage, the charge on the dot will fluctuate between m and $m+1$ electrons giving rise to a peak in the conductance. The

oscillations in conductance as a function of gate voltage are called Coulomb blockade oscillations. At sufficiently low temperatures, these oscillations turn into sharp peaks. In Coulomb blockade regime $kT \ll \Delta \ll E_c$, the tunneling occurs through a single resonance in the dot. Here, T is the temperature, Δ is the mean single particle level spacing and E_c is the charging energy. Ultrasmall metallic grains are small pieces of metals of size $\sim 2 - 10$ nm. The level separation for nm-size metallic grains is smaller than in quantum dots of similar size and thus experiments can easily probe the Coulomb blockade regime in quantum dots. Also, some of the phenomena observed in nm-size metallic grains are strikingly similar to those seen in quantum dots suggesting that quantum dots are generic systems for exploring physics of small coherent structures [Gu-98, Al-00a].

Although the quantum dots contain many electrons, their properties cannot be obtained by using thermodynamic limit. The description of transport through a quantum dot at low temperatures in terms of local material constants breaks down and the whole structure must be treated as a single coherent entity. The quantum limits of electrical conduction are revealed in quantum dots and conductivity exhibits statistical properties which reflect the presence of one-body chaos, quantum interference and electron-electron interaction. The transport properties of a quantum dot can be measured by coupling it to leads and passing current through the dot. The conductance through the dots displays mesoscopic fluctuations as a function of gate voltage, magnetic field and shape deformation. The techniques used to describe these fluctuations include semiclassical methods, random matrix theory and supersymmetric methods [Al-00a].

Mesoscopic fluctuations are universal dictated only by a few basic symmetries of the system. It is now widely appreciated that the universal conductance fluctuations are intimately related to the universal statistics of finite isolated quantum systems whose classical analogs are chaotic [Ko-01, Ko-03, Pa-07]. In describing transport through these coherent systems, we are interested in quantum manifestations of classical chaos. Scattering of electrons from impurities or irregular boundaries leads to single particle dynamics that are mostly chaotic. RMT describes the statistical fluctuations in the universal regime i.e., at energy scales below the Thouless energy $E = g\Delta$, g is the Thouless conductance. In this universal regime RMT addresses questions

about statistical behavior of eigenvalues and eigenfunctions rather than their individual description. We consider a closed mesoscopic system (quantum dot or small metallic grain) with chaotic single particle dynamics and with large Thouless conductance g . Such a structure is described by an effective Hamiltonian which comprises of a mean field and two-body interactions preserving spin degree of freedom. For chaotic isolated mesoscopic systems, randomness of single particle energies leads to randomness in effective interactions that are two-body in nature. Hence it is important to invoke the ideas of embedded ensembles to understand and also predict properties of these systems theoretically.

A realistic Hamiltonian for mesoscopic systems conserves total spin S and therefore includes a mean field one-body part, (random) two-body interaction, pairing H_p and exchange interaction \hat{S}^2 . In order to obtain physical interpretation of the \hat{S}^2 operator, we consider the space exchange or the Majorana operator M that exchanges the spatial coordinates of the particles and leaves the spin unchanged, i.e.,

$$M|i, \alpha; j, \beta\rangle = |j, \alpha; i, \beta\rangle. \quad (3.5.1)$$

In Eq. (3.5.1), labels i, j and α, β , respectively denote the spatial and spin labels. As the embedding algebra for EGOE(1+2)-s is $U(2\Omega) \supset U(\Omega) \otimes SU(2)$ and $|i, \alpha; j, \beta\rangle = (a_{i,\alpha}^\dagger a_{j,\beta}^\dagger)|0\rangle$, we have

$$2M = C_2[U(\Omega)] - \Omega \hat{n}. \quad (3.5.2)$$

In Eq. (3.5.2), $C_2[U(\Omega)] = \sum_{i,j,\alpha,\beta} a_{i,\alpha}^\dagger a_{j,\alpha} a_{j,\beta}^\dagger a_{i,\beta}$ is the quadratic Casimir invariant of the $U(\Omega)$ group,

$$C_2[U(\Omega)] = \hat{n}(\Omega + 2) - \frac{\hat{n}^2}{2} - \hat{S}^2. \quad (3.5.3)$$

Combining Eqs. (3.5.2) and (3.5.3), we have finally

$$M = -\hat{S}^2 - \hat{n} \left(\frac{\hat{n}}{4} - 1 \right). \quad (3.5.4)$$

Therefore, the interaction generated by the \hat{S}^2 operator is the exchange interaction with a number dependent term. This number dependent term becomes important when the particle number m changes. The H operator for isolated mesoscopic sys-

tems in universal regime has the form (with λ_p and λ_s being positive),

$$\{\hat{H}(\lambda_0, \lambda_1, \lambda_p, \lambda_s)\} = \hat{h}(1) + \lambda_0 \{\hat{V}^{s=0}(2)\} + \lambda_1 \{\hat{V}^{s=1}(2)\} - \lambda_p H_p - \lambda_s \hat{S}^2. \quad (3.5.5)$$

The constant part arising due to charging energy E_c that depends on the number of fermions in the system can be easily incorporated in our model when required. For more details on two-body ensembles and mesoscopic systems see [Gu-98, Al-00a, Ko-01, Mi-00]. Before proceeding further, it is important to mention that, with the analytical formula for the propagator $P(\Omega, m, S)$ given by Eq. (2.3.12), EGOE(1+2)-s generates odd-even staggering in gs energies and also explains preponderance of gs with spin 0 (m even) for mesoscopic systems in a simple way. In other words, random interaction disfavor magnetized ground states; see Fig. 2.2. It is important to mention that even with the best available computing facilities, it is not yet feasible to numerically study the properties of large systems ($\Omega \gg 10$) modeled by EGOE(1+2)-s. As the minimum spin gs is favored by random interactions, the Stoner transition will be delayed in presence of a strong random two-body part in the Hamiltonian. The standard Stoner picture of ferromagnetism in itinerant systems is based on the competition between one-body kinetic energy [$h(1)$ in Eq. (3.5.5)] and the exchange interaction (\hat{S}^2). The probability $P(S > 0)$ for the gs to be with $S > 0$ (for m even) is studied as a function of λ in Eq. (3.5.5) with $\lambda_p = 0$ and the results are given in Fig. 3.5. Thus EGOE(1+2)-s also explains the strong bias for low-spin ground states and the delayed gs magnetization by random two-body interactions.

3.5.2 Conductance peak spacing (Δ_2) distribution

Coulomb blockade oscillations yield detailed information about the energy and wavefunction statistics of mesoscopic systems. We consider a closed mesoscopic system and study the distribution $P(\Delta_2)$ of spacing Δ_2 between two neighboring conductance peaks at temperatures less than the average level spacing. Also our focus is in the strong interaction regime [$\lambda_0 = \lambda_1 = \lambda \geq 0.3$ in Eq. (3.5.5)] and we use fixed sp energies ϵ_i . The spacing Δ_2 between the peaks in conductance as a function of the gate voltage for $T \ll \Delta$ is second derivative of gs energies with respect to the number

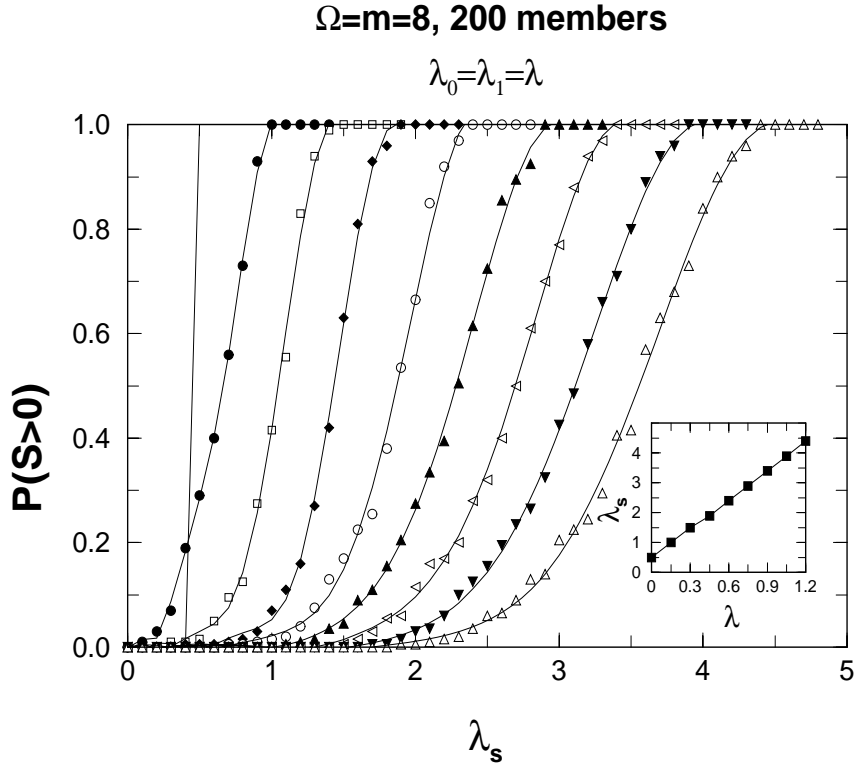


Figure 3.5: Probability $P(S > 0)$ for ground states to have $S > 0$ as a function of exchange interaction strength λ_s for $\lambda = 0$ to 1.2 in steps of 0.15 ; used here is $\hat{H}(\lambda, \lambda, 0, \lambda_s)$ defined by Eq. (3.5.5). The calculations are for 200 member EGOE(2)-s ensemble with $\Omega = m = 8$. Inset of figure shows the minimum exchange interaction strength λ_s required for the ground states to have $S > 0$ with 100% probability as a function of λ . It is seen from the results that the probability $P(S > 0)$ for gs to have $S > 0$ is very small when $\lambda > \lambda_s$ and it increases with increasing λ_s . The results clearly bring out the demagnetizing effect of random interaction. Similar calculations have been performed in the past for smaller systems with $\Omega = m = 6$ [Ko-06, Ja-01].

of particles,

$$\Delta_2 = E_{gs}^{(m+1)} + E_{gs}^{(m-1)} - 2 E_{gs}^{(m)}. \quad (3.5.6)$$

In Eq. (3.5.6), $E_{gs}^{(m)}$ is the gs energy for a m fermion system. The distribution $P(\Delta_2)$ has been used in the study of the distribution of conductance peak spacings in chaotic quantum dots [Al-05, Al-00, Al-01, Al-01a].

Let us first consider non-interacting spinless finite Fermi systems i.e., $H = h(1)$ and say the sp energies are ϵ_i ; $i = 1, 2, \dots, N$. Then Eq. (3.5.6) gives, by applying Pauli principle, $\Delta_2 = \epsilon_{m+1} - \epsilon_m$, irrespective of whether m is even or odd. For chaotic systems it is possible to consider sp energies drawn from GOE eigenvalues [Al-05, Al-00, Al-01, Al-01a]. Therefore $P(\Delta_2)$ corresponds to GOE spacing distribution $P_W(\Delta_2)$

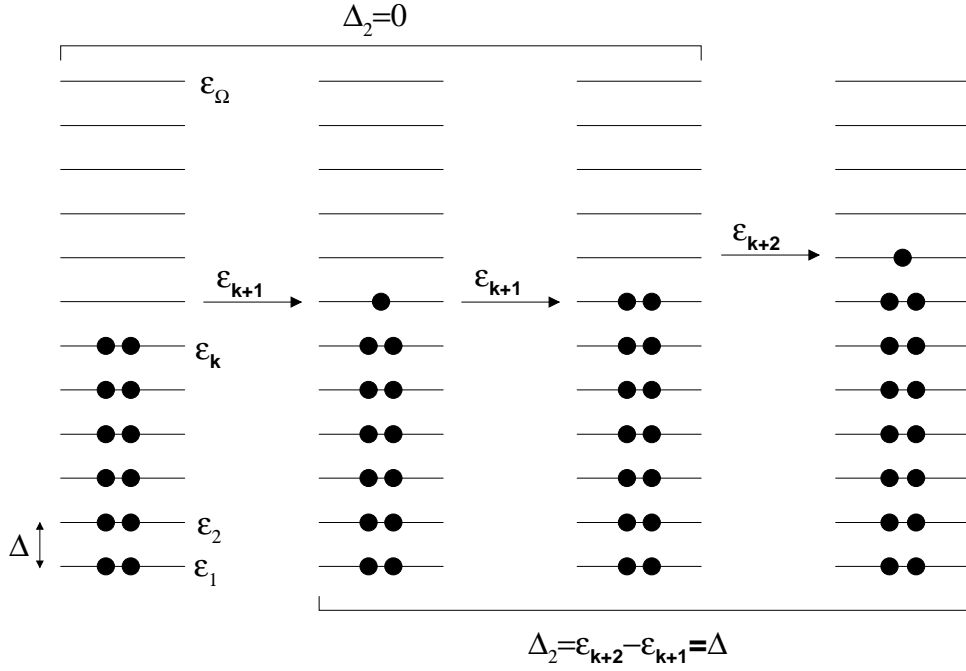


Figure 3.6: Figure showing Δ_2 values for systems with spin degree of freedom. For even-odd-even transitions, $\Delta_2 = 0$ and for odd-even-odd transitions, $\Delta_2 = \Delta$. See text for details.

- the Wigner distribution. However recent experiments showed that $P(\Delta_2)$ is a Gaussian in many situations [Pa-98]. This calls for inclusion of two-body interactions and hence the importance of EGOE(1+2) (in [Al-00, Al-01, Al-01a] this is called RIMM) in the study of conductance fluctuations in mesoscopic systems. It was shown by Alhassid et al [Al-00, Al-01, Al-01a] that EGOE(1+2) indeed generates Gaussian form for $P(\Delta_2)$.

As discussed in Sec. 3.5.1, Hamiltonian for interacting electron systems conserves total spin S and thus it is important to consider sp levels that are doubly degenerate; i.e., spin degree of freedom should be included in H . Again, we start with non-interacting finite Fermi systems with sp energies ϵ_i , $i = 1, 2, \dots, \Omega$ and drawn from a GOE; total number of sp states $N = 2\Omega$. In this scenario Δ_2 depends on whether m is odd or even. For m odd, say $m = 2k + 1$, the $(m - 1)$ fermion gs energy $E_{gs}^{(m-1)} = 2 \sum_{i=1}^k \epsilon_i$, $E_{gs}^{(m)} = E_{gs}^{(m-1)} + \epsilon_{k+1}$ and $E_{gs}^{(m+1)} = E_{gs}^{(m-1)} + 2 \epsilon_{k+1}$ resulting in $\Delta_2 = 0$. Similar analysis for even $m = 2k$ yields $\Delta_2 = \epsilon_{k+1} - \epsilon_k$; note that $E_{gs}^{(m)} = 2 \sum_{i=1}^k \epsilon_i$, $E_{gs}^{(m-1)} = E_{gs}^{(m)} - \epsilon_k$ and $E_{gs}^{(m+1)} = E_{gs}^{(m)} + \epsilon_{k+1}$. For odd m , Δ_2 corresponds to even-odd-even transition and $P(\Delta_2)$ is a delta function. For even m , we have odd-even-odd transitions with $P(\Delta_2)$ following Wigner distribution. Figure 3.6 gives a pictorial illus-

tration for Δ_2 calculation for systems with spin. Therefore, by applying Pauli principle and using Eq. (3.5.6) gives $\Delta_2 = 0$ for m odd and $\Delta_2 = \epsilon_{k+1} - \epsilon_k$ for even m ($k = m/2$). As we need to include, for real systems, both even and odd m 's, inclusion of spin degree of freedom gives bimodal distribution for $P(\Delta_2)$,

$$P(\Delta_2) = \frac{1}{2} [\delta(\Delta_2) + P_W(\Delta_2)] . \quad (3.5.7)$$

Convolution of this bimodal form with a Gaussian has been used in the analysis of data for quantum dots obtained for situations that correspond to weak interactions [Lu-01]. This shows that spin degree of freedom and pairing correlations are important for mesoscopic systems. Hence, it is imperative to study $P(\Delta_2)$ with a Hamiltonian that includes mean field one-body part, (random) two-body interaction, exchange interaction and pairing (defined by H_p). Therefore we have carried out EGOE(1+2)-s calculations using the Hamiltonian given in Eq. (3.5.5) (with λ_p and λ_s being positive) and constructed $P(\Delta_2)$ by combining Δ_2 values obtained for both even and odd m values. Before discussing these model calculations let us mention that very recently, for small metallic grains, $P(\Delta_2)$ results are reported in [Sc-08]. These authors use a H consisting of pairing and exchange interactions just as in Eq. (3.5.5) but with sp energies of $h(1)$ drawn from GOE and a two-body interaction that is a function of m . More importantly a microscopic theory is used in [Sc-08] to construct $P(\Delta_2)$ at finite temperatures. When the pairing interaction is dominant (compared to exchange interaction), the distribution is found to be bimodal whereas the distribution becomes unimodal for strong exchange interaction. Following our discussion in the previous sections, here we present results for the distribution of Δ_2 defined by Eq. (3.5.6) with two values for m and using H defined by Eq. (3.5.5). We use fixed $h(1)$ as in the previous sections and $\lambda = 0.3$. Therefore our focus is in the strong interaction regime. Though our calculations are restrictive and the model is simpler, we will show that they reproduce all the essential features of $P(\Delta_2)$ reported in [Sc-08].

Using 1000 member EGOE(1+2)-s with H defined by Eq. (3.5.5), gs energies are calculated for $\lambda = 0.3$ and for various values of λ_p and λ_s by diagonalizing the Hamiltonian in good spin basis for $\Omega = 6$ and $m = 3, 4, 5$ and 6. Then Δ_2 is computed using Eq. (3.5.6) for $m = 4$ and 5 and combining these, normalized histograms for $P(\Delta_2)$

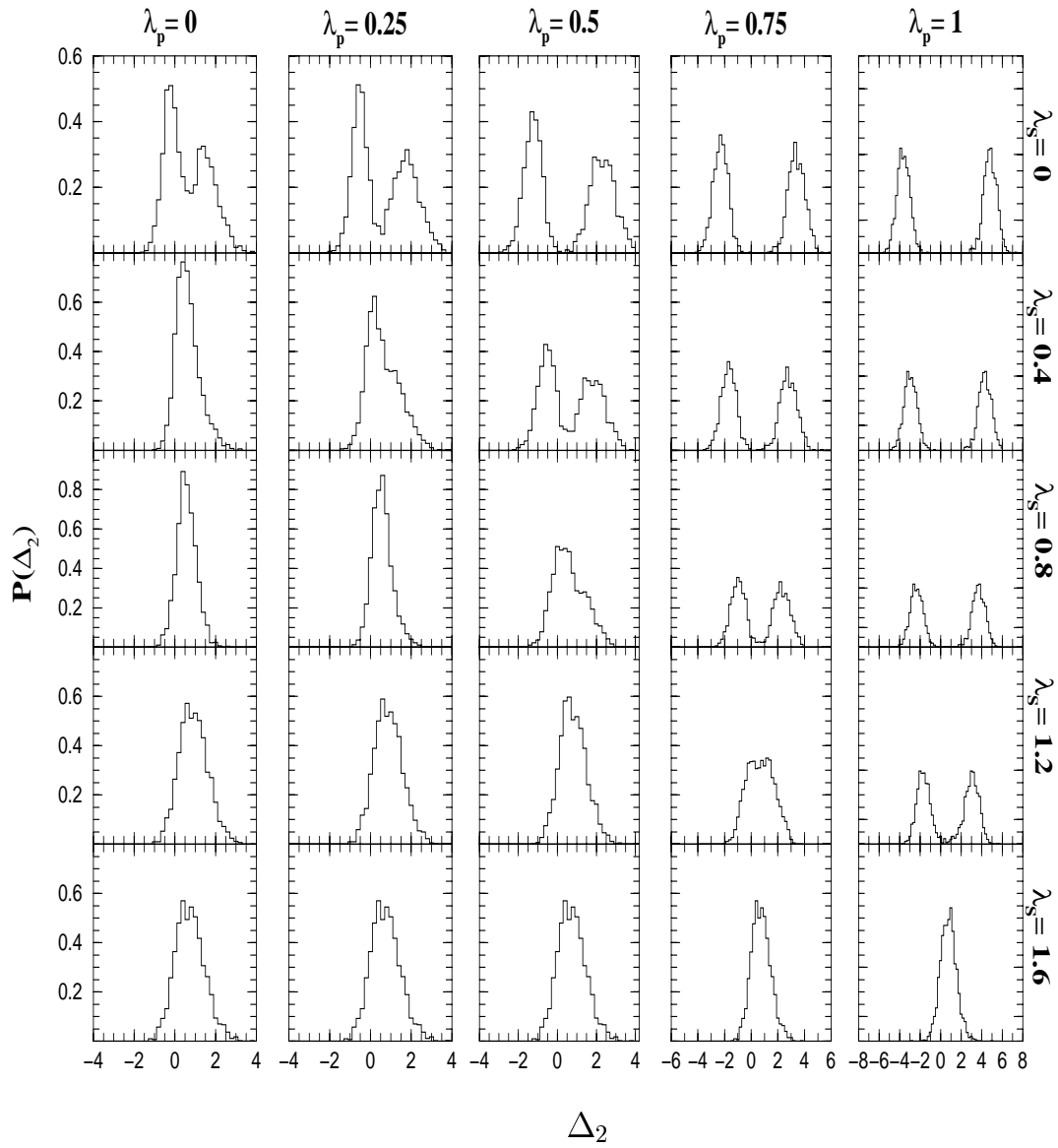


Figure 3.7: $P(\Delta_2)$ vs Δ_2 for various values of the pairing strength λ_p and exchange interaction strength λ_s for the EGOE(1+2)-**s** system defined in the text. The distributions $P(\Delta_2)$ are constructed (with bin size 0.2) by combining the results for Δ_2 with $m = 4$ and 5. See text for further details.

are constructed. Results in Fig. 3.7 show that strong pairing correlations ($\lambda_s = 0$) give rise to bimodal form for $P(\Delta_2)$ with the two modes well separated. Increasing the exchange interaction reduces the separation between the two parts and they overlap when exchange interaction is dominant and pairing is weak. In other words, pairing correlations help distinguish between m even and m odd in Eq. (3.5.6). These conclusions are close to the results in Fig. 1 of [Sc-08]. A qualitative understanding of these results follows from the centroids $\langle \Delta_2 \rangle$ of $P(\Delta_2)$ for each m generated by H_p

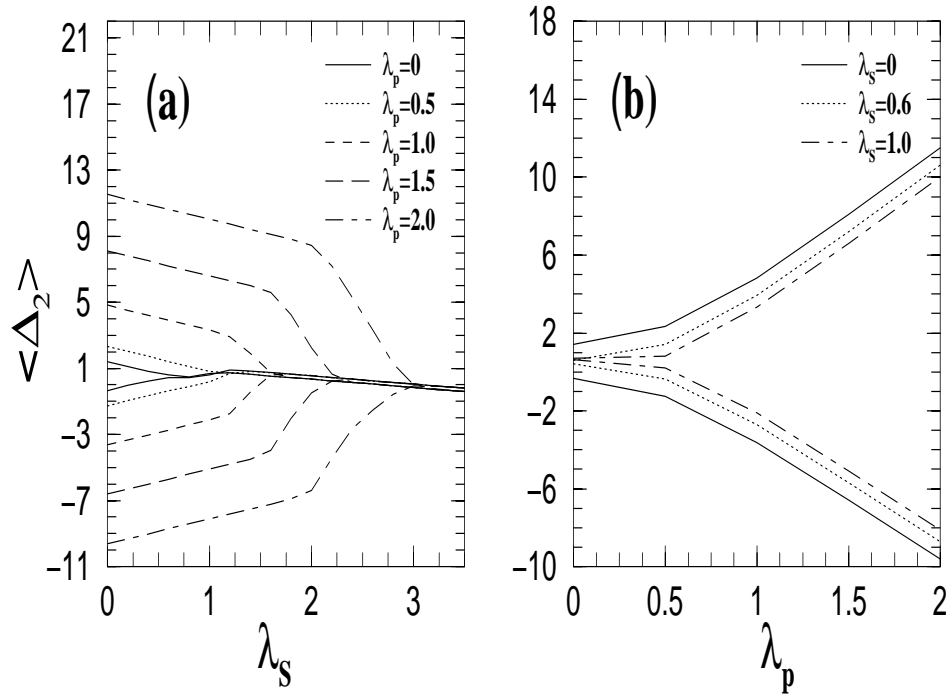


Figure 3.8: Average peak spacing $\langle \Delta_2 \rangle$ (a) as a function of exchange interaction strength λ_S for several values of pairing strength λ_p and (b) as a function of λ_p for several values of λ_S , for a 1000 member ensemble with $\Omega = 6$. The curves in the upper part correspond to $m = 4$ ($3 \rightarrow 4 \rightarrow 5$) and those in the lower part to $m = 5$ ($4 \rightarrow 5 \rightarrow 6$) in Eq. (3.5.6). See text for details.

and \hat{S}^2 terms in H . When pairing is relatively stronger ($\lambda_p \gg \lambda_S$), gs has minimum spin and thus $v = 0(1)$ for m even(odd) and when pairing is weaker ($\lambda_S \gg \lambda_p$), gs has maximum spin ($S = m/2$) and thus $v = m$. Using the pairing eigenvalues $E_p(m, v, S)$ given by Eq. (3.2.10), it is easily seen that for weak pairing, $\langle \Delta_2 \rangle = -\lambda_S/2$ for both m even and odd and for strong pairing, $\langle \Delta_2 \rangle = (\Omega + 1)\lambda_p - 3/2\lambda_S$ and $-\Omega\lambda_p + 3/2\lambda_S$ for even m and odd m , respectively. Therefore, for fixed λ_S , spacing between the peaks for $m = 4$ and $m = 5$ increases with sufficiently large λ_p values as seen in Fig. 3.7.

Figure 3.8(a) shows the variation of average peak spacing with exchange interaction strength λ_S for several λ_p values. The curves in the upper part correspond to $m = 4$ and those in the lower part to $m = 5$. As the exchange strength increases, the average peak spacing $\langle \Delta_2 \rangle$ is almost same for odd-even-odd and even-odd-even transitions. Value of average peak spacing and its variation with λ_S is different for odd-even-odd and even-odd-even transitions when pairing correlations are strong. The curve for fixed value of λ_p can be divided into two linear regions whose slopes can be determined considering only exchange interactions i.e., $E_{gs} = C_0 - \lambda_S S(S+1)$. For weak exchange interaction strength, gs spin is $0(1/2)$ for m even(odd) and thus

for this linear region, $\langle \Delta_2 \rangle / \lambda_S \propto -3/2(3/2)$. The linear region where exchange interactions are dominant, $\langle \Delta_2 \rangle / \lambda_S \propto -1/2$ as gs spin is $m/2$. Figure 3.8(b) shows the variation of average peak spacing with pairing strength for several λ_S values. It clearly shows that the separation between the distributions becomes larger with increasing λ_p . These results are in good agreement with the numerically obtained results for the $P(\Delta_2)$ variation as a function of λ_p and λ_S in Fig. 3.7. Thus, EGOE(1+2)-s with H defined in Eq. (3.5.5) explains the interplay between exchange (favoring ferromagnetism) and pairing (favoring superconductivity) interaction in the Gaussian domain as expected in mesoscopic systems and can be used for investigating transport properties of mesoscopic systems.

3.6 Summary

Going beyond the results reported in Chapter 2 for the random matrix ensemble EGOE(1+2)-s, in the present chapter, further results are presented with focus on pairing correlations. Firstly, in the space defined by EGOE(1+2)-s ensemble, pairing symmetry defined by the algebra $U(2\Omega) \supset Sp(2\Omega) \supset SO(\Omega) \otimes SU_S(2)$ is identified and some of its properties are discussed. Using numerical calculations it is shown that in the strong coupling limit, partial densities defined over pairing subspaces are close to Gaussian form and propagation formulas for their centroids and variances are derived. As a part of understanding pairing correlations in finite Fermi systems, we have shown that pair transfer strength sums (used in nuclear structure) as a function of excitation energy (for fixed S), a statistic for onset of chaos (used in nuclei [Ho-07]), follows, for low spins, the form derived for spinless fermion systems i.e., it is close to a ratio of Gaussians. This is demonstrated using three detailed examples. Going further, we have considered a quantity in terms of gs energies, giving conductance peak spacings in mesoscopic systems at low temperatures, and studied its distribution over EGOE(1+2)-s by including both pairing and exchange interactions. We have shown that the random matrix model reproduces the main results that are observed recently in a realistic calculation for small metallic grains. Finally, results reported in this chapter establish that EGOE(1+2)-s can be used as a random matrix model for studying pairing correlations in finite quantum systems.

Chapter 4

EGUE(2)- $SU(4)$: Group Theoretical Results

4.1 Introduction

Spin-isospin $SU(4)$ supermultiplet scheme for nuclei was introduced by Wigner [Wi-37] and there is good evidence for the goodness of this symmetry in some parts of the nuclear chart [Pa-78, Va-95, Na-01, Va-05, Ko-07a, Va-99, Va-07] and also more recently there is new interest in $SU(4)$ symmetry for heavy $N \sim Z$ nuclei [Va-95, Na-01, Va-05, Ko-07a]. Therefore, it is important to define and study EGE's generated by random two-body interactions with $SU(4)$ symmetry [EGUE(2)- $SU(4)$]. Given m fermions (nucleons) in Ω number of sp orbitals with spin and isospin degrees of freedom, for $SU(4)$ scalar Hamiltonians, the symmetry algebra is $U(4\Omega) \supset U(\Omega) \otimes SU(4)$ and all the states within an $SU(4)$ [but not $U(\Omega)$] irrep will be degenerate in energy. In the past, applying Wigner-Racah algebra of the embedding algebra $U(2\Omega) \supset U(\Omega) \otimes SU(2)$ some analytical results are derived for EGUE(2)-s; see Appendix C for some details. Going beyond the spin ensemble (discussed in Chapters 2, 3 and Appendix C), our purpose in the present chapter is to define EGUE(2)- $SU(4)$, develop analytical formulation for solving the ensemble and derive analytical formulas, for the lower order moments of the one-point (density of eigenvalues) and two-point (defining level fluctuations) functions, for some simple class of $SU(4)$ irreps. In addition, analytical formulation developed in the chapter allows one to consider all these, numerically, for any $SU(4)$ [or $U(\Omega)$] irrep. Using these, studied are: ensemble averaged spec-

tral variances, expectation values of the quadratic Casimir invariant of $SU(4)$ algebra, four periodicity in the gs energies and lower order cross-correlations in energy centroids and spectral variances generated by this ensemble. Before proceeding further, let us mention that a preliminary report of some of the results in this chapter is given in [Ma-09a] and all the details are published in the long paper [Ma-10b].

4.2 Preliminaries of $U(4\Omega) \supset U(\Omega) \otimes SU(4)$ Algebra

Although all the results in this section are well-known [Pa-78, He-69, He-74a], we will discuss these here for completeness and also for introducing various quantities and notations used in the reminder of the chapter^a.

4.2.1 Generators of $U(\Omega)$ and $SU(4)$ algebras

Let us begin with m fermions distributed in 4Ω number of sp states. Then the spectrum generating algebra is $U(4\Omega)$. Associating two quantum numbers i (i -space) and α (α -space) to each sp state, the sp states are denoted by $|i, \alpha\rangle$, where $i = 1, 2, \dots, \Omega$ and $\alpha = 1, 2, 3, 4$. In nuclear applications, the i -space corresponds to the orbital space and the α -space corresponds to the spin(**s**)-isospin(**t**) space, then $|\alpha\rangle = |m_s, m_t\rangle = |\frac{1}{2}, \frac{1}{2}\rangle, |\frac{1}{2}, -\frac{1}{2}\rangle, |-\frac{1}{2}, \frac{1}{2}\rangle$ and $|-\frac{1}{2}, -\frac{1}{2}\rangle$, respectively. From now on in this section we will present results both in single state representation defined by $|i, \alpha\rangle$ states and also in the spin-isospin representation defined by $|i; \mathbf{s} = \frac{1}{2}, m_s; \mathbf{t} = \frac{1}{2}, m_t\rangle$ states. For the EGUE(2)- $SU(4)$ ensemble, the former will suffice. However the later (spin-isospin) representation is useful for understanding the physical relevance of the ensemble. In the single state representation, the $(4\Omega)^2$ number of operators $C_{i\alpha; j\beta}$ generate $U(4\Omega)$ algebra and with respect to this algebra, all the m fermion states transform as the ir-rep $\{1^m\}$. In terms of the creation operators $a_{i,\alpha}^\dagger$ and the annihilation operators $a_{j,\beta}$, the generators $C_{i\alpha; j\beta}$ and their commutation relations are,

$$C_{i\alpha; j\beta} = a_{i,\alpha}^\dagger a_{j,\beta}; \quad [C_{i\alpha; j\beta}, C_{k\alpha'; l\beta'}] = C_{i\alpha; l\beta'} \delta_{jk} \delta_{\beta\alpha'} - C_{k\alpha'; j\beta} \delta_{li} \delta_{\beta'\alpha}. \quad (4.2.1)$$

It is possible to define commuting unitary transformations in the i -space and α -space separately and then we have $U(\Omega)$ and $U(4)$ algebras describing unitary trans-

^aWe use different notations in this chapter for mathematical ease

formations in the two respective spaces. With this we have the direct product group-subgroup structure $U(4\Omega) \supset U(\Omega) \otimes U(4)$. We can easily write the generators A_{ij} and $B_{\alpha\beta}$ for the $U(\Omega)$ and $U(4)$ algebras, respectively, using the fact that the generators of $U(\Omega)$ are scalars in α -space and similarly the $U(4)$ generators in the i -space,

$$A_{ij} = \sum_{\alpha=1}^4 C_{i\alpha;j\alpha}, \quad B_{\alpha\beta} = \sum_{i=1}^{\Omega} C_{i\alpha;i\beta}. \quad (4.2.2)$$

Their commutation relations can be derived using Eq. (4.2.1) by summing over the appropriate indices,

$$\begin{aligned} [A_{ij}, A_{kl}] &= A_{il}\delta_{jk} - A_{kj}\delta_{li}, \\ [B_{\alpha\beta}, B_{\alpha'\beta'}] &= B_{\alpha\beta'}\delta_{\beta\alpha'} - B_{\alpha'\beta}\delta_{\alpha\beta'}. \end{aligned} \quad (4.2.3)$$

Also the A 's commute with the B 's. Instead of $U(4)$, it is possible to consider $SU(4)$ by making the generators B 's traceless [see Eq. (4.2.11) ahead].

In the orbital \times spin-isospin realization of the $U(4\Omega) \supset U(\Omega) \otimes SU(4)$ algebra, $SU(4)$ corresponds to the Wigner's supermultiplet algebra [Wi-37]. In this physically relevant spin-isospin representation, the $SU(4)$ generators can be written in terms of the one-body operators $\mathcal{A}_{ij;\mu_s,\mu_t}^{s,t}$ where,

$$\begin{aligned} \mathcal{A}_{ij;\mu_s,\mu_t}^{s,t} &= \left(a_i^\dagger \tilde{a}_j \right)_{\mu_s,\mu_t}^{s,t} \\ &= \sum_{m_s(m'_s), m_t(m'_t)} \left\langle \frac{1}{2}m_s \frac{1}{2}m'_s \middle| s \mu_s \right\rangle \left\langle \frac{1}{2}m_t \frac{1}{2}m'_t \middle| t \mu_t \right\rangle a_{i;\frac{1}{2},m_s;\frac{1}{2},m_t}^\dagger \tilde{a}_{j;\frac{1}{2},m'_s;\frac{1}{2},m'_t}. \end{aligned} \quad (4.2.4)$$

Note that $\tilde{a}_{j;\frac{1}{2},\mu_s;\frac{1}{2},\mu_t} = (-1)^{1+\mu_s+\mu_t} a_{j;\frac{1}{2},-\mu_s;\frac{1}{2},-\mu_t}$. The operators $\mathcal{A}_{ij;\mu_s,\mu_t}^{s,t}$ generate $U(4\Omega)$ algebra. Similarly, the operators $\mathcal{A}_{ij}^{0,0}$ (Ω^2 in number) and $\sum_i \mathcal{A}_{ii;\mu_s,\mu_t}^{s,t}$ (16 in number) generate the $U(\Omega)$ and $U(4)$ algebras, respectively. The 16 generators of $U(4)$ can be written in terms of the number operator \hat{n} , the three spin generators S_μ^1 , the three isospin generators T_μ^1 and the nine components $(\sigma\tau)_{\mu,\mu'}^{1,1}$ of the Gamow-Teller operator $\sigma\tau$. Dropping the number operator, we obtain the $SU(4)$ algebra. Given a one-body operator \mathcal{O} , it can be expressed in terms of the creation and annihilation

operators,

$$\mathcal{O} = \sum_{i,j,m_s,m_t,m'_s,m'_t} \left\langle i; \frac{1}{2}, m_s; \frac{1}{2}, m_t \mid \mathcal{O} \mid j; \frac{1}{2}, m'_s; \frac{1}{2}, m'_t \right\rangle a_{i;\frac{1}{2},m_s,\frac{1}{2},m_t}^\dagger a_{j;\frac{1}{2},m'_s,\frac{1}{2},m'_t}. \quad (4.2.5)$$

Starting with Eq. (4.2.5), applying the angular-momentum algebra [Ed-74] and using Eq. (4.2.4), will give [Ko-06b]

$$\hat{n} = 2 \sum_i \mathcal{A}_{ii;0,0}^{0,0}, \quad S_\mu^1 = \sum_i \mathcal{A}_{ii;\mu,0}^{1,0}, \quad (4.2.6)$$

$$T_\mu^1 = \sum_i \mathcal{A}_{ii;0,\mu}^{0,1}, \quad (\sigma\tau)_{\mu,\mu'}^{1,1} = \sum_i \mathcal{A}_{ii;\mu,\mu'}^{1,1}.$$

Commutation relations for the $SU(4)$ generators in the spin-isospin (sometimes called spherical) representation are,

$$\begin{aligned} \left[S_\mu^1, S_{\mu'}^1 \right] &= -\sqrt{2} \langle 1 \mu \ 1 \mu' \mid 1 \mu + \mu' \rangle S_{\mu+\mu'}^1, \\ \left[T_\mu^1, T_{\mu'}^1 \right] &= -\sqrt{2} \langle 1 \mu \ 1 \mu' \mid 1 \mu + \mu' \rangle T_{\mu+\mu'}^1, \\ \left[S_\mu^1, (\sigma\tau)_{\mu',\mu''}^{1,1} \right] &= -\sqrt{2} \langle 1 \mu \ 1 \mu' \mid 1 \mu + \mu' \rangle (\sigma\tau)_{\mu+\mu',\mu''}^{1,1}, \\ \left[T_\mu^1, (\sigma\tau)_{\mu',\mu''}^{1,1} \right] &= -\sqrt{2} \langle 1 \mu \ 1 \mu'' \mid 1 \mu + \mu'' \rangle (\sigma\tau)_{\mu',\mu+\mu''}^{1,1}, \\ \left[(\sigma\tau)_{\mu_1,\mu_2}^{1,1}, (\sigma\tau)_{\mu_3,\mu_4}^{1,1} \right] &= \sqrt{2} (-1)^{\mu_1+1} \langle 1 \mu_2 \ 1 \mu_4 \mid 1 \mu_2 + \mu_4 \rangle \delta_{\mu_1,-\mu_3} T_{\mu_2+\mu_4}^1 \\ &\quad + \sqrt{2} (-1)^{\mu_2+1} \langle 1 \mu_1 \ 1 \mu_3 \mid 1 \mu_1 + \mu_3 \rangle \delta_{\mu_2,-\mu_4} S_{\mu_1+\mu_3}^1. \end{aligned} \quad (4.2.7)$$

Now we will consider the quadratic Casimir invariants (C_2) of $U(\Omega)$ and $SU(4)$ and their physical interpretation. However we will not consider here the cubic (C_3) and quartic (C_4) invariants of $SU(4)$ although they are needed for some purposes as discussed ahead; see for example [Pa-78] for C_3 and C_4 operators.

4.2.2 Quadratic Casimir operators of $U(\Omega)$ and $SU(4)$ and the Majorana operator

In the $|i, \alpha\rangle$ representation it is easy to write down the quadratic Casimir invariant of $U(4)$,

$$C_2[U(4)] = \sum_{\alpha, \beta} B_{\alpha, \beta} B_{\beta, \alpha} = 4\hat{n} + \sum_{i, j, \alpha, \beta} a_{i, \alpha}^\dagger a_{j, \beta}^\dagger a_{j, \alpha} a_{i, \beta}. \quad (4.2.8)$$

The operator $C_2[U(4)]$ commutes with the generators $B_{\alpha, \beta}$ or equivalently with \hat{n} , S_μ^1 , T_μ^1 and $(\sigma\tau)_{\mu, \mu'}^{1,1}$. Just as $C_2[U(4)]$, the quadratic Casimir invariant of $U(\Omega)$ is,

$$C_2[U(\Omega)] = \sum_{i, j} A_{ij} A_{ji} = \hat{n} \Omega - \sum_{i, j, \alpha, \beta} a_{i, \alpha}^\dagger a_{j, \beta}^\dagger a_{j, \alpha} a_{i, \beta}. \quad (4.2.9)$$

Combining Eqs. (4.2.8) and (4.2.9) we have

$$C_2[U(\Omega)] + C_2[U(4)] = \hat{n}(\Omega + 4). \quad (4.2.10)$$

It is also easy to see that the $C_2[SU(4)]$ can be written in terms of $C_2[U(4)]$ and $C_2[U(\Omega)]$,

$$\begin{aligned} C_2[SU(4)] &= \sum_{\alpha, \beta} B'_{\alpha, \beta} B'_{\beta, \alpha}; \quad B'_{\alpha, \beta} = B_{\alpha, \beta} - \frac{\text{Tr}(B)}{4} \delta_{\alpha, \beta}, \quad \text{Tr}(B) = \sum_{\alpha} B_{\alpha, \alpha} \\ &= C_2[U(4)] - \frac{\hat{n}^2}{4} \\ &= - \left[C_2[U(\Omega)] - \hat{n}(\Omega + 4) + \frac{\hat{n}^2}{4} \right]. \end{aligned} \quad (4.2.11)$$

In the angular-momentum coupled representation, $C_2[SU(4)] = S^2 + T^2 + (\sigma\tau) \cdot (\sigma\tau)$. In order to obtain a physical interpretation for $C_2[SU(4)]$, we will consider the space exchange or the Majorana operator \widehat{M} , with strength κ , that exchanges the spatial coordinates of the particles (the index i) and leaves the index α (equivalently spin-isospin quantum numbers) unchanged. Then [Pa-78],

$$\widehat{M} |i, \alpha; j, \beta\rangle = \kappa |j, \alpha; i, \beta\rangle. \quad (4.2.12)$$

As $|i, \alpha; j, \beta\rangle = a_{i,\alpha}^\dagger a_{j,\beta}^\dagger |0\rangle$, Eq. (4.2.12) gives, with κ a constant,

$$\begin{aligned}
\widehat{M} &= \frac{\kappa}{2} \left[\sum_{i,j,\alpha,\beta} \left(a_{j,\alpha}^\dagger a_{i,\beta}^\dagger \right) \left(a_{i,\alpha}^\dagger a_{j,\beta}^\dagger \right)^\dagger \right] \\
&= \frac{\kappa}{2} \left[\sum_{i,j} \left(\sum_{\alpha} a_{j,\alpha}^\dagger a_{i,\alpha} \right) \left(\sum_{\beta} a_{i,\beta}^\dagger a_{j,\beta} \right) - \Omega \sum_{j,\alpha} a_{j,\alpha}^\dagger a_{j,\alpha} \right] \\
&= \frac{\kappa}{2} \{ C_2 [U(\Omega)] - \Omega \hat{n} \} .
\end{aligned} \tag{4.2.13}$$

Eqs. (4.2.11) and (4.2.13) allow us to write the \widehat{M} operator in terms of $C_2 [SU(4)]$.

Then, we have

$$\widehat{M} = \kappa \left\{ 2\hat{n} \left(1 + \frac{\hat{n}}{16} \right) - \frac{1}{2} C_2 [SU(4)] \right\} . \tag{4.2.14}$$

Using Eq. (4.2.14) one can identify the $SU(4)$ [or $U(4)$] irrep for gs, assuming that the Hamiltonian is represented by the Majorana operator. Towards this end, now we will consider the $SU(4)$ and $U(\Omega)$ irreps and the reduction of the $SU(4)$ irreps to (S, T) .

4.2.3 $SU(4)$ and $U(\Omega)$ irreps and identification of the ground state

$U(\Omega)$ or $SU(4)$ irreps

With m fermions in 4Ω sp states, we can decompose the basis space with dimension $\binom{4\Omega}{m}$ into irreps of $U(4)$ [or $SU(4)$] and $U(\Omega)$ and further the $U(4)$ irreps into (S, T) . Firstly, the $U(4)$ irreps are represented by the Young tableaux (see Fig. 4.2) or the partitions $\{F\}$,

$$\{F\} = \{F_1, F_2, F_3, F_4\} , \quad F_1 \geq F_2 \geq F_3 \geq F_4 \geq 0 , \quad m = \sum_{i=1}^4 F_i . \tag{4.2.15}$$

Note that F_α are the eigenvalues of $B_{\alpha\alpha}$ defined in Eq. (4.2.2). As the total m -particle wavefunctions are antisymmetric, the $U(\Omega)$ irreps $\{f\}$ are uniquely defined by $\{F\}$ and $\{f\} = \{\widetilde{F}\}$ (alternatively $\{F\} = \{\widetilde{f}\}$) which is obtained by changing rows to columns in the Young tableaux $\{F\}$; see for example [Pa-78, Wy-70, Ha-62]. Due to this symmetry constraint, $F_j \leq \Omega$, $j = 1, 2, 3, 4$ and $f_i \leq 4$, $i = 1, 2, \dots, \Omega$. Given the $U(4)$ irrep $\{F\}$, the corresponding $SU(4)$ irrep $\{F'\}$, which is three rowed Young tableaux, can be defined

by

$$\{F'\} = \{F'_1, F'_2, F'_3\} = \{F_1 - F_4, F_2 - F_4, F_3 - F_4\}. \quad (4.2.16)$$

The $\{F\} \rightarrow (S, T)$ reductions can be obtained using group theoretical methods [Wy-70, Ha-62]. Alternatively a physically intuitive procedure, easy to implement on a machine, is as follows. First, the $\{F\} \rightarrow (S, T)$ reductions for a symmetric $U(4)$ irrep $\{F\} = \{F_1, 0, 0, 0\}$ can be obtained by distributing $m = F_1$ identical bosons in the four spin-isospin orbitals labeled by $|m_s m_t\rangle$. From these distributions, the S_z and T_z eigenvalues $M_S = \sum_i m_i(m_s)_i$ and $M_T = \sum_i m_i(m_t)_i$ and the corresponding degeneracies $d(m : M_S, M_T)$ follow easily. Here m_i are the number of bosons in the i th orbit with $m_s = (m_s)_i$ and $m_t = (m_t)_i$. Let us denote the number of times (S, T) appears in a given $\{F\}$ by $D(\{F\} : S, T)$. It is easy to see that $D(\{m, 0, 0, 0\} : S, T)$ is given by the double difference,

$$\begin{aligned} D(\{m, 0, 0, 0\} : S, T) &= d(m : M_S = S, M_T = T) - d(m : M_S = S, M_T = T + 1) \\ &\quad - d(m : M_S = S + 1, M_T = T) + d(m : M_S = S + 1, M_T = T + 1). \end{aligned} \quad (4.2.17)$$

Carrying out this exercise on a machine for many m values, we obtain the following (well known in literature) general result,

$$\{m, 0, 0, 0\} \rightarrow (S, T) = \left(\frac{m}{2}, \frac{m}{2}\right), \left(\frac{m}{2} - 1, \frac{m}{2} - 1\right), \dots, (0, 0) \text{ or } \left(\frac{1}{2}, \frac{1}{2}\right). \quad (4.2.18)$$

It is important to note that here $D(\{m, 0, 0, 0\} : S, T) = 1$ for all allowed (S, T) values (i.e., multiplicity is unity). The reductions for a general $U(4)$ irrep $\{F\} = \{F_1, F_2, F_3, F_4\}$ follow by writing $\{F\}$ as a determinant involving only totally symmetric irreps with the multiplication of the elements in the determinant replaced by outer products. Then we have [Wy-70, Ja-81]

$$\{F\} = |\mathcal{F}_{ij}|, \quad \mathcal{F}_{ij} = \{F_i + j - i, 0, 0, 0\}; \quad \{0\} = 1, \quad \{-x, 0, 0, 0\} = 0. \quad (4.2.19)$$

Substituting the dimensions for symmetric irreps in the above determinant gives the

dimension formula for $U(4)$ irreps,

$$d_4(\{F\}) = |d_{ij}|, \quad d_{ij} = \binom{F_i + j - i + 3}{3}. \quad (4.2.20)$$

Also the corresponding (S, T) values and their multiplicities can be obtained by substituting the (S, T) values for \mathcal{F}_{ij} in the determinant in Eq. (4.2.19) and evaluating the determinant by applying angular-momentum coupling rules. Note that $d_4(\{F\}) = \sum_{S,T} (2S+1)(2T+1) D(\{F\} : S, T)$. In carrying out the algebra we can exploit the equivalence between $SU(4)$ and $U(4)$ irreps and employ just 3 rowed $U(4)$ irreps. This procedure is used in constructing Tables 4.1 and 4.2. For a realistic system such as the atomic nucleus, given the Ω value and the number of valence nucleons m , we can enumerate all the allowed $U(4)$ or $SU(4)$ irreps using Eqs. (4.2.15) and (4.2.16). Table 4.1 gives all the possible $U(4)$ irreps for $\Omega = 10$ and $m = 0 - 6$ along with their spin-isospin structure.

Assuming that the Majorana operator is the Hamiltonian with κ in Eq. (4.2.14) negative, we can identify the $SU(4)$ irreps labeling gs as follows. Using the formulas for the eigenvalues of $C_2[U(4)]$ and $C_2[U(\Omega)]$,

$$\langle C_2[U(4)] \rangle^{\{F\}} = \sum_{i=1}^4 F_i(F_i + 5 - 2i), \quad \langle C_2[U(\Omega)] \rangle^{\{f\}} = \sum_{i=1}^{\Omega} f_i(f_i + \Omega + 1 - 2i), \quad (4.2.21)$$

and applying Eq. (4.2.14), we can order the $SU(4)$ irreps. For physical systems, generally, the $U(\Omega)$ (spatial) irrep for the ground states should be the most symmetric one. The symmetric irrep, as seen from Eq. (4.2.21), will have the largest eigenvalue for $C_2[U(\Omega)]$. From Eqs. (4.2.13) and (4.2.14), then it follows that the $SU(4)$ irrep for gs should be the one with the lowest eigenvalue for $C_2[SU(4)]$ and these eigenvalues can be obtained by combining Eq. (4.2.11) with Eq. (4.2.21). Now, for a given (m, T_z) with $T = |T_z|$ and $T_z = (N-Z)/2$ for a nucleus with N neutrons and Z protons, enumerating $\{F\} \rightarrow (S, T)$ reductions, we can determine the $U(4)$ irreps labeling gs, by applying Eq. (4.2.14) with κ negative. In Table 4.2, $U(4)$ and $U(\Omega)$ irreps for gs are listed for $\Omega = 10$ and $m = 4 - 11$ for all T_z values. As it is well known and also seen from Table 4.2, for the Majorana operator or equivalently for the $SU(4)$ invariant Hamiltonians, for $N=Z$ even-even ($m = 4r$), $N=Z$ odd-odd ($m = 4r + 2$) and $N=Z \pm 1$ ($m = 4r \pm 1$) odd-A nuclei,

Table 4.1: $m \rightarrow \{F\} \rightarrow (S, T)$ reductions for $\Omega = 10$ and $m = 0 - 6$. In the table, r in $(S, T)^r$ gives the multiplicity of the irrep (S, T) .

m	$\{F_1, F_2, F_3, F_4\}$	(S, T)
0	$\{0, 0, 0, 0\}$	$(0, 0)$
1	$\{1, 0, 0, 0\}$	$(\frac{1}{2}, \frac{1}{2})$
2	$\{1, 1, 0, 0\}$	$(1, 0), (0, 1)$
	$\{2, 0, 0, 0\}$	$(1, 1), (0, 0)$
3	$\{1, 1, 1, 0\}$	$(\frac{1}{2}, \frac{1}{2})$
	$\{2, 1, 0, 0\}$	$(\frac{3}{2}, \frac{1}{2}), (\frac{1}{2}, \frac{3}{2}), (\frac{1}{2}, \frac{1}{2})$
	$\{3, 0, 0, 0\}$	$(\frac{3}{2}, \frac{3}{2}), (\frac{1}{2}, \frac{1}{2})$
4	$\{1, 1, 1, 1\}$	$(0, 0)$
	$\{2, 1, 1, 0\}$	$(1, 1), (1, 0), (0, 1)$
	$\{2, 2, 0, 0\}$	$(2, 0), (1, 1), (0, 2), (0, 0)$
	$\{3, 1, 0, 0\}$	$(2, 1), (1, 2), (1, 1), (1, 0), (0, 1)$
	$\{4, 0, 0, 0\}$	$(2, 2), (1, 1), (0, 0)$
5	$\{2, 1, 1, 1\}$	$(\frac{1}{2}, \frac{1}{2})$
	$\{2, 2, 1, 0\}$	$(\frac{3}{2}, \frac{1}{2}), (\frac{1}{2}, \frac{3}{2}), (\frac{1}{2}, \frac{1}{2})$
	$\{3, 1, 1, 0\}$	$(\frac{3}{2}, \frac{3}{2}), (\frac{3}{2}, \frac{1}{2}), (\frac{1}{2}, \frac{3}{2}), (\frac{1}{2}, \frac{1}{2})$
	$\{3, 2, 0, 0\}$	$(\frac{5}{2}, \frac{1}{2}), (\frac{3}{2}, \frac{3}{2}), (\frac{3}{2}, \frac{1}{2}), (\frac{1}{2}, \frac{5}{2}), (\frac{1}{2}, \frac{3}{2}), (\frac{1}{2}, \frac{1}{2})$
	$\{4, 1, 0, 0\}$	$(\frac{5}{2}, \frac{3}{2}), (\frac{3}{2}, \frac{5}{2}), (\frac{3}{2}, \frac{3}{2}), (\frac{3}{2}, \frac{1}{2}), (\frac{1}{2}, \frac{5}{2}), (\frac{1}{2}, \frac{3}{2}), (\frac{1}{2}, \frac{1}{2})$
	$\{5, 0, 0, 0\}$	$(\frac{5}{2}, \frac{5}{2}), (\frac{3}{2}, \frac{3}{2}), (\frac{1}{2}, \frac{1}{2})$
6	$\{2, 2, 1, 1\}$	$(1, 0), (0, 1)$
	$\{2, 2, 2, 0\}$	$(1, 1), (0, 0)$
	$\{3, 1, 1, 1\}$	$(1, 1), (0, 0)$
	$\{3, 2, 1, 0\}$	$(2, 1), (2, 0), (1, 2), (1, 1)^2, (1, 0), (0, 2), (0, 1)$
	$\{3, 3, 0, 0\}$	$(3, 0), (2, 1), (1, 2), (1, 0), (0, 3), (0, 1)$
	$\{4, 1, 1, 0\}$	$(2, 2), (2, 1), (1, 2), (1, 1), (1, 0), (0, 1)$
	$\{4, 2, 0, 0\}$	$(3, 1), (2, 2), (2, 1), (2, 0), (1, 3), (1, 2), (1, 1)^2, (0, 2), (0, 0)$
	$\{5, 1, 0, 0\}$	$(3, 2), (2, 3), (2, 2), (2, 1), (1, 2), (1, 1), (1, 0), (0, 1)$
	$\{6, 0, 0, 0\}$	$(3, 3), (2, 2), (1, 1), (0, 0)$

the $U(\Omega)$ irreps for the gs, with lowest T , are $\{4^r\}$, $\{4^r, 2\}$, $\{4^r, 1\}$ and $\{4^r, 3\}$ with spin-isospin structure (see Table 4.1) being $(0, 0)$, $(1, 0) \oplus (0, 1)$, $(\frac{1}{2}, \frac{1}{2})$ and $(\frac{1}{2}, \frac{1}{2})$, respectively. For convenience, we introduce the notation $\{f_m^{(p)}\}$ where

$$\{f_m^{(p)}\} = \{4^r, p\}; \quad m = 4r + p \text{ and } p = \text{mod}(m, 4) \quad (4.2.22)$$

and this is used in the reminder of the chapter. We shall see ahead that for the special $U(\Omega)$ irreps in Eq. (4.2.22), analytical formulas are much simpler than for a general $U(\Omega)$ irrep.

Table 4.2: $U(4)$ and $U(\Omega)$ irreps F_m and f_m , respectively, with the smallest value for $\langle C_2[SU(4)] \rangle^{\tilde{f}_m}$ for a given (m, T_z) value in the $(2p1f)$ -shell $[\Omega = 10]$. For the results in the Table, isospin $T = |T_z|$.

m	$ T_z $	$F_m = \tilde{f}_m$	f_m	m	$ T_z $	$F_m = \tilde{f}_m$	f_m
4	0	{1, 1, 1, 1}	{4}	9	$\frac{1}{2}$	{3, 2, 2, 2}	{4, 4, 1}
	1	{2, 1, 1, 0}	{3, 1}		$\frac{3}{2}$	{3, 3, 2, 1}	{4, 3, 2}
	2	{2, 2, 0, 0}	{2, 2}		$\frac{5}{2}$	{4, 3, 1, 1}	{4, 2, 2, 1}
5	$\frac{1}{2}$	{2, 1, 1, 1}	{4, 1}	10	$\frac{1}{2}$	{4, 4, 1, 0}	{3, 2, 2, 2}
	$\frac{3}{2}$	{2, 2, 1, 0}	{3, 2}		$\frac{3}{2}$	{5, 4, 0, 0}	{2, 2, 2, 2, 1}
	$\frac{5}{2}$	{3, 2, 0, 0}	{2, 2, 1}		0	{3, 3, 2, 2}	{4, 4, 2}
6	0	{2, 2, 1, 1}	{4, 2}	11	1	{3, 3, 2, 2}	{4, 4, 2}
	1	{2, 2, 1, 1}	{4, 2}		2	{4, 3, 2, 1}	{4, 3, 2, 1}
	2	{3, 2, 1, 0}	{3, 2, 1}		3	{4, 4, 1, 1}	{4, 2, 2, 2}
	3	{3, 3, 0, 0}	{2, 2, 2}		4	{5, 4, 1, 0}	{3, 2, 2, 2, 1}
7	$\frac{1}{2}$	{2, 2, 2, 1}	{4, 3}	12	$\frac{1}{2}$	{5, 5, 0, 0}	{2, 2, 2, 2, 2}
	$\frac{3}{2}$	{3, 2, 1, 1}	{4, 2, 1}		$\frac{3}{2}$	{3, 3, 3, 2}	{4, 4, 3}
	$\frac{5}{2}$	{3, 3, 1, 0}	{3, 2, 2}		$\frac{5}{2}$	{4, 3, 2, 2}	{4, 4, 2, 1}
	$\frac{7}{2}$	{4, 3, 0, 0}	{2, 2, 2, 1}		$\frac{7}{2}$	{4, 4, 2, 1}	{4, 3, 2, 2}
8	0	{2, 2, 2, 2}	{4, 4}	13	$\frac{1}{2}$	{5, 4, 1, 1}	{4, 2, 2, 2, 1}
	1	{3, 2, 2, 1}	{4, 3, 1}		$\frac{3}{2}$	{5, 5, 1, 0}	{3, 2, 2, 2, 2}
	2	{3, 3, 1, 1}	{4, 2, 2}		$\frac{5}{2}$	{6, 5, 0, 0}	{2, 2, 2, 2, 2, 1}
	3	{4, 3, 1, 0}	{3, 2, 2, 1}				
	4	{4, 4, 0, 0}	{2, 2, 2, 2}				

Having described some of the essential properties of the $U(\Omega) \otimes SU(4)$ algebra, now we will introduce the EGUE(2)- $SU(4)$ random matrix ensemble and analyze in some detail its properties. From now on we denote the irreps $\{f\}$ and $\{F\}$ as f and F , respectively when there is no confusion.

4.3 Definition and Basic Properties of EGUE(2)- $SU(4)$

4.3.1 Definition of EGUE(2)- $SU(4)$

Let us begin with the normalized two-particle states $|f_2 \nu_2; F_2 \beta_2\rangle$ where the $U(4)$ irreps $F_2 = \{1^2\}$ and $\{2\}$ and the corresponding $U(\Omega)$ irreps f_2 are $\{2\}$ (symmetric) and $\{1^2\}$ (antisymmetric), respectively. Similarly ν_2 are the additional quantum numbers that belong to f_2 and β_2 belong to F_2 . As f_2 uniquely defines F_2 , from now on we will drop F_2 unless they are explicitly needed and also we will use the $f_2 \leftrightarrow F_2$ equivalence

whenever needed. With $A^\dagger(f_2 \nu_2 \beta_2)$ and $A(f_2 \nu_2 \beta_2)$ denoting creation and annihilation operators for the normalized two-particle states, a general two-body Hamiltonian operator \hat{H} that is $SU(4)$ scalar can be written as

$$\hat{H} = \hat{H}_{\{2\}} + \hat{H}_{\{1^2\}} = \sum_{f_2, \nu_2^i, \nu_2^f, \beta_2; f_2=\{2\}, \{1^2\}} H_{f_2 \nu_2^i \nu_2^f}(2) A^\dagger(f_2 \nu_2^f \beta_2) A(f_2 \nu_2^i \beta_2). \quad (4.3.1)$$

In Eq. (4.3.1), the two-body matrix elements $H_{f_2 \nu_2^i \nu_2^f}(2) = \langle f_2 \nu_2^f \beta_2 | \hat{H} | f_2 \nu_2^i \beta_2 \rangle$ are independent of the β_2 's. The uniform summation over β_2 in Eq. (4.3.1) ensures that \hat{H} is $SU(4)$ scalar and therefore it will not connect states with different f_2 's. However, \hat{H} is not a $SU(4)$ invariant operator. Just as the two-particle states, we can denote the m -particle states by $|f_m \nu_m^f \beta_m^F\rangle; F_m = \tilde{f}_m$. Action of \hat{H} on these states generates states that are degenerate with respect to β_m^F but not ν_m^f . Therefore for a given f_m , there will be $d_\Omega(f_m)$ number of levels each with $d_4(\tilde{f}_m)$ number of degenerate states. Formula for the dimension $d_\Omega(f_m)$ is [Wy-70],

$$d_\Omega(f_m) = \prod_{i < j=1}^{\Omega} \frac{f_i - f_j + j - i}{j - i}, \quad (4.3.2)$$

where, $f_m = \{f_1, f_2, \dots\}$. Equation (4.3.2) also gives $d_4(F_m)$ with the product ranging from $i = 1$ to 4 and replacing f_i by F_i . As \hat{H} is a $SU(4)$ scalar, the m -particle H matrix will be a direct sum of matrices with each of them labeled by the f_m 's with dimension $d_\Omega(f_m)$. Thus

$$H(m) = \sum_{f_m} H_{f_m}(m) \oplus. \quad (4.3.3)$$

Figure 4.1 shows an example for Eq. (4.3.3). As seen from Eq. (4.3.1), the H matrix in two-particle spaces is a direct sum of two matrices $H_{f_2}(2)$, one in the $f_2 = \{2\}$ space and the other in $\{1^2\}$ space. Similarly, for the 6 particle example shown in Fig. 4.1, there are 9 f_m 's and therefore the H matrix is a direct sum of 9 matrices. It should be noted that the matrix elements of $H_{f_m}(m)$ matrices receive contributions from both $H_{\{2\}}(2)$ and $H_{\{1^2\}}(2)$.

Embedded random matrix ensemble EGUE(2)- $SU(4)$ for a m fermion systems with a fixed f_m , i.e., $\{H_{f_m}(m)\}$, is generated by the ensemble of H operators given in Eq. (4.3.1) with $H_{\{2\}}(2)$ and $H_{\{1^2\}}(2)$ matrices replaced by independent GUE ensem-

$\{4,2\}, 5$ 19305	0	0	0	0	0	0	0	0
0	$\{4,1^2\}, 9$ 17160	0	0	0	0	0	0	0
0	0	$\{3^2\}, 9$ 9075	0	0	0	0	0	0
0	0	0	$\{3,2,1\}, 15$ 21120	0	0	0	0	0
0	0	0	0	$\{3,1^3\}, 21$ 9240	0	0	0	0
0	0	0	0	0	$\{2^3\}, 21$ 4950	0	0	0
0	0	0	0	0	0	$\{2^2,1^2\}, 25$ 6930	0	0
0	0	0	0	0	0	0	$\{2,1^4\}, 33$ 2310	0
0	0	0	0	0	0	0	0	$\{1^6\}, 45$ 210

Figure 4.1: Direct sum matrix structure for a $SU(4)$ scalar Hamiltonian. The example in the figure is for $m = 6$ particles in $\Omega = 10$ sp orbitals. The $U(\Omega)$ irreps and the corresponding eigenvalues for the quadratic Casimir invariant of $SU(4)$ along with the dimensions for the diagonal blocks are shown in the figure. For example, for the block that corresponds to the irrep $f_m = \{3, 2, 1\}$, we have $\langle C_2[SU(4)] \rangle_{\tilde{f}_m} = 15$ and $d_\Omega = 21120$. As shown in the figure (with all the off-diagonal blocks having all matrix elements zero), $H(m) = \sum_{f_m} H_{f_m}(m) \oplus$ and for each diagonal block, we have a EGUE(2)- $SU(4)$ matrix ensemble labeled by (m, f_m) .

bles of random matrices,

$$\{H(2)\} = \{H_{\{2\}}(2)\}_{\text{GUE}} \oplus \{H_{\{1^2\}}(2)\}_{\text{GUE}}. \quad (4.3.4)$$

Random variables defining the real and imaginary parts of the matrix elements of $H_{f_2}(2)$ are independent Gaussian variables with zero center and variance given by (with bar representing ensemble average),

$$\overline{H_{f_2 v_2^1 v_2^2}(2) H_{f_2' v_2^3 v_2^4}(2)} = \delta_{f_2 f_2'} \delta_{v_2^1 v_2^4} \delta_{v_2^2 v_2^3} (\lambda_{f_2})^2. \quad (4.3.5)$$

Also, the independence of the $\{H_{\{2\}}(2)\}$ and $\{H_{\{1^2\}}(2)\}$ GUE ensembles imply,

$$\begin{aligned} & \overline{\left[H_{\{2\}v_2^1 v_2^2}(2) \right]^P} \overline{\left[H_{\{1^2\}v_2^3 v_2^4}(2) \right]^Q} = 0 \text{ for } P \text{ or } Q \text{ odd,} \\ & = \left\{ \overline{\left[H_{\{2\}v_2^1 v_2^2}(2) \right]^P} \right\} \left\{ \overline{\left[H_{\{1^2\}v_2^3 v_2^4}(2) \right]^Q} \right\} \text{ for } P \text{ and } Q \text{ even.} \end{aligned} \quad (4.3.6)$$

Action of \hat{H} defined by Eq. (4.3.1) on m -particle basis states with a fixed f_m , along with Eqs. (4.3.4)-(4.3.6) generates EGUE(2)- $SU(4)$ ensemble $\{H_{f_m}(m)\}$; it is labeled by the $U(\Omega)$ irrep f_m with matrix dimension $d_\Omega(f_m)$.

4.3.2 Matrix structure

For a better understanding of the size of the EGUE(2)- $SU(4)$ matrices and the number of independent matrix elements they contain, let us consider the example of 8 fermions in $N = 24$ sp states. For spinless fermion systems, we have EGUE(2) with a two-particle GUE of dimension 276 and the number of independent variables [denoted by $i_2(0)$] is 76176. These generate the m fermion EGUE(2) ensemble with H matrices of dimension $d(8) = 735471$. For fermions with spin symmetry, we have EGUE(2)-**s** with $\Omega = 12$. This ensemble is generated by independent GUE's in two-particle spin $s = 0$ and $s = 1$ spaces with dimensions 78 and 66, respectively. Then the number of independent variables [denoted by $i_2(2)$] for this system is 10440. The H matrix dimensions for EGUE(2)-**s** ensembles for the 8 particle system with spins $S = 0, 1, 2, 3$ and 4 are $d(8, S) = 70785, 113256, 51480, 9009$, and 495, respectively. Going further, with $SU(4)$ symmetry we have EGUE(2)- $SU(4)$ ensembles with $\Omega = 6$. These ensembles are generated by two independent GUE's in $f_2 = \{2\}$ and $\{1^2\}$ spaces with dimensions 21 and 15 respectively. Then the number of independent variables [denoted by $i_2(4)$] for this system is 666. The H matrix dimensions for EGUE(2)- $SU(4)$ ensembles for the 8 particle system with $f_8 = \{2^2, 1^4\}, \{2^3, 1^2\}, \{2^4\}, \{3, 1^5\}, \{3, 2, 1^3\}, \{3, 2^2, 1\}, \{3^2, 1^2\}, \{3^2, 2\}, \{4, 1^4\}, \{4, 2, 1^2\}, \{4, 2^2\}, \{4, 3, 1\}$, and $\{4^2\}$ are 15, 105, 105, 21, 384, 1050, 1176, 1470, 315, 2430, 2520, 4410, and 1764, respectively. Thus i_2 will be considerably reduced as the symmetry increases (with fixed N), i.e., $i_2(4) \ll i_2(2) \ll i_2(0)$. Similarly the H matrix dimensions decrease as we go from EGUE(2) to EGUE(2)-**s** to EGUE(2)- $SU(4)$. For further insight, let us consider the fraction of independent ma-

trix elements $\mathcal{J}(m, f_m)$, for $m \gg 2$ for the EGUE(2)- $SU(4)$ ensemble, defined as the ratio of $i_2(4)$ to the total number (without counting the hermitian conjugates) of matrix elements,

$$\mathcal{J}(m, f_m) = \frac{i_2(4)}{[d_\Omega(f_m)]^2}. \quad (4.3.7)$$

Similarly, for EGUE(2) and EGUE(2)-**s** ensembles, we can define the fraction of independent matrix elements as $\mathcal{J}(m) = i_2(0)/[d(m)]^2$ and $\mathcal{J}(m, S) = i_2(2)/[d(m, S)]^2$, respectively. In our above example, for EGUE(2), EGUE(2)-**s** with $S = 0$ and EGUE(2)- $SU(4)$ with $f_8 = \{4^2\}$, we have $\mathcal{J} = 1.4 \times 10^{-7}$, 2×10^{-6} , and 2×10^{-4} , respectively. Therefore the H matrices with more symmetry are characterized by relatively large fraction of independent matrix elements.

Due to the two-body selection rules, many of the m -particle matrix elements of the EGUE(2)'s will be zero. In order to understand the sparse nature of the EGUE matrices we employ the sparsity index \mathbf{S} with \mathbf{S}^{-1} defined as the ratio of number of m -particle states that are directly coupled by the two-body interaction to the m -particle matrix dimension. The number of many-particle states that are coupled by the two-body interaction, i.e., the connectivity factor $K(m, f_m)$, is given by the spectral variances; see Chapter 2 and [Ja-97]. Therefore, for the EGUE(2)- $SU(4)$ ensemble,

$$\mathbf{S}^{-1}(m, f_m) = \frac{K(m, f_m)}{d_\Omega(f_m)}. \quad (4.3.8)$$

Similarly, $\mathbf{S}^{-1}(m) = K(m)/d(m)$ for EGUE(2) and $\mathbf{S}^{-1}(m, S) = K(m, S)/d(m, S)$ for EGUE(2)-**s**. Formulas for the $K(m)$ and $K(m, S)$ are given in ([Fl-96], [Ko-05]) and ([Ko-07], Chapter 2), respectively. For EGUE(2)- $SU(4)$, given the two-particle variances to be $\lambda_{f_2}^2 = \lambda^2$, the variances $\overline{\langle \hat{H}^2 \rangle}^{m, f_m}$ in m -particle space are $\sigma^2(m, f_m) = \lambda^2 K(m, f_m)$ with $K(m, f_m)$ propagating the two-particle variances to m -particle spaces. Results in Table 4.6 ahead give formulas for the variance propagator $K(m, f_m)$ for the $U(\Omega)$ irreps $f_m^{(p)}$. For example, $K(m = 4r, f_m = \{4^r\}) = r(\Omega - r + 4) \{2r(2\Omega - 2r + 9) - \Omega - 8\}$, and $K(m = 4r + 1, f_m = \{4^r, 1\}) = r(\Omega - r + 4) \{4r(2\Omega - 2r + 7) + 2\Omega - 15\}/2$. For the 8 particle example (with $N = 24$) considered before, the connectivity factors K are 4284, 1440, and 864, respectively for EGUE(2), EGUE(2)-**s** with $S = 0$ and EGUE(2)- $SU(4)$ with $f_8 = \{4^2\}$. These give $\mathbf{S}^{-1} = 5.8 \times 10^{-3}$, 0.02, and 0.49, respectively for these

ensembles. Therefore as symmetry increases, in general, the many-particle EGUE matrices will become more dense. Consequences of this will be discussed further in Section 4.7.

4.3.3 Matrix construction

Before proceeding to the analytical formulation, we will briefly outline a method for numerical construction of EGUE(2)- $SU(4)$ ensemble for a given (Ω, m, f_m) . Consider m fermions in Ω number of sp orbitals each four-fold degenerate. Then in the spin-isospin representation, the sp states are denoted by $|i; \frac{1}{2}, m_s; \frac{1}{2}, m_t\rangle$ as discussed before, where $i = 1, 2, \dots, \Omega$. We arrange the sp states in such a way that the first Ω states have $(m_s, m_t) = (\frac{1}{2}, \frac{1}{2})$, $\Omega + 1$ to 2Ω sp states have $(m_s, m_t) = (\frac{1}{2}, -\frac{1}{2})$, $2\Omega + 1$ to 3Ω sp states have $(m_s, m_t) = (-\frac{1}{2}, \frac{1}{2})$ and $3\Omega + 1$ to 4Ω sp states have $(m_s, m_t) = (-\frac{1}{2}, -\frac{1}{2})$. In this single state representation we denote the sp states as $|k_r\rangle$, $r = 1, 2, \dots, 4\Omega$. Now distributing in all possible ways the m fermions in these 4Ω sp states will generate the m -particle configurations $\mathbf{m} = [m(k_1), m(k_2), \dots, m(k_{4\Omega})]$, with $m(k_r) = 0$ or 1 and $\sum_{r=1}^{4\Omega} m(k_r) = m$. The corresponding (M_S, M_T) values are $M_S = [\sum_{r=1}^{\Omega} m(k_{r1}) + \sum_{r=2=\Omega+1}^{2\Omega} m(k_{r2}) - \sum_{r=3=2\Omega+1}^{3\Omega} m(k_{r3}) - \sum_{r=4=3\Omega+1}^{4\Omega} m(k_{r4})]/2$ and $M_T = [\sum_{r=1}^{\Omega} m(k_{r1}) - \sum_{r=2=\Omega+1}^{2\Omega} m(k_{r2}) + \sum_{r=3=2\Omega+1}^{3\Omega} m(k_{r3}) - \sum_{r=4=3\Omega+1}^{4\Omega} m(k_{r4})]/2$. The m -particle H matrix in the basis defined by \mathbf{m} 's with $(M_S^{min}, M_T^{min}) = (0, 0)$ will contain states with all (S, T) values for even m and similarly with $(M_S^{min}, M_T^{min}) = (\frac{1}{2}, \frac{1}{2})$ for odd m . The dimension of this basis space, called $\mathcal{D}(M_S^{min}, M_T^{min})$, is $\sum_{f_m} d_{\Omega}(f_m) \sum_{S,T} D(\tilde{f}_m : S, T)$. In the (st) coupled representation the two-particle matrix elements of \hat{H} are

$$\langle (i, j)s, m_s, t, m_t | \hat{H} | (k, l)s', m_{s'}, t', m_{t'} \rangle .$$

As the $SU(4)$ irreps $\{2\} \rightarrow (st) = (11) \oplus (00)$ and $\{1^2\} \rightarrow (10) \oplus (01)$, it is easy to put these matrix elements in one to one correspondence with the two-body matrix elements $H_{f_2 v_2^i v_2^f}(2)$ in Eq. (4.3.1). Applying angular-momentum algebra, it is then possible to transform these matrix elements into two-body matrix elements $\langle k_c k_d | \hat{H} | k_a k_b \rangle$ in the single state representation. Then the construction of the m -particle H matrix in the \mathbf{m} -basis with (M_S^{min}, M_T^{min}) defined above reduces to the problem of EGUE(2) for spinless fermion systems. The construction of EGUE(2) for spinless fermion sys-

tems on a machine is straightforward. For instance, the dimensions of the matrices $\mathcal{D}(M_S^{min} = 0, M_T^{min} = 0)$ for $m = 6, 8$ and 12 , with $\Omega = 6$, are 17000, 79875, and 263844, respectively. On the other hand, the total m -particle matrix dimensions are $d(6) = 134596$, $d(8) = 735471$, and $d(12) = 2704156$. Therefore, the \mathbf{m} -basis formulation reduces the matrix dimensions considerably.

After constructing this matrix, it is possible to generate the H matrix defined over a fixed f_m space, for some special f_m 's easily, using the $C_2[SU(4)]$ operator as the projection operator; eigenvalues of $C_2[SU(4)]$ will in general have degeneracies with respect to f_m . Some of the special irreps that can be identified uniquely by $C_2[SU(4)]$ are the following: (a) for $m = 4r$, the irreps $\{4^r\}$, $\{4^{r-1}, 3, 1\}$ and $\{4^{r-1}, 2^2\}$ with eigenvalues 0, 8, and 12, respectively; (b) for $m = 4r + 2$, the irreps $\{4^r, 2\}$ and $\{4^{r-1}, 3, 2, 1\}$ with eigenvalues 5, and 15, respectively; (c) for $m = 4r + 1$, the irreps $\{4^r, 1\}$, $\{4^{r-1}, 3, 2\}$ and $\{4^{r-1}, 3, 1^2\}$ with eigenvalues 3, 9, and 13, respectively; and (d) for $m = 4r + 3$, the irreps $\{4^r, 3\}$, $\{4^r, 2, 1\}$, and $\{4^{r-1}, 3^2, 1\}$ with eigenvalues 3, 9, and 13, respectively. For convenience, we denote these special irreps by f_m^s . It should be noted that $f_m^{(p)}$ belong to f_m^s . For the $C_2[SU(4)]$ operator, the m -particle matrix in the \mathbf{m} -basis can be constructed by identifying the two-particle matrix elements, in single state representation, using Eqs. (4.2.8)-(4.2.11). Diagonalizing this matrix gives a direct sum of unitary matrices and the unitary matrix that corresponds to a given f_m^s can be identified from the eigenvalues of $C_2[SU(4)]$. Applying the unitary transformation defined by this unitary matrix, the m -particle H matrix with $(M_S, M_T) = (0, 0)$ for even m [$(M_S, M_T) = (\frac{1}{2}, \frac{1}{2})$ for odd m] can be transformed to the basis with good f_m^s . This method can be successfully implemented on a machine for the irreps f_m^s . Results in Section 4.2 are sufficient for constructing EGUE(2)- $SU(4)$ for these irreps. It is important to note that the $C_2[SU(4)]$ alone will not suffice to identify the matrices corresponding to all the f_m 's. To distinguish them, we need to construct the m -particle matrices for the cubic and quartic Casimir invariants of $SU(4)$ algebra and these are more complicated. Numerical investigations of EGUE(2)- $SU(4)$ by matrix construction are impractical as the dimensions $\mathcal{D}(M_S^{min}, M_T^{min})$ are prohibitively large (even for $\Omega = 6$ and $m = 6$, $\mathcal{D} = 17000$). Therefore our focus in this chapter is in developing analytical formulation for solving the EGUE(2)- $SU(4)$ ensemble (Secs. 4.4 and 4.5 and Appendix F) and using this we have carried out some numerical investigations (Secs. 4.6 and 4.7).

4.4 $U(4\Omega) \supset U(\Omega) \otimes SU(4)$ Wigner-Racah Algebra for Solving EGUE(2)- $SU(4)$

Analytical solutions for EGUE(2)- $SU(4)$ follow, as discussed before for EGUE(k) and EGUE(2)- s (see Sec. 1.2.3 and Appendix C), from the tensorial decomposition of the \hat{H} operator [equivalently $A^\dagger A$ in Eq. (4.3.1)] with respect to $U(\Omega) \otimes SU(4)$. As \hat{H} is a $SU(4)$ scalar, it transforms as the irrep $\{0\}$ with respect to the $SU(4)$ algebra. However with respect to $SU(\Omega)$, the tensorial characters, in the Young tableaux notation, for $f_2 = \{2\}$ are $F_\nu = \{0\}, \{21^{\Omega-2}\}$ and $\{42^{\Omega-2}\}$ with $\nu = 0, 1$, and 2 , respectively. Note that F_ν follow from the Kronecker product of the $U(\Omega)$ irreps $\{2\}$ and $\{2^{\Omega-1}\}$ as A^\dagger and A transform as these irreps. Similarly for $f_2 = \{1^2\}$, $F_\nu = \{0\}, \{21^{\Omega-2}\}$ and $\{2^2 1^{\Omega-4}\}$ with $\nu = 0, 1, 2$, respectively. Then we can introduce unitary tensors B 's,

$$B(f_2 F_\nu \omega_\nu) = \sum_{v_2^i, v_2^f, \beta_2} A^\dagger(f_2 v_2^f \beta_2) A(f_2 v_2^i \beta_2) \left\langle f_2 v_2^f \overline{f_2} \overline{v_2^i} \mid F_\nu \omega_\nu \right\rangle \left\langle F_2 \beta_2 \overline{F_2} \overline{\beta_2} \mid \{0\}0 \right\rangle, \quad (4.4.1)$$

and expand \hat{H} in terms of these tensor operators. In Eq. (4.4.1), $\langle f_2 --- \rangle$ are $SU(\Omega)$ Wigner coefficients and $\langle F_2 --- \rangle$ are $SU(4)$ Wigner coefficients. Some properties of the Wigner coefficients are discussed in Appendix E. Note that in Eq. (4.4.1), irreps $\overline{f_2}$ are complex conjugate of the irreps f_2 [Bu-81]. For example, for the $U(\Omega)$ irrep $f = \{2^r\}$, the irrep that corresponds to \overline{f} is $\{2^{\Omega-r}\}$. Similarly, $\overline{f} = \{4^{\Omega-r}\}$ for $f = \{4^r\}$, $\overline{f} = \{4^{\Omega-r-2}, 2, 1\}$ for $f = \{4^r, 3, 2\}$ and so on. Using the orthonormal properties of the Wigner coefficients appearing in Eq. (4.4.1) and the action of operators A and A^\dagger on the vacuum and two-particle states respectively, it can be proved that the tensors B 's are orthonormal with respect to the traces over fixed f_2 spaces,

$$\langle \langle B(f_2 F_\nu \omega_\nu) B(f_2' F_\nu' \omega_\nu') \rangle \rangle^{f_2} = \delta_{f_2 f_2'} \delta_{F_\nu F_\nu'} \delta_{\omega_\nu \omega_\nu'}. \quad (4.4.2)$$

Expanding \hat{H} in terms of B 's will give the expansion coefficients W 's,

$$\hat{H} = \sum_{f_2, F_\nu, \omega_\nu} W(f_2 F_\nu \omega_\nu) B(f_2 F_\nu \omega_\nu), \quad (4.4.3)$$

and they can be written in terms of the $H(2)$ matrix elements using Eq. (4.4.2),

$$\begin{aligned} W(f_2 \mathbf{F}_v \omega_v) &= \langle \langle \hat{H} B(f_2 \mathbf{F}_v \omega_v) \rangle \rangle^{f_2} \\ &= \sum_{v_2^i, v_2^f} \sqrt{d_4(\tilde{f}_2)} \langle f_2 v_2^f \tilde{f}_2 \overline{v_2^i} | \mathbf{F}_v \omega_v \rangle H_{f_2 v_2^i v_2^f}(2). \end{aligned} \quad (4.4.4)$$

Now the most significant result is that the W 's are also independent Gaussian variables just as $H(2)$'s with ensemble averaged variances given by,

$$\overline{W(f_2 \mathbf{F}_v \omega_v) W(f_2' \mathbf{F}_v' \omega_v')} = \delta_{f_2 f_2'} \delta_{\mathbf{F}_v \mathbf{F}_v'} \delta_{\omega_v \omega_v'} (\lambda_{f_2})^2 d_4(F_2). \quad (4.4.5)$$

Above result is derived using Eq. (4.3.5) and (4.4.4). As we will see ahead, Eq. (4.4.5) and the (m, f_m) -space matrix elements of H as given by the Wigner-Eckart theorem applied using $SU(\Omega) \otimes SU(4)$ Wigner-Racah algebra, will completely solve EGUE(2)- $SU(4)$.

Analysis of the random matrix ensemble EGUE(2)- $SU(4)$ involves construction of the one-point function $\overline{\rho^{m, f_m}(E)}$, the ensemble averaged density of eigenvalues given by Eq. (2.3.1) with $\Gamma = f_m$ and the two-point and other higher point functions defining fluctuations. The two-point function is given by,

$$S^{m, \Gamma: m', \Gamma'}(E, E') = \overline{\rho^{m, \Gamma}(E) \rho^{m', \Gamma'}(E')} - \left\{ \overline{\rho^{m, \Gamma}(E)} \right\} \left\{ \overline{\rho^{m', \Gamma'}(E')} \right\}, \quad (4.4.6)$$

with $\rho^{m, \Gamma}(E)$ defining fixed- (m, Γ) density of eigenvalues. The two-point function $S^{m, \Gamma: m', \Gamma'}$ generates 'self-correlations' when $m = m'$ and $\Gamma = \Gamma'$ and 'cross-correlations' between states with $m \neq m'$ and/or $\Gamma \neq \Gamma'$. For EGUE(2)- $SU(4)$ ensemble, $\Gamma = f_m$. In Chapter 6, Γ corresponds to the m -particle spin S . Therefore, for EGUE(2)- $SU(4)$, the two-point function $S^{m f_m: m' f_{m'}}$ generates self-correlations when $m = m'$ and $f_m = f_{m'}$ and cross-correlations between states with $m = m'$ and $f_m \neq f_{m'}$ and also between states with $m \neq m'$ and $f_m \neq f_{m'}$. It should be emphasized that with $m = m'$ it is possible to have $f_m \neq f_{m'}$ and this should not be confused as $f_m = f_{m'}$ (confusion may arise if one substitutes the numerical value for $m = m'$). Towards deriving the forms for the one and two-point functions (discussion of higher point functions is beyond the scope of the present thesis), the moment approach is adopted and the lower or-

der moments are analyzed. By definition, all odd moments of $\overline{\rho^{m,f_m}(E)}$ will vanish and therefore the lower order moments of interest are the ensemble averaged spectral variances $\overline{\langle \hat{H}^2 \rangle^{m,f_m}}$ and the fourth moment $\overline{\langle \hat{H}^4 \rangle^{m,f_m}}$ giving the excess parameter $\gamma_2(m, f_m)$ where,

$$\gamma_2(m, f_m) = \left[\overline{\langle \hat{H}^2 \rangle^{m,f_m}} \right]^{-2} \left[\overline{\langle \hat{H}^4 \rangle^{m,f_m}} \right] - 3. \quad (4.4.7)$$

Similarly the two lower order normalized bivariate moments of the two-point function are Σ_{rr} , $r = 1, 2$ give the covariances in energy centroids and spectral variances respectively. The formulas for these are given by,

$$\begin{aligned} \Sigma_{11}(m, \Gamma; m', \Gamma') &= \frac{\overline{\langle H \rangle^{m,\Gamma} \langle H \rangle^{m',\Gamma'}}}{\left[\left\{ \overline{\langle H^2 \rangle^{m,\Gamma}} \right\} \left\{ \overline{\langle H^2 \rangle^{m',\Gamma'}} \right\} \right]^{1/2}}, \\ \Sigma_{22}(m, \Gamma; m', \Gamma') &= \frac{\overline{\langle [H]^2 \rangle^{m,\Gamma} \langle H^2 \rangle^{m',\Gamma'}}}{\left\{ \overline{\langle H^2 \rangle^{m,\Gamma}} \right\} \left\{ \overline{\langle H^2 \rangle^{m',\Gamma'}} \right\}} - 1, \end{aligned} \quad (4.4.8)$$

with $\Gamma = f_m$ and $\Gamma' = f_{m'}$ for EGUE(2)- $SU(4)$. For $m = m'$ and $f_m = f_{m'}$, the Σ_{11} and Σ_{22} give the first two terms in the normal mode decomposition of the level motion in the ensemble [Br-81, Pa-00] and hence they are of importance. Similarly for $(m = m', f_m \neq f_{m'})$ and $(m \neq m', f_m \neq f_{m'})$, the Σ_{11} and Σ_{22} are important as they generate non-zero cross-correlations that are zero if the m -particle H matrices for each f_m are represented by independent GUE's.

In order to derive the analytical results for the moments of the one and two-point functions, the basic quantity that is needed is the ensemble averaged covariance between any two m -particle matrix elements of H , i.e.,

$$\begin{aligned} &\overline{H_{f_m v_m^i v_m^f} H_{f_{m'} v_{m'}^i v_{m'}^f}} \\ &= \overline{\left\langle f_m F_m v_m^f \beta \mid \hat{H} \mid f_m F_m v_m^i \beta \right\rangle \left\langle f_{m'} F_{m'} v_{m'}^f \beta' \mid \hat{H} \mid f_{m'} F_{m'} v_{m'}^i \beta' \right\rangle}. \end{aligned} \quad (4.4.9)$$

Using the expansion given by Eq. (4.4.3) and applying Eq. (4.4.5) for the ensemble

average of the product of two W 's, $\overline{H H}$ reduces to the matrix elements of the unit tensors B 's. Wigner-Eckart theorem in $SU(\Omega)$ and $SU(4)$ spaces will give [He-74a],

$$\begin{aligned}
& \langle f_m F_m v_m^f \beta | B(f_2 \mathbf{F}_v \omega_v) | f_m F_m v_m^i \beta \rangle \\
&= \sum_{\rho} \langle f_m || B(f_2 \mathbf{F}_v) || f_m \rangle_{\rho} \langle f_m v_m^i \mathbf{F}_v \omega_v | f_m v_m^f \rangle_{\rho} \\
&= \frac{1}{\sqrt{d_{\Omega}(f_2) d_4(\tilde{f}_2)}} \sum_{\rho} \langle f_m ||| B(f_2 \mathbf{F}_v) ||| f_m \rangle_{\rho} \langle f_m v_m^i \mathbf{F}_v \omega_v | f_m v_m^f \rangle_{\rho}; \tag{4.4.10}
\end{aligned}$$

$$\langle f_m ||| B(f_2 \mathbf{F}_v) ||| f_m \rangle_{\rho} = \sum_{f_{m-2}} F(m) \frac{\mathcal{N}_{f_{m-2}}}{\mathcal{N}_{f_m}} \frac{U(f_m \overline{f_2} f_m f_2; f_{m-2} \mathbf{F}_v)_{\rho}}{U(f_m \overline{f_2} f_m f_2; f_{m-2} \{0\})},$$

where the summation is over the multiplicity index ρ and this arises as $f_m \otimes \mathbf{F}_v$ gives in general more than once the irrep f_m . In Eq. (4.4.10), $F(m) = -m(m-1)/2$ and $U(---)$ are the $SU(\Omega)$ Racah coefficients. Similarly, the standard double-barred matrix elements (called reduced matrix elements) are changed into triple-barred matrix elements in Eq. (4.4.10) for convenience. The formula for the dimension $d_{\Omega}(f_m)$ is given by Eq. (4.3.2) and the dimension \mathcal{N}_{f_m} of f_m with respect to the S_m group is [Wy-70],

$$\mathcal{N}_{f_m} = \frac{m! \prod_{i=1}^r (\ell_i - \ell_k)}{\ell_1! \ell_2! \dots \ell_r!}; \quad \ell_i = f_i + r - i. \tag{4.4.11}$$

Here, r denotes total number of rows in the Young tableaux for f_m . Correlations generated by EGUE(2)- $SU(4)$ between states with (m, f_m) and $(m', f_{m'})$ follow from the covariances between the m -particle matrix elements of H . Applying Eqs. (4.4.9), (4.4.3), (4.4.5) and (4.4.10) in that order, the final expression for $\overline{H H}$ is,

$$\begin{aligned}
& \overline{H_{f_m v_m^i v_m^f} H_{f_{m'} v_{m'}^i v_{m'}^f}} \\
&= \sum_{f_2, \mathbf{F}_v, \omega_v} \frac{(\lambda_{f_2})^2}{d_{\Omega}(f_2)} \sum_{\rho, \rho'} \langle f_m ||| B(f_2 \mathbf{F}_v) ||| f_m \rangle_{\rho} \langle f_{m'} ||| B(f_2 \mathbf{F}_v) ||| f_{m'} \rangle_{\rho'} \tag{4.4.12} \\
&\times \langle f_m v_m^i \mathbf{F}_v \omega_v | f_m v_m^f \rangle_{\rho} \langle f_{m'} v_{m'}^i \mathbf{F}_v \omega_v | f_{m'} v_{m'}^f \rangle_{\rho'}.
\end{aligned}$$

In the following section, we will consider $\overline{\langle \hat{H}^2 \rangle^{m, f_m}}$ and $\overline{\langle \hat{H}^r \rangle^{m, f_m} \langle \hat{H}^r \rangle^{m', f_{m'}}}$; $r = 1, 2$. It is important to mention here that in evaluating these moments, the Wigner coefficients appearing in Eq. (4.4.12) will eventually disappear due to the orthonormal properties of these coefficients [see Eqs. (E6a) and (E6b)] and therefore the final results for these moments will involve only the $SU(\Omega)$ Racah coefficients given in Eq. (4.4.10). In Appendix F, we will consider $\overline{\langle \hat{H}^4 \rangle^{m, f_m}}$ and the algebra here is more complicated giving additional Racah coefficients than in Eq. (4.4.10).

From now onwards, we drop the “hat” symbol over the H operator when there is no confusion.

4.5 Exact Expressions for Spectral Variances, Lower Order Cross-correlations and Analytical Results for Lowest $U(\Omega)$ Irreps

4.5.1 Covariances in energy centroids $\overline{\langle H \rangle^{m, f_m} \langle H \rangle^{m', f_{m'}}}$

Firstly the ensemble averaged energy centroid $\overline{\langle H \rangle^{m, f_m}} = 0$ by the definition of EGUE(2)- $SU(4)$ ensemble. As $\langle H \rangle^{m, f_m}$ is the trace of H (divided by the dimensionality) in (m, f_m) space, only $F_v = \{0\}$ will generate this. Therefore for $\overline{\langle H \rangle \langle H \rangle}$, the Wigner coefficients in Eq. (4.4.12) and the ratio of the U -coefficients in Eq. (4.4.10) will be unity. Then trivially,

$$\begin{aligned} \overline{\langle H \rangle^{m, f_m} \langle H \rangle^{m', f_{m'}}} &= F(m) F(m') \sum_{f_2} \frac{(\lambda_{f_2})^2}{d_\Omega(f_2)} \sum_{f_{m-2}} \frac{\mathcal{N}_{f_{m-2}}}{\mathcal{N}_{f_m}} \sum_{f_{m'-2}} \frac{\mathcal{N}_{f_{m'-2}}}{\mathcal{N}_{f_{m'}}} \\ &= \sum_{f_2} \frac{(\lambda_{f_2})^2}{d_\Omega(f_2)} P^{f_2}(m, f_m) P^{f_2}(m', f_{m'}), \end{aligned} \quad (4.5.1)$$

where,

$$P^{f_2}(m, f_m) = F(m) \sum_{f_{m-2}} \frac{\mathcal{N}_{f_{m-2}}}{\mathcal{N}_{f_m}}. \quad (4.5.2)$$

Table 4.3 gives the expression for $P^{f_2}(m, f_m)$ for the irreps $f_m^{(p)}$. It is possible to derive Eq. (4.5.1) using the trace propagation formula for the energy centroids [Pa-78],

$$E_c(m, f_m) = \langle H \rangle^{m, f_m} = a_0 + a_1 m + a_2 m^2 + a_3 \langle C_2[SU(4)] \rangle^{\tilde{f}_m}$$

$$\begin{aligned}
\Rightarrow E_c(m, f_m) &= \frac{3m^2 + 12m - 4 \langle C_2 [SU(4)] \rangle^{\tilde{f}_m}}{16} \langle H \rangle^{2, \{2\}} \\
&+ \frac{5m^2 - 20m + 4 \langle C_2 [SU(4)] \rangle^{\tilde{f}_m}}{16} \langle H \rangle^{2, \{1^2\}}.
\end{aligned} \tag{4.5.3}$$

Note that $\langle C_2 [SU(4)] \rangle^{\tilde{f}_m} = \langle C_2 [U(4)] \rangle^{\tilde{f}_m} - m^2/4$ with $\langle C_2 [U(4)] \rangle^{\tilde{f}_m}$ given by Eq. (4.2.21).

We have verified that Eq. (4.5.3) reproduces the results given in Table 4.3.

Table 4.3: $P^{f_2}(m, f_m)$ for $f_m = f_m^{(p)} = \{4^r, p\}$ and $f_2 = \{2\}$ and $\{1^2\}$. See Eq. (4.5.2) for the definition of $P^{f_2}(m, f_m)$.

$f_m^{(p)}$	$P^{f_2}(m, f_m^{(p)})$	
	$f_2 = \{2\}$	$f_2 = \{1^2\}$
$\{4^r\}$	$-3r(r+1)$	$-5r(r-1)$
$\{4^r, 1\}$	$-\frac{3r}{2}(2r+3)$	$-\frac{5r}{2}(2r-1)$
$\{4^r, 2\}$	$-(3r^2 + 6r + 1)$	$-5r^2$
$\{4^r, 3\}$	$-\frac{3}{2}(r+2)(2r+1)$	$-\frac{5r}{2}(2r+1)$

4.5.2 Spectral variances $\overline{\langle H^2 \rangle^{m, f_m}}$

Writing $\overline{\langle H^2 \rangle^{m, f_m}}$ explicitly in terms of the m -particle H matrix elements,

$$\overline{\langle H^2 \rangle^{m, f_m}} = \frac{1}{d_\Omega(f_m)} \sum_{v_m^1, v_m^2} \overline{H_{f_m v_m^1 v_m^2} H_{f_m v_m^2 v_m^1}}, \tag{4.5.4}$$

and then applying Eqs. (4.4.10) and (4.4.12) and the orthonormal properties of the $SU(\Omega)$ Wigner coefficients (see Appendix E) lead to

$$\begin{aligned}
\overline{\langle H^2 \rangle^{m, f_m}} &= \sum_{f_2} \frac{(\lambda_{f_2})^2}{d_\Omega(f_2)} \sum_{v=0,1,2} \sum_{\rho} \left| \langle f_m ||| B(f_2, \mathbf{F}_v) ||| f_m \rangle_{\rho} \right|^2 \\
&= \sum_{f_2} \frac{(\lambda_{f_2})^2}{d_\Omega(f_2)} \sum_{v=0,1,2} \mathcal{Q}^v(f_2 : m, f_m).
\end{aligned} \tag{4.5.5}$$

The functions $\mathcal{Q}^\nu(f_2 : m, f_m)$ involve $SU(\Omega)$ U -coefficients and the explicit expression is,

$$\begin{aligned} \mathcal{Q}^\nu(f_2 : m, f_m) &= [F(m)]^2 \sum_{f_{m-2}, f'_{m-2}} \frac{\mathcal{N}_{f_{m-2}}}{\mathcal{N}_{f_m}} \frac{\mathcal{N}_{f'_{m-2}}}{\mathcal{N}_{f_m}} X_{UU}(f_2; f_{m-2}, f'_{m-2}; \mathbf{F}_\nu); \\ X_{UU}(f_2; f_{m-2}, f'_{m-2}; \mathbf{F}_\nu) &= \\ \sum_{\rho} \frac{U(f_m, \overline{f_2}, f_m, f_2; f_{m-2}, \mathbf{F}_\nu)_\rho U(f_m, \overline{f_2}, f_m, f_2; f'_{m-2}, \mathbf{F}_\nu)_\rho}{U(f_m, \overline{f_2}, f_m, f_2; f_{m-2}, \{0\}) U(f_m, \overline{f_2}, f_m, f_2; f'_{m-2}, \{0\})}. \end{aligned} \quad (4.5.6)$$

Tabulations for X_{UU} (also for Y_{UU} defined ahead) or equivalently $SU(\Omega)$ U -coefficients, though in a complex form, are available in [He-74a]. However to gain insight into the spectral variances and the cross-correlations Σ_{rr} , we derive analytical results by restricting ourselves to the physically relevant (in nuclear structure; see Section 4.2) irreps $f_m^{(p)}$.

Summation over the multiplicity index ρ appearing in Eq. (4.5.6) [also Eq. (4.5.17) ahead] arises naturally in applications to physical problems as all the physically relevant results should be independent of ρ which is a label for equivalent $SU(\Omega)$ irreps. Hecht derived formulas for the sums in X_{UU} (also Y_{UU} defined ahead) in the context of spectral distribution methods in nuclei [He-74a]. Tabulations for $X_{UU}(f_2; f_{m-2}, f'_{m-2}; \mathbf{F}_\nu)$ are collected in Table 4.4 and they are given in terms of the so-called axial distances τ_{ij} for the boxes i and j in a given Young tableaux. Given a Young tableaux $\{f_m\}$, the axial distance τ_{ij} between the last box in row i and the last box in row j is $\tau_{ij} = f_i - f_j + j - i$, with f_k being the number of boxes in the row k . The f_{m-2} irreps are obtained by removing the two-particle symmetric ($f_2 = \{2\}$) or anti-symmetric ($f_2 = \{1^2\}$) irreps from f_m . Figure 4.2 shows all the allowed f_{m-2} 's for the irreps $f_m^{(p)}$. In the figure, a and b (or c) denote the last boxes in the rows a and b (or c), respectively, that are to be removed from the Young tableaux $\{4^r, p\}$ to obtain the allowed f_{m-2} irreps for $f_2 = \{2\}$ and $\{1^2\}$. It is seen that unlike for EGUE(2)-s studied in [Ko-07], for the EGUE(2)- $SU(4)$ ensemble we need a much wider variety of X_{UU} 's. Results in Table 4.4 (also Table 4.7) for any f_m are given in terms of the following func-

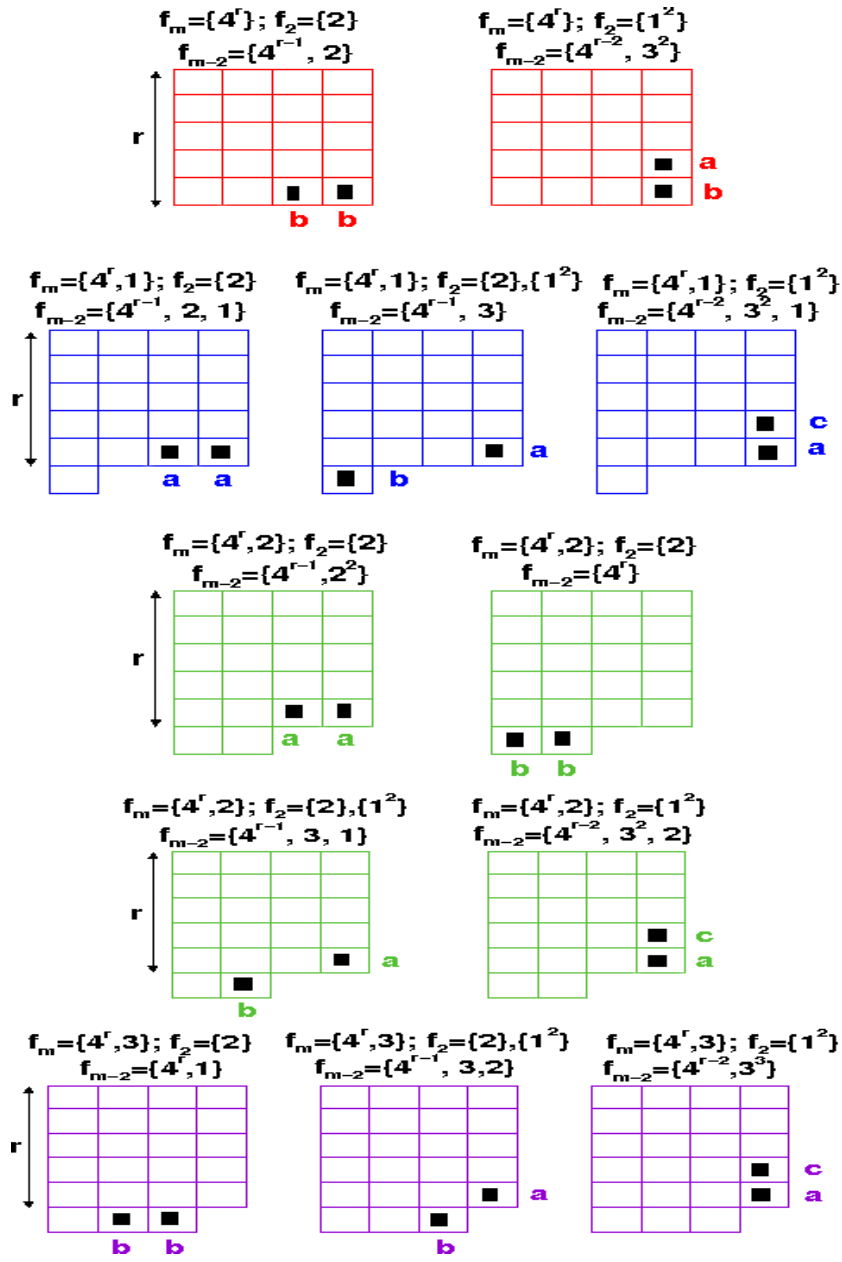


Figure 4.2: Schematic representation of the Young tableaux $f_m = f_m^{(p)} = \{4^r, p\}$ with $p = 0, 1, 2$ and 3. Shown are the boxes with filled squares denoted by a , b and c whose removal from the irrep f_m generates the irreps f_{m-2} by action of $\overline{f_2}$ where $f_2 = \{2\}$ and $\{1^2\}$.

tions,

$$\Pi_a^{(b)} = \prod_{i=1,2,\dots,\Omega; i \neq a, i \neq b} (1 - 1/\tau_{ai}) , \quad (4.5.7a)$$

$$\Pi_b^{(a)} = \prod_{i=1,2,\dots,\Omega; i \neq a, i \neq b} (1 - 1/\tau_{bi}) .$$

$$\Pi'_a = \prod_{i=1,2,\dots,\Omega; i \neq a} (1 - 1/\tau_{ai}) , \quad (4.5.7b)$$

$$\Pi''_a = \prod_{i=1,2,\dots,\Omega; i \neq a} (1 - 2/\tau_{ai}) .$$

$$\Pi_a^{(bc)} = \prod_{i=1,2,\dots,\Omega; i \neq a, i \neq b, i \neq c} (1 - 1/\tau_{ai}) ; \quad a \neq b \neq c . \quad (4.5.7c)$$

In [He-74a], the functions $\Pi_a^{(b)}$ and $\Pi_b^{(a)}$ are called Π_a and Π_b , respectively and sometimes this (Π_a, Π_b) notation is confusing. Further, we have introduced the functions Π'_a , Π''_a and $\Pi_a^{(bc)}$. These and the notation $\Pi_a^{(b)}$ and $\Pi_b^{(a)}$ simplify considerably the formulas given by Hecht [He-74a] and therefore the results in Table 4.4 (also Table 4.7) are much easier to use in practice. Table 4.5 gives τ_{ab} , $\Pi_a^{(b)}$, $\Pi_b^{(a)}$, Π'_a , Π''_a and $\Pi_a^{(bc)}$ for the irreps $f_m^{(p)}$ which are required for deriving analytical formulas for the corresponding $X_{UU}(f_2; f_{m-2}, f'_{m-2}; \mathbf{F}_v)$ and also $Y_{UU}(f_{m-2}, f'_{m-2}; \mathbf{F}_v)$ defined ahead. Also given in the table are $\mathcal{N}_{f_{m-2}}/\mathcal{N}_{f_m}$ obtained by simplifying Eq. (4.4.11). Combining the results in Tables 4.4 and 4.5 and carrying out simplifications, final formulas for $\langle H^2 \rangle^{m, f_m}$ are obtained and they are given in Table 4.6. In principle, the operator generating $\langle H^2 \rangle^{m, f_m}$ for any two or (1+2)-body H , will be a polynomial of maximum body rank 4 in the number operator \hat{n} and the quadratic, cubic and quartic invariants of the $SU(4)$ algebra. The expansion coefficients in the resulting formula will involve $\langle H^2 \rangle^{m, f_m}$ with $m = 0$ to 4 [Pa-73, Pa-72] and they can be calculated by constructing the ensemble, for a fixed Ω , on a computer. Using these inputs, the propagation equation can be used to compute spectral variances for any (m, f_m) . However Eqs. (4.5.5) and (4.5.6) give the ensemble averaged variances directly in terms of $SU(\Omega)$ U -coefficients.

Table 4.4: Formulas for $X_{UU}(f_2; f_{m-2}, f'_{m-2}; \mathbf{F}_v)$ defined in Eq. (4.5.6). Note that $\{f(ab)\}\{f(ab)\}$ entries satisfy the $a \leftrightarrow b$ symmetry correctly. Similarly the entries $\{f(ab)\}\{f(ac)\}$ are independent of $b \leftrightarrow c$ interchange as required by the X_{UU} function. See text for details.

$\{f_{m-2}\}\{f'_{m-2}\}$	$X_{UU}(\{1^2\}; f_{m-2}, f'_{m-2}; \{2, 1^{\Omega-2}\})$
$\{f(ab)\}\{f(ab)\}$	$\frac{\Omega(\Omega-1)}{2(\Omega-2)} \left\{ \left(1 + \frac{1}{\tau_{ab}}\right) \frac{1}{\Pi_b^{(a)}} + \left(1 - \frac{1}{\tau_{ab}}\right) \frac{1}{\Pi_a^{(b)}} - \frac{4}{\Omega} \right\}$

Table 4.4 – continued

$\{f(ab)\} \{f(ac)\}$	$\frac{\Omega(\Omega-1)}{2(\Omega-2)} \left\{ \frac{1}{\Pi_a^{(bc)}} - \frac{4}{\Omega} \right\}$
$\{f(cd)\} \{f(ab)\}$	$-\frac{2(\Omega-1)}{(\Omega-2)}$
$\{f_{m-2}\} \{f'_{m-2}\}$	$X_{UU}(\{1^2\}; f_{m-2}, f'_{m-2}; \{2^2, 1^{\Omega-4}\})$
$\{f(ab)\} \{f(ab)\}$	$\frac{\Omega}{(\Omega-2)} \left\{ 1 + \frac{(\Omega-1)(\Omega-2)}{2\Pi_a^{(b)}\Pi_b^{(a)}} - \frac{(\Omega-1)}{2} \right.$ $\times \left[\left(1 + \frac{1}{\tau_{ab}}\right) \frac{1}{\Pi_b^{(a)}} + \left(1 - \frac{1}{\tau_{ab}}\right) \frac{1}{\Pi_a^{(b)}} \right] \left. \right\}$
$\{f(ab)\} \{f(ac)\}$	$\frac{\Omega(\Omega-1)}{2(\Omega-2)} \left\{ \frac{2}{\Omega-1} - \frac{1}{\Pi_a^{(bc)}} \right\}$
$\{f(cd)\} \{f(ab)\}$	$\frac{\Omega}{(\Omega-2)}$
$\{f_{m-2}\} \{f'_{m-2}\}$	$X_{UU}(\{2\}; f_{m-2}, f'_{m-2}; \{2, 1^{\Omega-2}\})$
$\{f(ab)\} \{f(ab)\}$	$\frac{\Omega(\Omega+1)}{2(\Omega+2)} \left\{ \frac{(\tau_{ab}-1)^2}{\tau_{ab}(\tau_{ab}+1)} \frac{1}{\Pi_b^{(a)}} + \frac{(\tau_{ab}+1)^2}{\tau_{ab}(\tau_{ab}-1)} \frac{1}{\Pi_a^{(b)}} - \frac{4}{\Omega} \right\}$
$\{f(aa)\} \{f(aa)\}$	$\frac{2\Omega(\Omega+1)}{(\Omega+2)} \left\{ \frac{1}{\Pi'_a} - \frac{1}{\Omega} \right\}$
$\{f(aa)\} \{f(bb)\}$	
or	$-\frac{2(\Omega+1)}{(\Omega+2)}$
$\{f(aa)\} \{f(bc)\}$	
$\{f(aa)\} \{f(ab)\}$	$\frac{\Omega(\Omega+1)}{(\Omega+2)} \left\{ \frac{(\tau_{ab}+1)}{(\tau_{ab}-1)} \frac{1}{\Pi_a^{(b)}} - \frac{2}{\Omega} \right\}$
$\{f(ab)\} \{f(ac)\}$	$\frac{\Omega(\Omega+1)}{2(\Omega+2)} \left\{ \frac{(\tau_{ab}+1)(\tau_{ac}+1)}{(\tau_{ab}-1)(\tau_{ac}-1)} \frac{1}{\Pi_a^{(bc)}} - \frac{4}{\Omega} \right\}$
$\{f(ab)\} \{f(cd)\}$	$-\frac{2(\Omega+1)}{(\Omega+2)}$
$\{f_{m-2}\} \{f'_{m-2}\}$	$X_{UU}(\{2\}; f_{m-2}, f'_{m-2}; \{4, 2^{\Omega-2}\})$

Table 4.4 – continued

$\{f(ab)\} \{f(ab)\}$	$\frac{\Omega(\Omega+1)}{2} \left\{ \frac{1}{\Pi_a^{(b)} \Pi_b^{(a)}} + \frac{2}{(\Omega+1)(\Omega+2)} \right.$
	$\left. - \frac{1}{(\Omega+2)} \left[\frac{(\tau_{ab}-1)^2}{\tau_{ab}(\tau_{ab}+1)} \frac{1}{\Pi_b^{(a)}} + \frac{(\tau_{ab}+1)^2}{\tau_{ab}(\tau_{ab}-1)} \frac{1}{\Pi_a^{(b)}} \right] \right\}$
$\{f(aa)\} \{f(aa)\}$	$\frac{\Omega}{(\Omega+2)} \left\{ 1 - 2(\Omega+1) \frac{1}{\Pi'_a} + \frac{(\Omega+1)(\Omega+2)}{2} \frac{1}{\Pi''_a} \right\}$
$\{f(aa)\} \{f(bb)\}$	
or	$\frac{\Omega}{(\Omega+2)}$
$\{f(aa)\} \{f(bc)\}$	
$\{f(aa)\} \{f(ab)\}$	$\frac{\Omega}{(\Omega+2)} \left\{ 1 - \frac{(\Omega+1)(\tau_{ab}+1)}{(\tau_{ab}-1)\Pi_a^{(b)}} \right\}$
$\{f(ab)\} \{f(ac)\}$	$\frac{\Omega}{(\Omega+2)} \left\{ 1 - \frac{(\Omega+1)(\tau_{ab}+1)(\tau_{ac}+1)}{2(\tau_{ab}-1)(\tau_{ac}-1)} \frac{1}{\Pi_a^{(bc)}} \right\}$
$\{f(ab)\} \{f(cd)\}$	$\frac{\Omega}{(\Omega+2)}$

4.5.3 Cross-correlations in energy centroids $\Sigma_{11}(m, f_m; m', f_{m'})$

Analysis of the random matrix ensembles with various symmetries involves construction of the one-point function $\overline{\rho^{m,\Gamma}(E)}$ given by Eq. (2.3.1) and the two-point and other higher point functions defining fluctuations. Covariances in energy centroids $\Sigma_{11}(m, f_m; m', f_{m'})$ follow from Eqs. (4.4.8), (4.5.1) and (4.5.5),

$$\Sigma_{11}(m, f_m; m', f_{m'}) = \frac{\sum_{f_2} \frac{(\lambda_{f_2})^2}{d_\Omega(f_2)} P^{f_2}(m, f_m) P^{f_2}(m', f_{m'})}{\left[\left\{ \overline{\langle H^2 \rangle^{m, f_m}} \right\} \left\{ \overline{\langle H^2 \rangle^{m', f_{m'}}} \right\} \right]^{1/2}}. \quad (4.5.8)$$

For the irreps $f_m^{(p)}$, formulas for the functions $P^{f_2}(m, f_m)$ and the variances $\overline{\langle H^2 \rangle^{m, f_m}}$ are given in Tables 4.3 and 4.6, respectively. Table 4.4 gives X_{UU} required for calculating the covariances for any general f_m . To gain some insight into the structure

Table 4.5: Axial distances τ_{ab} and the functions $\Pi_a^{(b)}$, $\Pi_b^{(a)}$, Π'_a and Π''_a for the irreps $f_m^{(p)}$ shown in Fig. 4.2. For the situations with $f(ac)$, $\tau_{ab} \rightarrow \tau_{ac}$, $\Pi_a^{(b)} \rightarrow \Pi_a^{(c)}$ and $\Pi_b^{(a)} \rightarrow \Pi_c^{(a)}$. Also for $f(bb)$, $\Pi'_a \rightarrow \Pi'_b$ and $\Pi''_a \rightarrow \Pi''_b$. For $f_2 = \{1^2\}$ and for $f_m^{(p)} = \{4^r, p\}$ with $p \neq 0$, we need $\Pi_a^{(bc)}$ (see Fig. 4.2 for a, b and c) and for the examples in the Table, we have $\Pi_a^{(bc)} = 5r/[2(4 + \Omega - r)]$.

$f_m^{(p)}$	f_2	f_{m-2}	τ_{ab}	$\frac{1}{\Pi_a^{(b)}}$	$\frac{1}{\Pi_b^{(a)}}$	$\frac{1}{\Pi'_a}$	$\frac{1}{\Pi''_a}$	$\frac{\mathcal{N}_{f_{m-2}}}{\mathcal{N}_{f_m}}$
$\{4^r\}$	$\{2\}$	$\{4^{r-1}, 2\}$	–	–	–	$\frac{4 + \Omega - r}{4r}$	$\frac{(4 + \Omega - r)(3 + \Omega - r)}{6r(r + 1)}$	$\frac{3(r + 1)}{2(4r - 1)}$
		$\rightarrow f(bb)$						
	$\{1^2\}$	$\{4^{r-2}, 3^2\}$	+1	$\frac{5 + \Omega - r}{5(r - 1)}$	$\frac{4 + \Omega - r}{2r}$	–	–	$\frac{5(r - 1)}{2(4r - 1)}$
		$\rightarrow f(ab)$						
$\{4^r, 1\}$	$\{2\}$	$\{4^{r-1}, 2, 1\}$	–	–	–	$\frac{4(4 + \Omega - r)}{15r}$	$\frac{(4 + \Omega - r)(3 + \Omega - r)}{5r(r + 1)}$	$\frac{5(r + 1)}{4(4r + 1)}$
		$\rightarrow f(aa)$						
		$\{4^{r-1}, 3\}$	+4	$\frac{4 + \Omega - r}{5r}$	$\frac{5(\Omega - r)}{r + 4}$	–	–	$\frac{r + 4}{4(4r + 1)}$
		$\rightarrow f(ab)$						
	$\{1^2\}$	$\{4^{r-1}, 3\}$	+4	$\frac{4 + \Omega - r}{5r}$	$\frac{5(\Omega - r)}{r + 4}$	–	–	$\frac{r + 4}{4(4r + 1)}$
		$\rightarrow f(ab)$						
		$\{4^{r-2}, 3^2, 1\}$	–1	$\frac{8(4 + \Omega - r)}{15r}$	$\frac{5(5 + \Omega - r)}{24(r - 1)}$	–	–	$\frac{9(r - 1)}{4(4r + 1)}$
		$\rightarrow f(ac)$						

Table 4.5 – (continued)

$f_m^{(p)}$	f_2	f_{m-2}	τ_{ab}	$\frac{1}{\Pi_a^{(b)}}$	$\frac{1}{\Pi_b^{(a)}}$	$\frac{1}{\Pi_a'}$	$\frac{1}{\Pi_a''}$	$\frac{\mathcal{N}_{f_{m-2}}}{\mathcal{N}_{f_m}}$
$\{4^r, 2\}$	$\{2\}$	$\{4^r\}$	–	–	–	$\frac{3(1+\Omega-r)}{2(r+3)}$	$\frac{6(\Omega-r)(1+\Omega-r)}{(r+3)(r+4)}$	$\frac{(r+3)(r+4)}{6(4r+1)(4r+2)}$
		$\rightarrow f(bb)$						
		$\{4^{r-1}, 2^2\}$	–	–	–	$\frac{3(4+\Omega-r)}{10r}$	$\frac{3(3+\Omega-r)(4+\Omega-r)}{10r(r+1)}$	$\frac{10r(r+1)}{3(4r+1)(4r+2)}$
		$\rightarrow f(aa)$						
		$\{4^{r-1}, 3, 1\}$	+3	$\frac{4+\Omega-r}{5r}$	$\frac{2(1+\Omega-r)}{r+3}$	–	–	$\frac{5r(r+3)}{2(4r+1)(4r+2)}$
		$\rightarrow f(ab)$						
		$\{4^{r-1}, 3, 1\}$	+3	$\frac{4+\Omega-r}{5r}$	$\frac{2(1+\Omega-r)}{r+3}$	–	–	$\frac{5r(r+3)}{2(4r+1)(4r+2)}$
		$\rightarrow f(ab)$						
		$\{4^{r-2}, 3^2, 2\}$	–1	$\frac{3(4+\Omega-r)}{5r}$	$\frac{2(5+\Omega-r)}{9(r-1)}$	–	–	$\frac{15r(r-1)}{2(4r+1)(4r+2)}$
		$\rightarrow f(ac)$						
$\{4^r, 3\}$	$\{2\}$	$\{4^r, 1\}$	–	–	–	$\frac{2(2+\Omega-r)}{3(r+2)}$	$\frac{(1+\Omega-r)(2+\Omega-r)}{(r+2)(r+3)}$	$\frac{(r+2)(r+3)}{(4r+2)(4r+3)}$
		$\rightarrow f(bb)$						
		$\{4^{r-1}, 3, 2\}$	+2	$\frac{4+\Omega-r}{5r}$	$\frac{(2+\Omega-r)}{r+2}$	–	–	$\frac{5r(r+2)}{(4r+2)(4r+3)}$
		$\rightarrow f(ab)$						
		$\{4^{r-1}, 3, 2\}$	+2	$\frac{4+\Omega-r}{5r}$	$\frac{(2+\Omega-r)}{r+2}$	–	–	$\frac{5r(r+2)}{(4r+2)(4r+3)}$
		$\rightarrow f(ab)$						
		$\{4^{r-2}, 3^3\}$	–1	$\frac{4(4+\Omega-r)}{5r}$	$\frac{(5+\Omega-r)}{4(r-1)}$	–	–	$\frac{5r(r-1)}{(4r+2)(4r+3)}$
		$\rightarrow f(ac)$						

of $\Sigma_{11}(m, f_m; m', f_{m'})$, we consider the dilute limit defined by $\Omega \rightarrow \infty$, $r \gg 1$ and $r/\Omega \rightarrow 0$. Then the variance formulas in Table 4.6 take a simple form for all $f_m^{(p)}$,

$$\overline{\langle H^2 \rangle^{m, f_m^{(p)}}} = -\frac{\Omega^2}{2} \left[\lambda_{\{2\}}^2 P^{\{2\}}(m, f_m^{(p)}) + \lambda_{\{1^2\}}^2 P^{\{1^2\}}(m, f_m^{(p)}) \right]. \quad (4.5.9)$$

Combining Eqs. (4.5.8) and (4.5.9), we have

$$\Sigma_{11}(m, f_m^{(p)}; m', f_{m'}^{(p)}) \xrightarrow{\Omega \rightarrow \infty, r \gg 1} \frac{4}{\Omega^4} \frac{\sum_{f_2} \lambda_{f_2}^2 P^{f_2}(m, f_m^{(p)}) P^{f_2}(m', f_{m'}^{(p)})}{\left[\left\{ \sum_{f_2} \lambda_{f_2}^2 P^{f_2}(m, f_m^{(p)}) \right\} \left\{ \sum_{f_2} \lambda_{f_2}^2 P^{f_2}(m', f_{m'}^{(p)}) \right\} \right]^{1/2}}. \quad (4.5.10)$$

Thus, $\Sigma_{11}(m, f_m^{(p)}; m', f_{m'}^{(p)})$ will be zero as $\Omega \rightarrow \infty$ and there will be no cross-correlations. However for finite Ω , there will be correlations between energy centroids of different states and some examples are discussed ahead.

Table 4.6: Ensemble averaged spectral variances $\overline{\langle H^2 \rangle^{m, f_m^{(p)}}}$ for various $f_m = f_m^{(p)}$.

$f_m^{(p)}$	$\overline{\langle H^2 \rangle^{m, f_m^{(p)}}}$
$\{4^r\}$	$\frac{r(\Omega - r + 4)}{2} \left[\lambda_{\{2\}}^2 3(r+1)(\Omega - r + 3) + \lambda_{\{1^2\}}^2 5(r-1)(\Omega - r + 5) \right]$
$\{4^r, 1\}$	$\frac{r(\Omega - r + 4)}{4} \left[\lambda_{\{2\}}^2 \{6r(\Omega - r + 1) + 9\Omega + 15\} + \lambda_{\{1^2\}}^2 5\{2r(\Omega - r + 5) - \Omega - 9\} \right]$
$\{4^r, 2\}$	$\lambda_{\{2\}}^2 \frac{1}{2} \left[3r^4 - 6(\Omega + 2)r^3 + (3\Omega^2 + 6\Omega - 5)r^2 + (\Omega + 2)(6\Omega + 17)r + \Omega(\Omega + 1) \right] + \lambda_{\{1^2\}}^2 \frac{5r}{2} (\Omega - r + 4) \{(\Omega + 4)r - r^2 - 3\}$
$\{4^r, 3\}$	$\frac{1}{4} \left[\lambda_{\{2\}}^2 3(r+2)(\Omega - r + 2)(2r\Omega - 2r^2 + 6r + \Omega + 1) + \lambda_{\{1^2\}}^2 5r(\Omega - r + 4)(2r\Omega - 2r^2 + 6r + \Omega - 1) \right]$

4.5.4 Cross-correlations in spectral variances $\Sigma_{22}(m, f_m; m', f_{m'})$

Expression for $\Sigma_{22}(m, f_m; m', f_{m'})$ given by Eq. (4.4.8) involves evaluation of

$$\overline{\langle H^2 \rangle^{m, f_m} \langle H^2 \rangle^{m', f_{m'}}}.$$

As the two-body H operator defined in Eq. (4.3.1) is a sum of H 's in two-particle spaces defined by $f_2 = \{2\}$ and $\{1^2\}$, we have $H(2) = H_{\{2\}}(2) + H_{\{1^2\}}(2)$. The H_{f_2} 's are independent and the variables defining the matrix elements of H_{f_2} are independent Gaussian variables with zero center and variance given by Eq. (4.3.5). Expanding $\overline{\langle H^2 \rangle^{m, f_m} \langle H^2 \rangle^{m', f_{m'}}}$ and using Eqs. (4.3.5) and (4.3.6), we obtain

$$\begin{aligned} & \overline{\langle H^2 \rangle^{m, f_m} \langle H^2 \rangle^{m', f_{m'}}} \\ &= \overline{\langle (H_{\{2\}})^2 \rangle^{m, f_m} \langle (H_{\{2\}})^2 \rangle^{m', f_{m'}}} + \overline{\langle (H_{\{1^2\}})^2 \rangle^{m, f_m} \langle (H_{\{1^2\}})^2 \rangle^{m', f_{m'}}} \\ &+ \left\{ \overline{\langle (H_{\{2\}})^2 \rangle^{m, f_m}} \right\} \left\{ \overline{\langle (H_{\{1^2\}})^2 \rangle^{m', f_{m'}}} \right\} + \left\{ \overline{\langle (H_{\{1^2\}})^2 \rangle^{m, f_m}} \right\} \left\{ \overline{\langle (H_{\{2\}})^2 \rangle^{m', f_{m'}}} \right\} \\ &+ 4 \overline{\langle H_{\{2\}} H_{\{1^2\}} \rangle^{m, f_m} \langle H_{\{1^2\}} H_{\{2\}} \rangle^{m', f_{m'}}}. \end{aligned} \tag{4.5.11}$$

Similarly, expanding $\overline{\langle H^2 \rangle^{m, f_m} \langle H^2 \rangle^{m', f_{m'}}}$ gives,

$$\begin{aligned} \left\{ \overline{\langle H^2 \rangle^{m, f_m}} \right\} \left\{ \overline{\langle H^2 \rangle^{m', f_{m'}}} \right\} &= \left\{ \overline{\langle (H_{\{2\}})^2 \rangle^{m, f_m}} \right\} \left\{ \overline{\langle (H_{\{2\}})^2 \rangle^{m', f_{m'}}} \right\} \\ &+ \left\{ \overline{\langle (H_{\{2\}})^2 \rangle^{m, f_m}} \right\} \left\{ \overline{\langle (H_{\{1^2\}})^2 \rangle^{m', f_{m'}}} \right\} \\ &+ \left\{ \overline{\langle (H_{\{1^2\}})^2 \rangle^{m, f_m}} \right\} \left\{ \overline{\langle (H_{\{2\}})^2 \rangle^{m', f_{m'}}} \right\} \\ &+ \left\{ \overline{\langle (H_{\{1^2\}})^2 \rangle^{m, f_m}} \right\} \left\{ \overline{\langle (H_{\{1^2\}})^2 \rangle^{m', f_{m'}}} \right\}. \end{aligned} \tag{4.5.12}$$

Using Eqs. (4.5.11) and (4.5.12) in the expression for Σ_{22} given by Eq. (4.4.8), the numerator simplifies to give

$$\begin{aligned}
& \overline{\langle H^2 \rangle^{m,f_m} \langle H^2 \rangle^{m',f_{m'}}} - \left\{ \overline{\langle H^2 \rangle^{m,f_m}} \right\} \left\{ \overline{\langle H^2 \rangle^{m',f_{m'}}} \right\} \\
&= \left\{ \overline{\langle (H_{\{2\}})^2 \rangle^{m,f_m} \langle (H_{\{2\}})^2 \rangle^{m',f_{m'}}} - \left[\overline{\langle (H_{\{2\}})^2 \rangle^{m,f_m}} \right] \left[\overline{\langle (H_{\{2\}})^2 \rangle^{m',f_{m'}}} \right] \right\} \\
&+ \left\{ \overline{\langle (H_{\{1^2\}})^2 \rangle^{m,f_m} \langle (H_{\{1^2\}})^2 \rangle^{m',f_{m'}}} - \left[\overline{\langle (H_{\{1^2\}})^2 \rangle^{m,f_m}} \right] \left[\overline{\langle (H_{\{1^2\}})^2 \rangle^{m',f_{m'}}} \right] \right\} \\
&+ 4 \overline{\langle H_{\{2\}} H_{\{1^2\}} \rangle^{m,f_m} \langle H_{\{1^2\}} H_{\{2\}} \rangle^{m',f_{m'}}} \\
&= X_{\{2\}} + X_{\{1^2\}} + 4 X_{\{1^2\}\{2\}} .
\end{aligned} \tag{4.5.13}$$

Then, we have

$$\Sigma_{22}(m, f_m; m', f_{m'}) = \frac{X_{\{2\}} + X_{\{1^2\}} + 4 X_{\{1^2\}\{2\}}}{\left[\overline{\langle H^2 \rangle^{m,f_m}} \right] \left[\overline{\langle H^2 \rangle^{m',f_{m'}}} \right]} . \tag{4.5.14}$$

To evaluate $X_{\{2\}}$ and $X_{\{1^2\}}$, we use Eq. (4.4.3) and carry out the ensemble averaging over W 's using the fact that W 's are Gaussian random variables with zero center and variance given by Eq. (4.4.5). Then, Eq. (4.4.10) and the sum rules for $SU(\Omega)$ Wigner coefficients [see Eqs. (E6a) and (E6b)] will give,

$$X_{f_2} = \frac{2(\lambda_{f_2})^4}{[d_\Omega(f_2)]^2} \sum_{v=0,1,2} [d(\mathbf{F}_v)]^{-1} \mathcal{Q}^v(f_2 : m, f_m) \mathcal{Q}^v(f_2 : m', f_{m'}) . \tag{4.5.15}$$

Similarly, we have

$$\begin{aligned}
X_{\{1^2\}\{2\}} &= \frac{\lambda_{\{2\}}^2 \lambda_{\{1^2\}}^2}{d_\Omega(\{2\}) d_\Omega(\{1^2\})} \\
&\times \sum_{v=0,1} [d(\mathbf{F}_v)]^{-1} R^v(\{1^2\}\{2\} : m, f_m) R^v(\{1^2\}\{2\} : m', f_{m'}) .
\end{aligned} \tag{4.5.16}$$

Note that $\mathcal{Q}^\vee(f_2 : m, f_m)$ are defined in Eq. (4.5.6). The functions $R^\vee(\{1^2\}\{2\} : m, f_m)$ also involve $SU(\Omega)$ U -coefficients and the explicit expression for R^\vee is,

$$R^\vee(\{1^2\}\{2\} : m, f_m) = [F(m)]^2 \sum_{f_{m-2}, f'_{m-2}} \frac{\mathcal{N}_{f_{m-2}}}{\mathcal{N}_{f_m}} \frac{\mathcal{N}_{f'_{m-2}}}{\mathcal{N}_{f_m}} Y_{UU}(f_{m-2}, f'_{m-2}; \mathbf{F}_\vee);$$

$$Y_{UU}(f_{m-2}, f'_{m-2}; \mathbf{F}_\vee) =$$

$$\sum_\rho \frac{U(f_m, \{1^{\Omega-2}\}, f_m, \{1^2\}; f_{m-2}, \mathbf{F}_\vee)_\rho U(f_m, \{2^{\Omega-1}\}, f_m, \{2\}; f'_{m-2}, \mathbf{F}_\vee)_\rho}{U(f_m, \{1^{\Omega-2}\}, f_m, \{1^2\}; f_{m-2}, \{0\}) U(f_m, \{2^{\Omega-1}\}, f_m, \{2\}; f'_{m-2}, \{0\})}.$$
(4.5.17)

In $Y_{UU}(f_{m-2}, f'_{m-2}; \mathbf{F}_\vee)$, f_{m-2} comes from $f_m \otimes \{1^{\Omega-2}\}$ and f'_{m-2} comes from $f_m \otimes \{2^{\Omega-1}\}$. In Eq. (4.5.16), the summation is over $\nu = 0$ and 1 only as $\nu = 2$ parts for $f_2 = \{2\}$ and $\{1^2\}$ are different. Here $d(\mathbf{F}_\vee)$ are dimension of the irrep \mathbf{F}_\vee , and we have $d(\{0\}) = 1$, $d(\{21^{\Omega-2}\}) = \Omega^2 - 1$, $d(\{42^{\Omega-2}\}) = \Omega^2(\Omega + 3)(\Omega - 1)/4$, and $d(\{2^21^{\Omega-4}\}) = \Omega^2(\Omega - 3)(\Omega + 1)/4$. Tables for $X_{UU}(f_2; f_{m-2}, f'_{m-2}; \mathbf{F}_\vee)$ are already discussed before (see Table 4.4). Formulas for $Y_{UU}(f_{m-2}, f'_{m-2}; \mathbf{F}_\vee)$ are tabulated in Table 4.7 and they also involve τ_{ab} , $\Pi_a^{(b)}$, $\Pi_b^{(a)}$, Π'_a , Π''_a and $\Pi_a^{(bc)}$ introduced before.

Table 4.7: Formulas for $Y_{UU}(f_{m-2}, f'_{m-2}; \mathbf{F}_\vee)$ defined in Eq. (4.5.17). Note that $\{f(ab)\}\{f(ab)\}$ entries satisfy the $a \leftrightarrow b$ symmetry. See text for details.

$\{f_{m-2}\}\{f'_{m-2}\}$	$Y_{UU}(f_{m-2}, f'_{m-2}; \{2, 1^{\Omega-2}\})$
$\{f(ab)\}\{f(ab)\}$	$-\frac{\Omega}{2} \left[\frac{(\Omega^2 - 1)}{(\Omega^2 - 4)} \right]^{1/2} \left\{ \left(1 + \frac{1}{\tau_{ab}} \right) \frac{1}{\Pi_a^{(b)}} \right.$ $\left. + \left(1 - \frac{1}{\tau_{ab}} \right) \frac{1}{\Pi_b^{(a)}} - \frac{4}{\Omega} \right\}$
$\{f(ab)\}\{f(ac)\}$	$-\frac{\Omega}{2} \left[\frac{(\Omega^2 - 1)}{(\Omega^2 - 4)} \right]^{1/2} \left\{ \left(1 + \frac{1}{\tau_{ac}} \right) \frac{1}{\Pi_a^{(b)}} - \frac{4}{\Omega} \right\}$
$\{f(ab)\}\{f(aa)\}$	$-\Omega \left[\frac{(\Omega^2 - 1)}{(\Omega^2 - 4)} \right]^{1/2} \left\{ \frac{1}{\Pi_a^{(b)}} - \frac{2}{\Omega} \right\}$
$\{f(ab)\}\{f(cc)\}$	
or	$2 \left[\frac{(\Omega^2 - 1)}{(\Omega^2 - 4)} \right]^{1/2}$
$\{f(ab)\}\{f(cd)\}$	

Using the results in Tables 4.4 and 4.7 and simplifying Eqs. (4.5.6) and (4.5.17), expressions for $\mathcal{Q}^v(f_2 : m, f_m)$ and $R^v(\{1^2\}\{2\} : m, f_m)$ are derived for the irreps $f_m^{(p)}$. It is found that, with P^{f_2} defined in Eq. (4.5.2),

$$\begin{aligned}\mathcal{Q}^{v=0}(f_2 : m, f_m^{(p)}) &= \left[P^{f_2}(m, f_m^{(p)}) \right]^2, \\ R^{v=0}(\{1^2\}\{2\} : m, f_m^{(p)}) &= P^{\{1^2\}}(m, f_m^{(p)}) P^{\{2\}}(m, f_m^{(p)}).\end{aligned}\quad (4.5.18)$$

The final results for $\mathcal{Q}^{v=1,2}(f_2 : m, f_m^{(p)})$ and $R^{v=1}(\{1^2\}\{2\} : m, f_m^{(p)})$ are given in Tables 4.8 and 4.9, respectively. Formulas in these Tables are verified numerically in many examples by directly programming Tables 4.4 and 4.7. In the dilute limit ($\Omega \rightarrow \infty$, $r \gg 1$, $r/\Omega \rightarrow 0$), the cross term $X_{\{1^2\}\{2\}}$ will be very small compared to the direct terms X_{f_2} . Dominant contribution to X_{f_2} comes from $\mathcal{Q}^{v=2}(f_2 : m, f_m^{(p)})$ which has the form $-\Omega^4 P^{f_2}(m, f_m^{(p)})/4$ (while the other terms i.e., $\mathcal{Q}^{v=1}(f_2 : m, f_m^{(p)})$ and $R^{v=1}(\{1^2\}\{2\} : m, f_m^{(p)})$ have Ω^2 dependence). Then in the dilute limit, for the irreps $f_m^{(p)}$, simplifying the results given in Tables 4.8 and 4.9, the covariances in spectral variances take a simple form,

$$\begin{aligned}\Sigma_{22}(m, f_m^{(p)}; m', f_{m'}^{(p)}) &\xrightarrow{\Omega \rightarrow \infty, r \gg 1, r/\Omega \rightarrow 0} \\ &= \frac{8}{\Omega^4} \frac{\sum_{f_2} \lambda_{f_2}^4 P^{f_2}(m, f_m^{(p)}) P^{f_2}(m', f_{m'}^{(p)})}{\left\{ \sum_{f_2} \lambda_{f_2}^2 P^{f_2}(m, f_m^{(p)}) \right\} \left\{ \sum_{f_2} \lambda_{f_2}^2 P^{f_2}(m', f_{m'}^{(p)}) \right\}}.\end{aligned}\quad (4.5.19)$$

As $\Omega \rightarrow \infty$, $\Sigma_{22}(m, f_m^{(p)}; m', f_{m'}^{(p)}) \rightarrow 0$ and there will be no correlations. For finite Ω , there will be correlations between states with different or same (m, f_m) and examples for these are discussed ahead.

Table 4.8: $\mathcal{Q}^v(f_2 : m, f_m)$ for $f_m = f_m^{(p)}$ and $v = 1$ and 2. See Eq. (4.5.6) for the definition of \mathcal{Q}^v .

$f_m^{(p)}$	f_2	v	$\mathcal{Q}^v(f_2 : m, f_m^{(p)})$
$\{4^r\}$	$\{2\}$	1	$\frac{9r(r+1)^2(\Omega-r)(\Omega+1)(\Omega+4)}{2(\Omega+2)}$
		2	$\frac{3r\Omega(r+1)(\Omega-r+1)(\Omega-r)(\Omega+4)(\Omega+5)}{4(\Omega+2)}$
	$\{1^2\}$	1	$\frac{25r(r-1)^2(\Omega-r)(\Omega-1)(\Omega+4)}{2(\Omega-2)}$

Table 4.8 – continued

$f_m^{(p)}$	f_2	ν	$\mathcal{Q}^\nu(f_2 : m, f_m^{(p)})$
		2	$\frac{5r\Omega(r-1)(\Omega+3)(\Omega+4)(\Omega-r)(\Omega-r-1)}{4(\Omega-2)}$
$\{4^r, 1\}$	$\{2\}$	1	$\frac{3r(\Omega+1)}{8(\Omega+2)} \left[-12(\Omega+4)r^3 + 12(\Omega-3)(\Omega+4)r^2 \right.$ $\left. + (33\Omega^2 + 100\Omega - 108)r + 20\Omega(\Omega+4) \right]$
		2	$\frac{3r\Omega}{8(\Omega+2)} (\Omega-r+1)(\Omega+4) \left[-2(\Omega+5)r^2 \right.$ $\left. + 2(\Omega-2)(\Omega+5)r + \Omega(3\Omega+11) - 10 \right]$
	$\{1^2\}$	1	$-\frac{5r(\Omega-1)}{8(\Omega-2)} \left[20(\Omega+4)r^3 - 20(\Omega^2+5\Omega+4)r^2 \right.$ $\left. + (25\Omega^2 + 132\Omega + 20)r - 12\Omega(\Omega+4) \right]$
		2	$\frac{5r\Omega(\Omega+4)}{8(\Omega-2)} \left[2(\Omega+3)r^3 - 2(2\Omega^2+5\Omega-3)r^2 \right.$ $\left. + (2\Omega^3 + 5\Omega^2 + \Omega - 6)r - \Omega^3 - 6\Omega^2 + 13\Omega - 6 \right]$
	$\{2\}$	1	$\frac{(\Omega+1)}{4(\Omega+2)} \left[-8(3r^2+6r+1)^2 + (3r+4)(6r^2+13r+1)\Omega^2 \right.$ $\left. - 2(9r^4 - 79r^2 - 88r - 2)\Omega \right]$
		2	$\frac{\Omega}{4(\Omega+2)} \left[3(\Omega+4)(\Omega+5)r^4 - 6(\Omega-1)(\Omega+4)(\Omega+5)r^3 \right.$ $\left. + \Omega(\Omega+4)(3\Omega^2+3\Omega-56)r^2 \right.$ $\left. + (\Omega-1)(\Omega+4)(6\Omega^2+29\Omega+15)r \right.$ $\left. + \Omega(\Omega-1)(\Omega+2)(\Omega+3) \right]$
$\{4^r, 2\}$	$\{2\}$	1	$-\frac{5r(\Omega-1)}{4(\Omega-2)} \left[10(\Omega+4)r^3 - 10\Omega(\Omega+4)r^2 \right.$ $\left. + \Omega(5\Omega+38)r - 3\Omega(\Omega+4) \right]$
		2	$-\frac{5r\Omega(\Omega+4)(\Omega-r-1)}{4(\Omega-2)} \left[3(\Omega-1) - r(\Omega-r-1)(\Omega+3) \right]$
	$\{1^2\}$	1	$-\frac{3(r+2)(\Omega+1)}{8(\Omega+2)} \left[12(r+2)(2r+1)^2 - \Omega^2(12r^2+27r+8) \right.$ $\left. + 4(3r^3 - 3r^2 - 19r - 4)\Omega \right]$
		2	$-\frac{3\Omega(r+2)(\Omega+4)(\Omega-r-1)}{8(\Omega+2)} \left[2r^2(\Omega+5) - 2\Omega r(\Omega+5) \right.$ $\left. - \Omega(\Omega+3) \right]$
	$\{2\}$	1	$-\frac{5r(\Omega-1)}{8(\Omega-2)} \left[20(\Omega+4)r^3 - 20r^2(\Omega^2+3\Omega-4) \right.$ $\left. + r(-5\Omega^2+12\Omega+20) - 2\Omega(\Omega+4) \right]$
		2	

Table 4.8 – continued

$f_m^{(p)}$	f_2	v	$\mathcal{Q}^v(f_2 : m, f_m^{(p)})$
		2	$-\frac{5r\Omega(\Omega+4)(\Omega-r-1)}{8(\Omega-2)} [2(\Omega+3)r^2 - 2r(\Omega^2 + \Omega - 6) - \Omega(\Omega-3)]$

Table 4.9: $R^{v=1}(\{1^2\}\{2\} : m, f_m)$ for $f_m = f_m^{(p)}$. See Eq. (4.5.17) for the definition of $R^{v=1}$.

$f_m^{(p)}$	$R^{v=1}(\{1^2\}\{2\} : m, f_m^{(p)})$
$\{4^r\}$	$-\frac{15r}{2} \sqrt{\frac{\Omega^2-1}{\Omega^2-4}} (r^2-1)(\Omega-r)(\Omega+4)$
$\{4^r, 1\}$	$\frac{15r}{8} \sqrt{\frac{\Omega^2-1}{\Omega^2-4}} [4r^3(\Omega+4) - 4r^2(\Omega+4)(\Omega-1) - 3r(\Omega+2)^2 + 4\Omega(\Omega+4)]$
$\{4^r, 2\}$	$-\frac{5r}{4} \sqrt{\frac{\Omega^2-1}{\Omega^2-4}} [-6r^3(\Omega+4) - 3\Omega(\Omega+6) + 6r^2(\Omega-2)(\Omega+4) + r(9\Omega^2 + 28\Omega - 8)]$
$\{4^r, 3\}$	$-\frac{15r}{8} (r+2) \sqrt{\frac{\Omega^2-1}{\Omega^2-4}} [-4r^2(\Omega+4) + 4r(\Omega-1)(\Omega+4) + \Omega^2 - 4]$

4.6 Numerical Results for Spectral Variances, Expectation Values of $C_2[SU(4)]$ and Four Periodicity in GS

Employing the analytical formulation described in Secs. 4.4 and 4.5 along with the results in Table 4.6 for $f_m = f_m^{(p)}$ irreps and Table 4.4 for general f_m irreps, numerical calculations are carried out for $\langle H^2 \rangle^{m, f_m}$. In our examples, we have chosen $\Omega = 6$ and $\Omega = 10$ and they correspond to nuclear $(2s1d)$ and $(2p1f)$ shells, respectively. Results for spectral variances are used to analyze expectation values of $C_2[SU(4)]$ and the four periodicity in the gs energies. Conclusions from these studies are summarized at the end.

4.6.1 Spectral variances

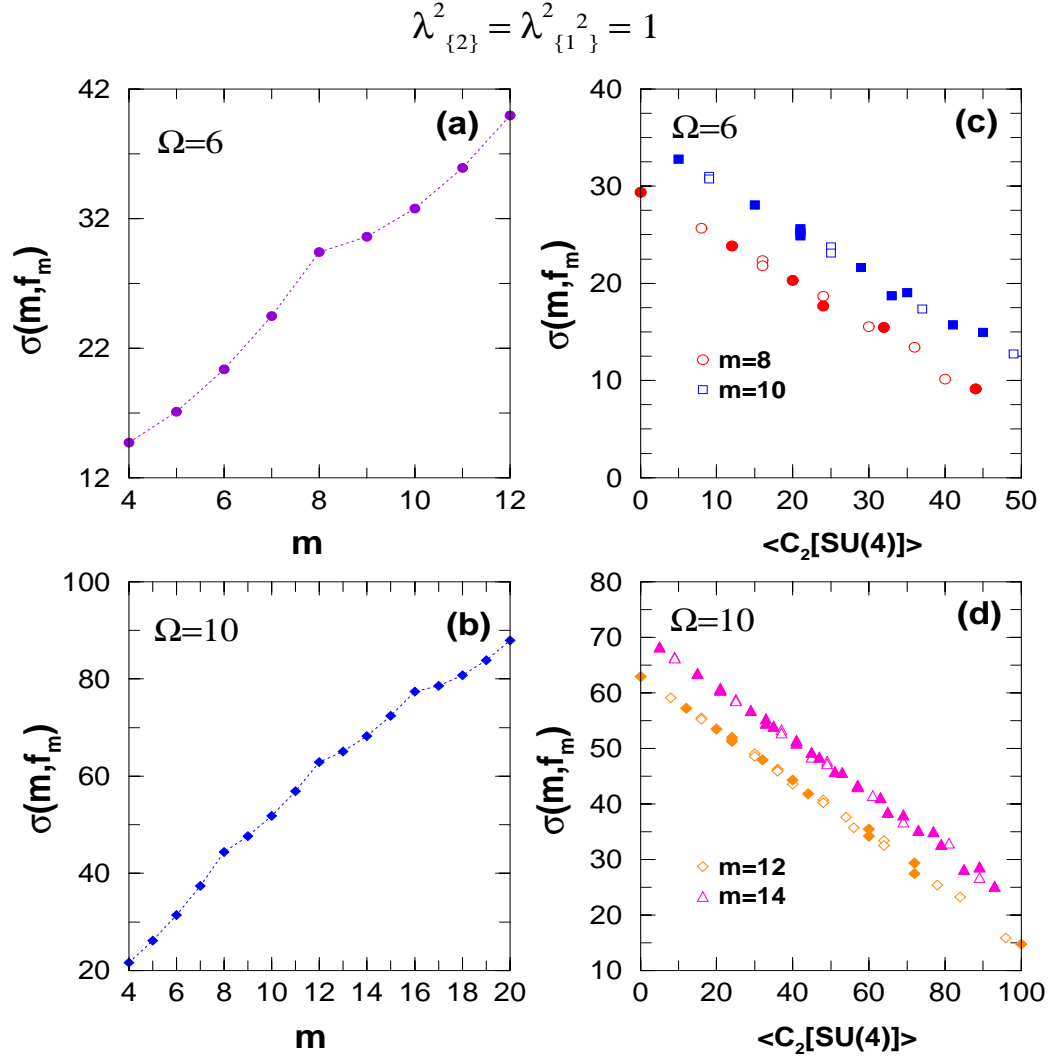


Figure 4.3: Variation of spectral widths $\left[\overline{\langle H^2 \rangle^{m, f_m}} \right]^{1/2}$ as a function of m with fixed f_m and similarly variation as a function of f_m with fixed m . (a) $\Omega = 6$, $f_m = f_m^{(p)}$, (b) $\Omega = 10$, $f_m = f_m^{(p)}$, (c) $\Omega = 6$ and $m = 8$ and 10 , and (d) $\Omega = 10$ and $m = 12$ and 14 . Note that $f_m^{(p)} = \{4^r, p\}$ where $m = 4r + p$. Similarly, instead of showing f_m in (c) and (d) we have used $\langle C_2[SU(4)] \rangle_{\tilde{f}_m}$. We have marked by filled symbols in (c) and (d) the irreps f_m that give $(S, T) = (0, 0)$ for $m = 4r$ systems and $(S, T) = (1, 0) \oplus (0, 1)$ for $m = 4r + 2$ systems. See text for details.

Figures 4.3(a) and (b) show variation in the spectral widths $\sigma(m, f_m) = [\overline{\langle H^2 \rangle^{m, f_m}}]^{1/2}$ as a function of the particle number m with fixed $f_m = f_m^{(p)}$. Notice the peaks at $m = 4r$; $r = 2, 3, \dots$. Except for this structure, there are no other differences between $\{4^r\}$ and $\{4^r, 2\}$ systems or equivalently between even-even and odd-odd $N=Z$ nuclei. Figures 4.3(c) and (d) show variation in the spectral widths $\sigma(m, f_m)$ as a function of

f_m with fixed m values. Results are shown for $m = 8$ and 10 for $\Omega = 6$ and $m = 12$ and 14 for $\Omega = 10$. In the figures, we have used the physically more appropriate $\langle C_2[SU(4)] \rangle^{\tilde{f}_m}$ label for the x -axis instead of showing f_m . It is clearly seen that the variation in the spectral widths is almost linear. Considering the eigenvalue density to be Gaussian [extrapolating from the results known for EGUE(2), EGOE(2) and EGOE(2)-s] and neglecting the dimension effects, energy of the lowest state that belong to a given f_m follows from the Jacquod and Stone prescription [Pa-08, Ja-01]. This gives

$$E_{gs}(f_m) - E_c(m, f_m) \propto -\sigma(m, f_m). \quad (4.6.1)$$

This follows from Eq. (4.6.4) given ahead if we restrict it to a given f_m . Combining Eq. (4.6.1) with the results in Figs. 4.3(c) and (d), we can identify the irreps that label the gs generated by EGUE(2)- $SU(4)$. As $\sigma(m, f_m)$ vs $\langle C_2[SU(4)] \rangle^{\tilde{f}_m}$ curves are linear, clearly EGUE(2)- $SU(4)$ generates gs labeled by the irreps that have lowest $\langle C_2[SU(4)] \rangle^{\tilde{f}_m}$. Therefore random interactions, which are $SU(4)$ scalar, carry the properties of $C_2[SU(4)]$, the $SU(4)$ invariant or the Majorana force. In Figs. 4.3(c) and (d), we have marked the irreps that give $(S, T) = (0, 0)$ for $m = 4r$ and $(S, T) = (1, 0) \oplus (0, 1)$ for $m = 4r + 2$ systems. If we restrict to these irreps, the second irrep is forbidden in both cases i.e., there is a gap between the lowest and next allowed irrep. This implies that even with random interactions we obtain gs with $f_m = f_m^{(p)}$. We will further substantiate this result by calculating the expectation values $\langle C_2[SU(4)] \rangle^E$ and also analyzing the four periodicity in E_{gs} .

4.6.2 Expectation values $\langle C_2[SU(4)] \rangle^E$

In order to examine the extent to which random interactions with $SU(4)$ symmetry carry the properties of the Majorana operator, we have studied expectation values (smoothed with respect to E) of the quadratic Casimir invariant of $SU(4)$ using the Hamiltonian H_α ,

$$\{H_\alpha\} = C_2[SU(4)] + \alpha\{H\}. \quad (4.6.2)$$

where $\{H\}$ is defined by Eq. (4.3.1) with $\lambda_{\{2\}}^2 = \lambda_{\{1^2\}}^2 = 1$. In order to study $\langle C_2[SU(4)] \rangle^E$, we decompose it in terms of $\langle C_2[SU(4)] \rangle^{\tilde{f}_m}$ (see Eq. (3.4.6) and [Pa-78]),

$$\langle C_2[SU(4)] \rangle^E = \sum_{f_m} \frac{I_{\mathcal{G}}^{m,f_m}(E)}{I^m(E)} \langle C_2[SU(4)] \rangle^{\tilde{f}_m}; \quad (4.6.3a)$$

$$I^m(E) = \sum_{f_m} I_{\mathcal{G}}^{m,f_m}(E) = \sum_{f_m} d_{\Omega}(f_m) d_4(\tilde{f}_m) \rho_{\mathcal{G}}^{m,f_m}(E). \quad (4.6.3b)$$

In Eq. (4.6.3a), $I^{m,f_m}(E)$ are partial eigenvalue densities defined over a fixed f_m space, $I^{m,f_m}(E) = \langle \langle \delta(H - E) \rangle \rangle^{m,f_m}$ and $I^m(E)$ is the total eigenvalue density. Equation (4.6.3a) is exact if we remove \mathcal{G} , as f_m (equivalently \tilde{f}_m) label the eigenstates of $C_2[SU(4)]$. For smoothed expectation values, based on the $SU(4)$ partial densities that are studied within the nuclear shell-model (with $\Omega = 6$) [Pa-73, Pa-72], we assume that $\rho^{m,f_m}(E)$ will be close to a Gaussian (\mathcal{G}). Numerical calculations of γ_2 using H matrix construction as discussed in Section 4.3.3 or using the analytical formulation discussed in Appendix F, will verify this assumption. However, at present both these methods are not feasible in practice. For the Hamiltonian in Eq. (4.6.2), the centroid of $\rho_{\mathcal{G}}^{m,f_m}(E)$ is $\langle C_2[SU(4)] \rangle^{\tilde{f}_m}$ and the variance is $\overline{\langle H^2 \rangle}^{m,f_m}$.

As an example, for $\Omega = 6$ and $m = 8$ and 10 , the expectation values are calculated as a function of energy for various values of α in Eq. (4.6.2) and the results are shown in Figs. 4.4(a) and (b). It is seen that with the increase in the strength α , fluctuations decrease and the staircase form for $\alpha \sim 0$ turns into a smooth curve for $\alpha \gtrsim \alpha_c = 0.3$. This conclusion remains same even when we consider $U(\Omega)$ irreps with $(S, T) = (0, 0)$ for m even and $(S, T) = (1, 0) \oplus (0, 1)$ for m odd. Then the normalization for $I_{\mathcal{G}}^{m,f_m}(E)$ is $d_{\Omega}(f_m) \times d_{g_s}$. Note that the degeneracy $d_{g_s} = 1, 6$, and 4 , respectively for $m = 4r$ (even-even nuclei), $m = 4r + 2$ (odd-odd nuclei) and $m = 4r + 1$ or $4r + 3$ (odd-A nuclei). Just as for EGOE(1+2) and EGOE(1+2)-s, it is expected that the transition point $\alpha_c \propto \Omega/K(m, f_m)$ and the variance propagator $K(m, f_m)$, as mentioned in Section 4.3.2, follows from the formulas in Table 4.6 for $f_m^{(p)}$ irreps and for general irreps from Eq. (4.5.5) and Table 4.4 with $\lambda_{\{1^2\}}^2 = \lambda_{\{2\}}^2 = 1$. From the results in Table 4.6, for the $f_m^{(p)}$ irreps, it follows that in the dilute limit, $K(m, f_m) \rightarrow m^2 \Omega^2$. Thus, $\alpha_c \propto 1/m^2 \Omega$ and this result is same as those derived before for EGOE(1+2) and EGOE(1+2)-s; see Chapter 2 for details. Therefore, with fixed m , $\alpha_c = 0.3$ for $\Omega = 6$ corresponds to $\alpha_c \sim 0.2$ for

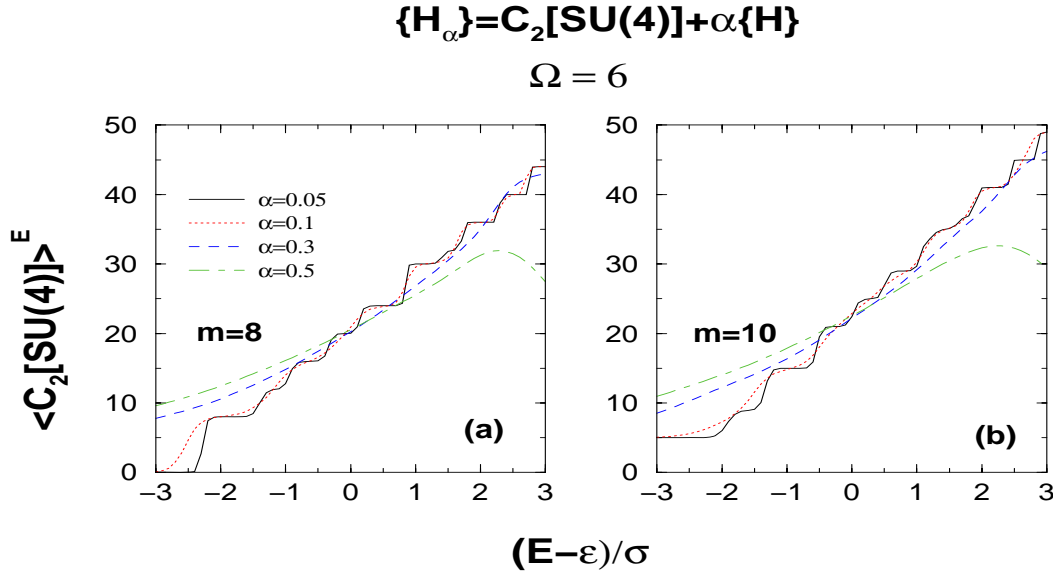


Figure 4.4: Expectation values of the quadratic Casimir invariant of $SU(4)$ as a function of excitation energy for the H_α Hamiltonian ensemble defined in Eq. (4.6.2). Results are shown for four values of interaction strength α : (a) for $m = 8$ and (b) for $m = 10$. Note that the energies are zero centered with respect to the centroid ϵ and scaled with the width σ defined by first and second moments of the total density of states. All the results are for $\Omega = 6$. Similar results are obtained even when we consider, in Eq. (4.6.3b), the irreps f_m that give $(S, T) = (0, 0)$ for $m = 8$ and $(S, T) = (1, 0) \oplus (0, 1)$ for $m = 10$.

$\Omega = 10$. We have verified this by comparing the numerical results for $\Omega = 6$ and 10.

Results in Figs. 4.4(a) and (b) confirm that even with random interactions that are $SU(4)$ scalar, ground states have lowest value for $\langle C_2[SU(4)] \rangle^E$ and therefore they carry the property of the Majorana force. Also beyond a critical strength (α_c) of the random part in Eq. (4.6.2), expectation values will be smooth with respect to energy.

4.6.3 Four-periodicity in the ground state energies

An evidence for effective space symmetry for nuclear ground states is derived from the four periodicity in the gs energies E_{gs} per particle [Pa-78]. An important question is: will this feature survive even in the presence of random interactions. To test this, as a model, we consider the Hamiltonian H_α in Eq. (4.6.2) where α is the strength of the random interaction with $SU(4)$ symmetry. For the strength $\alpha = 0$, H reduces to the quadratic Casimir invariant of the $SU(4)$ group and this, as it is well-known, produces oscillations in $E_{gs}(m)/m$ with minima at $m = 4r$ (this is called four periodicity) as seen clearly from Fig. 4.5. When the strength α is non-zero, for given number of particles m , all the irreps f_m , with $(S, T) = (0, 0)$ for $m = 4r$, $(S, T) = (1, 0) \oplus (0, 1)$ for

$$\Omega = 10$$

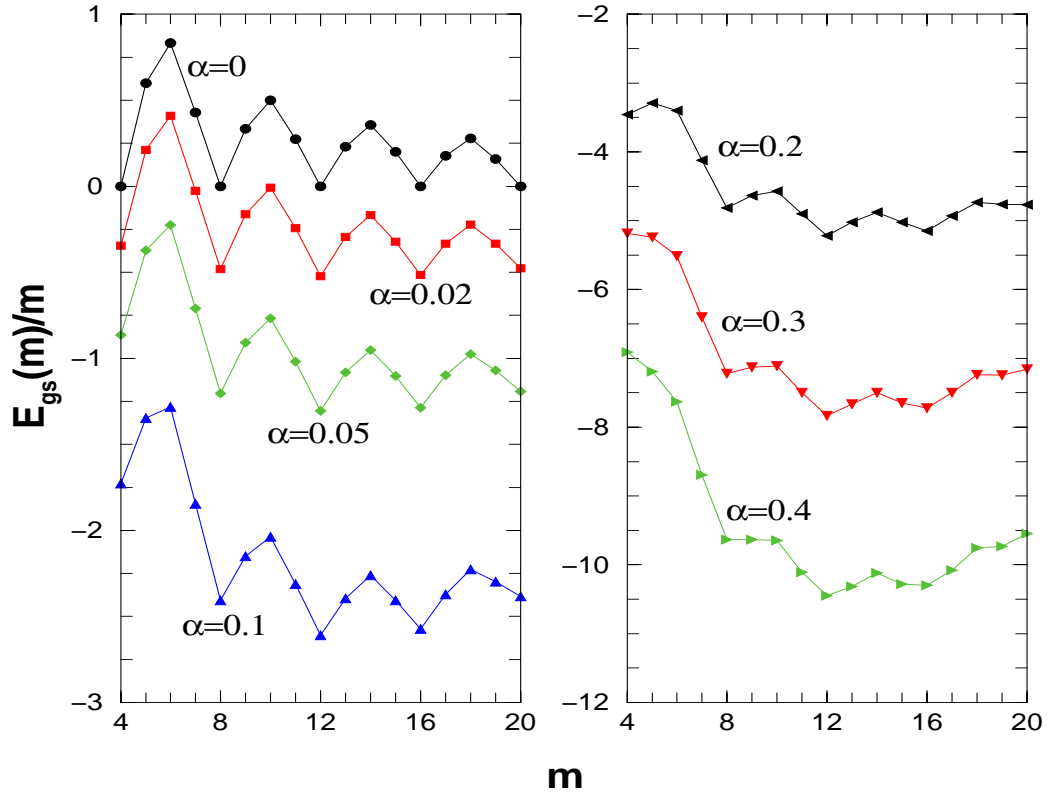


Figure 4.5: Ground state energy $E_{gs}(m)$ per particle m as a function of m for different values of the interaction strength α in Eq. (4.6.2). Results are shown for $\alpha \leq 0.4$. The variation of $E_{gs}(m)/m$ shown in the figure brings out the four periodicity effect in the gs energies. See text for details.

$m = 4r + 2$ and $(S, T) = (\frac{1}{2}, \frac{1}{2})$ for $m = 4r + 1$ and $4r + 3$, contribute to the sum in Eq. (4.6.3b) in generating the total density of states. Using Eq. (4.6.3b), $E_{gs}(m)$ for a fixed m is determined numerically by inverting the integral,

$$\frac{1}{2} = \int_{-\infty}^{E_{gs}(m)} \sum_{f_m} d\Omega(f_m) \rho_{\mathcal{G}}^{m, f_m}(E) dE. \quad (4.6.4)$$

This is known as “Ratcliff procedure” in nuclear physics literature [Ra-71, Wo-86]. We show in Fig. 4.5, the variation of $E_{gs}(m)/m$ vs m for different interaction strengths α . In the calculations, $\Omega = 10$ and $m = 4 - 20$. It is clearly seen that the four periodicity produced by $C_2[SU(4)]$ is preserved by random Hamiltonian H_α for $\alpha \leq 0.2$. The kinks in the spectral widths at $m = 4r$ as a function of m as seen from Fig. 4.3(a) and (b) and similarly, their monotonic decrease with $\langle C_2[SU(4)] \rangle^{\tilde{f}_m}$ as seen from Fig. 4.3(c) and (d), together explain the four periodicity in the gs energies.

Beyond $\alpha = 0.2$, this structure starts disappearing as the difference Δ between the centroids, produced by $C_2[SU(4)]$ for the lowest two irreps, becomes comparable to the width of the gs irrep $\{4^r\}$; $m = 4r$. Therefore, with a regular part that is close to $C_2[SU(4)]$, random interactions that are not too strong [$\alpha \lesssim \alpha'_c = 0.2$ in Eq. (4.6.2)] generate, in the $\Omega = 10$ example, ground states that are spatially symmetric. Thus, $\alpha_c \sim \alpha'_c$ (see Section 4.6.2 for α_c) and therefore, the region of onset of smooth behavior for $\langle C_2[SU(4)] \rangle^{\tilde{f}_m}$ also marks the onset of diminishing four periodicity effect in the gs energies. As $\alpha_c \propto 1/m^2\Omega$, the four periodicity effect should diminish faster for large m and this is clearly seen from Fig. 4.5.

4.6.4 Conclusions

Thus, ensemble averaged spectral variances $\overline{\langle H^2 \rangle^{m, f_m}}$, expectation values $\langle C_2[SU(4)] \rangle^E$ and the four periodicity in $E_{gs}(m)/m$ discussed in Secs. 4.6.1-4.6.3 establish that random interactions with $SU(4)$ symmetry keep intact all the essential features of the Majorana force (see Section 4.8 for further discussion on the importance of this result). Therefore the EGUE(2)- $SU(4)$ and the corresponding EGOE(2)- $SU(4)$ ensemble should be useful in nuclear structure.

4.7 Numerical Results for Correlations in Energy Centroids and Spectral Variances

Using the results in Tables 4.3, 4.6, 4.8 and 4.9 for $f_m = f_m^{(p)}$ irreps and Tables 4.4 and 4.7 for general f_m irreps, the self and cross-correlations in energy centroids and spectral variances [i.e., Σ_{11} and Σ_{22} in Eq. (4.4.8)] are calculated. See [Br-81, Fl-00, Pa-00] for a detailed discussion on the significance of self-correlations (they affect level motion in the ensemble) and [Pa-07, Ko-07, Ko-06] on the significance of the cross-correlations (they will vanish for GE's) generated by embedded ensembles. Results for Σ_{11} and Σ_{22} are discussed in Secs. 4.7.1-4.7.3 and a summary is given at the end.

4.7.1 Self-correlations

Results for self-correlations ($m = m'$, $f_m = f_{m'}$) are shown in Table 4.10 for $f_m = f_m^{(p)}$ and $\Omega = 6$ and 10. For $\Omega = 6$ we have, $[\Sigma_{11}]^{1/2} \sim 12 - 28\%$ and $[\Sigma_{22}]^{1/2} \sim 7 - 15\%$ as

m changes from 6 to 12. Similarly, for $\Omega = 10$ and m ranging from 12 to 20, they decrease to 10 – 22% for $[\Sigma_{11}]^{1/2}$ and 4 – 9% for $[\Sigma_{22}]^{1/2}$. We can also infer from Table 4.10 that as m increases, the self-correlations also increase. Therefore, fluctuations in the level motion in the ensemble increase with m and as a result the ensemble averages deviate from spectral averages with increasing m . This feature has been studied before for EGOE(2) and EGOE(2)-s [Br-81, Fl-00, Le-08].

Further significance of the magnitude of the self-correlations follows by comparing the results with the corresponding ones for EGUE(2) and EGUE(2)-s for fixed number of sp states (N). Using the analytical formulas given in [Ko-05] for EGUE(2), $[\Sigma_{11}(m, m)]^{1/2}$ and $[\Sigma_{22}(m, m)]^{1/2}$ are calculated for various values of m with $N = 24$ and 40 and the results are shown in third and sixth columns of Table 4.10. Similarly, using the formulas in [Ko-07] for EGUE(2)-s, $[\Sigma_{11}(m, S; m, S)]^{1/2}$ and $[\Sigma_{22}(m, S; m, S)]^{1/2}$ with $S = 0$ for even m and $S = 1/2$ for odd m are calculated for various values of m with $N = 24$ ($\Omega = 12$) and 40 ($\Omega = 20$) and the results are shown in fourth and seventh columns of Table 4.10. It is seen from Table 4.10 that the magnitude of the covariances in energy centroids and spectral variances increases by a factor 3 when we go from EGUE(2) \rightarrow EGUE(2)-s \rightarrow EGUE(2)- $SU(4)$.

As discussed in Section 4.3, the fraction of independent matrix elements \mathcal{I} increases with symmetry and also the sparsity (\mathbf{S}) decreases and therefore the EGUE(2)- $SU(4)$ matrices will be dense leading to a more complete mixing of the basis states compared to EGUE(2) and EGUE(2)-s. Therefore there is a correlation between (i) increase in fluctuations defined by Σ_{11} and Σ_{22} and (ii) the matrices $H_{f_m}(m)$ becoming more dense as we go from EGUE(2) \rightarrow EGUE(2)-s \rightarrow EGUE(2)- $SU(4)$. See Section 4.8 for further discussion.

4.7.2 Cross-correlations

Results for cross-correlations in energy centroids $\Sigma_{11}(m, f_m; m', f_{m'})$ and spectral variances $\Sigma_{22}(m, f_m; m', f_{m'})$ with $f_m = f_m^{(p)}$ as a function of m and m' are shown in Fig. 4.6 for both $\Omega = 6$ and 10. It is seen that $[\Sigma_{11}]^{1/2}$ and $[\Sigma_{22}]^{1/2}$ increase almost linearly with m . At $m = 4r$, $r = 2, 3, \dots$ there is a slight dip in $[\Sigma_{11}]^{1/2}$ as well as in $[\Sigma_{22}]^{1/2}$. For $\Omega = 6$ we have, $[\Sigma_{11}]^{1/2} \sim 10 - 24\%$ and $[\Sigma_{22}]^{1/2} \sim 6 - 12\%$. Similarly, for $\Omega = 10$ these decrease to 5 – 16% for $[\Sigma_{11}]^{1/2}$ and 2 – 6% for $[\Sigma_{22}]^{1/2}$. The decrease in Σ 's

Table 4.10: Variation in the self-correlations in energy centroids (Σ_{11}) and spectral variances (Σ_{22}) with symmetry. See text for details.

N	m	$[\Sigma_{11}]^{1/2}$			$[\Sigma_{22}]^{1/2}$		
		EGUE(2)	EGUE(2)- s	EGUE(2)- <i>SU</i> (4)	EGUE(2)	EGUE(2)- s	EGUE(2)- <i>SU</i> (4)
24	6	0.017	0.043	0.125	0.0056	0.017	0.069
	7	0.021	0.055	0.144	0.0059	0.019	0.076
	8	0.026	0.066	0.160	0.0064	0.021	0.083
	9	0.031	0.081	0.196	0.0069	0.025	0.099
10	0.037	0.094	0.229	0.0077	0.028	0.117	
11	0.044	0.112	0.256	0.0087	0.034	0.134	
12	0.051	0.128	0.276	0.0099	0.039	0.148	
40	12	0.0139	0.038	0.105	0.00222	0.0079	0.035
	13	0.0157	0.044	0.120	0.00234	0.0086	0.039
	14	0.0176	0.048	0.134	0.00247	0.0093	0.044
	15	0.0196	0.054	0.146	0.00262	0.0103	0.049
	16	0.0218	0.06	0.156	0.0028	0.0112	0.053
	17	0.0241	0.067	0.174	0.003	0.0125	0.061
	18	0.0267	0.073	0.192	0.00324	0.0138	0.069
	19	0.0294	0.081	0.206	0.00352	0.0156	0.078
	20	0.0325	0.088	0.218	0.00385	0.0174	0.085

$$\lambda_{\{2\}}^2 = \lambda_{\{1\}^2}^2 = 1$$

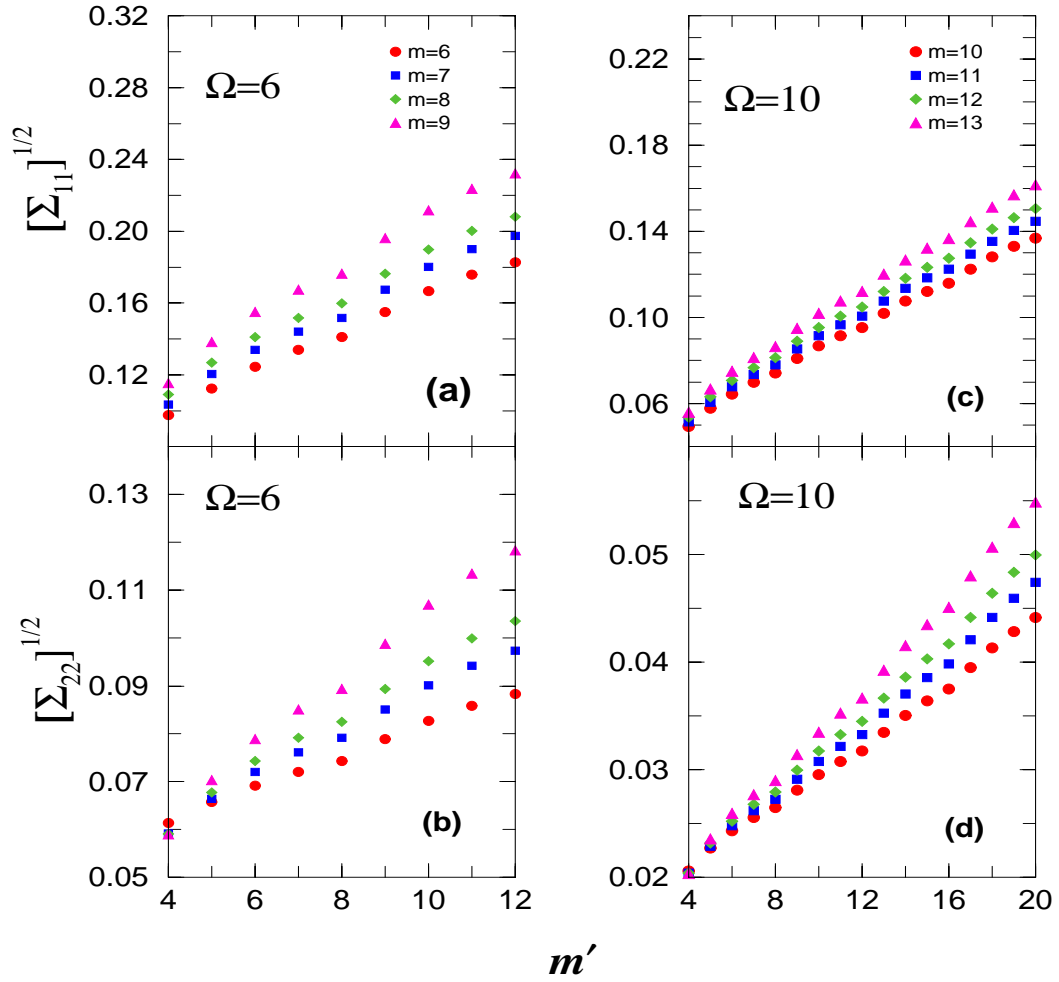


Figure 4.6: Self and cross-correlations in energy centroids and spectral variances as a function of m and m' (with fixed f_m and $f_{m'}$) for $\Omega = 6$ and $\Omega = 10$ examples: (a) $[\Sigma_{11}(m, f_m; m', f_{m'})]^{1/2}$ for $\Omega = 6$; (b) $[\Sigma_{22}(m, f_m; m', f_{m'})]^{1/2}$ for $\Omega = 6$; (c) $[\Sigma_{11}(m, f_m; m', f_{m'})]^{1/2}$ for $\Omega = 10$; (d) $[\Sigma_{22}(m, f_m; m', f_{m'})]^{1/2}$ for $\Omega = 10$. Results in the figure are for $f_m = f_m^{(p)}$ and $f_{m'} = f_{m'}^{(p)}$. See text for details.

with increasing Ω is in agreement with the results obtained for EGOE(2) for spinless fermions and EGOE(2)-s. Similarly, the covariances in spectral variances are always smaller compared to those for energy centroids.

Figures 4.7(a) and (b) show cross-correlations in energy centroids Σ_{11} and spectral variances Σ_{22} as a function of f_m and $f_{m'}$ with fixed $m = m'$. Results are shown for the first, second and fourth lowest $U(\Omega)$ irreps, ordered according to $\langle C_2[SU(4)] \rangle^{\tilde{f}_m}$, with all other f_m 's for $m = 8$ and 10 with $\Omega = 6$. The correlations grow with increase in $\langle C_2[SU(4)] \rangle^{\tilde{f}_m}$. It is important to note that there is no correlation between variation

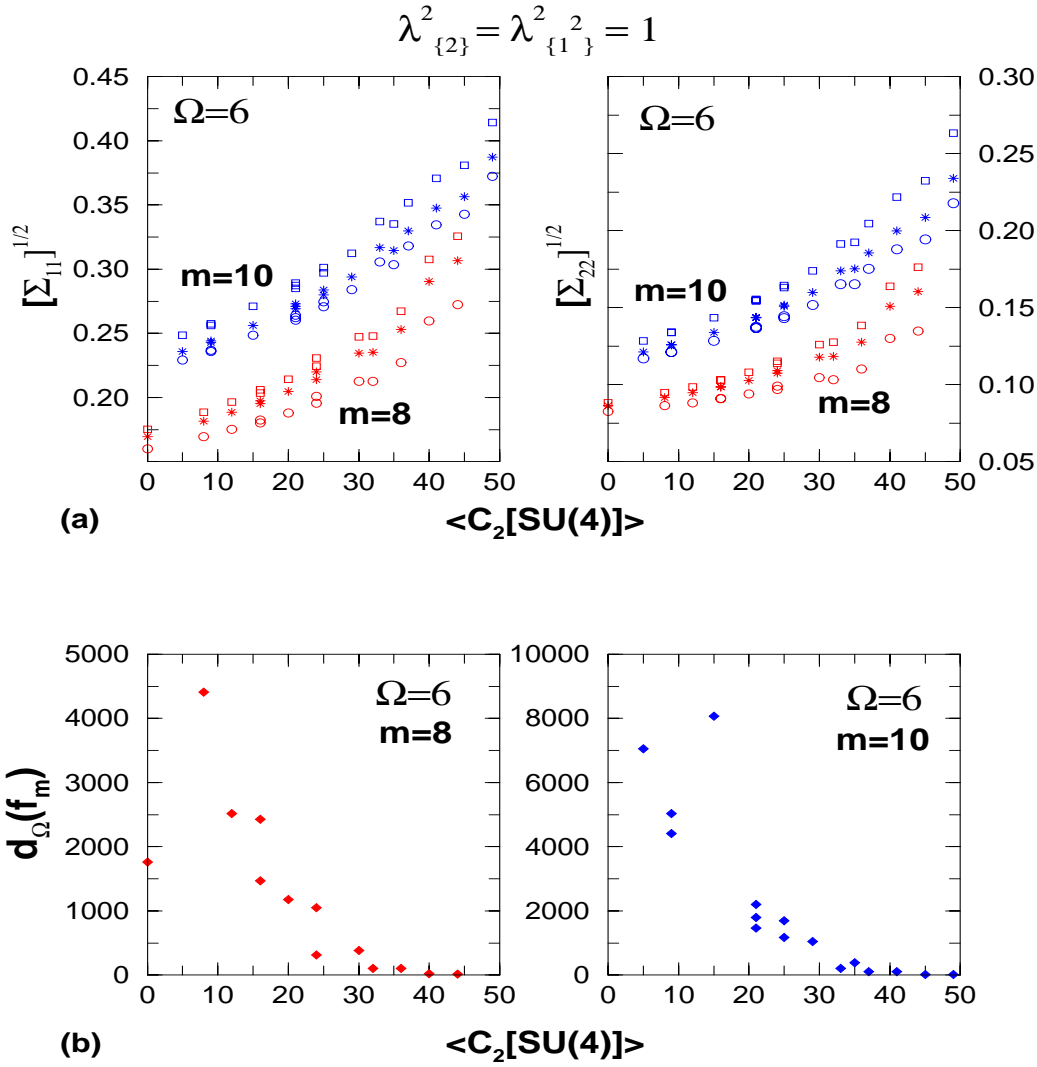


Figure 4.7: (a) Self and cross-correlations in energy centroids $[\Sigma_{11}(m, f_m; m', f_{m'})]^{1/2}$ and spectral variances $[\Sigma_{22}(m, f_m; m', f_{m'})]^{1/2}$ as a function of f_m and $f_{m'}$ (with fixed $m = m'$). Results are shown for the first (circle), second (star) and fourth (square) lowest $U(\Omega)$ irreps (ordered according to $\langle C_2[SU(4)] \rangle^{\tilde{f}_m}$) with all other irreps for $m = m' = 8$ (red) and 10 (blue) as a function of $\langle C_2[SU(4)] \rangle^{\tilde{f}_m}$. (b) Dimension $d_{\Omega}(f_m)$ for $m = 8, 10$ vs the eigenvalue of $C_2[SU(4)]$ in the corresponding $SU(4)$ irrep. Note that for a given value of the eigenvalue of $C_2[SU(4)]$ in some cases there are more than one f_m with the same eigenvalue. All results are for $\Omega = 6$.

in covariances with the variation in the f_m dimensions; see Figs. 4.7(a) and (b).

The increase in the cross-correlations with m' for fixed f_m and similar increase with $\langle C_2[SU(4)] \rangle^{\tilde{f}_m}$ with fixed m , seen from Figs. 4.6 and 4.7, could possibly be exploited in deriving experimental signatures for cross-correlations. Note that the cross-correlations will be zero if we replace EGUE by GUE for $H_{f_m}(m)$ matrix.

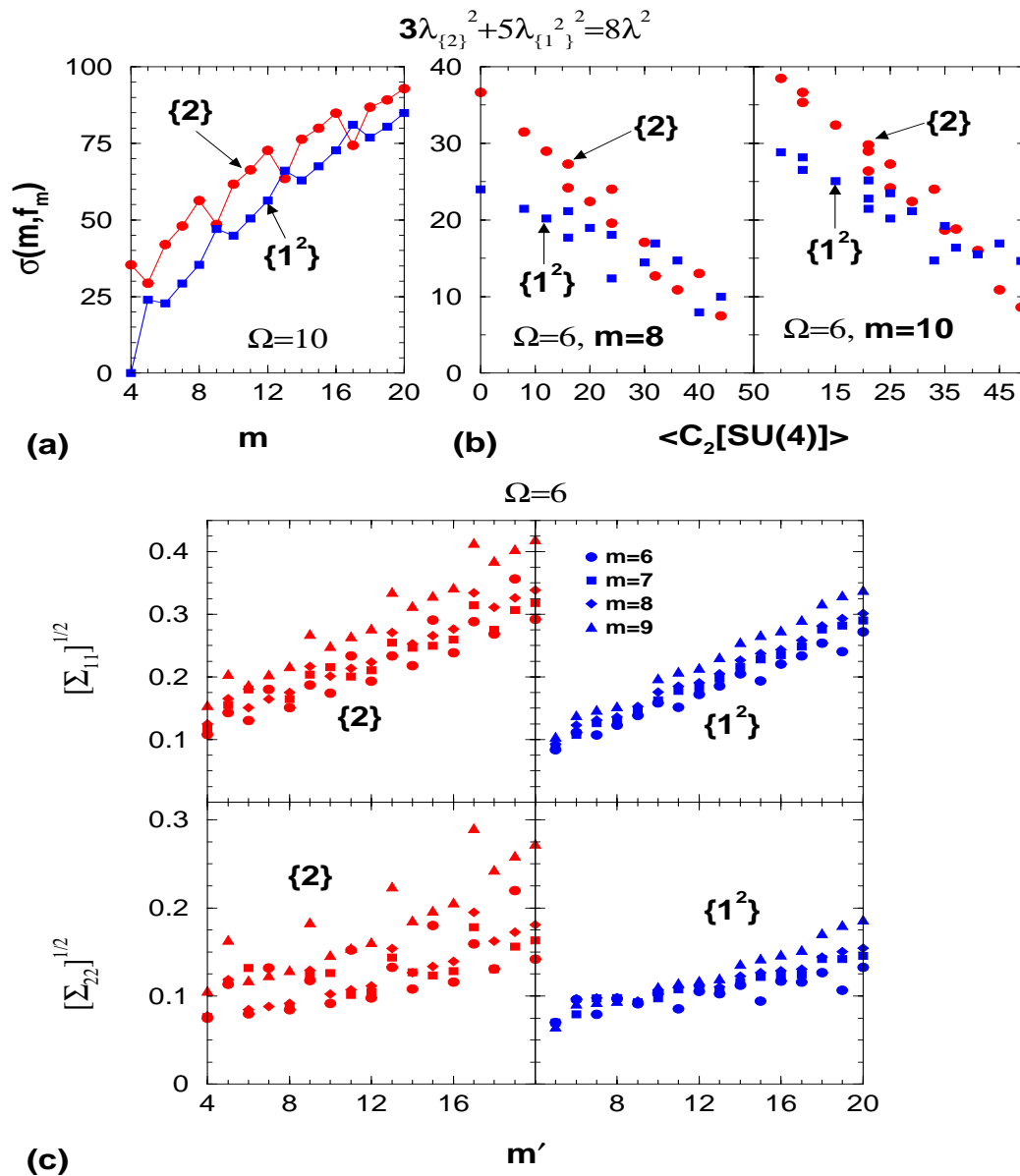


Figure 4.8: (a) Variation of spectral widths $\sigma(m, f_m)$ as a function of m with $f_m = f_m^{(p)}$. (b) Variation of spectral widths as a function of $\langle C_2[SU(4)] \rangle^{\tilde{f}_m}$ for $m = 8$ and 10 . In (c), results are shown for the covariances in energy centroids $[\Sigma_{11}]^{1/2}$ and spectral variances $[\Sigma_{22}]^{1/2}$ for some values of m and m' with $f_m = f_m^{(p)}$ and $f_{m'} = f_{m'}^{(p)}$. For the calculations in (a), $\Omega = 10$ and for (b) and (c), $\Omega = 6$. Note that in the figures $\lambda_{\{2\}}^2 = 8/3$, $\lambda_{\{1^2\}}^2 = 0$ is denoted as ' $\{2\}$ ' and similarly $\lambda_{\{2\}}^2 = 0$, $\lambda_{\{1^2\}}^2 = 8/5$ is denoted as ' $\{1^2\}$ '. See text for details.

4.7.3 Results for $\lambda_{\{2\}}^2 \neq \lambda_{\{1^2\}}^2$

All the discussion in the Secs. 4.6, 4.7.1, and 4.7.2 is restricted to $\lambda_{\{1^2\}}^2 = \lambda_{\{2\}}^2$, i.e., for equal strengths for the symmetric and anti-symmetric parts of the interaction. For completeness, we have studied the variation of widths and covariances when $\lambda_{\{1^2\}}^2 \neq \lambda_{\{2\}}^2$ by fixing the value for the ensemble averaged two-particle spectral vari-

ance $\sigma_{H(2)}^2(2)$ to a constant and then varying $\lambda_{\{2\}}$ (or equivalently $\lambda_{\{1^2\}}$). The two-particle spectral variance for $\Omega \gg 1$ is $\sigma_{H(2)}^2(2) = \Omega^2 [3\lambda_{\{2\}}^2 + 5\lambda_{\{1^2\}}^2]/16$. Therefore calculations are carried out with the constraint $[3\lambda_{\{2\}}^2 + 5\lambda_{\{1^2\}}^2] = 8\lambda^2$. All our previous results correspond to $\lambda_{\{2\}}^2 = \lambda_{\{1^2\}}^2 = \lambda^2 = 1$. Now we will discuss some results for the extreme cases: (i) $\lambda_{\{1^2\}}^2 = 0$, $\lambda_{\{2\}}^2 = 8/3$ (denoted by $\{2\}$ in Fig. 4.8 and this corresponds to $H = H_{\{2\}}$) and (ii) $\lambda_{\{1^2\}}^2 = 8/5$, $\lambda_{\{2\}}^2 = 0$ (denoted by $\{1^2\}$ in Fig. 4.8 and this corresponds to $H = H_{\{1^2\}}$). Figure 4.8(a) shows that the spectral widths have peaks at $m = 4r$ and $m = 4r + 1$ for $H_{\{2\}}$ and $H_{\{1^2\}}$, respectively. The peak for $H_{\{2\}}$ is much larger and for $H_{\{1^2\}}$ it appears at a wrong place when compared to the results shown in Fig. 4.3 for $H = H_{\{2\}} \oplus H_{\{1^2\}}$. Similarly, it is seen from Fig. 4.8(b) that the variation in the spectral widths $\sigma(m, f_m) = [\langle H^2 \rangle^{m, f_m}]^{1/2}$ as a function of f_m show more fluctuations as compared to a good linear behavior for $\lambda_{\{1^2\}}^2 = \lambda_{\{2\}}^2$. Figure 4.8(c) shows self and cross-correlations $\Sigma_{11}(m, f_m; m', f_{m'})$ and $\Sigma_{22}(m, f_m; m', f_{m'})$ with $f_m = f_m^{(p)}$ as a function of m and m' . Results for $H_{\{2\}}$ and $H_{\{1^2\}}$ show more fluctuations and more importantly, the magnitude of correlations for $H_{\{2\}}$ is much larger and for $H_{\{1^2\}}$ somewhat smaller compared to the results for $H = H_{\{2\}} \oplus H_{\{1^2\}}$. From this exercise, we can conclude that the results for spectral widths and lower order correlations will deviate strongly from those reported in Secs. 4.6 and 4.7 ($\lambda_{\{1^2\}}^2 = \lambda_{\{2\}}^2 = \lambda^2$) when $\lambda_{\{1^2\}}^2$ differs significantly from $\lambda_{\{2\}}^2$.

4.7.4 Conclusions

Increase in the magnitude of self-correlations in energy centroids and spectral variances, defined by Σ_{11} and Σ_{22} and the matrices $H_{f_m}(m)$ becoming more dense as we go from $\text{EGUE}(2) \rightarrow \text{EGUE}(2)\text{-}\mathbf{s} \rightarrow \text{EGUE}(2)\text{-}SU(4)$ is an important result that deserves more investigation. The cross-correlations increase with m' for fixed f_m and also with $\langle C_2[SU(4)] \rangle^{\tilde{f}_m}$ with fixed m . For $\lambda_{\{2\}}^2 \neq \lambda_{\{1^2\}}^2$, results for spectral widths and lower order correlations will deviate strongly from those with $\lambda_{\{2\}}^2 = \lambda_{\{1^2\}}^2$ only when $\lambda_{\{1^2\}}^2$ differs significantly from $\lambda_{\{2\}}^2$.

4.8 Summary

We have introduced in this chapter a new embedded ensemble, $\text{EGUE}(2)\text{-}SU(4)$, and it is defined for two-body Hamiltonians preserving $SU(4)$ symmetry for a system of

m fermions in Ω number of levels each four-fold degenerate. We have developed, for this ensemble, an analytical formulation based on the Wigner-Racah algebra of the embedding $U(\Omega) \otimes SU(4)$ algebra. Explicit formulas are derived for spectral variances and covariances in energy centroids and spectral variances for $U(\Omega)$ irreps of the type $f_m^{(p)} = \{4^r, p\}$, $p = 0, 1, 2$ and 3 . Results in Tables 4.3, 4.6, 4.8 and 4.9 allow one to calculate these for any m and Ω . For general $U(\Omega)$ irreps f_m , the analytical formulation in Secs. 4.3-4.5 and the formulas in the Tables 4.4 and 4.7 (obtained by simplifying the tabulations due to Hecht [He-74a]), allows one to carry out numerical calculations and codes for the same are developed. The analytical formulas in the Tables led to simple expressions for the covariances in energy centroids and spectral variances in the dilute limit for the irreps $f_m^{(p)}$. Using the formulation in Secs. 4.3-4.5 and the results in Tables 4.3-4.9, several numerical calculations are carried out and the results are presented in Secs. 4.6 and 4.7 and in Figs. 4.3-4.8. Main conclusions from these are as follows:

- (i) Expectation values $\langle C_2[SU(4)] \rangle^E$ studied in Section 4.6.2 by constructing Gaussian partial densities with centroids given by $\langle C_2[SU(4)] \rangle^{\tilde{f}_m}$ and variances given by $\overline{\langle H^2 \rangle^{m, \tilde{f}_m}}$ and similarly, the four periodicity in the gs energies studied in Section 4.6.3, establish that random interactions with $SU(4)$ symmetry keep intact the essential features of the Majorana force. This conclusion is quite similar to the result derived for EGOE(2)- J (also called TBRE some times), the embedded ensemble with angular-momentum J symmetry. This ensemble is generated by (see also Sec. 7.4) random interactions that are J scalar [$SO(3)$ scalar] and it is found that, for systems with even number of fermions, there is $J^\pi = 0^+$ preponderance in the ground states. This feature has been investigated in many different ways [Zh-04, Zh-04a, Ze-04, Pa-04]. It should be noted that the $SO(3)$ invariant operator is J^2 and it gives (with $H = J^2$) $J = 0$ as gs, a property generated also by random interactions.
- (ii) As shown in Section 4.7.1, there is increase in the magnitude of self-correlations in energy centroids and spectral variances, defined by Σ_{11} and Σ_{22} in direct correlation with the $H_{f_m}(m)$ matrices becoming more dense (implying stronger mixing) as we go from EGUE(2) \rightarrow EGUE(2)-**s** \rightarrow EGUE(2)- $SU(4)$. Further inves-

tigation of this feature may provide additional justification for the recent claim by Papenbrock and Weidenmüller [Pa-05] that symmetries are responsible for chaos in nuclear shell-model spaces.

- (iii) As shown in Section 4.7.2, there is a significant increase in cross-correlations with particle number m for a fixed $U(\Omega)$ irrep f_m and similarly with $\langle C_2[SU(4)] \rangle^{\tilde{f}_m}$ for fixed m . This could be used as a signature for experimental detection of cross-correlations generated by EGUE(2)- $SU(4)$.

Finally, we conclude that the results presented in the present chapter represent a first detailed analytical study of an embedded ensemble with a non-trivial symmetry that is relevant in nuclear structure.

Chapter 5

EGOE(1+2)- π : Density of States and Parity Ratios

5.1 Introduction

Parity is an important symmetry for finite quantum systems such as nuclei and atoms. In this chapter, we consider EGOE that includes parity explicitly and address three important questions related to parity in nuclear structure. These are as follows:

- (i) Parity ratios of nuclear level densities is an important ingredient in nuclear astrophysical applications. Recently, a method based on non-interacting Fermi-gas model for proton-neutron systems has been developed and the parity (π) ratios as a function of excitation energy in large number of nuclei of astrophysical interest have been tabulated [Mo-07]. The method is based on the assumption that the probability to occupy s out of N given sp states follow Poisson distribution in the dilute limit ($m \ll N, N \rightarrow \infty$ where m is the number of particles). Then the ratio of the partition functions for the +ve and -ve parity states is given by the simple formula $Z_- / Z_+ = \tanh f$, where f is average number of particles in the +ve parity states. Starting with this, an iterative method is developed with inputs from the Fermi-Dirac distribution for occupancies including pairing effects and the Fermi-gas form for the total level density. In the examples studied in [Mo-07], parity ratios are found to equilibrate only around 5 – 10 MeV excitation energy. However, ab-initio interacting particle theory for parity

ratios is not yet available.

- (ii) A closely related question is about the form of the density of states defined over spaces with fixed- π . In general, fixed- π density of states can be written as a sum of appropriate partial densities. In the situation that the form of the partial densities is determined by a few parameters (as it is with a Gaussian or a Gaussian with one or two corrections), it is possible to derive a theory for these parameters and using these, one can construct fixed- π density of states and calculate parity ratios. Such a theory with interactions in general follows from random matrix theory [Ko-10].
- (iii) There is the important recognition in the past few years that random interactions generate regular structures [Ze-04, Zh-04a, Pa-07, Ho-10]. It was shown in [Zh-04] that shell-model for even-even nuclei gives preponderance of +ve parity ground states. A parameter-free EGOE with parity has been defined and analyzed recently by Papenbrock and Weidenmüller [Pa-08] to address the question of ‘preponderance of ground states with positive parity’ for systems with even number of fermions. They show that in the dilute limit, +ve parity ground states appear with only 50% probability. Thus, a random matrix theory describing shell-model results is not yet available.

With the success of the embedded random matrix ensembles, one can argue that the EE generated by parity preserving random interaction may provide generic results for the three nuclear structure quantities mentioned above. For nuclei, the GOE versions of EE are relevant. Then, with a chaos producing two-body interaction preserving parity in the presence of a mean-field, we have embedded Gaussian orthogonal ensemble of one plus two-body interactions with parity [hereafter called EGOE(1+2)- π]. This model contains two mixing parameters and a gap between the +ve and -ve parity sp states and it goes much beyond the simpler model considered in [Pa-08]. In the random matrix model used in the present chapter, proton-neutron degrees of freedom and angular momentum (J) are not considered. Let us add that in the present chapter for the first time a random matrix theory for parity ratios is attempted. All the results presented in this chapter are published in [Ma-11a].

5.2 EGOE(1+2)- π Ensemble

Given N_+ number of positive parity sp states and similarly N_- number of negative parity sp states, let us assume, for simplicity, that the +ve and -ve parity states are degenerate and separated by energy Δ ; see Fig. 5.1. This defines the one-body part $h(1)$ of the Hamiltonian H with $N = N_+ + N_-$ sp states. The matrix for the two-body part $V(2)$ of H [we assume H is (1+2)-body] will be a 3×3 block matrix in two-particle spaces as there are three possible ways to generate two-particle states with definite parity: (i) both fermions in +ve parity states; (ii) both fermions in -ve parity states; (iii) one fermion in +ve and other fermion in -ve parity states. They will give the matrices A , B , and C , respectively in Fig. 5.1. For parity preserving interactions only the states (i) and (ii) will be mixed and mixing matrix is D in Fig. 5.1. Note that the matrices A , B and C are symmetric square matrices while D is in general a rectangular mixing matrix. Consider N sp states arranged such that the states 1 to N_+ have +ve parity and states $N_+ + 1$ to N have -ve parity. Then the operator form of H preserving parity is,

$$\begin{aligned}
 H &= h(1) + V(2); \\
 h(1) &= \sum_{i=1}^{N_+} \epsilon_i^{(+)} \hat{n}_i^{(+)} + \sum_{i=N_++1}^N \epsilon_i^{(-)} \hat{n}_i^{(-)}; \quad \epsilon_i^{(+)} = 0, \quad \epsilon_i^{(-)} = \Delta, \\
 V(2) &= \sum_{\substack{i,j,k,l=1 \\ (i < j, k < l)}}^{N_+} \langle v_k v_l | V | v_i v_j \rangle a_k^\dagger a_l^\dagger a_j a_i \\
 &+ \sum_{\substack{i',j',k',\ell'=N_++1 \\ (i' < j', k' < \ell')}}^N \langle v_{k'} v_{\ell'} | V | v_{i'} v_{j'} \rangle a_{k'}^\dagger a_{\ell'}^\dagger a_{j'} a_{i'} \\
 &+ \sum_{i'',k''=1}^{N_+} \sum_{j'',\ell''=N_++1}^N \langle v_{k''} v_{\ell''} | V | v_{i''} v_{j''} \rangle a_{k''}^\dagger a_{\ell''}^\dagger a_{j''} a_{i''}
 \end{aligned} \tag{5.2.1}$$

$$+ \sum_{\substack{P, Q = 1 \\ (P < Q)}}^{N_+} \sum_{\substack{R, S = N_+ + 1 \\ (R < S)}}^N \left[\langle v_P v_Q | V | v_R v_S \rangle a_P^\dagger a_Q^\dagger a_S a_R + \text{h.c.} \right].$$

In Eq. (5.2.1), v_i 's are sp states with $i = 1, 2, \dots, N$ (the first N_+ states are +ve parity and remaining -ve parity). Similarly, $\langle \dots | V | \dots \rangle$ are the two-particle matrix elements, \hat{n}_i are number operators and a_i^\dagger and a_i are creation and annihilation operators, respectively. Note that the four terms in the RHS of the expression for $V(2)$ in Eq. (5.2.1) correspond, respectively, to the matrices A , B , C and D shown in Fig. 5.1.

Many-particle states for m fermions in the N sp states can be obtained by distributing m_1 fermions in the +ve parity sp states (N_+ in number) and similarly, m_2 fermions in the -ve parity sp states (N_- in number) with $m = m_1 + m_2$. Let us denote each distribution of m_1 fermions in N_+ sp states by \mathbf{m}_1 and similarly, \mathbf{m}_2 for m_2 fermions in N_- sp states. Many-particle basis defined by $(\mathbf{m}_1, \mathbf{m}_2)$ with m_2 even will form the basis for +ve parity states and similarly, with m_2 odd for -ve parity states. In the $(\mathbf{m}_1, \mathbf{m}_2)$ basis with m_2 even (or odd), the H matrix construction reduces to the matrix construction for spinless fermion systems. The method of construction for spinless fermion systems is well known (see Chapter 1) and therefore it is easy to construct the many-particle H matrices in +ve and -ve parity spaces. The matrix dimensions d_+ for +ve parity and d_- for -ve parity spaces are given by,

$$d_+ = \sum_{m_1, m_2 (m_2 \text{ even})} \binom{N_+}{m_1} \binom{N_-}{m_2}, \quad d_- = \sum_{m_1, m_2 (m_2 \text{ odd})} \binom{N_+}{m_1} \binom{N_-}{m_2}. \quad (5.2.2)$$

Some examples for the dimensions d_+ and d_- are given in Table 5.1.

The EGOE(1+2)- π ensemble is defined by choosing the matrices A , B and C to be independent GOE's with matrix elements variances v_a^2 , v_b^2 , and v_c^2 , respectively. Similarly the matrix elements of the mixing D matrix are chosen to be independent (independent of A , B and C matrix elements) zero centered Gaussian variables with variance v_d^2 . Without loss of generality we choose $\Delta = 1$ so that all the v 's are in Δ units. This general EGOE(1+2)- π model will have too many parameters ($v_a^2, v_b^2, v_c^2, v_d^2, N_+, N_-, m$) and therefore it is necessary to reduce the number of parameters. A numerically tractable and physically relevant (as discussed ahead) re-

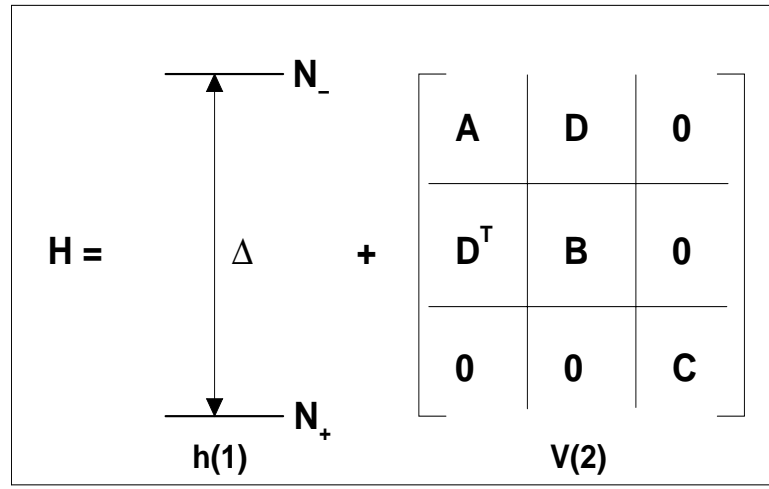


Figure 5.1: Parity preserving one plus two-body H with a sp spectrum defining $h(1)$ along with a schematic form of the $V(2)$ matrix. Dimension of the matrices A , B and C are $N_+(N_+ - 1)/2$, $N_-(N_- - 1)/2$, and N_+N_- , respectively. Note that D^T is the transpose of the matrix D . See text for details.

Table 5.1: Hamiltonian matrix dimensions d_+ and d_- for various values of (N_+, N_-, m) .

N_+	N_-	m	d_+	d_-	N_+	N_-	m	d_+	d_-
6	6	6	452	472	8	8	4	924	896
7	5	6	462	462			5	2184	2184
7	7	5	1001	1001			6	3976	4032
		6	1484	1519	10	6	4	900	920
		7	1716	1716			5	2202	2166
8	6	5	1016	986			6	4036	3972
		6	1499	1504	6	10	4	900	920
9	5	5	1011	911			5	2166	2202
		6	1524	1479			6	4036	3972
5	10	4	665	700	9	9	6	9240	9324
		5	1501	1502	10	8	6	9268	9296
					10	10	5	7752	7752
							6	19320	19440

striction is to choose the matrix elements variances of the diagonal blocks A , B and C to be same and then we have the EGOE(1+2)- π model defined by (N_+, N_-, m) and the variance parameters (τ, α) where

$$\frac{v_a^2}{\Delta^2} = \frac{v_b^2}{\Delta^2} = \frac{v_c^2}{\Delta^2} = \tau^2, \quad \frac{v_d^2}{\Delta^2} = \alpha^2. \quad (5.2.3)$$

Thus EGOE(1+2)- π we employ is

$$\begin{aligned} A: \text{GOE}(0: \tau^2), B: \text{GOE}(0: \tau^2), C: \text{GOE}(0: \tau^2), D: \text{GOE}(0: \alpha^2); \\ A, B, C, D \text{ are independent GOE's.} \end{aligned} \quad (5.2.4)$$

Note that the D matrix is a GOE only in the sense that the matrix elements D_{ij} are all independent zero centered Gaussian variables with variance α^2 . In the limit $\tau^2 \rightarrow \infty$ and $\alpha = \tau$, the model defined by Eqs. (5.2.1), (5.2.3) and (5.2.4) reduces to the simpler model analyzed in [Pa-08].

Starting with the EGOE(1+2)- π ensemble defined by Eqs. (5.2.1), (5.2.3) and (5.2.4), we have numerically constructed the ensemble in many-particle +ve and -ve parity spaces with dimensions d_+ and d_- given by Eq. (5.2.2) for several values of (N_+, N_-, m) and varying the parameters τ and α . Before discussing the results of the numerical calculations, we present the results for the energy centroids, variances and also the shape parameters (skewness and excess) defining the normalized fixed- (m_1, m_2) partial densities $\rho^{m_1, m_2}(E) = \langle \delta(H - E) \rangle^{m_1, m_2}$. These will allow us to understand some of the numerical results. Let us add that the fixed- π eigenvalue densities $I_{\pm}(E)$ are sum of the appropriate partial densities as given by Eq. (5.4.4) ahead. Note that the densities $I_{\pm}(E)$ are normalized to d_{\pm} .

5.3 Energy Centroids, Variances, Skewness and Excess

Parameters for Fixed- (m_1, m_2) Partial Densities

Let us call the set of +ve parity sp states as unitary orbit #1 and similarly the set of -ve parity sp states as unitary orbit #2; unitary orbits notation and their significance was discussed in [Ko-10]. For convenience, from now on, we denote the sp states by the roman letters (i, j, \dots) and unitary orbits by greek letters (α, β, \dots) . Note that $\alpha = 1$ corresponds to the +ve parity unitary orbit and $\alpha = 2$ corresponds to the -ve parity unitary orbit (with this notation, $N_1 = N_+$ and $N_2 = N_-$). The sp states that belong to a unitary orbit α are denoted as $i_{\alpha}, j_{\alpha}, \dots$. Propagation formulas for the energy centroids and variances of the partial densities $\rho^{m_1, m_2}(E)$ follow from the unitary decomposition of $V(2)$ with respect to the sub-algebra $U(N_+) \oplus U(N_-)$ contained in $U(N)$. The operator $V(2)$ decomposes into three parts $V(2) \rightarrow V^{[0]} + V^{[1]} + V^{[2]}$.

The $V^{[0]}$ generates the energy centroids $\langle V \rangle^{m_1, m_2}$, $V^{[1]}$ corresponds to the ‘algebraic’ mean-field generated by V and $V^{[2]}$ is the remaining irreducible two-body part. Extending the unitary decomposition for the situation with a single orbit for spinless fermions (see Appendix A) and also using the detailed formulation given in [Ch-71], we obtain the following formulas for the $V^{[v]}$ ’s. The $V^{[0]}$ is given by (with $\alpha = 1, 2$ and $\beta = 1, 2$)

$$\begin{aligned}
V^{[0]} &= \sum_{\alpha \geq \beta} \frac{\hat{n}_\alpha (\hat{n}_\beta - \delta_{\alpha\beta})}{(1 + \delta_{\alpha\beta})} V_{\alpha\beta}; \\
V_{\alpha\alpha} &= \binom{N_\alpha}{2}^{-1} \sum_{i>j} V_{i_\alpha j_\alpha i_\alpha j_\alpha}, \\
V_{\alpha\beta} &= (N_\alpha N_\beta)^{-1} \sum_{i,j} V_{i_\alpha j_\beta i_\alpha j_\beta}; \quad \alpha \neq \beta.
\end{aligned} \tag{5.3.1}$$

Then the traceless part \tilde{V} is given by

$$\begin{aligned}
\tilde{V} &= V - V^{[0]} = V^{[1]} + V^{[2]}; \\
(\tilde{V})_{i_\alpha j_\beta i_\alpha j_\beta} &= V_{i_\alpha j_\beta i_\alpha j_\beta} - V_{\alpha\beta}, \\
(\tilde{V})_{ijkl} &= V_{ijkl} \quad \text{for all others.}
\end{aligned} \tag{5.3.2}$$

Now the $V^{[1]}$ part is

$$\begin{aligned}
V^{[1]} &= \sum_{i_\alpha, j_\alpha} \hat{\xi}_{i_\alpha j_\alpha} a_{i_\alpha}^\dagger a_{j_\alpha}; \\
\hat{\xi}_{i_\alpha j_\alpha} &= \sum_{\beta} \frac{\hat{n}_\beta - \delta_{\alpha\beta}}{N_\beta - 2\delta_{\alpha\beta}} \zeta_{i_\alpha j_\alpha}(\beta), \quad \zeta_{i_\alpha j_\alpha}(\beta) = \sum_{k_\beta} \tilde{V}_{k_\beta i_\alpha k_\beta j_\alpha}.
\end{aligned} \tag{5.3.3}$$

It is important to stress that, with spherical (j) orbits and no radial degeneracy (as used in many nuclear structure studies), $V^{[1]}$ part will not exist. Finally, the $V^{[2]}$ part

is as follows,

$$\begin{aligned}
V^{[2]} &= \tilde{V} - V^{[1]}; \\
V_{i_\alpha j_\beta i_\alpha j_\beta}^{[2]} &= \tilde{V}_{i_\alpha j_\beta i_\alpha j_\beta} - \left[\frac{\zeta_{i_\alpha j_\alpha}(\beta)}{N_\beta - 2\delta_{\alpha\beta}} + \frac{\zeta_{i_\beta j_\beta}(\alpha)}{N_\alpha - 2\delta_{\alpha\beta}} \right], \\
V_{k_\alpha i_\beta k_\alpha j_\beta}^{[2]} &= \tilde{V}_{k_\alpha i_\beta k_\alpha j_\beta} - \frac{\zeta_{i_\beta j_\beta}(\alpha)}{N_\alpha - 2\delta_{\alpha\beta}}; \quad i_\beta \neq j_\beta, \\
V_{ijk\ell}^{[2]} &= \tilde{V}_{ijk\ell} \text{ for all others.}
\end{aligned} \tag{5.3.4}$$

Given the $U(N) \supset U(N_+) \oplus U(N_-)$ unitary (tensorial) decomposition, by intuition and using Eq. (A3), it is possible to write the propagation formulas for the energy centroids and variances of $\rho^{m_1, m_2}(E)$. Note that these are essentially traces of H and H^2 over the space defined by the two-orbit configurations (m_1, m_2) ; see Eqs. (5.3.5) and (5.3.6) ahead. A direct approach to write the propagation formulas for centroids and variances for a multi-orbit configuration was given in detail first by French and Ratcliff [Fr-71]. The formula for the variance given in [Fr-71] is cumbersome and it is realized later [Ch-71] that they can be made compact by applying group theory (see also [Ko-01, Wo-86, Ko-10]). We have adopted the group theoretical approach for the two-orbit averages and obtained formulas. Propagation formula for the fixed- (m_1, m_2) energy centroids is,

$$E_c(m_1, m_2) = \langle H \rangle^{m_1, m_2} = m_2 \Delta + \sum_{\alpha \geq \beta} \frac{m_\alpha(m_\beta - \delta_{\alpha\beta})}{(1 + \delta_{\alpha\beta})} V_{\alpha\beta}. \tag{5.3.5}$$

First term in Eq. (5.3.5) is generated by $h(1)$ and is simple because of the choice of the sp energies as shown in Fig. 5.1. Propagation formula for fixed- (m_1, m_2) variances is,

$$\begin{aligned}
\sigma^2(m_1, m_2) &= \langle H^2 \rangle^{m_1, m_2} - [\langle H \rangle^{m_1, m_2}]^2 \\
&= \sum_\alpha \frac{m_\alpha(N_\alpha - m_\alpha)}{N_\alpha(N_\alpha - 1)} \sum_{i_\alpha, j_\alpha} [\xi_{i_\alpha, j_\alpha}(m_1, m_2)]^2
\end{aligned} \tag{5.3.6}$$

$$\begin{aligned}
& + \sum'_{\alpha, \beta, \gamma, \delta} \frac{m_\alpha(m_\beta - \delta_{\alpha\beta})(N_\gamma - m_\gamma)(N_\delta - m_\delta - \delta_{\gamma\delta})}{N_\alpha(N_\beta - \delta_{\alpha\beta})(N_\gamma - \delta_{\gamma\alpha} - \delta_{\gamma\beta})(N_\delta - \delta_{\delta\alpha} - \delta_{\delta\beta} - \delta_{\delta\gamma})} (X); \\
& \xi_{i_\alpha, j_\alpha}(m_1, m_2) = \sum_\beta \frac{m_\beta - \delta_{\alpha\beta}}{N_\beta - 2\delta_{\alpha\beta}} \zeta_{i_\alpha j_\alpha}(\beta), \quad X = \sum' \left(V_{i_\alpha j_\beta k_\gamma \ell_\delta}^{[2]} \right)^2.
\end{aligned}$$

The ‘prime’ over summations in Eq. (5.3.6) implies that the summations are not free sums. Note that $(\alpha, \beta, \gamma, \delta)$ take values $(1, 1, 1, 1)$, $(2, 2, 2, 2)$, $(1, 2, 1, 2)$, $(1, 1, 2, 2)$ and $(2, 2, 1, 1)$. Similarly, in the sum over (i_α, j_β) , $i \leq j$ if $\alpha = \beta$ and otherwise the sum is over all i and j . Similarly, for (k_γ, ℓ_δ) . Using $E_c(m_1, m_2)$ and $\sigma^2(m_1, m_2)$, the fixed-parity energy centroids and spectral variances [they define $I_\pm(E)$] can be obtained as follows,

$$\begin{aligned}
E_c(m, \pm) &= \langle H \rangle^{m, \pm} = \frac{1}{d_\pm} \sum'_{m_1, m_2} d(m_1, m_2) E_c(m_1, m_2), \\
\sigma^2(m, \pm) &= \langle H^2 \rangle^{m, \pm} - [\langle H \rangle^{m, \pm}]^2; \\
\langle H^2 \rangle^{m, \pm} &= \frac{1}{d_\pm} \sum'_{m_1, m_2} d(m_1, m_2) [\sigma^2(m_1, m_2) + E_c^2(m_1, m_2)].
\end{aligned} \tag{5.3.7}$$

The ‘prime’ over summations in Eq. (5.3.7) implies that m_2 is even(odd) for +ve(–ve) parity.

It should be pointed out that the formulas given by Eqs. (5.3.5), (5.3.6) and (5.3.7) are compact and easy to understand compared to Eqs. (10)-(14) of [Pa-08] and also those that follow from Eqs. (129) and (133) of [Fr-71] where unitary decomposition is not employed. We have verified Eqs. (5.3.5) and (5.3.6) by explicit construction of the H matrices in many examples. In principle, it is possible to obtain a formula for the ensemble averaged variances using Eq. (5.3.6); the ensemble averaged centroids derive only from $h(1)$. Simple asymptotic formulas for ensemble averaged variances follow by neglecting the δ -functions that appear in Eq. (5.3.6) and replacing $(V_{ijkl}^{[2]})^2$ by τ^2 and α^2 appropriately. Then the final formula for the ensemble averaged fixed-

(m_1, m_2) variances is,

$$\begin{aligned} \overline{\sigma^2(m_1, m_2)} &\approx m \left[\sum_{\alpha=1}^2 m_{\alpha} (N_{\alpha} - m_{\alpha}) \right] \tau^2 + \left[\binom{m_1}{2} \binom{\tilde{m}_2}{2} + \binom{m_2}{2} \binom{\tilde{m}_1}{2} \right] \alpha^2 \\ &+ \left[\binom{m_1}{2} \binom{\tilde{m}_1}{2} + \binom{m_2}{2} \binom{\tilde{m}_2}{2} + m_1 m_2 \tilde{m}_1 \tilde{m}_2 \right] \tau^2. \end{aligned} \quad (5.3.8)$$

Here, $\tilde{m}_1 = N_1 - m_1$ and $\tilde{m}_2 = N_2 - m_2$. In Table 5.2, we compare the results obtained from Eq. (5.3.8) with those obtained for various 100 member ensembles using Eq. (5.3.6) and the agreements are quite good. Therefore, in many practical applications, one can use Eq. (5.3.8).

In practice, fixed- π state densities are constructed as a sum of the partial densities $\rho^{m_1, m_2}(E)$ as discussed in Sec. 5.4.1 ahead. Going beyond the first two moments $M_1(m_1, m_2) = \langle H \rangle^{m_1, m_2}$ and $M_2(m_1, m_2) = \langle H^2 \rangle^{m_1, m_2}$, it is possible to consider the third and fourth moments $M_3(m_1, m_2) = \langle H^3 \rangle^{m_1, m_2}$ and $M_4(m_1, m_2) = \langle H^4 \rangle^{m_1, m_2}$ respectively of $\rho^{m_1, m_2}(E)$. The skewness and excess parameters $\gamma_1(m_1, m_2)$ and $\gamma_2(m_1, m_2)$ give information about the shape of the partial densities and they are close to zero implies Gaussian form. The partial densities $\rho^{m_1, m_2}(E)$ determine the total +ve and -ve parity state densities $I_{\pm}(E)$; see Eq. (5.4.4) ahead. By extending the binary correlation approximation to evaluate averages over two-orbit configurations, we have derived formulas for $\gamma_1(m_1, m_2)$ and $\gamma_2(m_1, m_2)$. All the details are discussed in Chapter 7. Exact results for skewness $\gamma_1(m, \pm)$ and excess $\gamma_2(m, \pm)$ parameters for fixed- π eigenvalue densities $I_{\pm}(E)$ are compared with the binary correlation results in Table 7.1 and it is clearly seen from the results in Table 7.1 that in all the examples considered, the binary correlation results are quite close to the exact results. In addition, the following results are inferred from the results in Chapter 7.

It is seen from Eq. (7.2.19), $\gamma_1(m_1, m_2)$ will be non-zero only when $\alpha \neq 0$ and the τ dependence is weak. Also, it is seen that for $N_+ = N_-$, $\gamma_1(m_1, m_2) = -\gamma_1(m_2, m_1)$. Similarly, Eq. (7.2.20) shows that for $N_+ = N_-$, $\gamma_2(m_1, m_2) = \gamma_2(m_2, m_1)$. In the dilute limit, with some approximations as discussed after Eq. (7.2.20), the expression for $\gamma_2(m_2, m_1)$ is given by Eq. (7.2.21). This shows that, for $\alpha \ll \tau$, $\gamma_2(m_2, m_1) = C_1 / [\langle X^2 \rangle^{m_1, m_2}]^2$ with $C_1 \sim -9\tau^4 N^4 m^3 / 16$ for $m_1 = m_2 = m/2$ and $N_1 = N_2 = N$. Eval-

Table 5.2: Ensemble averaged fixed- (m_1, m_2) widths $\sigma(m_1, m_2)$ and the total spectral width σ_t for different (τ, α) values. For each (τ, α) , the $\sigma(m_1, m_2)$ are given in the table and they are obtained using the exact propagation formula Eq. (5.3.6) for each member of the ensemble. In all the calculations, 100 member ensembles are employed. Numbers in the bracket are obtained by using the asymptotic formula given in Eq. (5.3.8). Last row for each (N_+, N_-) gives the corresponding σ_t values. All the results are given for 6 particle systems and the dimensions $d(m_1, m_2)$ are also given in the table. See text for details.

(N_+, N_-)	m_1	m_2	$d(m_1, m_2)$	$(\tau, \alpha/\tau)$			
				(0.1, 0.5)	(0.1, 1.5)	(0.2, 0.5)	(0.2, 1.5)
(8, 8)	0	6	28	1.36(1.39)	3.21(3.21)	2.73(2.77)	6.41(6.42)
	1	5	448	1.76(1.79)	2.70(2.72)	3.52(3.57)	5.41(5.44)
	2	4	1960	2.05(2.09)	2.48(2.50)	4.11(4.17)	4.96(5.01)
	3	3	3136	2.16(2.19)	2.42(2.45)	4.31(4.38)	4.84(4.90)
	4	2	1960	2.05(2.09)	2.48(2.50)	4.11(4.17)	4.95(5.01)
	5	1	448	1.76(1.79)	2.70(2.72)	3.52(3.57)	5.41(5.44)
	6	0	28	1.37(1.39)	3.21(3.21)	2.75(2.77)	6.42(6.42)
				2.29(2.32)	2.68(2.71)	4.24(4.30)	5.08(5.13)
(6, 10)	0	6	210	1.67(1.70)	2.70(2.72)	3.34(3.41)	5.41(5.44)
	1	5	1512	2.04(2.07)	2.48(2.51)	4.08(4.15)	4.97(5.02)
	2	4	3150	2.19(2.22)	2.41(2.44)	4.37(4.44)	4.82(4.88)
	3	3	2400	2.11(2.14)	2.43(2.46)	4.22(4.28)	4.86(4.91)
	4	2	675	1.84(1.87)	2.60(2.62)	3.67(3.73)	5.20(5.24)
	5	1	60	1.46(1.48)	3.06(3.06)	2.92(2.96)	6.12(6.13)
	6	0	1	1.30(1.30)	3.90(3.90)	2.60(2.60)	7.81(7.79)
				2.31(2.33)	2.65(2.67)	4.30(4.36)	5.02(5.07)
(10, 10)	0	6	210	1.97(2.01)	4.16(4.19)	3.95(4.01)	8.33(8.37)
	1	5	2520	2.44(2.49)	3.63(3.66)	4.90(4.98)	7.25(7.32)
	2	4	9450	2.76(2.81)	3.36(3.40)	5.53(5.61)	6.71(6.79)
	3	3	14400	2.87(2.92)	3.28(3.32)	5.74(5.83)	6.56(6.64)
	4	2	9450	2.76(2.81)	3.36(3.40)	5.53(5.61)	6.71(6.79)
	5	1	2520	2.44(2.49)	3.63(3.66)	4.90(4.98)	7.25(7.32)
	6	0	210	1.97(2.01)	4.16(4.19)	3.95(4.01)	8.33(8.37)
				2.95(2.99)	3.54(3.57)	5.62(5.70)	6.83(6.91)

uating $\overline{\langle X^2 \rangle^{m_1, m_2}}$ in the dilute limit then gives $\gamma_2 \sim -4/m$. Similarly, for $\tau \ll \alpha$, we have $\gamma_2(m_2, m_1) = C_2 / [\overline{\langle D\tilde{D} \rangle^{m_1, m_2}} + \overline{\langle \tilde{D}D \rangle^{m_1, m_2}}]^2$ with $C_2 \sim -\alpha^4 N^4 m^3 / 16$ and this gives $\gamma_2 \sim -4/m$. Therefore, in the $\tau \ll \alpha$ and $\tau \gg \alpha$ limit, the result for γ_2 is same as the result for spinless fermion EGOE(2) [Mo-73, Mo-75] and this shows that for a range of (τ, α) values, $\rho^{m_1, m_2}(E)$ will be close to Gaussian. Moreover, to the extent that Eq. (7.2.21) applies, the density $\rho^{m_1, m_2}(E)$ is a convolution of the densities generated

by $X(2)$ and $D(2)$ operators. Let us add that the binary correlation results presented in Chapter 7, with further extensions, will be useful in the study of partitioned EGOE discussed in [Ko-01, Ko-99]. Now we present some numerical results.

5.4 Numerical Results and Discussion

In order to proceed with the calculations, we need to have some idea of the range of the parameters $(\tau, \alpha, m/N_+, N_+/N_-)$. Towards this end, we have used realistic nuclear effective interactions in $sdfp$ [No-09] and $fp_{g_{9/2}}$ [So-02] spaces and calculated the variances $v_a^2, v_b^2, v_c^2, v_d^2$ for these interactions. Note that it is easy to identify the matrices A, B, C and D given the interaction matrix elements $\langle (j_1 j_2)JT | V | (j_3 j_4)JT \rangle$. To calculate the mean-squared matrix elements v^2 's, we put the diagonal two-particle matrix elements to be zero and use the weight factor $(2J+1)(2T+1)$. Assuming that $\Delta = 3$ MeV and 5 MeV (these are reasonable values for $A = 20 - 80$ nuclei), we obtain $\tau \sim 0.09 - 0.24$ and $\alpha \sim (0.9 - 1.3) \times \tau$. These deduced values of α and τ clearly point out that one has to go beyond the highly restricted ensemble employed in [Pa-08] and it is necessary to consider the more general EGOE(1+2)- π defined in Sec. 5.2. Similarly, for $sdfp$ and $fp_{g_{9/2}}$ spaces $N_+/N_- \sim 0.5 - 2.0$. Finally, for nuclei with m number of valence nucleons (particles or holes) where $sdfp$ or $fp_{g_{9/2}}$ spaces are appropriate, usually $m \lesssim N_+$ or N_- , whichever is lower. Given these, we have selected the following examples: $(N_+, N_-, m) = (8, 8, 4), (8, 8, 5), (10, 6, 4), (10, 6, 5), (6, 10, 4), (6, 10, 5), (8, 8, 6), (6, 6, 6), (7, 7, 7)$ and $(7, 7, 6)$. To go beyond the matrix dimensions ~ 5000 with 100 members is not feasible at present with the HPC cluster that is used for all the calculations. Most of the discussion in this chapter is restricted to $N = N_+ + N_- = 16$ and $m \ll N$ as in this dilute limit, it is possible to understand the ensemble results better. Following the nuclear examples mentioned above, we have chosen $\tau = 0.05, 0.1, 0.2, 0.3$ and $\alpha/\tau = 0.5, 1.0, 1.5$. We will make some comments on the results for other (τ, α) values at appropriate places.

Now we will present the results for (i) the form of the +ve and -ve parity state densities $I_+(E)$ and $I_-(E)$, respectively, (ii) the parity ratios $I_-(E)/I_+(E)$ vs E where E is the excitation energy of the system and (iii) the probability for +ve parity ground states generated by the EGOE(1+2)- π ensemble.

5.4.1 Gaussian form for fixed- π state densities

Using the method discussed in Sec. 5.2, we have numerically constructed in +ve and -ve parity spaces EGOE(1+2)- π ensembles of random matrices consisting of 100 Hamiltonian matrices in large number of examples, i.e. for (N_+, N_-, m) and (τ, α) parameters mentioned above. Diagonalizing these matrices, ensemble averaged eigenvalue (state) densities,

$$\overline{I_{\pm}(E)} = \overline{\langle\langle\delta(H - E)\rangle\rangle^{\pm}}, \quad (5.4.1)$$

are constructed. From now on, we drop the “overline” symbol when there is no confusion. Results are shown for $(N_+, N_-, m) = (8, 8, 4), (8, 8, 5), (10, 6, 5)$ and $(6, 10, 5)$ for several values of (τ, α) in Figs. 5.2, 5.3 and 5.4. To construct the fixed-parity eigenvalue densities, we first make the centroids $E_c(m, \pm)$ of all the members of the ensemble to be zero and variances $\sigma^2(m, \pm)$ to be unity, i.e., for each member we have the standardized eigenvalues $\hat{E} = [E - E_c(m, \pm)]/\sigma(m, \pm)$. Then, combining all the \hat{E} and using a bin-size $\Delta\hat{E} = 0.2$, histograms for $I_{\pm}(E)$ are generated. It is seen that the state densities are multimodal for small τ values and for $\tau \geq 0.1$, they are unimodal and close to a Gaussian. Note that in our examples, $\alpha = (0.5 - 1.5) \times \tau$.

For $V(2) = 0$, the eigenvalue densities will be a sum of spikes at $0, 2\Delta, 4\Delta, \dots$ for +ve parity densities and similarly at $\Delta, 3\Delta, 5\Delta, \dots$ for -ve parity densities. As we switch on $V(2)$, the spikes will spread due to the matrices A, B and C in Fig. 5.1 and mix due to the matrix D . The variance $\sigma^2(m_1, m_2)$ can be written as,

$$\sigma^2(m_1, m_2) = \sigma^2(m_1, m_2 \rightarrow m_1, m_2) + \sigma^2(m_1, m_2 \rightarrow m_1 \pm 2, m_2 \mp 2). \quad (5.4.2)$$

The internal variance $\sigma^2(m_1, m_2 \rightarrow m_1, m_2)$ is due to A, B and C matrices and it receives contribution only from the τ parameter. Similarly, the external variance $\sigma^2(m_1, m_2 \rightarrow m_1 \pm 2, m_2 \mp 2)$ is due to the matrix D and it receives contribution only from the α parameter. When we switch on $V(2)$, as the ensemble averaged centroids generated by $V(2)$ will be zero, the positions of the spikes will be largely unaltered. However, they will start spreading and mixing as τ and α increase. Therefore, the density will be multimodal with the modes well separated for very small (τ, α) values. Some examples for this are shown in Fig. 5.5. As τ and α start increasing from zero,

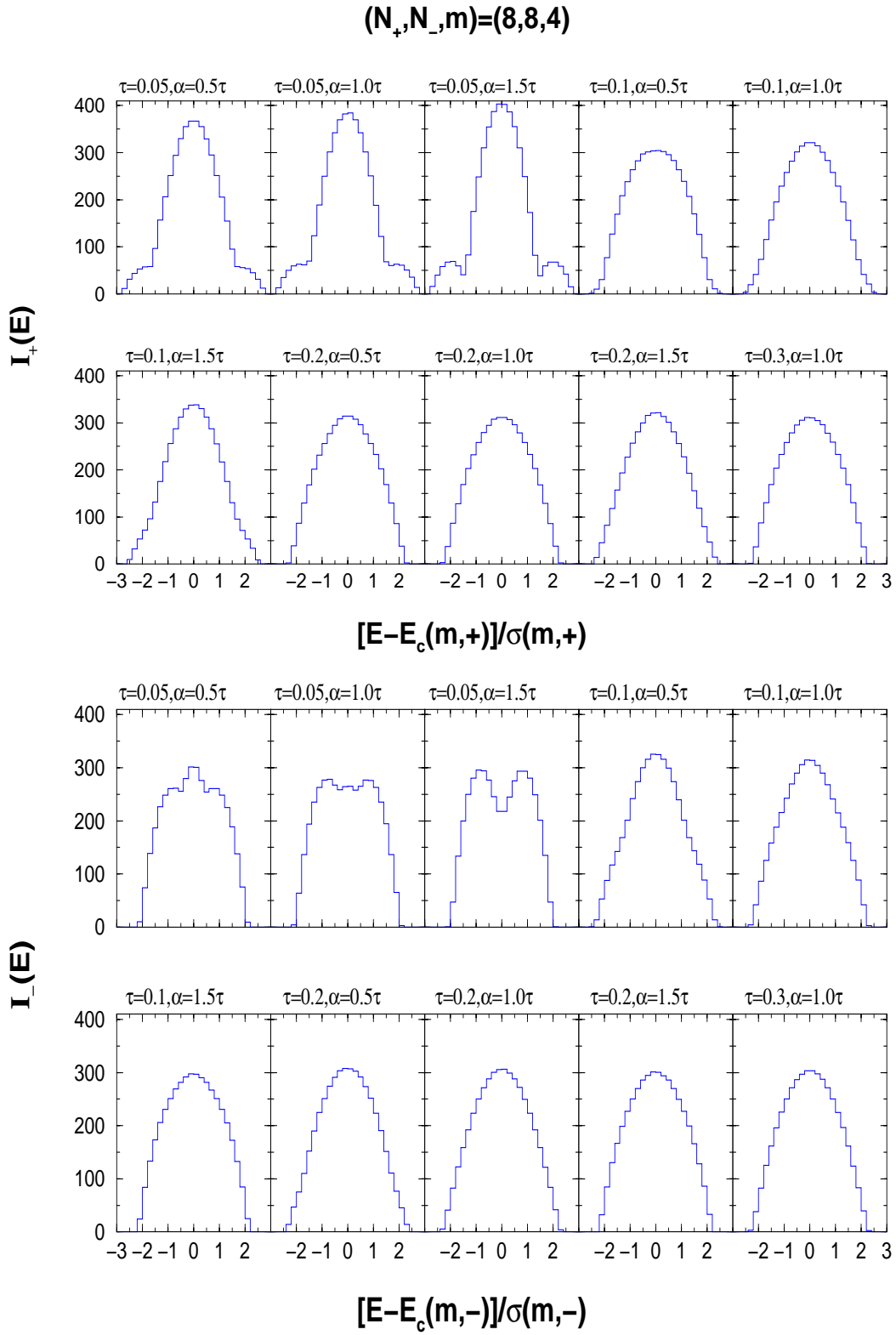


Figure 5.2: Positive and negative parity state densities for various (τ, α) values for $(N_+, N_-, m) = (8, 8, 4)$ system. See text for details.

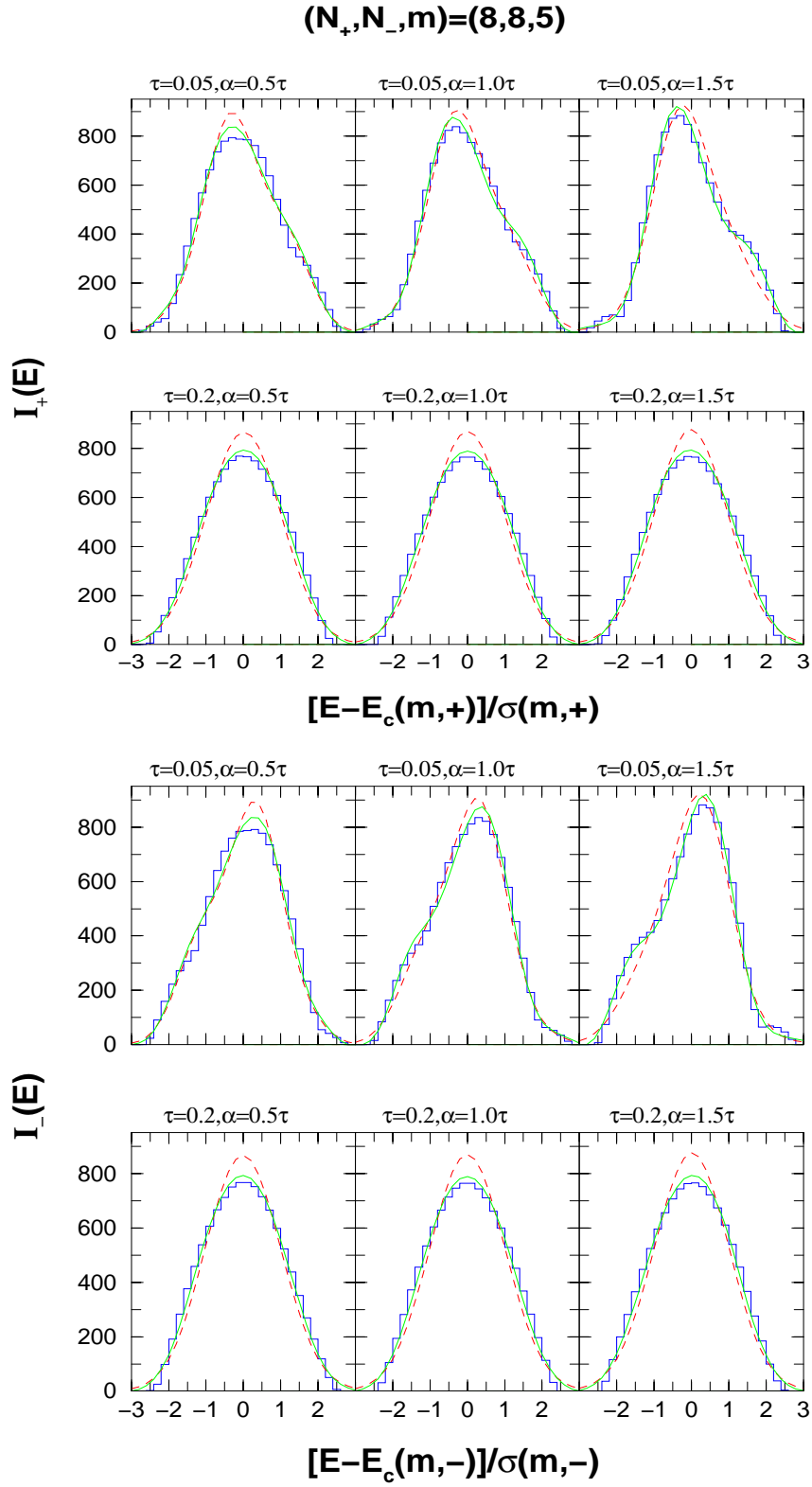


Figure 5.3: Positive and negative parity state densities for various (τ, α) values for $(N_+, N_-, m) = (8, 8, 5)$ system. Histograms are numerical ensemble results. The dashed (red) curve corresponds to Gaussian form for $\rho^{m_1, m_2}(E)$ in Eq. (5.4.4) and similarly, solid (green) curve corresponds to Edgeworth corrected Gaussian form with $\gamma_1(m_1, m_2)$ and $\gamma_2(m_1, m_2)$ obtained using the results in Chapter 7. See text for details.

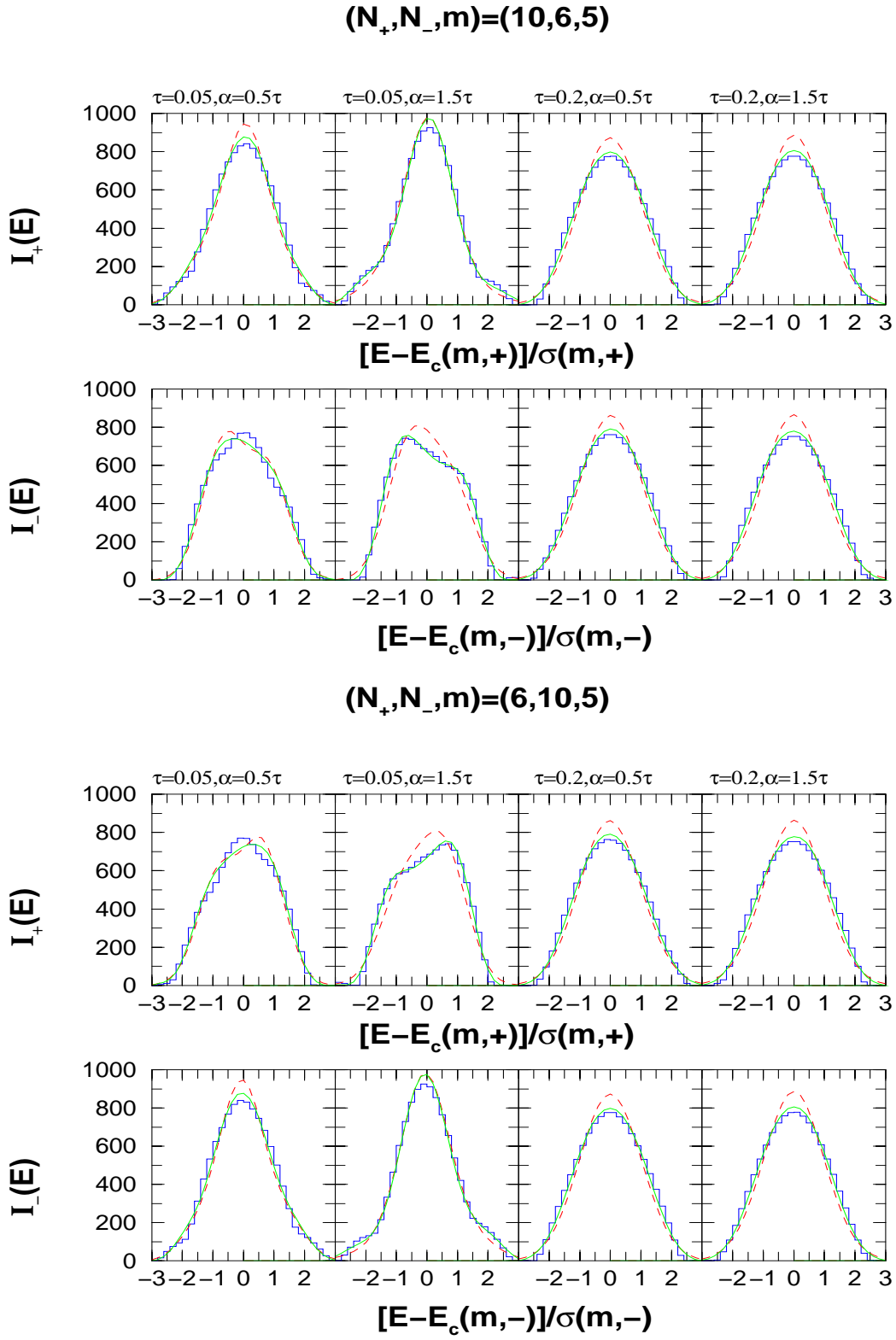


Figure 5.4: Positive and negative parity state densities for various (τ, α) values for $(N_+, N_-, m) = (10, 6, 5)$ and $(6, 10, 5)$ systems. Histograms are numerical ensemble results. The dashed (red) curve corresponds to Gaussian form for $\rho^{m_1, m_2}(E)$ in Eq. (5.4.4) and similarly, solid (green) curve corresponds to Edgeworth corrected Gaussian form with $\gamma_1(m_1, m_2)$ and $\gamma_2(m_1, m_2)$ obtained using the results in Chapter 7. See text for details.

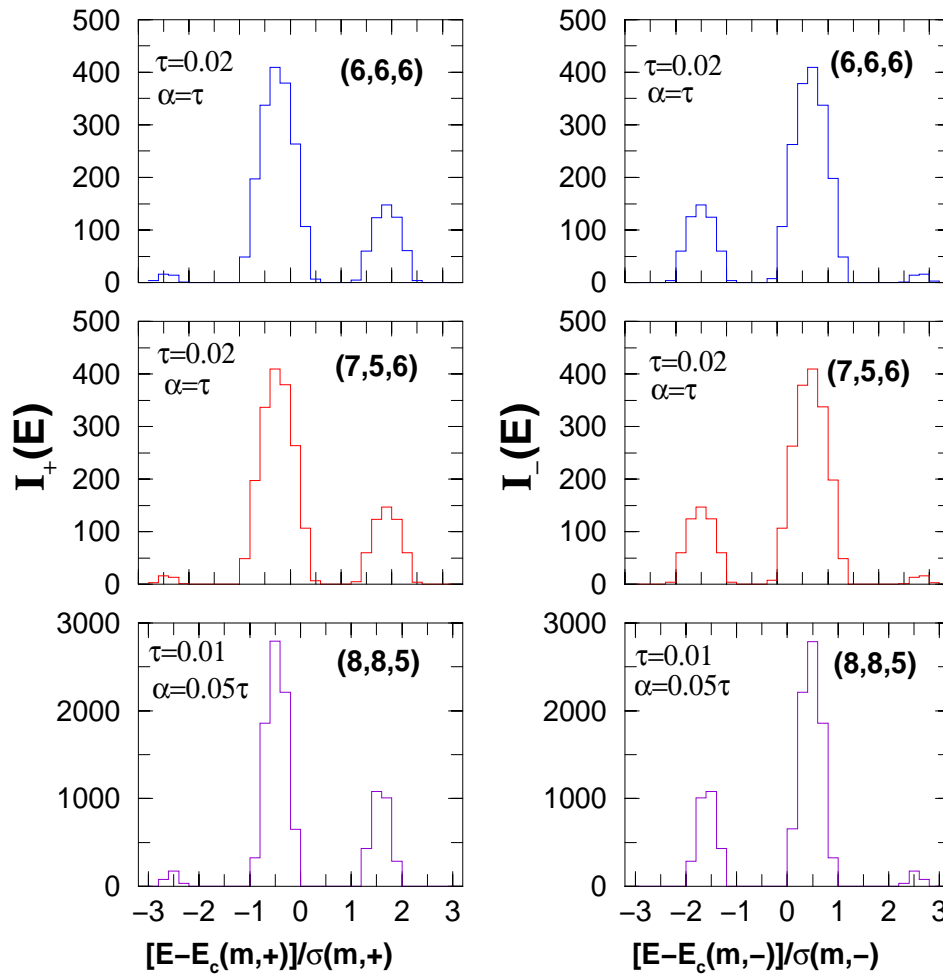


Figure 5.5: Positive and negative parity state densities for some small values of (τ, α) . The (N_+, N_-, m) values are given in the figures. See text for details.

the spikes spread and will start overlapping for $\sigma(m_1, m_2) \gtrsim \Delta$. This is the situation with $\tau = 0.05$ shown in Figs. 5.2, 5.3 and 5.4. However, as τ increases (with $\alpha \sim \tau$), the densities start becoming unimodal as seen from the $\tau = 0.1$ and 0.2 examples. Also, the m dependence is not strong as seen from the Figs. 5.2, 5.3 and 5.4. Now we will discuss the comparison of the ensemble results with the smoothed densities constructed using $E_c(m_1, m_2)$, $\sigma^2(m_1, m_2)$, $\gamma_1(m_1, m_2)$ and $\gamma_2(m_1, m_2)$.

As the particle numbers in the examples shown in Figs. 5.2, 5.3 and 5.4 are small, the excess parameter $\gamma_2^\pi(m) \sim -0.7$ to -0.8 (skewness parameter $\gamma_1^\pi(m) \sim 0$ in all our examples). Therefore the densities are not very close to a Gaussian form. It has been well established that the ensemble averaged eigenvalue density takes Gaussian form in the case of spinless fermion (as well as boson) systems and also for the embedded ensembles extending to those with good quantum numbers; see Chapter 2

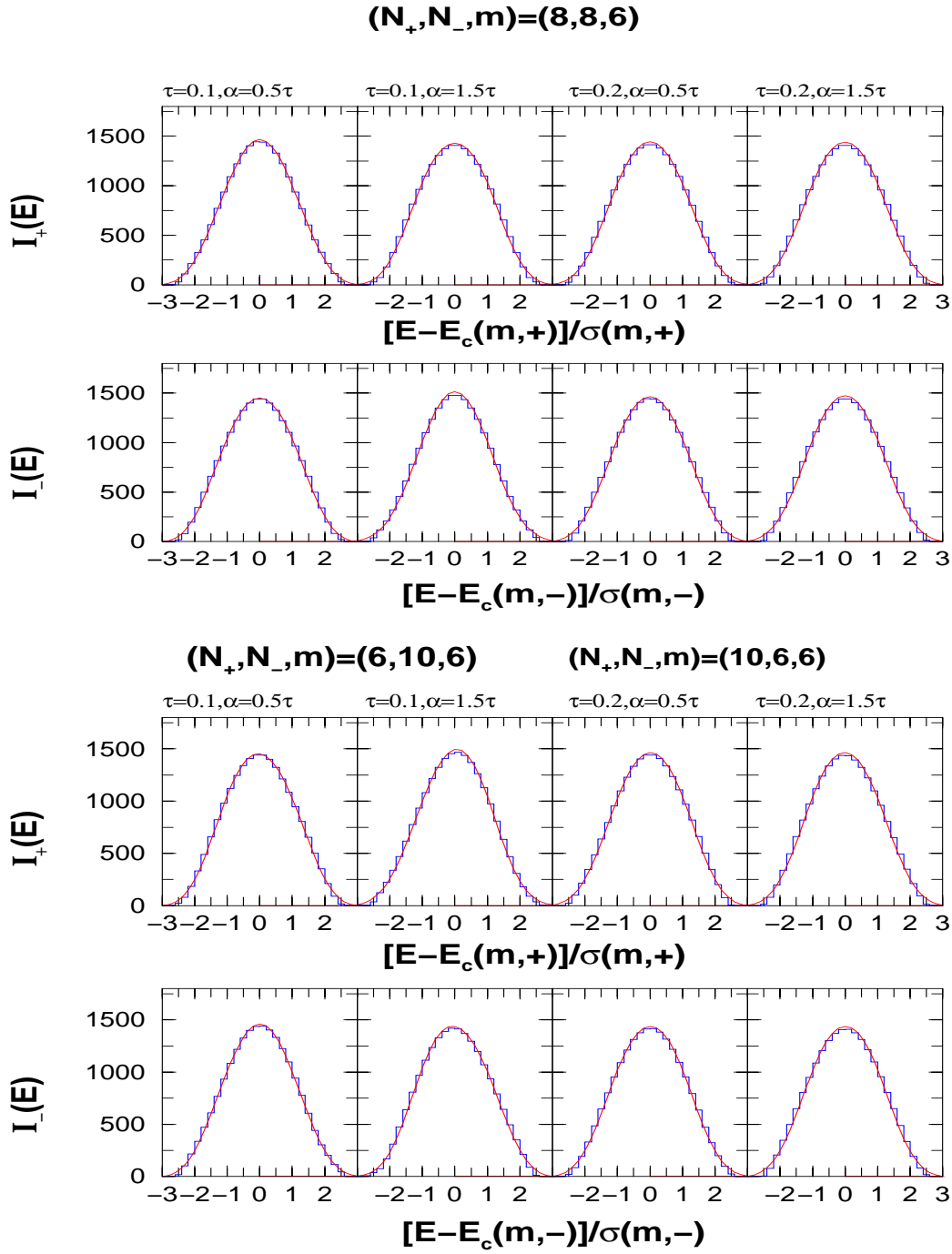


Figure 5.6: Positive and negative parity state densities for various (τ, α) values for $(N_+, N_-, m) = (8, 8, 6)$, $(6, 10, 6)$ and $(10, 6, 6)$ systems. Smoothed curves (solid red lines) are obtained using fixed- (m_1, m_2) partial densities. See text for details.

and [Ko-01, Go-11]. Thus, it can be anticipated that Gaussian form is generic for the state densities or more appropriately, for the partial densities $\rho^{m_1, m_2}(E)$ generated by EGOE(1+2)- π for sufficiently large values of (τ, α) . Results for the fixed- π densities for $(N_+, N_-, m) = (8, 8, 6)$, $(6, 10, 6)$ and $(10, 6, 6)$ systems are shown in Fig. 5.6. The

smoothed +ve and –ve parity densities are a sum of the partial densities $\rho^{m_1, m_2}(E)$,

$$\rho_{\pm}(E) = \frac{1}{d_{\pm}} \sum_{m_1, m_2}^I d(m_1, m_2) \rho^{m_1, m_2}(E). \quad (5.4.3)$$

Note that the summation in Eq. (5.4.3) is over m_2 even for +ve parity density and similarly over m_2 odd for –ve parity density. Here $\rho_{\pm}(E)$ as well as $\rho^{m_1, m_2}(E)$ are normalized to unity. However, in practice, the densities normalized to dimensions are needed and they are denoted, as used earlier, by $I_{\pm}(E)$ and $I^{m_1, m_2}(E)$, respectively,

$$I_{\pm}(E) = d_{\pm} \rho_{\pm}(E) = \sum_{m_1, m_2}^I I^{m_1, m_2}(E); \quad I^{m_1, m_2}(E) = d(m_1, m_2) \rho^{m_1, m_2}(E). \quad (5.4.4)$$

We employ the Edgeworth (ED) form that includes γ_1 and γ_2 corrections to the Gaussian partial densities $\rho_{\mathcal{G}}^{m_1, m_2}(E)$. Then

$$\rho^{m_1, m_2}(E) \rightarrow \rho_{\mathcal{G}}^{m_1, m_2}(E) \rightarrow \rho_{ED}^{m_1, m_2}(E)$$

and in terms of the standardized variable \hat{E} , the ED form $\eta_{ED}(\hat{E})$ is given by Eq. (2.3.2). Using Eqs. (5.4.3) and (2.3.2) with exact centroids and variances given by the propagation formulas in Sec. 5.3 and the binary correlation results for γ_1 and γ_2 as given by the formulas in Chapter 7, the smoothed +ve and –ve parity state densities are constructed. We put $\eta_{ED}(\hat{E}) = 0$ when $\eta_{ED}(\hat{E}) < 0$. It is clearly seen from Fig. 5.6 that the sum of partial densities, with the partial densities represented by ED corrected Gaussians, describe extremely well the exact fixed- π densities. Therefore, for the (τ, α) values in the range determined by nuclear *sdfp* and *fp_{g9/2}* interactions, i.e. $\tau \sim 0.1 - 0.3$ and $\alpha \sim 0.5\tau - 2\tau$, the partial densities can be well represented by ED corrected Gaussians and total densities are also close to ED corrected Gaussians. Unlike Fig. 5.6, densities in Figs. 5.2, 5.3 and 5.4 show, in many cases, strong departures from Gaussian form. Therefore, it is important to test how well Eq. (5.4.4) with ED corrected Gaussian for $\rho^{m_1, m_2}(E)$ describes the numerical results for $I_{\pm}(E)$. We show this comparison for all the densities in Figs. 5.3 and 5.4. It is clearly seen that the agreements with ED corrected Gaussians are good in all the cases. Therefore, the large deviations from the Gaussian form for $I_{\pm}(E)$ arise mainly because of the distribution of the centroids [this involves dimensions of the (m_1, m_2) configu-

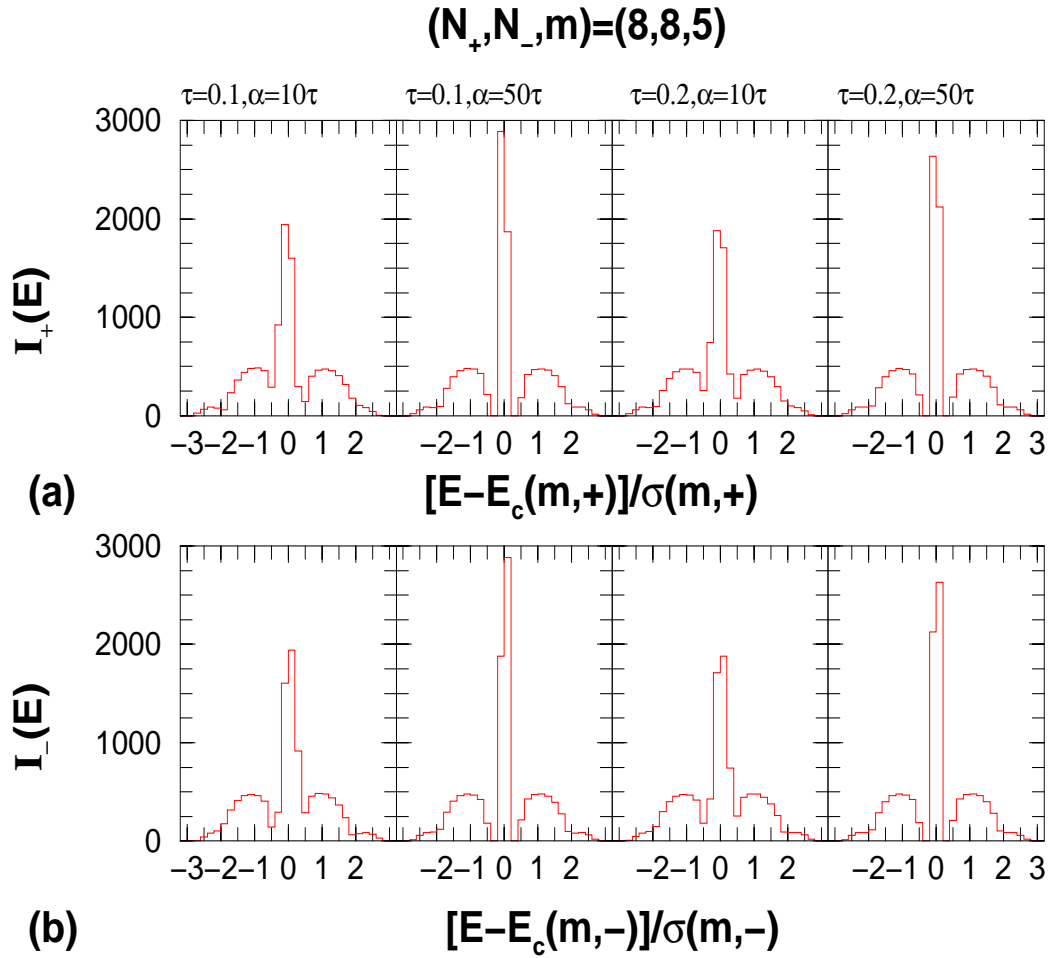


Figure 5.7: (a) Positive and (b) negative parity state densities for some small values of τ and large α values for $(N_+, N_-, m) = (8, 8, 5)$ system. See text for details.

rations] of the partial densities involved. It is possible that the agreements in Figs. 5.3 and 5.4 may become more perfect if we employ, for the partial densities, some non-canonical forms defined by the first four moments as given for example in [Gr-95a, Te-06a]. However, as these forms are not derived using any random matrix ensemble, we haven't used these for the partial densities in our present investigation. In conclusion, for the physically relevant range of (τ, α) values, the propagation formulas for centroids and variances given by Eqs. (5.3.5) and (5.3.6) or alternatively with $E_c(m_1, m_2) = m_2 \Delta$ and Eq. (5.3.8) along with the EGOE(1+2)- π ensemble averaged $\gamma_1(m_1, m_2)$ and $\gamma_2(m_1, m_2)$ estimates as given in Chapter 7 can be used to construct fixed- π state densities for larger (N_+, N_-, m) systems. Finally, for a small value of τ but α very large, the densities again become multi-modal and some examples for this are shown in Fig. 5.7. The situation here is similar to the model discussed in [Le-94].

5.4.2 Parity ratios for state densities

As stated in the beginning of this chapter, parity ratio of state densities at a given excitation energy (E) is a quantity of considerable interest in nuclear structure. For the systems shown in Figs. 5.2, 5.3 and 5.4 and also for many other systems, we have studied the parity ratios and the results are shown in Figs. 5.8-5.11. As the parity ratios need to be calculated at a given value of excitation energy E , we measure the eigenvalues in both +ve and -ve parity spaces with respect to the absolute gs energy E_{gs} of the $N = N_+ + N_-$ system. Thus, E_{gs} is defined by taking all the +ve and -ve parity eigenvalues of all members of the ensemble and choosing the lowest of all these. The gs energy can also be determined by averaging the +ve and -ve parity gs energies over the ensemble and then the gs energy is minimum of the two. It is seen that the results for parity ratios are essentially independent of the choice of E_{gs} and thus we employ absolute gs energy in our calculations. We use the ensemble averaged total (+ve and -ve eigenvalues combined) spectrum width σ_t of the system for scaling. The total widths σ_t can be calculated also by using $E_c(m_1, m_2)$ and $\sigma^2(m_1, m_2)$. Examples for σ_t are shown in Table 5.2 and they are in good agreement with the results obtained using the simple formula given by Eq. (5.3.8). We use the variable $E = (E - E_{gs})/\sigma_t$ for calculating parity ratios. Starting with E_{gs} and using a bin-size of $\Delta E = 0.2$, we have calculated the number of states $I_+(E)$ with +ve parity and also the number of states $I_-(E)$ with -ve parity in a given bin and then the ratio $I_-(E)/I_+(E)$ is the parity ratio. Note that the results in Figs. 5.8-5.11 are shown for $E = 0 - 3$ as the spectrum span is $\sim 5.5\sigma_t$. To go beyond the middle of the spectrum, for real nuclei, one has to include more sp levels (also a finer splitting of the +ve and -ve parity levels may be needed) and therefore, N_+ and N_- change. Continuing with this, one obtains the Bethe form for nuclear level densities [Ko-10].

General observations from Figs. 5.8-5.11 are as follows. (i) The parity ratio $I_-(E)/I_+(E)$ will be zero up to an energy E_0 . (ii) Then, it starts increasing and becomes larger than unity at an energy E_m . (iii) From here on, the parity ratio decreases and saturates quickly to unity from an energy E_1 . In these examples, $E_0 \lesssim 0.4$, $E_m \sim 1$ and $E_1 \sim 1.5$. It is seen that the curves shift towards left as τ increases. Also the position of the peak shifts to much larger value of E_m and equilibration gets delayed as

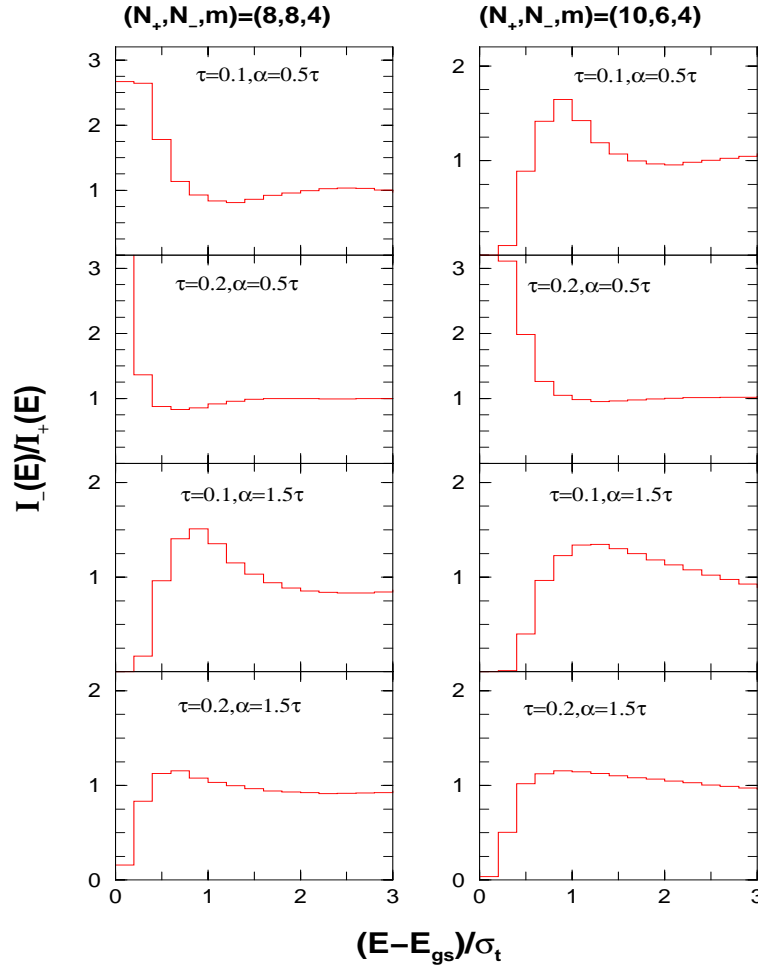
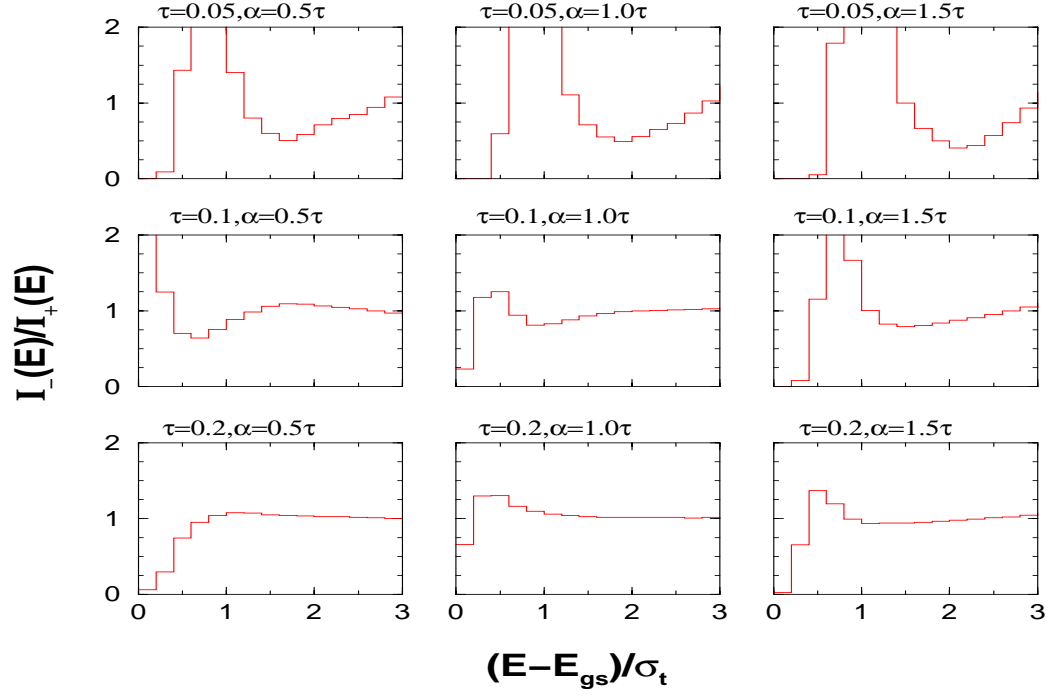


Figure 5.8: Parity ratios for various (τ, α) values for $(N_+, N_-, m) = (8, 8, 4)$ and $(10, 6, 4)$ systems. See text for details.

α increases for a fixed τ value. Therefore for larger τ , the energies (E_0, E_m, E_1) are smaller compared to those for a smaller τ . The three transition energies also depend on (N_+, N_-, m) . We have also verified, as shown in Fig. 5.10, that the general structure of the parity ratios will remain same even when we change $\Delta \rightarrow -\Delta$ (i.e., -ve parity sp states below the +ve parity sp states). For $(N_+, N_-, m) = (8, 8, 4)$ system, results for $\Delta = 1$ are given in Fig. 5.8 and they are almost same as the results with $\Delta = -1$ given in Fig. 5.10. The general structures (i)-(iii) are clearly seen in the numerical examples shown in [Mo-07] where a method based on the Fermi-gas model has been employed. If $\sigma_t \sim 6 - 8$ MeV, equilibration in parities is expected around $E \sim 8 - 10$ MeV and this is clearly seen in the examples in [Mo-07]. It is also seen from Fig. 5.9 that equilibration is quite poor for very small values of τ and therefore comparing with the results in [Mo-07], it can be argued that very small values of τ are ruled out

$$(N_+, N_-, m) = (6, 10, 4)$$



$$(N_+, N_-, m) = (6, 10, 5)$$

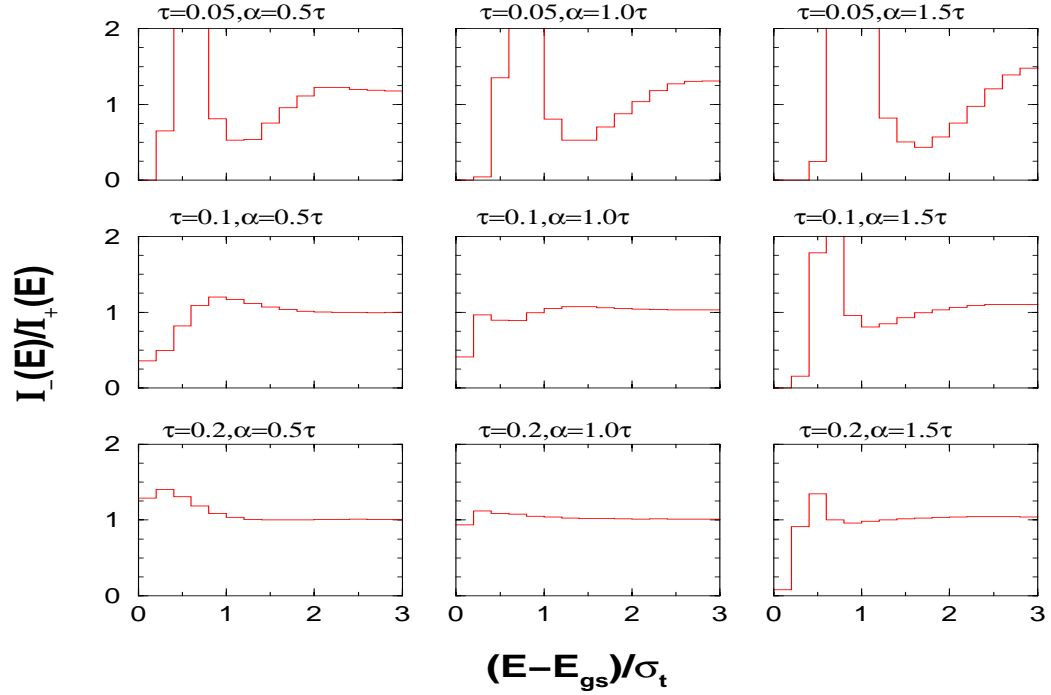


Figure 5.9: Parity ratios for various (τ, α) values for $(N_+, N_-, m) = (6, 10, 4)$ and $(6, 10, 5)$ systems. See text for details.

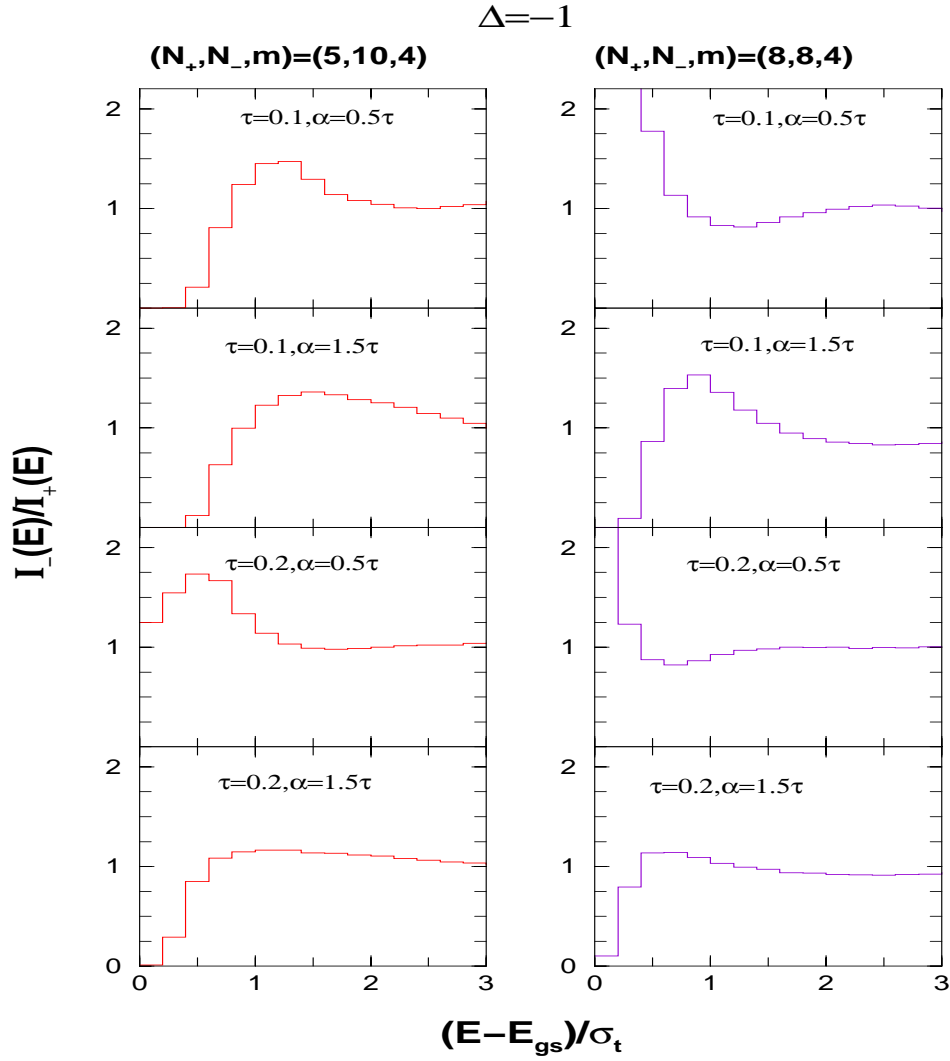


Figure 5.10: Parity ratios for some values of (τ, α) with $\Delta = -1$ for $(N_+, N_-, m) = (5, 10, 4)$ and $(8, 8, 4)$ systems. See text for details.

for nuclei. Hence, it is plausible to conclude that generic results for parity ratios can be derived using EGOE(1+2)- π with reasonably large (τ, α) values. Let us add that the interpretations in [Mo-07] are based on the occupancies of the sp orbits while in the present chapter, they are in terms of τ and α parameters.

Using the smoothed $I_{\pm}(E)$, constructed as discussed in Sec. 5.4.1, smoothed forms for parity ratios are calculated as follows. Starting with the absolute gs energy E_{gs} and using a bin-size of $\Delta E = 0.2$, +ve and -ve parity densities in a given energy bin are obtained and their ratio is the parity ratio at a given E . We have chosen the examples where I_+ and I_- are close to Gaussians. It is seen from Fig. 5.11 that the agreement with exact results is good for $E \gtrsim 0.5$. However, for smaller E , to obtain a

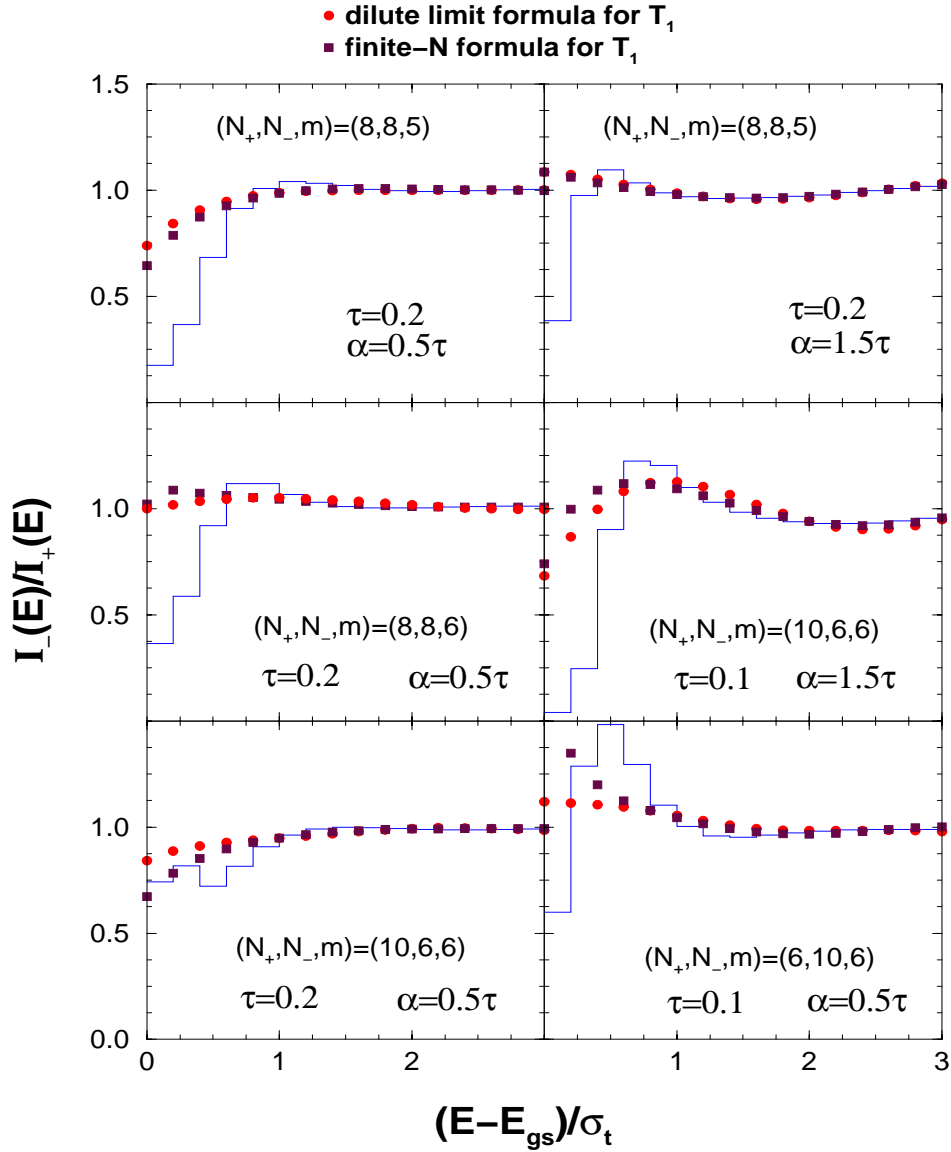


Figure 5.11: Parity ratios for various (τ, α) values and for various (N_+, N_-, m) systems. Filled circles (red) and squares (brown) are obtained using fixed- (m_1, m_2) partial densities with dilute limit formula and finite- N formula for the functions $F(\cdots)$ given in Eqs. (H14) and (H23) respectively that are required to calculate T_1 in Eq. (7.2.8); see Chapter 7 and Appendix H for details.

good agreement one should have a better prescription for determining the tail part of the $\rho^{m_1, m_2}(E)$ distributions. Developing the theory for this is beyond the scope of the present thesis as this requires more complete analytical treatment of the ensemble.

5.4.3 Probability for +ve parity ground states

Papenbrock and Weidenmüller used the $\tau \rightarrow \infty$, $\alpha = \tau$ limit of EGOE(1+2)- π for several (N_+, N_-, m) systems to study the probability (R_+) for +ve parity ground states

over the ensemble [Pa-08]. As stated before, this exercise was motivated by shell-model results with random interaction giving preponderance of +ve parity ground states [Zh-04]. The numerical calculations in [Pa-08] showed considerable variation (18 – 84%) in R_+ . In addition, they gave a plausible proof that in the dilute limit [$m \ll (N_+, N_-)$], R_+ will approach 50%. Combining these, they argued that the observed preponderance of +ve parity ground states could be a finite size (finite N_+ , N_- , m) effect. For the extended EGOE(1+2)- π considered in the present chapter, where the $\tau \rightarrow \infty$ and $\alpha = \tau$ restriction is relaxed, as we will discuss now, R_+ can reach 100%.

For EGOE(1+2)- π with $\tau \sim 0$, clearly one will get $R_+ = 100\%$ (for even m and $m \ll N_+, N_-$) and therefore it is of interest to study R_+ variation with (τ, α) . We have carried out calculations using a 200 member ensemble for $(N_+, N_-, m) = (6, 6, 6)$ and 100 member ensembles for $(8, 8, 5)$, $(6, 6, 6)$, $(6, 10, 4)$ and $(6, 10, 5)$ systems. In these calculations, we use $\alpha = \tau$ and 1.5τ . The results are shown in Fig. 5.12. For $\alpha = \tau$, the results are as follows. For $\tau \lesssim 0.04$, we have $R_+ \sim 100\%$ and then R_+ starts decreasing with some fluctuations between $\tau = 0.1$ and 0.2 . The origin of these fluctuations is not clear. As $\tau > 1$ is not realistic, we have restricted the R_+ calculations to $\tau \leq 1$. We see from the figure that EGOE(1+2)- π generates $R_+ \gtrsim 50\%$ for $\tau \leq 0.3$ independent of (N_+, N_-, m) . Also, R_+ decreases much faster with τ and reaches $\sim 30\%$ for $\tau = 0.5$ for $(N_+, N_-, m) = (6, 6, 6)$. For $m < (N_+, N_-)$, the decrease in R_+ is slower. If we increase α , from the structure of the two-particle H matrix in Fig. 5.1, we can easily infer that the width of the lowest +ve parity (m_1, m_2) unitary configuration becomes much larger compared to the lowest –ve parity unitary configuration (see Table 5.2 for examples). Therefore, with increasing α we expect R_+ to increase and this is clearly seen in Fig. 5.12. Thus $\alpha \gtrsim \tau$ is required for R_+ to be large. A quantitative description of R_+ requires the construction of +ve and –ve parity state densities more accurately in the tail region and the theory for this is not yet available.

5.5 Summary

In the present chapter, we have introduced a generalized EGOE(1+2)- π ensemble for identical fermions and its construction follows from EGOE(1+2) for spinless fermion systems. Using this generalized EE, we have not only studied R_+ , as it was done by Papenbrock and Weidenmüller [Pa-08] using a simpler two-body ensemble with par-

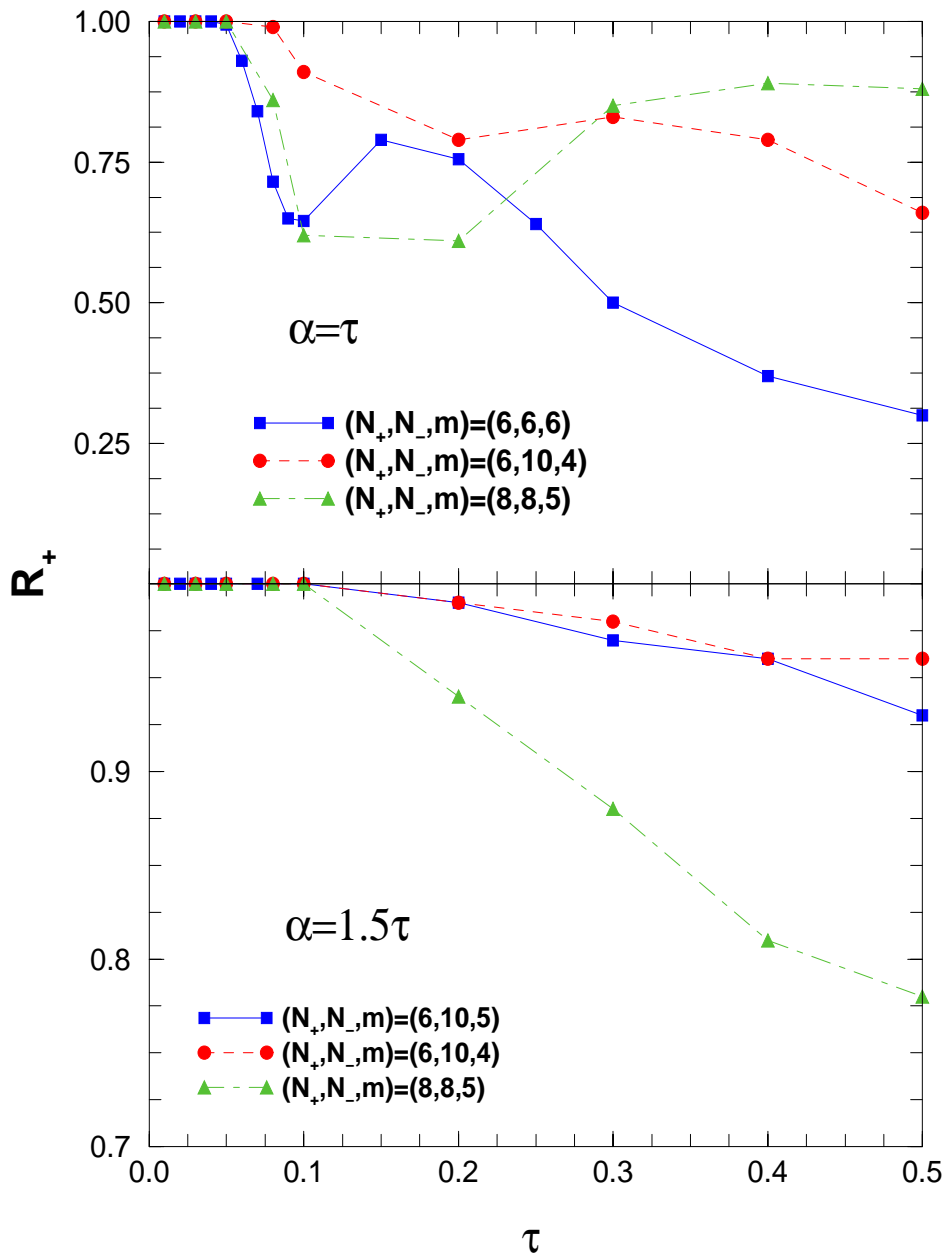


Figure 5.12: Probability (R_+) for +ve parity ground states for various (τ, α) values and for various (N_+, N_-, m) systems. See text for details.

ity, but also studied the form of fixed- π state densities and parity ratios which are important nuclear structure quantities. Numerical examples (see Figs. 5.2-5.4 and 5.6), with the range of the various parameters in the model fixed using realistic nuclear effective interactions, are used to show that the fixed- π state densities in finite dimensional spaces are of Gaussian form for sufficiently large values of the mixing parameters (τ, α) . The random matrix model also captures the essential features of parity ratios as seen in the method based on non-interacting Fermi-gas model reported

in [Mo-07]. We also found preponderance of +ve parity ground states for $\tau \lesssim 0.5$ and $\alpha \sim 1.5\tau$. In addition, for constructing fixed- π Gaussian densities we have derived an easy to understand propagation formula [see Eq. (5.3.6)] for the spectral variances of the partial densities $\rho^{m_1, m_2}(E)$ that generate I_+ and I_- . Similarly, for calculating the corrections to the Gaussian forms, formulas for skewness γ_1 and excess γ_2 of the partial densities $\rho^{m_1, m_2}(E)$ are derived using the binary correlation approximation (see Chapter 7 for the formulas). The smoothed densities constructed using Edgeworth corrected Gaussians are shown to describe the numerical results for $I_{\pm}(E)$ [for (τ, α) values in the range defined by nuclear *sdfp* and *fp_{g9/2}* interactions - see beginning of Sec. 5.4] and also the parity ratios at energies away from the gs. Numerical results presented for parity ratios at lower energies show that a better theory for the tails of the partial densities is needed (see Figs. 5.8-5.11). Thus, the results in the present chapter represent considerable progress in analyzing EGOE(1+2)- π ensemble going much beyond the analysis presented in [Pa-08].

Chapter 6

BEGOE(1+2)-s: Spectral Properties

6.1 Introduction

In the present chapter, our focus is on embedded ensembles for boson systems. As already emphasized in Chapter 1, unlike for fermion systems, there are only a few BEE investigations for finite interacting spinless boson systems [Ag-01, Ag-02, Ch-03, Ch-04]. Going beyond the embedded ensembles for spinless boson systems, our purpose in this chapter is to introduce and analyze spectral properties of embedded Gaussian orthogonal ensemble of random matrices for boson systems with spin degree of freedom [BEGOE(2)-s and also BEGOE(1+2)-s] and for Hamiltonians that conserve the total spin of the m -boson systems. Here the spin is, for example, as the F -spin in the proton-neutron interacting boson model (pn IBM) of atomic nuclei [Ca-05]. Just as the earlier BEE studies for spinless boson systems, a major motivation for the study undertaken in the present chapter is the possible applications of generalized BEEs to ultracold atoms. The BEGOE(1+2)-s with spin- $\frac{1}{2}$ bosons is a simple yet non-trivial extension of BEGOE(1+2). This ensemble is useful in obtaining several physical conclusions, like spin dependence of the order to chaos transition marker in level fluctuations, the spin of the gs, the spin ordering of excited states and pairing correlations in the gs region generated by random interactions, that explicitly require inclusion of spin degree of freedom. These are discussed in Secs. 6.3, 6.5 and 6.6.

It should be emphasized that the present chapter opens a new direction in defining and analyzing embedded ensembles for boson systems with symmetries. There are now many studies of spinor BEC using Hamiltonians conserving the total spin

with the bosons carrying $\mathbf{s} = 1$ (also higher) degree of freedom [Pe-10, Yi-07]. Also, there are several studies of the properties of a mixture of two species of atoms which correspond to pseudospin- $\frac{1}{2}$ bosons (i.e., two-component boson systems) with $m_s = \pm \frac{1}{2}$ distinguishing the two species; see for example [Al-03, Sh-10]. However, the Hamiltonians appropriate for these studies do not conserve the total spin (as the system does not have true $\frac{1}{2}$ -spins). BEE with good M_S are appropriate in understanding the statistical properties of these systems. These explorations are beyond the scope of the present thesis. Extensions of BEGOE(1+2)- \mathbf{s} with $\mathbf{s} = \frac{1}{2}$ to boson ensembles with integer spin $\mathbf{s} = 1$ and to BEGOE(1+2)- M_S are briefly discussed in Appendix G for completeness. All the results presented in this chapter are reported in [Ma-11]. Now, we begin with the definition and construction of BEGOE(1+2)- \mathbf{s} .

6.2 Definition and Construction of BEGOE(1+2)- \mathbf{s}

Let us consider a system of m ($m > 2$) bosons distributed in Ω number of sp orbitals each with spin $\mathbf{s} = \frac{1}{2}$. Then the number of sp states is $N = 2\Omega$. The sp states are denoted by $|i, m_s = \pm \frac{1}{2}\rangle$ with $i = 1, 2, \dots, \Omega$ and the two-particle symmetric states are denoted by $|(ij)s, m_s\rangle$ with $s = 0$ or 1 . It is important to note that for EGOE(1+2)- \mathbf{s} , the embedding algebra is $U(2\Omega) \supset U(\Omega) \otimes SU(2)$ with $SU(2)$ generating spin; see Secs. 6.5 and 6.6 ahead. The dimensionalities of the two-particle spaces with $s = 0$ and $s = 1$ are $\Omega(\Omega - 1)/2$ and $\Omega(\Omega + 1)/2$, respectively. For one plus two-body Hamiltonians preserving m -particle spin S , the one-body Hamiltonian is $\hat{h}(1) = \sum_{i=1}^{\Omega} \epsilon_i n_i$ where the orbitals i are doubly degenerate, n_i are number operators and ϵ_i are sp energies. The two-body Hamiltonian $\hat{V}(2)$ preserving m -particle spin S is defined by the symmetrized two-body matrix elements $V_{ijkl}^s = \langle (kl)s, m_s | \hat{V}(2) | (ij)s, m_s \rangle$ with $s = 0, 1$ and they are independent of the m_s quantum number; note that for $s = 0$, only $i \neq j$ and $k \neq l$ matrix elements exist. Thus $\hat{V}(2) = \hat{V}^{s=0}(2) + \hat{V}^{s=1}(2)$ and the sum here is a direct sum. The BEGOE(2)- \mathbf{s} ensemble for a given (m, S) system is generated by first defining the two parts of the two-body Hamiltonian to be independent GOE(1)'s in the two-particle spaces [one for $\hat{V}^{s=0}(2)$ and other for $\hat{V}^{s=1}(2)$]. Now the $V(2)$ ensemble defined by $\{\hat{V}(2)\} = \{\hat{V}^{s=0}(2)\} + \{\hat{V}^{s=1}(2)\}$ is propagated to the (m, S) -spaces by using the geometry (direct product structure) of the m -particle spaces. By adding the

$\hat{h}(1)$ part, the BEGOE(1+2)-**s** is defined by the operator

$$\{\hat{H}\}_{\text{BEGOE}(1+2)\text{-}\mathbf{s}} = \hat{h}(1) + \lambda_0 \{\hat{V}^{s=0}(2)\} + \lambda_1 \{\hat{V}^{s=1}(2)\}. \quad (6.2.1)$$

Here λ_0 and λ_1 are the strengths of the $s = 0$ and $s = 1$ parts of $\hat{V}(2)$, respectively. The mean-field one-body Hamiltonian $\hat{h}(1)$ in Eq. (6.2.1) is defined by sp energies ϵ_i with average spacing Δ . As already mentioned in Chapter 2, we put $\Delta = 1$ so that λ_0 and λ_1 are in the units of Δ and choose $\epsilon_i = i + 1/i$. Thus BEGOE(1+2)-**s** is defined by the five parameters $(\Omega, m, S, \lambda_0, \lambda_1)$. The H matrix dimension $d_b(\Omega, m, S)$ for a given (m, S) is

$$d_b(\Omega, m, S) = \frac{(2S+1)}{(\Omega-1)} \binom{\Omega + m/2 + S - 1}{m/2 + S + 1} \binom{\Omega + m/2 - S - 2}{m/2 - S}, \quad (6.2.2)$$

and they satisfy the sum rule $\sum_S (2S+1) d_b(\Omega, m, S) = \binom{N+m-1}{m}$. For example: (i) $d_b(4, 10, S) = 196, 540, 750, 770, 594$ and 286 for spins $S = 0 - 5$; (ii) $d_b(4, 11, S) = 504, 900, 1100, 1056, 780$ and 364 for $S = 1/2 - 11/2$; (iii) $d_b(5, 10, S) = 1176, 3150, 4125, 3850, 2574$ and 1001 for $S = 0 - 5$; (iv) $d_b(6, 12, S) = 13860, 37422, 50050, 49049, 36855, 20020$ and 6188 for $S = 0 - 6$; and (v) $d_b(6, 16, S) = 70785, 198198, 286650, 321048, 299880, 235620, 151164, 72675$ and 20349 for $S = 0 - 8$.

Given ϵ_i and V_{ijkl}^s , the many-particle Hamiltonian matrix for a given (m, S) can be constructed using the M_S representation (M_S is the S_z quantum number) and for spin projection the S^2 operator is used as it was done for fermion systems in Chapter 2. Alternatively, it is possible to construct the H matrix directly in a good S basis using angular-momentum algebra as it was done for fermion systems in [Tu-06]. We have employed the M_S representation for constructing the H matrices with $M_S = M_S^{min} = 0$ for even m and $M_S = M_S^{min} = \frac{1}{2}$ for odd m and they will contain states with all S values. The dimension of this basis space is $\mathcal{D}(\Omega, m, M_S^{min}) = \sum_S d_b(\Omega, m, S)$. For example, $\mathcal{D}(4, 10, 0) = 3136$, $\mathcal{D}(4, 11, \frac{1}{2}) = 4704$, $\mathcal{D}(5, 10, 0) = 15876$, $\mathcal{D}(6, 12, 0) = 213444$ and $\mathcal{D}(6, 16, 0) = 1656369$.

To construct the many-particle Hamiltonian matrix for a given (m, S) , first the sp states $|i, m_s = \pm \frac{1}{2}\rangle$ are arranged in such a way that the first Ω states have $m_s = \frac{1}{2}$ and the remaining Ω states have $m_s = -\frac{1}{2}$ so that the sp states are $|r\rangle = |i = r, m_s = \frac{1}{2}\rangle$ for $r \leq \Omega$ and $|r\rangle = |i = r - \Omega, m_s = -\frac{1}{2}\rangle$ for $r > \Omega$. Using the direct product structure

of the many-particle states, the m -particle configurations \mathbf{m} , in occupation number representation, are

$$\mathbf{m} = \left| \prod_{r=1}^{N=2\Omega} m_r \right\rangle = |m_1, m_2, \dots, m_\Omega, m_{\Omega+1}, m_{\Omega+2}, \dots, m_{2\Omega}\rangle, \quad (6.2.3)$$

where $m_r \geq 0$ with $\sum_{r=1}^N m_r = m$ and $M_S = \frac{1}{2} [\sum_{r=1}^{\Omega} m_r - \sum_{r'=\Omega+1}^{2\Omega} m_{r'}]$. To proceed further, the (1+2)-body Hamiltonian defined by ϵ_i and $V_{ijkl}^{s=0,1}$ is converted into the $|i, m_s = \pm \frac{1}{2}\rangle$ basis. Then the sp energies ϵ'_i with $i = 1, 2, \dots, N$ are $\epsilon'_i = \epsilon'_{i+\Omega} = \epsilon_i$ for $i \leq \Omega$. Similarly, V_{ijkl}^s are changed to $V_{im_i, jm_j, km_k, lm_l} = \langle im_i, jm_j | V(2) | km_k, lm_l \rangle$ using,

$$\begin{aligned} V_{i\frac{1}{2}, j\frac{1}{2}, k\frac{1}{2}, l\frac{1}{2}} &= V_{i-\frac{1}{2}, j-\frac{1}{2}, k-\frac{1}{2}, l-\frac{1}{2}} = V_{ijkl}^{s=1}, \\ V_{i\frac{1}{2}, j-\frac{1}{2}, k\frac{1}{2}, l-\frac{1}{2}} &= \frac{\sqrt{(1+\delta_{ij})(1+\delta_{kl})}}{2} [V_{ijkl}^{s=1} + V_{ijkl}^{s=0}], \end{aligned} \quad (6.2.4)$$

with all the other matrix elements being zero except for the symmetries,

$$V_{im_i, jm_j, km_k, lm_l} = V_{km_k, lm_l, im_i, jm_j} = V_{jm_j, im_i, lm_l, km_k} = V_{im_i, jm_j, lm_l, km_k}. \quad (6.2.5)$$

Using $(\epsilon'_r, V_{im_i, jm_j, km_k, lm_l})$'s, construction of the m -particle H matrix in the basis defined by Eq. (6.2.3) reduces to the problem of BEGOE(1+2) for spinless boson systems and hence Eq. (1.3.3) will give the formulas for the non-zero matrix elements; see Sec. 1.3 for details. Now diagonalizing the S^2 matrix in the basis defined by Eq. (6.2.3) will give the unitary transformation required to change the H matrix in M_S basis into good S basis. Following this method, we have numerically constructed BEGOE(1+2)- \mathbf{s} in many examples and analyzed various spectral properties generated by this ensemble. In addition, we have also derived some analytical results as discussed ahead in Secs. 6.4 and 6.6. These results are also used to validate the BEGOE(1+2)- \mathbf{s} numerical code we have developed. In addition, we have also verified the code by comparing the results with those [Ch-10] obtained by directly programming the operations that give Eq. (1.3.3). In this chapter, we deal with both BEGOE(2)- \mathbf{s} and BEGOE(1+2)- \mathbf{s} and the focus is on the dense limit defined by $m \rightarrow \infty$, $\Omega \rightarrow \infty$, $m/\Omega \rightarrow \infty$ and S is fixed. Now we will discuss these results.

6.3 Numerical Results for Eigenvalue Density and Level Fluctuations in the Dense Limit

We begin with the ensemble averaged fixed- (m, S) eigenvalue density $\rho^{m,S}(E)$, the one-point function for eigenvalues. First we present the results for BEGOE(2)-**s** ensemble defined by $\hat{h}(1) = 0$ in Eq. (6.2.1) and then the Hamiltonian operator is,

$$\{\hat{H}\}_{\text{BEGOE}(2)\text{-s}} = \lambda_0 \{\hat{V}^{s=0}(2)\} + \lambda_1 \{\hat{V}^{s=1}(2)\}. \quad (6.3.1)$$

We have considered a 500 member BEGOE(2)-**s** ensemble with $\Omega = 4$ and $m = 10$ and similarly a 100 member ensemble with $\Omega = 4$ and $m = 11$. Here and in all other numerical results presented in the present chapter, we use $\lambda_0 = \lambda_1 = \lambda$. In the construction of the ensemble averaged eigenvalue densities, the spectra of each member of the ensemble is first zero centered and scaled to unit width (therefore the densities are independent of the λ parameter). The eigenvalues are then denoted by \hat{E} . Given the fixed- (m, S) energy centroids $E_c(m, S)$ and spectral widths $\sigma(m, S)$, $\hat{E} = [E - E_c(m, S)]/\sigma(m, S)$. Then the histograms for the density are generated by combining the eigenvalues \hat{E} from all the members of the ensemble. Results are shown in Fig. 6.1 for a few selected S values. The calculations have been carried out for all S values (the results for other S values are close to those given in the figure) and also for many other BEGOE(2)-**s** examples. It is clearly seen that the eigenvalue densities are close to Gaussian (denoted by \mathcal{G} below) with the ensemble averaged skewness (γ_1) and excess (γ_2) being very small; $|\gamma_1| \sim 0$, $|\gamma_2| \sim 0.1 - 0.27$. The agreements with Edgeworth (ED) corrected Gaussians are excellent. The ED form that includes γ_1 and γ_2 corrections is given by ρ_{ED} in Eq. (2.3.2).

For the analysis of level fluctuations (equivalent to studying the two-point function for the eigenvalues), each spectrum in the ensemble is unfolded using a sixth order polynomial correction to the Gaussian and then the smoothed density is $\overline{\eta(\hat{E})} = \eta_{\mathcal{G}}(\hat{E}) \{1 + \sum_{\zeta \geq 3}^{\zeta_0} (\zeta!)^{-1} S_{\zeta} \text{He}_{\zeta}(\hat{E})\}$ with $\zeta_0 = 6$ [Le-08, Pa-00]. The parameters S_{ζ} are determined by minimizing $\Delta^2 = \sum_{i=1}^{d_b(\Omega, m, S)} [F(E_i) - \overline{F(E)}]^2$. The distribution function $F(E) = \int_{-\infty}^E \eta(x) dx$ and similarly $\overline{F(E)}$ is defined. We require that the continuous function $\overline{F(E)}$ passes through the mid-points of the jumps in the discrete $F(E)$ and

BEGOE(2)-s

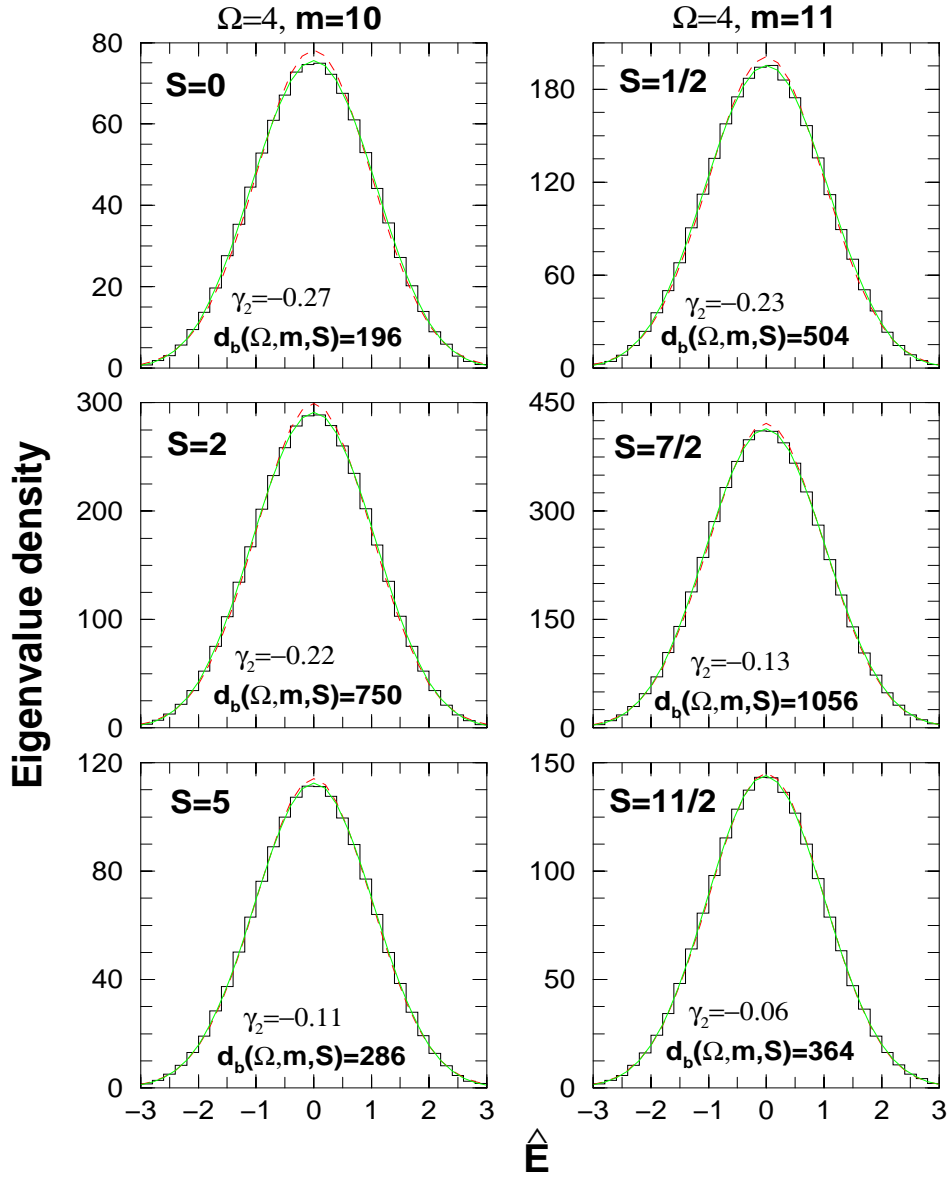


Figure 6.1: Ensemble averaged eigenvalue density $\rho^{m,S}(\hat{E})$ vs \hat{E} for BEGOE(2)-s ensembles with $\Omega = 4$, $m = 10$ and $\Omega = 4$, $m = 11$. In the figure, histograms constructed with a bin size 0.2 are BEGOE(2)-s results and they are compared with Gaussian (dashed red) and Edgeworth (ED) corrected Gaussian (solid green) forms. The ensemble averaged values of the excess parameter (γ_2) are also shown in the figure. In the plots, the area under the curves is normalized to the dimensions $d_b(\Omega, m, S)$. See text for further details.

therefore, $F(E_i) = (i - 1/2)$. The ensemble averaged Δ_{RMS} is ~ 3 for $\zeta_0 = 3$, ~ 1 for $\zeta_0 = 4$ and ~ 0.8 for $\zeta_0 = 6$ with some variation with respect to S . As $\Delta_{RMS} \sim 0.88$ for GOE, this implies GOE fluctuations set in when we add 6th order corrections to the asymptotic Gaussian density. Using the unfolded energy levels of all the mem-

bers of the BEGOE(2)-**s** ensemble, the nearest neighbor spacing distribution (NNSD) that gives information about level repulsion and the Dyson-Mehta $\overline{\Delta}_3(L)$ statistic that gives information about spectral rigidity are studied. Results for the same systems used in Fig. 6.1 are shown in Fig. 6.2 with $S = 2$ and 5 for $m = 10$ and $S = 7/2$ and $11/2$ for $m = 11$ (for other spins, the results are similar). In the calculations, middle 80% of the eigenvalues from each member are employed. It is clearly seen from the figures that the NNSD are close to GOE (Wigner) form and the widths of the NNSD are ~ 0.288 (GOE value is ~ 0.272). The $\overline{\Delta}_3(L)$ values show some departures from GOE for $L \gtrsim 30$ for $S = S_{max}$ and this could be because the matrix dimensions are small for $S = S_{max}$ in our examples (also the systems considered are not strictly in the dense limit and numerical examples with much larger m and Ω with $m \gg \Omega$ are currently not feasible). It is useful to add that $S = S_{max}$ states are important for boson systems with random interactions as discussed in Secs. 6.4-6.6 ahead. In conclusion, sixth order unfolding removes essentially all the secular behavior and then the fluctuations follow closely GOE. This is similar to the result known before for spinless boson systems [Le-08, Ch-03].

Going beyond BEGOE(2)-**s**, calculations are also carried out for BEGOE(1+2)-**s** systems using Eq. (6.2.1) with $\lambda_0 = \lambda_1 = \lambda$. We have verified the Gaussian behavior for the eigenvalue density for BEGOE(1+2)-**s**; an example is shown in Fig. 6.3(a). This result is essentially independent of λ . In addition, we have also verified that BEGOE(1+2)-**s** also generates level fluctuations close to GOE for $\lambda \gtrsim 0.1$ for $\Omega = 4$ and $m = 10, 11$ systems; Figs. 6.3(b) and 6.3(c) show the results for $\lambda = 0.1$ for $\Omega = 4, m = 11, S = 7/2$ system. Going beyond this, in Fig. 6.4, we show the NNSD results, for a 100 member BEGOE(1+2)-**s** ensemble with $\Omega = 4, m = 10$ and total spins $S = 0, 2$ and 5, by varying λ from 0.01 to 0.1 to demonstrate that as λ increases from zero, there is generically Poisson to GOE transition. A similar study is reported in Chapter 2 for fermion systems. As discussed there, for very small λ , the NNSD will be Poisson (as we use sp energies to be $\epsilon_i = i + 1/i$, the $\lambda = 0$ limit will not give strictly a Poisson). Moreover, as discussed in detail in Chapter 2, the variance of the NNSD can be written in terms of a parameter Λ (Λ is a parameter in a 2×2 random matrix model that generates Poisson to GOE transition) with $\Lambda = 0$ giving Poisson, $\Lambda \gtrsim 1$ GOE and $\Lambda = 0.3$ the transition point λ_c that marks the onset of GOE fluctuations. We show in

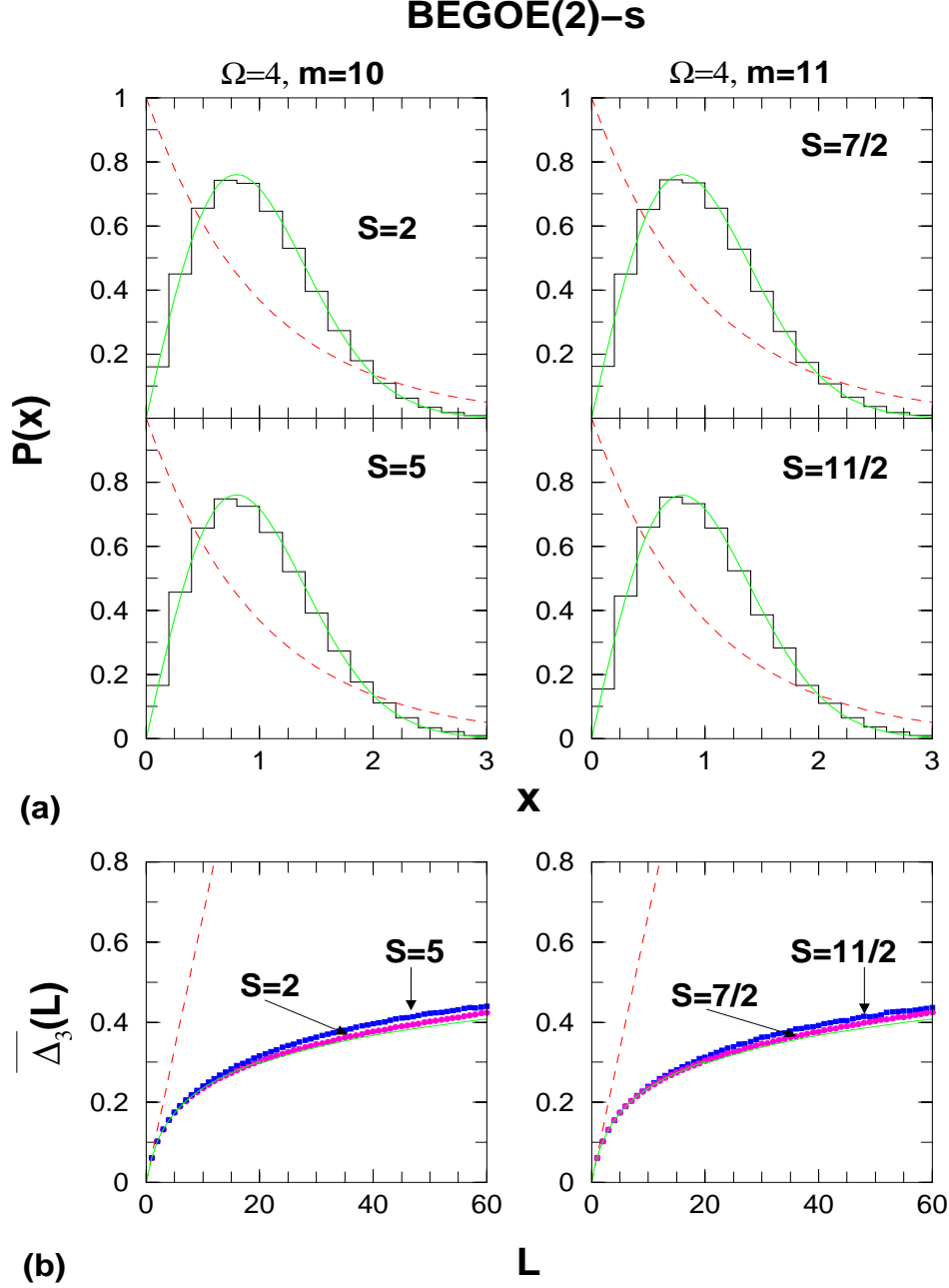


Figure 6.2: (a) Ensemble averaged nearest neighbor spacing distribution (NNSD) and (b) Dyson-Mehta statistic $\overline{\Delta}_3(L)$ vs L for $L \leq 60$. Results are for the same systems considered in Fig. 6.1; first column gives the results for $(\Omega = 4, m = 10)$ and the second column for $(\Omega = 4, m = 11)$ systems. The NNSD histograms from BEGOE(2)-s are compared with Poisson (dashed red) and GOE (Wigner) forms (solid green) and similarly the $\overline{\Delta}_3(L)$ results. In the NNSD graphs, the bin-size is 0.2 and x is the nearest neighbor spacing in the units of local mean spacing. See text and Fig. 6.1 for further details.

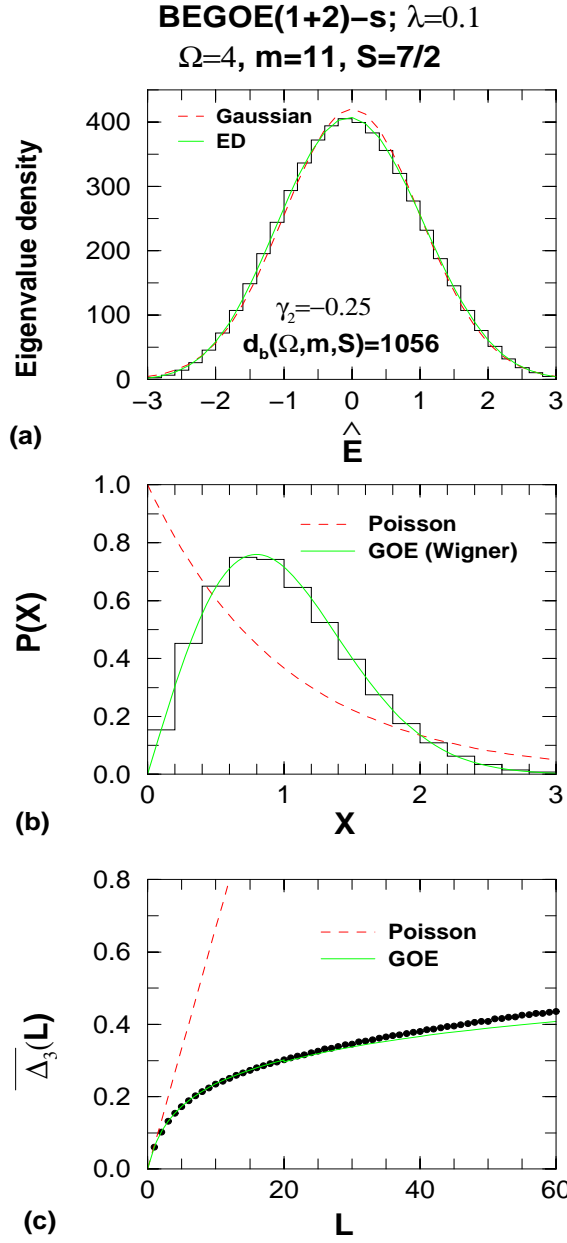


Figure 6.3: (a) Ensemble averaged eigenvalue density $\rho^{m,S}(\hat{E})$, (b) NNSD and (c) $\overline{\Delta_3(L)}$ vs. L for a 100 member BEGOE(1+2)-s ensemble for $\Omega = 4$, $m = 11$ and $S = 7/2$ system with $\lambda_0 = \lambda_1 = \lambda = 0.1$ in Eq. (6.2.1). For all other details, see text and Figs. 6.1 and 6.2.

Fig. 6.4, for each λ , the deduced value of Λ from the variance of the NNSD (Fig. 6.2 gives the results for $\lambda \rightarrow \infty$). As seen from the Fig. 6.4, $\lambda_c = 0.039, 0.0315, 0.0275$ for $S = 0, 2$, and 5 , respectively. Thus λ_c decreases with increasing spin S and this is opposite to the situation for fermion systems. For a fixed Ω value, as discussed in Chapter 2, the λ_c is inversely proportional to K , where K is the number of many-particle states [defined by $h(1)$] that are directly coupled by the two-body interaction. For fermion

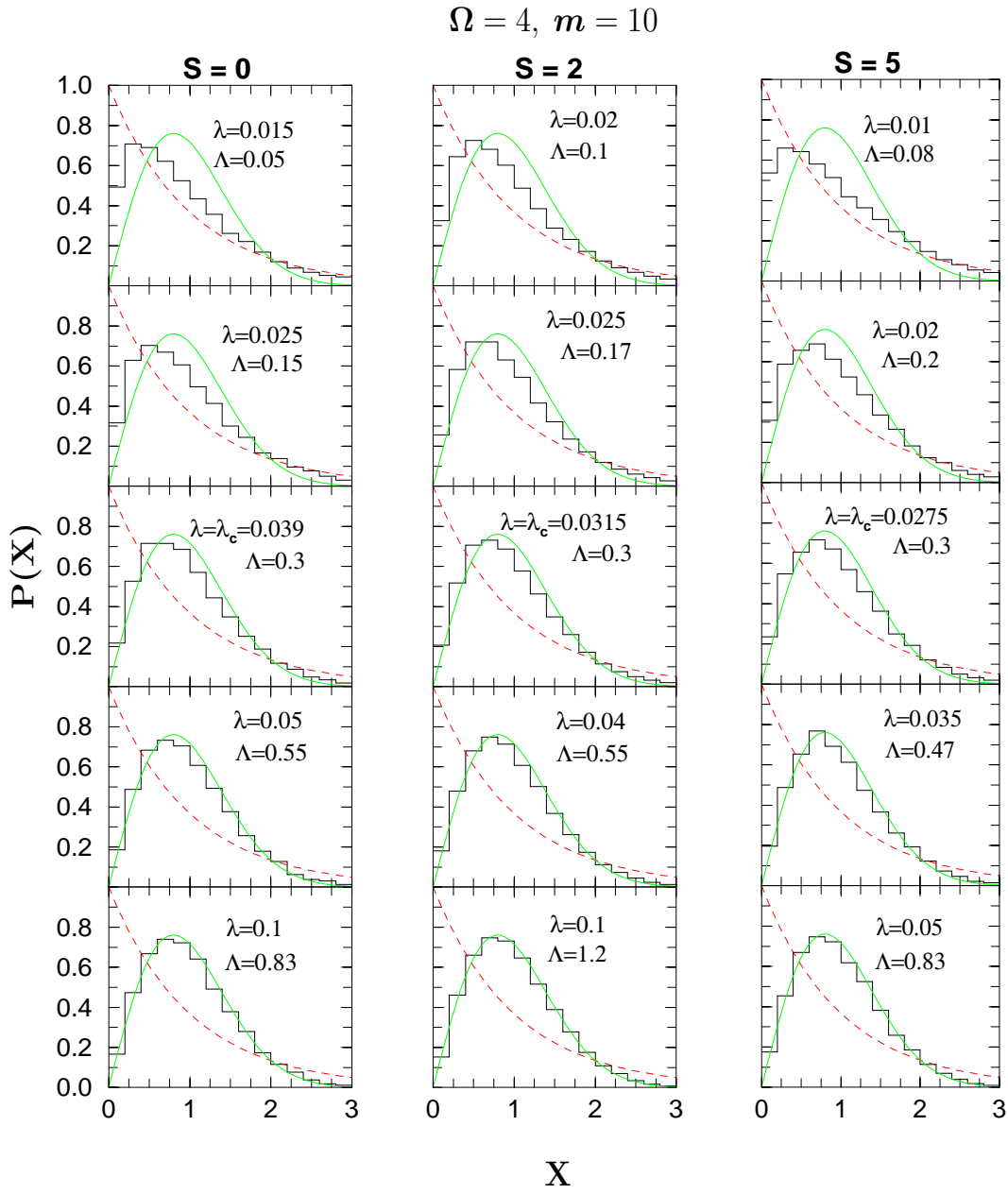


Figure 6.4: NNSD for a 100 member BEGOE(1+2)-s ensemble with $\Omega = 4$, $m = 10$ and spins $S = 0, 2$ and 5 . Calculated NNSD are compared to the Poisson (red dashed) and Wigner (GOE) (green solid) forms. Values of the interaction strength λ and the transition parameter Λ are given in the figure. The values of Λ are deduced as discussed in Chapter 2. The chaos marker λ_c corresponds to $\Lambda = 0.3$ and its values, as shown in the figure, are $0.039, 0.0315, 0.0275$ for $S = 0, 2$, and 5 , respectively. Bin-size for the histograms is 0.2 .

systems, K is proportional to the variance propagator but not for boson systems as discussed in [Ch-03]. At present, for BEGOE(1+2)-s we don't have a formula for K . However, if we use the variance propagator $Q(\Omega, m, S)$ for the boson systems [see Eq. (6.4.7) and Fig. 6.5 ahead], then qualitatively we understand the decrease in λ_c with

increasing spin.

Finally, it is well-known that the Gaussian form for the eigenvalue density is generic for embedded ensembles of spinless boson (also fermion) systems; see Chapter 1. In addition, ensemble averaged fixed- (m, S) eigenvalue densities for the fermion EGOE(1+2)-**s** are shown to take Gaussian form; see Chapter 2. Hence, from the results shown in Figs. 6.1 and 6.3(a), it is plausible to conclude that the Gaussian form is generic for BEE (also EE) with good quantum numbers. With the eigenvalue density being close to Gaussian, it is useful to derive formulas for the energy centroids and ensemble averaged spectral variances. These in turn, as already discussed in Chapter 4, will also allow us to study the lowest two moments of the two-point function. From now on, we will drop the “hat” over the operators H , $h(1)$ and $V(2)$ when there is no confusion.

6.4 Energy Centroids, Spectral Variances and Ensemble Averaged Spectral Variances and Covariances

6.4.1 Propagation formulas for energy centroids and spectral variances

Given a general (1+2)-body Hamiltonian $H = h(1) + V(2)$, which is a typical member of BEGOE(1+2)-**s**, the energy centroids will be polynomials in the number operator and the S^2 operator. As H is of maximum body rank 2, the polynomial form for the energy centroids is $\langle H \rangle^{m,S} = E_c(m, S) = a_0 + a_1 m + a_2 m^2 + a_3 S(S+1)$. Solving for the a 's in terms of the centroids in one and two-particle spaces, the propagation formula for the energy centroids is,

$$\begin{aligned} \langle H \rangle^{m,S} = E_c(m, S) &= \left[\langle h(1) \rangle^{1, \frac{1}{2}} \right] m + \lambda_0 \langle \langle V^{s=0}(2) \rangle \rangle^{2,0} \frac{P^0(m, S)}{4\Omega(\Omega-1)} \\ &+ \lambda_1 \langle \langle V^{s=1}(2) \rangle \rangle^{2,1} \frac{P^1(m, S)}{4\Omega(\Omega+1)}; \end{aligned}$$

$$\begin{aligned} P^0(m, S) &= [m(m+2) - 4S(S+1)] , \quad P^1(m, S) = [3m(m-2) + 4S(S+1)] , \\ \langle h(1) \rangle^{1, \frac{1}{2}} &= \bar{\epsilon} = \Omega^{-1} \sum_{i=1}^{\Omega} \epsilon_i , \end{aligned} \tag{6.4.1}$$

$$\langle\langle V^{s=0}(2)\rangle\rangle^{2,0} = \sum_{i<j} V_{ijij}^{s=0}, \quad \langle\langle V^{s=1}(2)\rangle\rangle^{2,1} = \sum_{i\leq j} V_{ijij}^{s=1}.$$

For the energy centroid of a two-body Hamiltonian [member of a BEGOE(2)-s], the $h(1)$ part in Eq. (6.4.1) will be absent.

Just as for the energy centroids, polynomial form for the spectral variances

$$\sigma_{H=h(1)+V(2)}^2(m, S) = \langle H^2 \rangle^{m,S} - [E_c(m, S)]^2$$

is $\sum_{p=0}^4 a_p m^p + \sum_{q=0}^2 b_q m^q S(S+1) + c_0[S(S+1)]^2$. It is well-known that the propagation formulas for fermion systems will give the formulas for the corresponding boson systems by applying $\Omega \rightarrow -\Omega$ transformation [Ko-79a, Ko-80, Ko-81, Cv-82, Ko-05]. Applying this transformation to the propagation equation for the spectral variances for fermion systems with spin given by Eq. (B2), we obtain the propagation equation for $\sigma_{H=h(1)+V(2)}^2(m, S)$ in terms of inputs that contain the sp energies ϵ_i defining $h(1)$ and the two-particle matrix elements V_{ijkl}^s . The final result is,

$$\begin{aligned} \sigma_{H=h(1)+V(2)}^2(m, S) &= \langle H^2 \rangle^{m,S} - [E_c(m, S)]^2 \\ &= \frac{(\Omega - 2)mm^* + 2\Omega \langle S^2 \rangle}{(\Omega - 1)\Omega(\Omega + 1)} \sum_i \tilde{\epsilon}_i^2 \\ &\quad + \frac{m^* P^0(m, S)}{2(\Omega - 1)\Omega(\Omega + 1)} \sum_i \tilde{\epsilon}_i \lambda_{i,i}(0) \\ &\quad + \frac{(\Omega - 2)m^* P^1(m, S) + 8\Omega(m - 1) \langle S^2 \rangle}{2(\Omega - 1)\Omega(\Omega + 1)(\Omega + 2)} \sum_i \tilde{\epsilon}_i \lambda_{i,i}(1) \\ &\quad + P^{v=1,s=0}(m, S) \sum_{i,j} \lambda_{i,j}^2(0) + P^{v=1,s=1}(m, S) \sum_{i,j} \lambda_{i,j}^2(1) \\ &\quad + \frac{P^2(m, S)P^0(m, S)}{4(\Omega - 1)\Omega(\Omega + 1)(\Omega + 2)} \sum_{i,j} \lambda_{i,j}(0)\lambda_{i,j}(1) \\ &\quad + P^{v=2,s=0}(m, S) \langle (V^{v=2,s=0})^2 \rangle^{2,0} + P^{v=2,s=1}(m, S) \langle (V^{v=2,s=1})^2 \rangle^{2,1}. \end{aligned} \tag{6.4.2}$$

The propagators $P^{v,s}$'s, which are used later, are

$$\begin{aligned}
P^{v=1,s=0}(m, S) &= \frac{[(m+2)m^*/2 - \langle S^2 \rangle] P^0(m, S)}{8(\Omega-2)(\Omega-1)\Omega(\Omega+1)}, \\
P^{v=1,s=1}(m, S) &= \frac{8\Omega(m-1)(\Omega+2m-4)\langle S^2 \rangle + (\Omega-2)P^2(m, S)P^1(m, S)}{8(\Omega-1)\Omega(\Omega+1)(\Omega+2)^2}, \\
P^{v=2,s=0}(m, S) &= [m^*(m^*-1) - \langle S^2 \rangle] P^0(m, S) / [8\Omega(\Omega+1)], \\
P^{v=2,s=1}(m, S) &= \left\{ [\langle S^2 \rangle]^2 (3\Omega^2 + 7\Omega + 6)/2 + 3m(m-2)m^*(m^*+1) \right. \\
&\times (\Omega-1)(\Omega-2)/8 + [\langle S^2 \rangle/2] [(5\Omega+3)(\Omega-2)mm^* + \Omega(\Omega-1)(\Omega+1) \\
&\times (\Omega-6)] \} / [(\Omega-1)\Omega(\Omega+2)(\Omega+3)]; \\
P^2(m, S) &= 3(m-2)m^*/2 + \langle S^2 \rangle, \quad m^* = \Omega + m/2, \quad \langle S^2 \rangle = S(S+1).
\end{aligned} \tag{6.4.3}$$

The inputs in Eq. (6.4.2) are given by,

$$\begin{aligned}
\tilde{\epsilon}_i &= \epsilon_i - \bar{\epsilon}, \\
\lambda_{i,i}(s) &= \sum_j V_{ijij}^s (1 + \delta_{ij}) - (\Omega)^{-1} \sum_{k,l} V_{klkl}^s (1 + \delta_{kl}), \\
\lambda_{i,j}(s) &= \sum_k \sqrt{(1 + \delta_{ki})(1 + \delta_{kj})} V_{kikj}^s \quad \text{for } i \neq j, \\
V_{ijij}^{v=2,s} &= V_{ijij}^s - [\langle V(2) \rangle^{2,s} + (\lambda_{i,i}(s) + \lambda_{j,j}(s)) (\Omega - 2(-1)^s)^{-1}], \\
V_{kikj}^{v=2,s} &= V_{kikj}^s - (\Omega - 2(-1)^s)^{-1} \sqrt{(1 + \delta_{ki})(1 + \delta_{kj})} \lambda_{i,j}^s \quad \text{for } i \neq j, \\
V_{ijkl}^{v=2,s} &= V_{ijkl}^s \quad \text{for all other cases.}
\end{aligned} \tag{6.4.4}$$

Eqs. (6.4.1) and (6.4.2) can be applied to individual members of the BEGOE(1+2) ensemble. On the other hand, it is possible to use these to obtain ensemble averaged spectral variances and ensemble averaged covariances in energy centroids just as it was done before for fermion systems; see Chapter 2 for details. Now we will consider these.

6.4.2 Ensemble averaged spectral variances for BEGOE(2)-s

In the present subsection, we restrict to $H = V(2)$ i.e., BEGOE(2)-s and consider BEGOE(1+2)-s at the end.

For the ensemble averaged spectral variances generated by H , only the fourth, fifth, seventh and eighth terms in Eq. (6.4.2) will contribute. Evaluating the ensemble averages of the inputs in these four terms, we obtain,

$$\begin{aligned}
 \overline{\sum_{i,j} \lambda_{i,j}^2(0)} &= \lambda_0^2(\Omega - 1)(\Omega - 2)(\Omega + 2), \\
 \overline{\sum_{i,j} \lambda_{i,j}^2(1)} &= \lambda_1^2(\Omega - 1)(\Omega + 2)^2, \\
 \overline{\langle (H^{v=2,s=0})^2 \rangle^{2,0}} &= \lambda_0^2 \frac{(\Omega - 3)(\Omega^2 + \Omega + 2)}{2(\Omega - 1)}, \\
 \overline{\langle (H^{v=2,s=1})^2 \rangle^{2,1}} &= \lambda_1^2 \frac{(\Omega - 1)(\Omega + 2)}{2}.
 \end{aligned} \tag{6.4.5}$$

Note that these inputs follow from the results for EGOE(2)-s for fermions given in Chapter 2 by interchanging $s = 0$ with $s = 1$. Now the final expression for the ensemble averaged variances is

$$\begin{aligned}
 \overline{\sigma_H^2(m, S)} &= \sum_{s=0,1} \lambda_s^2(\Omega - 1)(\Omega - (-1)^s 2)(\Omega + 2) P^{v=1,s}(m, S) \\
 &+ \lambda_0^2 \frac{(\Omega - 3)(\Omega^2 + \Omega + 2)}{2(\Omega - 1)} P^{v=2,s=0}(m, S) \\
 &+ \lambda_1^2 \frac{(\Omega - 1)(\Omega + 2)}{2} P^{v=2,s=1}(m, S).
 \end{aligned} \tag{6.4.6}$$

In most of the numerical calculations, we employ $\lambda_0 = \lambda_1 = \lambda$ and then $\overline{\sigma_H^2(m, S)}$ takes the form,

$$\overline{\sigma_H^2(m, S)} \xrightarrow{\lambda_0=\lambda_1=\lambda} \lambda^2 Q(\Omega, m, S). \tag{6.4.7}$$

Expression for the variance propagator $Q(\Omega, m, S)$ follows easily from Eqs. (6.4.1), (6.4.3) and (6.4.6). In Fig. 6.5, we show a plot of $Q(\Omega, m, S)/Q(\Omega, m, S_{max})$ vs S/S_{max}

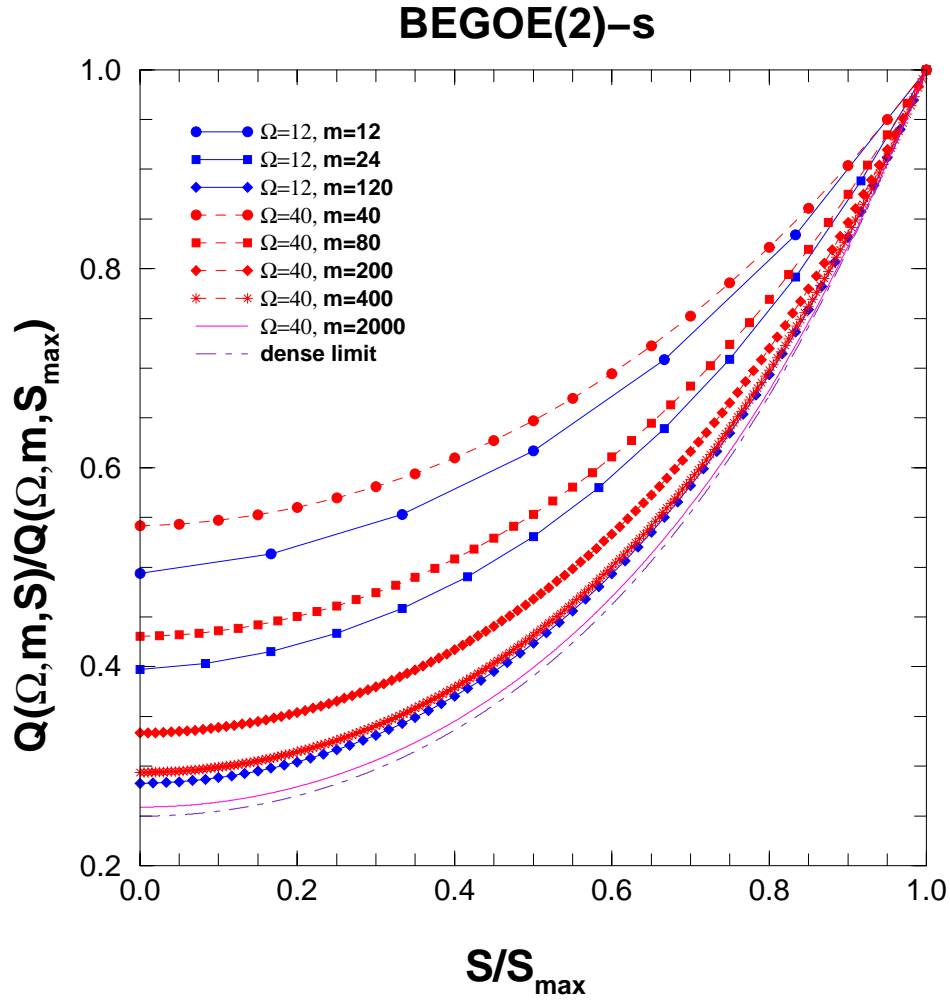


Figure 6.5: BEGOE(2)-s variance propagator $Q(\Omega, m, S)/Q(\Omega, m, S_{\max})$ vs S/S_{\max} for various values of Ω and m . Formula for $Q(\Omega, m, S)$ follows from Eqs. (6.4.3), (6.4.6) and (6.4.7). Note that the results in the figure are for $\lambda_0 = \lambda_1 = \lambda$ in Eq. (6.3.1) and therefore independent of λ . Dense limit (dot-dashed) curve corresponds to the result given by Eq. (6.4.10) with $m = 2000$.

for various Ω and m values. It is clearly seen that the propagator value increases as spin increases and this is just opposite to the result for fermion systems (see Fig. 2.2). An important consequence of this is BEGOE(2)-s gives ground states with $S = S_{\max}$ [for fermion EGOE(2)-s, the ground states with random interactions have $S = 0$; see Figs. 2.2 and 3.5]. This result follows from Eq. (4.6.1) with f_m replaced by S .

Before proceeding further, let us remark that for the BEGOE(1+2)-s Hamiltonian $\{H\} = h(1) + \{V(2)\}$, assuming that $h(1)$ is fixed, we have $\overline{\sigma_H^2} = \sigma_{h(1)}^2 + \overline{\sigma_{V(2)}^2}$. The first term $\sigma_{h(1)}^2$ is given by the first term of Eq. (6.4.2) and the second term is given by Eq. (6.4.6). In the situation $h(1)$ is represented by an ensemble independent of $\{V(2)\}$, we have to replace $\sigma_{h(1)}^2$ by $\overline{\sigma_{h(1)}^2}$ in $\overline{\sigma_H^2}$.

6.4.3 Ensemble averaged covariances in energy centroids and spectral variances for BEGOE(2)-s

Normalized covariances in energy centroids Σ_{11} and spectral variances Σ_{22} are defined by Eq. (4.4.8) with $\Gamma = S$. These define the lowest two moments of the two-point function, $\mathbf{S}^{m,S;m',S'}(E, W)$; see Eq. (4.4.6). For $(m, S) = (m', S')$ they will give information about fluctuations and in particular about level motion in the ensemble [Pa00]. For $(m, S) \neq (m', S')$, the covariances (cross-correlations) are non-zero for BEGOE while they will be zero for independent GOE representation for the m boson Hamiltonian matrices with different m or S . Note that the Ω value has to be same for both (m, S) and (m', S') systems so that the Hamiltonian in two-particle spaces remains same. Now we will discuss analytical and numerical results for Σ_{11} and numerical results for Σ_{22} for large values of (Ω, m) and they are obtained using the results in Secs. 6.4.1 and 6.4.2.

Trivially, the ensemble average of the energy centroids $E_c(m, S)$ will be zero [note that H is two-body for BEGOE(2)-s]; i.e., $\overline{\langle H \rangle^{m,S}} = 0$. However the covariances in the energy centroids of H are non-zero and Eq. (6.4.1) gives,

$$\overline{\langle H \rangle^{m,S} \langle H \rangle^{m',S'}} = \frac{\lambda_0^2}{16\Omega(\Omega-1)} P^0(m, S) P^0(m', S') + \frac{\lambda_1^2}{16\Omega(\Omega+1)} P^1(m, S) P^1(m', S'). \quad (6.4.8)$$

Equations (6.4.6), (6.4.7) and (6.4.8) allow us to calculate Σ_{11} for any (Ω, m, S) . For $m = m'$ and $S = S'$, the $[\Sigma_{11}]^{1/2}$ gives the width ΔE_c of the fluctuations in the energy centroids. In the numerical calculations, we use $\lambda_0 = \lambda_1 = \lambda$ and therefore, Σ_{11} and Σ_{22} are independent of λ . Figure 6.6 gives some numerical results for ΔE_c and it is seen that : (i) for $m \gg \Omega$, the ΔE_c is $\sim 20\%$ for $S = 0$ and it goes down to $\sim 15\%$ for $S = S_{max} = m/2$ for $\Omega = 12$; (ii) going from $\Omega = 12$ to 40, ΔE_c decreases to $\sim 2-7\%$; (iii) for fixed (m, Ω) , there is decrease in ΔE_c with increasing S value; (iv) for fixed (m, S) and very large m value, there is a sharp decrease in ΔE_c with increasing Ω up to $\Omega \sim 20$ and then it slowly converges to zero. It is possible to understand these results and the results for cross-correlations $[\Sigma_{11}(m, S : m', S')]^{1/2}$, with $(m, S) \neq (m', S')$ as shown in Fig. 6.7, using the asymptotic structure of $Q(\Omega, m, S)$.

BEGOE(2)-s

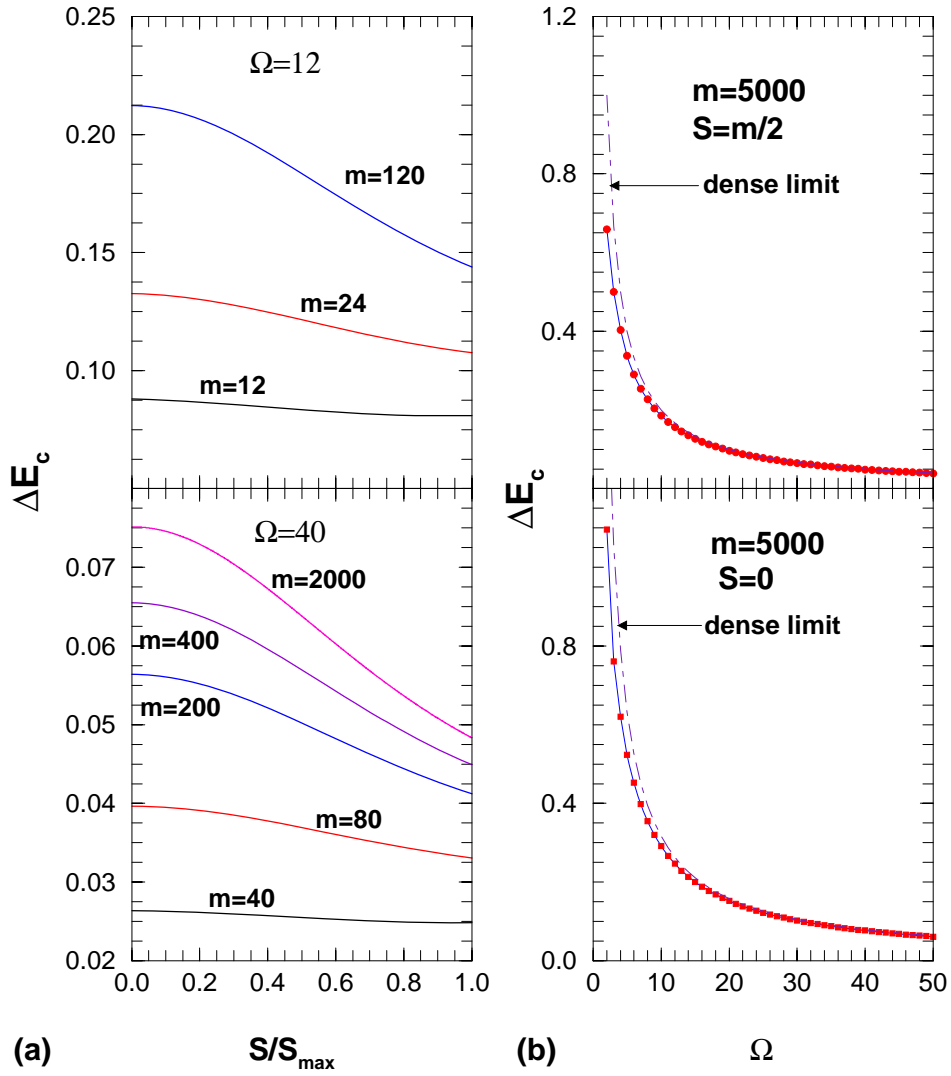


Figure 6.6: (a) Self-correlations $\Sigma_{11}^{1/2}$ in energy centroids, giving width ΔE_c of the fluctuations in energy centroids scaled to the spectrum width, as a function of spin S for different values of m and Ω . (b) Self-correlations as a function of Ω for 5000 bosons with minimum spin ($S = 0$) and maximum spin ($S = 2500$). Dense limit (dot-dashed) curves for $S = 0$ and $S = m/2$ in (b) correspond to the results given by Eq. (6.4.12). See text for details.

Let us consider the dense limit defined by $m \rightarrow \infty$, $\Omega \rightarrow \infty$ and $m/\Omega \rightarrow \infty$. Firstly the $P^{v,s}(m, S)$ in Eq. (6.4.3) take the simpler forms, with $\mathcal{S}^2 = S(S+1)$,

$$\begin{aligned}
 P^{v=1,s=0} &= \frac{(m^2 - 4\mathcal{S}^2)^2}{32\Omega^4}, & P^{v=1,s=1} &= \frac{64m^2\mathcal{S}^2(3m^2 + 4\mathcal{S}^2)^2}{32\Omega^4}, \\
 P^{v=2,s=0} &= \frac{(m^2 - 4\mathcal{S}^2)^2}{32\Omega^2}, & P^{v=2,s=1} &= \frac{3m^4 + 40m^2\mathcal{S}^2 + 48(\mathcal{S}^2)^2}{32\Omega^2}.
 \end{aligned} \tag{6.4.9}$$

BEGOE(2)-s

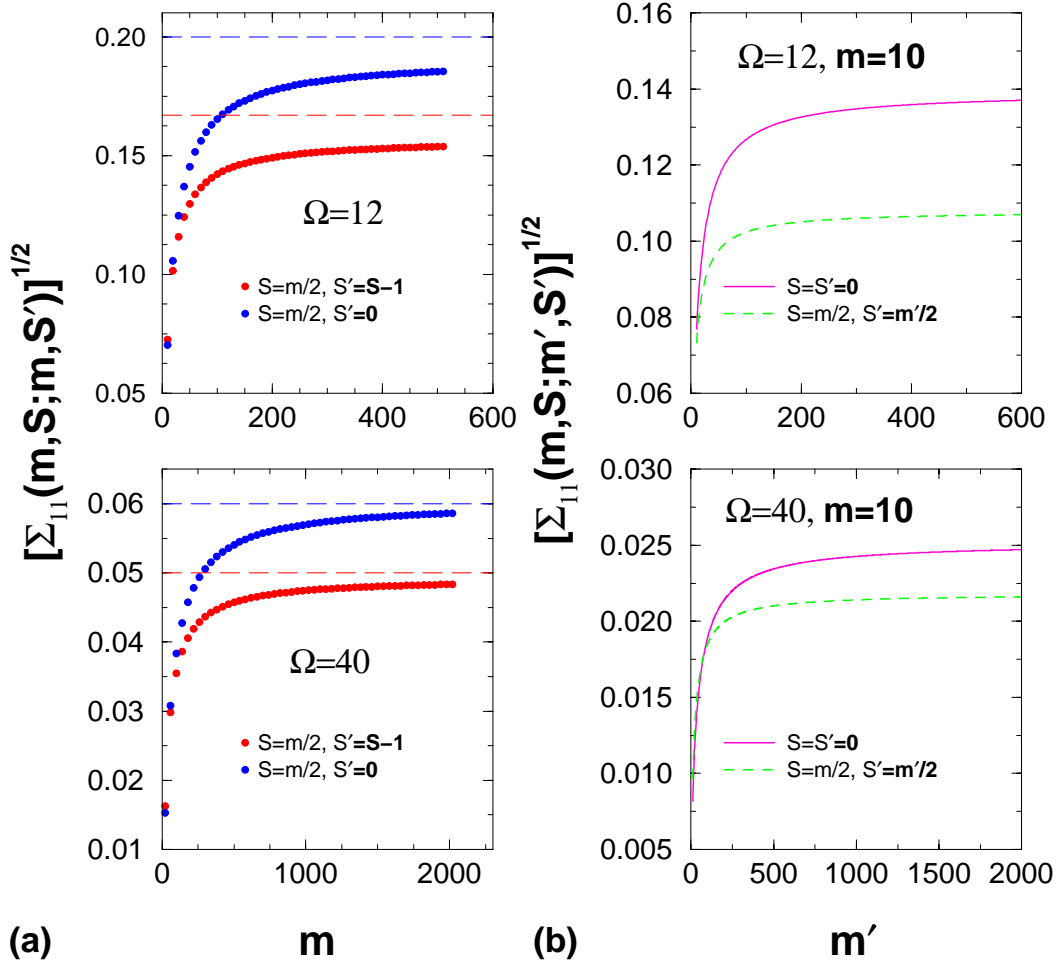


Figure 6.7: Cross-correlations $\Sigma_{11}^{1/2}$ in energy centroids for various BEGOE(2)-s systems. (a) $\Sigma_{11}^{1/2}$ vs m with $m = m'$ but different spins ($S \neq S'$). (b) $\Sigma_{11}^{1/2}$ vs m' with $m = 10$ and $S = S' = 0$ and $S = 5, S' = m'/2$. The dashed lines in (a) are the dense limit results. See text for details.

Using these in Eq. (6.4.6), with $\lambda_0 = \lambda_1 = \lambda$, we have

$$\begin{aligned} \overline{\sigma_H^2(m, S)} &= \lambda^2 \frac{(m^2 + 4\mathcal{S}^2)^2}{16} \\ \Rightarrow \left[\overline{\sigma_H^2(m, S_{max})} \right]^{-1} \overline{\sigma_H^2(m, S)} &= \left[\frac{m/(m+2) + \mathcal{S}^2/\mathcal{S}_{max}^2}{m/(m+2) + 1} \right]^2. \end{aligned} \quad (6.4.10)$$

The dense limit result given by Eq. (6.4.10) with $m = 2000$ is compared with the exact results in Fig. 6.5. Firstly, it should be noted that for the applicability of Eq. (6.4.10), Ω should be sufficiently large and $m \gg \Omega$. Also, the result is independent of Ω . Com-

paring with the $\Omega = 12$ and $\Omega = 40$ results, it is seen that the dense limit result is very close to the $\Omega = 40$ results for $m \gtrsim 200$. Thus for sufficiently large value of Ω and $m \gtrsim 5\Omega$, the dense limit result describes quite well the exact results.

Simplifying $\overline{\langle H \rangle^{m,S} \langle H \rangle^{m',S'}}$ gives in the dilute limit,

$$\begin{aligned} & \overline{\langle H \rangle^{m,S} \langle H \rangle^{m',S'}} \\ &= \frac{\lambda^2}{16\Omega^2} [(m^2 - 4\mathcal{S}^2) \{(m')^2 - 4(\mathcal{S}')^2\} + (3m^2 + 4\mathcal{S}^2) \{3(m')^2 + 4(\mathcal{S}')^2\}] . \end{aligned} \quad (6.4.11)$$

Then $[\Sigma_{11}]^{1/2}$, with $m = m'$ and $S = S'$ (for $\lambda_0 = \lambda_1$) giving ΔE_c , is

$$[\Sigma_{11}]^{1/2} = \Delta E_c = \frac{\sqrt{2(5m^4 + 8m^2\mathcal{S}^2 + 16(\mathcal{S}^2)^2)}}{\Omega(m^2 + 4\mathcal{S}^2)} . \quad (6.4.12)$$

Eq. (6.4.12) gives $[\Sigma_{11}]^{1/2}$ to be $\sqrt{10}/\Omega$ and $2/\Omega$ for $S = 0$ and $S = S_{max}$ and these dense limit results are well verified by the results in Fig. 6.6(b). Similarly, Eqs. (6.4.10) and (6.4.11) will give $[\Sigma_{11}]^{1/2}$ to be $\sqrt{6}/\Omega$ for $(m = m' : S = S_{max}, S' = 0)$ and $2/\Omega$ for $(m = m' : S = S_{max}, S' = S_{max} - 1)$. The upper and lower dashed lines in Fig. 6.7(a) for $\Omega = 12$ (similarly for $\Omega = 40$) correspond to these two dense limit results, respectively. It is seen that the dense limit results are close to exact results for $\Omega = 40$ but there are deviations for $\Omega = 12$. Also, for $\Omega = 40$, the agreements are good only for $m \gtrsim 80$ and these are similar to the results discussed earlier with reference to Fig. 6.5.

Unlike for the covariances in energy centroids, we do not have at present complete analytical formulation for the covariances in spectral variances. However, for a given member of BEGOE(2)-s, generating numerically (on a computer) the ensembles $\{V^{s=0}(2)\}$ and $\{V^{s=1}(2)\}$ and applying Eqs. (6.4.1) and (6.4.2) to each member of the ensemble will give $\overline{\langle H^2 \rangle^{m,S}} = \overline{\sigma^2(m, S)} + \overline{[E_c(m, S)]^2}$. This procedure has been used with 500 members and results for Σ_{22} are obtained for various (Ω, m, S) values. For some examples, results are shown in Fig. 6.8 for both self-correlations giving the width $\Delta \langle H^2 \rangle^{m,S}$ of variances and cross-correlations $[\Sigma_{22}]^{1/2}$ with $(m, S) \neq (m', S')$. It is seen that $[\Sigma_{22}]^{1/2}$ are always much smaller than $[\Sigma_{11}]^{1/2}$ just as for EGOE(2) for spinless fermion systems [Ko-06a]. It is seen from Fig. 6.8(a) that for $\Omega = 12$, width of the fluctuations in the variances $\langle H^2 \rangle^{m,S}$ are $\sim 3 - 5\%$. Similarly for large m , with Ω very

BEGOE(2)-s

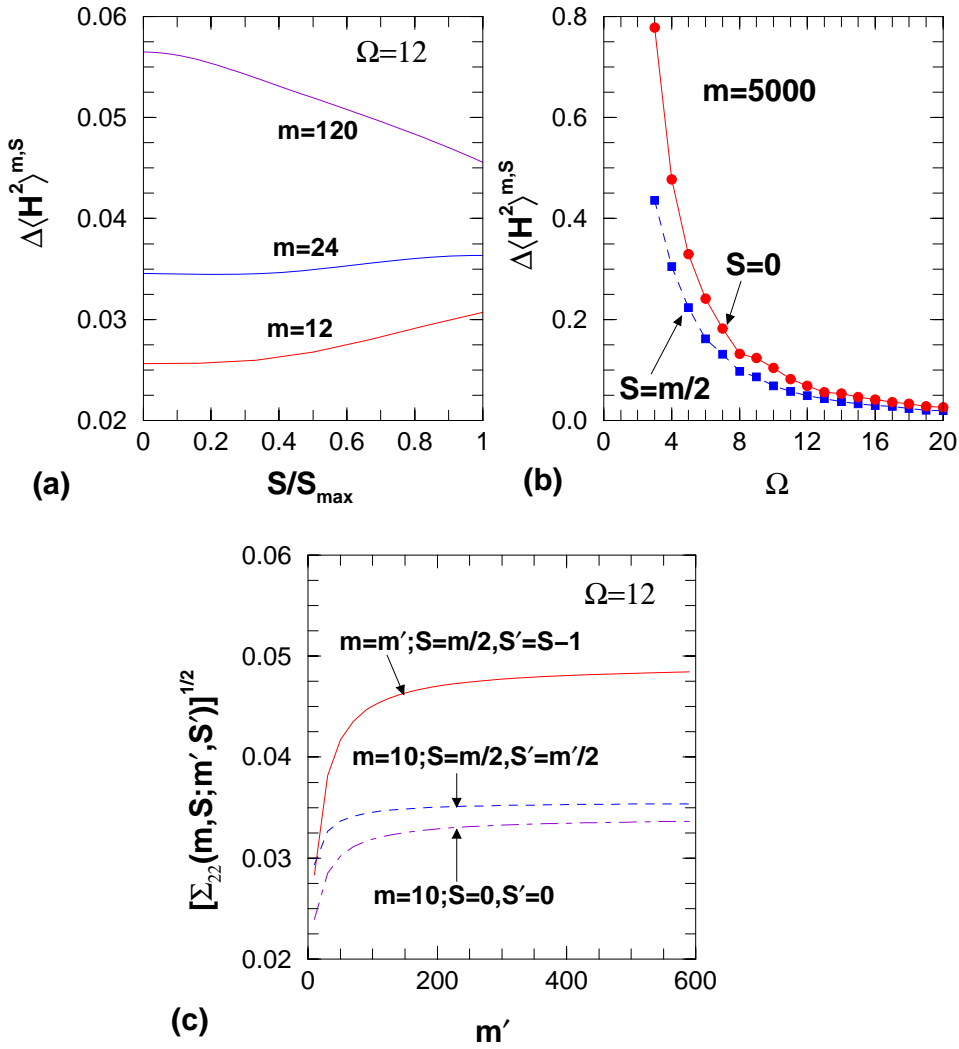


Figure 6.8: Correlations in spectral variances $\Sigma_{22}^{1/2}$ for various BEGOE(2)-s systems. (a) Self-correlations, giving width $\Delta \langle H^2 \rangle_{m,S}$ of the spectral variances, as a function of spin S for $m = 12, 24$ and 120 with $\Omega = 12$. (b) Self-correlations as a function of Ω for 5000 bosons with $S = 0$ and 2500. (c) Three examples for cross-correlation in spectral variances with same or different particle numbers and same or different spins. All the results are obtained using 500 member ensembles. See text for details.

small, the widths are quite large but they decrease fast with increasing Ω as seen from Fig. 6.8(b). Finally, for $\Omega = 12$, the cross-correlations are $\sim 4\%$. Finally, let us add that it is important to identify measures involving Σ_{11} and Σ_{22} that can be tested using some experiments so that evidence for BEGOE(2) operation in real quantum systems can be established.

6.5 Preponderance of $S_{max} = m/2$ Ground States and Natural Spin Order : Role of Exchange Interaction

6.5.1 Introduction to regular structures with random interactions

Johnson et al [Jo-98] discovered in 1998 that the nuclear shell-model with random interactions generates, with high probability, 0^+ ground states in even-even nuclei (also generates odd-even staggering in binding energies, the seniority pairing gap etc.) and similarly, Bijker and Frank [Bi-00] found that the interacting boson model (*sd*IBM) of atomic nuclei [in this model, one considers identical bosons carrying angular-momentum $\ell = 0$ (called *s* bosons) and $\ell = 2$ (called *d* bosons)] with random interactions generates vibrational and rotational structures with high probability. Starting with these, there are now many studies on regular structures in many-body systems generated by random interactions. See for example [Zh-04a,Ze-04,We-09] for reviews on the subject and Sec. 5.4.3 for results on preponderance of +ve parity ground states. More recently, the effect of random interactions in the *pn*-*sd*IBM with *F*-spin quantum number has been studied by Yoshida et al [Yo-09]. Here, proton and neutron bosons are treated as the two components of a spin $\frac{1}{2}$ boson and this spin is called *F*-spin. Yoshida et al found that random interactions conserving *F*-spin generate predominance of maximum *F*-spin (F_{max}) ground states. It should be noted that the low-lying states generated by *pn*-*sd*IBM correspond to those of *sd*IBM and all *sd*IBM states will have $F = F_{max}$. Thus random interactions preserve the property that the low-lying states generated by *pn*-*sd*IBM are those of *sd*IBM. Similarly, using shell-model with isospin conserving interactions (here protons and neutrons correspond to the two projections of isospin $t = \frac{1}{2}$), Kirson and Mizrahi [Ki-07] showed that random interactions generate natural isospin ordering. Denoting the lowest energy state (les) for a given many nucleon isospin T by $E_{les}(T)$, the natural isospin ordering corresponds to $E_{les}(T_{min}) \leq E_{les}(T_{min} + 1) \leq \dots$; for even-even $N=Z$ nuclei, $T_{min} = 0$. Therefore, one can ask if BEGOE(1+2)-**s** generates a spin ordering.

As an application of BEGOE(1+2)-**s**, we present here results for the probability of gs spin to be $S = S_{max}$ and also for natural spin ordering (NSO). Here NSO corresponds to $E_{les}(S_{max}) \leq E_{les}(S_{max} - 1) \dots$. In this analysis, we add the Majorana force

or the space exchange operator to the Hamiltonian in Eq. (6.2.1). Note that S in BEGOE(1+2)- \mathbf{s} is similar to F -spin in the pn - sd IBM. First we will derive the exchange interaction and then present some numerical results.

6.5.2 $U(\Omega)$ algebra and space exchange operator

In terms of boson creation (b^\dagger) and annihilation (b) operators, the sp states for $(\Omega)^m$ systems are $|i, m_s \pm \frac{1}{2}\rangle = b_{i, \frac{1}{2}, m_s}^\dagger |0\rangle$ with $i = 1, 2, \dots, \Omega$. It can be easily identified that the $4\Omega^2$ number of one-body operators $A_{ij;\mu}^r$,

$$A_{ij;\mu}^r = \left(b_i^\dagger \tilde{b}_j \right)_\mu^r ; \quad r = 0, 1, \quad (6.5.1)$$

generate $U(2\Omega)$ algebra. In Eq. (6.5.1), $\tilde{b}_{i, \frac{1}{2}, m_s} = (-1)^{\frac{1}{2} + m_s} b_{i, \frac{1}{2}, -m_s}$. The $U(2\Omega)$ irreducible representations are denoted trivially by the particle number m as they must be symmetric irreps $\{m\}$. The Ω^2 number of operators A_{ij}^0 generate $U(\Omega)$ algebra and similarly there is a $U(2)$ algebra generated by the number operator \hat{n} and the spin generators S_μ^1 ,

$$\hat{n} = \sqrt{2} \sum_i A_{ii}^0 ; \quad S_\mu^1 = \frac{1}{\sqrt{2}} \sum_i A_{ii;\mu}^1. \quad (6.5.2)$$

Then we have the group-subgroup algebra $U(2\Omega) \supset U(\Omega) \otimes SU(2)$ with $SU(2)$ generated by S_μ^1 . Note that $S_0 = S_0^1$, $S_+ = -\sqrt{2}S_1^1$ and $S_- = \sqrt{2}S_{-1}^1$. As the $U(2)$ irreps are two-rowed, the $U(\Omega)$ irreps have to be two-rowed and they are labeled by $\{m_1, m_2\}$ with $m = m_1 + m_2$ and $S = (m_1 - m_2)/2$; $m_1 \geq m_2 \geq 0$. Thus with respect to $U(\Omega) \otimes SU(2)$ algebra, many boson states are labeled by $|\{m_1, m_2\}, \xi\rangle$ or equivalently by $|(m, S), \xi\rangle$, where ξ are extra labels required for a complete specification of the states. The quadratic Casimir operator of the $U(\Omega)$ algebra is,

$$C_2[U(\Omega)] = 2 \sum_{i,j} A_{ij}^0 \cdot A_{ji}^0 \quad (6.5.3)$$

and its eigenvalues are $\langle C_2[U(\Omega)] \rangle^{\{m_1, m_2\}} = m_1(m_1 + \Omega - 1) + m_2(m_2 + \Omega - 3)$ or equivalently,

$$\langle C_2[U(\Omega)] \rangle^{(m, S)} = \frac{m}{2} (2\Omega + m - 4) + 2S(S + 1). \quad (6.5.4)$$

Note that the Casimir invariant of $SU(2)$ is \hat{S}^2 with eigenvalues $S(S+1)$. Now we will show that the space exchange or the Majorana operator \widehat{M} is simply related to $C_2[U(\Omega)]$.

Majorana operator \widehat{M} acting on a two-particle state exchanges the spatial coordinates of the particles (index i) and leaves the spin quantum numbers (m_s) unchanged. The operator form of \widehat{M} is

$$\widehat{M} = \frac{\kappa}{2} \sum_{i,j,m_s,m'_s} \left(b_{j,m_s}^\dagger b_{i,m'_s}^\dagger \right) \left(b_{i,m_s}^\dagger b_{j,m'_s}^\dagger \right)^\dagger. \quad (6.5.5)$$

Equation (6.5.5) gives, with κ a constant,

$$\widehat{M} = \frac{\kappa}{2} \{C_2[U(\Omega)] - \Omega \hat{n}\}. \quad (6.5.6)$$

Then, combining Eqs. (6.5.4) and (6.5.6), we have

$$\widehat{M} = \kappa \left\{ \hat{n} \left(\frac{\hat{n}}{4} - 1 \right) + \hat{S}^2 \right\}. \quad (6.5.7)$$

As seen from Eq. (6.5.7), exchange interaction with $\kappa > 0$ generates gs with $S = S_{min} = 0(\frac{1}{2})$ for even(odd) m (this is opposite to the result for ‘fermion systems’ where the exchange interaction generates gs with $S = S_{max} = m/2$ [Ma-10, Ja-01]). Now we will study the interplay between random interactions and the Majorana force in generating gs spin structure in boson systems. Note that for states with boson number fixed, $\widehat{M} \propto \hat{S}^2$ as seen from Eq. (6.5.7) and therefore, from now on, we refer to \hat{S}^2 as the exchange interaction just as in Chapter 3.

6.5.3 Numerical results for $S_{max} = m/2$ ground states and natural spin order

In order to understand the gs structure in BEGOE(1+2)-s, we have studied $P(S = S_{max})$, the probability for the gs to be with spin $S_{max} = m/2$, by adding the exchange term $\lambda_S S^2$ with $\lambda_S > 0$ to the Hamiltonian in Eq. (6.2.1) i.e., using

$$\{H\}_{\text{BEGOE}(1+2)\text{-s:Exch}} = h(1) + \lambda \left[\{V^{s=0}(2)\} + \{V^{s=1}(2)\} \right] + \lambda_S S^2. \quad (6.5.8)$$

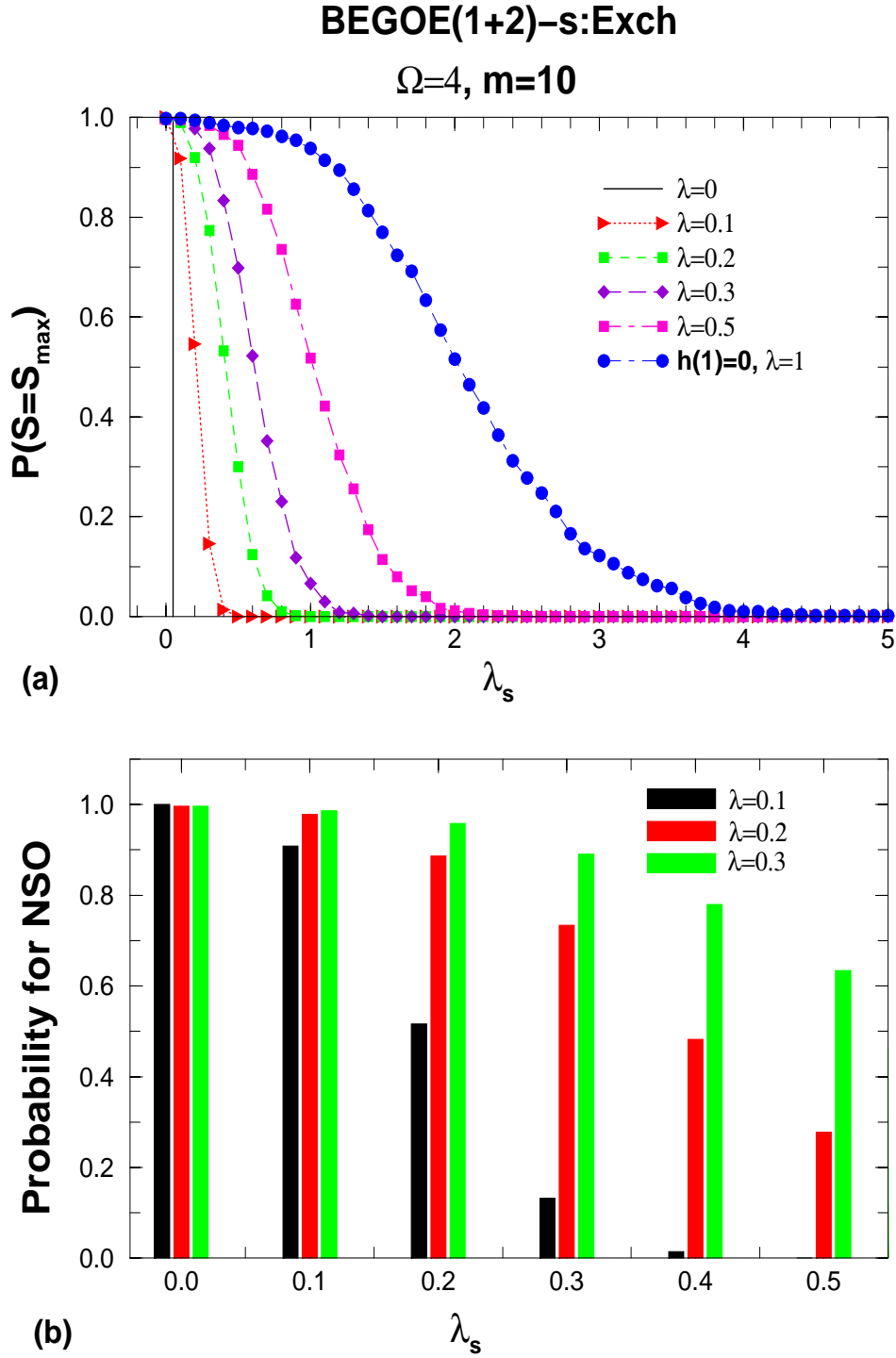


Figure 6.9: (a) Probability for ground states to have spin $S = S_{\max}$ as a function of the exchange interaction strength $\lambda_s \geq 0$. (b) Probability for natural spin order (NSO) as a function of λ_s . Results are shown for a 500 member BEGOE(1+2)-s : Exch ensemble generated by Eq. (6.5.8) for a system with $\Omega = 4$ and $m = 10$. Values of the interaction strength λ are shown in the figure.

Note that the operator S^2 is simple in the (m, S) basis. Fig. 6.9(a) gives probability $P(S = S_{max})$ for the ground states to have spin $S = S_{max}$ as a function of exchange interaction strength λ_S for $\lambda_0 = \lambda_1 = \lambda = 0, 0.1, 0.2, 0.3$ and 0.5 and also for $h(1) = 0$ with $\lambda = 1$. Similarly, Fig. 6.9(b) shows the results for NSO. Calculations are carried out for $(\Omega = 4, m = 10)$ system using a 500 member ensemble and the mean-field Hamiltonian $h(1)$ is as defined in Sec. 6.2.

Preponderance of $S_{max} = m/2$ ground states

Let us begin with pure random two-body interactions. Then $h(1) = 0$ in Eq. (6.5.8). Now in the absence of the exchange interaction ($\lambda_S = 0$), as seen from Fig. 6.9(a), ground states will have $S = S_{max}$ i.e., the probability $P(S = S_{max}) = 1$. The variance propagator (see Fig. 6.5) derived earlier gives a simple explanation for this by applying the Jacquod and Stone prescription given by Eq. (4.6.1) with f_m replaced by S for BEGOE(1+2)-s. Thus pure random interactions generate preponderance of $S = S_{max}$ ground states. On the other hand, as discussed in Sec. 6.5.2, the exchange interaction acts in opposite direction by generating $S = S_{min}$ ground states. Therefore, by adding the exchange interaction to the $\{V(2)\}$ ensemble, $P(S = S_{max})$ starts decreasing as the strength λ_S ($\lambda_S > 0$) starts increasing. For the example considered in Fig. 6.9(a), for $\lambda_S > 4$, we have $P(S = S_{max}) \sim 0$. The complete variation with λ_S is shown in Fig. 6.9(a) marked $h(1) = 0$ and $\lambda = 1$.

Similarly, on the other end, for $\lambda = 0$ in Eq. (6.5.8), we have $H = h(1)$ in the absence of the exchange interaction. In this situation, as all the bosons can occupy the lowest sp state, gs spin $S = S_{max}$. Therefore, $P(S = S_{max}) = 1$. When the exchange interaction is turned on, $P(S = S_{max})$ remains unity until λ_S equals the spacing between the lowest two sp states divided by m . As in our example, the sp energies are $\epsilon_i = i + 1/i$, we have $P(S = S_{max}) = 1$ for $\lambda_S < 0.05$. Then $P(S = S_{max})$ drops to zero for $\lambda_S \geq 0.05$. This variation with λ_S is shown in Fig. 6.9(a) marked $\lambda = 0$. Figure 6.9(a) also shows the variation of $P(S = S_{max})$ with λ_S for several values of λ between 0.1 and 0.5. It is seen that there is a critical value (λ_S^c) of λ_S after which $P(S = S_{max}) = 0$ and its value increases with λ . Also, the variation of $P(S = S_{max})$ with λ_S becomes slower as λ increases.

In summary, results in Fig. 6.9(a) clearly show that with random interactions there

is preponderance of $S = S_{max} = m/2$ ground states. This is unlike for fermions where there is preponderance of $S = S_{min} = 0(\frac{1}{2})$ ground states for m even(odd); see Fig. 3.5. With the addition of the exchange interaction, $P(S = S_{max})$ decreases and finally goes to zero for $\lambda_S \geq \lambda_S^c$ and the value of λ_S^c increases with λ . We have also carried out calculations for $(\Omega = 4, m = 11)$ system using a 100 member ensemble and the results are close to those given in Fig. 6.9(a). All these explain the results given in [Yo-09] where random interactions are employed within *pn-sdIBM*.

Natural spin ordering

For the system considered in Fig. 6.9(a), for each member of the ensemble, eigenvalue of the lowest state for each spin S is calculated and using these, we have obtained total number of members N_λ having NSO as a function of λ_S for $\lambda = 0.1, 0.2$ and 0.3 using the Hamiltonian given in Eq. (6.5.8). As stated in Sec. 6.5.1, the NSO here corresponds to (as $S = S_{max}$ is the spin of the gs of the system) $E_{les}(S_{max}) < E_{les}(S_{max}-1) < E_{les}(S_{max}-2) < \dots$. The probability for NSO is $N_\lambda/500$ and the results are shown in Fig. 6.9(b). In the absence of the exchange interaction, as seen from Fig. 6.9(b), NSO is found in all the members independent of λ . Thus random interactions strongly favor NSO. The presence of exchange interaction reduces the probability for NSO. Comparing Figs. 6.9(a) and (b), it is clearly seen that with increasing exchange interaction strength, probability for gs state spin to be $S = S_{max}$ is preserved for much larger values of λ_S (with a fixed λ) compared to the NSO. Therefore for preserving both $S = S_{max}$ gs and the NSO with high probability, the λ_S value has to be small. We have also verified this for the $(\Omega = 4, m = 11)$ system. Finally, it is plausible to argue that the results in Fig. 6.9 obtained using BEGOE(1+2)-s are generic for boson systems with spin. Now we will turn to pairing in BEGOE(2)-s.

6.6 Pairing in BEGOE(2)-s

Pairing correlations are known to be important not only for fermion systems (see Chapter 3) but also for boson systems [Pe-10]. An important issue that is raised in the recent years is: to what extent random interactions carry features of pairing. See Chapter 3 and [Zh-04a, Ze-04, Ho-07] for some results for fermion systems. In order to address this question for boson systems, first we will identify the pairing algebra in

(Ω, m, S) spaces of BEGOE(2)-**s**. Then we will consider expectation values of the pairing Hamiltonian in the eigenstates generated by BEGOE(2)-**s** as they carry signatures of pairing.

6.6.1 $U(2\Omega) \supset [U(\Omega) \supset SO(\Omega)] \otimes SU_S(2)$ Pairing symmetry

In constructing BEGOE(2)-**s**, it is assumed that spin is a good symmetry and thus the m -particle states carry spin (S) quantum number. Now, following the $SO(5)$ pairing algebra for fermions [Fl-64], it is possible to consider pairs that are vectors in spin space. The pair creation operators $P_{i;\mu}$ for the level i and the generalized pair creation operators (over the Ω levels) P_μ , with $\mu = -1, 0, 1$, in spin coupled representation, are

$$P_\mu = \frac{1}{\sqrt{2}} \sum_i \left(b_i^\dagger b_i^\dagger \right)_\mu^1 = \sum_i P_{i;\mu}, \quad (P_\mu)^\dagger = \frac{1}{\sqrt{2}} \sum_i (-1)^{1-\mu} (\tilde{b}_i \tilde{b}_i)_{-\mu}^1. \quad (6.6.1)$$

Therefore in the space defining BEGOE(2)-**s**, the pairing Hamiltonian H_p and its two-particle matrix elements are,

$$H_p = \sum_\mu P_\mu (P_\mu)^\dagger, \quad \langle (k\ell)s | H_p | (ij)s \rangle = \delta_{s,1} \delta_{i,j} \delta_{k,\ell}. \quad (6.6.2)$$

With this, we will proceed to identify and analyze the pairing algebra. It is easy to verify that the $\Omega(\Omega-1)/2$ number of operators $C_{ij} = A_{ij}^0 - A_{ji}^0$, $i > j$ generate a $SO(\Omega)$ subalgebra of the $U(\Omega)$ algebra; $A_{ij;\mu}^r$ are defined in Eq. (6.5.1). Therefore we have $U(2\Omega) \supset [U(\Omega) \supset SO(\Omega)] \otimes SU(2)$. We will show that the irreps of $SO(\Omega)$ algebra are uniquely labeled by the seniority quantum number ν and a reduced spin \tilde{s} similar to the reduced isospin introduced in the context of nuclear shell-model [Fl-52] and they in turn define the eigenvalues of H_p . The quadratic Casimir operator of the $SO(\Omega)$ algebra is,

$$C_2[SO(\Omega)] = 2 \sum_{i>j} C_{ij} \cdot C_{ji}. \quad (6.6.3)$$

Carrying out angular-momentum algebra [Ed-74] it can be shown that,

$$C_2[SO(\Omega)] = C_2[U(\Omega)] - 2 H_p - \hat{n}. \quad (6.6.4)$$

The quadratic Casimir operator of the $U(\Omega)$ algebra is given in Eq. (6.5.3). Before discussing the eigenvalues of the pairing Hamiltonian H_p , let us first consider the irreps of $SO(\Omega)$.

Given the two-rowed $U(\Omega)$ irreps $\{m_1, m_2\}$; $m_1 + m_2 = m$, $m_1 - m_2 = 2S$, it should be clear that the $SO(\Omega)$ irreps should be of $[\nu_1, \nu_2]$ type and for later simplicity we use $\nu_1 + \nu_2 = \nu$ and $\nu_1 - \nu_2 = 2\tilde{s}$. The quantum number ν is called seniority and \tilde{s} is called reduced spin; see also Appendix D. The $SO(\Omega)$ irreps for a given $\{m_1, m_2\}$ can be obtained as follows. First expand the $U(\Omega)$ irrep $\{m_1, m_2\}$ in terms of totally symmetric irreps,

$$\{m_1, m_2\} = \{m_1\} \times \{m_2\} - \{m_1 + 1\} \times \{m_2 - 1\} . \quad (6.6.5)$$

Note that the irrep multiplication in Eq. (6.6.5) is a Kronecker multiplication [Ko-06c, Wy-70]. For a totally symmetric $U(\Omega)$ irrep $\{m'\}$, the $SO(\Omega)$ irreps are given by the well-known result

$$\{m'\} \rightarrow [\nu] = [m'] \oplus [m' - 2] \oplus \dots \oplus [0] \text{ or } [1] . \quad (6.6.6)$$

Finally, reduction of the Kronecker product of two symmetric $SO(\Omega)$ irreps $[\nu_1]$ and $[\nu_2]$, $\Omega > 3$ into $SO(\Omega)$ irreps $[\nu_1, \nu_2]$ is given by (for $\nu_1 \geq \nu_2$) [Ko-06c, Wy-70],

$$[\nu_1] \times [\nu_2] = \sum_{k=0}^{\nu_2} \sum_{r=0}^{\nu_2-k} [\nu_1 - \nu_2 + k + 2r, k] \oplus . \quad (6.6.7)$$

Combining Eqs. (6.6.5), (6.6.6) and (6.6.7) gives the $\{m_1, m_2\} \rightarrow [\nu_1, \nu_2]$ reductions. It is easy to implement this procedure on a computer.

Given the space defined by $|\{m_1, m_2\}, [\nu_1, \nu_2], \alpha\rangle$, with α denoting extra labels needed for a complete specification of the state, the eigenvalues of $C_2[SO(\Omega)]$ are [Ko-06c]

$$\langle C_2[SO(\Omega)] \rangle^{\{m_1, m_2\}, [\nu_1, \nu_2]} = \nu_1(\nu_1 + \Omega - 2) + \nu_2(\nu_2 + \Omega - 4) . \quad (6.6.8)$$

Now changing $\{m_1, m_2\}$ to (m, S) and $[\nu_1, \nu_2]$ to (ν, \tilde{s}) and using Eqs. (6.6.4) and (6.5.4) will give the formula for the eigenvalues of the pairing Hamiltonian H_p . The final

result is,

$$E_p(m, S, v, \tilde{s}) = \langle H_p \rangle^{m, S, v, \tilde{s}} = \frac{1}{4}(m - v)(2\Omega - 6 + m + v) + [S(S + 1) - \tilde{s}(\tilde{s} + 1)] . \quad (6.6.9)$$

This is same as the result that follows from Eq. (18) of [Fl-64] for fermions by using $\Omega \rightarrow -\Omega$ symmetry; see also Eq. (D4). From now on, we denote the $U(\Omega)$ irreps by (m, S) and $SO(\Omega)$ irreps by (v, \tilde{s}) . In Table 6.1, for $(\Omega, m) = (4, 10), (5, 8)$ and $(6, 6)$ systems, given are the $(m, S) \rightarrow (v, \tilde{s})$ reductions, the pairing eigenvalues given by Eq. (6.6.9) in the spaces defined by these irreps and also the dimensions of the $U(\Omega)$ and $SO(\Omega)$ irreps. The dimensions $d_b(\Omega, m, S)$ of the $U(\Omega)$ irreps (m, S) are given by Eq. (6.2.2). Similarly, the dimension $\mathbf{d}(v_1, v_2) \Leftrightarrow \mathbf{d}(v, \tilde{s})$ of the $SO(\Omega)$ irreps $[v_1, v_2]$ follow from Eqs. (6.6.6) and (6.6.7) and they will give

$$\begin{aligned} \mathbf{d}(v_1, v_2) &= \mathbf{d}(v_1)\mathbf{d}(v_2) - \sum_{k=0}^{v_2-1} \sum_{r=0}^{v_2-k} \mathbf{d}(v_1 - v_2 + k + 2r, k); \\ \mathbf{d}(v) &= \binom{\Omega + v - 1}{v} - \binom{\Omega + v - 3}{v - 2}. \end{aligned} \quad (6.6.10)$$

Note that in general the $SO(\Omega)$ irreps (v, \tilde{s}) can appear more than once in the reduction of $U(\Omega)$ irreps (m, S) . For example, $(2, 1)$ irrep of $SO(\Omega)$ appears twice in the reduction of the $U(\Omega)$ irrep $(10, 1)$.

It is useful to remark that just as the fermionic $SO(5)$ pairing algebra for nucleons in j orbits [Pa-65, He-65, Fl-64], there will be a $SO(4, 1)$ complementary pairing algebra corresponding to the $SO(\Omega)$ subalgebra. The ten operators $P_\mu^1, (P_\mu^1)^\dagger, S_\mu^1$ and \hat{n} form the $SO(4, 1)$ algebra. Their commutation relations follow from the basic two commutation relations,

$$\begin{aligned} \left[P_{\mu_1}^1, (P_{\mu_2}^1)^\dagger \right] &= -(\Omega + \hat{n} + 2\mu S_0^1) \quad \text{for } \mu_1 = \mu_2 = \mu \\ &= 2\sqrt{2}(-1)^{\mu_2} \langle 1\mu_1 1 - \mu_2 | 1\mu_1 - \mu_2 \rangle S_{\mu_1 - \mu_2}^1 \quad \text{for } \mu_1 \neq \mu_2, \end{aligned} \quad (6.6.11)$$

$$\left[\sqrt{2} P_{\mu_1}^1, \left(b^\dagger \tilde{b} \right)_{\mu_2}^s \right] = \sqrt{6(2s+1)} (-1)^{s+1} \langle 1\mu_1 s \mu_2 | 1\mu_1 + \mu_2 \rangle$$

$$\times \begin{Bmatrix} 1 & \frac{1}{2} & \frac{1}{2} \\ \frac{1}{2} & 1 & s \end{Bmatrix} P_{\mu_1 + \mu_2}^1 ; \quad s = 0, 1.$$

It is possible, in principle, to exploit this algebra to derive properties of the eigenstates defined by the pairing Hamiltonian.

6.6.2 Pairing expectation values

Pairing expectation values are defined by $\langle H_p \rangle^{S,E} = \langle m, S, E | H_p | m, S, E \rangle$ for eigenstates with energy E and spin S generated by a Hamiltonian H for a system of m bosons in Ω number of sp orbitals (for simplicity, we have dropped Ω and m labels in $\langle H_p \rangle^{S,E}$). In our analysis, H is a member of BEGOE(2)-**s**. As we will be comparing the results for all spins at a given energy E , for each member of the ensemble the eigenvalues for all spins are zero centered and normalized using the m -particle energy centroid $E_c(m) = \langle H \rangle^m$ and spectrum width $\sigma(m) = [\langle H^2 \rangle^m - \{E_c(m)\}^2]^{1/2}$. Then the eigenvalues E for all S are changed to $\hat{E} = [E - E_c(m)]/\sigma(m)$. Using the method described in Sec. 6.2, the H_p matrix is constructed in good M_S basis and transformed into the eigenbasis of a given S for each member of the BEGOE(2)-**s** ensemble. Then the ensemble average of the diagonal elements of the H_p matrix will give the ensemble averaged pairing expectation values $\overline{\langle H_p \rangle^{S,E}} \Leftrightarrow \overline{\langle H_p \rangle^{S,\hat{E}}}$. Using this procedure for a 500 member BEGOE(2)-**s** ensemble with $\Omega = 4$, $m = 10$ and $S = 0 - 5$, results for $\overline{\langle H_p \rangle^{S,\hat{E}}}$ as a function of energy \hat{E} (with \hat{E} as described above) and spin S are obtained and they are shown as a 3D histogram in Fig. 6.10. From Table 6.1, it is seen that the maximum value of the eigenvalues $E_p(m, S, \nu, \tilde{s})$ increases with spin S for a fixed- (Ω, m) . The values are 28, 32, 34, 42, 48, and 60 for $S = 0 - 5$, respectively for $\Omega = 4$ and $m = 10$. Numerical results in Fig. 6.10 also show that for states near the lowest \hat{E} value, $\overline{\langle H_p \rangle^{S,\hat{E}}}$ increases with spin S . Thus random interactions preserve this property of the pairing Hamiltonian in addition to generating $S = S_{max}$ ground states as discussed in Sec. 6.5.3. It is useful to remark that random interactions will not generate $S = S_{max}$ ground states with $(\nu, \tilde{s}) = (m, m/2)$ as required for example in the *pn-sd*IBM. This needs explicit inclusion of pairing and exchange terms in the

Hamiltonians defined by Eqs. (6.2.1) and (6.3.1).

Table 6.1: Classification of states in the $U(2\Omega) \supset [U(\Omega) \supset SO(\Omega)] \otimes SU_5(2)$ limit for $(\Omega, m) = (4, 10), (5, 8)$ and $(6, 6)$. Given are $U(\Omega)$ labels (m, S) and $SO(\Omega)$ labels (ν, \tilde{s}) with the corresponding dimensions $d_b(\Omega, m, S)$ and $\mathbf{d}(\nu, \tilde{s})$, respectively, and also the pairing eigenvalues $E_p = E_p(m, S, \nu, \tilde{s})$. Note that $\sum_{\nu, \tilde{s}} r \mathbf{d}(\nu, \tilde{s}) = d_b(\Omega, m, S)$; here r denotes multiplicity of the $SO(\Omega)$ irreps and in the table, they are shown only for the cases when $r > 1$.

Ω	m	$(m, S)_{d_b(\Omega, m, S)}$	$(\nu, \tilde{s})^r \mathbf{d}_{(\nu, \tilde{s})}$	E_p	Ω	m	$(m, S)_{d_b(\Omega, m, S)}$	$(\nu, \tilde{s})^r \mathbf{d}_{(\nu, \tilde{s})}$	E_p
4	10	$(10, 0)_{196}$	$(2, 0)_6$	28	5	8	$(8, 0)_{490}$	$(0, 0)_1$	24
			$(4, 1)_{30}$	22				$(2, 1)_{14}$	19
			$(6, 2)_{70}$	12				$(4, 2)_{55}$	10
			$(6, 0)_{14}$	18				$(4, 0)_{35}$	16
			$(8, 1)_{54}$	8				$(6, 1)_{220}$	7
			$(10, 0)_{22}$	0				$(8, 0)_{165}$	0
		$(10, 1)_{540}$	$(2, 1)_9^2$	28			$(8, 1)_{1260}$	$(2, 1)_{14}$	21
			$(4, 2)_{25}^2$	20				$(4, 2)_{55}$	12
			$(6, 3)_{49}$	8				$(4, 1)_{81}^2$	16
			$(4, 1)_{30}$	24				$(6, 2)_{260}$	5
			$(6, 2)_{70}$	14				$(6, 1)_{220}$	9
			$(6, 1)_{42}^2$	18				$(8, 1)_{455}$	0
			$(8, 2)_{90}$	6				$(2, 0)_{10}$	23
			$(8, 1)_{54}$	10				$(6, 0)_{84}$	11
			$(10, 1)_{66}$	0			$(8, 2)_{1500}$	$(4, 2)_{55}^2$	16
			$(0, 0)_1$	32				$(6, 3)_{140}$	3
			$(4, 0)_{10}$	26				$(6, 2)_{260}$	9
			$(8, 0)_{18}$	12				$(8, 2)_{625}$	0
		$(10, 2)_{750}$	$(4, 2)_{25}^2$	24				$(2, 1)_{14}^2$	25
			$(6, 3)_{49}$	12				$(4, 1)_{81}$	20
			$(6, 2)_{70}^2$	18				$(6, 1)_{220}$	13
			$(8, 3)_{126}$	4				$(0, 0)_1$	30
			$(8, 2)_{90}$	10				$(4, 0)_{35}$	22

Table 6.1 – continued

Ω	m	$(m, S)_{d_b(\Omega, m, S)}$	$(\nu, \tilde{s})^r_{\mathbf{d}_{(\nu, \tilde{s})}}$	E_p	Ω	m	$(m, S)_{d_b(\Omega, m, S)}$	$(\nu, \tilde{s})^r_{\mathbf{d}_{(\nu, \tilde{s})}}$	E_p
			$(10, 2)_{110}$	0			$(8, 3)_{1155}$	$(6, 3)_{140}$	9
			$(2, 1)_9$	32				$(8, 3)_{595}$	0
			$(4, 1)_{30}^2$	28				$(4, 2)_{55}$	22
			$(6, 1)_{42}$	22				$(6, 2)_{260}$	15
			$(8, 1)_{54}$	14				$(2, 1)_{14}$	31
			$(2, 0)_6$	34				$(4, 1)_{81}$	26
			$(6, 0)_{14}$	24				$(2, 0)_{10}$	33
		$(10, 3)_{770}$	$(6, 3)_{49}^2$	18			$(8, 4)_{495}$	$(8, 4)_{285}$	0
			$(8, 4)_{81}$	2				$(6, 3)_{140}$	17
			$(8, 3)_{126}$	10				$(4, 2)_{55}$	30
			$(10, 3)_{154}$	0				$(2, 1)_{14}$	39
			$(4, 2)_{25}^2$	30				$(0, 0)_1$	44
			$(6, 2)_{70}$	24	6	6	$(6, 0)_{490}$	$(2, 0)_{15}$	14
			$(8, 2)_{90}$	16				$(4, 1)_{175}$	6
			$(2, 1)_9^2$	38				$(6, 0)_{300}$	0
			$(4, 1)_{30}$	34			$(6, 1)_{1134}$	$(2, 1)_{20}^2$	14
			$(6, 1)_{42}$	28				$(4, 2)_{105}$	4
			$(0, 0)_1$	42				$(4, 1)_{175}$	8
			$(4, 0)_{10}$	36				$(6, 1)_{729}$	0
		$(10, 4)_{594}$	$(8, 4)_{81}$	10				$(0, 0)_1$	20
			$(10, 4)_{198}$	0				$(4, 0)_{84}$	10
			$(6, 3)_{49}$	26			$(6, 2)_{1050}$	$(4, 2)_{105}$	8
			$(8, 3)_{126}$	18				$(6, 2)_{735}$	0
			$(4, 2)_{25}$	38				$(2, 1)_{20}$	18
			$(6, 2)_{70}$	32				$(4, 1)_{175}$	12
			$(2, 1)_9$	46				$(2, 0)_{15}$	20
			$(4, 1)_{30}$	42			$(6, 3)_{462}$	$(6, 3)_{336}$	0
			$(2, 0)_6$	48				$(4, 2)_{105}$	14
		$(10, 5)_{286}$	$(10, 5)_{121}$	0				$(2, 1)_{20}$	24

Table 6.1 – continued

Ω	m	$(m, S)_{d_b(\Omega, m, S)}$	$(\nu, \tilde{s})^r_{\mathbf{d}_{(\nu, \tilde{s})}}$	E_p	Ω	m	$(m, S)_{d_b(\Omega, m, S)}$	$(\nu, \tilde{s})^r_{\mathbf{d}_{(\nu, \tilde{s})}}$	E_p
			$(8, 4)_{81}$	20				$(0, 0)_1$	30
			$(6, 3)_{49}$	36					
			$(4, 2)_{25}$	48					
			$(2, 1)_9$	56					
			$(0, 0)_1$	60					

For a given spin S , the pairing expectation values as a function of E are expected, for two-body ensembles, to be given by a ratio of expectation value density Gaussian (the first two moments given by $\langle H_p H \rangle^{m, S}$ and $\langle H_p H^2 \rangle^{m, S}$) and the eigenvalue density Gaussian with normalization given by $\langle H_p \rangle^{m, S}$ and this itself will be a Gaussian; see Chapters 2 and 3 for details. Let us denote the expectation value density centroid by $E_c(m, S : H_p)$ and width by $\sigma(m, S : H_p)$. Then the ratio of Gaussians [see Eq. (3.4.2)] will give

$$\begin{aligned}
 \overline{\langle H_p \rangle^{S, \hat{E}}} &= \frac{\langle H_p \rangle^{m, S}}{\hat{\sigma}(m, S)} \exp \frac{\hat{\epsilon}^2(m, S)}{2 [1 - \hat{\sigma}^2(m, S)]} \\
 &\times \exp \left\{ \frac{(\hat{\sigma}^2(m, S) - 1)}{2 \hat{\sigma}^2(m, S)} \left[\hat{E} - \frac{\hat{\epsilon}(m, S)}{1 - \hat{\sigma}^2(m, S)} \right]^2 \right\}.
 \end{aligned} \tag{6.6.12}$$

Here, $\hat{\epsilon}(m, S) = \{E_c(m, S : H_p) - E_c(m, S)\} / \sigma(m, S)$, $\hat{\sigma}(m, S) = \sigma(m, S : H_p) / \sigma(m, S)$ and $\hat{E} = [\sigma(m) / \sigma(m, S)] \{\hat{\mathbf{E}} - \mathcal{E}\}$; $\mathcal{E} = [E_c(m, S) - E_c(m)] / \sigma(m)$. The Gaussian form given by Eq. (6.6.12) is clearly seen in Fig. 6.10 and this also gives a quantitative description of the results. Note that in our example, $\hat{\epsilon}(10, S) = 0.001, 0.001, 0.001, 0.002, 0.002, 0.003$ and $\hat{\sigma}(10, S) = 1.045, 1.047, 1.053, 1.062, 1.073, 1.082$, respectively for $S = 0 - 5$.

6.7 Summary

In the present chapter, we have introduced the BEGOE(1+2)-**s** ensemble and a method for constructing BEGOE(1+2)-**s** for numerical calculations has been described. Numerical examples are used to show that, like the spinless BEGOE(1+2), the spin BEGOE(1+2)-**s** ensemble also generates Gaussian density of states in the

BEGOE(2) – s

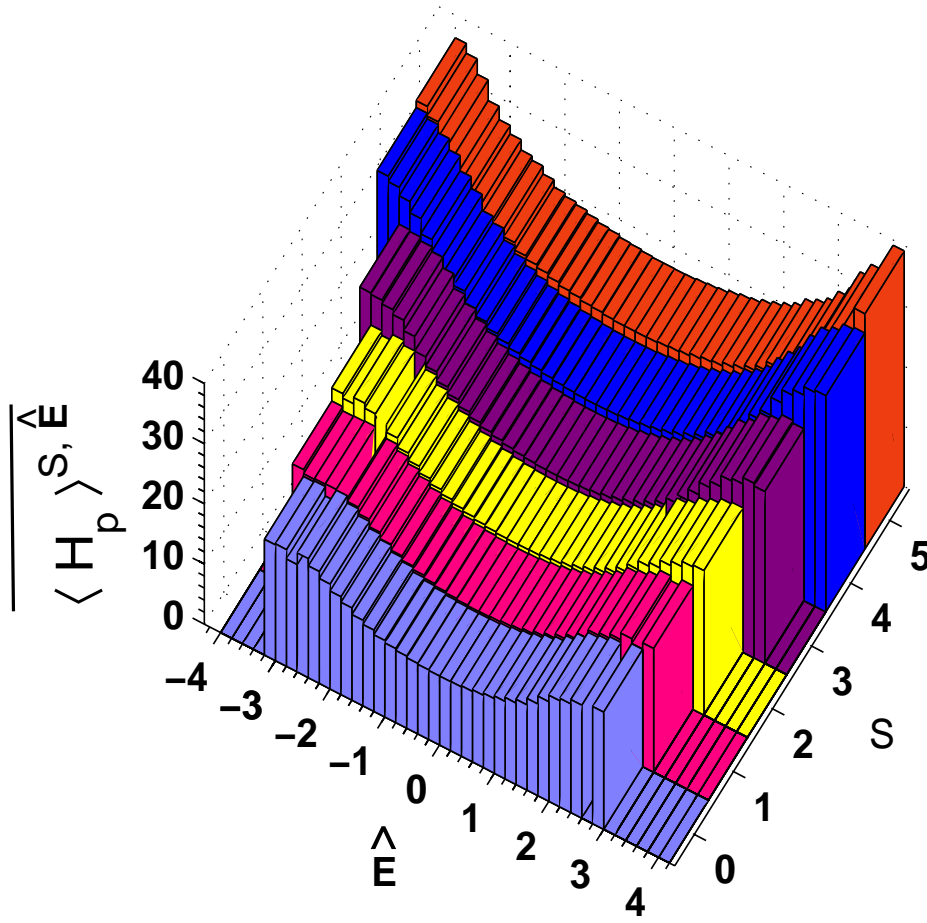


Figure 6.10: Ensemble averaged pairing expectation values $\overline{\langle H_p \rangle^{S, \hat{E}}}$ vs \hat{E} and S , shown as a 3D histogram, for a 500 member BEGOE(2)-s ensemble with $\Omega = 4$ and $m = 10$. The bin-size is 0.2 for \hat{E} . Note that the \hat{E} label in this figure is different from the \hat{E} used in Figs. 6.1 and 6.3(a).

dense limit. Similarly, BEGOE(2)-s exhibits GOE level fluctuations. On the other hand, BEGOE(1+2)-s exhibits Poisson to GOE transition as the interaction strength λ is increased and the transition marker λ_c is found to decrease with increasing spin. Moreover, ensemble averaged covariances in energy centroids and spectral variances for BEGOE(2)-s between spectra with different particle numbers and spins are studied using the propagation formulas derived for the energy centroids and spectral variances. For $\Omega = 12$ systems, the cross-correlations in energy centroids are $\sim 15\%$ and they reduce to $\sim 4\%$ for spectral variances. We have also derived the exact formula for the ensemble averaged fixed- (m, S) spectral variances and demonstrated

that the variance propagator gives a simple explanation for the preponderance of spin $S = S_{max}$ ground states generated by random interactions as in *pn-sdIBM*. It is also shown, by including exchange interaction \hat{S}^2 in BEGOE(1+2)-s, that random interactions preserving spin symmetry strongly favor NSO (just as with isospin in nuclear shell-model). These results are comprehensive and give a mathematical foundation for the results in [Yo-09]. In addition, we have identified the pairing $SO(\Omega)$ symmetry and showed using numerical examples that random interactions exhibit pairing correlations in the gs region and also they generate a Gaussian form for the variation of the pairing expectation values with respect to energy.

Chapter 7

Higher Order Traces and their Applications

7.1 Introduction

Embedded ensembles operating in many-particle spaces generate forms for distributions of various physical quantities with respect to energy and other quantum numbers; several examples for these are already discussed in Chapters 2-6. The separation of the energy evolution of various observables into a smoothed and a fluctuating part provides a basis for statistical spectroscopy. In statistical spectroscopy, methods are developed to determine various moments defining the distributions (predicted by EGEs) for the smoothed parts (valid in the chaotic region) without recourse to many-particle Hamiltonian construction. Parameters defining many of the important spectral distributions, generated by EGEs, involve traces of product of four (or even more) two-body (or one-body or a mixture of one and two-body) operators [Da-80, Ko-10]. For example, they are required for calculating nuclear structure matrix elements for β and $0\nu - \beta\beta$ decay and also for establishing Gaussian density of states generated by various extended two-body ensembles.

Propagation formulas for the moments $M_r = \langle H^r \rangle^m$, $r = 3, 4$ and also for traces over multi-orbit configurations for a given one plus two-body Hamiltonian $H = h(1) + V(2)$ follow from the results, derived using diagrammatic methods, given in [Wo-86, No-72, Ay-74, Po-75, Ch-78, Ka-95] many years back. These results extend to traces of product of four operators each of maximum body-rank 2. From now on,

we refer to these traces as fourth order traces or averages. The propagation formulas derived using diagrammatic methods contain very large number of complicated terms (in particular for fourth order averages) and carrying out analytically ensemble averaging of all these terms is proved to be impractical (we are not aware if anyone was successful in the past). Some idea of the difficulty in carrying out simplifications can be seen from the attempt in [Pl-97]. Ensemble averages from trace propagation formulas is feasible for the second order moments and we have already presented examples for these in Chapters 2, 5 and 6. An alternative is to program the exact formulas and evaluate the moments numerically for each member of EGE's by considering say 500 members in two-particle spaces. However, as pointed out by Terán and Johnson [Te-06] in their most recent attempt in this direction, these calculations for the fourth order averages are time consuming if not impractical. All the problems with the exact formulas have been emphasized in [Ko-10]. Because of these (in future with much faster computers it may be possible to use the exact formulas), we have adopted the binary correlation approximation, first used by Mon and French [Mo-73, Mo-75] and later by French et al [Fr-88, To-86] for deriving formulas for ensemble averaged traces and they are good in the dilute limit. All the "basic" binary correlation results for averages over one orbit and two orbit configurations are available in literature and for easy reference, we discuss these in Appendix H. Extending the binary correlation approximation method for two different operators and for traces over two orbit configurations, we have addressed two applications: (i) derived formulas for the skewness γ_1 and excess γ_2 parameters for EGOE(1+2)- π ensemble in the dilute limit; and (ii) we have derived formula for the fourth order trace defining correlation coefficient and sixth order traces defining the fourth order cumulants of the bivariate transition strength density generated by the transition operator relevant for $0\nu\text{-}\beta\beta$ decay (also β decay). The results for (i) and (ii) are presented in Secs. 7.2 and 7.3. In addition, we have derived formulas for cumulants (they also involve fourth order traces) over m -particle spaces that enter into the expansions for the energy centroids and spectral variances, up to order $[J(J+1)]^2$, for EGOE(2)- J i.e., embedded Gaussian orthogonal ensemble generated by random two-body interactions with angular momentum J symmetry for fermions in a single- j shell. The expansions for fixed- J centroids and variances involve traces of powers of operators H and J^2 . As H pre-

serves J symmetry, we use exact methods to evaluate these traces. More specifically, we have derived trace propagation formulas for the bivariate moments $\langle H^P(J^2)^Q \rangle^m$, $P + Q \leq 4$ and the results are presented in Sec. 7.4. All the results in Secs. 7.2 and 7.4 are published in [Ma-11a] and [Ko-08], respectively.

7.2 Application to EGOE(1+2)- π : Formulas for Skewness and Excess Parameters

For the EGOE(1+2)- π Hamiltonian, we have $H = h(1) + V(2) = h(1) + X(2) + D(2)$ with $X(2) = A \oplus B \oplus C$ is the direct sum of the spreading matrices A , B and C and $D(2) = D + \tilde{D}$ is the off-diagonal mixing matrix as defined in Chapter 5. Here, \tilde{D} is the transpose of the matrix D . The operator form for D is

$$D(2) = \sum_{\gamma, \delta} v_D^{\gamma\delta} \gamma_1^\dagger(2) \delta_2(2), \quad (7.2.1)$$

with $\overline{[v_D^{\gamma\delta}]^2} = v_D^2$. Note that the operator form of $X(2)$ is given by Eq. (H33) and then $v_X^2(i, j) = \tau^2$ with $i + j = 2$ and similarly, $v_D^2 = \alpha^2$; see Chapter 5 for further discussion on the (α, τ) parameters. Using this and the property that $h(1)$ conserves (m_1, m_2) symmetry and X preserves (m_1, m_2) symmetry, we apply the results in Appendix H and derive formulas for $M_r(m_1, m_2)$ with $r \leq 4$. These results are good in the dilute limit: $m_1, N_1, m_2, N_2 \rightarrow \infty$, $m/N_1 \rightarrow 0$ and $m/N_2 \rightarrow 0$ with $m = m_1$ or m_2 . With the sp energies defining the mean field $h(1)$ as in Chapter 5, the first moment M_1 of the partial densities $\rho^{m_1, m_2}(E)$ is trivially,

$$M_1(m_1, m_2) = \overline{\langle (h + V) \rangle^{m_1, m_2}} = m_2, \quad (7.2.2)$$

as $\langle h^r \rangle^{m_1, m_2} = (m_2)^r$ and $\overline{\langle V \rangle^{m_1, m_2}} = 0$. Applying the results in Appendix H in different ways, we derive formulas for the second, third and fourth order traces giving $M_r(m_1, m_2)$, $r = 2 - 4$. However, the presence of the mixing matrix D makes the application involved. The second moment M_2 is,

$$\begin{aligned} M_2(m_1, m_2) &= \overline{\langle (h + V)^2 \rangle^{m_1, m_2}} \\ &= \overline{\langle h^2 \rangle^{m_1, m_2}} + \overline{\langle V^2 \rangle^{m_1, m_2}} = (m_2)^2 + \overline{\langle V^2 \rangle^{m_1, m_2}}; \end{aligned}$$

Table 7.1: Exact results for skewness and excess parameters for fixed- π eigenvalue densities $I_{\pm}(E)$ compared with the binary correlation results (in the table, called 'Approx'). For exact results, we have used the eigenvalues obtained from EGOE(1+2)- π ensembles with 100 members. The binary correlation results are obtained using Eqs. (7.2.2)-(7.2.17) and extension of Eq. (5.3.7). See text for details.

(N_+, N_-, m)	$(\tau, \alpha/\tau)$	$\gamma_1(m, \pi)$				$\gamma_2(m, \pi)$			
		Exact	Approx	Exact	Approx	Exact	Approx	Exact	Approx
		$\pi = +$	$\pi = -$	$\pi = +$	$\pi = -$	$\pi = +$	$\pi = -$	$\pi = +$	$\pi = -$
(8, 8, 4)	(0.05, 0.5)	0.01	0	0	0	-0.05	-0.99	-0.05	-1.00
	(0.05, 1.0)	0.01	0	0	0	0.12	-1.08	0.13	-1.08
	(0.05, 1.5)	0.01	0	0	0	0.33	-1.16	0.34	-1.17
	(0.1, 0.5)	0	0	0	0	-0.84	-0.66	-0.84	-0.67
	(0.1, 1.0)	0	0	0	0	-0.70	-0.79	-0.71	-0.79
	(0.1, 1.5)	0	0	0	0	-0.51	-0.90	-0.51	-0.91
	(0.2, 0.5)	0	0	0	0	-0.83	-0.74	-0.84	-0.75
	(0.2, 1.0)	0	0	0	0	-0.84	-0.81	-0.84	-0.81
	(0.2, 1.5)	0	0	0	0	-0.74	-0.87	-0.74	-0.87
	(0.3, 1.0)	0	0	0	0	-0.85	-0.83	-0.85	-0.84

Table 7.1 – (continued)

(N_+, N_-, m)	$(\tau, \alpha/\tau)$	$\gamma_1(m, \pi)$				$\gamma_2(m, \pi)$			
		Exact		Approx		Exact		Approx	
		$\pi = +$	$\pi = -$	$\pi = +$	$\pi = -$	$\pi = +$	$\pi = -$	$\pi = +$	$\pi = -$
(8, 8, 5)	(0.05, 0.5)	0.15	-0.15	0.15	-0.15	-0.52	-0.52	-0.52	-0.52
	(0.05, 1.0)	0.16	-0.16	0.16	-0.16	-0.50	-0.50	-0.50	-0.50
	(0.05, 1.5)	0.18	-0.17	0.18	-0.18	-0.46	-0.46	-0.46	-0.46
	(0.2, 0.5)	-0.03	0.03	-0.03	0.03	-0.71	-0.71	-0.71	-0.71
	(0.2, 1.0)	-0.01	0.01	-0.01	0.01	-0.73	-0.73	-0.74	-0.74
(10, 6, 5)	(0.2, 1.5)	0.02	-0.02	0.02	-0.02	-0.72	-0.72	-0.73	-0.73
	(0.05, 0.5)	-0.06	0.09	-0.07	0.09	-0.26	-0.76	-0.26	-0.75
	(0.05, 1.5)	-0.04	0.15	-0.05	0.15	-0.01	-0.86	-0.01	-0.86
	(0.2, 0.5)	0.01	-0.04	0.01	-0.04	-0.73	-0.69	-0.73	-0.69
	(0.2, 1.5)	0.01	0.02	0.01	0.02	-0.69	-0.75	-0.70	-0.75
(6, 10, 5)	(0.05, 0.5)	-0.09	0.07	-0.09	0.07	-0.76	-0.26	-0.75	-0.26
	(0.05, 1.5)	-0.15	0.05	-0.15	0.05	-0.86	-0.01	-0.86	-0.01
	(0.2, 0.5)	0.04	-0.01	0.04	-0.01	-0.68	-0.73	-0.69	-0.73
	(0.2, 1.5)	-0.02	-0.01	-0.02	-0.01	-0.75	-0.69	-0.75	-0.70

$$\overline{\langle V^2 \rangle^{m_1, m_2}} = \overline{\langle X^2 \rangle^{m_1, m_2}} + \overline{\langle D\tilde{D} \rangle^{m_1, m_2}} + \overline{\langle \tilde{D}D \rangle^{m_1, m_2}}, \quad (7.2.3)$$

$$\overline{\langle X^2 \rangle^{m_1, m_2}} = \tau^2 \sum_{i+j=2} T(m_1, N_1, i) T(m_2, N_2, j),$$

$$\overline{\langle D\tilde{D} \rangle^{m_1, m_2}} = \alpha^2 \binom{m_1}{2} \binom{\tilde{m}_2}{2}, \quad \overline{\langle \tilde{D}D \rangle^{m_1, m_2}} = \alpha^2 \binom{\tilde{m}_1}{2} \binom{m_2}{2}.$$

The second line in Eq. (7.2.3) follows by using the fact that $X(2)$ and $D(2)$ are independent and $D(2)$ can correlate only with $\tilde{D}(2)$. In Eq. (7.2.3), the expression for $\overline{\langle X^2 \rangle^{m_1, m_2}}$ follows directly from Eq. (H34). The last two equations in Eq. (7.2.3) can be derived using Eq. (7.2.1) giving the definition of the operator $D(2)$ and using Eqs. (H2) and (H3) appropriately to contract the operators γ^\dagger with γ and δ with δ^\dagger . For the $T(\cdots)$'s in Eq. (7.2.3), we use Eq. (H8). Note that, Eq. (7.2.3) gives the binary correlation formula for $\overline{\sigma^2(m_1, m_2)}$. Similarly, the third moment M_3 is

$$\begin{aligned} M_3(m_1, m_2) &= \overline{\langle (h+V)^3 \rangle^{m_1, m_2}} \\ &= \overline{\langle h^3 \rangle^{m_1, m_2}} + 2 \overline{\langle h \rangle^{m_1, m_2} \langle V^2 \rangle^{m_1, m_2}} + \overline{\langle XhX \rangle^{m_1, m_2}} \\ &\quad + \overline{\langle Dh\tilde{D} \rangle^{m_1, m_2}} + \overline{\langle \tilde{D}hD \rangle^{m_1, m_2}} \\ &= (m_2)^3 + 2 m_2 \overline{\langle V^2 \rangle^{m_1, m_2}} + m_2 \overline{\langle X^2 \rangle^{m_1, m_2}} \\ &\quad + (m_2 + 2) \overline{\langle D\tilde{D} \rangle^{m_1, m_2}} + (m_2 - 2) \overline{\langle \tilde{D}D \rangle^{m_1, m_2}}. \end{aligned} \quad (7.2.4)$$

In Eq. (7.2.4), the last three terms on the RHS are evaluated by using the following properties of the operators X , D and \tilde{D} ,

$$X(2) |m_1, m_2\rangle \rightarrow |m_1, m_2\rangle, \quad D(2) |m_1, m_2\rangle \rightarrow |m_1 + 2, m_2 - 2\rangle, \quad (7.2.5)$$

$$\tilde{D}(2) |m_1, m_2\rangle \rightarrow |m_1 - 2, m_2 + 2\rangle.$$

Also, the fixed- (m_1, m_2) averages involving X^2 , V^2 , $D\tilde{D}$ and $\tilde{D}D$ in Eq. (7.2.4) follow from Eq. (7.2.3). Now, the formula for the fourth moment M_4 is,

$$\begin{aligned}
M_4(m_1, m_2) &= \overline{\langle (h + V)^4 \rangle^{m_1, m_2}} \\
&= \overline{\langle h^4 \rangle^{m_1, m_2}} + 3 \overline{\langle h^2 \rangle^{m_1, m_2} \langle V^2 \rangle^{m_1, m_2}} + \overline{\langle h^2 \rangle^{m_1, m_2} \langle X^2 \rangle^{m_1, m_2}} \\
&+ \overline{\langle Dh^2\tilde{D} \rangle^{m_1, m_2}} + \overline{\langle \tilde{D}h^2D \rangle^{m_1, m_2}} + 2 \overline{\langle hXhX \rangle^{m_1, m_2}} \\
&+ 2 \overline{\langle hDh\tilde{D} \rangle^{m_1, m_2}} + 2 \overline{\langle h\tilde{D}hD \rangle^{m_1, m_2}} + \overline{\langle V^4 \rangle^{m_1, m_2}} \\
&= (m_2)^4 + 3 (m_2)^2 \overline{\langle V^2 \rangle^{m_1, m_2}} + (m_2)^2 \overline{\langle X^2 \rangle^{m_1, m_2}} \\
&+ (m_2 + 2)^2 \overline{\langle D\tilde{D} \rangle^{m_1, m_2}} + (m_2 - 2)^2 \overline{\langle \tilde{D}D \rangle^{m_1, m_2}} \\
&+ 2 (m_2)^2 \overline{\langle X^2 \rangle^{m_1, m_2}} + 2 m_2 (m_2 + 2) \overline{\langle D\tilde{D} \rangle^{m_1, m_2}} \\
&+ 2 m_2 (m_2 - 2) \overline{\langle \tilde{D}D \rangle^{m_1, m_2}} + \overline{\langle V^4 \rangle^{m_1, m_2}}.
\end{aligned} \tag{7.2.6}$$

The first term in Eq. (7.2.6) is trivial. The next two terms follow from Eq. (7.2.3). The terms 4 – 8 in Eq. (7.2.6) are also simple and follow from Eq. (7.2.5). The expression for $\overline{\langle V^4 \rangle^{m_1, m_2}}$, which is non-trivial, is,

$$\begin{aligned}
\overline{\langle V^4 \rangle^{m_1, m_2}} &= \overline{\langle X^4 \rangle^{m_1, m_2}} + 3 \overline{\langle X^2 \rangle^{m_1, m_2}} \left\{ \overline{\langle D\tilde{D} \rangle^{m_1, m_2}} + \overline{\langle \tilde{D}D \rangle^{m_1, m_2}} \right\} \\
&+ \overline{\langle DX^2\tilde{D} \rangle^{m_1, m_2}} + \overline{\langle \tilde{D}X^2D \rangle^{m_1, m_2}} \\
&+ 2 \overline{\langle XDX\tilde{D} \rangle^{m_1, m_2}} + 2 \overline{\langle X\tilde{D}XD \rangle^{m_1, m_2}} + \overline{\langle (D + \tilde{D})^4 \rangle^{m_1, m_2}}.
\end{aligned} \tag{7.2.7}$$

The formula for the first term in Eq. (7.2.7) follows from Eq. (H39),

$$\overline{\langle X^4 \rangle^{m_1, m_2}} = 2 \left\{ \overline{\langle X^2 \rangle^{m_1, m_2}} \right\}^2 + T_1 ; \quad (7.2.8)$$

$$T_1 = \tau^4 \sum_{i+j=2, t+u=2} F(m_1, N_1, i, t) F(m_2, N_2, j, u) .$$

Combining Eqs. (7.2.7) and (7.2.8), we have,

$$\begin{aligned} & \overline{\langle V^4 \rangle^{m_1, m_2}} \\ &= 2 \left\{ \overline{\langle X^2 \rangle^{m_1, m_2}} \right\}^2 + T_1 + 3 \overline{\langle X^2 \rangle^{m_1, m_2}} \left\{ \overline{\langle D\tilde{D} \rangle^{m_1, m_2}} + \overline{\langle \tilde{D}D \rangle^{m_1, m_2}} \right\} \\ &+ \left\{ \overline{\langle DX^2\tilde{D} \rangle^{m_1, m_2}} + \overline{\langle \tilde{D}X^2D \rangle^{m_1, m_2}} \right\} \\ &+ 2 \left\{ \overline{\langle XDX\tilde{D} \rangle^{m_1, m_2}} + \overline{\langle X\tilde{D}XD \rangle^{m_1, m_2}} \right\} + \overline{\langle (D + \tilde{D})^4 \rangle^{m_1, m_2}} \\ &= 2 \left\{ \overline{\langle X^2 \rangle^{m_1, m_2}} \right\}^2 + 3 \overline{\langle X^2 \rangle^{m_1, m_2}} \left\{ \overline{\langle D\tilde{D} \rangle^{m_1, m_2}} + \overline{\langle \tilde{D}D \rangle^{m_1, m_2}} \right\} \\ &+ T_1 + T_2 + 2 T_3 + T_4 . \end{aligned} \quad (7.2.9)$$

To simplify the notations, we have introduced T_1 , T_2 , T_3 and T_4 in Eq. (7.2.9). The first and second terms in the RHS of the last step in Eq. (7.2.9) are completely determined by Eq. (7.2.3). Also, expression for T_1 is given in Eq. (7.2.8). Now, we will evaluate the terms T_2 , T_3 and T_4 . Firstly, using Eq. (7.2.5), we have

$$\begin{aligned} T_2 &= \overline{\langle DX^2\tilde{D} \rangle^{m_1, m_2}} + \overline{\langle \tilde{D}X^2D \rangle^{m_1, m_2}} \\ &= \left\{ \overline{\langle D\tilde{D} \rangle^{m_1, m_2}} \right\} \left\{ \overline{\langle X^2 \rangle^{m_1-2, m_2+2}} \right\} \\ &+ \left\{ \overline{\langle \tilde{D}D \rangle^{m_1, m_2}} \right\} \left\{ \overline{\langle X^2 \rangle^{m_1+2, m_2-2}} \right\} . \end{aligned} \quad (7.2.10)$$

Formulas for the averages involving X^2 , $D\tilde{D}$ and $\tilde{D}D$ in Eq. (7.2.10) are given by Eq. (7.2.3). Using Eqs. (H4) and (H5) appropriately to contract the operators D with \tilde{D}

across operator X along with the expression for $\overline{\langle X^2 \rangle^{m_1, m_2}}$ in Eq. (7.2.3), we have

$$\begin{aligned}
T_3 &= \overline{\langle XDX\tilde{D} \rangle^{m_1, m_2}} + \overline{\langle X\tilde{D}XD \rangle^{m_1, m_2}} \\
&= \tau^2 \alpha^2 \sum_{i+j=2} \left[\binom{m_1-i}{2} \binom{\tilde{m}_2-j}{2} + \binom{\tilde{m}_1-i}{2} \binom{m_2-j}{2} \right] \\
&\quad \times T(m_1, N_1, i) T(m_2, N_2, j).
\end{aligned} \tag{7.2.11}$$

Similarly, the expression for T_4 is as follows,

$$\begin{aligned}
T_4 &= \overline{\langle (D + \tilde{D})^4 \rangle^{m_1, m_2}} \\
&= \overline{\langle D^2 \tilde{D}^2 \rangle^{m_1, m_2}} + \overline{\langle \tilde{D}^2 D^2 \rangle^{m_1, m_2}} + \overline{\langle D \tilde{D} D \tilde{D} \rangle^{m_1, m_2}} \\
&\quad + \overline{\langle \tilde{D} D \tilde{D} D \rangle^{m_1, m_2}} + \overline{\langle D \tilde{D}^2 D \rangle^{m_1, m_2}} + \overline{\langle \tilde{D} D^2 \tilde{D} \rangle^{m_1, m_2}}.
\end{aligned} \tag{7.2.12}$$

As, in leading order, D can correlate only with \tilde{D} , we have

$$\begin{aligned}
\overline{\langle D^2 \tilde{D}^2 \rangle^{m_1, m_2}} &= \overline{\langle \textcolor{red}{D} \textcolor{blue}{D} \textcolor{red}{\tilde{D}} \textcolor{blue}{\tilde{D}} \rangle^{m_1, m_2}} + \overline{\langle \textcolor{red}{D} \textcolor{blue}{D} \textcolor{blue}{\tilde{D}} \textcolor{red}{\tilde{D}} \rangle^{m_1, m_2}} \\
&= \alpha^4 \sum_{\gamma, \delta, \kappa, \eta} \left\langle \gamma_1^\dagger(2) \delta_2(2) \kappa_1^\dagger(2) \eta_2(2) \delta_2^\dagger(2) \gamma_1(2) \eta_2^\dagger(2) \kappa_1(2) \right\rangle^{m_1, m_2} \\
&\quad + \alpha^4 \sum_{\gamma, \delta, \kappa, \eta} \left\langle \gamma_1^\dagger(2) \delta_2(2) \kappa_1^\dagger(2) \eta_2(2) \eta_2^\dagger(2) \kappa_1(2) \delta_2^\dagger(2) \gamma_1(2) \right\rangle^{m_1, m_2} \\
&= \alpha^4 \sum_{\gamma, \delta, \kappa, \eta} \left\langle \gamma_1^\dagger(2) \kappa_1^\dagger(2) \gamma_1(2) \kappa_1(2) \right\rangle^{m_1} \left\langle \delta_2(2) \eta_2(2) \delta_2^\dagger(2) \eta_2^\dagger(2) \right\rangle^{m_2} \\
&\quad + \alpha^4 \sum_{\gamma, \delta, \kappa, \eta} \left\langle \gamma_1^\dagger(2) \kappa_1^\dagger(2) \kappa_1(2) \gamma_1(2) \right\rangle^{m_1} \left\langle \delta_2(2) \eta_2(2) \eta_2^\dagger(2) \delta_2^\dagger(2) \right\rangle^{m_2} \\
&= 2 \alpha^4 \sum_{\gamma, \kappa} \left\langle \gamma_1^\dagger(2) \kappa_1^\dagger(2) \kappa_1(2) \gamma_1(2) \right\rangle^{m_1} \sum_{\delta, \eta} \left\langle \delta_2(2) \eta_2(2) \eta_2^\dagger(2) \delta_2^\dagger(2) \right\rangle^{m_2} \\
&= 2 \overline{\langle D \tilde{D} \rangle^{m_1, m_2}} \overline{\langle D \tilde{D} \rangle^{m_1-2, m_2+2}}.
\end{aligned} \tag{7.2.13}$$

In order to obtain the last step in Eq. (7.2.13), the operators $\kappa^\dagger \kappa$ and $\gamma^\dagger \gamma$ are contracted using Eq. (H2) that gives $\binom{m_1-2}{2}$ and $\binom{m_1}{2}$ respectively. Similarly, contracting operators $\eta \eta^\dagger$ and $\delta \delta^\dagger$ using Eq. (H3) gives $\binom{\tilde{m}_2-2}{2}$ and $\binom{\tilde{m}_2}{2}$ respectively. Combining these gives the last step in Eq. (7.2.13). Note that the correlated pairs of operators are represented using same color in Eq. (7.2.13). Also, the third binary pattern $\overline{\langle \textcolor{red}{D} \textcolor{red}{D} \textcolor{blue}{\tilde{D}} \textcolor{blue}{\tilde{D}} \rangle}^{m_1, m_2}$ is not considered as it will be $1/N_1$ or $1/N_2$ order smaller compared to the other two binary patterns shown in Eq. (7.2.13). Similarly, we obtain

$$\begin{aligned}
\overline{\langle \tilde{D}^2 D^2 \rangle}^{m_1, m_2} &= \overline{\langle \textcolor{red}{\tilde{D}} \textcolor{blue}{\tilde{D}} \textcolor{red}{D} \textcolor{red}{D} \rangle}^{m_1, m_2} + \overline{\langle \textcolor{blue}{\tilde{D}} \textcolor{red}{\tilde{D}} \textcolor{red}{D} \textcolor{red}{D} \rangle}^{m_1, m_2} \\
&= 2 \overline{\langle \tilde{D} D \rangle}^{m_1, m_2} \overline{\langle \tilde{D} D \rangle}^{m_1+2, m_2-2}, \\
\overline{\langle D \tilde{D} D \tilde{D} \rangle}^{m_1, m_2} &= \overline{\langle \textcolor{red}{D} \textcolor{red}{\tilde{D}} \textcolor{blue}{\tilde{D}} \textcolor{blue}{\tilde{D}} \rangle}^{m_1, m_2} + \overline{\langle \textcolor{red}{D} \textcolor{blue}{\tilde{D}} \textcolor{red}{\tilde{D}} \textcolor{red}{\tilde{D}} \rangle}^{m_1, m_2} \\
&= \left\{ \overline{\langle D \tilde{D} \rangle}^{m_1, m_2} \right\}^2 + \overline{\langle D \tilde{D} \rangle}^{m_1, m_2} \overline{\langle \tilde{D} D \rangle}^{m_1-2, m_2+2}, \\
\overline{\langle D \tilde{D} \tilde{D} D \rangle}^{m_1, m_2} &= \overline{\langle \textcolor{red}{D} \textcolor{red}{\tilde{D}} \textcolor{blue}{\tilde{D}} \textcolor{blue}{\tilde{D}} \rangle}^{m_1, m_2} + \overline{\langle \textcolor{red}{D} \textcolor{blue}{\tilde{D}} \textcolor{red}{\tilde{D}} \textcolor{red}{\tilde{D}} \rangle}^{m_1, m_2} \\
&= 2 \overline{\langle D \tilde{D} \rangle}^{m_1, m_2} \overline{\langle \tilde{D} D \rangle}^{m_1, m_2}, \\
\overline{\langle \tilde{D} D D \tilde{D} \rangle}^{m_1, m_2} &= \overline{\langle \textcolor{red}{\tilde{D}} \textcolor{red}{D} \textcolor{blue}{\tilde{D}} \textcolor{blue}{\tilde{D}} \rangle}^{m_1, m_2} + \overline{\langle \textcolor{blue}{\tilde{D}} \textcolor{red}{D} \textcolor{red}{\tilde{D}} \textcolor{red}{\tilde{D}} \rangle}^{m_1, m_2} \\
&= 2 \overline{\langle D \tilde{D} \rangle}^{m_1, m_2} \overline{\langle \tilde{D} D \rangle}^{m_1, m_2}, \\
\overline{\langle \tilde{D} D \tilde{D} D \rangle}^{m_1, m_2} &= \overline{\langle \textcolor{red}{\tilde{D}} \textcolor{red}{D} \textcolor{blue}{\tilde{D}} \textcolor{blue}{\tilde{D}} \rangle}^{m_1, m_2} + \overline{\langle \textcolor{blue}{\tilde{D}} \textcolor{red}{D} \textcolor{red}{\tilde{D}} \textcolor{red}{\tilde{D}} \rangle}^{m_1, m_2} \\
&= \left\{ \overline{\langle \tilde{D} D \rangle}^{m_1, m_2} \right\}^2 + \overline{\langle \tilde{D} D \rangle}^{m_1, m_2} \overline{\langle D \tilde{D} \rangle}^{m_1+2, m_2-2}.
\end{aligned} \tag{7.2.14}$$

Combining Eqs. (7.2.12)-(7.2.14), we have

$$\begin{aligned}
T_4 = & \left\{ \overline{\langle D\tilde{D} \rangle^{m_1, m_2}} \right\}^2 + \left\{ \overline{\langle \tilde{D}D \rangle^{m_1, m_2}} \right\}^2 \\
& + \overline{\langle D\tilde{D} \rangle^{m_1, m_2}} \left[2 \overline{\langle D\tilde{D} \rangle^{m_1-2, m_2+2}} + \overline{\langle \tilde{D}D \rangle^{m_1-2, m_2+2}} \right] \\
& + \overline{\langle \tilde{D}D \rangle^{m_1, m_2}} \left[2 \overline{\langle \tilde{D}D \rangle^{m_1+2, m_2-2}} + \overline{\langle D\tilde{D} \rangle^{m_1+2, m_2-2}} \right] \\
& + 4 \left\{ \overline{\langle D\tilde{D} \rangle^{m_1, m_2}} \right\} \left\{ \overline{\langle \tilde{D}D \rangle^{m_1, m_2}} \right\}.
\end{aligned} \tag{7.2.15}$$

Therefore, combining Eqs. (7.2.6), (7.2.8), (7.2.9), (7.2.10), (7.2.11) and (7.2.15), the expression for the fourth moment is,

$$\begin{aligned}
M_4(m_1, m_2) = & (m_2)^4 + 3 (m_2)^2 \overline{\langle V^2 \rangle^{m_1, m_2}} + 3 (m_2)^2 \overline{\langle X^2 \rangle^{m_1, m_2}} \\
& + (m_2 + 2)^2 \overline{\langle D\tilde{D} \rangle^{m_1, m_2}} + (m_2 - 2)^2 \overline{\langle \tilde{D}D \rangle^{m_1, m_2}} \\
& + 2 m_2 (m_2 + 2) \overline{\langle D\tilde{D} \rangle^{m_1, m_2}} + 2 m_2 (m_2 - 2) \overline{\langle \tilde{D}D \rangle^{m_1, m_2}} + 2 \left\{ \overline{\langle X^2 \rangle^{m_1, m_2}} \right\}^2 \\
& + 3 \overline{\langle X^2 \rangle^{m_1, m_2}} \left\{ \overline{\langle D\tilde{D} \rangle^{m_1, m_2}} + \overline{\langle \tilde{D}D \rangle^{m_1, m_2}} \right\} \\
& + \tau^4 \sum_{i+j=2, t+u=2} F(m_1, N_1, i, t) F(m_2, N_2, j, u) \\
& + \left\{ \overline{\langle D\tilde{D} \rangle^{m_1, m_2}} \right\} \left\{ \overline{\langle X^2 \rangle^{m_1-2, m_2+2}} \right\} \\
& + \left\{ \overline{\langle \tilde{D}D \rangle^{m_1, m_2}} \right\} \left\{ \overline{\langle X^2 \rangle^{m_1+2, m_2-2}} \right\} \\
& + 2 \tau^2 \alpha^2 \sum_{i+j=2} \left[\binom{m_1-i}{2} \binom{\tilde{m}_2-j}{2} + \binom{\tilde{m}_1-i}{2} \binom{m_2-j}{2} \right] \\
& \times T(m_1, N_1, i) T(m_2, N_2, j)
\end{aligned} \tag{7.2.16}$$

$$\begin{aligned}
& + \left\{ \overline{\langle D\tilde{D} \rangle^{m_1, m_2}} \right\}^2 + \left\{ \overline{\langle \tilde{D}D \rangle^{m_1, m_2}} \right\}^2 \\
& + \overline{\langle D\tilde{D} \rangle^{m_1, m_2}} \left[2 \overline{\langle D\tilde{D} \rangle^{m_1-2, m_2+2}} + \overline{\langle \tilde{D}D \rangle^{m_1-2, m_2+2}} \right] \\
& + \overline{\langle \tilde{D}D \rangle^{m_1, m_2}} \left[2 \overline{\langle \tilde{D}D \rangle^{m_1+2, m_2-2}} + \overline{\langle D\tilde{D} \rangle^{m_1+2, m_2-2}} \right] \\
& + 4 \left\{ \overline{\langle D\tilde{D} \rangle^{m_1, m_2}} \right\} \left\{ \overline{\langle \tilde{D}D \rangle^{m_1, m_2}} \right\}.
\end{aligned}$$

Equations (7.2.2), (7.2.3), (7.2.4), and (7.2.16), respectively give the first four non-central moments $[M_1(m_1, m_2), M_2(m_1, m_2), M_3(m_1, m_2)$ and $M_4(m_1, m_2)]$. In Eq. (7.2.16), we use Eq. (H8) for $T(\cdots)$'s and for $F(\cdots)$'s, we use Eq. (H14) and also Eq. (H23) in applications. The first four cumulants $[k_1(m_1, m_2), k_2(m_1, m_2), k_3(m_1, m_2), k_4(m_1, m_2)]$ can be calculated from these non-central moments using the formulas [St-87],

$$\begin{aligned}
k_1(m_1, m_2) &= M_1(m_1, m_2), \quad k_2(m_1, m_2) = M_2(m_1, m_2) - M_1^2(m_1, m_2), \\
k_3(m_1, m_2) &= M_3(m_1, m_2) - 3 M_2(m_1, m_2) M_1(m_1, m_2) + 2 M_1^3(m_1, m_2), \\
k_4(m_1, m_2) &= M_4(m_1, m_2) - 4 M_3(m_1, m_2) M_1(m_1, m_2) - 3 M_2^2(m_1, m_2) \\
&+ 12 M_2(m_1, m_2) M_1^2(m_1, m_2) - 6 M_1^4(m_1, m_2).
\end{aligned} \tag{7.2.17}$$

Then, the skewness and excess parameters are,

$$\gamma_1(m_1, m_2) = \frac{k_3(m_1, m_2)}{[k_2(m_1, m_2)]^{3/2}}, \quad \gamma_2(m_1, m_2) = \frac{k_4(m_1, m_2)}{[k_2(m_1, m_2)]^2}. \tag{7.2.18}$$

After carrying out the simplifications using Eqs. (7.2.2), (7.2.3), (7.2.4), (7.2.16) and (7.2.17), it is easily seen that,

$$\gamma_1(m_1, m_2) = \frac{2 \left[\overline{\langle D\tilde{D} \rangle^{m_1, m_2}} - \overline{\langle \tilde{D}D \rangle^{m_1, m_2}} \right]}{\left\{ \overline{\langle D\tilde{D} \rangle^{m_1, m_2}} + \overline{\langle \tilde{D}D \rangle^{m_1, m_2}} + \overline{\langle X^2 \rangle^{m_1, m_2}} \right\}^{3/2}}. \tag{7.2.19}$$

Thus, γ_1 will be non-zero only when $\alpha \neq 0$ and the τ dependence appears only in the denominator. Also, it is seen that for $N_+ = N_-$, $\gamma_1(m_1, m_2) = -\gamma_1(m_2, m_1)$. The expression for γ_2 is more cumbersome. Denoting $\mathcal{D} = \overline{\langle D\tilde{D} \rangle^{m_1, m_2}}$, $\tilde{\mathcal{D}} = \overline{\langle \tilde{D}D \rangle^{m_1, m_2}}$

and $\mathcal{X} = \overline{\langle X^2 \rangle^{m_1, m_2}}$ for brevity, we have

$$\gamma_2(m_1, m_2) + 1 = \frac{T_1 + T_2 + 2 T_3 + T_4 + (\tilde{\mathcal{D}} + \mathcal{D})(4 - \mathcal{X}) - 2 (\tilde{\mathcal{D}} + \mathcal{D})^2}{\{\tilde{\mathcal{D}} + \mathcal{D} + \mathcal{X}\}^2}. \quad (7.2.20)$$

The formulas for T 's, \mathcal{D} , $\tilde{\mathcal{D}}$ and \mathcal{X} given before together with Eq. (7.2.20) show that, for $N_+ = N_-$, $\gamma_2(m_1, m_2) = \gamma_2(m_2, m_1)$. With, $T_1 \sim \mathcal{X}^2 + C_1$, $T_2 = T_3 \sim \mathcal{X}(\tilde{\mathcal{D}} + \mathcal{D})$ and $T_4 \sim 3(\tilde{\mathcal{D}} + \mathcal{D})^2 + C_2$ which are good in the dilute limit ($|C_1/T_1|$ and $|C_2/T_4|$ will be close to zero), we have

$$\gamma_2(m_1, m_2) = \frac{C_1 + C_2 + 4 (\tilde{\mathcal{D}} + \mathcal{D})}{\{\tilde{\mathcal{D}} + \mathcal{D} + \mathcal{X}\}^2}. \quad (7.2.21)$$

Note that C_1 and \mathcal{X} depend only on τ . Similarly, C_2 and $(\tilde{\mathcal{D}}, \mathcal{D})$ depend only on α . The $(\tilde{\mathcal{D}} + \mathcal{D})$ term in the numerator will contribute to $\gamma_2(m_1, m_2)$ when $\tau = 0$ and α is very small. The approximation $T_2 = T_3 \sim \mathcal{X}(\tilde{\mathcal{D}} + \mathcal{D})$ is crucial in obtaining the numerator in Eq. (7.2.21) with no cross-terms involving the α and τ parameters. With this, we have k_4 to be the sum of k_4 's coming from $X(2)$ and $D(2)$ matrices [note that, as mentioned before, $X(2) = A \oplus B \oplus C$ and $D(2) = D + \tilde{D}$].

To test the accuracy of the formulas for M_r given by Eqs. (7.2.2), (7.2.3), (7.2.4) and (7.2.16), the binary correlation results for $\gamma_1(m, \pm)$ and $\gamma_2(m, \pm)$ are compared with exact results obtained using the eigenvalues from EGOE(1+2)- π ensembles with 100 members for several values of (N_+, N_-, m) and (τ, α) parameters in Table 7.1. Extension of Eq. (5.3.7) along with the results derived for $M_r(m_1, m_2)$ will give the binary correlation results for $\gamma_1(m, \pm)$ and $\gamma_2(m, \pm)$. It is clearly seen from the results in the Table that in all the examples considered, the binary correlation results are quite close to the exact results. Similar agreements are also seen in many other examples which are not shown in the table.

7.3 Application to $\beta\beta$ Decay: Formulas for the Bivariate Correlation Coefficient and Fourth Order Cumulants for the Transition Strength Density

7.3.1 Transition matrix elements and bivariate strength densities

Given a transition operator \mathcal{O} , the transition matrix elements are given by $|\langle f | \mathcal{O} | i \rangle|^2$, with i and f being the initial and final states. These are also generally called transition strengths. Operation of EGEs in many-particle spaces will lead to a theory for the smoothed part of transition strengths and the fluctuations in the locally renormalized strengths follow Porter-Thomas form for systems in the chaotic region. The transition matrix elements are needed in many applications. Examples are one-particle transfer [Po-91], E2 and M1 transition strengths in nuclei [Ha-82], dipole strengths in atoms [Fl-98], beta-decay [Ma-07], giant dipole resonances [Ma-98] and problems involving time-reversal non-invariance and parity [Fr-88, To-00]. Here, our focus is on $0\nu - \beta\beta$ decay. Half-life for 0ν double-beta decay (NDBD), for the 0_i^+ gs of a initial even-even nucleus decay to the 0_f^+ gs of the final even-even nucleus, with a few approximations, is given by [El-02]

$$\left[T_{1/2}^{0\nu}(0_i^+ \rightarrow 0_f^+) \right]^{-1} = G^{0\nu} |M^{0\nu}|^2 \frac{\langle m_\nu \rangle^2}{m_e^2}, \quad (7.3.1)$$

$$M^{0\nu} = M_{GT}^{0\nu} - \frac{g_V^2}{g_A^2} M_F^{0\nu} = \left\langle 0_f^+ \parallel \mathcal{O}(2 : 0\nu) \parallel 0_i^+ \right\rangle,$$

where $\langle m_\nu \rangle$ is effective neutrino mass and the $G^{0\nu}$ is an accurately calculable phase space integral [Bo-92, Do-93]. Similarly g_A and g_V are the weak axial-vector and vector coupling constants ($g_A/g_V = 1$ to 1.254). The nuclear matrix elements M_{GT} and M_F are matrix elements of Gamow-Teller and Fermi like two-body operators respectively. Forms for them will follow from the closure approximation which is well justified for NDBD [El-02]. As seen from Eq. (7.3.1), the NDBD half-lives are generated by the two-body transition operator $\mathcal{O}(2 : 0\nu)$. An experimental value of (bound on) $T_{1/2}^{0\nu}$ will give a value for (bound on) neutrino mass via Eq. (7.3.1) provided we know

the value of $|M^{0\nu}|^2$ generated by the NDBD two-body transition operator $\mathcal{O}(2 : 0\nu)$, connecting the ground states of the initial and final even-even nuclei involved.

Transition strengths multiplied by the eigenvalue densities at the two energies involved define the transition strength densities. With EGOE(1+2) operating in the Gaussian domain, it was established in the past that transition strength densities follow close to bivariate Gaussian form for spinless fermion systems and for operators that preserve particle number with the additional assumption that the transition operator and the Hamiltonian operator can be represented by independent EGOEs. With extensions of these results (without a EGOE basis), the bivariate Gaussian form is used in practical applications. Our purpose is to establish that for the $0\nu - \beta\beta$ decay (also for β decay), transition strength densities are close to bivariate Gaussian form and also to derive a formula for the bivariate correlation coefficient. We will address these two important questions so that the EGOE results can be applied to formulate a theory for calculating $0\nu - \beta\beta$ transition matrix elements [Ko-08a]. With space #1 denoting protons and similarly space #2 neutrons, the general form of the transition operator \mathcal{O} is,

$$\mathcal{O}(k_{\mathcal{O}}) = \sum_{\gamma, \delta} \nu_{\mathcal{O}}^{\gamma\delta}(k_{\mathcal{O}}) \gamma_1^{\dagger}(k_{\mathcal{O}}) \delta_2(k_{\mathcal{O}}); \quad k_{\mathcal{O}} = 2 \text{ for NDBD}. \quad (7.3.2)$$

Therefore, in order to derive the form for the transition strength densities generated by \mathcal{O} , it is necessary to deal with two-orbit configurations denoted by (m_1, m_2) , where m_1 is the number of particles in the first orbit (protons) and m_2 in the second orbit (neutrons). Now, the transition strength density $I_{\mathcal{O}}(E_i, E_f)$ is

$$\begin{aligned} I_{\mathcal{O}}^{(m_1^f, m_2^f), (m_1^i, m_2^i)}(E_i, E_f) \\ = I^{(m_1^f, m_2^f)}(E_f) \left| \left\langle (m_1^f, m_2^f) E_f \mid \mathcal{O} \mid (m_1^i, m_2^i) E_i \right\rangle \right|^2 I^{(m_1^i, m_2^i)}(E_i), \end{aligned} \quad (7.3.3)$$

and the corresponding bivariate moments are

$$\widetilde{M}_{PQ}(m_1^i, m_2^i) = \overline{\langle \mathcal{O}^{\dagger}(k_{\mathcal{O}}) H^Q(k_H) \mathcal{O}(k_{\mathcal{O}}) H^P(k_H) \rangle}^{m_1^i, m_2^i}. \quad (7.3.4)$$

Note that \widetilde{M} are in general non-central and non-normalized moments. The general

form of the operator $H(k_H)$ is given by Eq. (H33) and it preserves (m_1^i, m_2^i) 's. However, \mathcal{O} and its hermitian conjugate \mathcal{O}^\dagger do not preserve (m_1, m_2) i.e., $\mathcal{O}(k_\mathcal{O})|m_1, m_2\rangle = |m_1 + k_\mathcal{O}, m_2 - k_\mathcal{O}\rangle$ and $\mathcal{O}^\dagger(k_\mathcal{O})|m_1, m_2\rangle = |m_1 - k_\mathcal{O}, m_2 + k_\mathcal{O}\rangle$. Thus, given a (m_1^i, m_2^i) for an initial state, the (m_1^f, m_2^f) for the final state generated by the action of \mathcal{O} is uniquely defined and therefore, in the bivariate moments defined in Eq. (7.3.4), only the initial (m_1^i, m_2^i) is specified. For completeness, let us mention that given the marginal centroids (ϵ_i, ϵ_f) , widths (σ_i, σ_f) and the bivariate correlation coefficient ζ_{biv} , the normalized bivariate Gaussian is defined by,

$$\begin{aligned} \rho_{\text{biv-}\mathcal{G};\mathcal{O}}(E_i, E_f) &= \rho_{\text{biv-}\mathcal{G};\mathcal{O}}(E_i, E_f; \epsilon_i, \epsilon_f, \sigma_i, \sigma_f, \zeta_{biv}) \\ &= \frac{1}{2\pi\sigma_i\sigma_f\sqrt{(1-\zeta_{biv}^2)}} \\ &\times \exp -\frac{1}{2(1-\zeta_{biv}^2)} \left\{ \left(\frac{E_i - \epsilon_i}{\sigma_i} \right)^2 - 2\zeta_{biv} \left(\frac{E_i - \epsilon_i}{\sigma_i} \right) \left(\frac{E_f - \epsilon_f}{\sigma_f} \right) + \left(\frac{E_f - \epsilon_f}{\sigma_f} \right)^2 \right\}. \end{aligned} \quad (7.3.5)$$

7.3.2 Formulas for the bivariate moments

Using binary correlation approximation, we derive formulas for the first four moments $\widetilde{M}_{PQ}(m_1^i, m_2^i)$, $P + Q \leq 4$ of $I_\mathcal{O}^{(m_1^f, m_2^f), (m_1^i, m_2^i)}(E_i, E_f)$ for any $k_\mathcal{O}$ by representing $H(k_H)$ and $\mathcal{O}(k_\mathcal{O})$ operators by independent EGOEs and assuming $H(k_H)$ is a k_H -body operator preserving (m_1, m_2) 's. Note that the ensemble averaged k_H -particle matrix elements of $H(k_H)$ are $v_H^2(i, j)$ with $i + j = k_H$ [see Eq. (H33)] and similarly the ensemble average of $(v_\mathcal{O}^{\gamma\delta})^2$ is $v_\mathcal{O}^2$. From now on, we use $(m_1^i, m_2^i) = (m_1, m_2)$. Using Eq. (7.3.2) and applying the basic rules given by Eqs. (H2) and (H3), we have

$$\begin{aligned} \widetilde{M}_{00}(m_1, m_2) &= \overline{\langle \mathcal{O}^\dagger(k_\mathcal{O}) \mathcal{O}(k_\mathcal{O}) \rangle}^{m_1, m_2} \\ &= \sum_{\gamma, \delta} \overline{\left\{ v_\mathcal{O}^{\gamma\delta} \right\}^2} \left\langle \delta_2^\dagger(k_\mathcal{O}) \gamma_1(k_\mathcal{O}) \gamma_1^\dagger(k_\mathcal{O}) \delta_2(k_\mathcal{O}) \right\rangle^{m_1, m_2} \\ &= v_\mathcal{O}^2 \begin{pmatrix} \tilde{m}_1 \\ k_\mathcal{O} \end{pmatrix} \begin{pmatrix} m_2 \\ k_\mathcal{O} \end{pmatrix}. \end{aligned} \quad (7.3.6)$$

Trivially, $\widetilde{M}_{10}(m_1, m_2)$ and $\widetilde{M}_{01}(m_1, m_2)$ will be zero as $H(k_H)$ is represented by EGOE(k_H). Thus, $\widetilde{M}_{PQ}(m_1, m_2)$ are central moments. Moreover, by definition, all the odd-order moments, i.e., $\widetilde{M}_{PQ}(m_1, m_2)$ with $\text{mod}(P+Q, 2) \neq 0$, will be zero. Now, the \widetilde{M}_{11} is given by,

$$\begin{aligned}
\widetilde{M}_{11}(m_1, m_2) &= \overline{\langle \mathcal{O}^\dagger(k_{\mathcal{O}}) H(k_H) \mathcal{O}(k_{\mathcal{O}}) H(k_H) \rangle^{m_1, m_2}} \\
&= v_{\mathcal{O}}^2 \sum_{\alpha_1, \beta_1, \alpha_2, \beta_2, \gamma_1, \delta_2; i+j=k_H} v_H^2(i, j) \\
&\times \left\langle \gamma_1^\dagger(k_{\mathcal{O}}) \alpha_1(i) \beta_1^\dagger(i) \gamma_1(k_{\mathcal{O}}) \beta_1(i) \alpha_1^\dagger(i) \right\rangle^{m_1} \\
&\times \left\langle \delta_2(k_{\mathcal{O}}) \alpha_2(j) \beta_2^\dagger(j) \delta_2^\dagger(k_{\mathcal{O}}) \beta_2(j) \alpha_2^\dagger(j) \right\rangle^{m_2}.
\end{aligned} \tag{7.3.7}$$

Then, contracting over the $\gamma^\dagger \gamma$ and $\delta \delta^\dagger$ operators, respectively in the first and second traces in Eq. (7.3.7) using Eqs. (H4) and (H5) appropriately, we have

$$\begin{aligned}
\widetilde{M}_{11}(m_1, m_2) &= v_{\mathcal{O}}^2 \sum_{i+j=k_H} v_H^2(i, j) \begin{pmatrix} \tilde{m}_1 - i \\ k_{\mathcal{O}} \end{pmatrix} \begin{pmatrix} m_2 - j \\ k_{\mathcal{O}} \end{pmatrix} \\
&\times T(m_1, N_1, i) T(m_2, N_2, j).
\end{aligned} \tag{7.3.8}$$

Note that the formulas for the functions $T(\cdots)$'s appearing in Eq. (7.3.8) are given by Eqs. (H8), (H9) and (H10). Similarly, the functions $F(\cdots)$'s appearing ahead are given by Eqs. (H14) and (H23). For the marginal variances, we have

$$\begin{aligned}
\widetilde{M}_{20}(m_1, m_2) &= \overline{\langle \mathcal{O}^\dagger(k_{\mathcal{O}}) \mathcal{O}(k_{\mathcal{O}}) H^2(k_H) \rangle^{m_1, m_2}} \\
&= \widetilde{M}_{00}(m_1, m_2) \overline{\langle H^2(k_H) \rangle^{m_1, m_2}}, \\
\widetilde{M}_{02}(m_1, m_2) &= \overline{\langle \mathcal{O}^\dagger(k_{\mathcal{O}}) H^2(k_H) \mathcal{O}(k_{\mathcal{O}}) \rangle^{m_1, m_2}} \\
&= \widetilde{M}_{00}(m_1, m_2) \overline{\langle H^2(k_H) \rangle^{m_1+k_{\mathcal{O}}, m_2-k_{\mathcal{O}}}}.
\end{aligned} \tag{7.3.9}$$

In Eq. (7.3.9), the ensemble averages of $H^2(k_H)$ are given by Eq. (H34). Now, the correlation coefficient ζ_{biv} is

$$\zeta_{biv}(m_1, m_2) = \frac{\widetilde{M}_{11}(m_1, m_2)}{\sqrt{\widetilde{M}_{20}(m_1, m_2) \widetilde{M}_{02}(m_1, m_2)}}. \quad (7.3.10)$$

Clearly, ζ_{biv} will be independent of $v_{\mathcal{O}}^2$.

Proceeding further, we derive formulas for the fourth order moments \widetilde{M}_{PQ} , $P + Q = 4$. The results are as follows. Firstly, for $(PQ) = (40)$ and (04) , we have

$$\begin{aligned} \widetilde{M}_{40}(m_1, m_2) &= \overline{\langle \mathcal{O}^\dagger(k_{\mathcal{O}}) \mathcal{O}(k_{\mathcal{O}}) H^4(k_H) \rangle^{m_1, m_2}} \\ &= \widetilde{M}_{00}(m_1, m_2) \overline{\langle H^4(k_H) \rangle^{m_1, m_2}}, \\ \widetilde{M}_{04}(m_1, m_2) &= \overline{\langle \mathcal{O}^\dagger(k_{\mathcal{O}}) H^4(k_H) \mathcal{O}(k_{\mathcal{O}}) \rangle^{m_1, m_2}} \\ &= \widetilde{M}_{00}(m_1, m_2) \overline{\langle H^4(k_H) \rangle^{m_1 + k_{\mathcal{O}}, m_2 - k_{\mathcal{O}}}}. \end{aligned} \quad (7.3.11)$$

In Eq. (7.3.11), the ensemble averages of $H^4(k_H)$ are given by Eq. (H39). For $(PQ) = (31)$, we have

$$\begin{aligned} \widetilde{M}_{31}(m_1, m_2) &= \overline{\langle \mathcal{O}^\dagger(k_{\mathcal{O}}) H(k_H) \mathcal{O}(k_{\mathcal{O}}) H^3(k_H) \rangle^{m_1, m_2}} \\ &= \overline{\langle \mathcal{O}^\dagger(k_{\mathcal{O}}) \textcolor{blue}{H}(\textcolor{blue}{k}_H) \mathcal{O}(k_{\mathcal{O}}) \textcolor{blue}{H}(\textcolor{blue}{k}_H) \textcolor{red}{H}(\textcolor{red}{k}_H) \textcolor{red}{H}(\textcolor{red}{k}_H) \rangle^{m_1, m_2}} \\ &+ \overline{\langle \mathcal{O}^\dagger(k_{\mathcal{O}}) \textcolor{blue}{H}(\textcolor{blue}{k}_H) \mathcal{O}(k_{\mathcal{O}}) \textcolor{red}{H}(\textcolor{red}{k}_H) \textcolor{blue}{H}(\textcolor{blue}{k}_H) \textcolor{red}{H}(\textcolor{red}{k}_H) \rangle^{m_1, m_2}} \\ &+ \overline{\langle \mathcal{O}^\dagger(k_{\mathcal{O}}) \textcolor{blue}{H}(\textcolor{blue}{k}_H) \mathcal{O}(k_{\mathcal{O}}) \textcolor{red}{H}(\textcolor{red}{k}_H) \textcolor{red}{H}(\textcolor{red}{k}_H) \textcolor{blue}{H}(\textcolor{blue}{k}_H) \rangle^{m_1, m_2}}. \end{aligned} \quad (7.3.12)$$

Note that in Eq. (7.3.12), we use the same color for the binary correlated pairs of

operators. First and last terms on RHS of Eq. (7.3.12) are simple and this gives,

$$\begin{aligned}
\widetilde{M}_{31}(m_1, m_2) &= 2 \overline{\langle H^2(k_H) \rangle^{m_1, m_2}} \widetilde{M}_{11}(m_1, m_2) \\
&+ \overline{\langle \mathcal{O}^\dagger(k_{\mathcal{O}}) \textcolor{blue}{H}(\textcolor{blue}{k}_H) \mathcal{O}(k_{\mathcal{O}}) \textcolor{red}{H}(\textcolor{red}{k}_H) \textcolor{blue}{H}(\textcolor{blue}{k}_H) \textcolor{red}{H}(\textcolor{red}{k}_H) \rangle^{m_1, m_2}} \\
&= 2 \overline{\langle H^2(k_H) \rangle^{m_1, m_2}} \widetilde{M}_{11}(m_1, m_2) + v_{\mathcal{O}}^2 \sum_{i+j=k_H, t+u=k_H} v_H^2(i, j) v_H^2(t, u) \\
&\times \binom{m_2 - j}{k_{\mathcal{O}}} \binom{\widetilde{m}_1 - i}{k_{\mathcal{O}}} F(m_1, N_1, i, t) F(m_2, N_2, j, u) .
\end{aligned} \tag{7.3.13}$$

Similarly, we have

$$\begin{aligned}
\widetilde{M}_{13}(m_1, m_2) &= \overline{\langle \mathcal{O}^\dagger(k_{\mathcal{O}}) H^3(k_H) \mathcal{O}(k_{\mathcal{O}}) H(k_H) \rangle^{m_1, m_2}} \\
&= \overline{\langle \mathcal{O}^\dagger(k_{\mathcal{O}}) \textcolor{blue}{H}(\textcolor{blue}{k}_H) \textcolor{blue}{H}(\textcolor{blue}{k}_H) \textcolor{red}{H}(\textcolor{red}{k}_H) \mathcal{O}(k_{\mathcal{O}}) \textcolor{red}{H}(\textcolor{red}{k}_H) \rangle^{m_1, m_2}} \\
&+ \overline{\langle \mathcal{O}^\dagger(k_{\mathcal{O}}) \textcolor{blue}{H}(\textcolor{blue}{k}_H) \textcolor{red}{H}(\textcolor{red}{k}_H) \textcolor{blue}{H}(\textcolor{blue}{k}_H) \mathcal{O}(k_{\mathcal{O}}) \textcolor{red}{H}(\textcolor{red}{k}_H) \rangle^{m_1, m_2}} \\
&+ \overline{\langle \mathcal{O}^\dagger(k_{\mathcal{O}}) \textcolor{blue}{H}(\textcolor{blue}{k}_H) \textcolor{red}{H}(\textcolor{red}{k}_H) \textcolor{red}{H}(\textcolor{red}{k}_H) \mathcal{O}(k_{\mathcal{O}}) \textcolor{blue}{H}(\textcolor{blue}{k}_H) \rangle^{m_1, m_2}} \\
&= 2 \overline{\langle H^2(k_H) \rangle^{m_1 + k_{\mathcal{O}}, m_2 - k_{\mathcal{O}}}} \widetilde{M}_{11}(m_1, m_2) \\
&+ v_{\mathcal{O}}^2 \sum_{i+j=k_H, t+u=k_H} v_H^2(i, j) v_H^2(t, u) G(t, u) \\
&\times \binom{\widetilde{m}_1 - k_{\mathcal{O}} - t + i}{i} \binom{m_1 + k_{\mathcal{O}} - t}{i} \binom{\widetilde{m}_2 - u + k_{\mathcal{O}} + j}{j} \binom{m_2 - k_{\mathcal{O}} - u}{j} ; \\
G(t, u) &= \binom{\widetilde{m}_1 - t}{k_{\mathcal{O}}} \binom{m_2 - u}{k_{\mathcal{O}}} T(m_1, N_1, t) T(m_2, N_2, u) .
\end{aligned} \tag{7.3.14}$$

Finally, $\widetilde{M}_{22}(m_1, m_2)$ is given by,

$$\begin{aligned}
\widetilde{M}_{22}(m_1, m_2) &= \overline{\langle \mathcal{O}^\dagger(k_\mathcal{O}) H^2(k_H) \mathcal{O}(k_\mathcal{O}) H^2(k_H) \rangle^{m_1, m_2}} \\
&= \overline{\langle \mathcal{O}^\dagger(k_\mathcal{O}) \textcolor{blue}{H}(\textcolor{blue}{k}_H) \textcolor{blue}{H}(\textcolor{blue}{k}_H) \mathcal{O}(k_\mathcal{O}) \textcolor{red}{H}(\textcolor{red}{k}_H) \textcolor{red}{H}(\textcolor{red}{k}_H) \rangle^{m_1, m_2}} \\
&\quad + \overline{\langle \mathcal{O}^\dagger(k_\mathcal{O}) \textcolor{blue}{H}(\textcolor{blue}{k}_H) \textcolor{red}{H}(\textcolor{red}{k}_H) \mathcal{O}(k_\mathcal{O}) \textcolor{blue}{H}(\textcolor{blue}{k}_H) \textcolor{red}{H}(\textcolor{red}{k}_H) \rangle^{m_1, m_2}} \\
&\quad + \overline{\langle \mathcal{O}^\dagger(k_\mathcal{O}) \textcolor{blue}{H}(\textcolor{blue}{k}_H) \textcolor{red}{H}(\textcolor{red}{k}_H) \mathcal{O}(k_\mathcal{O}) \textcolor{red}{H}(\textcolor{red}{k}_H) \textcolor{blue}{H}(\textcolor{blue}{k}_H) \rangle^{m_1, m_2}} \\
&= \widetilde{M}_{00}(m_1, m_2) \overline{\langle H^2(k_H) \rangle^{m_1 + k_\mathcal{O}, m_2 - k_\mathcal{O}}} \overline{\langle H^2(k_H) \rangle^{m_1, m_2}} \\
&\quad + v_\mathcal{O}^2 \sum_{i+j=k_H, t+u=k_H} v_H^2(i, j) v_H^2(t, u) \binom{\widetilde{m}_1 - i - t}{k_\mathcal{O}} \binom{m_2 - u - j}{k_\mathcal{O}} \\
&\quad \times [F(m_1, N_1, i, t) F(m_2, N_2, j, u) \\
&\quad + T(m_1, N_1, i) T(m_1, N_1, t) T(m_2, N_2, j) T(m_2, N_2, u)] .
\end{aligned} \tag{7.3.15}$$

Given the $\widetilde{M}_{PQ}(m_1, m_2)$, the normalized central moments M_{PQ} are $M_{PQ} = \widetilde{M}_{PQ} / \widetilde{M}_{00}$.

7.3.3 Numerical results for bivariate correlation coefficient and fourth order cumulants

Firstly, the scaled moments \widehat{M}_{PQ} are

$$\widehat{M}_{PQ} = \frac{M_{PQ}(m_1, m_2)}{[M_{20}(m_1, m_2)]^{P/2} [M_{02}(m_1, m_2)]^{Q/2}} ; \quad P + Q \geq 2 . \tag{7.3.16}$$

Now the fourth order cumulants are [St-87],

$$\begin{aligned}
k_{40}(m_1, m_2) &= \widehat{M}_{40}(m_1, m_2) - 3 , \quad k_{04}(m_1, m_2) = \widehat{M}_{04}(m_1, m_2) - 3 , \\
k_{31}(m_1, m_2) &= \widehat{M}_{31}(m_1, m_2) - 3 \widehat{M}_{11}(m_1, m_2) , \\
k_{13}(m_1, m_2) &= \widehat{M}_{13}(m_1, m_2) - 3 \widehat{M}_{11}(m_1, m_2) , \\
k_{22}(m_1, m_2) &= \widehat{M}_{22}(m_1, m_2) - 2 \widehat{M}_{11}^2(m_1, m_2) - 1 .
\end{aligned} \tag{7.3.17}$$

Table 7.2: Correlation coefficients $\zeta_{biv}(m_1, m_2)$ for some nuclei with $k_{\mathcal{O}} = 2$ as appropriate for $0\nu - \beta\beta$ decay operator. Note that space #1 is for protons and space #2 for neutrons. The configuration spaces corresponding to N_1 or $N_2 = 20, 22, 30, 32, 44$ and 58 are r_3f , r_3g , r_4g , r_4h , r_5i , and r_6j , respectively with $f = {}^1f_{7/2}$, $g = {}^1g_{9/2}$, $h = {}^1h_{11/2}$, $i = {}^1i_{13/2}$, $j = {}^1j_{15/2}$, $r_3 = {}^1f_{5/2}$, $r_4 = {}^1g_{7/2}$, $r_5 = {}^1h_{9/2}$, $r_6 = {}^1i_{11/2}$, $r_3 = {}^1f_{5/2}$, $r_4 = {}^1g_{7/2}$, $r_5 = {}^1h_{9/2}$, $r_6 = {}^1i_{11/2}$, $r_3 = {}^1f_{5/2}$, $r_4 = {}^1g_{7/2}$, $r_5 = {}^1h_{9/2}$, $r_6 = {}^1i_{11/2}$, $r_3 = {}^1f_{5/2}$, $r_4 = {}^1g_{7/2}$, $r_5 = {}^1h_{9/2}$, $r_6 = {}^1i_{11/2}$. See text for details.

Nuclei	N_1	m_1	N_2	m_2	$\zeta_{biv}(m_1, m_2)$
${}^{76}_{32}\text{Ge}_{44}$	22	4	22	16	0.64
${}^{82}_{34}\text{Se}_{48}$	22	6	22	20	0.6
${}^{100}_{42}\text{Mo}_{58}$	30	2	32	8	0.57
${}^{128}_{52}\text{Te}_{76}$	32	2	32	26	0.62
${}^{130}_{52}\text{Te}_{78}$	32	2	32	28	0.58
${}^{150}_{60}\text{Nd}_{90}$	32	10	44	8	0.72
${}^{154}_{62}\text{Sm}_{92}$	32	12	44	10	0.76
${}^{180}_{74}\text{W}_{106}$	32	24	44	24	0.77
${}^{238}_{92}\text{U}_{146}$	44	10	58	20	0.83

Assuming $\nu_H^2(i, j)$ defining $H(2)$ are independent of (i, j) so that ζ_{biv} is independent of ν_H^2 , we have calculated the value of ζ_{biv} with $k_{\mathcal{O}} = 2$ for several $0\nu - \beta\beta$ decay candidate nuclei using Eq. (7.3.10) along with Eqs. (7.3.6), (7.3.8), (7.3.9) and (H34). For the function $T(\cdots)$, we use Eq. (H8). Note that $\nu_H^2(i, j)$ correspond to the variance of two-particle matrix elements from the p-p ($i = 2, j = 0$), n-n ($i = 0, j = 2$) and p-n ($i = 1, j = 1$) interactions. Results are given in Table 7.2. It is seen that $\zeta_{biv} \sim 0.6-0.8$. It is important to mention that $\zeta_{biv} = 0$ for GOE. Therefore, the transition strength density will be narrow in (E_i, E_f) plane. In order to establish the bivariate Gaussian form for the $0\nu - \beta\beta$ decay transition strength density, we have examined k_{PQ} , $P + Q = 4$. For a good bivariate Gaussian, $|k_{PQ}| \lesssim 0.3$. Using Eqs. (7.3.6), (7.3.8), (7.3.9), (7.3.11), (7.3.13)-(7.3.17) along with Eqs. (H34) and (H39), we have calculated the cumulants $k_{PQ}(m_1, m_2)$, $P + Q = 4$. These involve $T(\cdots)$ and $F(\cdots)$ functions. For set #1 calculations in Table 7.3, we use Eq. (H8) for $T(\cdots)$ and Eq. (H23) for $F(\cdots)$. For the set #2

Table 7.3: Cumulants k_{PQ} , $P + Q = 4$ for some nuclei listed in Table 7.2. The numbers in the brackets are for the strict dilute limit as explained in the text. Just as in the construction of Table 7.2, we use $v_H^2(i, j)$ independent of (i, j) . See Table 7.2 and text for details.

Nuclei	N_1	m_1	N_2	m_2	k_{40}	k_{04}	k_{13}	k_{31}	k_{22}
$^{100}_{42}\text{Mo}_{58}$	30	2	32	8	-0.45(-0.39)	-0.42(-0.38)	-0.24(-0.23)	-0.26(-0.25)	-0.20(-0.22)
$^{150}_{60}\text{Nd}_{90}$	32	10	44	8	-0.27(-0.22)	-0.29(-0.23)	-0.22(-0.18)	-0.20(-0.17)	-0.19(-0.18)
$^{154}_{62}\text{Sm}_{92}$	32	12	44	10	-0.24(-0.18)	-0.25(-0.18)	-0.19(-0.15)	-0.18(-0.15)	-0.17(-0.15)
$^{180}_{74}\text{W}_{106}$	32	24	44	24	-0.19(-0.08)	-0.20(-0.08)	-0.17(-0.08)	-0.15(-0.08)	-0.15(-0.08)
$^{238}_{92}\text{U}_{146}$	44	10	58	20	-0.18(-0.13)	-0.18(-0.13)	-0.15(-0.11)	-0.15(-0.11)	-0.13(-0.11)

calculations, shown in ‘brackets’ in Table 7.3, we use Eq. (H9) for $T(\cdots)$, Eq. (H14) for $F(\cdots)$ and replace everywhere $\binom{\tilde{m}_i+r}{s} \rightarrow \binom{N_i}{s}$ for any (r, s) with $i = 1, 2$. Then we have the strict dilute limit. We show in Table 7.3, bivariate cumulants for five heavy nuclei for both sets of calculations and they clearly establish that bivariate Gaussian is a good approximation. We have also examined this analytically in the dilute limit with $N_1, N_2 \rightarrow \infty$ and assuming $\nu_H^2(i, j)$ independent of (i, j) . With these, we have expanded k_{PQ} in powers of $1/m_1$ and $1/m_2$ using Mathematica. It is seen that all the k_{PQ} , $P + Q = 4$ behave as,

$$k_{PQ} = -\frac{4}{m_1} + O\left(\frac{1}{m_1^2}\right) + O\left(\frac{m_2^2}{m_1^3}\right) + \dots \quad (7.3.18)$$

Therefore, for $m_1 \gg 1$ and $m_2 \ll m_1^{3/2}$, the strength density approaches bivariate Gaussian form in general. It is important to recall that the strong dependence on m_1 in Eq. (7.3.18) is due to the nature of the operator \mathcal{O} i.e., $\mathcal{O}(k_{\mathcal{O}})|m_1, m_2\rangle = |m_1 + k_{\mathcal{O}}, m_2 - k_{\mathcal{O}}\rangle$. Thus, we conclude that bivariate Gaussian form is a good approximation for $0\nu - \beta\beta$ decay transition strength densities. With this, one can apply the formulation given in [Ko-08a] with the bivariate correlation coefficient ζ_{biv} given by Eqs. (7.3.10), (7.3.9) and (7.3.8). The values given by the two-orbit binary correlation theory for ζ_{biv} can be used as starting values in practical calculations.

For completeness, we have also calculated the correlation coefficient and fourth order moments for the transition operator relevant for β decay and the results presented in Table 7.4 confirm that bivariate Gaussian form is a good approximation for β decay transition strength densities. These results justify the assumptions made in [Ko-95].

7.4 EGOE(2)- J Ensemble: Structure of Centroids and Variances for Fermions in a Single- j Shell

7.4.1 Definition and construction of EGOE(2)- J

Shell-model corresponds to m fermions occupying sp j -orbits j_1, j_2, \dots and interacting via a two body interaction $H = V(2)$ that preserves total m -particle angular momenta J . For simplicity we restrict to identical nucleons and degenerate sp ener-

Table 7.4: Correlation coefficients $\zeta_{biv}(m_1, m_2)$ and cumulants k_{pq} , $P + Q = 4$ for some nuclei relevant for β decay [$k_\theta = 1$ in Eq. (7.3.2)]. The first four nuclei in the table are relevant for β^- transitions, next four nuclei are relevant for electron capture and the last two nuclei are relevant for β^+ transitions. The numbers in the brackets for k_{pq} are for the strict dilute limit as in Table 7.3. We assume $\nu_H^2(i, j)$ are independent of (i, j) just as in the calculations for generating Tables 7.2 and 7.3. See caption to Table 7.2 for other details.

Nuclei	N_1	m_1	N_2	m_2	$\zeta_{biv}(m_1, m_2)$	k_{40}	k_{04}	k_{13}	k_{31}	k_{22}
$^{62}_{27}\text{Co}_{35}$	20	7	30	15	0.72	-0.26(-0.18)	-0.27(-0.18)	-0.24(-0.16)	-0.23(-0.16)	-0.22(-0.16)
$^{64}_{27}\text{Co}_{37}$	20	7	30	17	0.73	-0.27(-0.16)	-0.27(-0.16)	-0.24(-0.15)	-0.23(-0.15)	-0.21(-0.15)
$^{62}_{26}\text{Fe}_{36}$	20	6	30	16	0.72	-0.28(-0.18)	-0.28(-0.18)	-0.24(-0.16)	-0.24(-0.16)	-0.22(-0.16)
$^{68}_{28}\text{Ni}_{40}$	20	8	30	20	0.72	-0.27(-0.14)	-0.27(-0.14)	-0.24(-0.13)	-0.23(-0.13)	-0.21(-0.13)
$^{65}_{32}\text{Ge}_{33}$	36	5	36	4	0.55	-0.45(-0.41)	-0.46(-0.42)	-0.35(-0.33)	-0.34(-0.32)	-0.34(-0.34)
$^{69}_{34}\text{Se}_{35}$	36	7	36	6	0.66	-0.36(-0.29)	-0.34(-0.30)	-0.28(-0.25)	-0.28(-0.25)	-0.27(-0.25)
$^{73}_{36}\text{Kr}_{37}$	36	9	36	8	0.72	-0.28(-0.23)	-0.28(-0.23)	-0.24(-0.20)	-0.24(-0.20)	-0.23(-0.20)
$^{77}_{38}\text{Sr}_{39}$	36	11	36	10	0.76	-0.24(-0.19)	-0.24(-0.19)	-0.21(-0.17)	-0.21(-0.17)	-0.20(-0.17)
$^{85}_{42}\text{Mo}_{43}$	36	15	36	14	0.79	-0.20(-0.14)	-0.21(-0.14)	-0.19(-0.13)	-0.18(-0.13)	-0.17(-0.13)
$^{93}_{46}\text{Pd}_{47}$	36	19	36	18	0.80	-0.19(-0.11)	-0.19(-0.11)	-0.18(-0.10)	-0.17(-0.10)	-0.16(-0.10)

gies. Firstly, the $V(2)$ matrix $[V(2)]$ in two-particle spaces is a direct sum of matrices, $[V(2)] = [V^{J_{12}}(2)] \oplus [V^{J'_{12}}(2)] \oplus [V^{J''_{12}}(2)] \oplus \dots$ where J_{12} are two-particle angular momenta. Now the $[V^{J_{12}}(2)]$ matrices are represented by GOE, i.e., $V(2)$ in two-particle spaces is a direct sum of GOE's. Let us consider the example of $j = (7/2, 5/2, 3/2, 1/2)$, i.e., the nuclear $2p1f$ shell. Here $J_{12} = 0 - 6$ and the corresponding matrix dimensions are 4, 3, 8, 5, 6, 2, and 2, respectively. This gives 94 independent matrix elements for the $\{V(2)\}$ ensemble and they are chosen to be Gaussian variables with zero center and variance unity (variance of the diagonal elements being 2); see Eq. (1.2.4). The EGOE(2)- J ensemble in m -particle spaces is then generated by propagating this $\{V(2)\}$ ensemble to a given (m, J) space by using the shell-model geometry, i.e., by the algebra $U(N) \supset SO_J(3)$ with a suitable sub-algebra in between, where $N = \sum_i (2j_i + 1)$. Then, the m -particle H matrix elements are linear combinations of two-particle matrix elements with the expansion coefficients being essentially fractional parentage coefficients. For the $(2p1f)^{m=8}$ system, the dimensions $D(m, J)$ are 347, 880, 1390, 1627, 1755, 1617, 1426, 1095, 808, 514, 311, 151, 73, 22, 6 for $J = 0$ to 14, respectively. As the shell-model geometry is complex, EGOE(2)- J is mathematically a difficult ensemble. In the case of a single- j shell, $J_{12} = 0, 2, 4, \dots, (2j - 1)$ and $\{V^{J_{12}}(2)\}$ are one dimensional. In general, nuclear shell-model codes can be used to construct EGOE(2)- J [Br-81, Ze-04, Zh-04, Pa-07].

For a $(j)^m$ system with H 's preserving angular momentum J symmetry, the operator form for a two-body H is,

$$H = \sum_{J_2=\text{even}, M_2} V_{J_2} A(j^2; J_2 M_2) [A(j^2; J_2 M_2)]^\dagger, \quad (7.4.1)$$

where $V_{J_2} = \langle (j^2) J_2 M_2 | H | (j^2) J_2 M_2 \rangle$ are independent of M_2 and $J_2 = 0, 2, 4, \dots, (2j - 1)$. The operator $A(j^2; J_2 M_2)$ creates a two-particle state. The EGOE(2)- J ensemble for the $(j)^m$ system is generated by assuming V_{J_2} 's to be independent Gaussian random variables with zero center and variance unity,

$$\rho_{V_{J_{2a}}, V_{J_{2b}}, \dots}(x_a, x_b, \dots) dx_a dx_b \dots = \rho_{V_{J_{2a}; \mathcal{G}}}(x_a) \rho_{V_{J_{2b}; \mathcal{G}}}(x_b) \dots dx_a dx_b \dots \quad (7.4.2)$$

One simple way to construct the EGOE(2)- J ensemble in m -particle spaces with a

fixed- J value is as follows. Consider the $N = (2j + 1)$ sp states $|jm\rangle$, $m = -j, -j + 1, \dots, j$. Now distributing m fermions in the $|jm\rangle$ orbits in all possible ways will give the configurations $[m_v] = |n_{v_1}, n_{v_2}, \dots, n_{v_m}\rangle$ where (v_1, v_2, \dots, v_m) are the filled orbits so that $n_{v_i} = 1$. We can select configurations such that $M = \sum_{i=1}^m n_{v_i} m_{v_i} = 0$ for even m and $M = 1/2$ for odd m . The number of $[m_v]$'s for $M = 0$, with m even, is $D(m, M = 0) = \sum_{J=0}^{J_{\max}} d(m, J)$ and similarly for odd m , $D(m, M = 1/2) = \sum_{J=1/2}^{J_{\max}} d(m, J)$. Converting V_{J_2} into the $|jm\rangle |jm'\rangle$ basis will give,

$$\begin{aligned} V_{m_1, m_2, m_3, m_4} &= \langle jm_3 jm_4 | V | jm_1 jm_2 \rangle \\ &= 2 \sum_{J_2=\text{even}, M_2} \langle jm_1 jm_2 | J_2 M_2 \rangle \langle jm_3 jm_4 | J_2 M_2 \rangle V_{J_2}, \end{aligned} \quad (7.4.3)$$

where $M_2 = m_1 + m_2 = m_3 + m_4$. The V matrix in the $[m_v]$ basis follows easily from the formalism used for EGOE(2) for spinless fermion systems when we use V_{m_1, m_2, m_3, m_4} matrix elements; see Chapter 1 for details. Starting with the J^2 operator and writing its one and two-body matrix elements in the $|jm\rangle |jm'\rangle$ basis, it is possible to construct the J^2 matrix in the $[m_v]$ basis. Diagonalizing this matrix will give (with $M_0 = 0$ for even m and $1/2$ for odd m) the C -coefficients in

$$|(j)^m \alpha JM_0\rangle = \sum_{[m_v]} C_{[m_v]}^{\alpha J} \phi_{[m_v]} \quad (7.4.4)$$

and we can identify the J -value of the eigenfunctions by using the eigenvalues $J(J+1)$. With this, the H matrix in the $|(j)^m \alpha JM_0\rangle$ basis is

$$\langle (j)^m \beta JM_0 | H | (j)^m \alpha JM_0 \rangle = \sum_{[m_v]_i, [m_v]_f} C_{[m_v]_i}^{\alpha J} C_{[m_v]_f}^{\beta J} \langle \phi_{[m_v]_f} | V | \phi_{[m_v]_i} \rangle. \quad (7.4.5)$$

The above procedure can be implemented on a computer easily. In our study we analyze EGOE(2)- J without explicitly constructing the H matrices in the m -particle spaces. In particular, we analyze the structure of fixed- J energy centroids $E_c(m, J)$ and spectral variances $\sigma^2(m, J)$ for $(j)^m$ systems.

Exact formulas for $E_c(m, J)$ and $\sigma^2(m, J)$ can be obtained from the results in [Ja-79, Ja-79a, Wo-86, Ve-81, Ve-82, Ve-84, No-72]. However, they are too complicated and

computationally extensive. An alternative is to use the bivariate Edgeworth form for $\rho(E, M)$ and seek expansions for the centroids and variances. The expansion coefficients then will involve fourth order traces over fixed- m spaces. We will derive the expansions in Sec. 7.4.2. Trace propagation formulas for the expansion coefficients are given in Sec. 7.4.3. Finally, in Sec. 7.4.4, we will discuss the structure of $E_c(m, J)$ and $\sigma^2(m, J)$ for $(j)^m$ systems.

7.4.2 Expansions for centroids $E_c(m, J)$ and variances $\sigma^2(m, J)$

Firstly, fixed- J averages of a J invariant operator \mathcal{O} follow from fixed- M averages using,

$$\begin{aligned} \langle \mathcal{O} \rangle^{m, J} &= \frac{\langle \langle \mathcal{O} \rangle \rangle^{m, M=J} - \langle \langle \mathcal{O} \rangle \rangle^{m, M=J+1}}{\mathcal{D}(m, M=J) - \mathcal{D}(m, M=J+1)} \\ &\simeq \left[- \frac{\partial \mathcal{D}(m, M)}{\partial M} \Big|_{M=J+1/2} \right]^{-1} \left[- \frac{\partial \langle \langle \mathcal{O} \rangle \rangle^M}{\partial M} \Big|_{M=J+1/2} \right]. \end{aligned} \quad (7.4.6)$$

Here, $\mathcal{D}(m, M)$ is fixed- M dimension. We use an expansion for the bivariate distribution $\rho^{H, m}(E, M)$ and obtain the expansion for various quantities in Eq. (7.4.6). Applying this to H and H^2 operators, we have derived expansions to order $[J(J+1)]^2$ for $E_c(m, J)$ and $\sigma^2(m, J)$. Now we present these results.

The operators H and J_z whose eigenvalues are E and M , respectively, commute and therefore the bivariate moments of $\rho^{H, m}(E, M)$ are just $M_{rs}(m) = \langle H^r J_z^s \rangle^m$; note that nuclear effective Hamiltonians are all J invariant. Now some important results are: (i) $M_{rs}(m) = 0$ for s odd and therefore all the cumulants $k_{rs}(m) = 0$ for s odd; (ii) the marginal densities $\rho(E)$ and $\rho(M)$ are close to Gaussian, the first one is a result of the fact that nuclear H 's can be represented by two-body random matrix ensembles giving $k_{40}(m) \sim -4/m$ and the second as J_z is a one-body operator giving $k_{04}(m) \sim -1/m$; (iii) the correlation coefficient $\zeta_{biv}(m) = k_{11}(m) = 0$ and hence the bivariate Gaussian in (E, M) is just $\rho_{\mathcal{G}}(E)\rho_{\mathcal{G}}(M)$; (iv) random matrix representation of H shows that $k_{22}(m) \sim -2/3m$ in the dilute limit and this follows from the results in Eqs. (7.4.15), (7.4.16) and (7.4.22); (v) as $k_{rs}(m) \sim 1/m$ for $r+s=4$, one can assume further that $k_{rs}(m) \sim 1/[m^{(r+s-2)/2}]$. With (i)-(v), it is possible to use bivariate

ED expansion for $\rho(E, M)$ and the system parameter that decides the convergence of the expansion is the particle number m ; see [Ko-01, Ko-84, St-87]. The expansion for $\eta(E, M)$ up to order $1/m^2$ follow from Eq. (12) and Table 2 of [Ko-84]. Using these and noting that $\hat{E} = He_1(\hat{E})$ and $\hat{E}^2 - 1 = He_2(\hat{E})$, the traces $\langle\langle (\hat{H})^p \rangle\rangle^{m,M}$, $p = 0, 1, 2$ are given by

$$\begin{aligned}
\langle\langle \hat{H} \rangle\rangle^{m,M} &= \mathcal{D}_{\mathcal{G}}(m, M) \left\{ \frac{k_{12}(m)}{2} He_2(\widehat{M}) + \frac{k_{14}(m)}{24} He_4(\widehat{M}) \right. \\
&\quad \left. + \frac{k_{04}(m)k_{12}(m)}{48} He_6(\widehat{M}) + O\left(\frac{1}{m^{5/2}}\right) \right\}, \\
\langle\langle \hat{H}^2 - 1 \rangle\rangle^{m,M} &= \mathcal{D}_{\mathcal{G}}(m, M) \left\{ \frac{k_{22}(m)}{2} He_2(\widehat{M}) + \frac{[k_{12}(m)]^2}{4} He_4(\widehat{M}) \right. \\
&\quad + \frac{k_{24}(m)}{24} He_4(\widehat{M}) + \frac{k_{14}(m)k_{12}(m)}{24} He_6(\widehat{M}) \\
&\quad + \frac{k_{22}(m)k_{04}(m)}{48} He_6(\widehat{M}) + \frac{k_{04}(m)[k_{12}(m)]^2}{96} He_8(\widehat{M}) \\
&\quad \left. + O\left(\frac{1}{m^3}\right) \right\}, \\
\mathcal{D}(m, M) &= \mathcal{D}_{\mathcal{G}}(m, M) \left\{ He_0(\widehat{M}) + \frac{k_{04}(m)}{24} He_4(\widehat{M}) \right. \\
&\quad \left. + \frac{k_{06}(m)}{720} He_6(\widehat{M}) + \frac{[k_{04}(m)]^2}{1152} He_8(\widehat{M}) + O\left(\frac{1}{m^3}\right) \right\}.
\end{aligned} \tag{7.4.7}$$

Here we have used the results that $\int He_r(\hat{E}) He_s(\hat{E}) \eta_{\mathcal{G}}(\hat{E}) d\hat{E} = r! \delta_{rs}$ and $\widehat{M} = M/\sigma_{J_z}(m)$ with $\sigma_{J_z}^2(m) = \langle J_z^2 \rangle^m$.

Using Eqs. (7.4.6) and (7.4.7) and carrying out some tedious algebra (and also verified using Mathematica) will give the following expansions to order $[J(J+1)]^2$,

$$\begin{aligned}
D(m, J) &\simeq \binom{N}{m} \frac{(2J+1)}{\sqrt{8\pi}\sigma_{J_z}^3(m)} \exp - \frac{(J+1/2)^2}{2\sigma_{J_z}^2(m)} \\
&\quad \times \left[1 + \frac{k_{04}(m)}{24} \left\{ \left[\frac{J(J+1)}{\sigma_{J_z}^2(m)} \right]^2 - 10 \frac{J(J+1)}{\sigma_{J_z}^2(m)} + 15 \right\} \right],
\end{aligned} \tag{7.4.8}$$

$$\begin{aligned}
\langle \hat{H} \rangle^{m,J} &= \frac{E_c(m, J) - E_c(m)}{\sigma(m)} \\
&= \left[\frac{k_{12}(m)}{2} \left(-3 + \frac{1}{4\sigma_{J_z}^2(m)} \right) + \frac{k_{14}(m)}{8} \left(5 - \frac{5}{6\sigma_{J_z}^2(m)} + \frac{1}{48\sigma_{J_z}^4(m)} \right) \right. \\
&\quad \left. + \frac{k_{04}(m)k_{12}(m)}{4} \left(-5 + \frac{5}{4\sigma_{J_z}^2(m)} - \frac{1}{24\sigma_{J_z}^4(m)} \right) \right] \\
&\quad + \frac{J(J+1)}{\sigma_{J_z}^2(m)} \left\{ \frac{k_{12}(m)}{2} + \frac{k_{14}(m)}{12} \left(-5 + \frac{1}{4\sigma_{J_z}^2(m)} \right) \right. \\
&\quad \left. + \frac{k_{04}(m)k_{12}(m)}{4} \left(5 - \frac{1}{3\sigma_{J_z}^2(m)} \right) \right\} \tag{7.4.9}
\end{aligned}$$

$$\begin{aligned}
&\quad + \frac{[J(J+1)]^2}{\sigma_{J_z}^4(m)} \left\{ \frac{k_{14}(m)}{24} - \frac{k_{04}(m)k_{12}(m)}{6} \right\} \\
&\simeq \left[-\frac{3k_{12}(m)}{2} \right] + \frac{k_{12}(m)}{2} \frac{J(J+1)}{\sigma_{J_z}^2(m)} + \left\{ \frac{k_{14}(m)}{24} - \frac{k_{04}(m)k_{12}(m)}{6} \right\} \frac{[J(J+1)]^2}{\sigma_{J_z}^4(m)}, \\
&\frac{\sigma^2(m, J)}{\sigma^2(m)} = \langle \hat{H}^2 \rangle^{m,J} - \left(\langle \hat{H} \rangle^{m,J} \right)^2 \\
&= \left[1 - \frac{3k_{22}(m)}{2} + \frac{3[k_{12}(m)]^2}{2} + \frac{5k_{24}(m)}{8} - \frac{5k_{14}(m)k_{12}(m)}{2} \right. \\
&\quad \left. - \frac{5k_{22}(m)k_{04}(m)}{4} + \frac{15k_{04}(m)[k_{12}(m)]^2}{4} \right] + \left[\frac{J(J+1)}{\sigma_{J_z}^2(m)} + \frac{1}{4\sigma_{J_z}^2(m)} \right] \\
&\quad \left\{ \frac{k_{22}(m)}{2} - [k_{12}(m)]^2 - \frac{5k_{24}(m)}{12} + \frac{5k_{14}(m)k_{12}(m)}{2} - 5k_{04}(m)[k_{12}(m)]^2 \right. \\
&\quad \left. + \frac{5k_{22}(m)k_{04}(m)}{4} \right\} + \left[\frac{J(J+1)}{\sigma_{J_z}^2(m)} + \frac{1}{4\sigma_{J_z}^2(m)} \right]^2 \left\{ \frac{k_{24}(m)}{24} - \frac{k_{14}(m)k_{12}(m)}{3} \right. \\
&\quad \left. - \frac{k_{22}(m)k_{04}(m)}{6} + \frac{5k_{04}(m)[k_{12}(m)]^2}{6} \right\} \tag{7.4.10}
\end{aligned}$$

$$\simeq \left[1 - \frac{3k_{22}(m)}{2} \right] + \left[\frac{k_{22}(m)}{2} \right] \frac{J(J+1)}{\sigma_{J_z}^2(m)} + \left\{ \frac{k_{24}(m)}{24} - \frac{k_{22}(m)k_{04}(m)}{6} \right\} \left[\frac{J(J+1)}{\sigma_{J_z}^2(m)} \right]^2.$$

The last step in Eq. (7.4.9) follows from the assumption that $\sigma_{J_z}^2(m) \gg 1$. Similarly, in the last step in Eq. (7.4.10), assuming that $\sigma_{J_z}^2(m) \gg 1$, we have neglected $1/4\sigma_{J_z}^2(m)$ terms and so also the terms with squares and products of cumulants that are expected to be small. Note that the expansions to order $J(J+1)$ were given before [Ko-02a] and the terms with $[J(J+1)]^2$ are new. From now on, we use the last forms in Eqs. (7.4.9) and (7.4.10) and apply them to $(j)^m$ systems in the present section. To proceed further, we need to define and evaluate the bivariate cumulants $k_{rs}(m)$.

Bivariate cumulants $k_{rs}(m)$ are defined in terms of the bivariate moments $\langle \tilde{H}^r J_z^s \rangle^m$ with $\tilde{H} = H - \langle H \rangle^m$,

$$\begin{aligned} k_{04}(m) &= \frac{\langle J_z^4 \rangle^m}{\sigma_{J_z}^4(m)} - 3, \quad k_{12}(m) = \frac{\langle \tilde{H} J_z^2 \rangle^m}{\sigma(m) \sigma_{J_z}^2(m)}, \\ k_{14}(m) &= \frac{\langle \tilde{H} J_z^4 \rangle^m}{\sigma(m) \sigma_{J_z}^4(m)} - \frac{6 \langle \tilde{H} J_z^2 \rangle^m}{\sigma(m) \sigma_{J_z}^2(m)}, \\ k_{22}(m) &= \frac{\langle \tilde{H}^2 J_z^2 \rangle^m}{\sigma_{J_z}^2(m) \sigma^2(m)} - 1, \\ k_{24}(m) &= \frac{\langle \tilde{H}^2 J_z^4 \rangle^m}{\sigma_{J_z}^4(m) \sigma^2(m)} - \frac{\langle J_z^4 \rangle^m}{\sigma_{J_z}^4(m)} - 6 \frac{\langle \tilde{H}^2 J_z^2 \rangle^m}{\sigma_{J_z}^2(m) \sigma^2(m)} \\ &\quad - 6 \frac{[\langle \tilde{H} J_z^2 \rangle^m]^2}{\sigma_{J_z}^4(m) \sigma^2(m)} + 6. \end{aligned} \tag{7.4.11}$$

Note that, $\sigma^2(m) = \langle \tilde{H}^2 \rangle^m$.

7.4.3 Propagation equations for bivariate cumulants $k_{rs}(m)$ for $(j)^m$ systems

To begin with, let us mention that the tensorial decomposition of the H and J^2 operators with respect to the $U(N)$, $N = 2j + 1$, algebra will be useful for deriving propagation equations for $k_{rs}(m)$. For the single- j shell situation, the H operator is defined by the two-body matrix elements $V_{J_2} = \langle (j)^2 J_2 | H | (j)^2 J_2 \rangle$ with J_2 being even taking

values $0, 2, \dots, 2j - 1$. Using the results in Appendix A, unitary decomposition for the operators H and J^2 are,

$$H = H^{v=0} + H^{v=2};$$

$$H^{v=0} = \frac{\hat{n}(\hat{n}-1)}{2} \bar{V}, \quad \bar{V} = \left(\frac{N}{2} \right)^{-1} \sum_{J_2} (2J_2 + 1) V_{J_2}, \quad (7.4.12)$$

$$H^{v=2} \Longleftrightarrow V_{J_2}^{v=2} = V_{J_2} - \bar{V}.$$

$$J^2 = (J^2)^{v=0} + (J^2)^{v=2};$$

$$(J^2)^{v=0} = \frac{\hat{n}(N-\hat{n})}{N(N-1)} j(j+1)(2j+1), \quad (7.4.13)$$

$$(J^2)^{v=2} \Longleftrightarrow (J^2)_{J_2}^{v=2} = J_2(J_2+1) - (2j-1)(j+1).$$

To proceed further, we write the cumulants defined in Eq. (7.4.11) in terms of $H^{v=2}$ and $(J^2)^{v=2}$. For this purpose, we use the equalities $\langle H^p J_z^2 \rangle^m = \langle H^p J^2 \rangle^m / 3$ and $\langle H^p J_z^4 \rangle^m = \langle H^p (J^2)^2 \rangle^m / 5 - \langle H^p (J^2) \rangle^m / 15$. Then the formulas are,

$$\begin{aligned} k_{12}(m) &= \frac{\langle H^{v=2} (J^2)^{v=2} \rangle^m}{3 \sigma(m) \sigma_{J_z}^2(m)}, \\ k_{14}(m) &= \frac{1}{\sigma(m) \sigma_{J_z}^4(m)} \left\{ \frac{1}{5} \langle (J^2)^{v=2} (J^2)^{v=2} H^{v=2} \rangle^m \right. \\ &\quad \left. - \left[\frac{4}{5} \sigma_{J_z}^2(m) + \frac{1}{15} \right] \langle (J^2)^{v=2} H^{v=2} \rangle^m \right\} \\ &\simeq \frac{1}{24 \sigma_{J_z}^8(m)} \left\{ \frac{1}{5} \langle (J^2)^{v=2} (J^2)^{v=2} H^{v=2} \rangle^m \right. \\ &\quad \left. - \frac{4}{5} \sigma_{J_z}^2(m) \langle (J^2)^{v=2} H^{v=2} \rangle^m \right\}, \end{aligned} \quad (7.4.14)$$

$$\begin{aligned}
k_{22}(m) &= \frac{\langle (H^{v=2})^2 (J^2)^{v=2} \rangle^m}{3\sigma_{J_z}^2(m) \sigma^2(m)}, \\
k_{24}(m) &= \frac{9}{5} - \frac{1}{5\sigma_{J_z}^2(m)} - \frac{\langle J_z^4 \rangle^m}{\sigma_{J_z}^4(m)} + \frac{\langle ((J^2)^{v=2})^2 (H^{v=2})^2 \rangle^m}{5\sigma_{J_z}^4(m) \sigma^2(m)} \\
&\quad - \frac{2[\langle (J^2)^{v=2} H^{v=2} \rangle^m]^2}{3\sigma_{J_z}^4(m) \sigma^2(m)} - \frac{\langle (J^2)^{v=2} (H^{v=2})^2 \rangle^m}{15\sigma_{J_z}^4(m) \sigma^2(m)} \\
&\quad - \frac{4\langle (J^2)^{v=2} (H^{v=2})^2 \rangle^m}{5\sigma_{J_z}^2(m) \sigma^2(m)}.
\end{aligned}$$

Simple trace propagation formulas that follows from the results in Appendix A are as follows,

$$\begin{aligned}
\sigma_{J_z}^2(m) &= \langle J_z^2 \rangle^m = \frac{1}{3} \langle (J^2)^{v=0} \rangle^m = \frac{m(N-m)}{N(N-1)} \frac{1}{3} j(j+1)(2j+1), \\
\langle J_z^4 \rangle^m &= \frac{9}{5} \sigma_{J_z}^4(m) - \frac{1}{5} \sigma_{J_z}^2(m) + \frac{1}{5} \langle (J^2)^{v=2} (J^2)^{v=2} \rangle^m;
\end{aligned} \tag{7.4.15}$$

$$\langle X^{v=2} Y^{v=2} \rangle^m = \frac{m(m-1)(N-m)(N-m-1)}{N(N-1)(N-2)(N-3)} \sum_{J_2} (2J_2+1) X_{J_2}^{v=2} Y_{J_2}^{v=2}.$$

Note that for $\sigma^2(m) = \langle H^{v=2} H^{v=2} \rangle^m$ is given by $X = Y = H$ in last equality in Eq. (7.4.15). Similarly, $\langle H^{v=2} (J^2)^{v=2} \rangle^m$ and $\langle (J^2)^{v=2} (J^2)^{v=2} \rangle^m$ are given by $X = H, Y = J^2$ and $X = Y = J^2$, respectively. From now on, we use the symbols $m^\times = (N-m)$ and $[X]_r = X(X-1)\dots(X-r+1)$, $X = m, N, m^\times$. Then, the propagation equation for $\langle (J^2)^{v=2} (J^2)^{v=2} H^{v=2} \rangle^m$ is [Ko-01],

$$\langle (J^2)^{v=2} (J^2)^{v=2} H^{v=2} \rangle^m = \frac{[m]_3 [m^\times]_3}{[N]_6} A + \left[\frac{[m]_2 [m^\times]_4 + [m]_4 [m^\times]_2}{[N]_6} \right] B, \tag{7.4.16}$$

where

$$\begin{aligned}
A &= \sum_{\Delta} (-1)^\Delta (2\Delta+1)^{-1/2} [\beta^\Delta ((J^2)^{v=2})]^2 \beta^\Delta (H^{v=2}), \\
B &= \langle \langle (J^2)^{v=2} (J^2)^{v=2} H^{v=2} \rangle \rangle^2 = \sum_{J_2} (2J_2+1) \left[(J^2)_{J_2}^{v=2} \right]^2 V_{J_2}^{v=2}.
\end{aligned} \tag{7.4.17}$$

Note that Δ symbol in Eq. (7.4.17) should not be confused with ' Δ ' used in Chapters 2-6. In Eq. (7.4.17), the term A is more complicated involving particle-hole matrix elements β^Δ of the $(J^2)^{\nu=2}$ and $H^{\nu=2}$ operators. The β^Δ for a $\nu = 2$ operator V , in the example of a single j shell is

$$\beta^\Delta(V) = -2 \sum_{J_2 = \text{even}} (-1)^\Delta \sqrt{2\Delta + 1} (2J_2 + 1) \left\{ \begin{matrix} j & j & J_2 \\ j & j & \Delta \end{matrix} \right\} V_{J_2}. \quad (7.4.18)$$

For $j \gg 1$, $(J^2)^{\nu=2}$ can be approximated as

$$(J^2)_{J_2}^{\nu=2} \simeq -2j(j+1)(2j+1) \left\{ \begin{matrix} j & j & J_2 \\ j & j & 1 \end{matrix} \right\}. \quad (7.4.19)$$

Substituting this in Eqs. (7.4.18) will give,

$$\beta^\Delta[(J^2)^{\nu=2}] = 2j(j+1)(2j+1)\sqrt{2\Delta+1} (-1)^\Delta \left[\frac{1}{3} \delta_{\Delta,1} + (-1)^{\Delta+1} \left\{ \begin{matrix} j & j & \Delta \\ j & j & 1 \end{matrix} \right\} \right]. \quad (7.4.20)$$

Now A in Eq. (7.4.16) takes a simple form,

$$\begin{aligned} A &= -8[j(j+1)(2j+1)]^2 \sum_{J_2} (2J_2 + 1) V_{J_2}^{\nu=2} X_{J_2}; \\ X_{J_2} &= \sum_{\Delta} (2\Delta + 1) \left\{ \begin{matrix} j & j & J_2 \\ j & j & \Delta \end{matrix} \right\} \left[\frac{1}{3} \delta_{\Delta,1} + (-1)^{\Delta+1} \left\{ \begin{matrix} j & j & \Delta \\ j & j & 1 \end{matrix} \right\} \right]^2 \\ &= \frac{1}{3} \left\{ \begin{matrix} j & j & J_2 \\ j & j & 1 \end{matrix} \right\} + 2 \left\{ \begin{matrix} j & j & 1 \\ j & j & 1 \end{matrix} \right\} \left\{ \begin{matrix} j & j & J_2 \\ j & j & 1 \end{matrix} \right\} + \left\{ \begin{matrix} j & j & J_2 \\ j & 1 & j \\ 1 & j & j \end{matrix} \right\} \\ &= -\frac{(J^2)_{J_2}^{\nu=2}}{6Y_j} + \frac{(J^2)_{J_2}^{\nu=2}[j(j+1)-1]}{Y_j^2} + \frac{(J^2)_{J_2}^{\nu=2}[(J^2)_{J_2}^{\nu=2}+2]}{4Y_j^2}, \end{aligned} \quad (7.4.21)$$

where $Y_j = j(j+1)(2j+1)$. Above simplifications are obtained using the results given in [Ed-74, Br-94] for angular-momentum recoupling coefficients. Going further, Eq.

(7.4.16) will give the expression for $\langle (J^2)^{\nu=2} (H^{\nu=2})^2 \rangle^m$ with A and B defined by

$$A = \sum_{\Delta} \frac{(-1)^{\Delta}}{(2\Delta + 1)^{\frac{1}{2}}} [\beta^{\Delta}(V^{\nu=2})]^2 \beta^{\Delta}((J^2)^{\nu=2}), \quad (7.4.22)$$

$$B = \sum_{J_2} (2J_2 + 1) (V_{J_2}^{\nu=2})^2 (J^2)_{J_2}^{\nu=2}.$$

Using the expression for β^{Δ} for a $\nu = 2$ operator from Eq. (7.4.18) and the simple formula for $\beta^{\Delta}((J^2)^{\nu=2})$ given by Eq. (7.4.20), the term A in Eq. (7.4.22) simplifies to,

$$A = 8j(j+1)(2j+1) \sum_{J_2, J'_2} (2J_2 + 1)(2J'_2 + 1) V_{J_2}^{\nu=2} V_{J'_2}^{\nu=2} \quad (7.4.23)$$

$$\times \left[\left\{ \begin{matrix} j & j & J_2 \\ j & j & 1 \end{matrix} \right\} \left\{ \begin{matrix} j & j & J'_2 \\ j & j & 1 \end{matrix} \right\} - \left\{ \begin{matrix} J'_2 & j & j \\ j & J_2 & 1 \end{matrix} \right\}^2 \right]$$

$$= \frac{2}{j(j+1)(2j+1)} \left[\sum_{J_2} (2J_2 + 1) V_{J_2}^{\nu=2} (J^2)_{J_2}^{\nu=2} \right]^2 \quad (7.4.24)$$

$$- 2 \sum_{J_2} (2J_2 + 1) (V_{J_2}^{\nu=2})^2 J_2(J_2 + 1).$$

Most complicated is the $k_{24}(m)$ cumulant that involves $\langle (J^2)^{\nu=2} (J^2)^{\nu=2} (H^{\nu=2}) (H^{\nu=2}) \rangle^m$. Equations (69) and (70) in [Wo-86] give a formula for this trace in a complex form. After carrying out the simplification of these equations and correcting errors at many places, it is seen that there will be 9 terms in the propagation equation. Table 7.5 gives the final result. We have verified that the results in Table 7.5 are correct by replacing $(J^2)^{\nu=2}$ with $H^{\nu=2}$ and then comparing with the formulas given in [No-72]. Results that are simple as in Table 7.5 for $k_{24}(m)$ for multi- j shell situation are not yet available and because of this, we have restricted our discussion to single- j shell in this section. For multi- j shell with realistic sp energies, the EGOE(1+2)- J is also called realistic TBRE (RTBRE) [Fl-00].

Table 7.5: Propagation equation for $\langle\langle (J^2)^{v=2} (J^2)^{v=2} H^{v=2} H^{v=2} \rangle\rangle^m$. Column 2 gives the input trace in a symbolic form and the corresponding expressions are given in the footnote. Column 3 gives the corresponding propagators. Multiplying the terms in column 2 with corresponding ones in column 3 and summing gives the propagation formula. Note that $N = 2j + 1$.

term	Input Trace	Propagator
#1	$J^1 H^1 H^1 J^1$	$\binom{N-8}{m-2} + \binom{N-8}{m-6} + 4\binom{N-8}{m-4}$
#2	$J^1 J^2 H^2 H^1$	$2\binom{N-8}{m-4} + \frac{4}{N} \left\{ \binom{N-8}{m-3} + \binom{N-8}{m-5} \right\} - \frac{24}{N} \binom{N-8}{m-4}$
#3	$J^1 H^2 H^2 J^1$	$\binom{N-8}{m-4} + \frac{4}{N} \left\{ \binom{N-8}{m-3} + \binom{N-8}{m-5} \right\} - \frac{8}{N} \binom{N-8}{m-4}$
#4	$J^1 \beta_J^2 \beta_H^2 H^1$	$-4\binom{N-8}{m-3} - 4\binom{N-8}{m-5} + 8\binom{N-8}{m-4}$
#5 ^a	$J^1 \beta_H^2 \beta_H^2 J^1$	$-2\binom{N-8}{m-3} - 2\binom{N-8}{m-5}$
#6 ^a	$H^1 \beta_J^2 \beta_J^2 H^1$	$-2\binom{N-8}{m-3} - 2\binom{N-8}{m-5}$
#7	$\beta_H^1 \beta_H^1 \beta_J^1 \beta_J^1$	$3\binom{N-8}{m-4}$
#8	$\beta_J^1 \beta_J^2 \beta_H^2 \beta_H^1$	$4\binom{N-8}{m-3} + 4\binom{N-8}{m-5} - 8\binom{N-8}{m-4}$
#9 ^a	$\beta_H^1 \beta_J^2 \beta_J^2 \beta_H^1$	$-8\binom{N-8}{m-4}$

$$\#1 = \langle\langle [(J^2)^{v=2}]^2 (H^{v=2})^2 \rangle\rangle^{m=2}, \quad \#2 = \left[\langle\langle (J^2)^{v=2} H^{v=2} \rangle\rangle^{m=2} \right]^2$$

$$\#3 = \langle\langle [(J^2)^{v=2}]^2 \rangle\rangle^{m=2} \langle\langle (H^{v=2})^2 \rangle\rangle^{m=2}$$

$$\#4 = \sum_{\Gamma, \Delta} (2\Gamma + 1) \left\{ \begin{matrix} j & j & \Gamma \\ j & j & \Delta \end{matrix} \right\} (J^2)_{\Gamma}^{v=2} \beta^{\Delta} ((J^2)^{v=2}) \beta^{\Delta} (H^{v=2}) V_{\Gamma}^{v=2}$$

$$\#7 = \sum_{\Delta} \frac{1}{(2\Delta + 1)} [\beta^{\Delta} (H^{v=2})]^2 [\beta^{\Delta} ((J^2)^{v=2})]^2$$

$$\#8 = \sum_{\Delta} \beta^{\Delta} ((J^2)^{v=2}) \beta^{\Delta} (H^{v=2}) \sum_{\Gamma_2, \Gamma_3} (2\Gamma_2 + 1)(2\Gamma_3 + 1) \left\{ \begin{matrix} \Delta & \Gamma_2 & \Gamma_3 \\ j & j & j \end{matrix} \right\}^2 (J^2)_{\Gamma_2}^{v=2} V_{\Gamma_3}^{v=2}$$

^aTerms $J^1 \beta_H^2 \beta_H^2 J^1$ and $H^1 \beta_J^2 \beta_J^2 H^1$ follow from appropriate permutations of $(J^2)^{v=2}$ and $H^{v=2}$ in the $J^1 \beta_J^2 \beta_H^2 H^1$ expression. Similarly $\beta_H^1 \beta_J^2 \beta_J^2 \beta_H^1$ follows by appropriate permutations in the $\beta_J^1 \beta_J^2 \beta_H^2 \beta_H^1$ expression.

7.4.4 Structure of centroids and variances

Centroids $E_c(m, J)$

In the dilute limit with $m \rightarrow \infty$, $N \rightarrow \infty$ and $m/N \rightarrow 0$, the centroids $E_c(M, J)$ given by Eq. (7.4.9) take a simple form. Firstly, the constant term in the expansion for $E_c(M, J)$ is [after simplifying $k_{12}(m)$ and $k_{14}(m)$],

$$E_c(m) - 3\sigma(m) \frac{k_{12}(m)}{2} \simeq \frac{m^2}{N^2} \sum_{J_2} (2J_2 + 1) V_{J_2}. \quad (7.4.25)$$

Similarly, the $J(J+1)$ term is

$$\sigma(m) \frac{k_{12}(m)}{2\sigma_{J_z}^2(m)} \simeq \frac{3}{2[j(j+1)]^2 N^2} \sum_{J_2} (2J_2 + 1) V_{J_2} (J^2)_{J_2}^{v=2}. \quad (7.4.26)$$

More remarkable is that the $[J(J+1)]^2$ term $\frac{\sigma(m)k_{14}(m)}{24\sigma_{J_z}^4(m)} - \frac{\sigma(m)k_{04}(m)k_{12}(m)}{6\sigma_{J_z}^4(m)}$ also takes a simple form. The results in Sec. 7.4.3 will give the expression for the first term as,

$$\begin{aligned} \sigma(m) \frac{k_{14}(m)}{24\sigma_{J_z}^4(m)} &= \sum_{J_2} (2J_2 + 1) V_{J_2}^{v=2} S_{J_2}; \\ S_{J_2} &\simeq \frac{9}{40m^2(N-m)^2 N^2 [j(j+1)]^4} \left\{ 3 \left[(J^2)_{J_2}^{v=2} \right]^2 (N-2m)^2 \right. \\ &\quad \left. - 4(J^2)_{J_2}^{v=2} j(j+1) [2N^2 - 2Nm + 2m^2] \right\}. \end{aligned} \quad (7.4.27)$$

Similarly, we can write the expression for $\frac{\sigma(m)k_{04}(m)k_{12}(m)}{6\sigma_{J_z}^4(m)}$ and in the dilute limit this reduces exactly to the second piece in the expression for S_{J_2} in Eq. (7.4.27). Therefore, in the dilute limit, the term multiplying $[J(J+1)]^2$ in the $E_c(m, J)$ expansion is,

$$\begin{aligned} \frac{\sigma(m)}{\sigma_{J_z}^4(m)} \left\{ \frac{k_{14}(m)}{24} - \frac{k_{04}(m)k_{12}(m)}{6} \right\} &= \sum_{J_2} (2J_2 + 1) V_{J_2}^{v=2} R_{J_2}; \\ R_{J_2} &\sim \frac{9(N-2m)^2}{40m^2(N-m)^2 N^2 [j(j+1)]^4} \left\{ 3 [J_2(J_2+1) - 2j(j+1)]^2 \right\}. \end{aligned} \quad (7.4.28)$$

It is already pointed out in [Ko-02a] that the constant term and the $J(J+1)$ term as given by Eqs. (7.4.25) and (7.4.26) are same as those derived by Mulhall et al [Mu-

00, Mu-02] using statistical mechanics approach that is completely different from the present moment method approach. For EGOE(2)- J ensemble, Eqs. (7.4.25)-(7.4.28) will give the distribution of the centroids over the ensemble as discussed in [Mu-02]. More remarkable is that the $[J(J+1)]^2$ term given by Eq. (7.4.28) is also very close to the formula given by Mulhall [Mu-02]. These results confirm that the approximations used in [Mu-00, Mu-02] are equivalent to the proposition that $\rho(E, M)$ is a Edgeworth corrected bivariate Gaussian as assumed in the present approach. The equivalence of Mulhall et al approach with the moment method approach in the dilute limit is further substantiated by the expansion for fixed- M occupancies; the results are given in Appendix I.

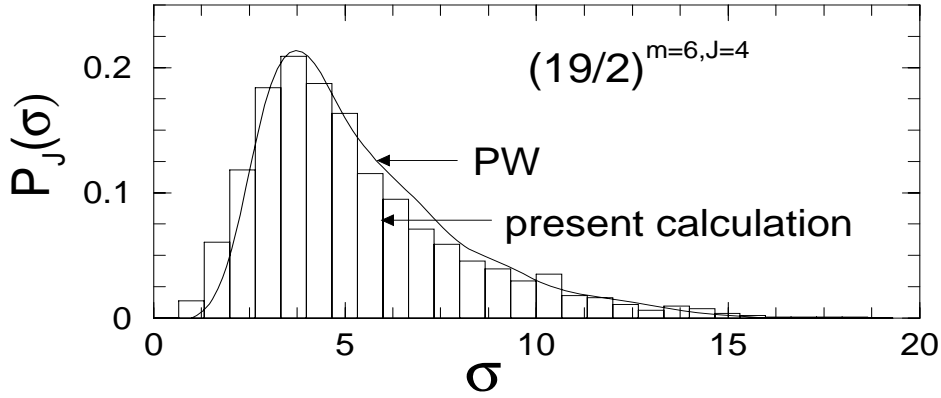


Figure 7.1: Probability distribution for widths σ for EGOE(2)- J ensemble; see text for details.

Variances $\sigma^2(m, J)$

In the dilute limit, simplifying $k_{22}(m)$ and $\sigma^2(m)$ will give

$$\begin{aligned} \sigma^2(m, J) = & \frac{m^2}{N^2} \sum_{J_2} (2J_2 + 1) (V_{J_2}^{v=2})^2 \\ & + \frac{3 J(J+1)}{2 N^2 [j(j+1)]^2} \sum_{J_2} (2J_2 + 1) (V_{J_2}^{v=2})^2 (J^2)^{v=2}. \end{aligned} \quad (7.4.29)$$

However to add $[J(J+1)]^2$ correction, we need to simplify $k_{24}(m)$ and this is quite cumbersome. A quantity of interest, as pointed out by Papenbrock and Weidenmüller [Pa-04] (PW) is the probability distribution for the spectral widths $\sigma = \{\langle H^2 \rangle^{m, J}\}^{1/2} = [\sigma^2(m, J) + E_c^2(m, J)]^{1/2}$ over the EGOE(2)- J ensemble. To compare with PW results, we have generated a EGOE(2)- J ensemble for $(\frac{19}{2})^{m=6}$ system with 2500 members, i.e

we have used 2500 sets of V_{J_2} 's. Using the formalism described in Secs. 7.4.2 and 7.4.3 we have calculated the bivariate cumulants $k_{rs}(m)$. For our example $\sigma_{J_z}(m) = 12.124$ and $k_{04}(m) = -0.229$. The ensemble averaged cumulants $\overline{k_{12}(m)}$, $\overline{k_{14}(m)} \sim 0$ as expected. However $\overline{k_{22}(m)} = -0.053$ and $\overline{k_{24}(m)} = -0.114$. With these, it is clear that the expansions to order $[J(J+1)]^2$ are needed. Equation (7.4.10) is found to be good for $J < 30$. We have calculated $\langle H^2 \rangle^{m,J}$ for each member of the ensemble and then $P_J(\sigma)$ vs σ histograms are constructed for various J values. Results for $J = 4$ are shown in Fig. 7.1. The calculated histogram is in good agreement with the exact curve given by PW [Pa-04]; in [Pa-04] a completely different formalism is used. Though not shown in Fig. 7.1, we have noticed that for $J = 0$, the widths given by the exact results (they are reported in [Pa-04]) are somewhat larger than the numbers given by the present formalism. This could be because $J = 0$ is at one extreme end of the Edgeworth expansion and therefore, the truncation to $1/m^2$ terms may not be adequate.

7.5 Summary

To summarize, by extending the binary correlation approximation method for two different operators and for traces over two-orbit configurations, we have derived formulas for γ_1 and γ_2 parameters for EGOE(1+2)- π ensemble. Note that EGOE(1+2)- π is defined by the embedding algebra $U(N) \supset U(N_+) \oplus U(N_-)$ with the Hamiltonian breaking the symmetry in a particular way as discussed in Chapter 5. In addition, we have derived formula for the fourth order trace defining correlation coefficient of the bivariate transition strength of the transition operator relevant for $0\nu\text{-}\beta\beta$ decay. We have also derived the formulas for the fourth order cumulants in order to establish bivariate Gaussian form of the transition strength densities. Here also the embedding algebra is $U(N) \supset U(N_p) \oplus U(N_n)$ with the Hamiltonian preserving the symmetry and the transition operator breaking the symmetry in a particular way. Going further, we have considered an application to EGOE(2)- J for fermions in a single- j shell. Here the embedding algebra is $U(2j+1) \supset SO_J(3)$. Expansions to order $[J(J+1)]^2$ for energy centroids $E_c(m, J)$ and spectral variances $\sigma^2(m, J)$ are obtained. Formulas are derived for fixed- m bivariate cumulants and they are used to show the expansion to order $[J(J+1)]^2$ explain the structure of fixed- J centroids and variances. These results are important in the subject of regular structures generated by random interactions.

Chapter 8

Hamiltonian Matrix Structure

8.1 Introduction

In Chapters 2-7, our focus is in analyzing extended embedded ensembles for isolated finite interacting quantum systems. As discussed in Chapter 1, the classical GOE is universally regarded as the model for fluctuation properties of generic chaotic quantum systems. However for a complete statistical description of systems such as nuclei and atoms, as the interactions for these systems are two-body, as already emphasized in the previous chapters, EGOE is expected to be most appropriate. On the other hand, banded random matrix ensembles (BRME) [Wi-55, Wi-57, Ca-90, Ca-93, Fy-91, Fy-92] are also employed by some groups. One can infer the appropriateness of GOE, BRME or EGOE representation, for describing statistical properties, by analyzing eigenvalue densities, strength functions, chaos measures such as information entropy, transition strength distributions, expectation values of operators, level and strength fluctuations and so on [Br-81, Ko-01, Fl-99, Go-01, Go-04]. However, an important question is: is it possible to infer the random matrix structure by directly examining the Hamiltonian matrix itself.

Some of the earlier studies of GOE and EGOE structure of nuclear shell-model Hamiltonian matrices were due to Gervois [Ge-68], French and Wong [Fr-70, Fr-71a, Wo-72] and Bohigas and Flores [Bo-71]. Similarly, for atoms, they were due to Rosenzweig and Porter [Ro-60] and Parikh [Pa-78a]. In many of these studies, the matrix dimensions are quite small (in most cases they are 10-50 dimensional). More recently (in the 90's) there has been renewed interest in examining Hamiltonian ma-

trices in nuclear and atomic examples as it is now possible to construct much larger size matrices and more importantly, because random matrix theory has been well established in the 80's. For example, characteristic features, in terms of GOE and EGOE, of the shell-model Hamiltonian matrix of ^{22}Na , $(J^\pi T) = (2^+ 0)$ with dimension $d = 307$, were studied by French et al [Fr-88, To-86]. Similarly, Zelevinsky et al analyzed GOE and BRME structure of ^{28}Si , $(J^\pi T) = (2^+ 0)$ and $(0^+ 0)$ shell-model Hamiltonian matrices, with $d = 3276$ and 839 , respectively [Ze-96]. On the other hand, Flambaum et al [Fl-94, Gr-95] using ls coupling studied, in terms of GOE and BRME, the structure of Hamiltonian matrices of CeI, $J^\pi = 4^\pm$, with dimension $d = 260$ for odd parity and 276 for even parity. Similarly, both ls and jj coupling schemes were investigated for Hamiltonian matrices of CeI, $J^\pi = 4^\pm$; PrI, $J^\pi = 11/2^\pm$, with dimension for PrI being $d = 887$ and 737 for odd and even parities, respectively, by Cummings and collaborators [Cu-01]. Going beyond these studies, our purpose in this chapter is to carry out a comprehensive analysis of the structure of nuclear Hamiltonian matrices, with two shell-model examples (^{22}Na , ^{24}Mg), by employing all the measures, for GOE, BRME and EGOE, that are introduced in the literature at various times. For comparison, we have employed SmI atomic example, as this appears to be, from the past analysis [An-03, An-05], the best atomic example for EGOE. All the results presented in this chapter are published in [Ma-10c].

8.2 Matrix Structure by Visualization

With the advances in computer graphics, it is now possible to visualize the coarse grained structure of the H matrices. Given the many-particle matrix elements H_{ij} (in $J^\pi T$ basis for nuclei and in J^π basis for atoms) one can make a plot of the squares of the matrix elements H_{ij}^2 as a function of (i, j) . In general, there are many choices for the indices i . Most commonly employed one for i are the basis states indices defined by the ordering of the basis states as used in the shell-model codes. Note that the Hamiltonian operator is one plus two body, i.e., $H = h(1) + V(2)$ and the basis states used for constructing the H matrix are the eigenstates of the one-body part $[h(1)]$ of H . This exercise has been carried out: (i) for lanthanide atoms CeI and PrI by Flambaum et al [Fl-94] and Cummings et al [Cu-01]; (ii) for the lanthanide atoms NdI, PmI and SmI by Angom and Kota [An-05a]; (iii) for ^{28}Si nucleus by Zelevinsky et al [Ze-96].

Alternatively it is also possible to plot the same as a function of the basis state energies $e_i = H_{ii}$. Physically the basis states indices do not carry any significant information. However the basis state energies e_i 's give the location of the corresponding strength functions [see Eq. (8.4.2) ahead] and hence they are more meaningful. This exercise has been carried out for the lanthanide atoms NdI, PmI and SmI by Angom and Kota [An-05]. Following this, for visualization we plot H_{ij} as a function of (e_i, e_j) .

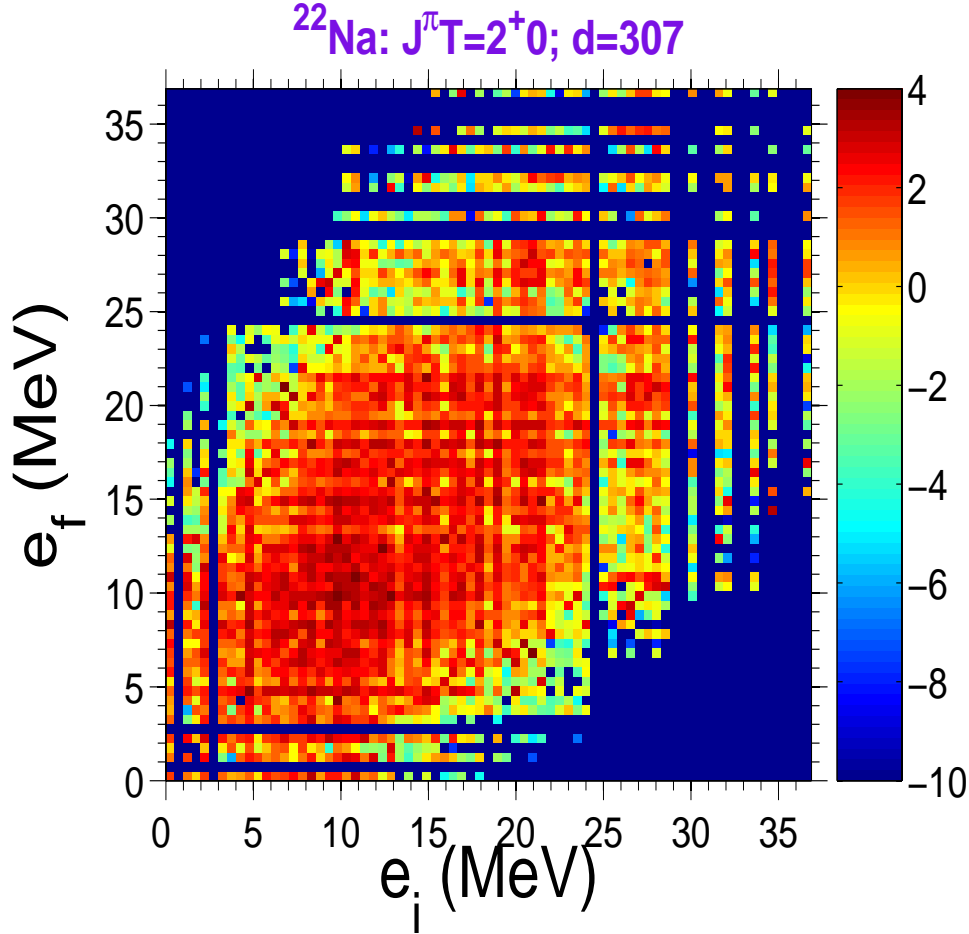


Figure 8.1: Intensity plot showing natural logarithm of the squares of the off-diagonal matrix elements $|\langle f | H | i \rangle|^2$ (whose value is determined by the color with scale as indicated in the figure) as a function of the single-particle basis state energies $e_i = \langle i | H | i \rangle$ and $e_f = \langle f | H | f \rangle$ for ^{22}Na nucleus. Note that diagonal matrix elements $\langle i | H | i \rangle$ are put to zero in calculating $\sum_{i,f} |\langle f | H | i \rangle|^2$ in a given bin. Bin-size is 0.5×0.5 . All matrix elements are in MeV units and d stands for the matrix dimension. Calculation used Kuo interaction with ^{17}O sp energies; see [Ko-98] for details.

We show in Figs. 8.1 and 8.2 for ^{22}Na ($J^\pi T = 2^+ 0$, $d = 307$) and ^{24}Mg ($J^\pi T = 0^+ 0$, $d = 325$) nuclei, respectively, the plot of squares of matrix elements H_{kl}^2 , by averaging over an area in the $e_k - e_l$ plane, as a function of the basis state energies (e_k, e_l) . For

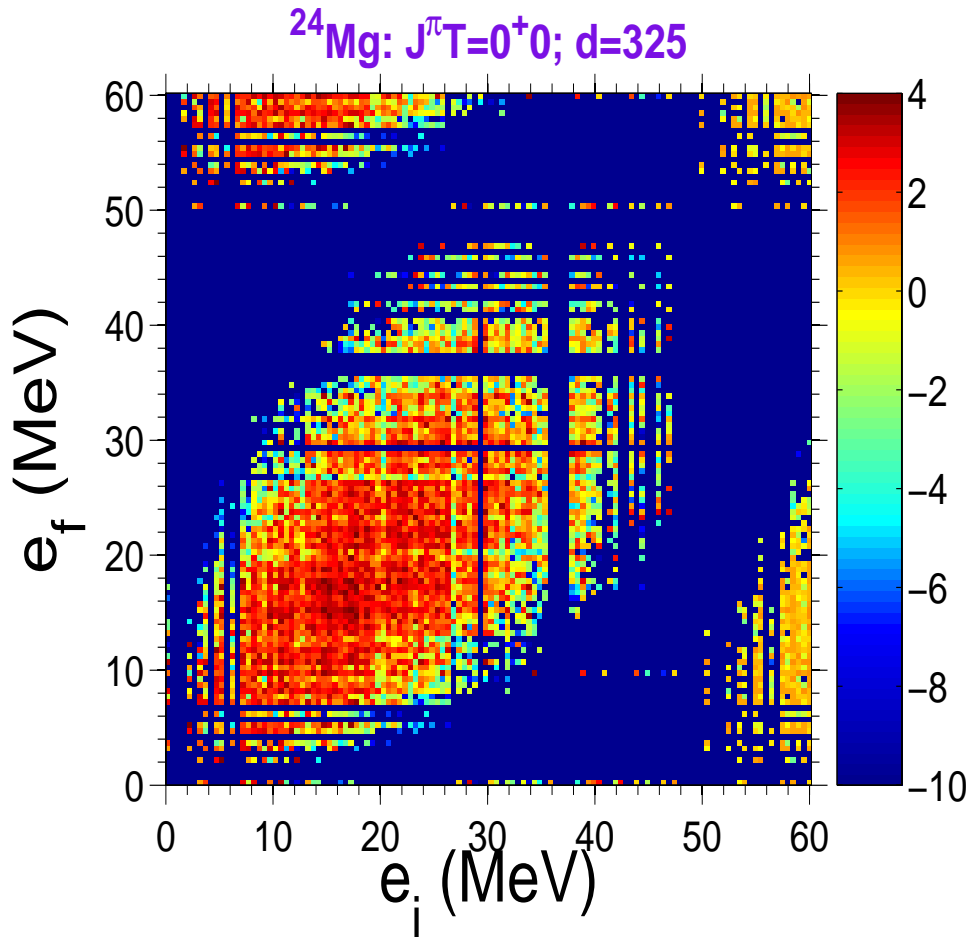


Figure 8.2: Same as Fig. 8.1 but for ^{24}Mg . Bin-size is 0.5×0.5 . All matrix elements are in MeV units. Calculation used Kuo interaction with ^{17}O sp energies; see [Ko-02] for details.

details of the nuclear shell-model calculations for ^{22}Na and ^{24}Mg see Refs. [Ko-98] and [Ko-02], respectively. In the plots, we employ a color code for better visualization. Similarly, in Fig. 8.3, H matrix plot for SmI ($J^\pi = 4^+$, $d = 7325$) atom is shown. Only the first 6300 basis states are taken into consideration in the plot as discussed in Ref. [An-05] and unlike in [An-05], we have used a color code for the plot for better visualization. For ^{22}Na and ^{24}Mg examples, the matrix is more spread compared to that for SmI . This is because, unlike in SmI example (also in many other atomic examples as discussed in [An-05]), in the nuclear shell-model all excitations within the model space are taken into account. Figs. 8.1 and 8.2 show a sparse, band-like structure with block structure within the band. As seen from Fig. 8.3 for SmI H matrix, there are prominent diagonal blocks and streaks of large matrix elements parallel to the diagonal but far away from the diagonal. Also, there is a sparse, band like structure

with block structures within the bands. It is seen from Figs. 8.1, 8.2 and 8.3 that, in general, strictly speaking the H matrices are neither GOE nor banded. Also, from the visualization in Figs. 8.1, 8.2 and 8.3, it is not possible to infer the two-body selection rules which form the basis for EGOE description.

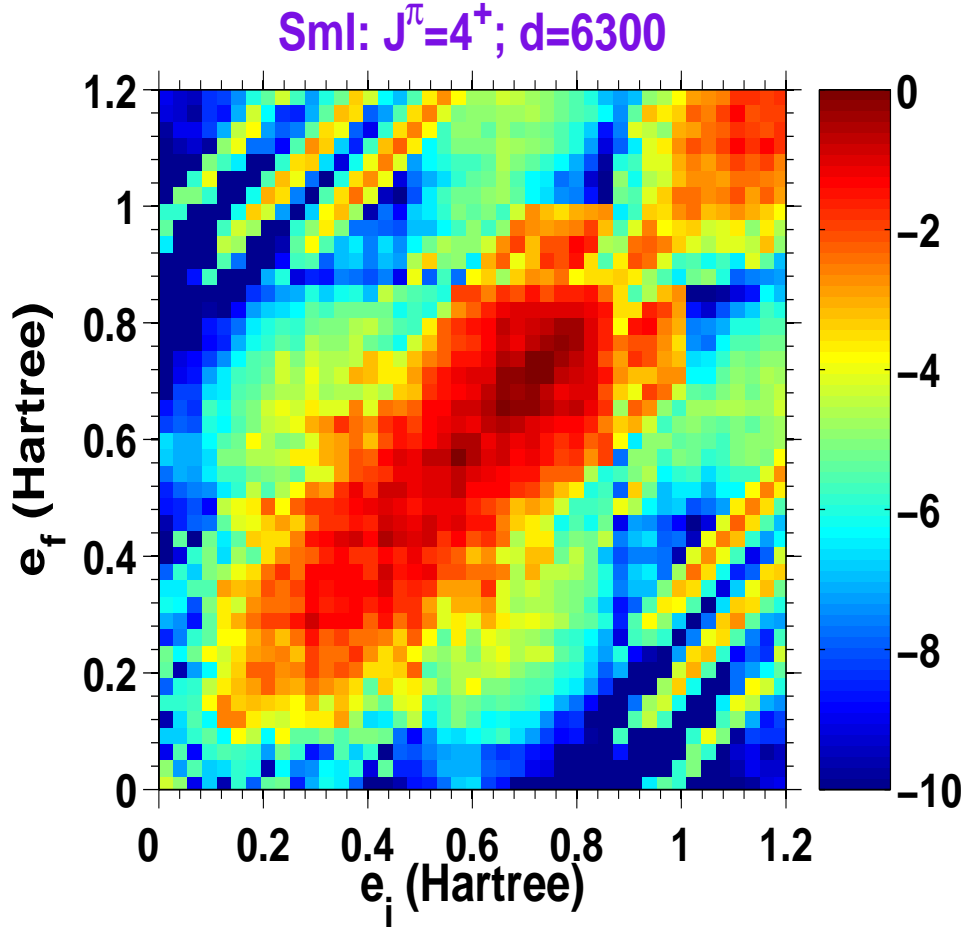


Figure 8.3: Same as Fig. 8.1 but for Sml. The bin-size used is 0.03×0.03 . The matrix construction was discussed in [An-05] and these results are used to construct the color plot. Note that all the matrix elements are in Hartree units.

In order to bring out the two-body selection rules clearly, we consider the following representation. In the nuclear shell-model, for m fermions distributed over r subshells with total angular momentum j_l , $l = 1, 2, \dots, r$, the many-particle states are labeled by the spherical configurations $\mathbf{m} = (m_1, m_2, \dots, m_r)$, total angular momentum J , isospin T and the multiplicity label α . Note that $m = \sum_{i=1}^r m_i$. The m -particle basis states $|\mathbf{m}\alpha JT\rangle$ can be ordered according to the \mathbf{m} 's. Then the H matrix will contain diagonal blocks which couple the states within same spherical configuration and off-

diagonal blocks which couple states with different spherical configurations. As the interaction is two-body in nature, there will be only two types of off-diagonal blocks containing non-zero matrix elements which can mix configurations differing in position of one or two particles. All other off-diagonal blocks will contain zero matrix elements. For visual demonstration of this result, we have shown in Chapter 1 in Fig. 1.3, a plot of the H matrix for the ^{24}Mg example displaying the structure due to the two-body selection rules. For this nucleus, there are 8 valence nucleons occupying the three spherical orbits ($1d_{5/2}$, $1d_{3/2}$, $2s_{1/2}$). Therefore the spherical configurations are (m_1, m_2, m_3) with m_1 number of nucleons in $1d_{5/2}$ orbit, m_2 in $1d_{3/2}$ orbit and m_3 in $2s_{1/2}$ orbit. There are 33 configurations generating the 325 dimensional ($J^\pi T = 0^+0$) H matrix. Their dimensions are 35, 34, 28, 27, 23, 20, 19, 15^2 , 14, 12, 10, 9^2 , 7^2 , 5, 4^4 , 3, 2^6 and 1^5 ; here d^n means there are n number of configurations with dimension d . The configurations are ordered such that the block matrices start from the maximum size (35×35) and go to the minimum (1×1). Figure 1.3 clearly shows the diagonal blocks and the off-diagonal blocks that involve change of occupancy of one and two nucleons, respectively. The regions that correspond to all other off-diagonal blocks are forbidden by the two-body selection rules. A similar figure was given earlier in [Pa-05] for ^{28}Si with $(J^\pi T) = (0^+0)$. Although Fig. 1.3 brings out clearly the structure due to two-body selection rules, it will not give any further insight into the EGOE structure of the matrix. Therefore, for a quantitative understanding of GOE, BRME and EGOE structures of the matrices, we employ various measures introduced in the literature for the structure of these ensembles. Now we will turn to this analysis.

8.3 Analysis in Terms of GOE and BRME

Hamiltonian matrices, prior to the actual diagonalization, are analyzed for the nuclear and atomic examples using measures defining GOE and BRME. To ascertain the GOE character, the distribution of off-diagonal elements is studied. As discussed in Sec. 8.2, the 3D matrix plots show a banded structure. In order to quantify the banded structure, we calculate the bandwidth and the sparsity parameters.

8.3.1 GOE structure: distribution of the off-diagonal matrix elements

Figure 8.4 shows the probability densities $P(x)$ for the off-diagonal matrix elements $x = \tilde{H}_{kl} = H_{kl}$, $k \neq l$ for ^{22}Na , ^{24}Mg and SmI examples. Figure shows that there are large number of small matrix elements and almost half of these are zeroes. This also implies the leading role of the diagonal matrix elements in forming the spectrum which we will discuss in detail in Sec. 8.4. For GOE, $P(x)$ should be a Gaussian. However, for large \tilde{H}_{kl} , it was found that the distribution $P(x)$ is well described by the Porter-Thomas ($P - T$) distribution [Fl-94],

$$P_{P-T}(x) = \frac{1}{2\sqrt{\pi w |x|}} \exp\left(-\frac{|x|}{w}\right); \quad x = \tilde{H}_{kl}, \quad w = \sqrt{\tilde{H}_{kl}^2}. \quad (8.3.1)$$

But, the agreement is not good when $\tilde{H}_{kl} \sim 0$. A better proposition is to use a generalized $P - T$ distribution as suggested first by Zelevinsky et al [Ze-96],

$$P_{\kappa}(x) = \frac{1}{2} [(2x_0)^{\kappa+1} \Gamma(\kappa+1)]^{-1} |x|^{\kappa} \exp\left(-\frac{|x|}{2x_0}\right). \quad (8.3.2)$$

Note that $x_0 = w/2(\kappa+1)$ and w is given in Eq. (8.3.1). Equation (8.3.2) is found to explain the distribution of the off-diagonal elements in the nuclear examples considered in [Ze-96]. Our examples substantiate this further as discussed below. Note that $\kappa = -1/2$ in Eq. (8.3.2) will give Eq. (8.3.1).

For ^{22}Na , ^{24}Mg and SmI examples that correspond to Figs. 8.1, 8.2, and 8.3, respectively, we have carried out fits to Eq. (8.3.2) with $\kappa = 0, -1/2, -1$ and -2 and found that there is good agreement for $\kappa = -1$ but not for the other values. The fits with $\kappa = -1$ are shown in Fig. 8.4 as continuous curves. In the fits to Eq. (8.3.2), a small region around $x = 0$ is not considered as $P_{\kappa}(x)$ will not be regular at $x = 0$ for $\kappa \leq -1$. Note that the deviations are larger for SmI example as compared to the nuclear examples. Therefore, our two nuclear examples (to some extent, even the atomic example) are in conformity with the conclusion of Zelevinsky et al. They state [Ze-96]: *Eq. (8.3.2) implies that the normally distributed quantities in the realistic cases are not the off-diagonal matrix elements themselves as would be the case in canonical ran-*

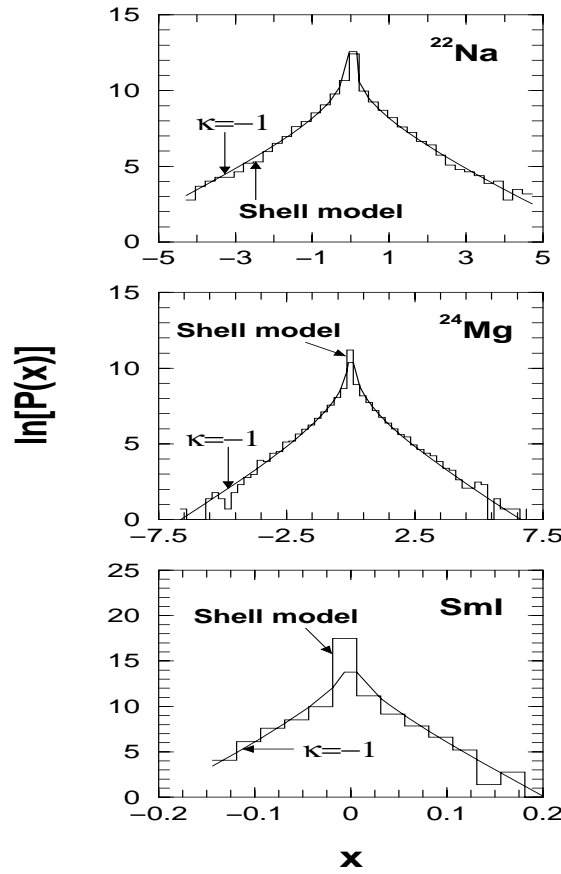


Figure 8.4: Plot showing distribution $P(x)$ of the off-diagonal matrix elements for ^{22}Na , ^{24}Mg and SmI. Note that $P(x)$ gives number of $x = \tilde{H}_{kl}$ in a given energy bin. The bin-size in the figures is 0.25 for ^{22}Na and ^{24}Mg and 0.025 for SmI. In the figure, exact results are shown as histograms and the best fits $P_{\kappa=-1}(x)$ are shown as continuous curves. The function $P(x)$ is normalized to $d(d-1)$, the number of off-diagonal matrix elements. Finally, note that the plots are for $\ln[P(x)]$ vs x . The units for x are MeV for ^{22}Na and ^{24}Mg and Hartree for SmI.

dom matrix ensembles but rather some quantities resembling square roots of them. As they have argued, it is possible that the multipole-multipole form of the nuclear interactions could be the physical reason for this. Hence, it is clear that GOE is not an appropriate representation for the nuclear (also atomic) Hamiltonian matrices.

8.3.2 BRME structure: bandwidths and sparsity

As seen from Figs. 8.1, 8.2 and 8.3, the H matrices have a band-like structure. We calculate a measure for sparsity and also the energy bandwidths for testing the BRME representation for the nuclear and atomic Hamiltonian examples.

Gribankina et al [Gr-95] and Cummings et al [Cu-01] defined the sparsity S as a function of Δ , the difference in the indices of the basis states connected by the Hamil-

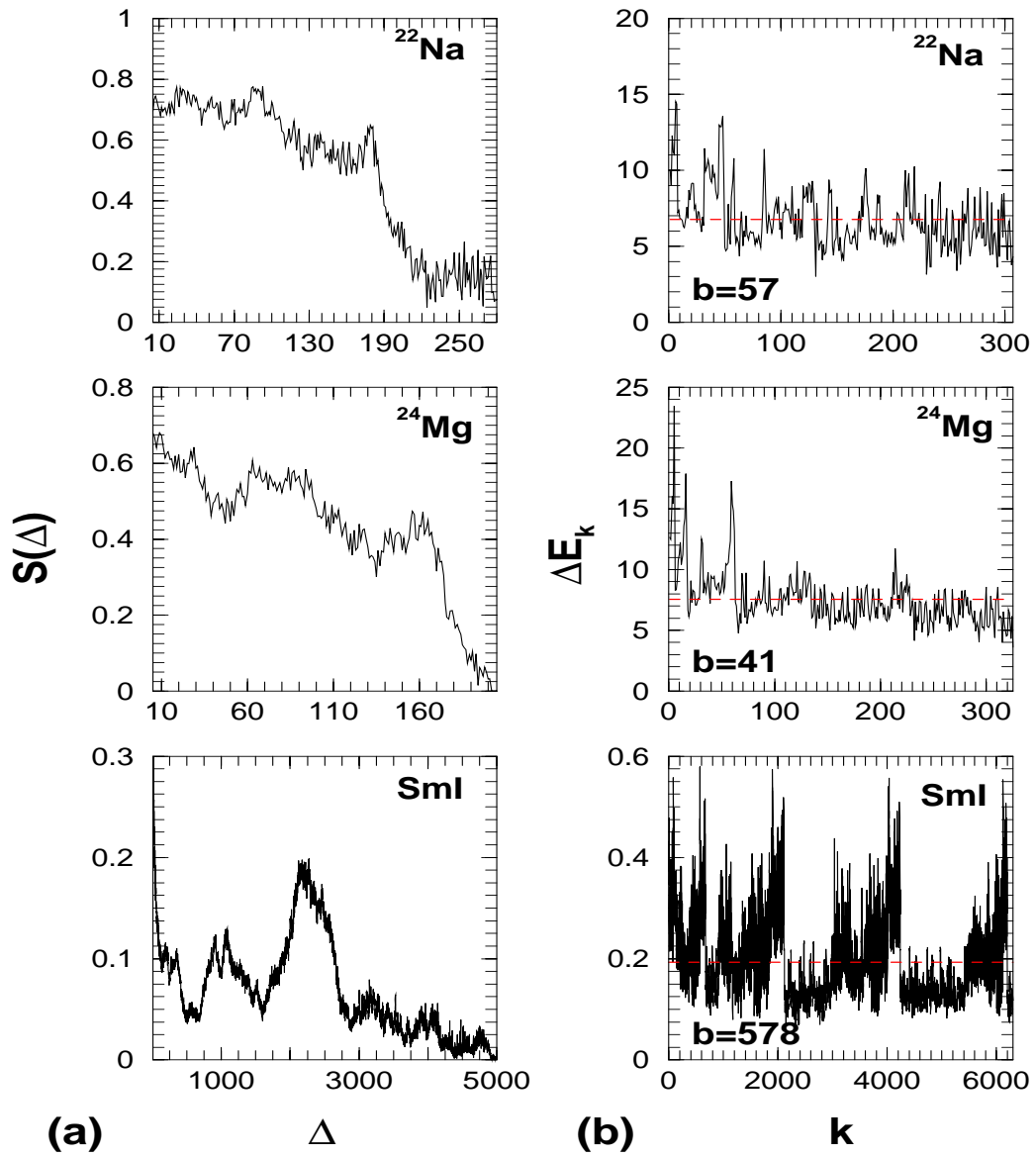


Figure 8.5: (a) Sparsity $S(\Delta)$ defined by Eq. (8.3.3) as a function of $\Delta = |k - l|$ for ^{22}Na , ^{24}Mg and SmI matrices. Results are shown for $\Delta \geq 5$. Note that for calculating sparsity, all the matrix elements whose absolute value is $\geq 10^{-5}$ and 10^{-8} , respectively for the nuclear and atomic examples are taken as non-zero. (b) Energy bandwidths ΔE_k defined by Eq. (8.3.4) as a function of state index k along with mean values of ΔE_k (dashed lines) for ^{22}Na , ^{24}Mg and SmI matrices. The units for ΔE_k are MeV for ^{22}Na and ^{24}Mg and Hartree for SmI . The values of the bandwidths b are shown in the figures.

tonian, as a measure for band-like structure. The definition of S is,

$$S(\Delta) = \frac{\text{number of } |H_{kl}| \neq 0}{\text{number of all } H_{kl}}, \quad |k - l| = \Delta. \quad (8.3.3)$$

For a BRME of bandwidth b , the sparsity $S = 1$ for $\Delta \leq b$ and zero for $\Delta > b$, thus it is a step function. Figure 8.5(a) shows the results for $S(\Delta)$ for the three examples ^{22}Na ,

^{24}Mg and SmI . In the nuclear examples, $S(\Delta)$ essentially decreases as a function of Δ with approximate linear dependence on Δ up to $\Delta \sim 150$ and then falls sharply to zero. However, there are sizeable fluctuations in S as a function of Δ . On the other hand, for SmI , the structure is quite different with large fluctuations and a peak at $\Delta \sim 2250$. The latter may be due to the large off-diagonal streaks seen in Fig. 8.3. Thus, $S(\Delta)$ shows clear deviation from band-like structure in all the examples. This is further substantiated by the energy bandwidths for the basis states and we will turn to this now.

Energy bandwidth b gives the energy interval in which the basis states are strongly mixed. The energy bandwidths ΔE_k for each basis state k are defined as [Fe-91],

$$\Delta E_k^2 = \frac{\sum_l (H_{kk} - H_{ll})^2 |H_{kl}|^2}{\sum_{l \neq k} |H_{kl}|^2}. \quad (8.3.4)$$

In Fig. 8.5(b) we show the results for ΔE_k for the ^{22}Na , ^{24}Mg and SmI examples. The value of the average bandwidth b is given as the ratio of the mean value of ΔE_k and the mean level spacing of the unperturbed energy levels D , i.e., $b = \overline{\Delta E_k} / D$; in general b can be energy dependent as D can be defined as the local mean spacing of the energy levels. The values of b are given in Fig. 8.5(b) and for all the three examples, b is smaller than the matrix dimension d by a factor of ~ 4 . The number b can also be calculated by fitting the mean squared matrix elements to the simple exponential ansatz [Fy-91, Fy-92],

$$\langle H_{kl}^2 \rangle_{|k-l|=\Delta} = H_0^2 \exp\left(-\frac{\Delta}{b}\right). \quad (8.3.5)$$

The values obtained using Eq. (8.3.5) are almost same as those obtained using Eq. (8.3.4). Significant observation from the figures is as follows. For a BRME, the bandwidth ΔE_k should be independent of k . However, there are significant fluctuations in the energy bandwidths in the nuclear examples and quite large fluctuations in SmI example. Note that it is impossible to reach a banded form even by reordering the basis states and this is due to the two-body selection rules. By combining the results for sparsity $S(\Delta)$ and the energy bandwidths ΔE_k shown in Fig. 8.5, we can conclude that BRME is not a good representation for the H matrices.

8.4 Analysis Using Measures for EGOE Structure

Going further, we analyze three measures for quantifying the EGOE structure of the H matrices for the two nuclear examples and the one atomic example in the present section.

8.4.1 Correlations between diagonal matrix elements and eigenvalues

Large number of numerical calculations in the past in the context of statistical nuclear spectroscopy have clearly indicated [Fr-83, Ko-89] that the joint probability distribution $\rho(E, e_k)$ of the diagonal matrix elements e_k and eigenvalues E is a bivariate Gaussian for EGOE. Therefore the marginal densities $\rho(E)$ and $\rho(e_k)$ will be close to Gaussians with same centroids but different widths. In addition, the widths of the conditional densities $\rho(E|e_k)$ will be independent of e_k . These results were used to derive a formula for the chaos measures, the number of principal components and information entropy in wavefunctions for embedded ensembles [Ko-01a]. The close to Gaussian form of $\rho(E)$ and $\rho(e_k)$ imply that the eigenvalues E and the diagonal elements of the H matrix (or equivalently the basis state energies) will be correlated. Flambaum et al examined, for CeI, eigenvalue spectrum vs the spectrum generated by e_k [Fl-94]. They found a close correlation between the two spectra.

There is recent interest in the topic of correlations between eigenvalues and diagonal matrix elements and several examples from nuclei and also random matrices have been discussed in [Sh-08, Yo-09a]. We show in Figs. 8.6 and 8.7, density of eigenvalues and density of diagonal matrix elements for the Hamiltonian matrices of ^{22}Na , ^{24}Mg and SmI. The distributions are compared with the Gaussian form $\rho_{\mathcal{G}}(\hat{x})$ and the Edgeworth (ED) corrected Gaussian form $\rho_{ED}(\hat{x})$; see Eq.(2.3.2) for definitions. Here, $\hat{x} = (x - x_c)/\sigma$ where x_c is the centroid and σ is the width of the distribution of x . It is clearly seen that the eigenvalue distributions for the two nuclear examples are quite close to $\rho_{\mathcal{G}}(\hat{x})$ while the densities of the diagonal matrix elements are, with some deviations, close to $\rho_{ED}(\hat{x})$. However, there are stronger deviations from $\rho_{ED}(\hat{x})$ for the SmI example, both for the eigenvalue density and the density of the diagonal elements. Here, the eigenvalue density has a secondary peak and the density of diagonal

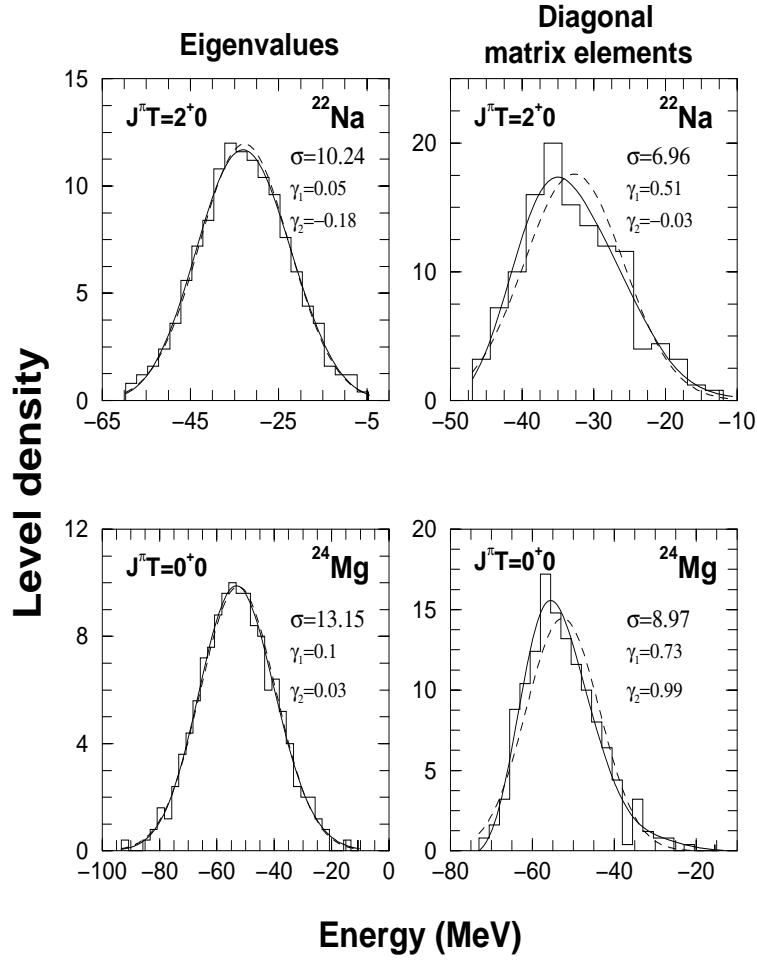


Figure 8.6: Plot showing density of eigenvalues and density of diagonal matrix elements for the Hamiltonian matrices of ^{22}Na and ^{24}Mg . Values of the widths σ , skewness γ_1 and excess γ_2 are given in the figures. The units for σ are MeV. The centroid $E_c = -32.77$ MeV for ^{22}Na and -52.59 MeV for ^{24}Mg . Histograms are the exact results with bin size 2.5 MeV for all the examples. The dashed curves are the Gaussians with centroid E_c given above and width σ whose value is given in the figure. Similarly continuous curves are Edgeworth corrected Gaussians defined in Eq. (2.3.2).

matrix elements displays a stronger bimodal form. Results in Fig. 8.6 reconfirm that in the nuclear examples, the eigenvalues and the diagonal matrix elements of the H matrix are highly correlated and their distributions are close to Gaussian forms. However, there are stronger deviations from this behavior for the SmI example.

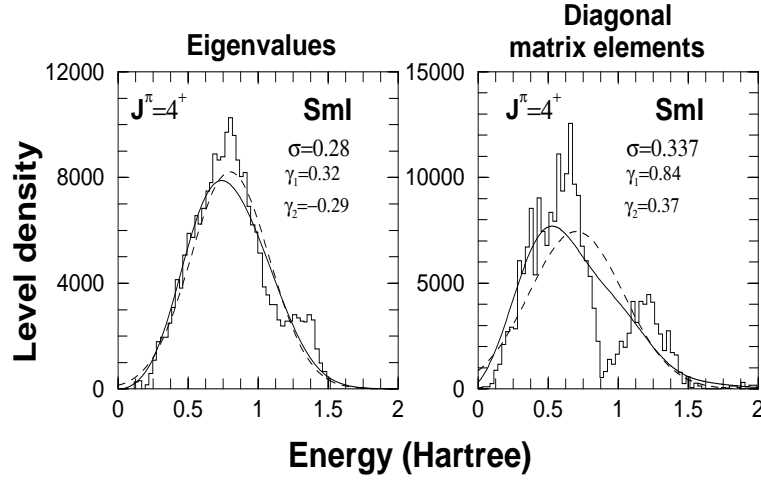


Figure 8.7: Same as Fig. 8.6 but for Sml matrix. The units for σ are Hartree. The centroid is $E_c = 0.7$ Hartree (all energies are given with respect to the lowest energy). Histograms are the exact results with bin size 0.028 Hartree. The eigenvalue density for Sml is constructed by scaling appropriately the data taken from Fig. 3 in [An-05].

8.4.2 Fluctuations in the basis states spreading widths

Going beyond the diagonal matrix elements, it is also useful to consider the basis state widths $\sigma(k)$ where

$$\sigma^2(k) = \langle k | H^2 | k \rangle - e_k^2 = \sum_{l \neq k} |\langle l | H | k \rangle|^2. \quad (8.4.1)$$

It should be noted that $\sigma(k)$ are the widths of the strength functions $F_k(E)$ and similarly e_k are their centroids. Given the mean field $h(1)$ basis states (denoted by $|k\rangle$) expanded in the H eigenvalue (E) basis, $|k\rangle = \sum_E C_k^E |E\rangle$, the strength functions $F_k(E)$ are defined by,

$$F_k(E) = \sum_{E'} |C_k^{E'}|^2 \delta(E - E') = |\mathcal{C}_k^E|^2 I(E). \quad (8.4.2)$$

In Eq. (8.4.2), $|\mathcal{C}_k^E|^2$ denotes the average of $|C_k^E|^2$ over the eigenstates with the same energy E and all the quantities are defined over good JT (nuclei) or J (atoms) spaces; the strength functions over good spin spaces are also defined in Chapter 2. The strength functions define the spreading of the basis states over the eigenstates and for EGOE the spreadings are of Gaussian form in the strong coupling limit; see [Fr-83, Ko-01] and Chapter 2. Also as stated above, the bivariate Gaussian form of $\rho(E, e_k)$ implies $\sigma^2(k)$ should be constant i.e., they are independent of k . We show in Fig. 8.8,

results for $\sigma(k)$ vs k for ^{22}Na , ^{24}Mg and SmI matrices. It is seen that the basis state widths $\sigma(k)$ are almost constant apart from small fluctuations in the nuclear examples. This result is in agreement with several previous numerical calculations [Ze-96, Fr-83, Ko-08]. Writing $\sigma(k) = \overline{\sigma(k)}(1 \pm \delta)$, it is seen that the relative rms deviation of the fluctuations from the mean values is 14% and 15% (i.e., $\delta = 0.14$ and 0.15 , respectively) and the mean values $\overline{\sigma(k)} = 7.5$ MeV and 9.6 MeV, respectively for ^{22}Na and ^{24}Mg matrices. For SmI, $\overline{\sigma(k)} = 0.14$ Hartree and $\delta = 0.25$. Therefore, the fluctuations in $\sigma(k)$ are much larger for SmI as compared to those for the nuclear examples.

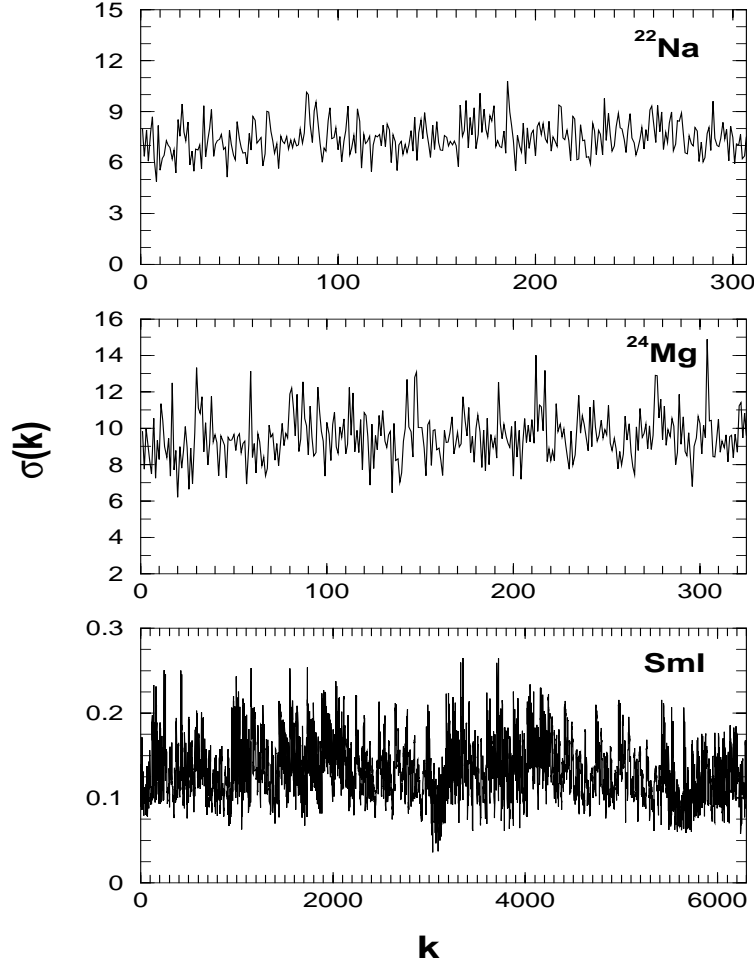


Figure 8.8: Plot showing the variation of width $\sigma(k)$ with the basis state index k for ^{22}Na , ^{24}Mg and SmI matrices. The units for $\sigma(k)$ are MeV for ^{22}Na and ^{24}Mg and Hartree for SmI.

It is possible to estimate the magnitude of the fluctuations in $\sigma(k)$. Say there are K number of many-particle states that are directly coupled by the two-body interaction. The connectivity factor K also defines the spectral variances; see [Fl-96, Fl-96a, Ja-01] and Chapter 2. Assuming that the coupling matrix elements are inde-

pendent Gaussian random variables with zero centroid and variance ν^2 , we have $\overline{\sigma^2(k)} = \nu^2 K$. Now the relative rms fluctuations in the $\sigma^2(k)$ are given by $\sqrt{2/K}$. Therefore, $\sigma(k) \sim [\overline{\sigma^2(k)}]^{1/2} (1 \pm 1/\sqrt{2K})$ giving δ defined above to be $1/\sqrt{2K}$. For embedded ensembles for spinless fermion systems with m fermions in N sp states, the connectivity factor $K \sim m(m-1)(N-m)(N-m-1)/4$ [Fl-96, Fl-96a]. For example, for 6 fermions in 12 sp states ($N = 12$, $m = 6$), $\delta \sim 0.05$. Going to embedded ensembles for fermion systems with spin ($\mathbf{s} = \frac{1}{2}$) degree of freedom and assuming that the variances of the matrix elements in the two-particle spin $s = 0$ and $s = 1$ channels to be ν_s^2 , we can relate ν_s to ν by demanding that the two-particle spectral variance in both the models is same. This gives $\nu_s^2 = \nu^2/4$ for large N . Using this scaling and the result for the connectivity factor $K(S) = K(\Omega, m, S) = P(\Omega, m, S)$ given in Chapter 2, we obtain $\delta \sim 0.1$ for 6 fermions in 6 sp orbits (so that $N = 12$) with total spin $S = 0$. Therefore, going from embedded ensembles for spinless fermion systems to systems with spin, relative rms fluctuations in the basis states variances change from 5% to 10% (see also Table 4.10). We expect the EGOE results for nuclei with JT symmetry to be larger than that of the embedded ensembles for spin systems and this explains the results in Fig. 8.8 for the nuclear examples.

8.4.3 Structure of the two-body part of the Hamiltonian in the eigenvalue basis

In general, it is possible to examine the H matrices in different bases. For example for $(2s1d)$ shell nuclei, the $U(24) \supset [U(6) \supset SU(3) \supset SO_L(3)] \otimes [SU(4) \supset SU_S(2) \otimes SU_T(2)] \supset SO_J(3) \otimes SU_T(2)$ basis [El-58] will be interesting. Similarly, Zuker et al [Zu-01] examined the structure of Lanczos tridiagonal H matrices for nuclei. Unlike examining the total H matrix, it was suggested in [Fr-88] that it may be useful to analyze the pure two-body part \mathbf{V} of H [\mathbf{V} is defined by dropping the diagonal matrix elements of the two-body part $V(2)$] as this part is responsible for chaos (note that the one-body part of H generates Poisson fluctuations). The two natural basis to consider are the shell-model mean-field basis and the H eigenvalue basis. The structure of \mathbf{V} in the mean-field basis is essentially same as that shown in Figs. 8.1, 8.2 and 8.3. Therefore new insight is expected from the structure of \mathbf{V} in the H eigenvalue basis. Unlike the mean-field basis or the $SU(3)$ basis mentioned above (or even any other

basis defined by a group symmetry), the H basis is expected to be the least biased and also it is the most natural basis. More importantly, EGOE has a prediction, as discussed ahead, for the structure of \mathbf{V} in the H basis. As the ^{22}Na nuclear example was discussed before [Fr-88, To-86] and the SmI example showed strong deviations from EGOE structure as discussed in Secs. 8.4.1 and 8.4.2, we restrict our discussion here to ^{24}Mg example.

For ^{24}Mg example, starting with the matrices for \mathbf{V} and H in the mean-field basis [H operator consists of two-body matrix elements due to Kuo [Ku-67] defining $V(2)$ and ^{17}O sp energies -4.15 MeV, 0.93 MeV and -3.28 MeV for $1d_{5/2}$, $1d_{3/2}$ and $2s_{1/2}$ orbits defining $h(1)$] we have constructed the matrix $\langle E_f | \mathbf{V} | E_i \rangle$. Using this we have analyzed the bivariate transition strength density generated by the operator \mathbf{V} (we put $\langle E_i | \mathbf{V} | E_i \rangle = 0$ as discussed in [Fr-88] so that we are dealing with the pure two-body part of H). Given the transition operator \mathbf{V} , transition strength density $I_{\mathbf{V}}^{H,m}(x, y)$ with the two variables x and y being eigenvalues of H is $I_{\mathbf{V}}^{H,m}(x, y) = I^{H,m}(y) |\langle m, y | \mathbf{V} | m, x \rangle|^2 I^{H,m}(x)$. The bivariate moments of this distribution are $\widetilde{M}_{pq} = \langle \langle \mathbf{V} H^q \mathbf{V} H^p \rangle \rangle^m$. Note that the normalization factor is M_{00} . Starting with \widetilde{M}_{pq} , we can obtain normalized moments, the central moments, reduced moments and also the reduced cumulants k_{rs} , $r + s \geq 3$. It is possible to write down the Edgeworth corrected bivariate Gaussian that includes the cumulants k_{rs} with $r + s = 3, 4$ [Fr-88, Ko-95]. Following the spinless EGOE results in [Fr-88, To-86] and the new results in Chapter 7, it can be argued that EGOE gives in general close to bivariate Gaussian form with Edgeworth corrections for $I_{\mathbf{V}}^{H,m}(x, y)$. Equation (J3) in Appendix J gives the bivariate Gaussian form with ED corrections. This prediction of EGOE is tested in Fig. 8.9 for ^{24}Mg . The spectrum span for this nucleus is from -93.29 to -10.06 MeV. The bivariate distribution $I_{\mathbf{V}}$ is shown in Fig. 8.9 and it is constructed using the bin-size 5×5 MeV². For comparison, we also show the corresponding ED corrected Gaussian distribution. The marginal centroids ϵ_i, ϵ_f are equal and their value is -50.44 MeV. Similarly, the marginal widths are 13.76 MeV and the bivariate correlation coefficient $\zeta_{biv} = 0.61$ MeV. Thus, it is clear that the matrix can not be represented by a GOE as $\zeta_{biv}^{GOE} = 0$. The bivariate cumulants ($k_{rs} = k_{sr}$ due to symmetry of the \mathbf{V} matrix) for $r + s \leq 4$ are $k_{21} = 0.035$, $k_{30} = 0.070$, $k_{22} = -0.092$, $k_{31} = -0.053$ and $k_{40} = -0.015$. The overall normalization is 12933.25 MeV². It is seen from Fig. 8.9 that the r.m.s.

matrix elements of \mathbf{V} in the H eigenvalue basis are well described by the EGOE bi-variate Gaussian form. This along with the previous [Fr-88, To-86] ^{22}Na example and all other results in Secs. 8.4.1 and 8.4.2 support the conjecture that EGOE is a good representation for nuclear Hamiltonians.

8.4.4 Comments on deviations from EGOE in the atomic example

Although both the nuclear and atomic shell-model Hamiltonians include a one-body and two-body parts, it is clearly seen that EGOE does not describe very well the atomic shell-model Hamiltonian while it is good for nuclei. Following are some of the differences in the two systems: (i) given the sp orbits and the number of valence fermions, only a few configurations (that correspond to single and double excitations with respect to the leading configuration) are included in atomic calculations [Fl-99, Cu-01, An-05] whereas all configurations allowed in the model space, just as in EGOE, are included in the nuclear examples; (ii) for atoms, both positive and negative parity (interwoven) sp orbits are included (and this is necessary) while in nuclear examples, orbits of only one parity are considered; (iii) the inter-configuration mixing is weak for atoms as discussed in earlier atomic calculations [Fl-99, Cu-01]; (iv) the Coulomb interaction is of long range while nuclear interactions are of short range. A simple plot of the distribution of the configuration centroids with degeneracy given by the dimensions shows multimodal structure for atoms (see Fig. 4 of [An-05]). However, for nuclear examples it is essentially an unimodal distribution and this difference can be ascribed to (i) and (ii). Random matrix model taking into account (i), (ii) and (iii) corresponds to partitioned EGOE [Ko-01]. A simpler version of this model shows that weak mixing between configurations generates bimodal (in general, multimodal) forms for density of states [Ko-99]. Similarly, in order to understand the effects due to (iv), the model considered by Bae et al [Ba-92] may be relevant. This model includes a parameter ξ , where ξ is the ratio of the radius of the many-body system to the range of the interaction. It will be useful to examine the statistical properties considered in the present chapter using both partitioned EGOE and the Bae et al model. However, this analysis is beyond the scope of the present thesis.

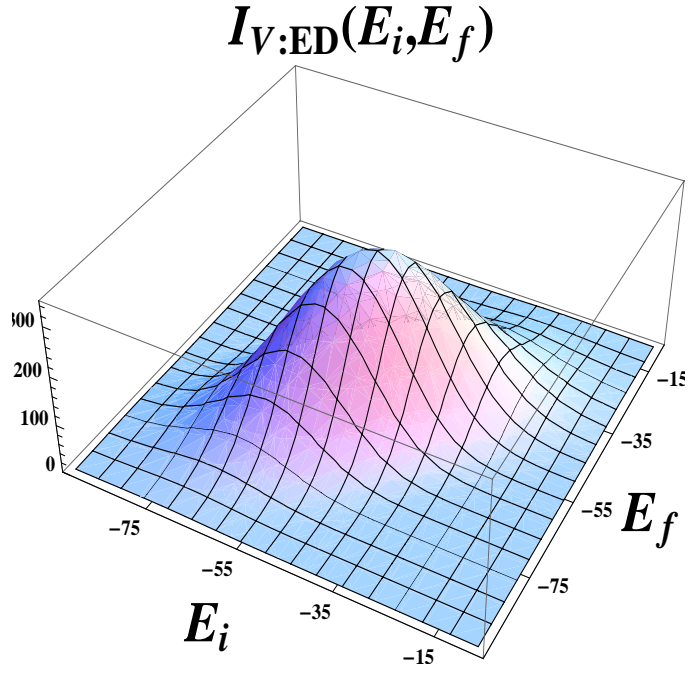
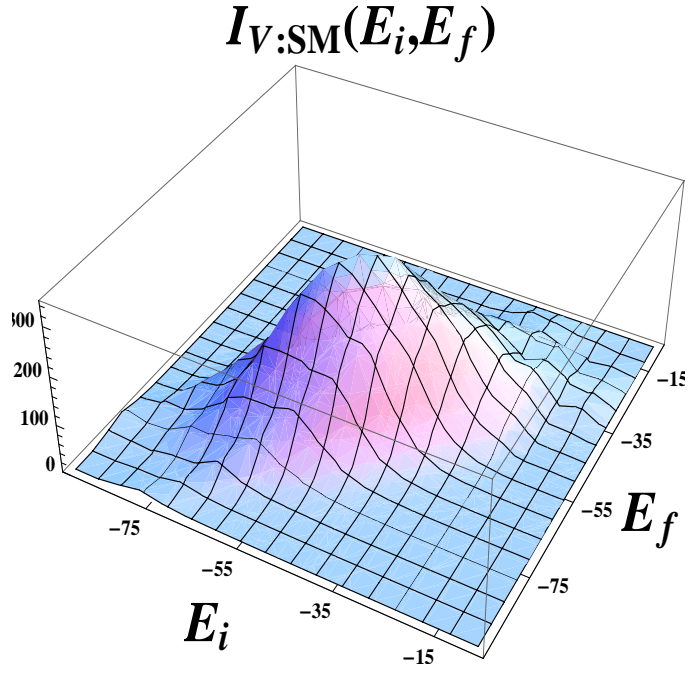


Figure 8.9: Plots showing the bivariate transition strength density for ^{24}Mg with $(J^\pi T) = (0^+ 0)$. Compared are the results from exact shell-model (denoted by $I_{V:SM}$ in the figure) with the Edgeworth corrected bivariate Gaussian $I_{V:ED}$ in Eq. (J3) obtained using the bivariate cumulants given in the text. The units for E_i and E_f are MeV.

8.5 Summary

In the present chapter, a comprehensive analysis of the structure of nuclear shell-model Hamiltonian matrices has been carried out by employing all available measures for GOE, BRME and EGOE random matrix ensembles. To this end, considered are ^{22}Na and ^{24}Mg nuclear examples and for comparison the SmI atomic example. In the nuclear examples, the matrix sizes are ~ 300 and comparing with some of the analysis carried out by Zelevinsky et al [Ze-96] and Papenbrock and Weidenmüller [Pa-07] where much larger size matrices are used, it is clearly seen from the results in Secs. 8.2-8.4 that the present examples are adequate for bringing out all the essential features of the nuclear shell model Hamiltonians and in particular, the EGOE structure. Results for SmI in Secs. 8.2-8.4 indicate that further investigations are needed for establishing the extent to which EGOE can be applied for describing statistical properties of atomic levels. For nuclear Hamiltonians, it is possible to argue, using chaos measures applied to the diagonal blocks in Fig. 1.3, that there is a local GOE structure (i.e., each diagonal block is close to a GOE with weak admixings between these blocks) in the matrices although there is a global EGOE structure [Pa-05]. This aspect was also recognized in the earlier studies of H matrices by French et al [Fr-88]. The study presented in Secs. 8.2-8.4 together with the previous analysis in [Pa-07, Fr-88, Ze-96] clearly establishes that EGOE is the best random matrix representation for nuclear shell-model Hamiltonians.

Chapter 9

Conclusions and Future Outlook

In this thesis, we have identified and systematically analyzed many different physically relevant EGEs with symmetries by considering a variety of quantities and measures that are important for finite interacting quantum systems such as nuclei, quantum dots, small metallic grains and ultracold atoms. The studies carried out and the main results obtained in the thesis are as follows.

Finite interacting Fermi systems with a mean-field and a chaos generating two-body interaction are modeled, more realistically, by one plus two-body embedded Gaussian orthogonal ensemble of random matrices with spin degree of freedom [called EGOE(1+2)-**s**]. Numerical calculations are used to demonstrate that, as λ , the strength of the interaction (measured in the units of the average spacing of the single particle levels defining the mean-field), increases, generically there is Poisson to GOE transition in level fluctuations, Breit-Wigner to Gaussian transition in strength functions (also called local density of states) and also a duality region where information entropy will be the same in both the mean-field and interaction defined basis. Spin dependence of the transition points λ_c , λ_F and λ_d , respectively, is described using the propagator for the spectral variances and the analytical formula for the propagator is derived. We have further established that the duality region corresponds to a region of thermalization. For this purpose we have compared the single particle entropy defined by the occupancies of the single particle orbitals with thermodynamic entropy and information entropy for various λ values and they are very close to each other at $\lambda = \lambda_d$. Chaos markers play an important role in quantum information science,

statistical nuclear spectroscopy and thermalization in finite quantum systems.

EGOE(1+2)-**s** also provides a model for understanding general structures generated by pairing correlations. In the space defined by EGOE(1+2)-**s** ensemble for fermions, pairing defined by the algebra $U(2\Omega) \supset Sp(2\Omega) \supset SO(\Omega) \otimes SU_S(2)$ is identified and some of its properties are derived. Using numerical calculations it is shown that in the strong coupling limit, partial densities defined over pairing subspaces are close to Gaussian form and propagation formulas for their centroids and variances are derived. As a part of understanding pairing correlations in finite Fermi systems, we have shown that pair transfer strength sums (used in nuclear structure) as a function of excitation energy (for fixed S), a statistic for onset of chaos, follows, for low spins, the form derived for spinless fermion systems, i.e., it is close to a ratio of Gaussians. Going further, we have considered a quantity in terms of ground state energies, giving conductance peak spacings in mesoscopic systems at low temperatures, and studied its distribution over EGOE(1+2)-**s** by including both pairing and exchange interactions. This model is shown to generate bimodal to unimodal transition in the distribution of conductance peak spacings consistent with the results obtained using realistic calculations for small metallic grains.

For m fermions in Ω number of single particle orbitals, each four-fold degenerate, we have introduced and analyzed in detail embedded Gaussian unitary ensemble of random matrices generated by random two-body interactions that are $SU(4)$ scalar [EGUE(2)- $SU(4)$]. Here, the $SU(4)$ algebra corresponds to the Wigner's supermultiplet $SU(4)$ symmetry in nuclei. Embedding algebra for the EGUE(2)- $SU(4)$ ensemble is $U(4\Omega) \supset U(\Omega) \otimes SU(4)$. Exploiting the Wigner-Racah algebra of the embedding algebra, analytical expression for the ensemble average of the product of any two m -particle Hamiltonian matrix elements is derived. Using this, formulas for a special class of $U(\Omega)$ irreps are derived for the ensemble averaged spectral variances and also for the covariances in energy centroids and spectral variances. On the other hand, simplifying the tabulations available for $SU(\Omega)$ Racah coefficients, numerical calculations are carried out for general $U(\Omega)$ irreps. Spectral variances clearly show, by applying the so-called Jacquod and Stone prescription, that the EGUE(2)- $SU(4)$ ensemble generates ground state structure just as the quadratic Casimir invariant (C_2) of $SU(4)$. This is further corroborated by the calculation of the expectation values of

$C_2[SU(4)]$ and the four periodicity in the ground state energies. Secondly, it is found that the covariances in energy centroids and spectral variances increase in magnitude considerably as we go from EGUE(2) for spinless fermions to EGUE(2) for fermions with spin to EGUE(2)- $SU(4)$ implying that the differences in ensemble and spectral averages grow with increasing symmetry. Also for EGUE(2)- $SU(4)$ there are, unlike for GUE, non-zero cross-correlations in energy centroids and spectral variances defined over spaces with different particle numbers and/or $U(\Omega)$ [equivalently $SU(4)$] irreps. In the dilute limit defined by $\Omega \rightarrow \infty$, $r \gg 1$ and $r/\Omega \rightarrow 0$, for the $\{4^r, p\}$ irreps, we have derived analytical results for these correlations. All correlations are non-zero for finite Ω and they tend to zero as $\Omega \rightarrow \infty$.

One plus two-body embedded Gaussian orthogonal ensemble of random matrices with parity [EGOE(1+2)- π] generated by a random two-body interaction (modeled by GOE in two particle spaces) in the presence of a mean-field, for spinless identical fermion systems, in terms of two mixing parameters and a gap between the positive ($\pi = +$) and negative ($\pi = -$) parity single particle states is introduced. Numerical calculations are used to demonstrate, using realistic values of the mixing parameters, that this ensemble generates Gaussian form (with corrections) for fixed parity state densities for sufficiently large values of the mixing parameters. The random matrix model also generates many features in parity ratios of state densities that are similar to those predicted by a method based on the Fermi-gas model for nuclei. We have also obtained a simple formula for the spectral variances defined over fixed- (m_1, m_2) spaces where m_1 is the number of fermions in the +ve parity single particle states and m_2 is the number of fermions in the -ve parity single particle states. The smoothed densities generated by the sum of fixed- (m_1, m_2) Gaussians with lowest two shape corrections describe the numerical results in many situations. The model also generates preponderance of +ve parity ground states for small values of the mixing parameters and this is a feature seen in nuclear shell-model results.

Turning to interacting boson systems, for m number of bosons, carrying spin ($\mathbf{s} = \frac{1}{2}$) degree of freedom, in Ω number of single particle orbitals, each doubly degenerate, we have introduced and analyzed embedded Gaussian orthogonal ensemble of random matrices generated by random two-body interactions that are spin (S) scalar [BEGOE(2)- \mathbf{s}]. The ensemble BEGOE(2)- \mathbf{s} is intermediate to the BEGOE(2) for

spinless bosons and for bosons with spin $\mathbf{s} = 1$ which is relevant for spinor BEC. Embedding algebra for the BEGOE(2)- \mathbf{s} ensemble and also for BEGOE(1+2)- \mathbf{s} that includes the mean-field one-body part is $U(2\Omega) \supset U(\Omega) \otimes SU(2)$ with $SU(2)$ generating spin. A method for constructing the ensembles in fixed- (m, S) spaces has been developed. Numerical calculations show that for BEGOE(2)- \mathbf{s} , the fixed- (m, S) density of states is close to Gaussian and level fluctuations follow GOE in the dense limit. For BEGOE(1+2)- \mathbf{s} , generically there is Poisson to GOE transition in level fluctuations as the interaction strength (measured in the units of the average spacing of the single particle levels defining the mean-field) is increased. The interaction strength needed for the onset of the transition is found to decrease with increasing S . Propagation formulas for the fixed- (m, S) space energy centroids and spectral variances are derived for a general one plus two-body Hamiltonian preserving spin. Derived also is the formula for the variance propagator for the fixed- (m, S) ensemble averaged spectral variances. Using these, covariances in energy centroids and spectral variances are analyzed. Variance propagator clearly shows that the BEGOE(2)- \mathbf{s} ensemble generates ground states with spin $S = S_{max}$. This is further corroborated by analyzing the structure of the ground states in the presence of the exchange interaction \hat{S}^2 in BEGOE(1+2)- \mathbf{s} . Natural spin ordering ($S_{max}, S_{max} - 1, S_{max} - 2, \dots, 0$ or $\frac{1}{2}$) is also observed with random interactions. Going beyond these, we have also introduced pairing symmetry in the space defined by BEGOE(2)- \mathbf{s} . Expectation values of the pairing Hamiltonian show that random interactions exhibit pairing correlations in the ground state region.

Parameters defining many of the important spectral distributions (valid in the chaotic region), generated by EGEs, involve traces of product of four two-body operators. For example, these higher order traces are required for calculating nuclear structure matrix elements for $\beta\beta$ decay and also for establishing Gaussian density of states generated by various embedded ensembles. Extending the binary correlation approximation method for two different operators and for traces over two-orbit configurations, we have derived formulas, valid in the dilute limit, for both skewness and excess parameters for EGOE(1+2)- π . In addition, we have derived a formula for the traces defining the correlation coefficient of the bivariate transition strength distribution generated by the two-body transition operator appropriate for calculat-

ing $0\nu\text{-}\beta\beta$ decay nuclear transition matrix elements and also for other higher order traces required for justifying the bivariate Gaussian form for the strength distribution. With applications in the subject of regular structures generated by random interactions, we have also derived expressions for the coefficients in the expansions to order $[J(J+1)]^2$ for the energy centroids $E_c(m, J)$ and spectral variances $\sigma^2(m, J)$ generated by EGOE(2)- J ensemble members for the single- j situation. These also involve traces of four two-body operators.

In order to establish random matrix structure of nuclear shell-model Hamiltonian matrices, we have presented a comprehensive analysis of the structure of Hamiltonian matrices based on visualization of the matrices in three dimensions as well as in terms of measures for GOE, banded and embedded random matrix ensembles. We have considered two nuclear shell-model examples, ^{22}Na with $J^\pi T = 2^+0$ and ^{24}Mg with $J^\pi T = 0^+0$ and, for comparison we have also considered SmI atomic example with $J^\pi = 4^+$. It is clearly established that the matrices are neither GOE nor banded. For the EGOE [strictly speaking, EGOE(2)- JT or EGOE(2)- J] structure we have examined the correlations between diagonal elements and eigenvalues, fluctuations in the basis states variances and structure of the two-body part of the Hamiltonian in the eigenvalue basis. Unlike the atomic example, nuclear examples show that the nuclear shell-model Hamiltonians can be well represented by EGOE.

In summary, in this thesis, large number of new results are obtained for embedded ensembles EGOE(1+2)-**s**, EGUE(2)- $SU(4)$, EGOE(1+2)- π and BEGOE(1+2)-**s**, with EGUE(2)- $SU(4)$ introduced for the first time in this thesis. Moreover, some results are presented for EGOE(2)- J and for the first time BEGOE(1+2)-**s** has been explored in detail in this thesis. In addition, formulas are derived, by extending the binary correlation approximation method, for higher order traces for embedded ensembles with $U(N) \supset U(N_1) \oplus U(N_2)$ embedding and some of these are needed for new applications of statistical nuclear spectroscopy. Results of the present thesis establish that embedded Gaussian ensembles can be used gainfully to study a variety of problems in many-body quantum physics.

Some of the future studies in embedded ensembles should include the following.

- It is important to examine the energy dependence of the transition markers

generated by EGOE(1+2)-s and this will give new information about onset of chaos in interacting many-particle systems as we increase the excitation energy. In addition, going beyond the strength functions and occupancies, the distribution of transition strengths, generated by a general one-body transition operator, that is a vector in the spin space should be studied. This is important for producing a better random matrix basis for the smoothed forms for transition strength densities.

- Going beyond the measures employed in Chapter 2, new entanglement measures, introduced in the context of quantum information science, should be analyzed to characterize complexity in quantum many-body systems; for disordered spin-1/2 lattice systems, entanglement and delocalization are found to be strongly correlated [Br-08, Pi-08]. Besides the entanglement measures, further analysis of the thermodynamic region generated by two-body ensembles (defined by λ_d in Fig. 2.11) using long-time averages of various complexity measures as discussed in [Ca-09, Ri-08] is needed. This, besides being important in QIS, should lead to a deeper understanding of wavefunction thermalization in generic isolated many-body quantum systems [Ko-11, Ca-09, Ri-08, Ge-00, Fl-00].
- It is possible to apply the Hamiltonian in Eq. (3.5.5) with sp energies drawn from GOE (or GUE), adding a particle number dependent term and also by varying the interaction strength λ . Analysis with this H will generalize the results in Fig. 3.7 and also those reported in [Sc-08]. Furthermore, it will be useful to consider a generalized pairing operator by extending Eq. (3.2.1) to $P = \sum_i \beta_i P_i$ where β_i are free parameters.
- For evaluating $\gamma_2(m, f_m)$ for EGUE(2)- $SU(4)$, even for $f_m^{(p)}$ irreps, the needed $SU(\Omega)$ Racah coefficients are not available in analytical form nor there are tractable methods for their numerical evaluation. The mathematical problem here is challenging and its solution will establish the Gaussian form of the eigenvalue densities generated by EGUE(2)- $SU(4)$.
- It will also be interesting to analyze EGOE/EGUE with $SU(4) - ST$ symmetry.

With this, it will be possible to understand the role of random interactions in generating the differences in the gs structure of even-even and odd-odd $N=Z$ nuclei.

- It is important to investigate $\text{EGOE}(1+2)-\pi$ for proton-neutron systems and then we will have four unitary orbits (two for protons and two for neutrons). This extended $\text{EGOE}(1+2)-\pi$ model with protons and neutrons occupying different sp states will be generated by a 10×10 block matrix for $V(2)$ in two-particle spaces with 14 independent variances. Therefore, parametrization of this ensemble is more complex.
- Further extension of $\text{BEGOE}(1+2)$ including $\mathbf{s} = 1$ (also spin 2 etc.) degree of freedom for bosons, as discussed in Appendix G, is relevant for spinor BEC studies [Pe-10, Yi-07] and this ensemble should be analyzed so that realistic applications of BEGOE can be attempted.
- Wavefunction structure should be analyzed for $\text{BEGOE}(1+2)-\mathbf{s}$ and with this, it is possible to address questions related to thermalization in finite interacting boson systems.
- Binary correlation theory for EGEs with symmetries [going beyond direct sum sub-algebra of $U(N)$] needs to be developed and then it is possible to derive results for the excess parameter γ_2 for $\text{EGOE}(2)-\mathbf{s}$ and $\text{EGUE}(2)-SU(4)$ ensembles.
- Extensions of binary correlation approximation to spinless boson systems and for boson systems with spin ($\mathbf{s} = 1/2$ and 1) will be interesting and may prove to be useful in ultracold atom studies.
- Binary correlation results presented for $\text{EGOE}(1+2)-\pi$ in Chapter 7 should be extended further for deriving spectral properties of partitioned EGOE [Ko-01, Ko-99].
- Applications of embedded ensembles to wider class of systems like quantum dots, BEC etc. should be carried out by deriving results for physically relevant quantities that can be confronted directly with experimental data.

- In systems like nuclei and quantum dots, it is important to find experimental signatures for cross-correlations (they are discussed in Chapters 4 and 6 and Appendix C) as they will give direct evidence for embedded ensembles. This requires identifying measures involving cross-correlations in lower order moments of the two-point function that can be used in data analysis.
- In future, it is important to analyze embedded ensembles with much larger matrix dimensions that are needed for particle number $m \geq 10$. This requires new numerical efforts.
- In literature and also in this thesis, embedded ensembles with only GOE and GUE embedding are explored. In future, embedded ensembles with GSE embedding (EGSE) should be attempted.
- New efforts in developing further the Wigner-Racah algebra for general $SU(N)$ groups are needed for more complete analytical tractability of embedded random matrix ensembles. For example, analytical form for the two-point function is not yet available even for the spinless EGOE/BEGOE.
- Starting with $U(N)$ algebra for m fermions/bosons in N sp states, we have identified EEs with embedding defined by some of the $U(N)$ sub-algebras. As $U(N)$ admits very large class of sub-algebras, it is possible to identify many more EEs that could be physically relevant and this exploration will enrich the subject of embedded random matrix ensembles.

Appendix A

Unitary decomposition for a one plus two-body Hamiltonian for spinless fermions

Let us consider a system of m fermions in N sp states with a (1+2)-body Hamiltonian $H = h(1) + V(2)$ where $h(1) = \sum_i \epsilon_i \hat{n}_i$ and $V(2)$ is defined by the two-body matrix elements $V_{ijkl} = \langle kl | V(2) | ij \rangle$. With respect to the $U(N)$ group, the two-body interaction $V(2)$ can be separated into scalar ($\nu = 0$), effective one-body ($\nu = 1$) and irreducible two-body ($\nu = 2$) parts. Then, we have [Ch-71, Ko-01a],

$$\begin{aligned}
 V^{\nu=0} &= \frac{\hat{n}(\hat{n}-1)}{2} \bar{V} ; \quad \bar{V} = \binom{N}{2}^{-1} \sum_{i < j} V_{ijij} , \\
 V^{\nu=1} &= \frac{\hat{n}-1}{N-2} \sum_{i,j} \zeta_{i,j} a_i^\dagger a_j ; \quad \zeta_{i,j} = \left[\sum_k V_{kikj} \right] - \left[(N)^{-1} \sum_{r,s} V_{rsrs} \right] \delta_{i,j} , \\
 V^{\nu=2} &= V - V^{\nu=0} - V^{\nu=1} \iff V_{ijkl}^{\nu=2} ; \\
 V_{ijij}^{\nu=2} &= V_{ijij} - \bar{V} - (N-2)^{-1} (\zeta_{i,i} + \zeta_{j,j}) , \\
 V_{jikk}^{\nu=2} &= V_{jikk} - (N-2)^{-1} \zeta_{j,k} \text{ for } j \neq k , \\
 V_{ijkl}^{\nu=2} &= V_{ijkl} \text{ for all other cases .}
 \end{aligned} \tag{A1}$$

Similar to Eq. (A1), the $h(1)$ operator will have $v = 0, 1$ parts,

$$\begin{aligned} h^{v=0} &= \bar{\epsilon} \hat{n}, \quad \bar{\epsilon} = (N)^{-1} \sum_i \epsilon_i, \\ h^{v=1} &= \sum_i \epsilon_i^1 \hat{n}_i, \quad \epsilon_i^1 = \epsilon_i - \bar{\epsilon}. \end{aligned} \tag{A2}$$

Then the propagation equations for the m -particle centroids and variances are,

$$\begin{aligned} E_c(m) &= \langle H \rangle^m = m \bar{\epsilon} + \binom{m}{2} \bar{V}, \\ \sigma^2(m) &= \langle H^2 \rangle^m - [E_c(m)]^2 \\ &= \frac{m(N-m)}{N(N-1)} \sum_{i,j} \left\{ \epsilon_i^1 \delta_{i,j} + \frac{m-1}{N-2} \zeta_{i,j} \right\}^2 \\ &\quad + \frac{m(m-1)(N-m)(N-m-1)}{N(N-1)(N-2)(N-3)} \left\langle \left\langle (V^{v=2})^2 \right\rangle \right\rangle^2. \end{aligned} \tag{A3}$$

Appendix B

Exact variance formula for a given member of EGOE(1+2)-s

For completeness, we reproduce here the formula for spectral variances generated by each member of EGOE(1+2)-s. Given a one plus two-body Hamiltonian H , the fixed- S spectral variance $\sigma^2(m, S) = \langle H^2 \rangle^{m,S} - [\langle H \rangle^{m,S}]^2$ will be a fourth order polynomial in m and $S(S+1)$ [Fr-69, No-86]. This gives

$$\sigma^2(m, S) = \sum_{p=0}^4 a_p m^p + \sum_{q=0}^2 b_q m^q S(S+1) + c_0 [S(S+1)]^2. \quad (\text{B1})$$

The parameters (a_i, b_i, c_i) follow from $\sigma^2(m, S)$ for $m \leq 4$ and to determine these inputs one has to construct H matrices for m up to 4. However an elegant method, allowing $\sigma^2(m, S)$ to be expressed in terms of $(\epsilon_i, V_{ijkl}^{s=0,1})$, is to use the embedding algebra $U(N) \supset U(\Omega) \otimes SU(2)$. With respect to this algebra, as pointed out in [Ko-79, Ko-02a], $h(1)$ decomposes into a scalar $\nu = 0$ part [given by the first term in the first equation in Eq. (2.3.3)] and an irreducible one-body part with $\nu = 1$. The $\nu = 0$ and $\nu = 1$ parts transform, in Young tableaux notation [He-74], as the irreps $[0]$ and $[21^{\Omega-2}]$ respectively of $U(\Omega)$. Similarly $V^s(2)$, $s = 0, 1$ decompose into $\nu = 0, 1$ and 2 parts. The scalar parts $V^{\nu=0:s=0,1}$ can be identified from Eq. (2.3.3) and they will not contribute to the variances. The effective one-body parts $V^{\nu=1:s=0,1}$, generated by $V_{ijkl}^{s=0,1}$, are defined by the induced single particle energies $\lambda_{i,j}(s)$ given ahead in Eq. (B2). The diagonal induced energies $\lambda_{i,i}(s)$ are identified for the first time in [Ko-79].

However for EGOE(1+2)-s it is possible to have $\lambda_{i,j}(s)$, $i \neq j$. Now the irreducible two-body part $V^{v=2:s=0} = V - V^{v=0:s=0} - V^{v=1:s=0}$ and similarly $V^{v=2:s=1}$ is defined. It should be noted that the two $v = 0$ parts of $V(2)$ transform as the $U(\Omega)$ irrep $[0]$ and the two $v = 1$ parts of $V(2)$ transform as the irrep $[21^{\Omega-2}]$. Similarly $V^{v=2:s=0}$ transforms as the irrep $[42^{\Omega-2}]$ and the $V^{v=2:s=1}$ as the irrep $[2^2 1^{\Omega-4}]$. Using these and the group theory of $U(N) \supset U(\Omega) \otimes SU(2)$ algebra as given by Hecht and Draayer [He-74], a compact and easy to understand expression for fixed- S variances emerges, with $\mathcal{S}^2 = S(S+1)$, $m^x = \Omega - m/2$, $X(m, S) = m(m+2) - 4S(S+1)$ and $Y(m, S) = m(m-2) - 4S(S+1)$,

$$\begin{aligned}
\sigma_{H=h(1)+V(2)}^2(m, S) &= \frac{(\Omega+2)mm^x - 2\Omega\mathcal{S}^2}{\Omega(\Omega-1)(\Omega+1)} \sum_i \tilde{\epsilon}_i^2 \\
&+ \frac{m^x X(m, S)}{2\Omega(\Omega-1)(\Omega+1)} \sum_i \tilde{\epsilon}_i \lambda_{i,i}(0) \\
&+ \frac{(\Omega+2)m^x [3Y(m, S) + 16\mathcal{S}^2] - 8\Omega(m-1)\mathcal{S}^2}{2\Omega(\Omega-1)(\Omega+1)(\Omega-2)} \sum_i \tilde{\epsilon}_i \lambda_{i,i}(1) \\
&+ \frac{[(m+2)m^x/2 + \mathcal{S}^2] X(m, S)}{8\Omega(\Omega-1)(\Omega+1)(\Omega+2)} \sum_{i,j} \lambda_{i,j}^2(0) \\
&+ \frac{1}{8\Omega(\Omega-1)(\Omega+1)(\Omega-2)^2} \{8\Omega(m-1)(\Omega-2m+4)\mathcal{S}^2 \\
&+ (\Omega+2) [3(m-2)m^x/2 - \mathcal{S}^2] [3Y(m, S) + 8\mathcal{S}^2]\} \sum_{i,j} \lambda_{i,j}^2(1) \\
&+ \frac{[3(m-2)m^x/2 - \mathcal{S}^2] X(m, S)}{4\Omega(\Omega-1)(\Omega+1)(\Omega-2)} \sum_{i,j} \lambda_{i,j}(0) \lambda_{i,j}(1) \\
&+ P_2^0(m, S) \left\langle (V^{v=2,s=0})^2 \right\rangle^{2,0} + P_2^1(m, S) \left\langle (V^{v=2,s=1})^2 \right\rangle^{2,1} ; \\
P_2^0(m, S) &= \frac{[m^x(m^x+1) - \mathcal{S}^2] X(m, S)}{8\Omega(\Omega-1)},
\end{aligned} \tag{B2}$$

$$P_2^1(m, S) = \frac{1}{\Omega(\Omega+1)(\Omega-2)(\Omega-3)} \left\{ (\mathcal{S}^2)^2 (3\Omega^2 - 7\Omega + 6)/2 + 3m(m-2)m^x(m^x-1) \right.$$

$$\left. \times (\Omega+1)(\Omega+2)/8 - \mathcal{S}^2 [(5\Omega-3)(\Omega+2)m^x m + \Omega(\Omega-1)(\Omega+1)(\Omega+6)]/2 \right\} ,$$

with

$$\tilde{\epsilon}_i = \epsilon_i - \bar{\epsilon} ,$$

$$\lambda_{i,i}(s) = \sum_j V_{ijij}^s (1 + \delta_{ij}) - (\Omega)^{-1} \sum_{k,l} V_{klkl}^s (1 + \delta_{kl}) ,$$

$$\lambda_{i,j}(s) = \sum_k \sqrt{(1 + \delta_{ki})(1 + \delta_{kj})} V_{kikj}^s \quad \text{for } i \neq j , \quad (\text{B3})$$

$$V_{ijij}^{v=2,s} = V_{ijij}^s - \left[\langle V(2) \rangle^{2,s} + (\lambda_{i,i}(s) + \lambda_{j,j}(s)) (\Omega + 2(-1)^s)^{-1} \right] ,$$

$$V_{kikj}^{v=2,s} = V_{kikj}^s - (\Omega + 2(-1)^s)^{-1} \sqrt{(1 + \delta_{ki})(1 + \delta_{kj})} \lambda_{i,j}^s \quad \text{for } i \neq j ,$$

$$V_{ijkl}^{v=2,s} = V_{ijkl}^s \quad \text{for all other cases .}$$

Equations (B2) and (B3) are tested, by using some members of the EGOE(1+2)-**s** ensemble, for all S values with $m = 6, 7$ and 8 and also for many different Ω values.

Appendix C

EGUE(2)-s ensemble

For m fermions occupying Ω number of sp orbitals each with spin $\mathbf{s} = \frac{1}{2}$ so that the number of sp states $N = 2\Omega$, we consider Hamiltonians that preserve total m -particle spin S . Then the m -particle states can be classified according to $U(N) \supset U(\Omega) \otimes SU(2)$ algebra with $SU(2)$ generating spin S . The $U(\Omega)$ irrep that corresponds to spin S is $f_m = \{2^p, 1^q\}$ where $m = 2p + q$ and $S = q/2$ and therefore the m -particle states are denoted by $|f_m \nu_m M\rangle$; ν_m are the additional quantum numbers that belong to f_m and M is the S_z quantum number. With this, a general two-body Hamiltonian operator preserving spin S can be written as,

$$\hat{H} = \sum_{f_2, \nu_2^i, \nu_2^f, m_2} V_{f_2 \nu_2^i \nu_2^f}(2) A^\dagger(f_2 \nu_2^f m_2) A(f_2 \nu_2^i m_2). \quad (C1)$$

Here, $A^\dagger(f_2 \nu_2 m_2)$ and $A(f_2 \nu_2 m_2)$ denote creation and annihilation operators for the normalized two-particle states and $V_{f_2 \nu_2^i \nu_2^f}(2) = \langle f_2 \nu_2^f s m_2 | \hat{H} | f_2 \nu_2^i s m_2 \rangle$ independent of the m_2 's. Note that the two-particle spin $s = 0$ and 1 and the corresponding $U(\Omega)$ irreps f_2 are $\{2\}$ (symmetric) and $\{1^2\}$ (antisymmetric), respectively. The EGUE(2)-s ensemble for a given (m, S) is generated by the action of \hat{H} on m -particle basis space with a GUE representation for the H matrix in two-particle spaces. Then, the two-particle matrix elements $V_{f_2 \nu_2^i \nu_2^f}(2)$ are independent Gaussian variables with zero center and variance given by,

$$\overline{V_{f_2 \nu_2^1 \nu_2^2}(2) V_{f_2' \nu_2^3 \nu_2^4}(2)} = \lambda_{f_2}^2 \delta_{f_2 f_2'} \delta_{\nu_2^1 \nu_2^4} \delta_{\nu_2^2 \nu_2^3}. \quad (C2)$$

Thus $V(2)$ is a direct sum of GUE matrices for $s = 0$ and $s = 1$. Just as for EGUE(2), tensorial decomposition of \hat{H} with respect to $U(\Omega) \otimes SU(2)$ algebra gives analytical results for the spin ensemble. As \hat{H} preserves S , it is a scalar in spin $SU(2)$ space. However with respect to $SU(\Omega)$, the tensorial characters for $f_2 = \{2\}$ are $F_v = \{0\}, \{21^{\Omega-2}\}$ and $\{42^{\Omega-2}\}$. Similarly for $f_2 = \{1^2\}$ they are $\{0\}, \{21^{\Omega-2}\}$ and $\{2^2 1^{\Omega-4}\}$. Here the unitary tensors B 's are

$$\begin{aligned} & B(f_2 \mathbf{F}_v \omega_v) \\ &= \sum_{v_2^i, v_2^f, m_2} \left\langle f_2 v_2^f \overline{f_2 v_2^i} \mid \mathbf{F}_v \omega_v \right\rangle \left\langle s m_2 \overline{s m_2} \mid 00 \right\rangle A^\dagger(f_2 v_2^f m_2) A(f_2 v_2^i m_2). \end{aligned} \quad (C3)$$

In Eq. (C3), $\langle f_2 --- \rangle$ are $SU(\Omega)$ Wigner coefficients and $\langle s --- \rangle$ are $SU(2)$ Wigner coefficients. Then we have $\hat{H}(2) = \sum_{f_2, \mathbf{F}_v, \omega_v} W(f_2 \mathbf{F}_v \omega_v) B(f_2 \mathbf{F}_v \omega_v)$. The expansion coefficients W 's are also independent Gaussian random variables, just as V 's, with zero center and variance given by

$$\overline{W(f_2 \mathbf{F}_v \omega_v) W(f_2' \mathbf{F}_v' \omega_v')} = \delta_{f_2 f_2'} \delta_{\mathbf{F}_v \mathbf{F}_v'} \delta_{\omega_v \omega_v'} (\lambda_{f_2})^2 (2s+1).$$

The m -particle H matrix will be a direct sum matrix with the diagonal blocks represented by f_m . Then $H(m) = \sum_{f_m} H_{f_m}(m) \oplus$ and the EGUE(2)- \mathbf{s} is generated for each $H_{f_m}(m)$.

Using Wigner-Eckart theorem, the matrix elements of B 's in f_m space can be decomposed as,

$$\begin{aligned} & \left\langle f_m v_m^f M \mid B(f_2 \mathbf{F}_v \omega_v) \mid f_m v_m^i M \right\rangle \\ &= \sum_{\rho} \left\langle f_m \parallel B(f_2 \mathbf{F}_v) \parallel f_m \right\rangle_{\rho} \left\langle f_m v_m^i \mathbf{F}_v \omega_v \mid f_m v_m^f \right\rangle_{\rho}, \end{aligned} \quad (C4)$$

where the summation is over the multiplicity index ρ and this arises as $f_m \otimes \mathbf{F}_v$ gives in general more than once the irrep f_m . Applying Eq. (C4) and the expansion of \hat{H} in terms of B 's, exact analytical formulas are derived for the ensemble averaged spectral variances, cross-correlations in energy centroids and also for the cross-correlations in spectral variances. In addition, the ensemble averaged excess parameter for the fixed- (m, S) density of states is given in terms of $SU(\Omega)$ Racah coefficients [Ko-07]. For finite m and $\Omega \rightarrow \infty$, some important results are: (i) the ensemble averaged variances,

to the leading order, just as for the spinless fermion systems [Be-01a], are same for both EGOE(2)-**s** and EGUE(2)-**s** and this is inferred from the exact analytical formulas available for both the ensembles [comparing Eq. (2.3.11) with Eq. (19) of [Ko-07]]; (ii) similarly it is seen that the cross-correlations in energy centroids for EGOE(2)-**s** are twice that of EGUE(2)-**s** to the leading order [Ko-06a, Be-01a] [as an aside, let us point out that Eqs. (2.3.4) and (2.3.11) give for EGOE(2)-**s**, the exact formula for the normalized cross-correlations in the energy centroids]; (iii) combining (ii) with the exact analytical results for spinless fermion EGUE(2)-**s** (see Sec. 1.2.3 for details), it is conjectured that the covariances in spectral variances for EGOE(2)-**s** are twice that of EGUE(2)-**s** to the leading order [note that for EGUE(2)-**s** an analytical result is available but not for EGOE(2)-**s**]; and (iv) combining the analytical results for the excess parameter for EGOE(2) and EGOE(2)-**s** (see Appendix H and Sec. 2.9 for details), it is expected that the density of eigenvalues will be Gaussian for EGUE(2)-**s**.

Appendix D

$U(2\Omega) \supset [U(\Omega) \supset SO(\Omega)] \otimes SU(2)$ pairing symmetry

With the $4\Omega^2$ number of one-body operators $u_\mu^r(i, j)$; $r = 0, 1$, defined in Sec. 3.2, generating $U(2\Omega)$ algebra, it is easily seen that the operators $u^0(i, j)$, which are Ω^2 in number, generate $U(\Omega)$ algebra. Similarly the operators $C(i, j) = u^0(i, j) - u^0(j, i)$, $i > j$, which are $\Omega(\Omega - 1)/2$ in number, generate the $SO(\Omega)$ sub-algebra of $U(\Omega)$. The spin operator $\hat{S} = S_\mu^1$, the number operator \hat{n} and the quadratic Casimir operators C_2 's of $U(\Omega)$ and $SO(\Omega)$ are

$$S_\mu^1 = \frac{1}{\sqrt{2}} \sum_{i=1}^{\Omega} u_\mu^1(i, i) ,$$

$$\hat{n} = \sum_i n_i, \quad n_i = \sqrt{2} u^0(i, i) ,$$
(D1)

$$C_2(U(\Omega)) = 2 \sum_{i,j} u^0(i, j) u^0(j, i) ,$$

$$C_2(SO(\Omega)) = 2 \sum_{i>j} C(i, j) C(j, i) .$$

The structure of $C_2(U(\Omega))$ in terms of the number operator and the $\hat{S} \cdot \hat{S} = \hat{S}^2$ operator is,

$$C_2(U(\Omega)) = \hat{n} \left(\Omega + 2 - \frac{\hat{n}}{2} \right) - 2\hat{S}^2 ,$$
(D2)

$$\langle C_2(U(\Omega)) \rangle^{m,S} = m \left(\Omega + 2 - \frac{m}{2} \right) - 2S(S+1) .$$

Note that $\langle C_2(U(\Omega)) \rangle^{\{f\}} = \sum_i f_i(f_i + \Omega + 1 - 2i)$. As $U(2\Omega) \supset U(\Omega) \otimes SU(2)$ with the $SU(2)$ algebra generating total spin S , the $U(\Omega)$ irreps are labeled by two column irreps $\{2^p 1^q\}$ with $m = 2p + q$, $S = q/2$. As a consequence, the $SO(\Omega)$ irreps are also of two column type and we will denote them by $[2^{\nu_1} 1^{\nu_2}]$. Here, $\nu_S = 2\nu_1 + \nu_2$ is called seniority and $\tilde{s} = \nu_2/2$ is called reduced spin. We also have [Wy-74]

$$\langle C_2(SO(\Omega)) \rangle^{\langle \omega \rangle} = \sum_i \omega_i(\omega_i + \Omega - 2i) \quad (D3)$$

$$\Rightarrow \langle C_2(SO(\Omega)) \rangle^{(2^{\nu_1} 1^{\nu_2})} = \nu_S \left(\Omega + 1 - \frac{\nu_S}{2} \right) - 2\tilde{s}(\tilde{s} + 1) .$$

After some commutator algebra it can be shown that,

$$2H_p = -C_2(SO(\Omega)) + \hat{n} \left(\Omega + 1 - \frac{\hat{n}}{2} \right) - 2\hat{S}^2, \quad (D4)$$

$$\langle H_p \rangle^{(m, S, \nu_S, \tilde{s})} = \frac{1}{4}(m - \nu_S)(2\Omega + 2 - m - \nu_S) + [\tilde{s}(\tilde{s} + 1) - S(S + 1)] ,$$

where the pairing Hamiltonian H_p is defined by Eq. (3.2.2). Classification of $U(2\Omega) \supset [U(\Omega) \supset SO(\Omega)] \otimes SU(2)$ states defined by (m, S, ν_S, \tilde{s}) quantum numbers is needed, i.e., $(m, S) \rightarrow (\nu_S, \tilde{s})$ reductions are required and they are obtained by group theory. Using the tabulations in [Wy-70], results are given in Tables D.1 and D.2 for: (i) $m \leq 4$, $\Omega \geq 4$ and (ii) $m = 6$, $\Omega = 6$ and $m = 5 - 8$, $\Omega = 8$, respectively.

Table D.1: $(m, S) \rightarrow (\nu_S, \tilde{s})$ reductions for $m \leq 4$ and $\Omega \geq 4$.

(m, S)	(ν_S, \tilde{s})
(0, 0)	(0, 0)
$(1, \frac{1}{2})$	$(1, \frac{1}{2})$
(2, 0)	(2, 0), (0, 0)
(2, 1)	(2, 1)
$(3, \frac{1}{2})$	$(3, \frac{1}{2}), (1, \frac{1}{2})$
$(3, \frac{3}{2})$	$\{(1, \frac{1}{2})_{\Omega=4}; (2, 1)_{\Omega=5}; (3, \frac{3}{2})_{\Omega \geq 6}\}$
(4, 0)	(4, 0), (2, 0), (0, 0)
(4, 1)	$\{(2, 0)_{\Omega=4}; (3, \frac{1}{2})_{\Omega=5}; (4, 1)_{\Omega \geq 6}\}, (2, 1)$
(4, 2)	$\{(0, 0)_{\Omega=4}; (1, \frac{1}{2})_{\Omega=5}; (2, 1)_{\Omega=6}; (3, \frac{3}{2})_{\Omega=7}; (4, 2)_{\Omega \geq 8}\}$

Table D.2: $(m, S) \rightarrow (\nu_S, \bar{s})$ irrep reductions for $(\Omega = 6; m = 6)$ and $(\Omega = 8; m = 5 - 8)$. Note that the dimensions $d_f(\Omega, m, S)$ of the (m, S) and $d(\Omega, \nu_S, \bar{s})$ of the (ν_S, \bar{s}) space are given as subscripts; $d_f(\Omega, m, S) = \sum_{\nu_S, \bar{s}} d(\Omega, \nu_S, \bar{s})$.

Ω	$(m, S)_{d_f(\Omega, m, S)}$	$(\nu_S, \bar{s})_{d(\Omega, \nu_S, \bar{s})}$
6	$(6, 0)_{175}$	$(6, 0)_{70}, (4, 0)_{84}, (2, 0)_{20}, (0, 0)_1$
	$(6, 1)_{189}$	$(4, 1)_{90}, (4, 0)_{84}, (2, 1)_{15}$
	$(6, 2)_{35}$	$(2, 1)_{15}, (2, 0)_{20}$
	$(6, 3)_1$	$(0, 0)_1$
8	$(5, \frac{1}{2})_{1008}$	$(5, \frac{1}{2})_{840}, (3, \frac{1}{2})_{160}, (1, \frac{1}{2})_8$
	$(5, \frac{3}{2})_{504}$	$(5, \frac{3}{2})_{448}, (3, \frac{3}{2})_{56}$
	$(5, \frac{5}{2})_{56}$	$(3, \frac{3}{2})_{56}$
	$(6, 0)_{1176}$	$(6, 0)_{840}, (4, 0)_{300}, (2, 0)_{35}, (0, 0)_1$
	$(6, 1)_{1512}$	$(6, 1)_{1134}, (4, 1)_{350}, (2, 1)_{28}$
	$(6, 2)_{420}$	$(4, 1)_{350}, (4, 2)_{70}$
	$(6, 3)_{28}$	$(2, 1)_{28}$
	$(7, \frac{1}{2})_{2352}$	$(7, \frac{1}{2})_{1344}, (5, \frac{1}{2})_{840}, (3, \frac{1}{2})_{160}, (1, \frac{1}{2})_8$
	$(7, \frac{3}{2})_{1344}$	$(5, \frac{1}{2})_{840}, (5, \frac{3}{2})_{448}, (3, \frac{3}{2})_{56}$
	$(7, \frac{5}{2})_{216}$	$(3, \frac{1}{2})_{160}, (3, \frac{3}{2})_{56}$
	$(7, \frac{7}{2})_8$	$(1, \frac{1}{2})_8$
	$(8, 0)_{1764}$	$(8, 0)_{588}, (6, 0)_{840}, (4, 0)_{300}, (2, 0)_{35}, (0, 0)_1$
	$(8, 1)_{2352}$	$(6, 0)_{840}, (6, 1)_{1134}, (4, 1)_{350}, (2, 1)_{28}$
	$(8, 2)_{720}$	$(4, 0)_{300}, (4, 1)_{350}, (4, 2)_{70}$
	$(8, 3)_{63}$	$(2, 0)_{35}, (2, 1)_{28}$
	$(8, 4)_1$	$(0, 0)_1$

Appendix E

Some properties of $SU(\Omega)$ Wigner coefficients

Some properties of the $SU(\Omega)$ Wigner coefficients used in Chapter 4 are given here and they are similar to those used for EGUE(2) and EGUE(2)-s in [Ko-05, Ko-07] and discussed in detail in [Bu-81]. Firstly (dropping the multiplicity index ρ everywhere for simplicity),

$$\langle f_a v_a f_b v_b | f_{ab} v_{ab} \rangle = (-1)^{\phi(f_a, f_b, f_{ab})} \langle f_b v_b f_a v_a | f_{ab} v_{ab} \rangle, \quad (\text{E1})$$

where ϕ is a function of (f_a, f_b, f_{ab}) that defines the phase for $a \rightarrow b$ interchange in the Wigner coefficient. With $|\overline{f_a v_a}\rangle$ denoting the time-reversal partner (complex conjugate) of $|f_a v_a\rangle$, we have

$$\langle f_a v_a f_b v_b | f_{ab} v_{ab} \rangle = \langle \overline{f_a v_a} \overline{f_b v_b} | \overline{f_{ab} v_{ab}} \rangle. \quad (\text{E2})$$

Similarly,

$$\langle f_a v_a f_b v_b | f_{ab} v_{ab} \rangle = (-1)^{\phi(f_a, f_b, f_{ab})} \sqrt{\frac{d_\Omega(f_{ab})}{d_\Omega(f_a)}} \langle f_{ab} v_{ab} \overline{f_b v_b} | f_a v_a \rangle. \quad (\text{E3})$$

In addition we also have,

$$\langle f_a v_a \overline{f_a v_a} | \{0\} 0 \rangle = \frac{1}{\sqrt{d_\Omega(f_a)}}, \quad (\text{E4})$$

$$\left[\left\langle f_a v_a \overline{f_a} \overline{v_b} \mid f_{ab} v_{ab} \right\rangle \right]^* = \left\langle f_a v_b \overline{f_a} \overline{v_a} \mid f_{ab} v_{ab} \right\rangle . \quad (\text{E5})$$

Orthonormal properties of the Wigner coefficients are,

$$\sum_{v_a, v_b} \left\langle f_a v_a f_b v_b \mid f_{ab} v_{ab} \right\rangle \left[\left\langle f_a v_a f_b v_b \mid f_{cd} v_{cd} \right\rangle \right]^* = \delta_{f_{ab}, f_{cd}} \delta_{v_{ab}, v_{cd}} , \quad (\text{E6a})$$

$$\sum_{f_{ab}, v_{ab}} \left\langle f_a v_a f_b v_b \mid f_{ab} v_{ab} \right\rangle \left\langle f_a v_c f_b v_d \mid f_{ab} v_{ab} \right\rangle = \delta_{v_a, v_c} \delta_{v_b, v_d} . \quad (\text{E6b})$$

Finally,

$$\begin{aligned} & \sum_{v_{ab}} \left\langle f_a v_a f_b v_b \mid f_{ab} v_{ab} \right\rangle \left\langle f_{ab} v_{ab} f_c v_c \mid f v \right\rangle \\ &= \sum_{f_{bc}, v_{bc}} \left\langle f_b v_b f_c v_c \mid f_{bc} v_{bc} \right\rangle \left\langle f_a v_a f_{bc} v_{bc} \mid f v \right\rangle U(f_a f_b f f_c; f_{ab} f_{bc}) . \end{aligned} \quad (\text{E7})$$

Appendix F

Excess parameter $\gamma_2(m, f_m)$ in terms of $SU(\Omega)$ Racah coefficients

The formula for $\gamma_2(m, f_m)$, given by Eq. (4.4.7), involves $\overline{\langle H^4 \rangle^{m, f_m}}$. As the Hamiltonian in Eq. (4.3.1) is a direct sum of matrices in $f_2 = \{2\}$ and $\{1^2\}$ spaces, we have

$$\overline{\langle H^4 \rangle^{m, f_m}} = \overline{\langle (H_{\{2\}} + H_{\{1^2\}})^4 \rangle^{m, f_m}}. \quad (\text{F1})$$

Expanding the RHS of Eq. (F1) using the cyclic invariance of the averages and applying the property that terms with odd powers of $H_{\{2\}}$ and $H_{\{1^2\}}$ will vanish [see Eq. (4.3.6)], we have

$$\begin{aligned} \overline{\langle H^4 \rangle^{m, f_m}} &= \overline{\langle (H_{\{2\}})^4 \rangle^{m, f_m}} + \overline{\langle (H_{\{1^2\}})^4 \rangle^{m, f_m}} + 4 \overline{\langle (H_{\{2\}})^2 (H_{\{1^2\}})^2 \rangle^{m, f_m}} \\ &\quad + 2 \overline{\langle H_{\{2\}} H_{\{1^2\}} H_{\{2\}} H_{\{1^2\}} \rangle^{m, f_m}}. \end{aligned} \quad (\text{F2})$$

Writing H in terms of the unit tensors B 's using Eq. (4.4.3), the first two terms in Eq. (F2) will give

$$\begin{aligned} &\overline{\langle H_{f_2}^4 \rangle^{m, f_m}} \\ &= \frac{1}{d_\Omega(f_m)} \sum_{v_1, v_2, v_3, v_4, \mathbf{F}_{v_1}, \mathbf{F}_{v_2}, \mathbf{F}_{v_3}, \mathbf{F}_{v_4}, \omega_{v_1}, \omega_{v_2}, \omega_{v_3}, \omega_{v_4}} \langle f_m v_1 | B(f_2 \mathbf{F}_{v_1} \omega_{v_1}) | f_m v_2 \rangle \end{aligned}$$

$$\begin{aligned}
& \times \langle f_m \nu_2 | B(f_2 \mathbf{F}_{\nu_2} \omega_{\nu_2}) | f_m \nu_3 \rangle \langle f_m \nu_3 | B(f_2 \mathbf{F}_{\nu_3} \omega_{\nu_3}) | f_m \nu_4 \rangle \\
& \times \langle f_m \nu_4 | B(f_2 \mathbf{F}_{\nu_4} \omega_{\nu_4}) | f_m \nu_1 \rangle \\
& \times \overline{W(f_2 \mathbf{F}_{\nu_1} \omega_{\nu_1}) W(f_2 \mathbf{F}_{\nu_2} \omega_{\nu_2}) W(f_2 \mathbf{F}_{\nu_3} \omega_{\nu_3}) W(f_2 \mathbf{F}_{\nu_4} \omega_{\nu_4})}.
\end{aligned} \tag{F3}$$

Using Eq. (4.4.5), it is easy to see that the term $\overline{\langle H_{f_2}^4 \rangle^{m, f_m}}$ will have non-zero contribution in three cases, (i) $\delta_{\mathbf{F}_{\nu_1}, \mathbf{F}_{\nu_2}} = 1, \delta_{\omega_{\nu_1}, \omega_{\nu_2}} = 1, \delta_{\mathbf{F}_{\nu_3}, \mathbf{F}_{\nu_4}} = 1, \delta_{\omega_{\nu_3}, \omega_{\nu_4}} = 1$; (ii) $\delta_{\mathbf{F}_{\nu_1}, \mathbf{F}_{\nu_4}} = 1, \delta_{\omega_{\nu_1}, \omega_{\nu_4}} = 1, \delta_{\mathbf{F}_{\nu_2}, \mathbf{F}_{\nu_3}} = 1, \delta_{\omega_{\nu_2}, \omega_{\nu_3}} = 1$; and (iii) $\delta_{\mathbf{F}_{\nu_1}, \mathbf{F}_{\nu_3}} = 1, \delta_{\omega_{\nu_1}, \omega_{\nu_3}} = 1, \delta_{\mathbf{F}_{\nu_2}, \mathbf{F}_{\nu_4}} = 1, \delta_{\omega_{\nu_2}, \omega_{\nu_4}} = 1$. The first two cases are equivalent due to cyclic invariance of the traces and they can be called direct terms whereas the third case involves cross-correlations and thus is called the exchange term. For (i) and (ii), applying the Wigner-Eckart theorem and carrying out simplifications using the properties of the Wigner coefficients (see Appendix E), the direct terms reduce to $2 \left[\overline{\langle H_{f_2}^2 \rangle^{m, f_m}} \right]^2$. Similarly, for the exchange term, reordering of the Wigner coefficients [see Eq. (E7)] yields an expression in terms of a new Racah coefficient. With these, we have

$$\begin{aligned}
\overline{\langle H_{f_2}^4 \rangle^{m, f_m}} &= 2 \left[\overline{\langle H_{f_2}^2 \rangle^{m, f_m}} \right]^2 + \lambda_{f_2}^4 [d_4(F_2)]^2 d_\Omega(f_m) \\
&\times \sum_{\mathbf{F}_{\nu_1}, \mathbf{F}_{\nu_2}, \rho_1, \rho_2, \rho_3, \rho_4} \frac{1}{\sqrt{d_\Omega(\mathbf{F}_{\nu_1}) d_\Omega(\mathbf{F}_{\nu_2})}} U(f_m \overline{f_m} f_m f_m; (\mathbf{F}_{\nu_1})_{\rho_1 \rho_3} (\mathbf{F}_{\nu_2})_{\rho_2 \rho_4}) \\
&\times \langle f_m || B(f_2 \mathbf{F}_{\nu_1}) || f_m \rangle_{\rho_1} \langle f_m || B(f_2 \mathbf{F}_{\nu_2}) || f_m \rangle_{\rho_2} \\
&\times \langle f_m || B(f_2 \mathbf{F}_{\nu_1}) || f_m \rangle_{\rho_3} \langle f_m || B(f_2 \mathbf{F}_{\nu_2}) || f_m \rangle_{\rho_4}.
\end{aligned} \tag{F4}$$

In Eq. (F4), the multiplicity labels appearing in the new U -coefficient [this is quite different from the U -coefficient appearing in Eq. (4.4.10)] can be easily understood from the corresponding labels in the reduced matrix elements. Similarly, we have

$$\overline{\langle H_{\{2\}}^2 H_{\{1^2\}}^2 \rangle^{m, f_m}} = \left\{ \overline{\langle H_{\{2\}}^2 \rangle^{m, f_m}} \right\} \left\{ \overline{\langle H_{\{1^2\}}^2 \rangle^{m, f_m}} \right\}, \tag{F5a}$$

$$\begin{aligned}
& \overline{\langle H_{\{2\}} H_{\{1^2\}} H_{\{2\}} H_{\{1^2\}} \rangle^{m, f_m}} = \lambda_{\{2\}}^2 \lambda_{\{1^2\}}^2 d_4(\{2\}) d_4(\{1^2\}) d_\Omega(f_m) \\
& \times \sum_{\mathbf{F}_{v_1}, \mathbf{F}_{v_2}, \rho_1, \rho_2, \rho_3, \rho_4} \frac{1}{\sqrt{d_\Omega(\mathbf{F}_{v_1}) d_\Omega(\mathbf{F}_{v_2})}} U(f_m \overline{f_m} f_m f_m; (\mathbf{F}_{v_1})_{\rho_1 \rho_3} (\mathbf{F}_{v_2})_{\rho_2 \rho_4}) \\
& \times \langle f_m \parallel B(\{2\} \mathbf{F}_{v_1}) \parallel f_m \rangle_{\rho_1} \langle f_m \parallel B(\{1^2\} \mathbf{F}_{v_2}) \parallel f_m \rangle_{\rho_2} \\
& \times \langle f_m \parallel B(\{2\} \mathbf{F}_{v_1}) \parallel f_m \rangle_{\rho_3} \langle f_m \parallel B(\{1^2\} \mathbf{F}_{v_2}) \parallel f_m \rangle_{\rho_4} .
\end{aligned} \tag{F5b}$$

Substituting the results in Eqs. (F4), (F5a) and (F5b) in Eq. (F2) gives $\overline{\langle H^4 \rangle^{m, f_m}}$. Using this and Eqs. (4.5.5) and (4.4.7), we have the analytical result for the excess parameter $\gamma_2(m, f_m)$. This involves $SU(\Omega)$ Racah coefficients with multiplicity labels and evaluation of these is in general complicated [Gl-05, Kl-09]. Similarly, evaluation of the reduced matrix elements in Eq. (F4) is also complicated. The only simple situation is, when the multiplicity labels are all unity. We denote the $U(\Omega)$ irreps that satisfy this as $f_m^{(g)}$ and we have verified that one of these irreps is $\{4^r\}$ where $m = 4r$. For these irreps, the expression for γ_2 is,

$$\begin{aligned}
& \left[\gamma_2(m, f_m^{(g)}) + 1 \right] = \left[\overline{\langle H^2 \rangle^{m, f_m^{(g)}}} \right]^{-2} \\
& \times \left\{ \sum_{f_a, f_b = \{2\}, \{1^2\}} \frac{\lambda_{f_a}^2 \lambda_{f_b}^2}{d_\Omega(f_a) d_\Omega(f_b)} \sum_{\mathbf{F}_{v_1}, \mathbf{F}_{v_2}} \frac{d_\Omega(f_m^{(g)})}{\sqrt{d_\Omega(\mathbf{F}_{v_1}) d_\Omega(\mathbf{F}_{v_2})}} \right. \\
& \left. \times U(f_m^{(g)} \overline{f_m^{(g)}} f_m^{(g)} f_m^{(g)}; \mathbf{F}_{v_1} \mathbf{F}_{v_2}) \mathcal{Q}^{v_1}(f_a : m, f_m^{(g)}) \mathcal{Q}^{v_2}(f_b : m, f_m^{(g)}) \right\} .
\end{aligned} \tag{F6}$$

The $\mathcal{Q}^v(f_2 : m, f_m)$ in Eq. (F6) are defined by Eq. (4.5.6). They can be calculated using X_{UU} given in Table 4.4. Therefore the only unknown in Eq. (F6) is the $SU(\Omega)$ Racah coefficient $U(f_m^{(g)} \overline{f_m^{(g)}} f_m^{(g)} f_m^{(g)}; \mathbf{F}_{v_1} \mathbf{F}_{v_2})$. There are many attempts in the past to derive analytical formulation and also to develop numerical methods for evaluating general $SU(N)$ Racah coefficients [Bi-68, Lo-70a, Lo-70, Bl-87, Bi-82, Se-88, Vi-95]. There are also attempts to derive analytical formulas for some simple class of Racah coefficients; see [Vi-95, Li-90] and references therein. In addition, there is a recent effort

to develop a new numerical method for evaluating $SU(N)$ Racah coefficients with multiplicities [Gl-05, Kl-09]. From all the attempts we made in trying to use these results, we conclude that further group theoretical work on $SU(N)$ Racah coefficients is needed to be able to derive analytical formulas for, or for evaluating numerically, the Racah coefficients appearing in Eq. (F6).

Appendix G

Further extensions of BEGOE(1+2)

For completeness, we briefly outline here extension of BEGOE(1+2) to BEGOE(1+2)- M_S and BEGOE(1+2)- p ; here p corresponds to spin $\mathbf{s} = 1$ bosons and M_S is the S_z quantum number for spin $\mathbf{s} = \frac{1}{2}$ bosons. We restrict our discussion to the definition and construction of these ensembles using the results for spinless BEGOE(1+2) discussed in Chapter 1.

BEBOE(1+2)- M_S

Consider a system of m bosons occupying Ω number of sp orbitals each with spin $\mathbf{s} = \frac{1}{2}$ so that the number of sp states $N = 2\Omega$. The sp states are denoted by $|v_i, m_{\mathbf{s}}\rangle$, $i = 1, 2, \dots, \Omega$ and $m_{\mathbf{s}} = \pm \frac{1}{2}$. The average spacing between the v_i states is assumed to be Δ and between two $m_{\mathbf{s}}$ states for a given v_i to be $\Delta_{m_{\mathbf{s}}}$. For constructing the H matrix in good M_S representation, we arrange the sp states $|i, m_{\mathbf{s}} = \pm \frac{1}{2}\rangle$ in such a way that the first Ω states have $m_{\mathbf{s}} = \frac{1}{2}$ and the remaining Ω states have $m_{\mathbf{s}} = -\frac{1}{2}$. Many-particle states for m bosons in the 2Ω sp states, arranged as explained above, can be obtained by distributing m_1 bosons in the $m_{\mathbf{s}} = \frac{1}{2}$ sp states (Ω in number) and similarly, m_2 fermions in the $m_{\mathbf{s}} = -\frac{1}{2}$ sp states (Ω in number) with $m = m_1 + m_2$. Thus, $M_S = (m_1 - m_2)/2$. Let us denote each distribution of m_1 fermions in $m_{\mathbf{s}} = \frac{1}{2}$ sp states by \mathbf{m}_1 and similarly, \mathbf{m}_2 for m_2 fermions in $m_{\mathbf{s}} = -\frac{1}{2}$ sp states. Many-particle basis defined by $(\mathbf{m}_1, \mathbf{m}_2)$ with $m_1 - m_2 = 2M_S$ will form the basis for BEGOE(1+2)- M_S . As the two-particle m_s can take values ± 1 and 0, the two-body part of the Hamiltonian preserving M_S will be $\hat{V}(2) = \lambda_0 \hat{V}^{m_s=0}(2) + \lambda_1 \hat{V}^{m_s=1}(2) + \lambda_{-1} \hat{V}^{m_s=-1}(2)$ with the corresponding two-particle matrix being a direct sum matrix generated by $\hat{V}^{m_s}(2)$. Therefore, the

Hamiltonian is

$$\hat{H} = \hat{h}(1) + \lambda_0 \{ \hat{V}^{m_s=0}(2) \} + \lambda_1 \{ \hat{V}^{m_s=1}(2) \} + \lambda_{-1} \{ \hat{V}^{m_s=-1}(2) \}. \quad (G1)$$

In Eq. (G1), the $\{ \hat{V}^{m_s}(2) \}$ ensembles in two-particle spaces are represented by independent GOE(1)'s [see Eq. (1.2.4)] and λ_{m_s} 's are their corresponding strengths. The action of the Hamiltonian operator defined by Eq. (G1) on the $(\mathbf{m}_1, \mathbf{m}_2)$ basis states with a given M_S generates the BEGOE(1+2)- M_S ensemble in m -particle spaces. Therefore, BEGOE(1+2)- M_S is defined by six parameters $(\Omega, m, \Delta_{m_s}, \lambda_0, \lambda_1, \lambda_{-1})$ [we put $\Delta = 1$ so that Δ_{m_s} and λ_{m_s} 's are in the units of Δ]. In the $(\mathbf{m}_1, \mathbf{m}_2)$ basis with a given M_S , the H matrix construction reduces to the matrix construction for spinless boson systems; see Chapter 1. The H matrix dimension for a given M_S is $\sum_{S \geq M_S} d_b(\Omega, m, S)$. Finally, pairing can also be introduced in this ensemble using the algebra $U(2\Omega) \supset SO(2\Omega) \supset SO(\Omega) \otimes SO(2)$ with $SO(2)$ generating M_S ; see [Ko-06c].

BE $GOE(1+2)$ - p

Let us begin with a system of m bosons distributed say in Ω number of sp orbitals each with spin $\mathbf{s} = 1$ so that the number of sp states $N = 3\Omega$. The sp states are denoted by $|i, m_s\rangle$ with $m_s = 0, \pm 1$ and $i = 1, 2, \dots, \Omega$. For a one plus two-body Hamiltonians preserving m -particle spin S , the one-body Hamiltonian $\hat{h}(1)$ is defined by the sp energies ϵ_i ; $i = 1, 2, \dots, \Omega$, with average spacing Δ . Similarly the two-body Hamiltonian $\hat{V}(2)$ is defined by the two-body matrix elements $\lambda_s V_{ijkl}^s = \langle (kl)s, m_s | \hat{V}(2) | (ij)s, m_s \rangle$ with the two-particle spins $s = 0, 1$ and 2 . These matrix elements are independent of the m_s quantum number. Note that the λ_s are parameters. For generating the many-particle states, firstly, the sp states are arranged such that the first Ω number of sp states have $m_s = 1$, next Ω number of sp states have $m_s = 0$ and the remaining Ω sp states have $m_s = -1$. Now, the many-particle states for m bosons can be obtained by distributing m_1 bosons in the $m_s = 1$ sp states, m_2 bosons in the $m_s = 0$ sp states and similarly, m_3 bosons in the $m_s = -1$ sp states with $m = m_1 + m_2 + m_3$. Thus, $M_S = (m_1 - m_3)$. Let us denote each distribution of m_1 bosons in $m_s = 1$ sp states by \mathbf{m}_1 , m_2 bosons in $m_s = 0$ sp states by \mathbf{m}_2 and similarly, \mathbf{m}_3 for m_3 bosons in $m_s = -1$ sp states. Many-particle basis defined by $(\mathbf{m}_1, \mathbf{m}_2, \mathbf{m}_3)$

will form a basis for $\text{BEGOE}(1+2)-p$. The V matrix in two-particle spaces will be a direct sum matrix and the $V(2)$ operator is $\hat{V}(2) = \lambda_0 \hat{V}^{s=0}(2) + \lambda_1 \hat{V}^{s=1}(2) + \lambda_2 \hat{V}^{s=2}(2)$ with three parameters $(\lambda_0, \lambda_1, \lambda_2)$. Now, $\text{BEGOE}(1+2)-p$ for a given (m, S) system is generated by defining the three parts of the two-body Hamiltonian to be independent $\text{GOE}(1)$'s in two-particle spaces and then propagating the $V(2)$ ensemble $\{\hat{V}(2)\} = \lambda_0 \{\hat{V}^{s=0}(2)\} + \lambda_1 \{\hat{V}^{s=1}(2)\} + \lambda_2 \{\hat{V}^{s=2}(2)\}$ to the m -particle spaces with a given spin S by using the geometry (direct product structure) of the m -particle spaces. The embedding algebra is $U(3\Omega) \supset G \supset G1 \otimes SO(3)$ with $SO(3)$ generating spin S . Thus $\text{BEGOE}(1+2)-p$ is defined by the operator

$$\hat{H} = \hat{h}(1) + \lambda_0 \{\hat{V}^{s=0}(2)\} + \lambda_1 \{\hat{V}^{s=1}(2)\} + \lambda_2 \{\hat{V}^{s=2}(2)\}. \quad (\text{G2})$$

The sp levels defined by $\hat{h}(1)$ will be triply degenerate. The action of the Hamiltonian operator defined by Eq. (G2) on $(\mathbf{m}_1, \mathbf{m}_2, \mathbf{m}_3)$ basis states with fixed- $(m, M_S = M_S^{min})$ generates the ensemble in (m, M_S) spaces. It is important to note that the construction of the m -particle H matrix in fixed- $(m, M_S = M_S^{min})$ spaces reduces to the problem of $\text{BEGOE}(1+2)$ for spinless boson systems and hence Eqs. (1.3.1)- (1.3.3) of Chapter 1 will apply. Then the \hat{S}^2 operator is used for projecting states with good S . Therefore, $\text{BEGOE}(1+2)-p$ ensemble is defined by five parameters $(\Omega, m, \lambda_0, \lambda_1, \lambda_2)$ with λ_s in units of Δ . Finally, it is important to mention that it is also possible to study the pairing symmetry in the space defined by $\text{BEGOE}(1+2)-p$ ensemble. For this, there are two possible algebras (each defining a particular type of pairing), $U(3\Omega) \supset [U(\Omega) \supset SO(\Omega)] \otimes [U(3) \supset SO(3)]$ and $U(3\Omega) \supset SO(3\Omega) \supset SO(\Omega) \otimes SO(3)$ and they can be studied in detail by extending the results for IBM-3 model in nuclear structure where $\Omega = 6$ [Ga-99, Ko-96]. Exploiting the group chain $U(3\Omega) \supset U(\Omega) \otimes [U(3) \supset SO(3)]$, it is possible to write the dimension formulas for the H matrices for a given (m, S) as it was done in Sec. 4.2.3 for $SU(4) - ST$ reductions.

Appendix H

Basic binary correlation results

We denote a k_H -body operator as,

$$H(k_H) = \sum_{\alpha, \beta} v_H^{\alpha\beta} \alpha^\dagger(k_H) \beta(k_H). \quad (\text{H1})$$

Here, $\alpha^\dagger(k_H)$ is the k_H particle creation operator and $\beta(k_H)$ is the k_H particle annihilation operator. Similarly, $v_H^{\alpha\beta}$ are matrix elements of the operator H in k_H particle space i.e., $v_H^{\alpha\beta} = \langle k_H \beta | H | k_H \alpha \rangle$ (it should be noted that Mon and French [Mo-73, Mo-75] used operators with daggers to denote annihilation operators and operators without daggers to denote creation operators). Following basic traces will be used throughout,

$$\sum_{\alpha} \alpha^\dagger(k) \alpha(k) = \binom{\hat{n}}{k} \Rightarrow \left\langle \sum_{\alpha} \alpha^\dagger(k) \alpha(k) \right\rangle^m = \binom{m}{k}. \quad (\text{H2})$$

$$\sum_{\alpha} \alpha(k) \alpha^\dagger(k) = \binom{N - \hat{n}}{k} \Rightarrow \left\langle \sum_{\alpha} \alpha(k) \alpha^\dagger(k) \right\rangle^m = \binom{\tilde{m}}{k}; \quad \tilde{m} = N - m. \quad (\text{H3})$$

$$\begin{aligned} \sum_{\alpha} \alpha^\dagger(k) B(k') \alpha(k) &= \binom{\hat{n} - k'}{k} B(k') \\ &\Rightarrow \left\langle \sum_{\alpha} \alpha^\dagger(k) B(k') \alpha(k) \right\rangle^m = \binom{m - k'}{k} B(k'). \end{aligned} \quad (\text{H4})$$

$$\sum_{\alpha} \alpha(k) B(k') \alpha^{\dagger}(k) = \binom{N - \hat{n} - k'}{k} B(k') \quad (\text{H5})$$

$$\Rightarrow \left\langle \sum_{\alpha} \alpha(k) B(k') \alpha^{\dagger}(k) \right\rangle^m = \binom{\tilde{m} - k'}{k} B(k').$$

Equation (H2) follows from the fact that the average should be zero for $m < k$ and one for $m = k$ and similarly, Eq. (H3) follows from the same argument except that the particles are replaced by holes. Equation (H4) follows first by writing the k' -body operator $B(k')$ in operator form using Eq. (H1), i.e.,

$$B(k') = \sum_{\beta, \gamma} v_B^{\beta\gamma} \beta^{\dagger}(k') \gamma(k'), \quad (\text{H6})$$

and then applying the commutation relations for the fermion creation and annihilation operators. This gives $\sum_{\beta, \gamma} v_B^{\beta\gamma} \beta^{\dagger}(k') \sum_{\alpha} \alpha^{\dagger}(k) \alpha(k) \gamma(k')$. Now applying Eq. (H2) to the sum involving α gives Eq. (H4). Eq. (H5) follows from the same arguments except one has to assume that $B(k')$ is fully irreducible $v = k'$ operator and therefore, it has particle-hole symmetry. For a general $B(k')$ operator, this is valid only in the $N \rightarrow \infty$ limit. Therefore, this equation has to be applied with caution.

Using the definition of the H operator in Eq. (H1), we have

$$\begin{aligned} \overline{\langle H(k_H) H(k_H) \rangle^m} &= \sum_{\alpha, \beta} \overline{\left\{ v_H^{\alpha\beta} \right\}^2} \left\langle \alpha^{\dagger}(k_H) \beta(k_H) \beta^{\dagger}(k_H) \alpha(k_H) \right\rangle^m \\ &= v_H^2 \left\langle \sum_{\alpha} \alpha^{\dagger}(k_H) \left\{ \sum_{\beta} \beta(k_H) \beta^{\dagger}(k_H) \right\} \alpha(k_H) \right\rangle^m \quad (\text{H7}) \\ &= v_H^2 T(m, N, k_H). \end{aligned}$$

Here, H is taken as EGOE(k_H) with all the k_H particle matrix elements being Gaussian variables with zero center and same variance for off-diagonal matrix elements (twice for the diagonal matrix elements). This gives $\overline{(v_H^{\alpha\beta})^2} = v_H^2$ to be independent of α, β labels. It is important to note that in the dilute limit, the diagonal terms [$\alpha = \beta$ in Eq. (H7)] in the averages are neglected (as they are smaller by at least one power of $1/N$) and the individual H 's are unitarily irreducible. These assumptions are no longer

valid for finite- N systems and hence, evaluation of averages is more complicated. In the dilute limit, we have

$$\begin{aligned}
T(m, N, k_H) &= \left\langle \sum_{\alpha} \alpha^{\dagger}(k_H) \left\{ \sum_{\beta} \beta(k_H) \beta^{\dagger}(k_H) \right\} \alpha(k_H) \right\rangle^m \\
&= \binom{\tilde{m} + k_H}{k_H} \left\langle \sum_{\alpha} \alpha^{\dagger}(k_H) \alpha(k_H) \right\rangle^m \\
&= \binom{\tilde{m} + k_H}{k_H} \binom{m}{k_H}.
\end{aligned} \tag{H8}$$

Note that, we have used Eq. (H3) to evaluate the summation over β and Eq. (H2) to evaluate summation over α in Eq. (H8). In the ‘strict’ $N \rightarrow \infty$ limit, we have

$$T(m, N, k_H) \xrightarrow{N \rightarrow \infty} \binom{m}{k_H} \binom{N}{k_H}. \tag{H9}$$

In order to incorporate the finite- N corrections, we have to consider the contribution of the diagonal terms. Then, we have,

$$\begin{aligned}
&T(m, N, k_H) \\
&= \left\langle \sum_{\alpha \neq \beta} \alpha^{\dagger}(k_H) \beta(k_H) \beta^{\dagger}(k_H) \alpha(k_H) \right\rangle^m + 2 \left\langle \sum_{\alpha} \alpha^{\dagger}(k_H) \alpha(k_H) \alpha^{\dagger}(k_H) \alpha(k_H) \right\rangle^m \\
&= \left\langle \sum_{\alpha} \alpha^{\dagger}(k_H) \left\{ \sum_{\beta} \beta(k_H) \beta^{\dagger}(k_H) \right\} \alpha(k_H) \right\rangle^m \\
&\quad + \left\langle \sum_{\alpha} \alpha^{\dagger}(k_H) \alpha(k_H) \alpha^{\dagger}(k_H) \alpha(k_H) \right\rangle^m \\
&= \binom{\tilde{m} + k_H}{k_H} \binom{m}{k_H} + \binom{m}{k_H} = \binom{m}{k_H} \left[\binom{\tilde{m} + k_H}{k_H} + 1 \right].
\end{aligned} \tag{H10}$$

Note that the prefactor ‘2’ in the second term of first line in Eq. (H10) comes because variance of the diagonal terms is twice that of the off-diagonal terms. Also, the trace $\sum_{\alpha} \alpha^{\dagger}(k_H) \alpha(k_H) \alpha^{\dagger}(k_H) \alpha(k_H) = \sum_{\alpha} \alpha^{\dagger}(k_H) \alpha(k_H)$ as the operator $\alpha^{\dagger}(k_H) \alpha(k_H)$

conserves the number of particles. Now we turn to evaluating fourth order averages.

For averages involving product of four operators of the form

$$\langle H(k_H)G(k_G)H(k_H)G(k_G) \rangle^m ,$$

with operators H and G independent and of body ranks k_H and k_G respectively, there are two possible ways of evaluating this trace. Either (a) first contract the H operators across the G operator using Eq. (H5) and then contract the G operators using Eq. (H4), or (b) first contract the G operators across the H operator using Eq. (H5) and then contract the H operators using Eq. (H5). Following (a), in the dilute limit, we get

$$\begin{aligned} & \overline{\langle H(k_H)G(k_G)H(k_H)G(k_G) \rangle^m} \\ &= \sum_{\alpha, \beta} \overline{\left\{ v_H^{\alpha\beta} \right\}^2} \left\langle \alpha^\dagger(k_H) \beta(k_H) G(k_G) \beta^\dagger(k_H) \alpha(k_H) G(k_G) \right\rangle^m \\ &= v_H^2 \binom{\tilde{m} + k_H - k_G}{k_H} \sum_{\alpha} \left\langle \alpha^\dagger(k_H) G(k_G) \alpha(k_H) G(k_G) \right\rangle^m \quad (\text{H11}) \\ &= v_H^2 \binom{\tilde{m} + k_H - k_G}{k_H} \binom{m - k_G}{k_H} \langle G(k_G) G(k_G) \rangle^m \\ &= v_H^2 v_G^2 \binom{\tilde{m} + k_H - k_G}{k_H} \binom{m - k_G}{k_H} \binom{\tilde{m} + k_G}{k_G} \binom{m}{k_G}. \end{aligned}$$

Similarly, following (b), in the dilute limit, we get

$$\begin{aligned} & \overline{\langle H(k_H)G(k_G)H(k_H)G(k_G) \rangle^m} \\ &= v_H^2 v_G^2 \binom{\tilde{m} + k_G - k_H}{k_G} \binom{m - k_H}{k_G} \binom{\tilde{m} + k_H}{k_H} \binom{m}{k_H}. \quad (\text{H12}) \end{aligned}$$

The result should be independent of the preference. In other words, the average should have the $k_H \leftrightarrow k_G$ symmetry. As seen from Eqs. (H11) and (H12), this symmetry is violated except for the trivial case of $k_H = k_G$. However, the $k_H \leftrightarrow k_G$ symmetry is valid for ‘strict’ $N \rightarrow \infty$ result and also for the result incorporating finite N

corrections as discussed below. In general, the final result can be expressed as,

$$\overline{\langle H(k_H)G(k_G)H(k_H)G(k_G) \rangle^m} = v_H^2 v_G^2 F(m, N, k_H, k_G). \quad (\text{H13})$$

In the ‘strict’ dilute limit, both Eqs. (H11) and (H12) reduce to give result for $F(m, N, k_H, k_G)$,

$$F(m, N, k_H, k_G) = \binom{m - k_H}{k_G} \binom{m}{k_H} \binom{N}{k_H} \binom{N}{k_G}, \quad (\text{H14})$$

In order to obtain finite- N corrections to $F(\dots)$, we have to contract over operators whose lower symmetry parts can not be ignored. The operator $H(k_H)$ contains irreducible symmetry parts $\mathcal{F}(s)$ denoted by $s = 0, 1, 2, \dots, k_H$ with respect to the unitary group $SU(N)$ decomposition of the operator. For a k_H -body number conserving operator [Ch-71, Mo-75],

$$H(k_H) = \sum_{s=0}^{k_H} \binom{m-s}{k_H-s} \mathcal{F}(s). \quad (\text{H15})$$

Here, the $\mathcal{F}(s)$ are orthogonal with respect to m -particle averages, i.e., $\langle \mathcal{F}(s) \mathcal{F}^\dagger(s') \rangle^m = \delta_{ss'}$. Now, the m -particle trace in Eq. (H11) with binary correlations will have four parts,

$$\begin{aligned} & \overline{\langle H(k_H)G(k_G)H(k_H)G(k_G) \rangle^m} \\ &= v_H^2 v_G^2 \sum_{\alpha, \beta, \gamma, \delta} \left\langle \alpha^\dagger(k_H) \beta(k_H) \gamma^\dagger(k_G) \delta(k_G) \beta^\dagger(k_H) \alpha(k_H) \delta^\dagger(k_G) \gamma(k_G) \right\rangle^m \\ &+ v_H^2 v_G^2 \sum_{\alpha, \gamma, \delta} \left\langle \alpha^\dagger(k_H) \alpha(k_H) \gamma^\dagger(k_G) \delta(k_G) \alpha^\dagger(k_H) \alpha(k_H) \delta^\dagger(k_G) \gamma(k_G) \right\rangle^m \\ &+ v_H^2 v_G^2 \sum_{\alpha, \beta, \gamma} \left\langle \alpha^\dagger(k_H) \beta(k_H) \gamma^\dagger(k_G) \gamma(k_H) \beta^\dagger(k_H) \alpha(k_H) \gamma^\dagger(k_G) \gamma(k_G) \right\rangle^m \\ &+ v_H^2 v_G^2 \sum_{\alpha, \delta} \left\langle \alpha^\dagger(k_H) \alpha(k_H) \delta^\dagger(k_G) \delta(k_G) \alpha^\dagger(k_H) \alpha(k_H) \delta^\dagger(k_G) \delta(k_G) \right\rangle^m \\ &= X + Y_1 + Y_2 + Z. \end{aligned} \quad (\text{H16})$$

Note that we have decomposed each operator into diagonal and off-diagonal parts. We have used the condition that the variance of the diagonal matrix elements is twice that of the off-diagonal matrix elements in the defining spaces to convert the restricted summations into unrestricted summations appropriately to obtain the four terms in the RHS of Eq. (H17). Following Mon's thesis [Mo-73] and applying unitary decomposition to $\gamma\delta^\dagger$ (also $\delta\gamma^\dagger$) in the first two terms and $\alpha\beta^\dagger$ (also $\beta\alpha^\dagger$) in the third term we get X , Y_1 and Y_2 . To make things clear, we will discuss the derivation for X term in detail before proceeding further. Applying unitary decomposition to the operators $\gamma^\dagger(k_G)\delta(k_G)$ and $\gamma(k_G)\delta^\dagger(k_G)$ using Eq. (H15), we have

$$X = v_H^2 v_G^2 \sum_{\alpha, \beta, \gamma, \delta} \sum_{s=0}^{k_G} \binom{m-s}{k_G-s}^2 \left\langle \alpha^\dagger(k_H)\beta(k_H)\mathcal{F}_{\gamma\delta}^\dagger(s)\beta^\dagger(k_H)\alpha(k_H)\mathcal{F}_{\gamma\delta}(s) \right\rangle^m. \quad (\text{H17})$$

Contracting the operators $\beta\beta^\dagger$ across \mathcal{F} 's using Eq. (H5) and operators $\alpha^\dagger\alpha$ across \mathcal{F} using Eq. (H4) gives,

$$X = v_H^2 v_G^2 \sum_{s=0}^{k_G} \binom{m-s}{k_G-s}^2 \binom{\tilde{m}+k_H-s}{k_H} \binom{m-s}{k_H} \sum_{\gamma, \delta} \left\langle \mathcal{F}_{\gamma\delta}^\dagger(s)\mathcal{F}_{\gamma\delta}(s) \right\rangle^m. \quad (\text{H18})$$

Inversion of the equation,

$$\sum_{\gamma, \delta} \left\langle \gamma^\dagger(k_G)\delta(k_G)\delta^\dagger(k_G)\gamma(k_G) \right\rangle^m = Q(m) = \sum_{s=0}^{k_G} \binom{m-s}{k_G-s}^2 \sum_{\gamma, \delta} \left\langle \mathcal{F}_{\gamma\delta}^\dagger(s)\mathcal{F}_{\gamma\delta}(s) \right\rangle^m, \quad (\text{H19})$$

gives,

$$\begin{aligned} & \binom{m-s}{k_G-s}^2 \sum_{\gamma, \delta} \left\langle \mathcal{F}_{\gamma\delta}^\dagger(s)\mathcal{F}_{\gamma\delta}(s) \right\rangle^m \\ &= \binom{m-s}{k_G-s}^2 \binom{N-m}{s} \binom{m}{s} [(k_G-s)!s!]^2 (N-2s+1) \\ & \times \sum_{t=0}^s \frac{(-1)^{t-s} [(N-t-k_G)!]^2}{(s-t)!(N-s-t+1)!t!(N-t)!} Q(N-t). \end{aligned} \quad (\text{H20})$$

It is important to mention that there are errors in the equation given in Mon's thesis and we have verified Eq. (H20) using Mathematica (Mon = Eq. (H20)/[(N-2s)!(s!)^2]).

For the average required in Eq. (H19), we have

$$Q(m) = \sum_{\gamma, \delta} \left\langle \gamma^\dagger(k_G) \delta(k_G) \delta^\dagger(k_G) \gamma(k_G) \right\rangle^m = \binom{\tilde{m} + k_G}{k_G} \binom{m}{k_G}. \quad (\text{H21})$$

Simplifying Eq. (H20) using Eq. (H21) and using the result in Eq. (H18) along with the series summation

$$\sum_{t=0}^s \frac{(-1)^{t-s} (N-t-k_G)! (k_G+t)!}{(s-t)! (t!)^2 (N-s-t+1)!} = \frac{k_G! (N-k_G-s)!}{(N+1-s)!} \binom{k_G}{s} \binom{N+1}{s}, \quad (\text{H22})$$

the expression for X is,

$$\begin{aligned} X &= v_H^2 v_G^2 F(m, N, k_H, k_G); \\ F(m, N, k_H, k_G) &= \sum_{s=0}^{k_G} \binom{m-s}{k_G-s}^2 \binom{\tilde{m} + k_H - s}{k_H} \binom{m-s}{k_H} \binom{\tilde{m}}{s} \binom{m}{s} \binom{N+1}{s} \\ &\times \frac{N-2s+1}{N-s+1} \binom{N-s}{k_G}^{-1} \binom{k_G}{s}^{-1}. \end{aligned} \quad (\text{H23})$$

Although not obvious, X has $k_H \leftrightarrow k_G$ symmetry and we have verified this explicitly for $k_H, k_G \leq 2$. Similarly, the terms Y_1 and Y_2 are given by,

$$\begin{aligned} Y_1 &= v_H^2 v_G^2 B(m, N, k_H, k_G), \quad Y_2 = v_H^2 v_G^2 B(m, N, k_G, k_H); \\ B(m, N, k_H, k_G) &= \sum_{s=0}^{k_G} \binom{m-s}{k_G-s}^2 \binom{\tilde{m} + k_H - s}{k_H} \binom{m-s}{k_H} \binom{\tilde{m}}{s} \binom{m}{s} \\ &\times \frac{N-2s+1}{N-s+1} \binom{N-s}{k_G}^{-1} \binom{k_G}{s}^{-1}. \end{aligned} \quad (\text{H24})$$

In order to derive Eq.(H24), we have used $Q(m) = \binom{m}{k_G}$ along with the series summation,

$$\sum_{t=0}^s \frac{(-1)^{t-s} (N-t-k_G)! k_G! t!}{(s-t)! (t!)^2 (N-s-t+1)!} = \frac{k_G! (N-k_G-s)!}{(N+1-s)!} \binom{k_G}{s}. \quad (\text{H25})$$

Note that Mon's thesis gives $\binom{m-s}{s}$ in place of $\binom{m-s}{k}$ with $k = k_H$ or k_G for X , Y_1 and Y_2

in Eqs. (H23) and (H24) and it should be a printing error. The expressions given in Eqs. (H23) and (H24) agree with the results given in Tomsovic's thesis [To-86]. Finally, the result for Z is

$$\begin{aligned}
Z &= v_H^2 v_G^2 \sum_{\alpha, \delta} \left\langle \alpha^\dagger(k_H) \alpha(k_H) \delta^\dagger(k_G) \delta(k_G) \alpha^\dagger(k_H) \alpha(k_H) \delta^\dagger(k_G) \delta(k_G) \right\rangle^m \\
&= v_H^2 v_G^2 \sum_{\alpha} \left\langle \alpha^\dagger(k_H) \alpha(k_H) \right\rangle^m \sum_{\delta} \left\langle \delta^\dagger(k_G) \delta(k_G) \right\rangle^m \\
&= v_H^2 v_G^2 C(m, N, k_H, k_G); \\
C(m, N, k_H, k_G) &= \binom{m}{k_H} \binom{m}{k_G}.
\end{aligned} \tag{H26}$$

Equation (H26) is in agreement with the result in Mon's thesis with $k_H = k_G = k$. However, it differs from the result given in Tomsovic's thesis. For a one-body operator, obviously $Z = m^2$ and this confirms that Eq. (H26) is correct. Therefore Eqs. (H16)-(H26) give the final formula for the trace $\overline{\langle H(k_H) G(k_G) H(k_H) G(k_G) \rangle^m}$. It is easily seen that dominant contribution to the average $\overline{\langle H(k_H) G(k_G) H(k_H) G(k_G) \rangle^m}$ comes from the X term and therefore, in all the applications, we use

$$\overline{\langle H(k_H) G(k_G) H(k_H) G(k_G) \rangle^m} = X = v_H^2 v_G^2 F(m, N, k_H, k_G). \tag{H27}$$

An immediate application of these averages is in evaluating the fourth order average $\langle H^4(k_H) \rangle^m$. There will be three different correlation patterns that will contribute to this average in the binary correlation approximation (we must correlate in pairs the operators for all moments of order > 2),

$$\begin{aligned}
\overline{\langle H^4(k_H) \rangle^m} &= \overline{\langle \textcolor{red}{H}(\textcolor{red}{k}_H) \textcolor{red}{H}(\textcolor{red}{k}_H) \textcolor{blue}{H}(\textcolor{blue}{k}_H) \textcolor{blue}{H}(\textcolor{blue}{k}_H) \rangle^m} \\
&+ \overline{\langle \textcolor{red}{H}(\textcolor{red}{k}_H) \textcolor{blue}{H}(\textcolor{blue}{k}_H) \textcolor{blue}{H}(\textcolor{blue}{k}_H) \textcolor{red}{H}(\textcolor{red}{k}_H) \rangle^m} \\
&+ \overline{\langle \textcolor{red}{H}(\textcolor{red}{k}_H) \textcolor{blue}{H}(\textcolor{blue}{k}_H) \textcolor{red}{H}(\textcolor{red}{k}_H) \textcolor{blue}{H}(\textcolor{blue}{k}_H) \rangle^m}.
\end{aligned} \tag{H28}$$

In Eq. (H28), we denote the correlated pairs of operators by same color in each pattern. The first two terms on the RHS of Eq. (H28) are equal due to cyclic invariance and follow easily from Eq. (H7),

$$\begin{aligned}\overline{\langle H(k_H)H(k_H)H(k_H)H(k_H) \rangle^m} &= \overline{\langle H(k_H)H(k_H)H(k_H)H(k_H) \rangle^m} \\ &= \left[\overline{\langle H^2(k_H) \rangle^m} \right]^2.\end{aligned}\tag{H29}$$

Similarly, the third term on the RHS of Eq. (H28) follows easily from Eq. (H27),

$$\overline{\langle H(k_H)H(k_H)H(k_H)H(k_H) \rangle^m} = \nu_H^4 F(m, N, k_H, k_H).\tag{H30}$$

Finally, $\overline{\langle H^4(k_H) \rangle^m}$ is given by,

$$\overline{\langle H^4(k_H) \rangle^m} = \nu_H^4 \left[2 \{T(m, N, k_H)\}^2 + F(m, N, k_H, k_H) \right].\tag{H31}$$

Simplifying $T(\dots)$ and $F(\dots)$ in ‘strict’ $N \rightarrow \infty$ limit and using Eqs. (H7) and (H31), the excess parameter for spinless EGOE(k_H) is,

$$\gamma_2(m) = \frac{\overline{\langle H^4(k_H) \rangle^m}}{\left[\overline{\langle H^2(k_H) \rangle^m} \right]^2} - 3 = \frac{\binom{m-k_H}{k_H}}{\binom{m}{k_H}} - 1 \xrightarrow{m \gg k_H} -\frac{k_H^2}{m}.\tag{H32}$$

Equation (H32) was first derived in [Mo-75]. As seen from Eq. (H32), state densities for spinless EGOE(k_H) approach Gaussian form for large m and they exhibit, as m increases from k_H , semicircle to Gaussian transition with $m = 2k_H$ being the transition point. The results for $\overline{\langle H^2(k_H) \rangle^m}$ and $\overline{\langle H^4(k_H) \rangle^m}$ easily extend, though not obvious, to averages over two-orbit spaces with operator H having fixed body ranks in the two spaces. It is useful to mention that the details for the two-orbit averages using binary correlation approximation are not available in literature. Now, we will discuss the two-orbit results.

In many nuclear structure applications and also for applications to interacting spin systems, fourth order traces over two orbit configurations are needed. Let us

consider m particles in two orbits with number of sp states being N_1 and N_2 respectively. Now the m -particle space can be divided into configurations (m_1, m_2) with m_1 particles in the #1 orbit and m_2 particles in the #2 orbit such that $m = m_1 + m_2$. Considering the operator H with fixed body ranks in m_1 and m_2 spaces such that (m_1, m_2) are preserved by this operators, the general form for H is,

$$H(k_H) = \sum_{i+j=k_H; \alpha, \beta, \gamma, \delta} \left[v_H^{\alpha\beta\gamma\delta}(i, j) \right] \alpha_1^\dagger(i) \beta_1(i) \gamma_2^\dagger(j) \delta_2(j). \quad (\text{H33})$$

Now, it is easily seen that, in the dilute limit,

$$\begin{aligned} & \overline{\langle H^2(k_H) \rangle^{m_1, m_2}} \\ &= \sum_{i+j=k_H} v_H^2(i, j) \sum_{\alpha, \beta, \gamma, \delta} \left\langle \alpha_1^\dagger(i) \beta_1(i) \gamma_2^\dagger(j) \delta_2(j) \beta_1^\dagger(i) \alpha_1(i) \delta_2^\dagger(j) \gamma_2(j) \right\rangle^{m_1, m_2} \\ &= \sum_{i+j=k_H} v_H^2(i, j) \sum_{\alpha, \beta} \left\langle \alpha_1^\dagger(i) \beta_1(i) \beta_1^\dagger(i) \alpha_1(i) \right\rangle^{m_1} \sum_{\gamma, \delta} \left\langle \gamma_2^\dagger(j) \delta_2(j) \delta_2^\dagger(j) \gamma_2(j) \right\rangle^{m_2} \\ &= \sum_{i+j=k_H} v_H^2(i, j) T(m_1, N_1, i) T(m_2, N_2, j). \end{aligned} \quad (\text{H34})$$

Note that $v_H^2(i, j) = \overline{[v_H^{\alpha\beta\gamma\delta}(i, j)]^2}$ and T 's are defined by Eqs. (H8) and (H9). The ensemble is defined such that $v_H^{\alpha\beta\gamma\delta}(i, j)$ are independent Gaussian random variables with zero center and the variances depend only on the indices i and j . The formula for $\overline{\langle H(k_H) H(k_H) \rangle^{m_1, m_2}}$ with finite (N_1, N_2) corrections is,

$$\overline{\langle H(k_H) H(k_H) \rangle^{m_1, m_2}} = \sum_{i+j=k_H} v_H^2(i, j) \binom{m_1}{i} \binom{m_2}{j} \left[\binom{\tilde{m}_1 + i}{i} \binom{\tilde{m}_2 + j}{j} + 1 \right]. \quad (\text{H35})$$

Similarly, with two operators H and G (with body ranks k_H and k_G respectively) that are independent and both preserving (m_1, m_2) , $\overline{\langle H(k_H) G(k_G) H(k_H) G(k_G) \rangle^{m_1, m_2}}$

is given by,

$$\overline{\langle H(k_H)G(k_G)H(k_H)G(k_G) \rangle^{m_1, m_2}} = \sum_{i+j=k_H, t+u=k_G} v_H^2(i, j) v_G^2(t, u) F(m_1, N_1, i, t) F(m_2, N_2, j, u). \quad (\text{H36})$$

Also, extending the single orbit results with finite- N corrections, we have,

$$\begin{aligned} & \overline{\langle H(k_H)G(k_G)H(k_H)G(k_G) \rangle^{m_1, m_2}} \\ &= \sum_{i+j=k_H, t+u=k_G} \sum_{\alpha_1, \beta_1, \gamma_1, \delta_1, \alpha_2, \beta_2, \gamma_2, \delta_2} v_H^2(i, j) v_G^2(t, u) \\ & \times \left\langle \alpha_1^\dagger(i) \beta_1(i) \gamma_1^\dagger(t) \delta_1(t) \beta_1^\dagger(i) \alpha_1(i) \delta_1^\dagger(t) \gamma_1(t) \right\rangle^{m_1} \\ & \times \left\langle \alpha_2^\dagger(j) \beta_2(j) \gamma_2^\dagger(u) \delta_2(u) \beta_2^\dagger(j) \alpha_2(j) \delta_2^\dagger(u) \gamma_2(u) \right\rangle^{m_2}. \end{aligned} \quad (\text{H37})$$

Applying Eqs. (H16)-(H26) to the two traces in Eq. (H37), we get

$$\begin{aligned} & \overline{\langle H(k_H)G(k_G)H(k_H)G(k_G) \rangle^{m_1, m_2}} = \sum_{i+j=k_H, t+u=k_G} v_H^2(i, j) v_G^2(t, u) \\ & \times [F(m_1, N_1, i, t) F(m_2, N_2, j, u) + B(m_1, N_1, i, t) B(m_2, N_2, j, u) \\ & + B(m_1, N_1, t, i) B(m_2, N_2, u, j) + C(m_1, N_1, i, t) C(m_2, N_2, j, u)] . \end{aligned} \quad (\text{H38})$$

The $F(\cdots)$'s appearing in Eq. (H38) are given by Eq. (H23). Also, the B 's and C 's are given by Eqs. (H24) and (H26) respectively. Finally, in the strict dilute limit as $F(\cdots)$'s dominate over B 's and C 's, we get back Eq. (H36). In all the applications discussed in Chapter 7, we use Eq. (H36). Now, using Eqs. (H34) and (H36), we have

$$\begin{aligned} & \overline{\langle H^4(k_H) \rangle^{m_1, m_2}} = 2 \left[\sum_{i+j=k_H} v_H^2(i, j) T(m_1, N_1, i) T(m_2, N_2, j) \right]^2 \\ & + \sum_{i+j=k_H, t+u=k_H} v_H^2(i, j) v_H^2(t, u) F(m_1, N_1, i, t) F(m_2, N_2, j, u). \end{aligned} \quad (\text{H39})$$

As a simple application of Eqs. (H34) and (H39), let us consider $\gamma_2(m, M_S)$ for EGOE(2)- M_S ensemble. For this ensembles, H will preserve M_S and it is defined for a system of m fermions carrying spin $\mathbf{s} = \frac{1}{2}$ degree of freedom (see also Appendix G). Then, we have two orbits with $N_1 = N_2 = \Omega$, $m_1 = m/2 + M_S$ and $m_2 = m/2 - M_S$. Here, orbit #1 corresponds to sp states with $m_{\mathbf{s}} = +\frac{1}{2}$ and orbit #2 corresponds to sp states with $m_{\mathbf{s}} = -\frac{1}{2}$. Note that the fixed- M_S dimension is $D(m, M_S) = \binom{\Omega}{m/2-M_S} \binom{\Omega}{m/2+M_S}$. By substituting $m_1 = m/2 + M_S$ and $m_2 = m/2 - M_S$, Eqs. (H34) and (H39) will give $\overline{\langle H^4(2) \rangle^{m, M_S}}$ and $\overline{\langle H^2(2) \rangle^{m, M_S}}$, respectively. Then, the fixed- (m, M_S) excess parameter $\gamma_2(m, M_S)$ in the dilute limit is given by,

$$\gamma_2(m, M_S) = \frac{\sum_{i+j=2, t+u=2} v_H^2(i, j) v_H^2(t, u) F(m_1, \Omega, i, t) F(m_2, \Omega, j, u)}{\left[\sum_{i+j=2} v_H^2(i, j) T(m_1, \Omega, i) T(m_2, \Omega, j) \right]^2} - 1, \quad (\text{H40})$$

with $T(\cdots)$'s and $F(\cdots)$'s given before.

Appendix I

Fixed- (m, M) occupation numbers

Our purpose here is to derive a simple expression for the occupation probabilities $\langle n_{m_{z_i}} \rangle^{mM}$ for m fermions in N sp states labeled by J_z quantum number m_{z_i} . Here, M are the eigenvalues of the J_z operator. As $\langle n_{m_{z_i}} \rangle^{mM}$ is an expectation value, we can write a polynomial expansion in terms of the J_z operator [Dr-77],

$$\langle n_{m_{z_i}} \rangle^{mM} = \sum_{\mu} \langle n_{m_{z_i}} P_{\mu}(\hat{J}_z) \rangle^m P_{\mu}(\widehat{M}), \quad (\text{I1})$$

where $\widehat{M} = M/\sigma_{J_z}(m)$, $\hat{J} = J_z/\sigma_{J_z}(m)$ and $P_{\mu}(M)$ are orthogonal polynomials defined by the density $\rho_{J_z}(M)$ which is close to a Gaussian. Retaining terms up to order 2, the expansion is,

$$\begin{aligned} \langle n_{m_{z_i}} \rangle^{mM} &= \langle n_{m_{z_i}} \rangle^m + \langle n_{m_{z_i}} \hat{J}_z \rangle^m \widehat{M} + \frac{(\langle n_{m_{z_i}} \hat{J}_z^2 \rangle^m - \langle n_{m_{z_i}} \rangle^m)(\widehat{M}^2 - 1)}{\langle J_z^4 \rangle^m - 1} \\ &= \langle n_{m_{z_i}} \rangle^m + \frac{\langle n_{m_{z_i}} J_z \rangle^m M}{\sigma_{J_z}^2(m)} \\ &+ \frac{1}{2} \left(\frac{\langle n_{m_{z_i}} J_z^2 \rangle^m}{\sigma_{J_z}^2(m)} - \langle n_{m_{z_i}} \rangle^m \right) \left(\frac{M^2}{\sigma_{J_z}^2(m)} - 1 \right). \end{aligned} \quad (\text{I2})$$

In the above expression we used $\langle \hat{J}_z^4 \rangle^m = 3$, the value for a Gaussian $\rho_{J_z}(M)$. Now the formulas for the traces in Eq. (I2) are as follows. Firstly,

$$\langle n_{m_{z_i}} \rangle^m = \frac{m}{N} \langle \langle n_{m_{z_i}} \rangle \rangle^1 = \frac{m}{N}. \quad (I3)$$

This implies $n_{m_{z_i}}^{v=0} = \hat{n}/N$. Also,

$$\langle n_{m_{z_i}} J_z \rangle^m = \frac{m(N-m)}{N(N-1)} \langle \langle n_{m_{z_i}} J_z \rangle \rangle^1, \quad (I4)$$

with $\langle \langle n_{m_{z_i}} J_z \rangle \rangle^1 = m_{z_i}$. Unitary decomposition of the number operator gives,

$$\langle n_{m_{z_i}} J_z^2 \rangle^m = \langle n_{m_{z_i}} \rangle^m \langle J_z^2 \rangle^m + \langle n_{m_{z_i}}^{v=1} J_z^2 \rangle^m, \quad (I5)$$

$$\langle n_{m_{z_i}}^{v=1} J_z^2 \rangle^m = \frac{m(N-m)(N-2m)}{N(N-1)(N-2)} \langle \langle n_{m_{z_i}}^{v=1} J_z^2 \rangle \rangle^1. \quad (I6)$$

Now,

$$\langle \langle n_{m_{z_i}}^{v=1} J_z^2 \rangle \rangle^1 = \langle \langle (n_{m_{z_i}} - n_{m_{z_i}}^{v=0}) J_z^2 \rangle \rangle^1 = m_{z_i}^2 - \frac{1}{N} \langle \langle J_z^2 \rangle \rangle^1, \quad (I7)$$

where we have used the result that $n_{m_{z_i}}^{v=0} = \hat{n}/N$ deduced from Eq. (I3). Thus,

$$\langle n_{m_{z_i}} J_z^2 \rangle^m / \sigma_{J_z}^2(m) = \langle n_{m_{z_i}} \rangle^m + \frac{(N-2m)(m_{z_i}^2 - \langle J_z^2 \rangle^1)}{(N-2)N \langle J_z^2 \rangle^1}. \quad (I8)$$

Substituting above traces in Eq. (I2) we have,

$$\langle n_{m_{z_i}} \rangle^{m,M} = \bar{m} + \frac{m_{z_i} M}{N \langle J_z^2 \rangle^1} - \frac{(\bar{m} - 1/2)(m_{z_i}^2 - \langle J_z^2 \rangle^1)(M^2 - \sigma_{J_z}^2(m))}{N^2 (\langle J_z^2 \rangle^1)^2 \bar{m} (1 - \bar{m})}, \quad (I9)$$

where $\bar{m} = m/N$. The expression for the occupation number $\langle n_{m_{z_i}} \rangle^{m,M}$ is close to that obtained in [Mu-00, Ze-04] where statistical mechanics approach has been employed. Thus, we have successfully reproduced the previously obtained results using moment method formalism.

Appendix J

Bivariate edgeworth expansion

Given the bivariate Gaussian, in terms of the standardized variables \hat{x} and \hat{y} ,

$$\eta_{\mathcal{G}}(\hat{x}, \hat{y}) = \frac{1}{2\pi\sqrt{1-\zeta^2}} \exp\left\{-\frac{\hat{x}^2 - 2\zeta\hat{x}\hat{y} + \hat{y}^2}{2(1-\zeta^2)}\right\}, \quad (J1)$$

the bivariate Edgeworth expansion for any bivariate distribution $\eta(\hat{x}, \hat{y})$ follows from,

$$\eta(\hat{x}, \hat{y}) = \exp\left\{\sum_{r+s \geq 3} (-1)^{r+s} \frac{k_{rs}}{r!s!} \frac{\partial^r}{\partial \hat{x}^r} \frac{\partial^s}{\partial \hat{y}^s}\right\} \eta_{\mathcal{G}}(\hat{x}, \hat{y}). \quad (J2)$$

Assuming that the bivariate reduced cumulants k_{r+s} behave as $k_{r+s} \propto \Upsilon^{-(r+s-2)/2}$ where Υ is a system parameter, and collecting in the expansion of Eq. (J2) all the terms that behave as $\Upsilon^{-P/2}$, $P = 1, 2, \dots$, we obtain the bivariate ED expansion to order $1/P$ [Ko-84, St-87],

$$\begin{aligned} \eta_{biv-ED}(\hat{x}, \hat{y}) = & \left\{ 1 + \left(\frac{k_{30}}{6} He_{30}(\hat{x}, \hat{y}) + \frac{k_{21}}{2} He_{21}(\hat{x}, \hat{y}) \right. \right. \\ & + \left. \frac{k_{12}}{2} He_{12}(\hat{x}, \hat{y}) + \frac{k_{03}}{6} He_{03}(\hat{x}, \hat{y}) \right) \\ & + \left(\left\{ \frac{k_{40}}{24} He_{40}(\hat{x}, \hat{y}) + \frac{k_{31}}{6} He_{31}(\hat{x}, \hat{y}) \right. \right. \\ & + \left. \left. \frac{k_{22}}{4} He_{22}(\hat{x}, \hat{y}) + \frac{k_{13}}{6} He_{13}(\hat{x}, \hat{y}) + \frac{k_{04}}{24} He_{04}(\hat{x}, \hat{y}) \right\} \right) \end{aligned} \quad (J3)$$

$$\begin{aligned}
& + \left\{ \frac{k_{30}^2}{72} He_{60}(\hat{x}, \hat{y}) + \frac{k_{30}k_{21}}{12} He_{51}(\hat{x}, \hat{y}) \right. \\
& + \left[\frac{k_{21}^2}{8} + \frac{k_{30}k_{12}}{12} \right] He_{42}(\hat{x}, \hat{y}) \\
& + \left[\frac{k_{30}k_{03}}{36} + \frac{k_{12}k_{21}}{4} \right] He_{33}(\hat{x}, \hat{y}) \\
& + \left[\frac{k_{12}^2}{8} + \frac{k_{21}k_{03}}{12} \right] He_{24}(\hat{x}, \hat{y}) + \frac{k_{12}k_{03}}{12} He_{15}(\hat{x}, \hat{y}) \\
& \left. + \frac{k_{03}^2}{72} He_{06}(\hat{x}, \hat{y}) \right\} \eta_{\mathcal{G}}(\hat{x}, \hat{y}) .
\end{aligned}$$

The bivariate Hermite polynomials $He_{m_1 m_2}(\hat{x}, \hat{y})$ in Eq. (J3) satisfy the recursion relation,

$$\begin{aligned}
(1 - \zeta^2) He_{m_1+1, m_2}(\hat{x}, \hat{y}) &= (\hat{x} - \zeta \hat{y}) He_{m_1, m_2}(\hat{x}, \hat{y}) \\
&- m_1 He_{m_1-1, m_2}(\hat{x}, \hat{y}) + m_2 \zeta He_{m_1, m_2-1}(\hat{x}, \hat{y}) .
\end{aligned} \tag{J4}$$

The polynomials $He_{m_1 m_2}$ with $m_1 + m_2 \leq 2$ are

$$\begin{aligned}
He_{00}(\hat{x}, \hat{y}) &= 1 , \\
He_{10}(\hat{x}, \hat{y}) &= (\hat{x} - \zeta \hat{y}) / (1 - \zeta^2) , \\
He_{20}(\hat{x}, \hat{y}) &= \frac{(\hat{x} - \zeta \hat{y})^2}{(1 - \zeta^2)^2} - \frac{1}{(1 - \zeta^2)} , \\
He_{11}(\hat{x}, \hat{y}) &= \frac{(\hat{x} - \zeta \hat{y})(\hat{y} - \zeta \hat{x})}{(1 - \zeta^2)^2} + \frac{\zeta}{1 - \zeta^2} .
\end{aligned} \tag{J5}$$

Note that $He_{m_1 m_2}(\hat{x}, \hat{y}) = He_{m_2 m_1}(\hat{y}, \hat{x})$.

Bibliography

- [Ag-01] T. Agasa, L. Benet, T. Rupp, and H.A. Weidenmüller, Eur. Phys. Lett. **56**, 340 (2001).
- [Ag-02] T. Agasa, L. Benet, T. Rupp, and H.A. Weidenmüller, Ann. Phys. (N.Y.) **298**, 229 (2002).
- [Al-91] Y. Alhassid and N. Whelan, Phys. Rev. Lett. **67**, 816 (1991).
- [Al-00] Y. Alhassid, Ph. Jacquod, and A. Wobst, Phys. Rev. B **61**, R13357 (2000).
- [Al-00a] Y. Alhassid, Rev. Mod. Phys. **72**, 895 (2000).
- [Al-01] Y. Alhassid, Ph. Jacquod, and A. Wobst, Physica E **9**, 393 (2001).
- [Al-01a] Y. Alhassid and A. Wobst, Phys. Rev. B **65**, 041304 (2001).
- [Al-05] Y. Alhassid, H.A. Weidenmüller, and A. Wobst, Phys. Rev. B **72**, 045318 (2005).
- [Al-03] E. Altman, W. Hofstetter, E. Demler, and M.D. Lukin, New J. Phys. **5**, 113 (2003).
- [An-10] G.W. Anderson, A. Guionnet, and O. Zeitouni, *An Introduction to Random Matrices* (Cambridge University Press, New York, 2010).
- [An-03] D. Angom and V.K.B. Kota, Phys. Rev. A **67**, 052508 (2003).
- [An-04] D. Angom, S. Ghosh, and V.K.B. Kota, Phys. Rev. E **70**, 016209 (2004).
- [An-05] D. Angom and V.K.B. Kota, Phys. Rev. A **71**, 042504 (2005).
- [An-05a] D. Angom and V.K.B. Kota, in the proceedings of the 3rd national conference on “Nonlinear Systems and Dynamics”, edited by M. Lakshmanan and R. Sahadevan (Chennai, India, 2006); http://www.cts.iitkgp.ernet.in/cts_html/ncnsd/paper06/125.pdf.
- [Ay-74] S. Ayik and J.N. Ginocchio, Nucl. Phys. A **221**, 285 (1974).
- [Ba-92] M.S. Bae, T. Otsuka, T. Mizusaki, and N. Fukunishi, Phys. Rev. Lett. **69**, 2349 (1992).
- [Ba-10] Z. Bai and J.W. Silverstein, *Spectral Analysis of Large Dimensional Random Matrices*, Second edition (Springer, New York, 2010).
- [Be-01] G. Benenti, G. Casati, and D.L. Shepelyansky, Euro. Phys. J. D **17**, 265 (2001).
- [Be-01a] L. Benet, T. Rupp, and H.A. Weidenmüller, Ann. Phys. **292**, 67 (2001).

- [Be-01b] L. Benet, T. Rupp, and H.A. Weidenmüller, Phys. Rev. Lett. **87**, 010601 (2001)
- [Be-03] L. Benet and H.A. Weidenmüller, J. Phys. A **36**, 3569 (2003).
- [Be-77] M.V. Berry and M. Tabor, Proc. R. Soc. London, Ser. A **356**, 375 (1977).
- [Be-81] M.V. Berry, Ann. Phys. (N.Y.) **131**, 163 (1981).
- [Bi-82] R.P. Bickerstaff, P.H. Butler, M.B. Butts, R.W. Haase, and M.F. Reid, J. Phys. A: Math. Gen. **15**, 1087 (1982).
- [Bi-68] L.C. Bidenharn and J.D. Louck, Comm. Math. Phys. **8**, 89 (1968).
- [Bi-00] R. Bijker and A. Frank, Phys. Rev. Lett. **84**, 420 (2000).
- [Bi-01] R. Bijker and A. Frank, Phys. Rev. C **64**, 061303 (2001).
- [Bl-87] R. Le Blanc and K.T. Hecht, J. Phys. A: Math. Gen. **20**, 4613 (1987).
- [Bo-92] F. Boehm and P. Vogel, *Physics of Massive Neutrinos*, Second edition (Cambridge University Press, Cambridge, 1992).
- [Bo-71] O. Bohigas and J. Flores, Phys. Lett. B **34**, 261 (1971).
- [Bo-83] O. Bohigas, R.U. Haq, and A. Pandey, in: *Nuclear Data for Science and Technology*, edited by K.H. Böckhoff (Reidel, Dordrecht, 1983), p. 809.
- [Bo-84] O. Bohigas, M.-J. Giannoni, and C. Schmit, J. Physique Lett. **45**, L-1015 (1984).
- [Bo-84a] O. Bohigas, M.-J. Giannoni, and C. Schmit, Phys. Rev. Lett. **52**, 1 (1984).
- [Bo-36] N. Bohr, Nature (London) **137**, 344 (1936).
- [Bo-98a] F. Borgonovi, I. Guarneri, and F.M. Izrailev, Phys. Rev. E **57**, 5291 (1998).
- [Bo-98b] F. Borgonovi, I. Guarneri, F.M. Izrailev, and G. Casati, Phys. Lett. A **247**, 140 (1998).
- [Br-06] Proceedings of the NATO Advanced Study Institute on *Applications of Random Matrices in Physics*, edited by É. Brézin, V. Kazakov, D. Serban, P. Wiegmann, and A. Zabrodin (Springer, The Netherlands, 2006).
- [Br-94] D.M. Brink and G. R. Satchler, *Angular Momentum*, Third edition (Oxford University Press, USA, 1994).
- [Br-81] T.A. Brody, J. Flores, J.B. French, P.A. Mello, A. Pandey, and S.S.M. Wong, Rev. Mod. Phys. **53**, 385 (1981).
- [Br-08] W.G. Brown, L.F. Santos, D.J. Starling, and L. Viola, Phys. Rev. E **77**, 021106 (2008).
- [Bu-81] P.H. Butler, *Point Group Symmetry Applications: Methods and Tables* (Plenum Press, New York, 1981).
- [Ca-00] E. Canetta and G. Maino, Phys. Lett. B **483**, 55 (2000).
- [Ca-05] M.A. Caprio and F. Iachello, Ann. Phys. (N.Y.) **318**, 454 (2005).

- [Ca-80] G. Casati, F. Valz-Gris and I. Guarneri, Lett. Nuovo Cimento Soc. Ital. Fis. **28**, 279 (1980).
- [Ca-90] G. Casati, F.M. Izrailev, and L. Molinary, Phys. Rev. Lett. **64**, 1851 (1990).
- [Ca-93] G. Casati, B.V. Chirikov, I. Guarneri, and F.M. Izrailev, Phys. Rev. E **48**, R1613 (1993).
- [Ca-09] A.C. Cassidy, D. Mason, V. Dunjko, and M. Olshanii, Phys. Rev. Lett. **102**, 025302 (2009).
- [Ch-71] F.S. Chang, J.B. French, and T.H. Thio, Ann. Phys. (N.Y.) **66**, 137 (1971).
- [Ch-78] B.D. Chang and S.S.M. Wong, Nucl. Phys. A **294**, 19 (1978).
- [Ch-03] N.D. Chavda, V. Potbhare, and V.K.B. Kota, Phys. Lett. A **311**, 331 (2003).
- [Ch-04] N.D. Chavda, V. Potbhare, and V.K.B. Kota, Phys. Lett. A **326**, 47 (2004).
- [Ch-10] N.D. Chavda, *Two-body Random Matrix Ensembles for Boson Systems with Spin*, in the proceedings of the National Seminar on “New Frontiers in Nuclear, Hadron and Mesoscopic Physics”, edited by V.K.B. Kota and A. Pratap (Allied Publishers, New Delhi, 2010), p. 38-50.
- [Co-82] A. Cortes, R.U. Haq, and A.P. Zuker, Phys. Lett. **B115**, 1 (1982).
- [Cu-01] A. Cummings, G. O’Sullivan, and D.M. Heffernan, J. Phys. B **34**, 3407 (2001).
- [Cv-82] P. Cvitanovic and A.D. Kennedy, Phys. Scr. **26**, 5 (1982).
- [Da-80] B.J. Dalton, S.M. Grimes, J.P. Vary, and S.A. Williams (ed.), *Moment Methods in Many Fermion Systems* (Plenum, New York, 1980).
- [De-91] J.M. Deutsch, Phys. Rev. A **43**, 2046 (1991).
- [Do-93] M. Doi and T. Kotani, Prog. Theo. Phys. **89**, 139 (1993).
- [Dr-77] J.P. Draayer, J.B. French, and S.S.M. Wong, Ann. Phys. (N.Y.) **106**, 472 (1977).
- [Dy-62] F.J. Dyson, J. Math. Phys. **3**, 140 (1962).
- [Dy-63] F.J. Dyson and M.L. Mehta, J. Math. Phys. **4**, 701 (1963).
- [Ed-74] A.R. Edmonds, *Angular Momentum in Quantum Mechanics* (Princeton, New Jersey, 1974).
- [El-02] S.R. Elliot and P. Vogel, Ann. Rev. Nucl. Part. Sci. **52**, 115 (2002).
- [El-58] J.P. Elliott, Proc. R. Soc. London **A245**, 128, 562 (1958).
- [Fe-91] M. Feingold, D.M. Leitner, and M. Wilkinson, Phys. Rev. Lett. **66**, 986 (1991).
- [Fl-94] V.V. Flambaum, A.A. Gribakina, G.F. Gribakin, and M.G. Kozlov, Phys. Rev. A **50**, 267 (1994).
- [Fl-96] V.V. Flambaum, G.F. Gribakin, and F.M. Izrailev, Phys. Rev. E **53**, 5729 (1996).
- [Fl-96a] V.V. Flambaum, F.M. Izrailev, and G. Casati, Phys. Rev. E **54**, 2136 (1996).

- [Fl-97] V.V. Flambaum and F.M. Izrailev, Phys. Rev. E **56**, 5144 (1997).
- [Fl-98] V.V. Flambaum, A.A. Gribakina, and G.F. Gribakin, Phys. Rev. A **58**, 230 (1998).
- [Fl-99] V.V. Flambaum, A.A. Gribakina, G.F. Gribakin, and I.V. Ponomarev, Physica D **131**, 205 (1999).
- [Fl-00] J. Flores, M. Horoi, M. Müller, and T.H. Seligman, Phys. Rev. E **63**, 026204 (2000).
- [Fl-52] B.H. Flowers, Proc. Royal Soc. (London) **A212**, 248 (1952).
- [Fl-64] B.H. Flowers and S. Szpikowski, Proc. Phys. Soc. **84**, 193 (1964).
- [Fo-10] P.J. Forrester, *Log-Gases and Random Matrices* (Princeton University Press, USA, 2010).
- [Fr-96] N. Frazier, B.A. Brown, and V. Zelevinsky, Phys. Rev. C **54**, 1665 (1996).
- [Fr-95] J.B. French, in *A Gift of Prophecy - Essays in the Celebration of the Life of R.E. Marshak*, edited by E.C.G. Sudarshan (World Scientific, Singapore, 1995), p. 156.
- [Fr-69] J.B. French, in *Isospin in Nuclear Physics*, edited by D.H. Wilkinson (North Holland, Amsterdam, 1969), p. 259.
- [Fr-70] J.B. French and S.S.M. Wong, Phys. Lett. B **33**, 449 (1970).
- [Fr-71] J.B. French and K.F. Ratcliff, Phys. Rev. C **3**, 94 (1971).
- [Fr-71a] J.B. French and S.S.M. Wong, Phys. Lett. B **35**, 5 (1971).
- [Fr-80] J.B. French, in *Moment Methods in Many Fermion Systems*, edited by B.J. Dalton, S.M. Grimes, J.P. Vary, and S.A. Williams (Plenum, New York, 1980), p. 91.
- [Fr-82] J.B. French and V.K.B. Kota, Ann. Rev. Nucl. Part. Sci. **32**, 35 (1982).
- [Fr-83] J.B. French and V.K.B. Kota, Phys. Rev. Lett. **51**, 2183 (1983).
- [Fr-88] J.B. French, V.K.B. Kota, A. Pandey, and S. Tomsovic, Ann. Phys. (N.Y.) **181**, 235 (1988).
- [Fr-06] J.B. French, S. Rab, J.F. Smith, R.U. Haq, and V.K.B. Kota, Can. J. Phys. **84**, 677 (2006).
- [Fy-91] Y.V. Fyodorov and A.D. Mirlin, Phys. Rev. Lett. **67**, 2405 (1991).
- [Fy-92] Y.V. Fyodorov and A.D. Mirlin, Phys. Rev. Lett. **69**, 1093 (1992).
- [Ga-99] J.E. García-Ramos and P. Van Isacker, Ann. Phys. (N.Y.) **274**, 45 (1999).
- [Ge-00] B. Georgeot and D.L. Shepelyansky, Phys. Rev. E **62**, 6366 (2000).
- [Ge-97] B. Georgeot and D.L. Shepelyansky, Phys. Rev. Lett. **79**, 4365 (1997).
- [Ge-68] A. Gervois, Phys. Lett. **B26**, 413 (1968).
- [Gi-80] J.N. Ginocchio, in *Moment Methods in Many Fermion Systems*, edited by B.J. Dalton, S.M. Grimes, J.P. Vary, and S.A. Williams (Plenum, New York, 1980), pp. 109.

- [Gl-05] S. Gliske, W.H. Klink, and T. Ton-That, *Acta Appl. Math.* **88**, 229 (2005).
- [Go-01] J.M.G. Gómez, K. Kar, V.K.B. Kota, J. Retamosa, and R. Sahu, *Phys. Rev. C* **64**, 034305 (2001).
- [Go-03] J.M.G. Gómez, K. Kar, V.K.B. Kota, R.A. Molina, and J. Retamosa, *Phys. Lett. B* **567**, 251 (2003).
- [Go-04] J.M.G. Gómez, K. Kar, V.K.B. Kota, R.A. Molina, and J. Retamosa, *Phys. Rev. C* **69**, 057302 (2004).
- [Go-11] J.M.G. Gómez, K. Kar, V.K.B. Kota, R.A. Molina, A. Relaño, and J. Retamosa, *Phys. Rep.* **499**, 103 (2011).
- [Gr-95] A.A. Gribankina, V.V. Flambaum, and G.F. Gribakin, *Phys. Rev. E* **52**, 5667 (1995).
- [Gr-95a] S.M. Grimes and T.N. Massey, *Phys. Rev. C* **51**, 606 (1995).
- [Gu-89] T. Guhr and H.A. Weidenmüller, *Ann. Phys.* **193**, 472 (1989).
- [Gu-98] T. Guhr, A. Müller-Groeling, and H. A. Weidenmüller, *Phys. Rep.* **299**, 189 (1998).
- [Ha-10] F. Haake, *Quantum Signatures of Chaos*, Third edition (Springer-Verlag, Heidelberg, 2010).
- [Ha-82] T.R. Halemane and J.B. French, *Phys. Rev. C* **25**, 2029 (1982).
- [Ha-62] M. Hamermesh, *Group Theory and its Application to Physical Problems* (Addison-Wesley, New York, 1962).
- [Ha-82a] R.U. Haq, A. Pandey, and O. Bohigas, *Phys. Rev. Lett.* **48**, 1086 (1982).
- [He-65] K.T. Hecht, *Nucl. Phys.* **63**, 177 (1965).
- [He-69] K.T. Hecht and S.C. Pang, *J. Math. Phys.* **10**, 1571 (1969).
- [He-74] K.T. Hecht and J.P. Draayer, *Nucl. Phys. A* **223**, 285 (1974).
- [He-74a] K.T. Hecht, *J. Math. Phys.* **15**, 2148 (1974).
- [He-07] S. Heusler, S. Müller, A. Altland, P. Braun, and F. Haake, *Phys. Rev. Lett.* **98**, 044103 (2007).
- [Ho-95] M. Horoi, V. Zelevinsky, and B.A. Brown, *Phys. Rev. Lett.* **74**, 5194 (1995).
- [Ho-07] M. Horoi and V. Zelevinsky, *Phys. Rev. C* **75**, 054303 (2007).
- [Ho-10] M. Horoi and V. Zelevinsky, *Phys. Rev. C* **81**, 034306 (2010).
- [Im-97] Y. Imry, *Introduction to Mesoscopic Physics* (Oxford University Press, New York, 1997).
- [Ja-79] C. Jacquemin and S. Spitz, *J. Phys. G* **5**, L95 (1979).
- [Ja-79a] C. Jacquemin and S. Spitz, *Z. Phys. A* **290**, 251 (1979).

- [Ja-97] Ph. Jacquod and D.L. Shepelyansky, Phys. Rev. Lett. **79**, 1837 (1997).
- [Ja-00] Ph. Jacquod and A.D. Stone, Phys. Rev. Lett. **84**, 3938 (2000).
- [Ja-01] Ph. Jacquod and A.D. Stone, Phys. Rev. B **64**, 214416 (2001).
- [Ja-02] Ph. Jacquod and I.A. Varga, Phys. Rev. Lett. **89**, 134101 (2002).
- [Ja-81] G. James and A. Kerber, *The Representation Theory of the Symmetric Group* (Addison-Wesley, New York, 1981).
- [Ja-01a] M. Janssen, *Fluctuations and Localization in Mesoscopic Electron Systems* (World Scientific Publishing Co. Pte. Ltd., Singapore, 2001).
- [Jo-98] C.W. Johnson, G.F. Bertsch, and D.J. Dean, Phys. Rev. Lett. **80**, 2749 (1998).
- [Ka-00] L. Kaplan, T. Papenbrock, and C.W. Johnson, Phys. Rev. C **63**, 014307 (2000).
- [Ka-94] J. Karwowski, Int. J. Quantum Chem. **51**, 425 (1994).
- [Ka-95] J. Karwowski, F. Rajadell, J. Planelles, and V. Mas, Atomic Data and Nuclear Data Tables **61**, 177 (1995).
- [Ki-07] M.W. Kirson and J.A. Mizrahi, Phys. Rev. C **76**, 064305 (2007).
- [Kl-09] W.H. Klink and T. Ton-That, Notices of the AMS, September (2009), p. 931.
- [Ko-79] V.K.B. Kota, Phys. Rev. C **20**, 347 (1979).
- [Ko-79a] V.K.B. Kota, J. de Physique-Letters **40**, L-579 (1979).
- [Ko-80] V.K.B. Kota and V. Potbhare, Phys. Rev. C **21**, 2637 (1980).
- [Ko-81] V.K.B. Kota, Ann. Phys. (N.Y.) **134**, 221 (1981).
- [Ko-84] V.K.B. Kota, Z. Phys. A **315**, 91 (1984).
- [Ko-89] V.K.B. Kota and K. Kar, Pramana-J. Phys. **32**, 647 (1989).
- [Ko-95] V.K.B. Kota and D. Majumdar, Z. Phys. A **351**, 377 (1995).
- [Ko-96] V.K.B. Kota, Ann. Phys. (N.Y.) **265**, 101 (1998).
- [Ko-98] V.K.B. Kota and R. Sahu, Phys. Lett. B **429**, 1 (1998).
- [Ko-99] V.K.B. Kota, D. Majumdar, R.U. Haq, and R.J. Leclair, Can. J. Phys. **77**, 893 (1999).
- [Ko-99a] V.K.B. Kota, R. Sahu, K. Kar, J.M.G. Gómez, and J. Retamosa, Phys. Rev. C **60**, 051306 (1999).
- [Ko-99b] V.K.B. Kota and S. Sumedha, Phys. Rev. E **60**, 3405 (1999).
- [Ko-00] V.K.B. Kota and R. Sahu, Phys. Rev. E **62**, 3568 (2000).
- [Ko-01] V.K.B. Kota, Phys. Rep. **347**, 223 (2001).
- [Ko-01a] V.K.B. Kota and R. Sahu, Phys. Rev. E **64**, 016219 (2001).

- [Ko-02] V.K.B. Kota and R. Sahu, Phys. Rev. E **66**, 037103 (2002).
- [Ko-02a] V.K.B. Kota and K. Kar, Phys. Rev. E **65**, 026130 (2002).
- [Ko-03] V.K.B. Kota, Ann. Phys. (N.Y.) **306**, 58 (2003).
- [Ko-04] V.K.B. Kota, High Energy Phys. and Nucl. Phys. (China) **28**, 1307 (2004).
- [Ko-05] V.K.B. Kota, J. Math. Phys. **46**, 033514 (2005).
- [Ko-06] V.K.B. Kota, N.D. Chavda, and R. Sahu, Phys. Lett. A **359**, 381 (2006).
- [Ko-06a] V.K.B. Kota, Int. J. Mod. Phys. E **15**, 1869 (2006).
- [Ko-06b] V.K.B. Kota and J.A. Castilho Alcarás, Nucl. Phys. A **764**, 181 (2006).
- [Ko-06c] V.K.B. Kota, in *Focus on Boson Research*, edited by A.V. Ling (Nova Science Publishers Inc., New York, 2006), p. 57-105.
- [Ko-07] V.K.B. Kota, J. Math. Phys. **48**, 053304 (2007).
- [Ko-07a] V.K.B. Kota, Prog. Theo. Phys. **118**, 893 (2007).
- [Ko-08] V.K.B. Kota, Manan Vyas, and K.B.K. Mayya, Int. J. Mod. Phys. E **17**, 318 (2008).
- [Ko-08a] V.K.B. Kota, *Nuclear Models and Statistical Spectroscopy for Double-Beta Decay*, in 'Neutrinoless Double Beta Decay', edited by V.K.B. Kota and U. Sarkar (Narosa Publishing House, New Delhi, India, 2008).
- [Ko-10] V.K.B. Kota and R.U. Haq, *Spectral Distributions in Nuclei and Statistical Spectroscopy* (World Scientific, Singapore, 2010).
- [Ko-11] V.K.B. Kota, A. Relaño, J. Retamosa, and Manan Vyas, arXiv:1102.0528.
- [Ku-67] T.T.S. Kuo, Nucl. Phys. **A103**, 71 (1967).
- [Ku-97] D. Kusnezov, Phys. Rev. Lett. **79**, 537 (1997).
- [Ku-00] D. Kusnezov, Phys. Rev. Lett. **85**, 3773 (2000).
- [Le-08] R.J. Leclair, R.U. Haq, V.K.B. Kota, and N.D. Chavda, Phys. Lett. A **372**, 4373 (2008).
- [Le-94] C.H. Lewenkopf and V.G. Zelevinsky, Nucl. Phys. A **569**, 183c (1994).
- [Li-90] X. Li and J. Paldus, J. Math. Phys. **31**, 1589 (1990).
- [Lo-70] J.D. Louck, Am. J. Phys. **38**, 3 (1970).
- [Lo-70a] J.D. Louck and L.C. Biedenharn, J. Math. Phys. **11**, 2368 (1970).
- [Lu-01] S. Lüscher, T. Heinzl, K. Ensslin, W. Wegscheider, and M. Bichler, Phys. Rev. Lett. **86**, 2118 (2001).
- [Ma-07] D. Majumdar and K. Kar, Pramana-J. Phys. **68**, 423 (2007).
- [Ma-98] D. Majumdar, K. Kar and A. Ansari, J. Phys. G **24**, 2103 (1998).

- [Ma-09] Manan Vyas, V.K.B. Kota, and N.D. Chavda, Phys. Lett. A **373**, 1434 (2009).
- [Ma-09a] Manan Vyas and V.K.B. Kota, in the proceedings of the conference on “Non-Hermitian Hamiltonians in Quantum Physics”, edited by S.R. Jain and Z. Ahmed, Pramana-J. Phys. **73**, 521 (2009).
- [Ma-10] Manan Vyas, *Random Interaction Matrix Ensembles in Mesoscopic Physics*, in the proceedings of the National Seminar on “New Frontiers in Nuclear, Hadron and Mesoscopic Physics”, edited by V.K.B. Kota and A. Pratap (Allied Publishers, New Delhi, 2010), p. 23-37; arXiv:1004.2761.
- [Ma-10a] Manan Vyas, V.K.B. Kota, and N.D. Chavda, Phys. Rev. E **81**, 036212 (2010).
- [Ma-10b] Manan Vyas and V.K.B. Kota, Ann. Phys. (N.Y.) **325**, 2451 (2010).
- [Ma-10c] Manan Vyas and V.K.B. Kota, Euro. Phys. J. A **45**, 111 (2010).
- [Ma-11] Manan Vyas, V.K.B. Kota, N.D. Chavda, and V. Potbhare, arXiv:1010.6054.
- [Ma-11a] Manan Vyas, V.K.B. Kota, and P.C. Srivastava, accepted for publication in Physical Review C; arXiv:1101.1711.
- [Ma-67] V.A. Marčenko and L.A. Pastur, Math. USSR-Sbornik **1**, 457 (1967).
- [Mc-79] S.W. McDonald and A.N. Kaufman, Phys. Rev. Lett. **42**, 1189 (1979).
- [Me-04] M.L. Mehta, *Random Matrices*, Third edition (Elsevier B.V., The Netherlands, 2004).
- [Me-05] C. Mejía-Monasterio, G. Benenti, G.G. Carlo, and G. Casati, Phys. Rev. A **71**, 062324 (2005).
- [Mi-10] G.E. Mitchell, A. Richter, and H. A. Weidenmüller, Rev. Mod. Phys. **82**, 2845 (2010),
- [Mi-00] A.D. Mirlin, Phys. Rep. **326**, 259 (2000).
- [Mo-07] D. Moclaj, T. Rauscher, G. Martínez-Pinedo, K. Langanke, L. Pacearescu, A. Faessler, F.-K. Thielemann, and Y. Alhassid, Phys. Rev. C **75**, 045805 (2007).
- [Mo-73] K.K. Mon, B.A. Dissertation, Princeton University, 1973.
- [Mo-75] K.K. Mon and J.B. French, Ann. Phys. (N.Y.) **95**, 90 (1975).
- [Mo-06] S. Montangero and L. Viola, Phys. Rev. A **73**, 040302(R) (2006).
- [Mu-02] D. Mulhall, Ph.D. Thesis, Michigan State University, 2002.
- [Mu-00] D. Mulhall, A. Volya and V. Zelevinsky, Phys. Rev. Lett. **85**, 4016 (2000).
- [Mu-06] L. Muñoz, E. Faleiro, R.A. Molina, A. Relaño, and J. Retamosa, Phys. Rev. E **73**, 036202 (2006).
- [Na-01] R.C. Nayak and V.K.B. Kota, Phys. Rev. C **64**, 057303 (2001).
- [Ne-29] J. von Neumann and E.P. Wigner, Phys. Z. **30**, 462 (1929).
- [No-72] M. Nomura, Prog. Theo. Phys. **48**, 110 (1972).

- [No-86] M. Nomura, J. Math. Phys. **27**, 536 (1986).
- [No-09] F. Nowacki and A. Poves, Phys. Rev. C **79**, 014310 (2009).
- [Ol-09] M. Olshanii and V. Yurovsky, arxiv:0911.5587.
- [Pa-81] A. Pandey, Ann. Phys. (N.Y.) **134**, 110 (1981).
- [Pa-02] T. Papenbrock, L. Kaplan, and G.F. Bertsch, Phys. Rev. B **65**, 235120 (2002).
- [Pa-04] T. Papenbrock and H.A. Weidenmüller, Phys. Rev. Lett. **93**, 132503 (2004).
- [Pa-05] T. Papenbrock and H.A. Weidenmüller, Nucl. Phys. A **757**, 422 (2005).
- [Pa-06] T. Papenbrock and H.A. Weidenmüller, Phys. Rev. C **73**, 014311 (2006).
- [Pa-07] T. Papenbrock and H.A. Weidenmüller, Rev. Mod. Phys. **79**, 997 (2007).
- [Pa-08] T. Papenbrock and H.A. Weidenmüller, Phys. Rev. C **78**, 054305 (2008).
- [Pa-11] T. Papenbrock, Z. Pluhař, J. Tithof, and H. A. Weidenmüller, Phys. Rev. E **83**, 031130 (2011).
- [Pa-72] J.C. Parikh and S.S.M. Wong, Nucl. Phys. A **182**, 593 (1972).
- [Pa-65] J.C. Parikh, Nucl. Phys. **63**, 214 (1965).
- [Pa-73] J.C. Parikh, Ann. Phys. **76**, 202 (1973).
- [Pa-78] J.C. Parikh, *Group Symmetries in Nuclear Structure* (Plenum, New York, 1978).
- [Pa-78a] J.C. Parikh, J. Phys. B **11**, 1881 (1978).
- [Pa-98] S.R. Patel, D.R. Stewart, C.M. Marcus, M. Gökçedağ, Y. Alhassid, A.D. Stone, C.I. Duruöz, and J.S. Harris, Jr., Phys. Rev. Lett. **80**, 4522 (1998).
- [Pa-00] K. Patel, M.S. Desai, V. Potbhare, and V.K.B. Kota, Phys. Lett. A **275**, 329 (2000).
- [Pe-10] G. Pelka, K. Byczuk, and J. Tworzydło, arXiv:1008.0529.
- [Pi-07] I. Pižorn, T. Prosen, and T.H. Seligman, Phys. Rev. B **76**, 035122 (2007).
- [Pi-08] I. Pižorn, T. Prosen, S. Mossmann, and T.H. Seligman, New J. Phys. **10**, 023020 (2008).
- [Pl-96] J. Planelles, F. Rajadell, J. Karwowski, and V. Mas, Phys. Rep. **267**, 161 (1996).
- [Pl-97] J. Planelles, F. Rajadell, and J. Karwowski, J. Phys. A **30**, 2181 (1997).
- [Pl-02] Z. Pluhař and H.A. Weidenmüller, Ann. Phys. (N.Y.) **297**, 344 (2002).
- [Po-65] C.E. Porter, *Statistical Theories of Spectra: Fluctuations* (Academic Press, New York, 1965).
- [Po-75] V. Potbhare, Ph.D. Thesis, University of Rochester, 1975.
- [Po-91] V. Potbhare and N. Tressler, Nucl. Phys. A **530**, 171 (1991).
- [Qu-74] C. Quesne and S. Spitz, Ann. Phys. (N.Y.) **85**, 115 (1974).

- [Qu-75] C. Quesne, J. Math. Phys. **16**, 2427 (1975).
- [Qu-77] C. Quesne and S. Spitz, J. Phys. Lett. (Paris) **38**, 337 (1977).
- [Ra-71] K.F. Ratcliff, Phys. Rev. C **3**, 117 (1971).
- [Ri-08] M. Rigol, V. Dunjko, and M. Olshanii, Nature (London) **452**, 854 (2008).
- [Ri-09] M. Rigol, Phys. Rev. Lett. **103**, 100403 (2009).
- [Ro-60] N. Rosenzweig and C.E. Porter, Phys. Rev. **120**, 1698 (1960).
- [Sa-10] L.F. Santos and M. Rigol, Phys. Rev. E **81**, 036206 (2010).
- [Sa-10a] L.F. Santos and M. Rigol, Phys. Rev. E **82**, 031130 (2010).
- [Sc-08] S. Schmidt and Y. Alhassid, Phys. Rev. Lett. **101**, 207003 (2008).
- [Se-88] B.G. Searle and P.H. Butler, J. Phys. A: Math. Gen. **21**, 1977 (1988).
- [Sh-08] J.J. Shen, A. Arima, Y.M. Zhao, and N. Yoshinaga, Phys. Rev. C **78**, 044305 (2008).
- [Sh-10] Yu Shi, Phys. Rev. A **82**, 023603 (2010).
- [So-02] O. Sorlin *et al.*, Phys. Rev. Lett. **88**, 092501 (2002).
- [Sr-94] M. Srednicki, Phys. Rev. E **50**, 888 (1994).
- [St-06] H.-J. Stöckmann, *Quantum Chaos: An Introduction* (Cambridge University Press, New York, 2006).
- [St-87] A. Stuart and J.K. Ord, *Kendall's Advanced Theory of Statistics : Distribution Theory* (Oxford University Press, New York, 1987).
- [Ta-93] I. Talmi, *Simple Models of Complex Nuclei: The Shell Model and Interacting Boson Model* (Harwood Academic Publishers, Switzerland, 1993).
- [Te-06] E. Terán and C.W. Johnson, Phys. Rev. C **73**, 024303 (2006).
- [Te-06a] E. Terán and C.W. Johnson, Phys. Rev. C **74**, 067302 (2006).
- [To-86] S. Tomsovic, Ph.D. Thesis, University of Rochester, 1986.
- [To-00] S. Tomsovic, M.B. Johnson, A.C. Hayes, and J.D. Bowman, Phys. Rev. C **62**, 054607 (2000).
- [Tu-04] A.M. Tulino and S. Verdú, *Random Matrix Theory and Wireless Communication* (now Publishers Inc., USA, 2004).
- [Tu-06] H.E. Türeci and Y. Alhassid, Phys. Rev. B **74**, 165333 (2006).
- [Ul-08] D. Ullmo, Rep. Prog. Phys. **71**, 026001 (2008).
- [Va-07] J.P. Valencia and H.C. Wu, AIP Conf. Proc. **947**, 283 (2007).
- [Va-95] P. Van Isacker, D.D. Warner, and D.S. Brenner, Phys. Rev. Lett. **74**, 4607 (1995).
- [Va-99] P. Van Isacker, O. Juillet, and F. Nowacki, Phys. Rev. Lett. **82**, 2060 (1999).

- [Va-05] P. Van Isacker, D.D. Warner, and A. Frank, Phys. Rev. Lett. **94**, 162502 (2005).
- [Ve-02] V. Velázquez and A.P. Zuker, Phys. Rev. Lett. **88**, 072502 (2002).
- [Ve-81] J.J.M. Verbaarschot and P.J. Brussaard, Phys. Lett. **B102**, 210 (1981).
- [Ve-82] J.J.M. Verbaarschot, Ph.D. Thesis, Fysisch Laboratorium, Utrecht, The Netherlands, 1982.
- [Ve-84] J.J.M. Verbaarschot and P.J. Brussaard, Nucl. Phys. **A423**, 77 (1984).
- [Vi-95] N. Ja. Vilenkin and A.U. Klimyk, *Representation of Lie Groups and Special Functions: Recent Advances* (Kluwer Academic, Dordrecht, The Netherlands, 1995).
- [Vo-08] A. Volya, Phys. Rev. Lett. **100**, 162501 (2008).
- [We-09] H. A. Weidenmüller and G. E. Mitchell, Rev. Mod. Phys. **81**, 539 (2009).
- [Wh-93] N. Whelan and Y. Alhassid, Nucl. Phys. A **556**, 42 (1993).
- [Wi-37] E.P. Wigner, Phys. Rev. **51**, 106 (1937).
- [Wi-55] E.P. Wigner, Ann. Math. **62**, 548 (1955).
- [Wi-57] E.P. Wigner, Ann. Math. **65**, 203 (1957).
- [Wi-61] E.P. Wigner, *The Probability of the Existence of a Self Reproducing Unit*, Reproduced from *The Logic of Personal Knowledge: Essays in Honor of Michael Polanyi, Chapter 19* (Routledge and Kegan Paul, London, 1961) in *Symmetries and Reflections: Scientific Essays of E.P. Wigner*, edited by W.J. Moore and M. Scriven, (Indiana University Press, Bloomington, 1967), reprinted by (Ox Bow Press, Connecticut, 1979), p. 200.
- [Wi-67] E.P. Wigner, SIAM Review **9**, 1 (1967).
- [Wi-28] J. Wishart, Biometrika **20A**, 32 (1928).
- [Wo-72] S.S.M. Wong and J. B. French, Nucl. Phys. A **198**, 188 (1972).
- [Wo-86] S.S.M. Wong, *Nuclear Statistical Spectroscopy* (Oxford University Press, New York, 1986).
- [Wr-10] M. Wright and R. Weiver, *New Directions in Linear Acoustics and Vibrations: Quantum Chaos, Random Matrix Theory and Complexity* (Cambridge University Press, New York, 2010).
- [Wy-70] B.G. Wybourne, *Symmetry Principles and Atomic Spectroscopy* (Wiley, New York, 1970).
- [Wy-74] B.G. Wybourne, *Classical Groups for Physicists* (Wiley, New York, 1974).
- [Yi-07] S.-K. Yip, Phys. Rev. A **75**, 023625 (2007).
- [Yo-09] N. Yoshida, Y.M. Zhao, and A. Arima, Phys. Rev. C **80**, 064324 (2009).
- [Yo-09a] N. Yoshinaga, A. Arima, J.J. Shen, and Y.M. Zhao, Phys. Rev. C **79**, 017301 (2009).

- [Ze-96] V. Zelevinsky, B.A. Brown, N. Frazier, and M. Horoi, Phys. Rep. **276**, 85 (1996).
- [Ze-04] V. Zelevinsky and A. Volya, Phys. Rep. **391**, 311 (2004).
- [Zh-04] Y.M. Zhao, A. Arima, N. Shimizu, K. Ogawa, N. Yoshinaga, and O. Scholten, Phys. Rev. C **70**, 054322 (2004).
- [Zh-04a] Y.M. Zhao, A. Arima, and N. Yoshinaga, Phys. Rep. **400** 1 (2004).
- [Zu-01] A.P. Zuker, L.W. Ndeuna, F. Nowacki, and E. Caurier, Phys. Rev. C **64**, 021304(R) (2001).